NATO Science for Peace and Security Series - C:
Environmental Security

Increasing Seismic Safety by Combining Engineering Technologies and Seismological Data

Edited by
Marco Mucciarelli
Marijan Herak
John Cassidy

Springer

NATO OTAN

This publication is supported by:

The NATO Science for Peace and Security Programme

Increasing Seismic Safety by Combining Engineering Technologies and Seismological Data

NATO Science for Peace and Security Series

This Series presents the results of scientific meetings supported under the NATO Programme: Science for Peace and Security (SPS).

The NATO SPS Programme supports meetings in the following Key Priority areas: (1) Defence Against Terrorism; (2) Countering other Threats to Security and (3) NATO, Partner and Mediterranean Dialogue Country Priorities. The types of meeting supported are generally "Advanced Study Institutes" and "Advanced Research Workshops". The NATO SPS Series collects together the results of these meetings. The meetings are co-organized by scientists from NATO countries and scientists from NATO's "Partner" or "Mediterranean Dialogue" countries. The observations and recommendations made at the meetings, as well as the contents of the volumes in the Series, reflect those of participants and contributors only; they should not necessarily be regarded as reflecting NATO views or policy.

Advanced Study Institutes (ASI) are high-level tutorial courses intended to convey the latest developments in a subject to an advanced-level audience

Advanced Research Workshops (ARW) are expert meetings where an intense but informal exchange of views at the frontiers of a subject aims at identifying directions for future action

Following a transformation of the programme in 2006 the Series has been re-named and re-organised. Recent volumes on topics not related to security, which result from meetings supported under the programme earlier, may be found in the NATO Science Series.

The Series is published by IOS Press, Amsterdam, and Springer, Dordrecht, in conjunction with the NATO Public Diplomacy Division.

Sub-Series

A.	Chemistry and Biology	Springer
B.	Physics and Biophysics	Springer
C.	Environmental Security	Springer
D.	Information and Communication Security	IOS Press
E.	Human and Societal Dynamics	IOS Press

http://www.nato.int/science
http://www.springer.com
http://www.iospress.nl

Series C: Environmental Security

Increasing Seismic Safety by Combining Engineering Technologies and Seismological Data

Edited by

Marco Mucciarelli
University of Basilicata, Department of Structures,
Soil Dynamics and Applied Geology,
Potenza, Italy

Marijan Herak
University of Zagreb, Faculty of Science, Department of Geophysics,
Zagreb, Croatia

and

John Cassidy
Natural Resources Canada, Geological Survey of Canada,
Sidney, BC, Canada

Published in cooperation with NATO Public Diplomacy Division

Proceedings of the NATO Advanced Research Workshop on
Increasing Seismic Safety by Combining Engineering Technologies
and Seismological Data
Dubrovnik, Croatia
19–21 September 2007

Library of Congress Control Number: 2008936835

ISBN 978-1-4020-9194-0 (PB)
ISBN 978-1-4020-9193-3 (HB)
ISBN 978-1-4020-9196-4 (e-book)

Published by Springer,
P.O. Box 17, 3300 AA Dordrecht, The Netherlands.

www.springer.com

Printed on acid-free paper

Contents

Introduction ix

Contributors xiii

Participant Sketches xvi

1 The Use of Ambient Noise for Building and Soil Characterisation . . . 1
Marijan Herak

1.1 The Need for Standardized Approach for Estimating the Local Site Effects Based on Ambient Noise Recordings 3
Kuvvet Atakan

1.2 Are Transients Carrying Useful Information for Estimating H/V Spectral Ratios? 17
Stefano Parolai, Matteo Picozzi, Angelo Strollo, Marco Pilz, Domenico Di Giacomo, Barbara Liss, and Dino Bindi

1.3 Basic Structure of QTS (HVSR) and Examples of Applications 33
Yutaka Nakamura

1.4 Ambient Noise and Site Response: From Estimation of Site Effects to Determination of the Subsoil Structure 53
Francisco J. Chávez-García

1.5 *In-Situ* Estimates of Material Damping from Environmental Noise Measurements 73
Dario Albarello and Francesco Baliva

1.6 Estimates of Vs30 Based on Constrained H/V Ratio Measurements Alone 85
Silvia Castellaro and Francesco Mulargia

1.7 Comparison of Recorded Dynamic Characteristics of Structures and Ground During Strong and Weak Shaking . . . 99
Mehmet Çelebi

1.8 HVSR Technique Improvement Using Redundant Wavelet Transform 117
Filippos Vallianatos and George Hloupis

2 Effect of Buildings on Free-Field Ground Motion 139
Marco Mucciarelli

2.1 Effect of Building-Building Interaction on "Free-Field" Ground Motion 141
Marco Mucciarelli, Rocco Ditommaso, Maria Rosaria Gallipoli, and Felice Ponzo

3 Role of Dynamic Properties on Building Vulnerability 147
Angelo Masi

3.1 How Far Ambient Noise Measurement May Help to Assess Building Vulnerability? 151
Claude Boutin and Stéphane Hans

3.2 Assessment of Seismic Capacity of Existing Buildings – Effects of Uncertainties 181
Dimitrios Baros, Miltiadis Kyrkos, Andreas Maravas, and Stavros Anagnostopoulos

3.3 Estimation of the Period of Vibration of Existing RC Building Types Based on Experimental Data and Numerical Results 207
Angelo Masi and Marco Vona

3.4 Retrofitting and Strengthening Evaluation from Stiffness Variations of a Damaged Building from Ambient Vibration Recordings 227
Mohammed N. Farsi, Bertrand Guillier, Jean-Luc Chatelain, and Sid-Ahmed Zermout

4 State-of-the-Art – Recent Advances and Applications 239
John F. Cassidy

4.1 Microtremor Soil-Structure Resonance Study in the Bovec Basin (NW Slovenia) Related to 1998 and 2004 Damaging Earthquakes 241
Andrej Gosar

4.2 Recent Earthquake Site Response Studies in Canada 257
John F. Cassidy and Sheri Molnar

4.3 Recent Applications of Ambient Vibration Measurements in Croatia 281
Marijan Herak

4.4 Applications to World Heritage Sites 293
Yutaka Nakamura, Jun Saita, and Tsutomu Sato

4.5 Two Applications of the HVSR Technique to Cultural Heritage and Historical Masonry 325
Domenico Liberatore, Marco Mucciarelli, Maria Rosaria Gallipoli, and Nicola Masini

4.6 Overview of Seismic Hazard Studies in Tunis City 337
Najla Bouden-Romdhane, Pierre Mechler, Anne-Marie Duval, and Sameh Anibi

4.7 An Empirical Geotechnical Seismic Site Response Procedure . . . 353
Adrian Rodriguez-Marek, Jonathan D. Bray, and Norm A. Abrahamson

5 Conclusions 381

Introduction

The current state-of-the-art allows seismologists to give statistical estimates of the probability of a large earthquake striking a given region, identifying the areas in which the seismic hazard is the highest. However, the usefulness of these estimates is limited, without information about local subsoil conditions and the vulnerability of buildings. Identifying the sites where a local amplification of seismic shaking will occur, and identifying the buildings that will be the weakest under the seismic shaking is the only strategy that allows effective defence against earthquake damage at **an** affordable cost, by applying selective reinforcement only to the structures that need it.

Unfortunately, too often the Earth's surface acted as a divide between seismologists and engineers. Now it is becoming clear that the building behaviour largely depends on the seismic input and the buildings on their turn act as seismic sources, in an intricate interplay that non-linear phenomena make even more complex. These phenomena are often the cause of observed damage enhancement during past earthquakes. While research may pursue complex models to fully understand soil dynamics under seismic loading, we need, at the same time, simple models valid on average, whose results can be easily transferred to end users without prohibitive expenditure. Very complex models require a large amount of data that can only be obtained at a very high cost or may be impossible to get at all.

Today, the interaction between engineers and seismologists is increasing, but still many questions remain unanswered. The idea of organizing the Advanced Research Workshop (ARW) in Dubrovnik, Croatia (19–21 September, 2007, http://nato.gfz.hr/Arw/Arw.html) came from recent discussions during meetings that put together seismologists and engineers: the NATO Science for Peace project named "Assessment of Seismic Site Amplification and Seismic Building Vulnerability in the FYR Macedonia, Croatia and Slovenia" (ASSASBV, more details at http://nato.gfz.hr), the ECEES Conference, Session STS-10 (http://www.usc.edu/dept/civil_eng/Earthquake_eng/ECEES_STS-E10/) and a joint seismologists-engineers workshop held in Italy (http://www.reluis.it/).

Under the title "Increasing Seismic Safety by Combining Engineering Technologies and Seismological Data", we grouped several topics to be discussed together by engineers and seismologists:

1. Can we use ambient noise building and soil characterisation to extract useful information for engineers?
2. How we can tell apart a frequency decrease due to distributed damage, concentrated damage, time-varying building and soil behaviour?
3. Which is the role of transients in ambient noise analysis?
4. Can we quantify the influence of existing buildings on ground-motion recordings (both noise and earthquake)?
5. To which extent soil-building resonance is a cause of damage enhancement?
6. How to couple soil and building non-linear behaviour?

The ARW aimed to bring together the most recent experience from highly qualified scientists, compare national experience and ongoing projects, and provide framework for discussion among participants.

The expected outcomes were guidelines that will help to make the most of current practice, new ideas to be put forward in future research and give the opportunity to devise new, larger projects on a trans-national basis.

Among the examples of possible practical results to be implemented following the outcome of the meeting are:

- Modification to existing building codes for soil classification
- Simplified approaches to building vulnerability and soil-building resonance, to be put in practice in megacities

However, it has to be pointed out that we did not want to reach consensus at all costs. Among the invited speakers, some are known for different points of view on some topics. The organisers believe that only from the comparison of contrasting theories it is possible to achieve advancements in knowledge. If a single idea was agreed upon, this was most welcome. But when contrasting views remained, they are fairly represented in workshop proceedings, so to stimulate further research. The conclusion of the ARW represent the current status of knowledge. On most question there is an unanimous answer, but in some cases different views are present and the disagreement is faithfully reported.

The Editors wish to acknowledge the support of the NATO Science committee that made possible the organisation of the workshop and the publication of this book.

Lectures Given

Wednesday, 19 September, 9:30–13:00

Marijan Herak – Marco Mucciarelli: Welcome speech and presentation of Project ASSASBV (NATO SfP 980857)

Kuvvet Atakan: The need for standardized H/V spectral ratio approach: Data collection, processing and interpretation
Paco Chavez-Garcia: Seismic noise, soil response, and subsoil structure
Yutaka Nakamura: Characteristics of H/V Spectrum

Wednesday, 19 September, 15:00–18:30

Dario Albarello: In situ estimate of seismic attenuation from noise measurements
Francesco Mulargia: Constrained single-station only HVSR estimates of Vs30 and deviations from 1-D subsoil geometry
Andrej Gosar: Microtremor study for assessing site effects in the Bovec basin (NW Slovenia) related to 1998 Mw 5.6 and 2004 Mw 5.2 earthquakes
John F. Cassidy: Earthquake Site Response Studies in Canada: Recent Advances and Applications

Thursday, 20 September, 9:30–13:00

Adrian Rodriguez-Marek: Geotechnical Site Classifications for Building Code Applications
John Douglas: Using seismological data to improve ground-motion predictions for engineering purposes
Adrian Rodriguez-Marek: Geotechnical Aspects of the August 15, 2007 Mw 8.0 Pisco, Peru Earthquake: Preliminary Observations
Pierre-Yves Bard: Modifications to seismic hazard due to urban environment: increase or decrease – Constraints from numerical and physical modelling

Thursday, 20 September, 15:00–18:30

Marco Mucciarelli: Effect of built environment on "free field" ground motion
Jun Saita: Vulnerability Assessment for Ground and Structures using Ambient Noise
Marijan Herak: Recent measurements of ambient vibrations in buildings in Croatia
Zoran Milutinović: Modal analysis of special structures using ambient vibration

Friday, 21 September, 9:30–13:00

Dominik H. Lang: The application of ambient seismic noise for engineering purposes
Claude Boutin: How far ambient noise measurements may help to assess building vulnerability?
Stavros A. Anagnostopoulos: Assessment of seismic capacity of existing buildings under uncertain soil properties
Najla Bouden Romdhane: Overview of Seismic Site Response Analysis in Tunis City

Friday, 21 September, 15:00–18:30

Mehmet Celebi: Comparison of recorded dynamic characteristics of structures and ground during strong and weak shaking

Angelo Masi: Estimation of the period of vibration of existing RC building types based on experimental data and numerical results
Sergey Tyagunov: Assessment of seismic vulnerability of built environment in earthquake prone areas
Domenico Liberatore/Marco Mucciarelli: Applications of the HVSR technique to cultural heritage and historical masonry
Final discussion and conclusion

Contributors

Norm A. Abrahamson Geosciences Department, Pacific Gas & Electric Company, San Francisco, CA 94177

Dario Albarello Dip. Di Scienze della Terra – Università di Siena – Via Laterina, 8 – 53100 Siena – Italy, albarello@unisi.it

Stavros A. Anagnostopoulos Department of Civil Engineering, University of Patras, 26500, Patras, Greece, saa@upatras.gr

Sameh Anibi Ecole Nationale d'Ingénieurs de Tunis, Department of Civil Engineering, Tunis, Tunisia

Kuvvet Atakan Department of Earth Sciences, University of Bergen, Norway, atakan@geo.uib.no

Francesco Baliva Dip. Di Scienze della Terra – Università di Siena – Via Laterina, 8 – 53100 Siena – Italy

Dimitrios Baros Department of Civil Engineering, University of Patras, 26500, Patras, Greece

D. Bindi Istituto Nazionale di Geofisica e Vulcanologia, via Bassini 15, 20133 Milano, Italy

Najla Bouden-Romdhane Ecole Nationale d'Ingénieurs de Tunis, Department of Civil Engineering, Tunis, Tunisia

Claude Boutin Université de Lyon, Laborataire Géomateriaux, Département Génic Civil et Biâtiment, URA CNRS 1652, claude.boutin@entpe.fr

Jonathan D. Bray Department of Civil and Environmental Engineering, University of California, Berkeley, CA 94720-1710

John F. Cassidy Geological Survey of Canada, Sidney, BC, Canada
and
University of Victoria, Victoria, BC, Canada, JCassidy@NRCan.gc.ca

Silvia Castellaro Dipartimento di Fisica, Università di Bologna, Viale Berti Pichat 8, 40127 Bologna, Italy

Mehmet Çelebi Earthquake Hazards Team, USGS, Menlo Park, CA. 94025, celebi@usgs.gov

Francisco J. Chávez-García Coordinación de Ingeniería Sismológica, Instituto de Ingeniería, Universidad Nacional Autónoma de México, Ciudad Universitaria, México, D.F. 04510, Mexico

Rocco Ditommaso DiSGG – Università della Basilicata, Potenza, Italy

Anne-Marie Duval CETE méditerranée, Nice, France

Maria Rosaria Gallipoli DiSGG – Università della Basilicata, Potenza, Italy, gallipoli@imaa.cnr.it

D. Di Giacomo GeoForschungsZentrum Potsdam, Telegrafenberg, 14473 Potsdam, Germany
and
Univertität Potsdam, Karl-Liebknecht-Strasse, 14476 Potsdam, Germany

Andrej Gosar Environmental Agency of Slovenia, Seismology and Geology Office, Dunajska 47, SI-1000 Ljubljana, Slovenia and University of Ljubljana, Faculty of Natural Sciences and Engineering, andrej.gosar@gov.si

S. Hans Ecole Nationale des Travaux Publics de l'Etat, rue Maurice Audin, 69518 Vaulx-en-Velin, France, stephane.hans@entpe.fr

Marijan Herak University of Zagreb, Faculty of Science, Department of Geophysics, Horvatovac bb, 10000 Zagreb, Croatia, herak@irb.hr

George Hloupis Department of Electronic and Computer Engineering, Brunel University, Uxbridge, Middlesex, UB83PH, United Kingdom

Miltiadis Kyrkos Department of Civil Engineering, University of Patras, 26500, Patras, Greece

D. Liberatore University of Basilicata, DiSGG, Potenza, Italy, domenico.liberatore @unibas.it

Andreas Maravas Department of Civil Engineering, University of Patras, 26500, Patras, Greece

Angelo Masi DiSGG, University of Basilicata, Campus Macchia Romana, Potenza, Italy, angelo.masi@unibas.it

N. Masini CNR, IBAM, Potenza, Italy, masini@iisf.pz.cnr.it

Pierre Mechler Département de Géophysique Appliquée, Université Paris 6

Sheri Molnar Natural Resources Canada, Sidney, BC, Canada, and University of Victoria, Victoria, BC, Canada

Marco Mucciarelli DiSGG – Università della Basilicata, Potenza, Italy, marco.mucciarelli@unibas.it

Francesco Mulargia Dipartimento di Fisica, Università di Bologna, Viale Berti Pichat 8, 40127 Bologna, Italy

Yutaka Nakamura President, System and Data Research Co., Ltd.; Visiting Professor, Department of Built Environment, Tokyo Institute Technology

S. Parolai GeoForschungsZentrum Potsdam, Telegrafenberg, 14473 Potsdam, Germany

M. Picozzi GeoForschungsZentrum Potsdam, Telegrafenberg, 14473 Potsdam, Germany

M. Pilz GeoForschungsZentrum Potsdam, Telegrafenberg, 14473 Potsdam, Germany

Felice Ponzo DiSGG – Università della Basilicata, Potenza, Italy

Adrian Rodriguez-Marek Department of Civil and Environmental Engineering, Washington State University, Pullman, WA 99164-2910

Jun Saita System and Data Research Co., Ltd., Tokyo, Japan

A. Strollo GeoForschungsZentrum Potsdam, Telegrafenberg, 14473 Potsdam, Germany
and
Univertität Potsdam, Karl-Liebknecht-Strasse, 14476 Potsdam, Germany

Filippos Vallianatos Department of Natural Resources and Environment, Technological Educational Institute of Crete, Romanou 3, 73133, Chania, Greece, fvallian@chania.teicrete.gr

Marco Vona DiSGG, University of Basilicata, Campus Macchia Romana, Potenza, Italy

Participant Sketches

The participants to the ARW as portrayed by Dr. Yutaka Nakamura.

1. Marco Vona, 2. Yutaka Nakamura, 3. Janez Roser, 4. Sergiey Tyagunov, 5. Marijan Herak, 6. Kresimir Kuk, 7. Maria Rosaria Gallipoli, 8. Angelo Masi, 9. Predrag Kvasnicka, 10. Davorka Herak, 11. John Douglas, 12. Adrian Rodiguez Marek, 13. Marco Mucciarelli, 14. Dario Albarello, 15. Francisco Chavez-Garcia, 16. Josip Stipcevic, 17. Stavros A. Anagnostopoulos, 18. Francesco Mulargia, 19. Pierre Yves Bard, 20. Andrej Gosar, 21. Claude Boutin, 22. Dominik Lang, 23. Zoran Milutinovic, 24. Jun Saita, 25. Mehmet Celebi, 26. Marco Mucciarelli, 27. Tatjana Olumceva, 28. Radmila Salic, 29. Kuvvet Atakan, 30. Nayla Bouden-Romdhane, 31. John Cassidy.

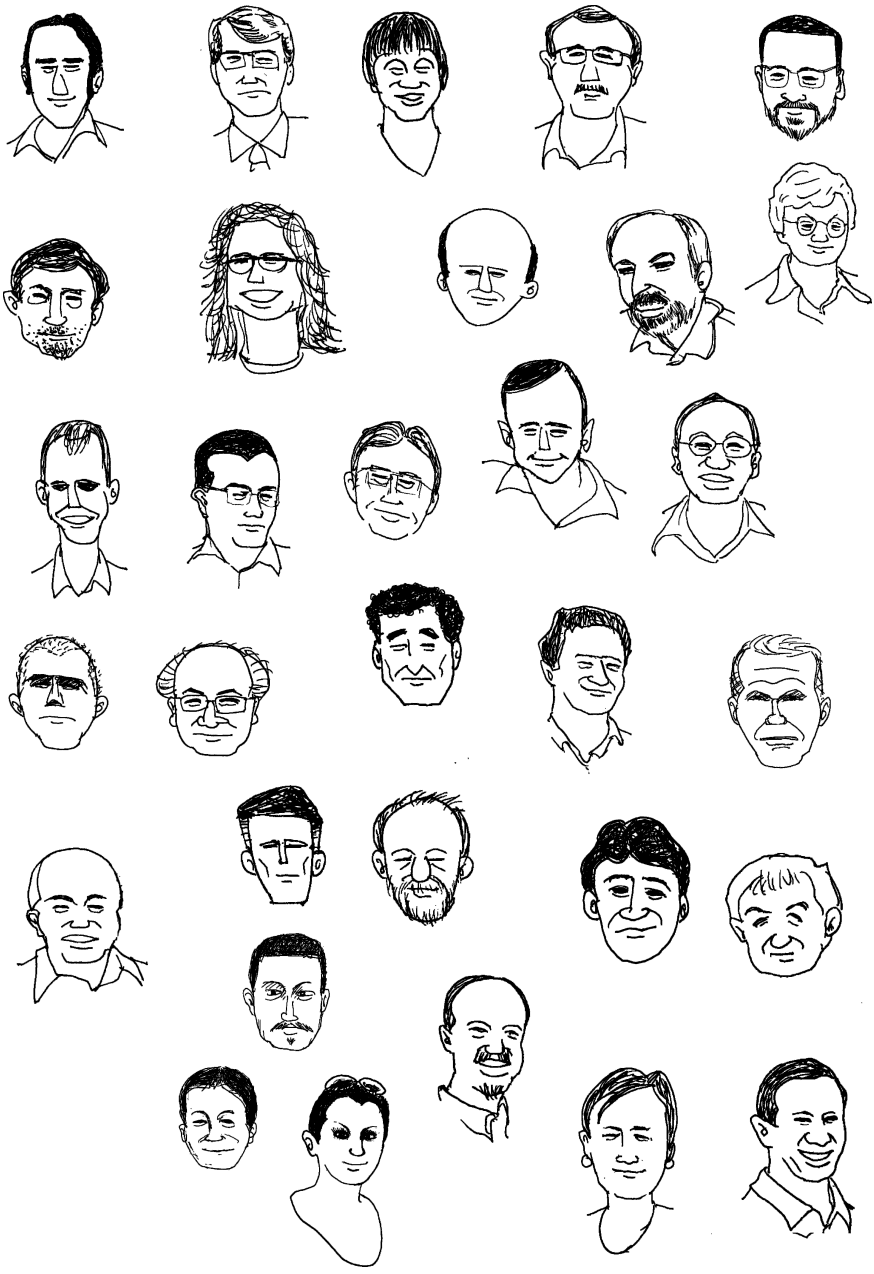

Chapter 1
The Use of Ambient Noise for Building and Soil Characterisation

Marijan Herak

1.1 Introduction

This chapter deals with diverse problems related to measurements of the ambient noise and their application for determination of soil or building properties. Although microtremors are studied since the first half of the 20th century, the number of investigations rapidly increased following the article by Nakamura in 1989. In the last two decades a host of methods and procedures emerged, some of which found their way into the everyday practice of seismologists and engineers dealing with the problems of site affects and soil-structure interaction.

Even though the theoretical background of the H/V ratio technique was initially not completely clear (and controversies still exist), its simplicity and low cost appealed to many. In his article in this chapter Y. Nakamura revisits the fundamental assumptions behind the concept of the H/V ratio and presents examples of its use. He clearly advocates the interpretation in terms of body waves, at least around the fundamental frequency of the soil.

It is quite safe to say that microtremor-based procedures are today methods of choice in practically all microzonation studies, at least as one of techniques used. It soon became clear that scientific community could not reach consensus not only on such fundamental questions as 'What is the composition of the signal we measure?', but also on the meaning of measured spectra. Can the observed curves be used to asses soil fundamental frequency? What about amplification – is this a tool to estimate the elusive site effects? Can we invert observations to learn about soil properties? The answer given by F. Chavez-Garcia in his contribution is: 'It depends ...'.

The hot topic of ambient noise was the matter of research in a number of international projects. K. Atakan was involved in the SESAME project, which aimed to

M. Herak
University of Zagreb, Faculty of Science, Department of Geophysics, Horvatovac bb, 10000 Zagreb, Croatia
e-mail: herak@irb.hr

M. Mucciarelli et al., (eds.), *Increasing Seismic Safety by Combining Engineering Technologies and Seismological Data,* NATO Science for Peace and Security Series C: Environmental Security, © Springer Science+Business Media B.V. 2009

asses how the instruments used, experimental conditions, and processing techniques influence the results. Their results are encouraging – with careful measurements and standardised interpretation steps, H/V ratios are stable in time and reliable. Some issues regarding measurement procedure, however, remain open. One of them is the extent to which transient signals affect results. Should we completely discard datasets 'contaminated' by passing cars or by other local sources of short duration? S. Parolai and colleagues present results of their ad-hoc experiment which indicate that such signals may amplify H/V ratio at low frequencies, and are not likely to degrade estimates of the fundamental frequency. Another view on transients (of long duration) is offered by F. Vallianatos and G. Hloupis who use wavelet transforms to detect them, thus improving reliability of the HVSR results.

New possibilities in exploiting seismic noise are described in the article written by D. Albarello and F. Baliva. Their results indicate that cross-correlation of noise recordings allows retrieval of the local Green's function along with the attenuation properties of subsoil. These results open new prospects for engineering and geotechnical application of environmental noise surveys.

One more use of H/V of microtremors is described by S. Castellaro and F. Mulargia. They propose a method to infer the ever-needed Vs30 by fitting the observed H/V spectrum to the theoretical one computed under assumption that the noise wavefield is composed of the fundamental mode Rayleigh waves. The authors find their technique superior and more informative than all popular array methods, allowing detection of deviations from 1-D subsoil geometry over lengths of a few meters!

Potential soil-building resonance is a matter of utmost importance for structural engineers. To assess it one needs to know fundamental frequencies of the building and of the soil, along with the corresponding damping. Ambient vibrations provide a convenient permanent source of shaking, and various methods have been proposed that use it for estimation of dynamic properties of buildings. The problem is – as M. Çelebi points out in his article – that fundamental period and damping significantly depend on the level of shaking. In particular, both periods and damping based on ambient data turned out to be underestimated if compared to values revealed during real earthquake. It is therefore important to monitor behaviour of buildings (especially the complex or irregular ones) during their life cycle, thus accumulating valuable data on building response to all kinds of excitation.

Chapter 1.1
The Need for Standardized Approach for Estimating the Local Site Effects Based on Ambient Noise Recordings

Kuvvet Atakan

Assessing local site effects reliably is one of the crucial aspects of seismic hazard, which usually cause amplification of ground motions and results in increasing the damage potential of a large earthquake. This phenomenon has been recognized for some time (e.g., Milne, 1898; Takahashi and Hirano, 1941; Gutenberg, 1957). The methods used to determine the site response can be categorized into two major groups, the analytical (theoretical) and the empirical methods. The analytical calculation of the site response, mainly based on inversion techniques, requires a very good knowledge of the geotechnical parameters to constrain the results. Empirical methods are somehow more effective in the sense that they are based on calculating the frequency spectrum directly from the recorded ground motion. Among the empirical methods, the spectral ratio of a sedimentary site with respect to a bedrock reference site, usually referred as the *standard spectral ratio technique*, is a widely used approach (e.g., Borcherdt, 1970; Borcherdt and Gibbs, 1976; Rogers et al., 1984). Effective use of this technique is demonstrated at different sites and geological conditions following large destructive earthquakes (e.g., Singh et al., 1988; Lermo et al., 1988; Borcherdt et al., 1989; Hough et al., 1990). Other methods include H/V spectral ratios (horizontal vs. vertical components) using single-station recordings (Nakamura, 1989; Lermo and Chávez-García, 1993; Field and Jacob, 1993; Lachet and Bard, 1994), and the cross-spectrum estimate (Safak, 1991; Field et al., 1992). There exists a number of review papers discussing the effectiveness of the different methods used in the site response estimate (e.g., Aki, 1988; Chin and Aki, 1991; Hartzell, 1992; Gutierrez and Singh, 1992; Yu et al., 1992; Aki, 1993; Bard, 1994; Atakan, 1995; Field and Jacob, 1995; Kudo, 1995; Mucciarelli et al., 2003; Atakan et al., 2004a). While most of the methods of site effects estimation use earthquake records, few are based on using microtremors. In the following we will focus on the latter, especially the spectral ratio of horizontal to vertical components

K. Atakan
Department of Earth Science, University of Bergen, Norway
e-mail: atakan@geo.uib.no

M. Mucciarelli et al., (eds.), *Increasing Seismic Safety by Combining Engineering Technologies and Seismological Data,* NATO Science for Peace and Security Series C: Environmental Security,

of ambient noise recordings. From here on we will refer to this technique simply as the *H/V method*. Other techniques using array measurements of ambient noise will not be treated in this section.

1.1.1 The history of H/V method

Starting from the late 1970s and throughout the 1980s and 1990s use of microtremors in estimating the local site effects have become increasingly popular. Application of the method on various locations and site conditions exists (e.g. Lermo and Chávez-García, 1993; Atakan and Havskov, 1996; Atakan et al., 1997). The popularity of the method is mainly due to its simple approach and its applicability by using a single three-component seismograph. It can be performed at various site conditions, the instruments and the analysis are simple, and it does not have any environmental consequence. However, there are a number of issues that are related to data collection, processing and interpretation, which will be treated separately in the following sections.

Microtremor measurements for site response estimates have long been one of the preferred approaches in Japan (Kanai, 1983). A clear evidence for a major control of seismic damage by local geology was already established in Japan following the 1923 Kanto earthquake (Kanai, 1951; Kanai et al., 1954). Since then, nearly all destructive earthquakes have brought additional evidence of the importance of site effects. The recognition of the H/V technique in Europe and USA came mainly after the paper by Nakamura (1989) where he applied H/V technique on microtremors and argued that the technique is capable of depicting the predominant frequency. Since then, the technique has been applied increasingly in developing countries and in areas of moderate seismicity due to its low cost. Additionally, the choice of the data type in estimating the site response using empirical techniques depends mainly on the tectonic setting and hence the earthquake activity rate of the area of interest. In actively deforming areas, such as the plate boundaries, recording strong motion in a reasonably short time is feasible, whereas in areas of low seismicity, even recording weak-motion requires considerable amount of time (Atakan et al., 1997). In the latter, recording ambient noise may be the only reasonable solution. For these reasons the use of microtremors in estimating local site effects has become increasingly popular over the years.

1.1.2 The nature of ambient noise

The terms microseisms (vibratory motion caused by the sea waves) and microtremors (cultural noise such as traffic, machinery etc.) are sometimes synonymously used for ambient noise. High frequency noise signals with periods below 2 s are customarily called "*microtremors*" and those above 2 s are called "*microseisms*"

(Kulhánek, 1990). The latter also referred sometimes as "*long-period microtremors*" (Yamanaka et al., 1994).

Both microtremors and microseisms are assumed to be transmitted along the bedrock-soil interface and are thus prone to amplifications by the sediment layers. However, it is important to note the difference between the microtremors induced by natural sources such as wind, oceanic disturbances and those triggered by local disturbances such as heavy traffic, industrial noise etc., which excite short-period Rayleigh waves in the vicinity of the recording stations, increasing significantly the noise level by a factor of 2–4 when compared to the background noise level (Nogoshi, 1978; Hough et al., 1992). Since the latter is associated with the very surficial sources, their energy is assumed not to reach any deeper than the uppermost layers of the sediments (soil). Other types of energy which may be included in the microtremors include short-period body-waves, higher mode surface waves, long-period surface waves and ultra-long-period surface waves (Horike, 1985; Matsushima and Okada, 1990; Cessaro, 1994; Yamanaka et al., 1994). Originated by the oceanic disturbances (Longuet-Higgings, 1950; Cessaro, 1994), these long-period waves propagate very efficiently through the granitic layer as R_g (Rayleigh-wave) and L_g (Love-wave) phases over continental paths (Ewing et al., 1957; Lermo and Chávez-García, 1994). Yamanaka et al. (1994) have demonstrated that the ellipticities of the Rayleigh waves correlate well with those from microtremors. This adds support to the hypothesis that the longer-period microtremors consists mainly of Rayleigh waves.

For practical purposes, we prefer the usage of the term "*ambient noise*" which simply describes all natural and artificial sources of noise generated near the surface of the earth in the vicinity of the recording instrument.

1.1.3 The H/V method

The technique is based on spectral ratio of horizontal to that of the vertical recording of ambient noise on a single site using a three component seismograph. As introduced by Nakamura (1989), the method was intended to achieve the amplification of the S-waves due to soft sediments by microtremor measurements. It is claimed that the spectral ratio of the horizontal to vertical components of the recorded ambient noise is equivalent to the ratio of the S-waves from an earthquake recorded on the surface of the sediments to that of the sediment-bedrock interface at the bottom of the sediment layer.

Let us define the problem in its simplest case, in a one dimensional flat single sediment (soil: denoted as sub-script "s") layer overlying bedrock (denoted as sub-script "b"). In this case the Fourier amplitude spectrum of the horizontal record on the surface (i.e. on top of the sediment layer) is H_s and at the bedrock sediment interface is H_b. The spectral ratio of the recorded signal on the surface (top of the sediment layer) with respect to that of the bedrock will then give the response of the

sediments. The spectral ratio on the horizontal components of the motion is denoted as S_h in the following way:

$$S_h = H_{s/}H_b \tag{1.1.1}$$

and for the vertical components as S_v

$$S_v = V_{s/}V_b \tag{1.1.2}$$

where, V_s is the spectrum of the vertical component as recorded on sediments and V_b on the bedrock. In addition to the above, Nakamura (1989) constructs a "transfer function" S_t expressed as:

$$S_t = S_{h/}S \tag{1.1.3}$$

Substituting (1.1.1) and (1.1.2) in Equation (1.1.3) we get:

$$S_t = (H_{s/}H_b)/(V_{s/}V_b) or S_t = H_s/V_s \tag{1.1.4}$$

Further expanding this equation results in the following:

$$\begin{aligned} S_t &= (H_{s/}H_b)/(V_{s/}V_b) = (H_{s/}H_b).(V_b/V_s) \\ S_t &= (H_s/V_s).(V_b/H_b) \end{aligned}$$

Therefore,

$$S_t = (H_s/V_s)/(H_b/V_b) \tag{1.1.5}$$

The validity of the H/V method using the above Equation (1.1.5) is dependent on two main assumptions. These are:

- *Assumption 1*: $H_b/V_b \approx 1$ – i.e. microtremor measurements on hard-rock show that the spectral ratio $H_b/V_b \approx 1$
- *Assumption 2*: $V_s \approx V_b$ – i.e. the vertical motion propagates undisturbed through the sediment layer

If these assumptions are correct, then $V_s \approx H_b$ and hence $H_s/V_s = H_s/H_b$. Empirical support to the first assumption is provided by a number of studies that checked the validity by applying the spectral ratio technique on stiff soil (Yamanaka et al., 1994) and bedrock conditions using weak-motion (Field and Jacob, 1995), strong-motion (Theodulidis et al., 1996), and using microtremors (Nakamura, 1989; Tenorio, 1997).

The capacity of the H/V method predicting the local site response is closely associated with its capacity to reproduce the S-wave amplification for the case of an earthquake record. In this sense the success of this depends on the assumption that the effect of Rayleigh wave ellipticity is negligible over the frequency range of interest (i.e. the ratio of the vertical to that of the horizontal component of the Rayleigh wave equals to 1 in the period range of 1–6 s).

The applicability of the technique is discussed by various authors (Kudo, 1995; Mucciarelli et al., 1997; Bard, 1998; Atakan et al., 2004b).

1.1.4 Theoretical basis of the H/V method

The theoretical basis of the H/V method still remains to be a subject for discussion (Lermo and Chávez-García 1993; 1994; Field and Jacob 1993; Lachet and Bard 1994; Dravinski et al. 1996; Fäh et al. 2001; Bonnefoy-Claudet et al. 2006).

Lermo and Chávez-García (1993) have tried to understand why H/V method which is based on ambient noise records composed mainly of weak Rayleigh waves, should also work for the S-wave records. They have applied Haskell's method, a special case of the propagator matrix method (Aki and Richards 1980) and found that, for large incidence angles, which ensure the existence of a vertical component for incidence S-waves, Nakamura's H/V ratio is a good estimate of the transfer function for horizontal components. For specific path and incidence angles the H/V results from S-waves are found to be in good agreement with the H/V on ambient noise measurements. The more vertical the incidence angle, the poorer is the fit. In a later paper, the same authors (Lermo and Chávez-García 1994) numerically modeled the ellipticity of Rayleigh waves and found that the ellipticity at the surface was in good agreement with the 1D vertical S-wave transfer function. Ellipticity in the sub-stratum on the other hand resulted to be near one at the fundamental frequency, but was different at higher modes. This seems to be the result of SV waves imitating the Rayleigh wave "ellipticity" around the resonant frequency for a certain range of incidence angles, but fail to do so at other frequencies.

Later studies have used more sophisticated ways of modeling the ambient noise as randomly distributed (both in time and space) point sources around the recording station (Field and Jacob 1993; Lachet and Bard 1994; Dravinski et al. 1996; Fäh et al. 2001; Bonnefoy-Claudet et al. 2006). Field and Jacob (1993) and Lachet and Bard (1994) managed successfully to match the modeled ambient noise H/V with the observations. Here however, it should be noted that the nature of the ambient noise is not only restricted to the surficial sources which do not have the pervasive energy to excite the entire sedimentary layer. Usually deeper sources are needed and such modeling from the nearby surface nodes may not be satisfactory. Lachet and Bard (1994) in their modeling of the polarization curves found a good correlation with the first peak of the H/V ratios. They further confirmed the results found by Lermo and Chávez-García (1993) on the comparison between the Rayleigh wave ellipticities on the surface and vertical S-wave transfer function. Lachet and Bard (1994) conclude that the H/V spectral ratios on ambient noise records allow assessing the fundamental frequency but fail to reproduce the higher modes. The amplification factors obtained were too sensitive to a variety of parameters, such as the velocity contrast, Poissons ratio and source-receiver distances and hence they were found not reliable.

Other theoretical investigations of the H/V method with 2D and 3D models of semi-circular and semi-spherical sedimentary basins were conducted to understand the various aspects of the wave propagation within the sedimentary layers (Dravinski et al. 1996; Moczo et al. 1997). Dravinski et al. (1996) demonstrated that the error in estimating the resonant frequency of the basin increases when approaching towards the center of the basin. Additionally, Moczo et al., (1997) showed that

the topographic anomalies next to the sediment valleys have to be taken into account when modeling the site response.

In studies of the ambient noise through theoretical modeling, Fäh et al. (2001) have tried the mode summation method and a finite difference technique which they have applied to investigate the spectral ratio between the horizontal and vertical components (H/V ratio) of ambient vibrations. They have explored the variation of the resonance frequency and the amplitude and shape of polarization as a function of the structure and the source positions. They have highlighted that the main problem in comparing the synthetics with the observations is the contribution of the SH waves on the observed H/V spectral ratios.

In a more recent approach Bonnefoy-Claudet et al. (2006) have modeled the ambient noise and have concluded that H/V ratio is mainly controlled by local surface sources and is due to the ellipticity of the fundamental Rayleigh waves. Furthermore their results indicate that the amplitude of H/V peak is not able to give a good estimate of site amplification factor.

1.1.5 Standardized approach

Recently a European project SESAME (Bard, 2004) was focused on studying the site effects assessment techniques using ambient vibrations. Within the framework of the project the reliability of the H/V spectral ratio technique in assessing the site effects is investigated in detail (Atakan et al., 2004b). The work was conducted in mainly three different lines with the following objectives: firstly to study the effect of the experimental conditions (Duval et al., 2004), secondly to find out the influence of the data processing (Atakan et al., 2004c) and finally compare the results from different techniques and data sets to empirically assess the reliability of its usage in microzonation studies (Theodulidis et al., 2004). These results indicate significant influences depending upon the instruments used (Guillier et al., 2008) experimental conditions (Chatelain et al., 2008) and the data processing routines. The studies concluded that by careful choice of instruments, controlled experimental setup and standardized processing routines reliable H/V results can be obtained. Under these conditions, the H/V ratios are stable in estimating the predominant frequencies. They do not however, completely reproduce the actual, frequency-dependent amplification factor. In the following we expand on these results.

Most of the earthquake risk is associated with the main population centers throughout the world where the earthquake is also high. In such a case, usually as part of microzontaion studies, conducting H/V measurements in cities becomes inevitable and requires both reliability of the results and rapidity of data collection. It is therefore important to understand which recording parameters influence the quality and reproducibility of the results. Some review in this topic may be found in dealing with the data acquisition system and the processing techniques as well (Duval, 1994; Nakamura, 1996; Mucciarelli et al., 1997; Atakan et al., 2004c; Guillier et al., 2008). However, in order to determine the influence of each of these

parameters, extensive experimental surveys are needed. Such a survey was conducted within the framework of the above mentioned European project, SESAME with the aim of evaluating the influence of experimental parameters in stability and reproducibility of H/V on ambient vibrations. This evaluation was conducted in a purely experimental process by means of various tests (Duval et al., 2004; Chatelain et al., 2008).

The first issue was to establish the impact of the digitizers, sensors and digitizer-sensor couples on stability, reliability and reproducibility of H/V measurements under laboratory conditions. This work was devoted to perform and analyze a set of tests in order to compare the performance of different instruments currently used (13 digitizers and 15 sensors). To reach this goal, three series of tests were conducted (Guillier et al., 2008):

- Tests on digitizers. Digitizer evaluation has been carried out through four different tests: sensitivity, internal noise evaluation, time stability and channel consistency.
- Tests on sensors. Sensor response has been evaluated for short period seismometers, long period seismometers and accelerometers.
- Tests on digitizer-sensor couples. These tests have been achieved collecting different measurements: individual recordings in the lab, simultaneous recordings in the lab and two simultaneous recordings in the free-field.

One of the main outcomes for the tested sensors is: the velocimeters are all usable (even the 4.5 Hz) whereas the accelerometers are not appropriate due to their insensitivity to noise measurements (Guillier et al., 2008).

The second issue was to establish the influence of the experimental conditions when recording ambient noise. The experimental tested parameters were classified in nine categories. Three types of parameters were distinguished:

- Parameters relative to the acquisition system and configuration: recording/instrument parameters in free-field microtremor records
- Parameters related to the characteristics of the site itself: in situ soil-sensor coupling; modified soil-sensor coupling; nearby structures; underground structures
- Parameters relative to the variation of external conditions: weather conditions; water table level, pore pressure; stability in time; noise sources

Each parameter has been tested against a reference recording. Similarity of the results (H/V amplitude and fundamental frequency) of both recordings, were checked using Student t-test (Chatelain et al., 2008). Based on the above statistical investigations, the tested parameters can be classified into three main categories: (i) the parameters that do not influence the result, (ii) those which influence the results only beyond some limits that can be easily controlled and (iii) those on which there is no possible control. One of the main conclusions is that no matter how strongly a parameter influences H/V amplitudes, the value of the frequency peak is usually not or slightly affected, with the noticeable exception of the wind in certain conditions.

Within the frame of the SESAME project practical recommendations as to data processing were proposed (Atakan et al., 2004b). The main purpose was to provide a consensus advice on several simple questions, which do not necessarily have trivial answers.

- What is the optimum time window length?
- What is the required number of noise windows to have a good reliability?
- What is the sensitivity to transients and should only stationary signal windows be used?
- How to merge the two horizontal components to get the "H" component?
- How to smooth the spectra?
- Should the averaging from all the windows be applied on H and V spectra or on the H/V spectral ratio?
- Should one prefer arithmetic or geometric averages?

There exist also less known processing techniques, which may present some interest and should be tested. While almost all authors limit their investigations to the spectral amplitude, Tokeshi et al. (1996) also analyzed the phase of the one-sided autocorrelogram of the horizontal components, and proposed a new way to derive the fundamental frequency, which corresponds to a change in the phase sign (from positive to negative). They recently performed time domain noise simulations (Tokeshi and Sugimura, 1998), and claim that, even for low impedance contrast structures where spectral peaks do not appear clearly, this technique is efficient in pointing out the right fundamental frequency.

On the other hand, Fäh et al. (1997) used a different way to derive average polarization curve: they did not smooth the spectra, so that the H/V values they obtained for every window presented a very large dispersion. They succeeded however in reaching meaningful averages by (i) considering a very large number of noise windows (500) and (ii) weighting every H/V value by the corresponding spectral energy. Finally, Teves-Costa et al. (1996) proposed to compute microtremor spectra with Maximum Entropy Methods, which has the advantage to provide more reliable estimates in the low frequency range with short noise windows.

Keeping in mind the importance of processing in the H/V results, development of robust software for data analysis applying the H/V technique became a necessity. A multiplatform processing software is developed (J-SESAME) with the aim of providing a standard procedure in processing the microtremor data using H/V method. Existing software that was previously used in processing the microtremor data using the H/V technique is tested and an optimum solution for the analysis is deduced. The software is available at: http://www.geo.uib.no/seismo/software/jsesame/jsesame.html. The details of this standard software can be found in Atakan et al. (2004c).

Another goal of the SESAME project was to perform a purely experimental assessment of the reliability of the H/V technique, by comparing its results with those of well established experimental techniques, based on a homogeneous data set of ambient noise and earthquake recordings (Theodulidis et al., 2004). In this work, comparison of H/V results with observed damage of recent earthquakes in Europe attempted. As a result (i) a homogeneous data set of noise and earthquake recordings

at many sites was created, (ii) the comparisons of experimentally and theoretically estimated transfer functions with the H/V spectral ratio of ambient vibrations technique were conducted and (iii) the comparison of damage distribution in modern urban areas with results from H/V spectral ratio were performed.

For selected sites H/V ratios of ambient noise were compared with H/V receiver functions of earthquake weak or/and strong motion recordings (Theodulidis et al., 2004), as well as with standard spectral ratios where data permitted. For a few sites – where geotechnical data was available – theoretically estimated transfer functions were compared with experimentally H/V ratios of ambient noise. In addition, for a few selected sites, which exhibited non-linearity during strong ground motion, H/V noise ratio was calculated to investigate the applicability of the latter. Ambient noise measurements were performed into the city of Thessaloniki, the town of Kalamata in Greece, the city of Rome and the towns of Palermo and Fabriano in Italy, and the town of Angra-do-Heroismo in Portugal. From the analyses of this data, it seems that in some cases (homogeneous building stock, distant event) the H/V ratio "fundamental" frequency may satisfactorily indicate areas of damage potential in urban environment. However, quantitative correlation between H/V spectral ratio "fundamental" frequency and damage is difficult to be established given the complexity of parameters involved. Correlation between the "fundamental" frequency and the near surface geology, on the other hand seems more reliable (Theodulidis et al., 2004).

1.1.6 Guidelines

In the framework of the European research project SESAME (Bard, 2004), guidelines on the H/V spectral ratio technique are prepared (Koller et al., 2004). These guidelines represent the state-of-the-art of the present knowledge of the H/V method and its applications, and are based on the consensus reached by a large group of participants. It reflects the synthesis of a considerable amount of data collection and subsequent analysis and interpretations. In general, due to the experimental character of the H/V method, the absolute values obtained for a given site require careful examination. In this respect visual inspection of the data both during data collection and processing is necessary. Especially during the interpretation of the results there should be frequent interaction with regard to the choices of the parameters for processing.

The guidelines are organized in two separate parts; the quick field reference and interpretation guidelines (Part I) and detailed technical guidelines (Part II). Part I aim to summarize the most critical factors that influence the data collection, analysis and interpretation and provide schematic recommendations on the interpretation of results. Part II includes a detailed description of the technical requirements, standard data processing and the interpretation of results.

The guidelines give a summary of the recommendations that should be taken into account in studies of local site effects using the H/V technique on ambient vibrations. The recommendations given apply basically for the case where the method is

used alone in assessing the natural frequency of sites of interest and are therefore based on a rather strict set of criteria. The recommended use of the H/V method is however, to combine several other geophysical and geotechnical approaches with sufficient understanding of the local geological conditions. In such a case, the interpretation of the H/V results can be improved significantly in the light of the complementary data.

The complete guidelines are available at: http://www.geo.uib.no/seismo/software/jsesame/SESAME-HV-User-Guidelines.pdf

References

Aki K (1988) Local site effects on strong ground motion: Proceedings of Earthquake Engineering and Soil Dynamics II, Park City, Utah, 27–30 June, American Society of Civil Engineers: 103–155.

Aki K (1993) Local site effects on weak and strong ground motion. In: F. Lund (ed.) New Horizons in Strong Motion: Seismic Studies and Engineering Practice: Tectonophysics, Vol. 218, pp. 93–111, Elsevier, the Netherlands.

Aki K and Richards PG (1980) Quantitative Seismology, Vol. 1, W.H. Freeman, San Francisco, CA.

Atakan K (1995) A review of the type of data and the techniques used in empirical estimation of local site response. Proceedings of the 5th International Conference on Seismic Zonation, Nice, France, 17–19 October: 1451–1460.

Atakan K and Havskov J (1996) Local site effects in the northern North Sea based on the single station spectral ratios of the OBS data. Terra Nova 8: 22–33.

Atakan K, Brandsdóttir B, Halldórsson P and Fridleifsson GO (1997) Site response as a function of near-surface geology in the South Iceland Seismic Zone. Natural Hazards 15: 139–164.

Atakan K, Ciudad-Real M and Torres R (2004a) Local site effects on microtremors, weak and strong ground motion in San Salvador, El Salvador. In: J.J. Bommer, W.I. Rose, D.L. Lopez, M.J. Carr, J.J. Major (eds.) Natural Hazards in El Salvador. Geological Society of America, Special Paper SPE375: 321–328, ISBN No. 0–8137–2375–2.

Atakan K, Duval AM, Theodulidis N, Bard PY and the SESAME Team (2004b) The H/V spectral ratio technique: Experimental conditions, data processing and empirical reliability assessment. Proceedings of the 13th World Conference on Earthquake Engineering. Paper No. 2268, 1–6 August, Vancouver, Canada.

Atakan K, Bard PY, Kind F, Moreno B, Roquette P, Tento A and the SESAME Team (2004c) J-SESAME: a standardized software solution for the H/V Spectral ratio technique. Proceedings of the 13th World Conference on Earthquake Engineering. Paper No. 2270, 1–6 August, Vancouver, Canada.

Bard PY (1994) Effects of surface geology on ground motion: recent results and remaining issues. Proceedings of the 10th European Conference on Earthquake Engineering, 1: 305–325.

Bard PY (1998) Microtremor measurements: a tool for site effect estimation?, State-of-the-art paper. Proceedings of the 2nd International Symposium on the Effects of Surface Geology on Seismic Motion, Yokohama, 1–3 December, Balkema, 3: 1251–1279.

Bard PY (2004) The SESAME project: an overview and main results. Proceedings of the 13th World Conference on Earthquake Engineering, 1–6 August, Vancouver, Canada. http://SESAME-FP5.obs.ujf-grenoble.fr

Bonnefoy-Claudet S, Cornou C, Bard PY, Cotton F, Moczo P, Kristek J and Fäh D (2006) H/V ratio: a tool for site effects evaluation. Results from 1-D noise simulations. Geophysical Journal International 167(2): 827–837.

Borcherdt RD (1970) Effects of local geology on ground motion near San Francisco Bay. Bulletin of the Seismological Society of America 60: 29–61.

Borcherdt RD and Gibbs JF (1976) Effects of local geological conditions in the region on ground motions and the intensities of the 1906 earthquakes. Bulletin of the Seismological Society of America 66: 467–500.

Borcherdt RD, Glassmoyer G, Der Kiureghian A and Cranswick E (1989) Results and data from seismologic and geologic studies following earthquakes of 7 December near Spitak, Armenia, S.S.R.: U.S. Geological Survey Open-File Report 89–163A.

Cessaro RK (1994) Sources of primary and secondary microseisms. Bulletin of the Seismological Society of America 84: 142–148.

Chatelain J.-L, Guillier B, Cara F, Duval A.-M, Atakan K, Bard P.-Y and the WP02 SESAME Team (2008) Evaluation of the influence of experimental conditions on H/V results from ambient noise recordings. Bulletin of Earthquake Engineering, Vol. 6, Issue 1, 33–74, doi: 10.1007/s10518-007-9040-7.

Chin BH and Aki K (1991) Simultaneous determination of source, path and recording site effects on strong ground motion during the Loma Prieta earthquake – A preliminary result on pervasive nonlinear site effect. Bulletin of the Seismological Society of America 81: 1859–1884.

Duval AM (1994) Détermination de la réponse d'un site aux séismes à l'aide du bruit de fond: évaluation expérimentale, Thèse de Doctorat, Université Pierre-et-Marie Curie, Paris (in French).

Duval AM, Chatelain JL, Guillier B and the SESAME Team (2004) Influence of experimental conditions on the H/V determinations using ambient vibrations (noise). Proceedings of the 13th World Conference on Earthquake Engineering. Paper No. 306, 1–6 August, Vancouver, Canada.

Dravinski M, Ding G and Wen KL (1996) Analysis of spectral ratios for estimating ground motion in deep basins. Bulletin of the Seismological Society of America 86: 646–654.

Ewing M, Jardetzky W and Press F (1957) Elastic Waves in Layered Media. McGraw-Hill, New York.

Fäh D, Rüttener E, Noack T and Kruspan P (1997) Microzonation of the city of Basel. Journal of Seismology 1: 87–102.

Fäh D, Kind F and Giardini D (2001) A theoretical investigation of average H/V ratios. Geophysical Journal International 145(2): 535–549, doi: 10.1046/j.0956–540x.2001.01406.x.

Field EH and Jacob KH (1993) The theoretical response of sedimentary layers to ambient seismic noise. Geophysical Research Letters 20: 2925–2928.

Field EH and Jacob KH (1995) A comparison and test of various site response estimation techniques, including three that are not reference site dependent. Bulletin of the Seismological Society of America 85: 1127–1143.

Field EH, Jacob KH and Hough SE (1992) Earthquake site response estimation: a weak motion case study. Bulletin of the Seismological Society of America 82: 2283–2307.

Guillier B, Atakan K, Chatelain J.-L, Havskov J, Ohrnberger M, Cara F, Duval A.-M, Zacharapoulos S, Teves-Costa P and the SESAME Team (2008) Influence of instruments on H/V spectral ratios of ambient vibrations. Bulletin of Earthquake Engineering, Vol. 6, Issue 1, 3–31, doi: 10.1007/s10518–007–9039–0.

Gutenberg B (1957) Effects of ground on earthquake motion. Bulletin of the Seismological Society of America 47: 221–250.

Gutierrez C and Singh SK (1992) A site effect study in Acapulco, Guerrero, Mexico; a comparison of results from strong-motion and microtremor data. Bulletin of the Seismological Society of America 82: 642–659.

Hartzell SH (1992) Site response estimation from earthquake data. Bulletin of the Seismological Society of America 82: 2303–2327.

Horike M (1985) Inversion of phase velocity of long period microtremors to the S-wave velocity structure down to the basement in urbanized areas. Journal of Physics of the Earth 33: 59–96.

Hough SE, Borcherdt RD, Friberg PA, Busby R, Field E and Jacob KH (1990) The role of sediment-induced amplification in the collapse of the Nimitz freeway during the October 17, 1989 Loma Prieta earthquake. Nature 344: 853–855.

Hough SE, Seeber L, Rovelli A, Malagnini L, DeCesare A, Selveggi G and Lerner-Lam (1992) Ambient noise and weak motion excitation of sediment resonances: results from the Tiber Valley, Italy. Bulletin of the Seismological Society of America 82: 1186–1205.

Kanai K (1951) Relation between the nature of surface layer and the amplitudes of the earthquake motion. Bulletin of Earthquake Research Institute-Tokyo University 30: 31–37.

Kanai K (1983) Engineering Seismology, University of Tokyo Press, Tokyo, 251 p.

Kanai K, Osada K, and Yoshizawa (1954) Observational study of earthquake motion in the depth of the ground. Bulletin of Earthquake Research Institute-Tokyo University 32: 361–370.

Koller M, Chatelain JL, Guillier B, Duval AM, Atakan K, Lacave C, Bard PY and the SESAME Participants (2004). Empirical evaluation of the Horizontal to vertical spectral ratio technique: Results from the SESAME Project. Proceedings of the 13th World Conference on Earthquake Engineering. Paper No. 3132, 1–6 August, Vancouver, Canada.

Kudo K (1995) Practical estimates of site response, State-of-the-Art report. Proceedings of the 5th International Conference on Seismic Zonation, Nice, October.

Kulhánek O (1990) Anatomy of Seismograms. Elsevier, Amsterdam.

Lachet C and Bard P-Y (1994) Numerical and theoretical investigations on the possibilities and limitations of Nakamura's technique. Journal of Physics of the Earth 42: 337–397.

Lermo JF and Chávez-García FJ (1993) Site effect evaluation using spectral ratios with only one station. Bulletin of the Seismological Society of America 83: 1574–1594.

Lermo JF and Chávez-García FJ (1994) Are microtremors useful in site response evaluation? Bulletin of the Seismological Society of America 84: 1350–1364.

Lermo JF, Rodriguez M and Singh SK (1988) The Mexico earthquake of September 19, 1985: Natural period of sites in the valley of Mexico from microtremor measurements and from strong motion data. Earthquake Spectra 4: 805–814.

Longuet-Higgings MS (1950) A theory on the origin of microseisms. Philosophical Transactions of the Royal Society of London 243: 1–35.

Matsushima T and Okada H (1990) Determination of deep geological structure under urban areas using long period microtremors. Butsuri-Tansa 43: 21–33.

Milne J (1898) Seismology (1st edition): London, Kegan Paul, Trench, Truber.

Moczo P, Bystrick E, Kristek J, Carcione JM and Bouchon M (1997) Hybrid modeling of P-SV seismic motion at inhomogeneous viscoelastic topographic structures. Bulletin of the Seismological Society of America 87: 1305–1323.

Mucciarelli M, Bettinali F, Zaninetti A, Mendez A, Vanini M and Galli P (1997) Refining Nakamura's technique: processing techniques and innovative instrumentation. Proceedings of the XXV E.S.C. General Assembly, Reykjavik: 411–416.

Mucciarelli M, Gallipoli MR and Arcieri M (2003) The stability of the horizontal-to-vertical spectral ratio of triggered noise and earthquake recordings. Bulletin of the Seismological Society of America 93: 1407–1412.

Nakamura Y (1989) A method for dynamic characteristics estimation of subsurface using microtremor on the ground surface: Quarterly Report of Railway Technical Research Institute, Vol. 30, no. 1: 25–33.

Nakamura Y (1996) Real-time information systems for hazards mitigation. Proceedings of the Xth World Conference on Earthquake Engineering, Acapulco, # 2134, Elsevier.

Nogoshi M (1978) On fundamental nature of microtremors. Min. Coll. Akita University Series A.

Rogers AM, Borcherdt RD, Covington PA and Perkins DM (1984) A comparative ground response study near Los Angeles using recordings of Nevada nuclear tests and the 1971 San Fernando earthquake. Bulletin of the Seismological Society of America 74: 1925–1949.

Safak E (1991) Problems with using spectral ratios to estimate site amplification. Proceedings of the Fourth International Conference on Seismic Zonation, Stanford, California, II: 277–284.

Singh SK, Lermo J, Dominguez T, Ordaz M, Espinoza JM, Mena F and Quass R, (1988) The Mexico earthquake of September 19, 1985: a study of amplification of seismic waves in the Valley of Mexico with respect to a hill zone site: Earthquake Spectra 4: 653–673.

Takahashi R and Hirano K (1941) Seismic vibrations of soft ground: Bulletin of the Earthquake Research Institute, Tokyo University 19: 534–543.

Tenorio C (1997) Site response evaluation: A review of the problems involved, estimation techniques and Nakamura's single station method, and Shallow crustal structure in Guatemala using P- and S-wave inversion. Unpublished Master Thesis, Department of solid Earth Physics, University of Bergen, 97p.

Teves-Costa P, Matias L and Bard PY (1996) Seismic behavior estimation of thin alluvium layers using microtremor recordings. Soil Dynamics and Earthquake Engineering 15: 201–209.

Theodulidis N, Bard PY, Archuleta R and Bouchon B (1996) Horizontal-to-vertical spectral ratio and geological conditions: The case of the Garner Valley downhole array in Southern California. Bulletin of the Seismological Society of America 86: 306–319.

Theodulidis N, Cultrera G, Tento A, Faeh D, Atakan K, Bard PY, Panou A and the SESAME Team (2004) Empirical evaluation of the Horizontal to vertical spectral ratio technique: Results from the SESAME Project. Proceedings of the 13th World Conference on Earthquake Engineering. Paper No. 2323, 1–6 August, Vancouver, Canada.

Tokeshi JC, Sugimura Y and Sasaki T (1996) Assessment of natural frequency from microtremor measurement using phase spectrum. Proceedings of the Xth World Conference on Earthquake Engineering, Acapulco, # 309, Elsevier.

Tokeshi JC and Sugimura Y (1998) A comparison of the Fourier phase spectral method with the Nakamura technique for a horizontally layered structure. Proceedings of the XIth European Conference on Earthquake Engineering, Paris, 6–11 September, Bisch, Labbé & Pecker Editors, Balkema.

Yamanaka H, Masayuki T, Hiroshi I and Masanori N (1994) Characteristics of long period microtremors and their applicability in exploration of deep sedimentary layers. Bulletin of the Seismological Society of America 84: 1831–1841.

Yu G, Anderson J and Siddharthan R (1992) On the characteristics of the nonlinear soil response. Bulletin of the Seismological Society of America 83: 218–244.

Chapter 1.2
Are Transients Carrying Useful Information for Estimating H/V Spectral Ratios?

Stefano Parolai, Matteo Picozzi, Angelo Strollo, Marco Pilz, Domenico Di Giacomo, Barbara Liss, and Dino Bindi

Abstract Defining a procedure to calculate the H/V spectral ratio of seismic noise has recently been the focus of several studies. Although some issues have been addressed and a general procedure to follow in choosing the optimal seismological equipment, carrying out the measurements and analyzing the data has been agreed upon by the majority of specialists in this field, some points still remain open. One open question is whether transients should be avoided when H/V spectral ratios are calculated. Starting from contradictory results of previous papers, an ad-hoc experiment at the Nauen test site (Germany) was conducted to verify the influence of transients on the H/V spectral ratio of seismic noise. We show, consistent with some previous studies, that transients generated by high frequency content sources can amplify spectral ratio peaks at low frequencies. After careful polarization analysis of the data and estimation of the spectral amplitude decay with distance, we provide an explanation in terms of the composition of the wavefield over certain distance ranges. Our results highlight the importance of a better understanding of the wavefield composition for better exploiting the potential of H/V spectral ratio method.

Keywords H/V spectral ratio · Seismic noise · Transients · Polarization · Nauen test site

1.2.1 Introduction

The Nakamura technique (Nakamura, 1989), first proposed by Nogoshi and Igarashi (1970, 1971), is today one of the most commonly applied methods for

S. Parolai (✉), M. Picozzi, A. Strollo, M. Pilz, D. Di Giacomo, and B. Liss
Helmholtz Centre Potsdam, GFZ German Research Centre for Geosciences Telegrafenberg, 14473 Potsdam, Germany

A. Strollo, D. Di Giacomo, and M. Pliz
Univertität Potsdam, Karl-Liebknecht Strasse, 14476 Potsdam, Germany

D. Bindi
Istituto Nazionale di Geofisica e Vulcanologia, via Bassini 15, 20133 Milano, Italy

M. Mucciarelli et al., (eds.), *Increasing Seismic Safety by Combining Engineering Technologies and Seismological Data,* NATO Science for Peace and Security Series C: Environmental Security,

microzonation studies of large urban areas (e.g. Parolai et al., 2001). A large number of studies using this rapid, economical, and therefore attractive technique have been published (e.g. Field and Jacob, 1993; Lermo and Chávez-García, 1994; Mucciarelli, 1998; Bard, 1999; Fäh et al., 2001). More recent studies (Fäh et al., 2003; Scherbaum et al., 2003; Arai and Tokimatsu, 2004; Parolai et al., 2005; Picozzi et al., 2005; Parolai and Galiana-Merino, 2006) proposed and tested the possibility of inverting the Horizontal-to-Vertical (H/V) spectral ratio of noise (alone or in a joint inversion scheme) for investigating the S-wave subsoil structure. All these studies require the a-priori assumption that the noise wavefield is generally dominated by surface waves. Moreover, attempts to provide standards for the analysis of seismic noise have only recently been carried out (Bard, 1999; SESAME, 2004; Picozzi et al., 2005). To this regard, a point frequently debated by the seismological community is whether only the stationary part of the recorded signal should be considered in the analysis, or could transients (e.g. due to human activities) also be considered (excluding obviously very strong and clipped signals). Most authors disregarded the non-stationary noise from the analysis (e.g. Horike et al., 2001), while others (e.g. Mucciarelli et al., 2003) showed that the H/V ratio of non-stationary noise might be more similar, especially in amplitude, to the H/V spectral ratio determined for small-size earthquakes. By applying an optimal filtering procedure to empirical data and using numerical simulations, Parolai and Galiana-Merino (2006) showed that transients might cause large variability in the H/V shape, depending on source type and distance from the receiver relative to the thickness of the sedimentary cover. However, they showed that when dealing with a sufficient number of real data, the H/V ratio is not biased by including transients. Recently, Chatelain et al. (2008) suggested to avoid the use of transients in the H/V analysis. Nevertheless, they showed that H/V does not significantly change if the sensor is located just a few meters from the major source of transients (in their case, cars on a highway). Furthermore, at only 2 m from the highway, the peak in the H/V spectral ratio is still visible, while it disappears when the sensor is placed directly on the highway. These results (except for those from the stations located directly on the highway) seem to be in agreement with the pioneering study of Taniguchi and Sawada (1979) who made systematic noise measurements close to a highway under constructions and observed that (1) the frequency peak in the transient spectra was stable independent of the mass of the source (a truck), hinting to the fact that the frequency of traffic-induced vibration is mainly determined by ground soil conditions, and (2) traffic-generated vibrations were dominated by Rayleigh waves. A recent investigation of the seismic noise wavefield induced by several source types can be found in Kim and Lee (2007).

Additional evidence of the role played by transients was reported by Mucciarelli (1998) who showed that when generating transients with a sledge hammer near the recording sensor, the H/V peak becomes more clear. This result, probably too often overlooked, stimulates many intriguing questions. Since the energy released by the blow of a sledge hammer peaks at frequencies much higher (50–70 Hz) than the fundamental resonance frequency of the site (1 Hz), how can the transients modify the H/V? Similarly, human generated seismic noise mainly affects fre-

quencies higher than 1–2 Hz, with cars generating signals with frequencies mainly between 10–20 Hz (e.g. Taniguchi and Sawada, 1979; McNamara and Buland, 2004). Therefore, the question arises if there is any important information carried by the transients that one could try to extract.

We endeavour to answer these questions, by analysing recordings of seismic noise that include transients generated by a sledge hammer. Vertical and horizontal sources have been simulated. We first calculate the H/V spectral ratio using only the stationary part of noise. Then, we calculate the H/V spectral ratio for the transients only. A comparison of the results, considering spectra inspection, polarization, and amplitude decay analysis is performed. Finally, a possible explanation of the observed phenomena in terms of wave propagation is proposed.

1.2.2 Data

The experiment was carried out at the Nauen test site (Germany) (http://www.geophysik.tu-berlin.de/menue/testfeld_nauen/), during a day with favourable weather conditions and absence of wind.

Seismic noise was recorded using a 24-bit digitizer (EarthDataLogger) connected to a Mark L4C-3D 1 Hz sensor. The sampling rate was fixed to 200 samples/s.

Transients were generated by a surface source at distances of 5, 10, 20, 30, 50, 75 and 100 m to the recorder. The source was a sledge hammer (5 kg) striking vertically a steel plate (vertical source) and horizontally (perpendicular to the radial line between the source and the geophone) a railway sleeper. Series of 5 vertical blows (separated from each other by a few seconds) were alternated with series of five horizontal blows. For each source-sensor distance, this energization scheme was repeated five times (i.e. five series of vertical and horizontal blows were recorded). Figures 1.2.1 and 1.2.2 show examples of recordings for the vertical, radial and transverse component of ground motion for the source distances 5 and 100 m, respectively.

1.2.3 Data processing

Using a visual inspection procedure, three different kinds of signal windows were selected from the continuous data stream. In particular, windows of signal containing only one series of vertical shots, only one series of horizontal shots and a couple of consecutive vertical and horizontal shots were extracted (Figures 1.2.1 and 1.2.2). The length of the signal windows varies between 20.48 s (for those including only a series) and 40.96 s (for those including a couple of vertical and horizontal blow series). The time series were corrected for trend in the data and tapered with a 5% cosine function at both ends. The Fast Fourier Transform (FFT) was calculated for each component, and the spectra were smoothed using a Konno and Ohmachi (1998) logarithmic window, with the coefficient b, which determines the bandwidth, fixed

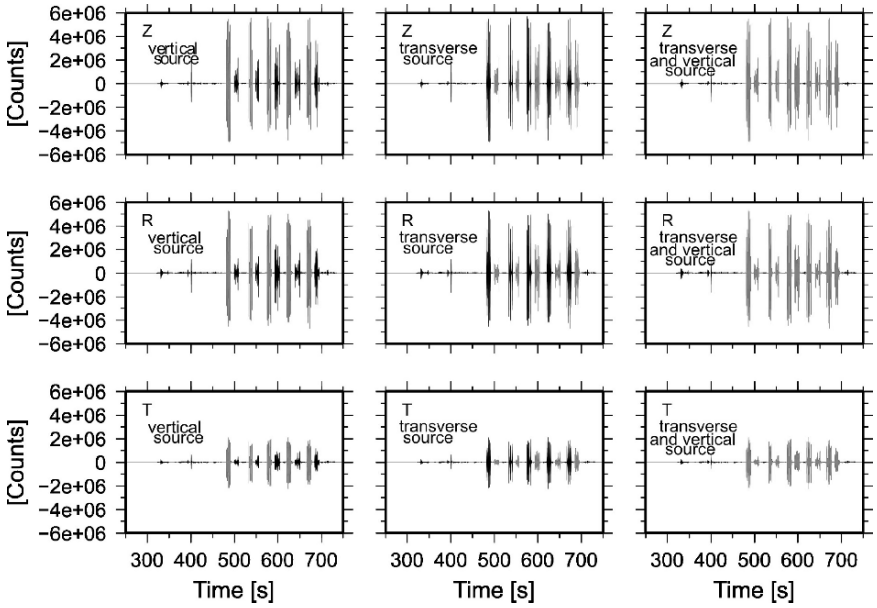

Fig. 1.2.1 Vertical (top), radial (middle) and transverse component (bottom) recordings of five series of alternated vertical and horizontal energization at 5 m distance from the sensor. Left panels highlight (gray) signal windows selected for the vertical energization. Central panels highlight (gray) signal windows selected for the transverse energization. Right panels show (gray) signal windows containing signals generated by vertical and horizontal sources. Please note that each transient in the panels is composed by five blows

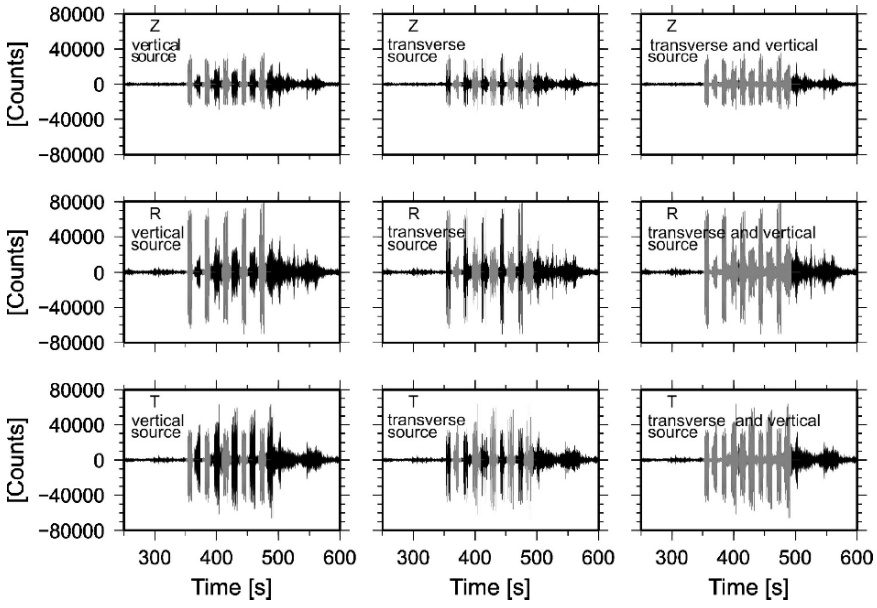

Fig. 1.2.2 Same as Figure 1.2.1, but for source-to-sensor distance of 100 m

to 40. The instrumental response correction was performed by considering the pole and zero configuration of the sensor. The same procedure was also applied to twenty 30-sec length stationary noise windows. Then, the Horizontal-to-Vertical spectral ratios (H/V) were calculated considering the root-mean-square (rms) spectra of the two horizontal components. The procedure was repeated for each source-sensor distance and source type (horizontal and vertical). Finally, the logarithmic average of the H/V spectral ratios was computed.

1.2.4 Amplitude Fourier spectra and H/V ratios

Figure 1.2.3 (left and middle frames) shows the average vertical and horizontal spectra of stationary noise and of the windows including transients, for vertical sources at different distances. The spectra are the logarithmic average of the five series. Figure 1.2.3 (right) shows the H/V results obtained for stationary noise and for transients generated at different source distances.

The former shows two peaks at around 0.2 and 1 Hz that are consistent with the H/V peaks obtained by M. Picozzi, 2007 (personnel communication) after analyzing data obtained from monitoring the site for one week. Since borehole measurements and geophysical surveys (geoelectric and georadar) carried out at the Nauen test site provide information about the structure of the upper 20 m only, the two peaks cannot be linked to any a-priori known impedance contrast below the site, that is strong enough to generate resonance peaks. Note that both peaks occur within the frequency band exploitable for the considered short period sensor (Strollo et al. 2008a, b), and therefore can be considered as reliable. However, since the lowest frequency peak, as shown in the following analysis, occurs at frequencies too low to be affected by the high frequency transients generated by the hammer blow, we will focus our attention mainly on the peak at around 1 Hz. Figure 1.2.3 suggests that the peak at 1 Hz is mainly related to a trough in the vertical component spectra, suggesting a link with the ellipticity of Rayleigh waves (Konno and Ohmachi, 1998).

Considering the transient windows, the spectral energy for both vertical and horizontal components of ground motion is concentrated at frequencies higher than 10 Hz, with a broader peak for the vertical component. The amplitude of the spectral peaks, occurring at about 30 Hz, decreases with distance due to the seismic wave attenuation, but at 100 m it is still higher than the spectral amplitude of the stationary noise.

It is remarkable that only when the source is located at a distance smaller than 20 m, do the spectra also show an increase in amplitude between 0.3 and 2 Hz. In particular, the largest amplitudes are of the radial component. The effect on the H/V (note that here only that obtained by averaging the radial and transverse component is shown) is also worth noting. In fact, while for short source-sensor distances (5 and 10 m) the peak around 1 Hz is strongly magnified (the large scattering in the results may be due to the fact that only 5 H/V spectral ratios have been averaged), for larger source distances it approaches the stationary noise H/V. Taking into account the amplitudes of the average spectra, this effect can mainly be related to the radial

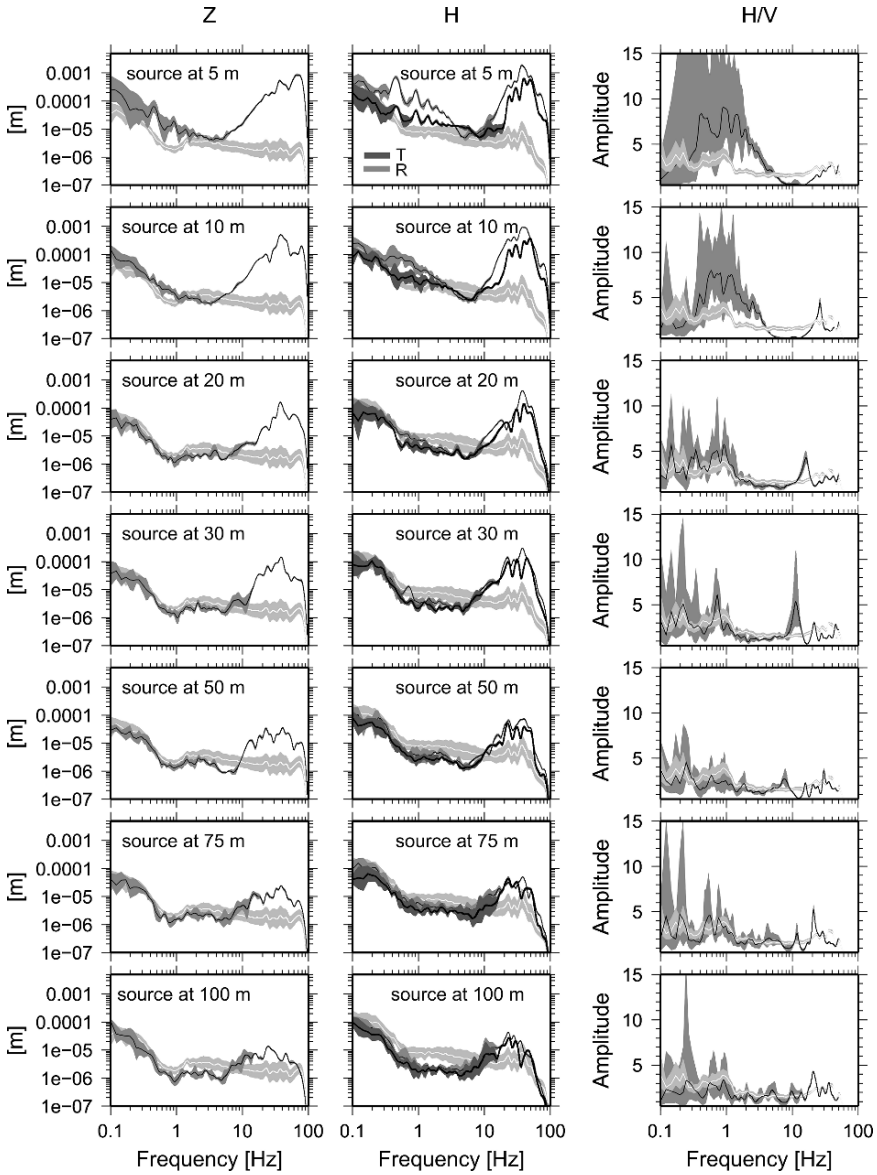

Fig. 1.2.3 Vertical and horizontal component Fourier Spectra (left and central panels, respectively) and H/V spectral ratio (right panels) calculated for increasing source-to-receiver distances (from top to bottom). Only results for vertical sources are shown here. Average spectra and H/V for stationary noise are shown with white lines and the 95% confidence interval is shown by light gray. Black lines indicate average spectra and H/V results for windows including transients. In the central panel, gray indicates the radial component, while dark gray indicates the transverse component

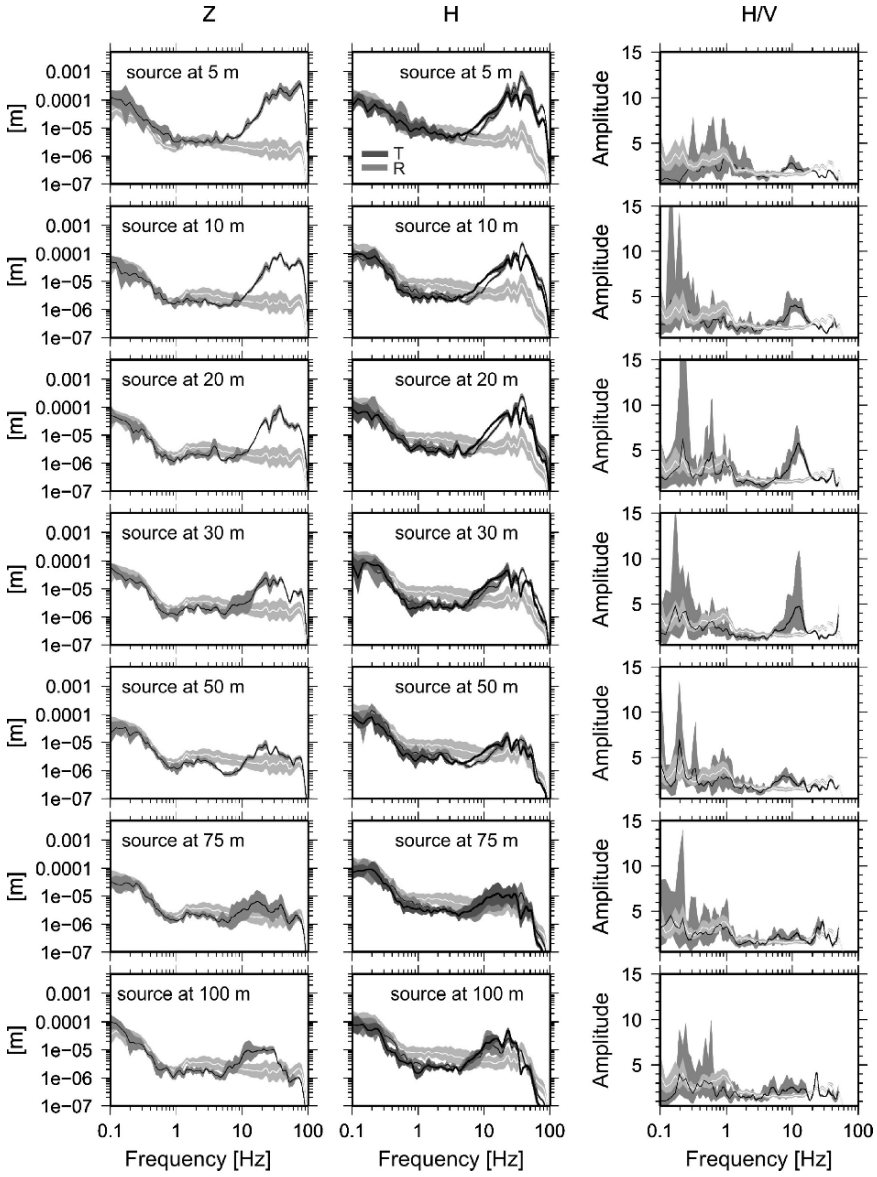

Fig. 1.2.4 As in Figure 1.2.3 but for horizontal sources

component behaviour. Some transient-related effects on the H/V shape are visible only at frequencies larger than 10 Hz.

Figure 1.2.4 shows the results obtained when only the horizontal sources are considered. The spectra of both horizontal and vertical components show large amplitudes at frequencies higher than 10 Hz. These amplitudes are, however, much smaller than those obtained using a vertical source. For example, the spectral

amplitudes of the signals generated by a horizontal source at a distance of 10 m are comparable with the amplitudes of a vertical source at 20 m. This is probably due to the less efficient energization in the horizontal direction and weak coupling of the sleeper with the soil. The spectral amplitude, as expected, decays with increasing source-to-station distance, and there is no large significant effect of the transients at frequencies around 1 Hz, neither when the short nor long source-to-station distances are considered. All the H/Vs show shapes similar to the stationary-noise H/V up to 10 Hz. Only at higher frequencies, and especially for the distance range 10–30 m, do transients appear to affect the H/V spectral ratio shape.

Figure 1.2.5 shows the results when vertical and horizontal sources are considered simultaneously. The results are similar to those obtained when considering only the vertical sources since the spectral amplitude of the waves they generated are higher.

1.2.5 Results and discussions

The evidence that the H/V spectral ratio is enhanced at frequencies around the resonance frequencies of the site when active sources are considered is in agreement with the results of Mucciarelli (1998). Indeed, the source-to-distance range used in the Mucciarelli (1998) test was larger (50 m) than the range of distances (5–10 m) we observed that provide the largest effects. Nevertheless, this can be explained by considering the numerical simulation results of Parolai and Galiana-Merino (2006), who showed that the influence of transients varies with the source-to-receiver distance relative to the thickness of the sediments.

In order to explain the mechanism generating the magnification of the H/V spectral ratio, we carried out further analyses. After having verified by time-frequency analysis (not shown here) that the increase of the spectral amplitude between 0.3 and 3 Hz (with well-defined peaks at 0.4 and 0.9 Hz), only results from vertical energization (i. e, neither in the stationary noise, nor when transverse sources are used), we focused the analysis only on the time series generated by the vertical impact of the sledge hammer. First, we filtered all the time series windows using a Gaussian filter (Dziewonski et al., 1969; Li et al., 1996; Shapiro and Singh, 1999)

$$H(\omega,\omega_0) = e^{-[(\omega-\omega_0)/(\alpha\omega_0)]^2}, \tag{1.2.1}$$

where ω_0 is the central angular frequency of the filter, α (fixed to 0.2) is the relative bandwidth and ω the angular frequency. Filtering is performed by first computing the Fourier transform of the trace, then multiplying the obtained complex spectrum by the Gaussian filter and then calculating the inverse Fourier transform of the filtered complex spectrum.

Second, the complex seismic traces (Taner et al., 1979; René et al., 1986; Parolai, 2008) are calculated for each component by

$$c(t) = r(t) + iq(t), \tag{1.2.2}$$

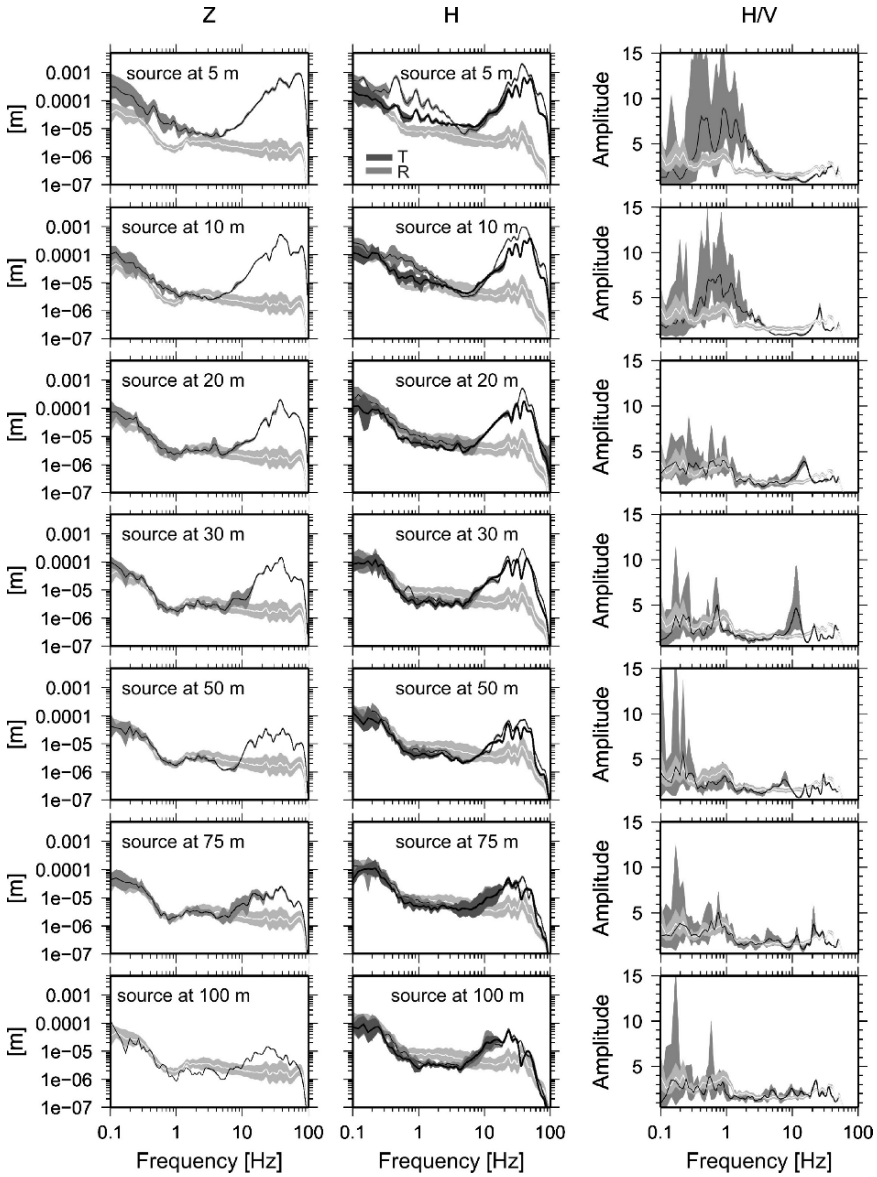

Fig. 1.2.5 As in Figure 1.2.3, but for the signal generated by vertical and horizontal sources

where $r(t)$ is the real seismic trace, i is the square root of -1, and $q(t)$ is the quadrature trace obtained as the Hilbert transform of the real trace. Finally, using complex seismic traces, we obtained instantaneous polarization attributes. Here we will focus on reciprocal ellipticity and phase differences, where positive and negative phase differences correspond to prograde and retrograde ground motion,

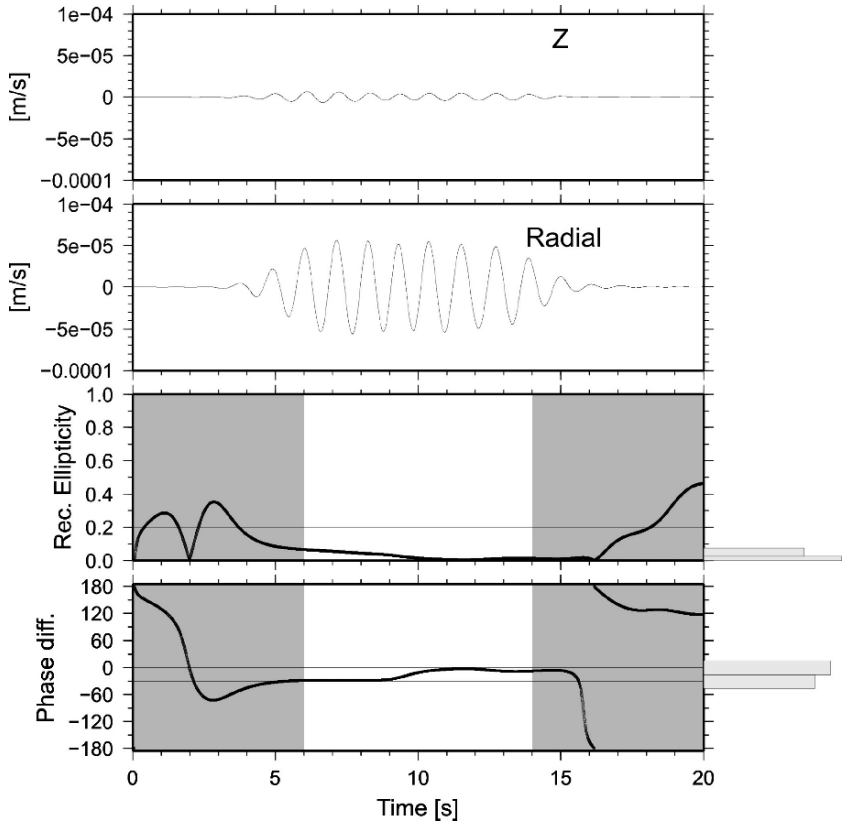

Fig. 1.2.6 The vertical (top panel) and the radial (second from the top) component of ground motion generated by a vertical source at 5 m distance after applying a Gaussian filter with a central frequency of 0.9 Hz. The reciprocal ellipticity (third panel from the top) versus time. The phase difference versus time (bottom panel). The white background indicates the time in which the vertical sources operated. The histograms are calculated considering the data falling within the area with white background

respectively; linear polarized waves have 0° (S-wave) or $|180°|$ (P-wave) phase differences, and a reciprocal ellipticity of 0. A reciprocal ellipticity of 1 corresponds to circular polarization.

Figure 1.2.6 shows the vertical- and radial-component seismograms filtered using the above described filter with a central frequency of 0.9 Hz. These time series include only five consecutive vertical shots. Outside of the time window, including the first and the last signal generated by the sledge-hammer impacts (e.g. occurring between about 5 and 15 s in Figure 1.2.6), small filter effects are observed. Within this time window, the radial component of ground motion is much larger than the vertical one, the reciprocal ellipticity is nearly 0 and the phase difference is close to 0°. Figure 1.2.7 shows the results for the radial and transverse components. The ground motion is predominant in the radial direction, with small reciprocal

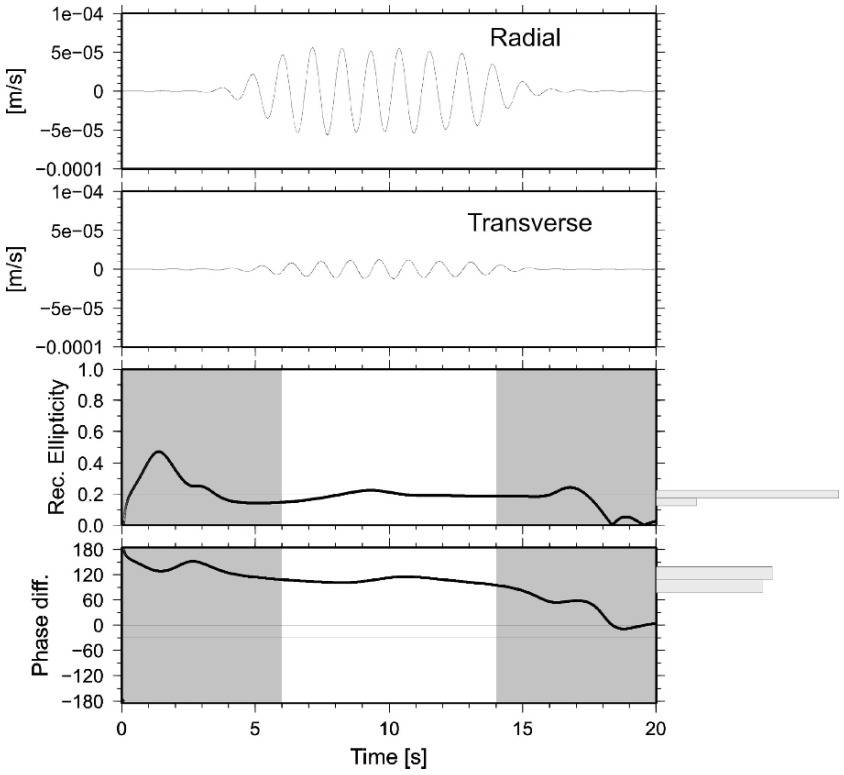

Fig. 1.2.7 Same as Figure 1.2.6, but for the radial and transverse components

ellipticity (0.2) and phase differences of nearly 120°. The results for the vertical and transverse components (Figure 1.2.8) show that the relatively small ground motion has reciprocal ellipticity that varies greatly (from 0.8 down to 0.3), whereas the phase difference is always around 90°.

Hence, the polarization analysis suggests that the spectral energy between 0.3 and 2 Hz observed at distances less than 20 m is carried out by waves linearly polarized in the radial direction. Plotting the radial component spectral amplitude at 0.9 Hz versus distance (scaled to the reference spectral amplitude at 5 m), a decay slightly larger than R^{-2}, where R is the source-to-station distance is observed for the first 30 m (Figure 1.2.9). At larger distances the spectral amplitudes are dominated by stationary seismic noise, and, therefore, do not decay any further.

In summary, considering that (1) body waves generated by a surficial source and recorded at the surface attenuate with R^{-2} (Richart et al., 1970), (2) substantial body waves affect the near field (Tokimatsu and Tamura, 1995; Tamura, 1996) and (3) we observe an increase in energy also on the vertical component (although much smaller than on the radial one), we believe that the contribution of surface waves to the observed spectral amplitudes can be discarded. Moreover, considering that a vertical source is expected to radiate a considerable amount of power as shear

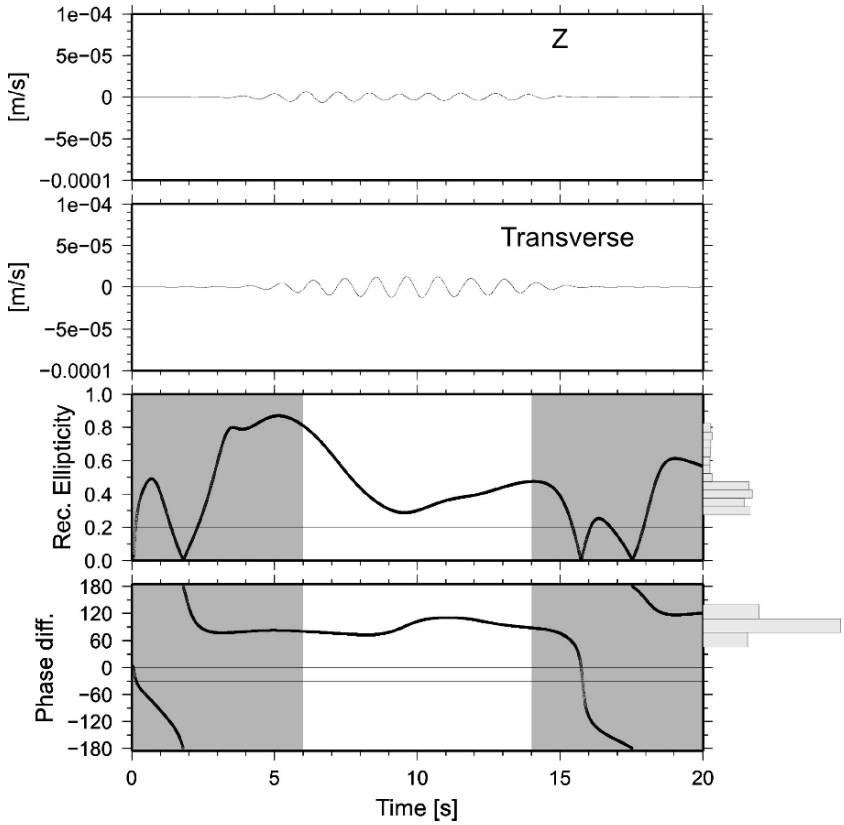

Fig. 1.2.8 Same as Figure 1.2.6, but for the vertical and transverse components

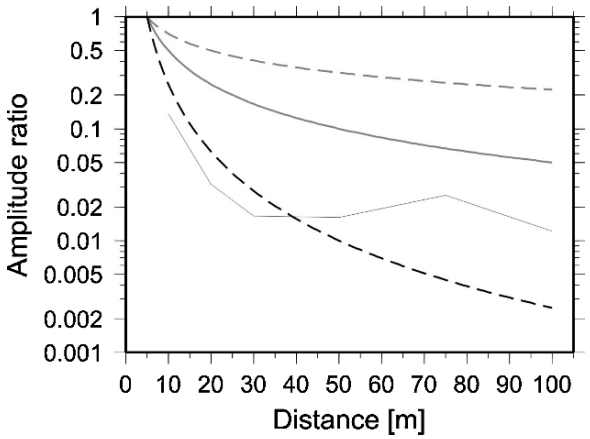

Fig. 1.2.9 The spectral amplitude decay for 0.9 Hz versus distance (thin light gray). The dashed black line indicates a R^{-2} decay. The thicker gray line indicates a R^{-1} decay. The dashed gray line indicates a $R^{-0.5}$ decay

waves (Miller and Pursey, 1955) and the results of the polarization analysis (a linearly polarized wave in the radial direction), we suggest that the wavefield in the frequency range between 0.3 and 2 Hz for sources at distances smaller than 20 m is dominated by SV waves.

The amplitude of the waves is relatively small with respect to higher frequencies, but a resonance mechanism is amplifying them over shorter distances. Although the resonance mechanism can still act when sources are further away, the spectral energy of the direct SV arrival (that decays with R^{-2}) is too small to make the spectral amplitudes larger than those of the stationary noise. The same mechanism could also explain why the 0.2 Hz resonance peak observed in the H/V for stationary noise is not affected by the transients.

Therefore, spectral amplitudes can be determined by the superimposition of spectral energy arriving directly from the source with a resonance mechanism. A similar effect for P waves is unlikely, because they are expected to have smaller amplitudes and because resonance should affect principally the vertical component of ground motion.

The lack of similar evidence when a transverse source is considered (and therefore generating SH waves more efficiently) could be explained by the lower spectral amplitude of the horizontal source signal. Note, in fact, that the spectral amplitudes (between 10 and 50 Hz) for a source-to-station distance of 10 m (Figure 1.2.4) are of the same order of magnitude than those generated by a vertical source at 20 m distance. The smaller spectral amplitudes do not allow, even in presence of resonance, to overstep the spectral amplitudes of stationary noise over the 0.3–2 Hz frequency range.

1.2.6 Conclusions

In this study we report on the results of an ad-hoc experiment performed to evaluate the influence of transients in H/V spectral ratio calculations. Consistent with previous studies (e.g. Mucciarelli, 1998), we observed that for certain distance ranges the peak in the H/V spectra ratio can be magnified when energy is added to the system. We proposed an explanation of the experimental evidence that agrees with the state-of-the-art knowledge in vibration studies and with the outcomes from previous empirical and numerical studies.

Our results suggest that including transients in the H/V spectral ratio should not worsen the estimation of the fundamental resonance frequency of a site. Since the mechanism generating a peak in the H/V spectral ratio may depend on the source position relevant to the thickness of the sedimentary column (Parolai and Galiana-Merino, 2006), a full understanding of the composition of the wavefield is mandatory before inverting the peak to obtain information about the sub-soil structure.

On the other hand, if including active sources can help in better highlighting the resonance effect of S-waves, the use of transients, consistent with Mucciarelli et al., (2003), might allow a H/V spectral ratio closer to the H/V spectral ratio of small earthquakes to be obtained.

We believe that these issues are worthy of the attention of the seismological community and further ad-hoc experiments should be planned in order to better understand the composition of the noise wavefield.

Acknowledgements K. Fleming kindly improved our English. Figures have been drawn using the GMT software (Wessel and Smith, 1991). R. Milkereit improved the figures.

References

Arai, H., and Tokimatsu, K. (2004). S-wave velocity profiling by inversion of microtremor H/V spectrum. Bulletin of the Seismological Society of America, 94, 1, 53–63.

Bard, P.Y. (1999). Microtremor measurements: a tool for site effect estimation? The Effects of Surface Geology on Seismic Motion, eds. K. Irikura, K. Kudo, H. Okada and T. Sasatani (Balkema, Rotterdam), 1251–1279.

Chatelain, J.C., Guillier, B., Cara, F., Duval, A.M., Atakan, K., Bard, P.Y., and The WP02 SESAME team (2008). Evaluation of the influence of experimental conditions on H/V results from ambient noise recordings. Bulletin of Earthquake Engineering, 6, 33–74, doi: 10.1007/s10518-007-9040-7.

Fäh, D., Kind, F., and Giardini, D. (2001). A theoretical investigation of average H/V ratios. Geophysical Journal International, 145, 535–549.

Fäh, D., Kind, F., and Giardini, D. (2003). Investigation of local S-wave velocity structures from average H/V ratios, and their use for the estimation of site effects. Journal of Seismology, 7, 449–467.

Dziewonski, A., Bloch, S., and Landisman, M. (1969). A technique for the analysis of transient seismic signals. Bulletin of the Seismological Society of America, 59, 427–444.

Field, E.H. and Jacob, K. (1993). The theoretical response of sedimentary layers to ambient seismic noise. Geophysical Research Letters, 20–24, 2925–2928.

Horike, M., Zhao, B., and Kawase, H. (2001). Comparison of site response characteristics inferred from microtremors and earthquakes shear waves. Bulletin of the Seismological Society of America, 81, 1526–1536.

Kim, D.S., and Lee, J.S. (2007). Propagation and attenuation characteristics of various ground vibrations. Soil Dynamics and Earthquake Engineering, 19, 115–126.

Konno, K., and Ohmachi, T. (1998). Ground-motion characteristic estimated from spectral ratio between horizontal and vertical components of microtremor. Bulletin of the Seismological Society of America, 88, 228–241.

Lermo, J., and Chávez-García, F.J. (1994). Are microtremors useful in site response evaluation? Bulletin of the Seismological Society of America, 84, 1350–1364.

Li, X.P., Zühlsdorf, L., and Liebhardt, G. (1996). Eliminating the effects of the surface weathered layer by using an inverse transform function. Scientific Drilling, 5, 233–242.

McNamara, D.E., and Buland, R.P. (2004). Ambient noise levels in the continental United States. Bulletin of the Seismological Society of America, 94, 1517–1527.

Miller, G.F., and Pursey, H. (1955). On the partition of energy between elastic waves in a semi–infinite solid. Proceedings of the Royal Society, London, Series A, 55–69.

Mucciarelli, M. (1998). Reliability and applicability range of the Nakamura's technique. Journal of Earthquake Engineering, 2, 4, 625–638.

Mucciarelli, M., Gallipoli, M.R., and Arcieri, M. (2003). The stability of the horizontal-to-vertical spectral ratio of triggered noise and earthquake recordings. Bulletin of the Seismological Society of America, 93, 1407–1412.

Nakamura. (1989). A method for dynamic characteristics estimations of subsurface using microtremors on the ground surface. Q. Rept. Railway Technical Research Institute Japan, 30, 25–33.

Nogoshi, M., and Igarashi, T. (1970). On the propagation characteristics estimations of subsurface using microtremors on the ground surface. Journal of Seismological Society of Japan, 23, 264–280.

Nogoshi, M., and Igarashi, T. (1971). On the amplitude characteristics of microtremor (part 2). Journal of Seismological Society of Japan, 24, 26–40.

Parolai, S., Bormann, P., and Milkereit, C. (2001). Assessment of the natural frequency of the sedimentary cover in the Cologne area (Germany) using noise measurements. Journal of Earthquake Engineering, 5, 4, 541–56.

Parolai, S., Picozzi, M., Richwalski, S.M., and Milkereit, C. (2005). Joint inversion of phase velocity dispersion and H/V ratio curves from seismic noise recordings using a genetic algorithm, considering higher modes. Geophys. Res. Lett., 32, L01303, doi: 10.1029/2004GL021115.

Parolai, S., and Galiana-Merino, J.J. (2006). Effect of transient seismic noise on estimates of H/V spectral ratios. Bulletin of the Seismological Society of America, 96, 228–236.

Parolai, S., Richwalski, S.M., Milkereit, C., and Fäh, D. (2006). S-wave velocity profiles for earthquake engineering purposes for the Cologne Area (Germany). Bulletin of Earthquake Engineering, 4, 65–94.

Parolai, S. (2008). Determination of dispersive phase velocities by Complex seismic trace Analysis of Surface Wave (CASW). Soil Dynamics and Earthquake Engineering in revision, doi: 10.1016/j.soildyn.2008.05.008

Picozzi, M., Parolai, S., and Richwalski, S.M. (2005). Joint inversion of H/V ratios and dispersion curves from seismic noise: Estimating the S-wave velocity of bedrock. Geophys. Res. Lett., 32, L1308, doi: 10.1029/2005GL022878.

René, R.M., Fitter, J.L., Forsyth, P.M., Kim, K.Y., Murray, D.J., Walters, J.K., and Westerman, J.D. (1986). Multicomponent seismic studies using complex trace analysis. Geophysics, 51, 6, 1235–1251.

Richart, F.E., Hall, J.R., and Woods, R.D. (1970). Vibration of Soils and Foundations. Englewood Cliffs, NJ: Prentice-Hall, 1970.

SESAME European project (2004). Guidelines for the implementation of the H/V spectral ratio technique on ambient vibrations measurements, processing and interpretation. Deliverable D23.12. http://sesame-fp5.obs.ujf-grenoble.fr/SES_TechnicalDoc.htm.

Scherbaum, F., Hinzen, K.-G., and Ohrnberger, M. (2003). Determination of shallow shear-wave velocity profiles in Cologne, Germany area using ambient vibrations. Geophysical Journal International, 152, 597–612.

Shapiro, N.M., and Singh, S.K. (1999). A systematic error in estimating surface-wave group velocity dispersion curve and a procedure for its correction. Bulletin of the Seismological Society of America, 89, 1138–1142.

Strollo, A., Bindi, D., Parolai, S., and Jäckel, K.-H. (2008a). On the suitability of 1 s geophone for ambient noise measurements in the 0.1–20 Hz frequency range: experimental outcomes. Bulletin of Earthquake Engineering, 6, 141–147, doi: 10.1007/s10518-008-9061-x.

Strollo A., Parolai, S., Jäckel K.-H., Marzorati, S., and Bindi, D. (2008b). Suitability of short-period sensors for retrieving reliable H/V peaks for frequencies less than 1 Hz. Bulletin of the Seismological Society of America, Vol. 98, No. 2, pp. 671–681, April 2008, doi: 10.1785/0120070055.

Tamura, S. (1996). Comparison of body and Rayleigh wave displacements generated by a vertical point force on a layered elastic medium. Proceedings of the 11th World Conference on Earthquake Engineering, Paper No. 1722.

Taner, M.T., Koehler, F., and Sheriff, R.E. (1979). Complex seismic trace analysis. Geophysics, 44, 6, 1041–1063.

Taniguchi, E., and Sawada, K. (1979). Attenuation with distance of traffic-induced vibrations. Soils and Foundations, 19, 2, 16–28.

Tokimatsu, K., and Tamura, S. (1995). Estimation of local site conditions in Kushiro city based on array observation of microtremors. Proceedings of the 3rd International Conference on Recent Advances in Geotechnical Earthquake Engineering and Soil Dynamics, 2, 599–602.

Wessel, P., and Smith, W.H.F. (1991). Free software helps map and display data. EOS Trans. AGU, 72,41,441,445–446.

Chapter 1.3
Basic Structure of QTS (HVSR) and Examples of Applications

Yutaka Nakamura

1.3.1 Introduction

Damages caused by the recent earthquakes are concluded as a direct result of local geological conditions affecting the ground motion. The best approach for understanding ground conditions is through direct observation of the seismic ground motion, but such studies are restricted to areas with relatively high seismicity. Because of these restrictions in other methods, such as only at high seismicity area and the availability of an adequate reference site, non-reference site methods have been applied to the site response studies. Microtremor is a very convenient tool to estimate the effect of surface geology on seismic motion without other geological information.

The H/V technique, alias QTS, Quasi-Transfer Spectra, fits very well to this description and it has received great attention from all over the world with its simplicity together with quick information about dynamic characteristics of ground and structures. Although several researchers claimed that the theoretical background of this technique is not clear, there have been many successful experimental studies performed. This method is attractive since it gives the ease of data collection and it can be applied in areas of low or even no seismicity.

The H/V technique was developed by the author with relating borehole investigations together with the strong motion records analysis, on the various geological site conditions. It was hypothesized that the vertical component of the ambient noise at the ground surface keeps the characteristics of basement ground, is relatively influenced by Rayleigh wave on the sediments and can therefore be used to remove both of the source and the Rayleigh wave effects from the horizontal components.

Y. Nakamura
President, System and Data Research Co., Ltd., Tokyo, Japan
Visiting Professor, Department of Built Environment, Interdisciplinary Graduate School of Science and Engineering, Tokyo Institute Technology, Japan

M. Mucciarelli et al., (eds.), *Increasing Seismic Safety by Combining Engineering Technologies and Seismological Data,* NATO Science for Peace and Security Series C: Environmental Security,

It is effective to identify the fundamental resonant frequency of a sedimentary layer, with implied amplification factors that are more realistic than those obtained from sediment to rock site ratios. It has been shown by many researchers (ex. Ohmachi et al., 1991; Lermo et al., 1992; Field and Jacob, 1993, 1995) that how such H/V ratio of noise can be used to identify the fundamental resonant frequency and amplification factor of sediments.

Looking to the examples in the study of Nogoshi and Igarashi (1971) which compared the H/V of Rayleigh wave with that of microtremor and concluded that microtremor was mostly composed of Rayleigh wave, some of theoretical studies (Lachet and Bard, 1994; Konno and Ohmachi, 1998; Bard, 1998) suggested that the peak on H/V can be explained with the fundamental mode of Rayleigh waves. If we think that this approach is true, microtremor should be considered to consist of only Rayleigh wave. On the other hand, if we check the examples given on Nogoshi and Igarashi (1971) carefully (which will be discussed later), we can clearly see that, at the peak frequency of H/V of Rayleigh wave, the energy of Rayleigh wave is very small, nearly zero. Rayleigh wave has its maximum energy at near trough frequency of H/V. Because of this, peak of the H/V of microtremor cannot be explained by the energy of Rayleigh wave. As it is explained by Nakamura (1989), the H/V of microtremor at peak frequency range can be explained with vertical incident SH wave.

1.3.2 Origin of the H/V technique

First of all the H/V spectral ratio was found from the strong motion records at various sites in Japan. On the soft ground, horizontal motion is larger than vertical motion. On the other hand, on the hard ground, both horizontal and vertical motions are similar to each other both on the maximum value and waveform.

First, horizontal to vertical ratio was derived from each maximum value and was compared with the softness of ground and the amplification factor. As shown in Figures 1.3.1 and 1.3.2, horizontal to vertical ratio of maximum value highly corresponds to these ground characteristics (Nakamura et al., 1983).

On the next step, the H/V spectral ratio of microtremor measured at anywhere was confirmed that it is able to estimate the predominant frequency and the

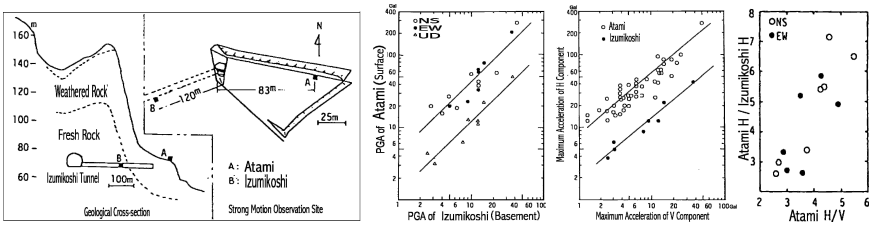

Fig. 1.3.1 Relation of maximum accelerations on surface and basement (Nakamura and Saito, 1983)

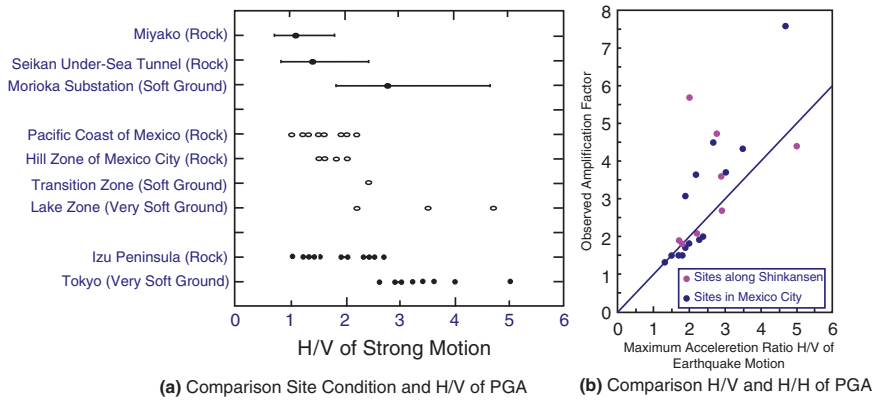

(a) Comparison Site Condition and H/V of PGA **(b)** Comparison H/V and H/H of PGA

Fig. 1.3.2 Comparisons between site condition and H/V of PGA, H/V and H/H of PGA

amplification factor. And as shown in Figure 1.3.3 the result of estimation is stable for the measured time and season (Nakamura, 1989).

From the background of the H/V technique, it is natural that the H/V spectral ratio of not only microtremor but also the earthquake motion can explain the characteristics, and the original paper (Nakamura, 1989) had pointed that the H/V spectral ratios of earthquake motion are almost similar to the amplification spectra as shown in Figure 1.3.4. And then as shown in Figure 1.3.5, it is confirmed that the H/V spectral ratios of microtremor and earthquake motion are similar to each other and mostly similar to the amplification spectrum (Sato et al., 2004).

1.3.3 Basic structure of the H/V spectral ratio

1. H/V Spectral Ratio Technique
   There is no reason to enlarge the amplitude of a particular frequency range and of a particular direction at the hard and uniform ground as imaged in Figure 1.3.6. It is natural that the vibration of hard ground is uniform for each frequency range and each direction. The measured results of microtremor and earthquake support it. On the other hand, under the situation of a soft ground deposition on the hard basement, it is important to grasp the amplification characteristics of the horizontal motion. At the frequency range amplified the horizontal motion, it seems vertical motion is not amplified. Meanwhile, at this kind of ground condition, it is important to consider the Rayleigh wave distributed on the ground surface. Earthquake disaster is caused mainly by the body wave and if the Rayleigh wave causes any damage, it must be a slight damage. That is to say that it is important to understand the phenomenon which the energy of the body wave trapped inside the soft surface layer. The phenomenon is the amplification of earthquake motion by so called the multiple reflections.

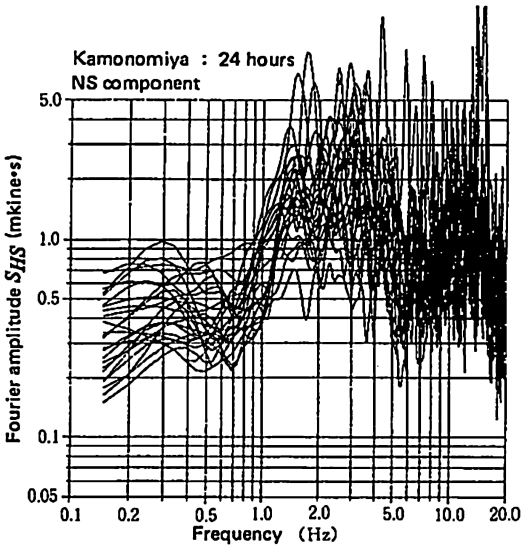

(a) A 24-hours Change in Horizontal Spectrum

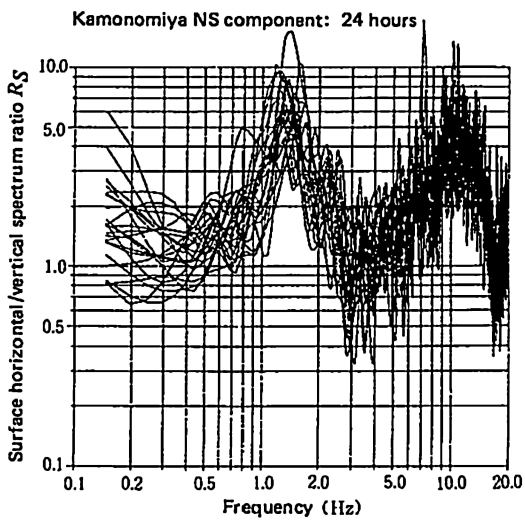

(b) A 24-hours Change in H/V Spectral Ratio

Fig. 1.3.3 Stability of H/V spectral ratio

From this view point, the Rayleigh wave plays as a noise and it is necessary to reject the effect of the Rayleigh wave. It is possible to understand that the surface layer behaves as a high-pass filter for the Rayleigh wave propagating in the surface layer as illustrated in Figure 1.3.7. Rayleigh wave can not propagate in the frequency range under the predominant frequency of surface ground (F_0), and

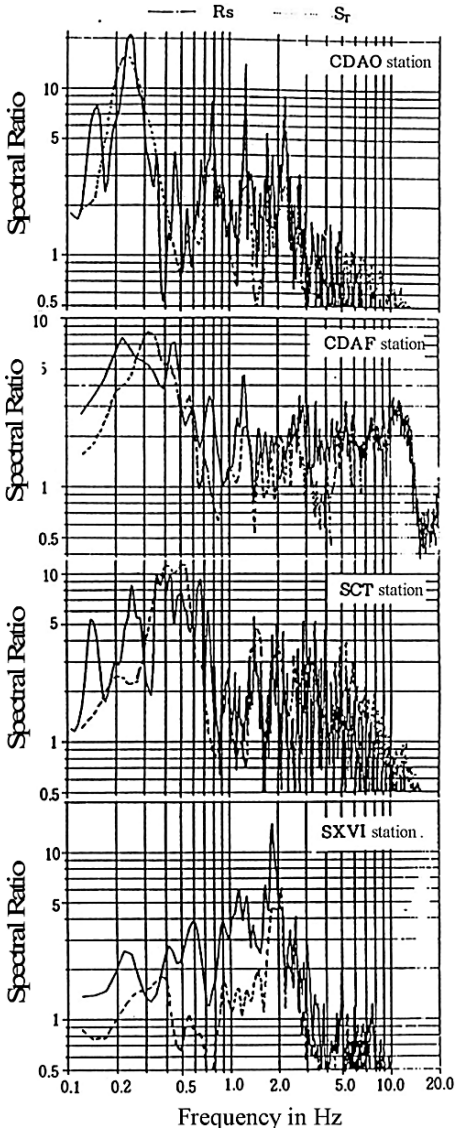

Fig. 1.3.4 Comparison between spectral ratios H/V(Rs) and H/H(St) at Mexico city

can transmit the energy peak around the frequency of minimum group velocity ($2F_0$, Airy phase). So the effect of multiple reflections of the SH wave is mainly composed around F_0.

Comparison of the vertical motions between the basement and the ground surface makes sure the existence of the Rayleigh wave. The focused frequency range is around F_0, the predominant frequency of the horizontal motion. The frequency of the vertical motion amplified by the multiple reflections is estimated as $V_p/V_s^* F_0$.

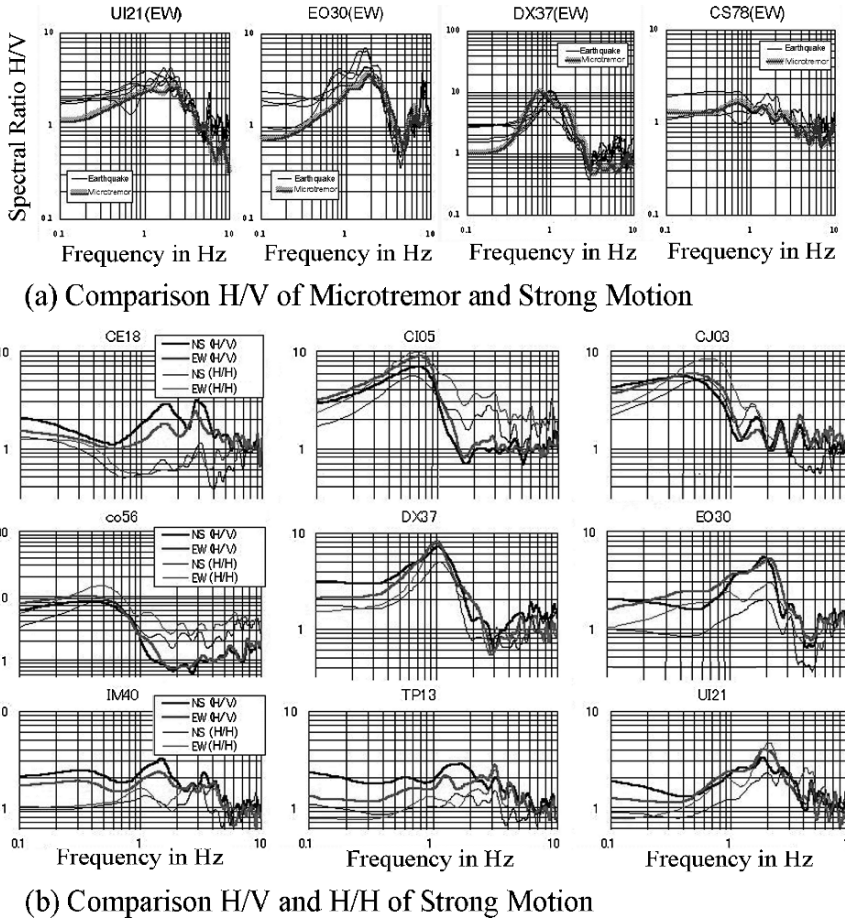

Fig. 1.3.5 Relation between H/V of strong motion, H/V of microtremor and H/H of strong motion

In case of the noticed soft ground, while V_s is about 50 to 200 m/s, V_p is around 1,000 m/s, near to the V_p of water $(= 1{,}500\,\mathrm{m/s})$. So the frequency that the vertical motion enlarged is 5–20 times for F_0. Corresponds to this, the frequency of maximum energy transmission of the Rayleigh wave is approximately $2F_0$. So it is important to judge that the Rayleigh wave effects much if the vertical motion of the ground surface is relatively larger than the basement at least the frequency range up to three times of F_0.

Many peaks are observed on the spectrum of measured microtremor in actual. In past, the analyzers had read the peak corresponding to the predominant frequency of surface layer based on their experiences and intuitions. It must be only a speculation because of their arbitrariness. It is necessary for extracting peak for the purpose exactly to reject the effect of the Rayleigh wave.

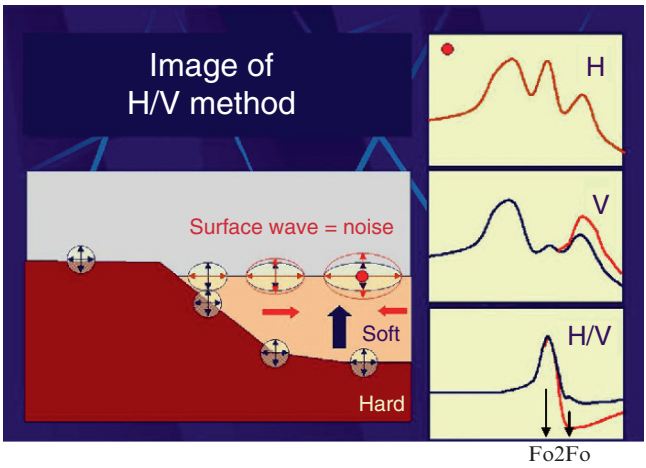

Fig. 1.3.6 Image of H/V method

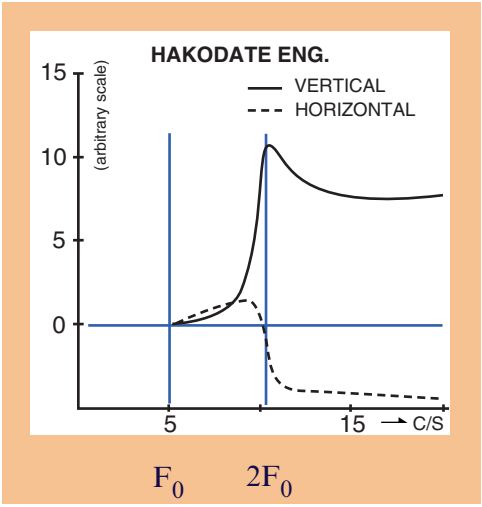

Fig. 1.3.7 An example of horizontal and vertical components of Rayleigh wave

The effect of the Rayleigh wave for the surface to the basement ratio of the horizontal motion R ($= A_{hs}/A_{hb}$: amplification characteristics) is estimated by the surface to the basement ratio of the vertical motion E ($= A_{vs}/A_{vb}$). Then the corrected amplification characteristic A_m is estimated as follows;

$$\begin{aligned} A_m &= R/E \\ &= (A_{hs}/A_{hb})/(A_{vs}/A_{vb}) \\ &= (A_{hs}/A_{vs})/(A_{hb}/A_{vb}) \end{aligned}$$

Using an observational fact that the ratio A_{hb} and A_{vb} is nearly equal to 1 for wide frequency range, A_m could be expressed as follows:

$$A_m \cong A_{hs}/A_{vs}.$$

This is the H/V spectral ratio. At present, however, there are many researchers who believe that the peak of the H/V can be explained by Rayleigh wave. Then the H/V of Rayleigh wave must be discussed.

2. H/V of Rayleigh Wave
For different wave-lengths, Ohta (1963) calculated H/V and phase velocity of Rayleigh waves for two layers model for various impedance ratio (varying between 1.2 and 4.5) and Poisson's ratio (varying between 0.25 and 0.49) both in sedimentary and basement layers. By using these calculated results, the relationship between the H/V of Rayleigh wave and the frequency is shown in Figure 1.3.8, and it shows the relations between impedance, peak and frequency. The frequency in this figure is normalized with the predominant frequency of surface layer, $F_0 = C_s/(4h)$. Group velocities calculated from phase velocities are normalized with S wave velocity and drawn with the frequency normalized with F_0. Figure 1.3.9 shows the distribution of group velocity versus frequency. As we follow this figure, if the impedance ratio is less than two, the energy of Rayleigh wave exists at the lower frequency range. Figure 1.3.10 shows the change of impedance ratio for frequencies of trough and peak of H/V and minimum group velocity of Rayleigh waves. The frequencies corresponding to the trough and minimum group velocity (for almost all impedance ratio values), change between 1.5 and 2. On the other hand, only for the peak frequency varies

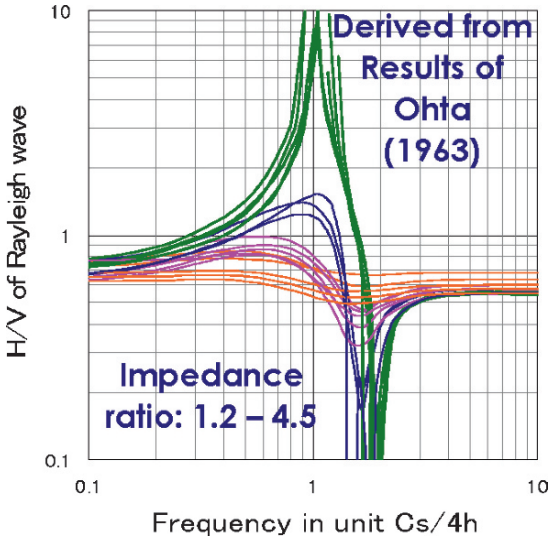

Fig. 1.3.8 H/V of Rayleigh waves for two layered ground

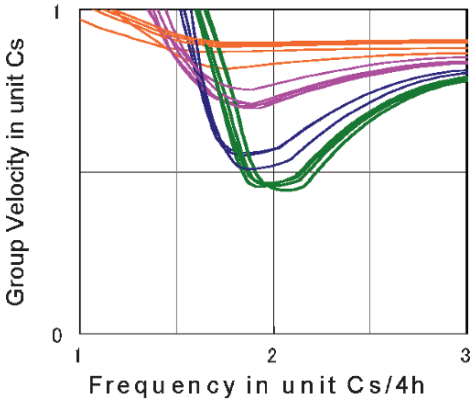

Fig. 1.3.9 Group velocities of Rayleigh waves for two layered ground

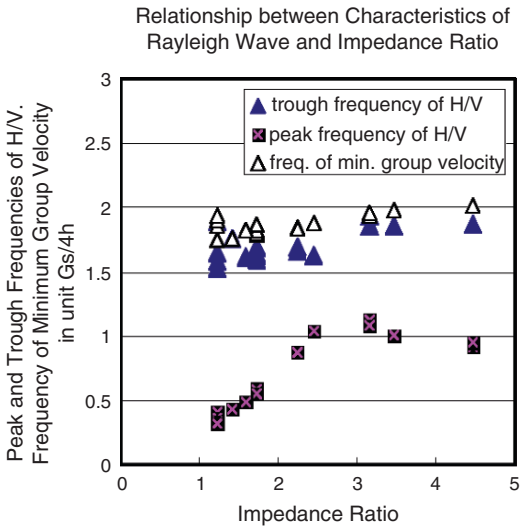

Fig. 1.3.10 Relationship between characteristics of Rayleigh wave and impedance ratio

in a wider range for different impedance ratio. The energy of the Rayleigh wave is almost zero at the peak frequency of H/V, and at the trough frequency of H/V the energy becomes to maximum. When the impedance ratio is greater than 2.5, the Rayleigh wave does not affect the H/V peak of ground motion. And on the other hand, when the impedance ratio is less than 2.5, the Rayleigh wave affects the H/V peak of ground motion.

3. Comparison between Microtremor and Rayleigh Wave for H/V
   Figure 1.3.11, modified after Nogoshi and Igarashi (1971), shows relationship between H, V and H/V for microtremor and for Rayleigh wave. It can be clearly seen from these figures that, the energy of Rayleigh wave does not appear on the peak of H/V of Rayleigh wave. We can easily see that there is no energy around

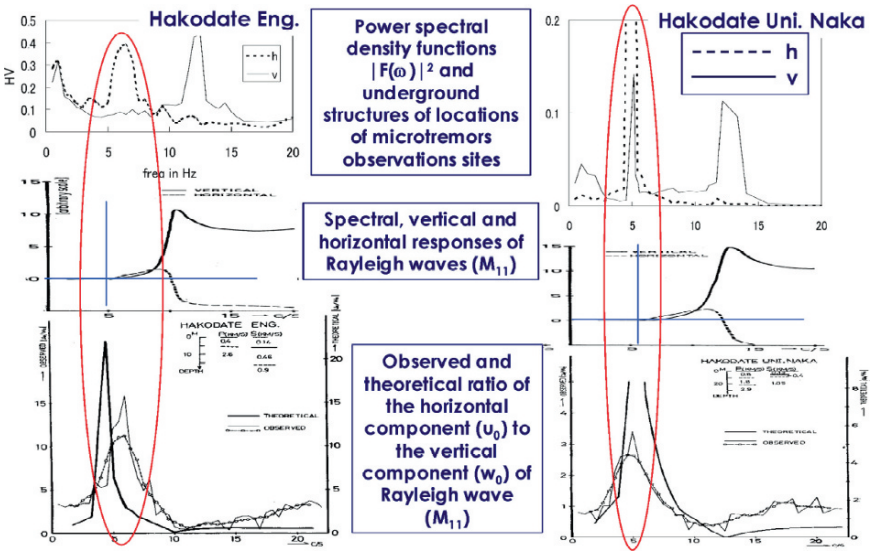

Fig. 1.3.11 Relation of H, V and H/V for microtremor and for Rayleigh wave (modified after Nogoshi and Igarashi, 1971)

the peak frequency of H/V and amplitude is almost zero for horizontal and zero for vertical components of Rayleigh waves. On the other hand, the energy of Rayleigh wave gets its maximum on later frequencies at minimum group velocity of Rayleigh wave and this is nearly equal to trough frequency which is almost two times of the H/V peak frequency. The peak of vertical component corresponds to Rayleigh wave, but the peak of horizontal component is not caused by Rayleigh waves. These figures show that the peak of the H/V is not caused by Rayleigh waves.

Figure 1.3.8 shows that the H/V of Rayleigh wave for a hard ground, corresponding impedance one, is estimated around 0.7, against 1.0 from microtremor measurement on rock sites. It also shows that the H/V spectral ratio of microtremor around the peak is not caused by the Rayleigh waves.

The H/V spectral ratio shows the amplification characteristics by the multiple reflections of the SH wave at least around F_0, and shows the characteristics contaminated by the Rayleigh wave around $2F_0$. In case of less effect of the Rayleigh wave it is possible to estimate not only preliminary peak but also secondary peak of amplification characteristics caused by multiple reflections with the H/V spectral ratio.

4. Comparison of the H/V spectral ratio between earthquake and Rayleigh wave
Figure 1.3.12(a) shows the H/V of strong ground motion of two different earthquakes recorded at the same site. Although the waveforms show different shape, if we take the H/V, they show similar shape. Another example can be found also in a paper of Okuma et al. (1999) which is given in Figure 1.3.12(b). The results show again that H/V gives similar characteristics for the different earthquakes

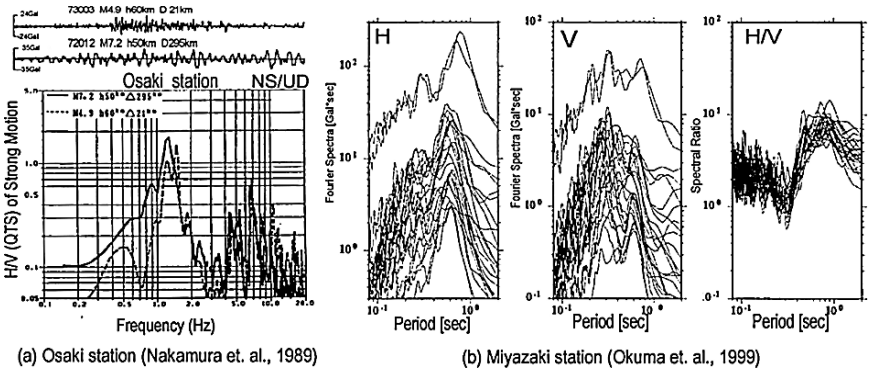

(a) Osaki station (Nakamura et. al., 1989) (b) Miyazaki station (Okuma et. al., 1999)

Fig. 1.3.12 H/V of strong ground motion for different earthquakes recorded at the same station

recorded at the same sites. If we think that the H/V of earthquake record can be explained by Rayleigh wave, we should see same characteristics for all directions of the site, but this is out of practice and it is proper to think that the H/V of earthquake motion indicate the transfer function of local surface ground, as same as the H/V of microtremor.

5. Numerical simulation for H/V
   The H/V indicates the transfer function of local surface ground. This was confirmed from the numerical simulation performed by Bonnefoy-Claudet et al. (2006) objecting the theory above mentioned contrary to their opinion. This paper is to consider the characteristics of H/V spectral ratio of microtremor experimentally using numerical ground model of two layer; basement and surface grounds with 6.5 of the impedance ratio. The first natural frequency of surface ground is set to 2 Hz. Various shape, location and depth of source are adopted for this analysis. In case of weak Rayleigh waves the peak corresponding to the second natural frequency 6 Hz appeared. The weaker the Rayleigh waves, the more correct the amplification factor. Consequently, it is natural to consider that the peak of 2 Hz is caused by the multiple reflections of S waves except strong affection of the Rayleigh waves near the source. The peak value at 2 Hz varies only between 5 and 8 for 6.5 of impedance ratio. This indicates the amplification factor can be estimated by the H/V peak value correctly.

6. Summary of the H/V characteristics
   Figure 1.3.13 shows the typical shape of the H/V spectral ratio. The characteristic of H/V for microtremor is summarized as follows. The first peak near F_0 consists of S-wave mainly. The first trough near $2F_0$ is caused by Rayleigh wave. Around F_0 there is almost no energy of Rayleigh waves, so the dispersion curves are unstable near F_0. Rayleigh wave are growing from F_0, and reach the first peak near the $2F_0$. It is verified that the H/V spectral ratio of both microtremor and strong motion is useful for estimation of at least fundamental frequency F_0 and its amplification factor. Consequently the excellent papers of Nogoshi and Igarashi (1971) and Suzuki (1933) have no relation to the H/V technique directory.

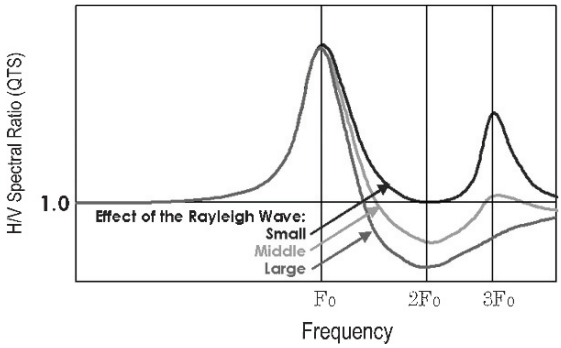

Fig. 1.3.13 Typical shape image of the H/V spectral ratio

1.3.4 Applications to hazard mitigation technology

From above discussions we can now conclude that peak of the spectral ratio H/V is caused by the multiple reflections of S waves. Alias QTS, Quasi Transfer Spectrum, represents the meaning coming from its name. Here, it should also be addressed the depth of the basement and the vulnerability of the surface ground related with QTS.

1. Basement depth
   The frequency F_0 related with QTS is:

$$F_0 = C_s/(4h),$$

   and the amplification factor A for this frequency is related to the impedance ratio. If densities for basement and surface layer are same then

$$A_0 = C_b/C_s,$$

   and the depth of basement h is

$$h = C_b/(4A_0F_0),$$

   where, C_b is S wave velocity of the basement.

   Figure 1.3.14 shows the depth of basement along the Shinkansen line estimated from microtremor for the case of basement velocity (C_b) is 600 m/s. The estimated results are compared with boring data and the results showed that, the contact line between alluvium and diluvium is the basement of QTS.

2. Vulnerability assessment
   Earthquake damage of structural members occurs at the time of exceeding the limit of the strain caused by deformation, and it causes the collapse if the stability of the structure lacked. Then the vulnerability index focused on the strain was defined (Nakamura, 1997) as imaged in Figure 1.3.15. K values in $10^{-6}/(\mathrm{cm/s^2})$ are defined to estimate the strain in the unit of 10^{-6} at particular parts of the

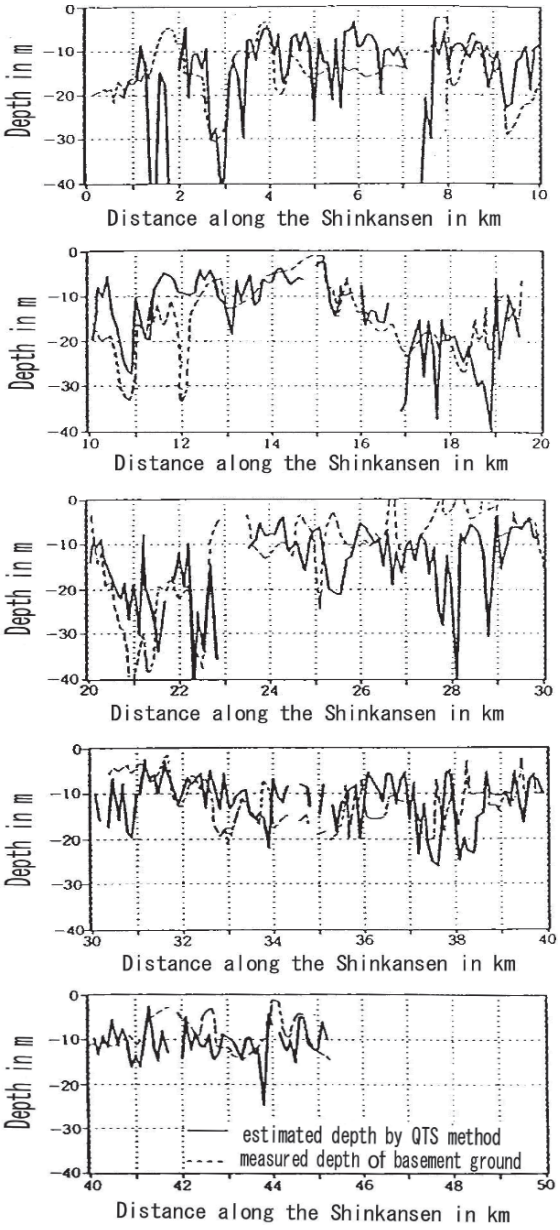

Fig. 1.3.14 Comparison between estimated depth and measured one (after Nakamura et al., 1970)

structures, by multiplying the maximum acceleration at the engineering basement and the K value.

These K values are defined for ground and various structures, as K_g value for ground, K_j value for embankment, K_s value for rigid frame structure and K_b value

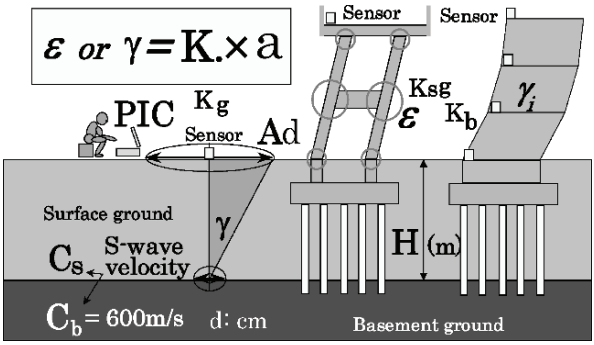

Fig. 1.3.15 Image of K values

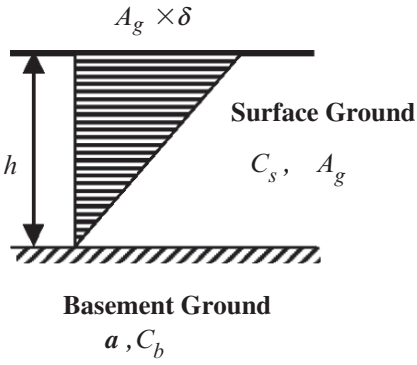

Fig. 1.3.16 Shear deformation of surface ground

for building. As peculiar K value, K_{d} value for derailment is defined. In this section, K_{g} is introduced. For other K values, refer the paper of Nakamura (1997).

(a) K_{g} for ground

For ground, shear strain γ of surface ground is noticed. In general, from $\gamma \cong 1{,}000 \times 10^{-6}$ surface ground begins to show non-linear characteristics and in $\gamma > 10{,}000 \times 10^{-6}$ large deformation and collapse will occur.

Simplifying the shear strain deformation of surface ground as shown in Figure 1.3.16, average shear strain γ of surface ground can be estimated by following formula:

$$\gamma = A_g \times \delta / h,$$

where, A_g is amplification factor, h is thickness of surface layer, and d is seismic displacement of the basement ground.

Putting S-wave velocities of basement ground and surface ground as C_b and C_s respectively, proper predominant frequency F_g of surface ground is approximately expressed as follows:

$$F_g = C_b/(4A_g \times h).$$

Acceleration of basement ground α_b is expressed as:

$$\alpha_b = (2\pi F_g)^2 \times \delta,$$

and γ is expressed by F_g, A_g and C_b:

$$\begin{aligned}\gamma &= (A_g \times \alpha_b/(2\pi F_g)^2) \times 4A_g \times F_g/C_b) \\ &= (A_g^2/F_g) \times \alpha_b/(\pi^2 C_b)).\end{aligned}$$

If the efficiency of applied dynamic force is assumed to be e% of static force, effective γ_e is expressed as:

$$\begin{aligned}\gamma_e &= K_g(e) \times \alpha_b \\ K_g(e) &= e \times A_g^2/F_g)/(\pi^2 C_b)/100.\end{aligned}$$

The value of C_b is expected to be nearly constant in a broad area and K_g is a proper value for measured point. Thus K_g can be considered as an index to indicate easiness of deformation of measured points which is expected useful to detect weak points of the ground. As we can consider $C_b = 600\,\mathrm{m/s}$, we obtain $1/(\pi^2 C_b) = 1.69 \times 10^{-6}$ (s/cm). If we put $e = 60\%$, then $K_g(e)$ is expressed as:

$$K_g(e) \cong A_g^2/F_g$$

The effective strain can be estimated by multiplying $K_g(e)$ value with maximum acceleration of basement ground in gal $(= \mathrm{cm/s^2})$.

Figure 1.3.17 shows the distribution of K_g-values obtained in San Francisco Bay Area after the 1989 Loma-Prieta Earthquake. For Marina district the result along a line from sea coast to hillside is shown. It shows K_g at the sites

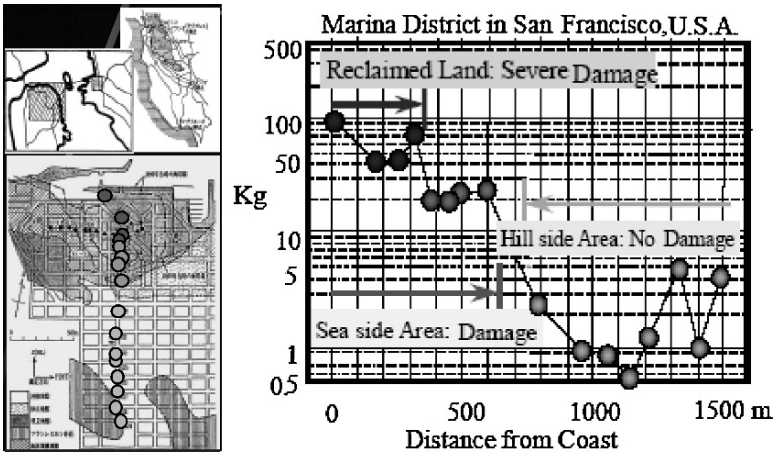

Fig. 1.3.17 Kg values measured after the 1989 Loma Prieta earthquake

where grounds deform much are bigger than 20 and K_g at the sites with no damage are very small. Considering the maximum basement accelerations around the area are estimated as 50 gal based on observations, $K_g = 1{,}000 \times 10^{-6}$ separates the areas liquefied or not.

(b) Derailment/overturn of trains
To study derailment/overturn of trains the work done per unit time (work rate or power) applied by earthquake motions is considered. Power w is proportional to the product of response acceleration $A \times \alpha_b$ and response velocity $A \times v_b$.

$$\begin{aligned} w &= m \times A \times \alpha_b \times A \times v_b \\ &= m \times A \times \alpha_b \times A \times \alpha_b/(2\pi F) \\ &= (m/(2\pi)) \times (A^2/F) \times \alpha_b^2 \\ &= (m/(2\pi)) \times K_d \times \alpha_b^2, \\ K_d &= A^2/F. \end{aligned}$$

Here m is mass of objects receiving seismic force for instance trains or stone. It may possible to adopt K_d-value not only for train derailment/overturn but also structure damage or jumping stone by strong motion.

F and A are directly related to the seismic motion applied to the train body. The dynamic characteristics of trains are known in general, F and A can be estimated from F_g and A_g when a train stays on the ground surface, or from F_{sg} and A_{sg} of both structures and ground when a train stays on the structure.

Site characteristics are reflected in K_d-value. In case of large K_d-value, power w and possibility of derailment/overturn are also large. Thus K_d-value is considered as an index to indicate the vulnerability on derailment/overturn of trains.

Figure 1.3.18 shows derailment/overturn of stopping electric vehicles at the JR-Takatori yard due to the 1995 Hyogo-Ken-Nanbu Earthquake. Severe derailments occur approximately on the points with bigger K_d-values.

Figure 1.3.19 shows derailments of running trains at the time of the 1995 Hyogo-Ken-Nanbu Earthquake and K_d-values near the derailment sites every 20 m approximately. It shows that whether trains derailed or not closely depends on K_d-values of the sites where trains were running.

1.3.5 Conclusion

The H/V spectral ratio, alias QTS, Quasi Transfer Spectrum, is overviewed from its origin to the application for practical disaster prevention. The H/V spectral ratio was found from the strong motion records at various sites in Japan. On the soft ground, horizontal motion is larger than vertical motion. On the other hand, on the hard ground, both horizontal and vertical motions are similar to each other both on

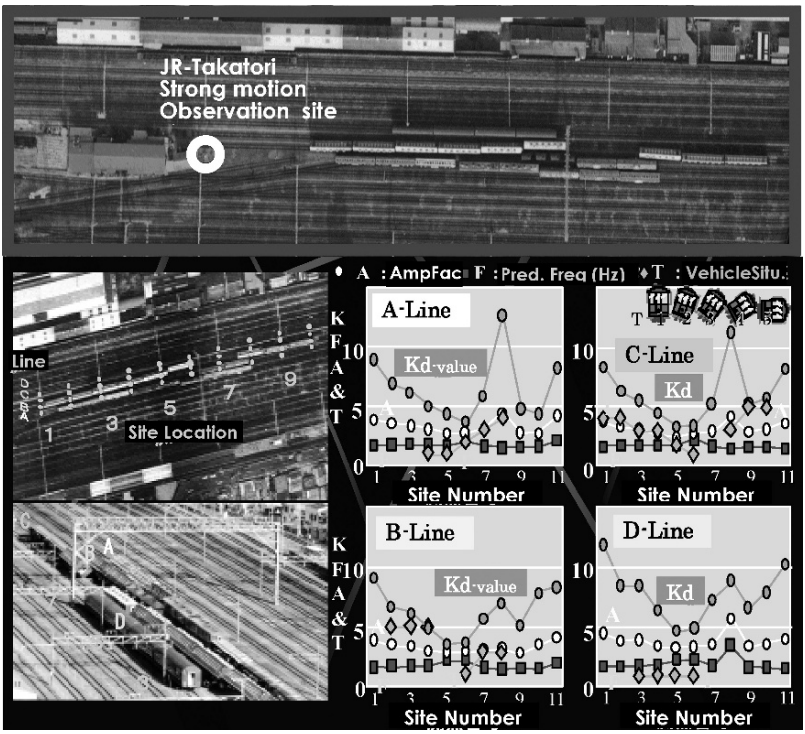

Fig. 1.3.18 Comparison between derailment/overturn of stopping vehicles and K_d values at the time of the 1995 Hyogo-Ken-Nanbu earthquake

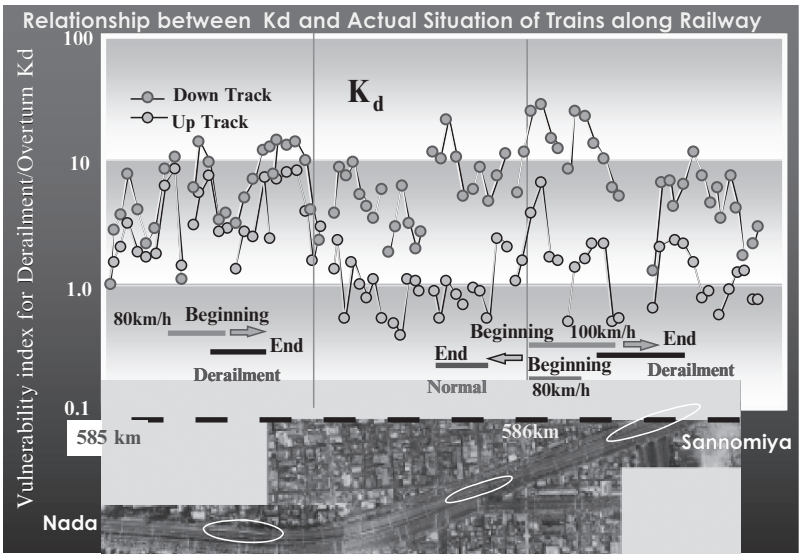

Fig. 1.3.19 Comparison between derailment of running trains and K_d values at the time of the 1995 Hyogo-Ken-Nanbu earthquake

the maximum value and waveform. It is proved in the present paper that the peak of H/V ratio (QTS), either for microtremor of for earthquakes cannot be explained with Rayleigh waves, since Rayleigh wave energy is very small for the peak frequency but high on the trough of H/V ratio. Author's explanation in Nakamura (1989) is correct for explaining this peak with SH waves. The H/V spectral ratio shows the amplification characteristics by the multiple reflections of the SH wave at least around F_0, and shows the characteristics contaminated by the Rayleigh wave around $2F_0$.

Based on this result, the way to estimate the basement depth and the vulnerability indices called K values were introduced. K values are simply derived from strains of ground and structures.

It seems to be possible to find the weak points previously with K values because of the high correlation between the earthquake damage and K values. There are research groups to establish the database on the vulnerability of structures. The H/V spectral ratio is already popular on the various research fields. It is happy that K values contribute to increase the earthquake-resistant capacity of the city with dissemination of the technique for investigation of the earthquake-resistant capacity.

References

Bard P.Y.: Microtremor Measurements: A Tool For Site Effect Estimation?, Manuscript for Proceedings of 2nd International Symposium on the Effect of Surface Geology on Seismic Motion, Yokohama, Japan, 1–3 December, 1998.

Bonnefoy-Claudet, S., Cornou, C., Bard, P.-Y., Cotton, F., Moczo, P., Kristek, J. and Fah, D.: H/V ratio: A tool for site effects evaluation. Results from 1-D noise simulations, Geophys. J. Int., 167, 827–837, 2006.

Field, E.H. and Jacob, K.H.: A comparison and test of various site response estimation techniques, including three that are not reference site dependent, Bull. Seism. Soc. Am., 85(4), 1127–1143, 1995.

Field, E.H. and Jacob, K.H.: The theoretical response of sedimentary layers to ambient seismic noise, Geophys. Res. Let., 20, 2925–2928, 1993.

Konno, K. and Ohmachi, T.: Ground-motion characteristics estimated from spectral ratio between horizontal and vertical components of microtremor, Bull. Seism. Soc. Am., 88(1), 228–241, 1998.

Lachet, C. and Bard, P.Y.: Numerical and theoretical investigations on the possibilities and limitations of Nakamura's technique, J. Phys. Earth, 42, 377–397, 1994.

Lermo, J., Francisco, S. and Chavez-Garcia, J.: Site effect evaluation using microtremors: a review(abstract), EOS, 73, 352, 1992.

Nakamura, Y. and Saito, A.: Estimations of Amplification Characteristics of Surface Ground and PGA using Strong Motion Records (in Japanese), Proceedings of the 17th JSCE Earthquake Engineering Symposium, pp. 25–28, 1983.

Nakamura, Y. and Samizo, M.: Site Effect Evaluation of Surface Ground using Strong Motion Records (in Japanese), Proceedings of 20th JSCE Earthquake Engineering Symposium, pp. 133–136, 1989.

Nakamura, Y. and Takizawa, T.: Evaluation of Liquefaction of Surface Ground using Microtremor (in Japanese), Proceedings of the 45th Annual Meeting of JSCE, I-519, pp. 1068–1069, 1990.

Nakamura, Y., Gurler, E.D. and Saita, J.: Dynamic Characteristics of Leaning Tower of Pisa Using Microtremor-Preliminary Results, Proceedings of the 25th JSCE Earthquake Engineering Symposium, Vol. 2, pp. 921–924, 1999.

Nakamura, Y., Saita, J. and Sato, T.: Development of Vulnerability Assessment Models using Microtremor/Strong Motion, 6th EqTAP Workshop in Kashikojima, Japan, December 2003.

Nakamura, Y.: A method for dynamic characteristics estimation of subsurface using microtremor on the ground surface, Quarterly Report of RTRI, 30(1), 25–33, 1989.

Nakamura, Y.: Clear Identification of Fundamental Idea of Nakamura's Technique and its Applications, 12WCEE, 2656, Auckland, New Zealand, 2000.

Nakamura, Y.: Real Time Information Systems for Seismic Hazards Mitigation UrEDAS, HERAS and PIC, Quarterly Report of RTRI, Vol. 37, No. 3, pp. 112–127, 1996.

Nakamura, Y.: Seismic Vulnerability Indices for Ground and Structures using Microtremor, World Congress on Railway Research in Florence, Italy, 1997.

Nogoshi, M. and Igarashi, T.: On the amplitude characteristics of microtremor – Part 2 (in Japanese with English abstract), J. Seism. Soc. Jpn., 24, 26–40, 1971.

Ohmachi, T., Nakamura, Y. and Toshinawa, T.: Ground Motion Characteristics in the San Francisco Bay Area detected by Microtremor Measurements, Proceedings of 2nd International Conference on Recent Adv. In Geot. Earth. Eng. And Soil Dyn., 11–15 March, St. Louis, Missouri, pp. 1643–1648, 1991.

Ohta, Y.: On the phase velocity and amplitude distribution of Rayleigh type waves in stratified double layer (in case of $\lambda \neq \mu$) (in Japanese with English abstract)", Zisin, 2(16), 12–25, 1963.

Okuma, Y., Harada, T., Yamazaki, F. and Matsuoka, M.: Strong Motion Network of Miyazaki Prefecture and Analysis of Records (in Japanese), Proceedings of 25th JSCE Earthquake Engineering Symposium, Vol. 1, pp. 173–176, 1999.

Sato, T., Saita, J. and Nakamura, Y.: Evaluation of the amplification characteristics of subsurface using microtremor and strong motion – the studies at Mexico City, 13th WCEE, Vancouver, Canada, 2004.

Suzuki, T.: Amplitude of Rayleigh waves on the surface of a stratified medium, Bull. Earthq Res. Inst., 11, 187–195, 1933.

Chapter 1.4
Ambient Noise and Site Response: From Estimation of Site Effects to Determination of the Subsoil Structure

Francisco J. Chávez-García

Abstract Damage distribution during large earthquakes is frequently conditioned by site effects. Site effect are best determined using earthquake data. However, that data is not always available and ambient noise measurements have been used as an inexpensive alternative. Microtremor measurements have been used along two paths to study site effects: estimation of a local transfer function, and estimation of the subsoil structure (once this structure is known, it is possible to compute expected ground motion amplification). Currently, the estimation of a transfer function uses H/V spectral ratios almost exclusively. Estimation of the subsoil structure exploits data from array measurements of microtremors applying techniques such as SPAC, ReMi and time domain analysis of cross-correlation. This paper discusses those two paths and shows the results that were obtained in two dissimilar examples: Parkway basin and Colima city. It is shown that results need to be validated; it is unsafe to use a single technique. In addition, it is clear that no single technique is adapted to all possible cases.

Keywords Site effects · Estimation of transfer function · H/V spectral ratios · Noise correlation · Subsoil structure

1.4.1 Introduction

Local amplification by surficial soft soils is a significant factor in destructive earthquake ground motion. Very often, damage distribution during large earthquakes has been correlated with subsoil conditions, which explains why site effects have received much attention during the last decades. Special theme conferences have been held dealing with this subject (for example, during August 2006, the Third

F.J. Chávez-García
Coordinación de Ingeniería Sismológica, Instituto de Ingeniería, Universidad Nacional Autónoma de México, Ciudad Universitaria, México, D.F. 04510, Mexico

M. Mucciarelli et al., (eds.), *Increasing Seismic Safety by Combining Engineering Technologies and Seismological Data,* NATO Science for Peace and Security Series C: Environmental Security,

International Symposium on the Effects of surface geology on seismic motion). There are many related aspects and a single article cannot do justice to such an ample subject (e.g., Aki, 1988). This paper will deal only with particular aspects of the use of ambient noise measurements for soil characterization.

Site effects are the modifications on incoming earthquake ground motion due to the irregular subsoil structure close to the surface. They are frequency dependent and the definition of how close is close to the surface depends strongly on the medium. If amplification is observed at high frequencies, then it is natural that we concentrate on very shallow layers. Conversely, when we observe amplification at low frequencies, it is usual that thick sedimentary deposits are involved and that soil characterization must reach larger depths. Earthquake ground motion may be amplified close to the free surface by purely geometrical effects (topographic effects). Irregular surface geometry will focus incoming energy at some places, increasing the amplitude of ground motion, and defocus it at other locations, decreasing observed motion. Topographic effects, however, are much smaller than amplification caused by the heterogeneity of soil properties. Seismic energy approaching the Earth's surface will travel through material with decreasing stiffness. Conservation of energy (or rather conservation of energy flux) requires that the waves remove energy from the interface between two materials at the same rate at which it arrives. Or, if the upper material has smaller wave velocity, the only way to do this is to increase the amplitude of the transmitted wave. Topographic amplification in a homogeneous medium usually does not exceed a factor of 2, even in the case of 3D topographies (e.g., Bouchon et al., 1996). This, rather tame amplification, contrasts with, for example, the effect of a rather thin (about 40 m), very soft clay layer near the surface in Mexico City. Measured average amplification there is a factor of 40. Naturally, most real cases involve both irregular geometry (not only at the free surface but also at the contact between different soil layers) and heterogeneous mechanical properties.

In this paper, I will explore the use of microtremors in two directions. One is the estimation of a local transfer function. The second is the use of microtremor measurements to estimate the subsoil structure and from there obtain site effects by modelling. Those two directions will be exemplified using two specific cases: Parkway basin (New Zealand) and Colima city (Mexico). These two sites are very different both in their location and in the results that were obtained using microtremors. Finally some conclusions and are given.

1.4.2 Estimating a transfer function using noise measurements

Local site effects are best characterized by a frequency transfer function. Seismic hazard studies may be able to provide an estimate of the expected earthquake motion on a real or fictitious rock outcrop using ground motion prediction models. If we assume linearity, it is possible to convolve this expected input motion with the estimated transfer function to predict ground motion at the sedimentary site.

Transfer functions may be estimated using spectral ratios of earthquake records, introduced by Borcherdt (1970). Their use is well substantiated by a seismic model and they have proven to be very reliable (e.g., Chávez-García et al., 1990). The use of microtremors to estimate a transfer function still lacks a similar seismic model. Microtremors have been used to estimate site effects using mainly three different techniques of analysis: direct interpretation of Fourier amplitudes or power spectral densities (e.g., Kanai and Tanaka, 1954; Katz, 1976; Katz and Bellon, 1978); computation of spectral ratios relative to a firm site reference station (Ohta et al., 1978; Kagami et al., 1982, 1986; Field et al., 1990); and computation of spectral ratios between horizontal components of motion relative to the vertical component recorded at the same site (Nakamura, 1989; Lermo and Chávez-García, 1994). These days, the first two techniques have been mostly abandoned, while the third one is doing ravages.

The use of H/V spectral ratio of microtremors to estimate a local transfer function has a weaker physical basis than spectral ratios relative to a reference site. However, it has been successful to estimate site effects. This success has been explained based on the assumption that microtremors consist of body waves (Nakamura, 1989). It is interesting to note that an explanation based on the assumption that microtremors consist essentially of surface waves is also successful (Fäh et al., 2001). This apparent contradiction is solved when we note that, for H/V to work, we must have large amplification and a simple geological structure. Local amplification is a property of the medium and it will impose its signature on whatever wave comes by. In addition, Rayleigh waves, for example, may be expressed as a particular superposition of body P and SV waves, i.e., they are of the same nature.

After the publication of Lermo and Chávez-García (1994), very many studies were made using H/V. A good review paper is that of Bard (1999). Most papers agree that the resonant frequency determined from microtremors H/V spectral ratios is useful and reliable (we must not forget, however, that there are cases where the concept of resonant frequency is not applicable). In addition, many papers have addressed the question of whether amplification level determined using H/V spectral ratios is useful or not. This discussion was very active a few years ago and has now subsided. For example, Horike et al. (2001) have shown among others that amplification computed from H/V of noise is reliable when local amplification is caused by a marked impedance contrast at a single interface and the amplification level is important. This means that, if H/V ratios are large, the results are usually dependable. However, when their amplitude is small it could indicate either that amplification is not significant (and then we need not worry about site effects) or that amplification is significant but not due to a single impedance contrast but resulting from a complex situation (e.g., velocity gradient). This is a large problem and one that has no general solution at present. As examples, this paper includes the discussion of two cases. In the first one, H/V spectral ratios of noise measurements closely follow reliable transfer functions. In the second, single station microtremor measurements were useless to investigate site effects.

1.4.3 Use of microtremors to estimate subsoil structure

Another approach that has been used to estimate site effects is to compute site response from the subsoil structure. Given that impedance contrast is the dominant factor, most studies limit themselves to vertical heterogeneities and are usually satisfied to determine a shear-wave velocity (Vs) profile at the site of interest. Of course, it is frequently possible to build 2D or 3D models putting together 1D profiles (e.g., Raptakis et al., 2000). The more reliable method to determine the structure and the properties of the subsoil materials is seismic prospecting. However, it is seldom used in site effect studies. It may be too cumbersome to apply in a city, or straightaway impossible to use because of cultural noise. In addition its cost is high when many locations have to be investigated. Ambient noise is much cheaper and we have seen many applications of its use to determine the subsoil structure, even if this objective requires measurements with arrays of stations.

Microtremor array data have been analysed with different techniques to determine a 1D soil profile at a site. Horike (1985) and Kagawa (1996), for example, have used *f-k* (frequency-wavenumber) spectra. Assuming a predominance of surface waves, phase velocity dispersion curves may be computed from *f-k* spectra estimated from the array (e.g., Aki and Richards, 1980). Phase velocity dispersion may in turn be inverted to obtain a Vs profile.

Another technique proposed recently is the ReMi approach (Louie, 2001), based on the stack proposed by McMechan and Yedlin (1981). The idea is to stack the signals recorded by an array of receivers (Louie proposes the use of a standard exploration seismograph) to obtain an image in the p-ω (slowness-frequency) plane. The procedure is straightforward and a programmed routine for the analysis of ballistic waves was included in the computer package by Herrmann (1987). However, the use of microtremor records, without a known direction of propagation, introduces an important uncertainty, and it becomes difficult to pick the phase velocity dispersion in the obtained diagram. In the better case, the result is a phase velocity dispersion curve that again has to be inverted using standard methods (e.g., Herrmann, 1987).

An older approach to determine subsoil structure using noise measurements is the SPatial AutoCorrelation (SPAC) technique (Aki, 1957). Again, microtremors need be dominated by surface waves. A circular array of seismographs with one at its centre is deployed and the azimuthal average of the noise correlation at a fixed distance (the radius of the circle) is computed. If the microtremor wavefield is stationary and isotropic, that average takes the form of a Bessel J_0 function with argument $\omega r/c$, where ω is the angular frequency, r is the circle radius and c is the phase velocity. It is then possible to invert the estimate of the Bessel function to determine the phase velocity dispersion curve and from that invert the Vs profile at the site. The details of the method have been presented in Ferrazzini et al. (1991) and Chouet et al. (1998), among others.

During many years the SPAC method was used with arrays with circular or semicircular geometry. Bettig et al. (2001) presented small corrections to be able to use it when the stations are off the perfect circular geometry by a small amount. A bolder approach is that of DeLuca et al. (1997), who used recorders arranged along a line,

installed with the purpose of recording an explosion. However, DeLuca et al. (1997) do not justify why SPAC would be valid for the geometry of their array, nor do they include any detail of their computations (e.g., how are average correlation coefficients computed). The paper by Ohori et al. (2002) is more complete. They present a derivation of the method that follows closely that of Asten (1976). In that derivation they clearly state that an azimuthal average is required; otherwise it not possible to obtain the Bessel function. However, when they apply the method to the data from their two T-shaped arrays, they neglect to explain how do they avoid the requirement to have an azimuthal average. A more radical approach was taken by Chávez-García et al. (2005) who showed that it is possible to use the SPAC method using data from single station pairs. The basis for this lies in the original paper by Aki (1957). If the microtremor wavefield is required to be isotropic and stationary both in time and space, then it is possible to replace the azimuthal average by a temporal one.

In the SPAC method, the data is analysed by computing cross-correlations in the frequency domain. Naturally, this operation can also be computed in time domain. As far back as 1968, Claerbout presented a scheme to produce reflection seismograms through the correlation of earthquake records. Baskir and Weller (1975), Nikolaev and Troitskiy (1987), Cole (1995) and Rickett (2001) showed that source–receiver type seismograms can be generated using cross-correlations of ambient seismic noise. Many recent papers have shown arguments, proofs and demonstrations that diffuse fields have time domain correlations closely related to the medium Green's function (e.g., Weaver and Lobkis, 2001; Snieder, 2004; Wapenaar, 2004; Roux et al., 2005; Sabra et al., 2005a).A brief historical review is given in the introduction section of Weaver and Lobkis (2005). This relation has been observed in ultrasonics (e.g., Lobkis and Weaver, 2001; Malcolm et al., 2004), acoustics (e.g., Sabra et al., 2005b), seismic coda (e.g., Campillo and Paul, 2003; Paul et al., 2005) and ambient seismic noise (e.g., Shapiro et al., 2005; Sabra et al., 2005c). The reason for a relation to exist between cross-correlation and the medium's Green's function for all these different types of signals is that they share a property called modal equipartition of the wavefield (Campillo, 2006). This means that when the wavefield consists of waves propagating in all directions and polarizations, with equal power in average, the power carried by S waves is $2\alpha^3/\beta^3$ times that of P waves, where α and β are the P and S-wave velocities. The randomness of the coda results from multiple scattering on randomly distributed scatterers and it has been shown that the diffusive regime for the coda emerges early, even if it only tends asymptotically to complete isotropy. Concerning ambient seismic noise, even if its actual origin cannot be pinpointed, we may safely assume that it is the result of the summation of the effects of many sources, distributed randomly at the surface of the Earth. Thus, seismic noise and seismic coda are equivalent once the waves that form it have reached the diffusive regime. Campillo (2006) presents a complete summary of these results.

In the following sections of this paper, I will show the application of these techniques and ideas at two, very different sites. The first one presents the case of a very small sedimentary basin in New Zealand. Site effects here were investigated using both earthquake and ambient noise data. The simplicity of the subsoil structure

and the large amplification that is observed led to good results with all the techniques that were used. A sharp contrast is observed with the case of Colima city, Mexico. Although local amplification is not negligible, the subsoil structure is complex, without a clear-cut impedance contrast producing the observed amplification. The case of Colima underscores the need to validate the results through the comparison between different techniques.

1.4.4 The case of Parkway basin, New Zealand

An example where the different techniques showed a very good agreement among them is Parkway basin, in North Island, New Zealand (Figure 1.4.1). This small valley was selected for study by the Institute of Geological and Nuclear Sciences, New Zealand, because it showed a strong resonance. Additionally, the basin is very small and it was possible to instrument it densely with portable instruments. Moreover, the seismicity rate allowed to record many useful earthquakes during the two and a half months that the temporal seismic network was operated. The estimate of site effects provided by earthquake data was later used as a standard against which to evaluate transfer functions determined using microtremors.

The determination of site effects using earthquake data for Parkway basin was presented in Chávez-García et al. (1999, 2002). The comparison between different techniques (spectral ratios relative to a reference site, Borcherdt 1970; spectral ratios between horizontal and vertical components, Lermo and Chávez-García 1993; and a parametric inversion of Fourier spectra, Field and Jacob (1995) allowed to fully validate the empirical transfer functions. These transfer functions allow in turn to evaluate the results of microtremors measurements. Figure 1.4.2 shows, for example, H/V spectral ratios computed for a few representative stations in the soft sediments within Parkway basin. The thin lines in this figure show the average H/V spectral ratios. Each curve corresponds to the average of H/V ratios computed from many 60-s noise windows. The number of windows varies between 46 (for station 04) and 71 (for stations 07, 16, 18). The thick lines are the average transfer functions derived from earthquake data spectral ratios between a sediment site and station 25, on rock. We observe a very good agreement for both dominant frequency and maximum amplification. A similar agreement was obtained for the other stations. Thus, in this case, H/V of microtremors provide a reliable estimate of the transfer function at each site.

Consider now the use of microtemors to determine subsoil structure. At Parkway we have used noise measurements coming from a variety of experiments. The results using noise windows from the 1995 experiment (1 Hz sensors, short time windows) with the SPAC two-station method were presented in Chávez-García et al. (2005), where the details are discussed. An example of the results is given in Figure 1.4.3, which shows the final phase velocity dispersion curve determined from microtremors (solid circles). The open diamonds show the dispersion curve obtained from the detailed f-k analysis of earthquake data recorded at Parkway for

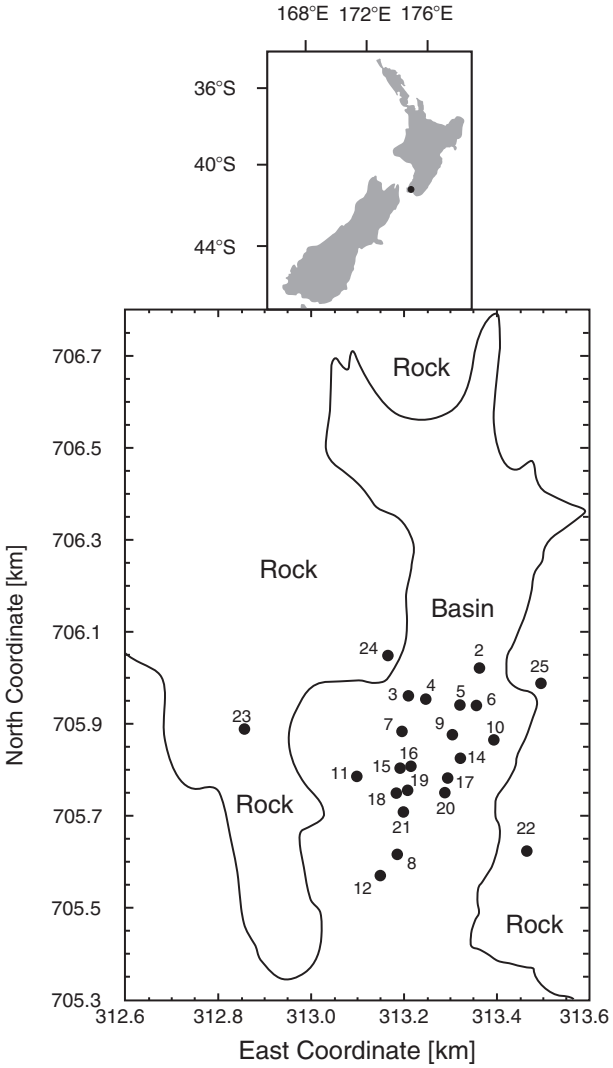

Fig. 1.4.1 Location map and distribution of the seismic stations of the 1995 temporal network in Parkway valley, New Zealand. The thin line shows the contact at the surface between soft-soil sediments and underlying rock. (Modified from Chávez-García et al., 1999.)

the 10 best recorded events (Chávez-García et al., 2002). Figure 1.4.3 also shows the phase velocity dispersion curve computed for the model established by Stephenson and Barker (2000) for this basin. The agreement among all three results is quite good for frequencies above 1.7 Hz, and poor for lower frequencies. Chávez-García et al. (2005) speculated that the SPAC method could not yield reliable results for frequencies smaller than the resonant frequency within the basin. Surface wave energy inside the basin is trapped within the sediments and only very little information can

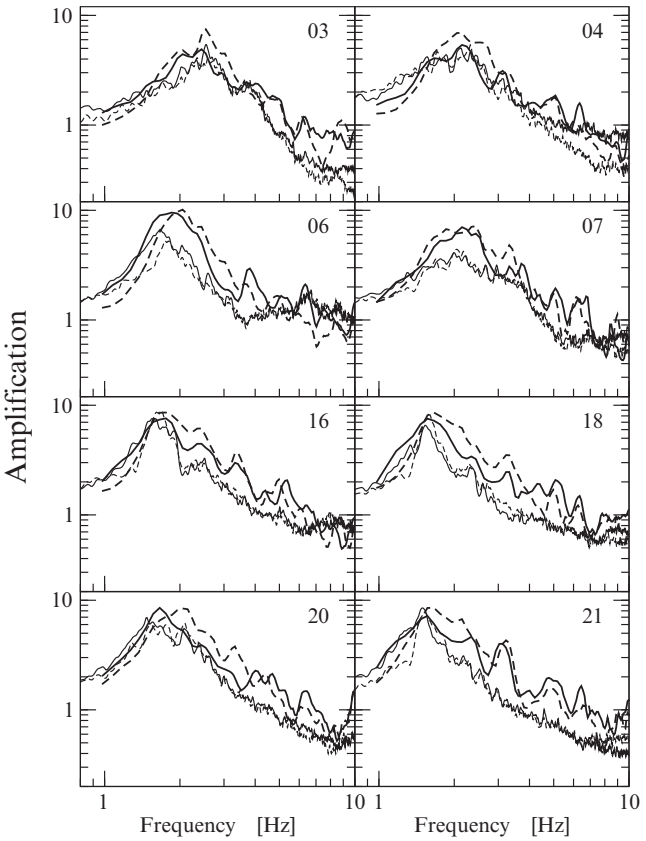

Fig. 1.4.2 Comparison between H/V of microtremors in Parkway with earthquake determined transfer functions. In each diagram the corresponding station number is indicated. Thick lines show the amplification computed from spectral ratios relative to a reference site using earthquake data (Chávez-García et al., 1999). Thin lines show the average H/V spectral ratio using 60-s noise windows. Solid lines correspond to NS component, while dashed lines indicate EW component

be retrieved from the underlying bedrock. Amplification in the basin, however, is due to the Vs contrast between sediments and bedrock. If we are unable to estimate the Vs of the bedrock it is not possible to compute the amplification, and the dispersion curves of Figure 1.4.3 do not allow to constrain this value.

Vs of the bedrock could not be determined with the data from the 1995 experiment. This could be due either to the limitations related to using 1 Hz seismometers or to having inter-stations distances that were not large enough. For this reason, a second round of measurements was made in 2003, where broad band sensors were used and a larger range of distances tested (although only five instruments were available). Details of the experiments and the results were given in Chávez-García et al. (2005, 2006). An example is shown in Figure 1.4.4, which compares the phase velocity dispersion curves obtained using the 1995 data, with that determined using

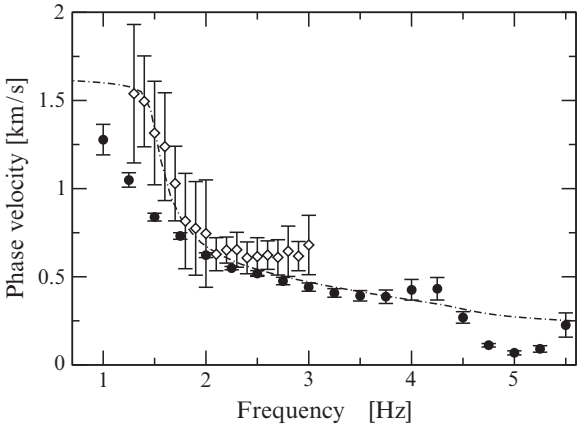

Fig. 1.4.3 Example of the results for Parkway using SPAC with data from the 1995 experiment. Solid circles show the phase-velocity dispersion curve inverted from the two station correlations of microtremors for all station pairs. Open diamonds show the phase velocity obtained from the detailed f–k analysis of earthquake data recorded by Parkway array for the ten best recorded events (Chávez-García et al., 2002). The dot-dash line shows the fundamental mode phase-velocity dispersion curve computed for the model established by Stephenson and Barker (2000) for Parkway basin. (Modified from Chávez-García et al., 2005.)

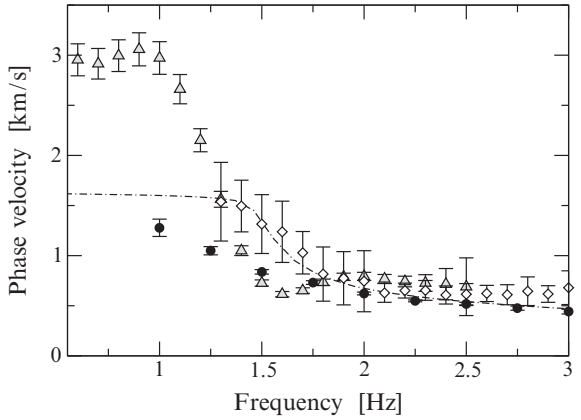

Fig. 1.4.4 Phase velocity dispersion determined at Parkway. The solid circles, open diamonds and dot-dash line repeat the same data shown in Figure 1.4.3. The grey triangles show the results using SPAC and broad band data from the 2003 experiment. (Modified from Chávez-García et al., 2005.)

broad band seismographs. We observe that the data from the new experiment were able to constrain the Vs of the bedrock at around 3 km/s. The combined data allows to compute the expected amplification, which is in very good agreement with that determined using earthquake data spectral ratios.

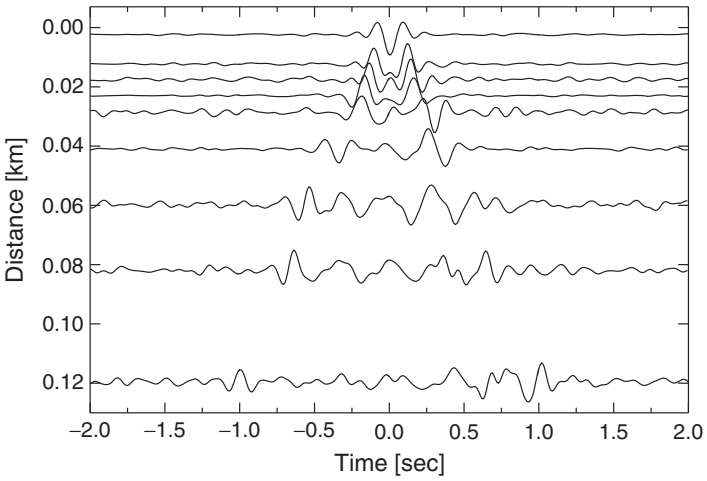

Fig. 1.4.5 Seismic section formed with the correlation functions computed in time domain for all station pairs from the linear arrays at Parkway (Chávez-García et al., 2007). Each trace is plotted at the corresponding interstation distance and is the average for all station pairs with that interstation distance. We observe a clear pulse, symmetric with respect to zero time. (After Chávez-García and Rodríguez, 2007.)

Finally, Figure 1.4.5 shows part of the results obtained from time domain cross-correlation analyses. This figure shows the cross-correlation functions computed from noise windows between station pairs separated between 5 to 120 m (see Chávez-García and Rodríguez, 2007 for the details). The result is shown as a seismic section where a clear pulse, symmetric with respect to zero time, appears at increasing time with increasing distance. The signal-to-noise ratio of this pulse decreases with increasing distance. Its phase velocity is between 250 and 300 m/s. When the interstation distance is much smaller than the dominant wavelength, we expect the cross-correlation function to degenerate to the autocorrelation function. The trace plotted at 5 m distance shows a single pulse that is symmetric about zero time, as expected for wavelengths between 50 and 150 m. The pulse has larger amplitudes than the rest of the trace between 2 and 7 Hz (by a factor between 5 and 10). In this frequency range, information on phase and/or group velocity may be retrieved from the seismic section shown, which in turn may be inverted to recover a Vs profile at the site.

We observe then that, in the case of Parkway basin, results from single noise microtremor measurements are in good agreement with earthquake data. The Vs profile may be inverted from dispersion curves estimated using either SPAC or time domain cross-correlation. In addition, the computed transfer functions are in good agreement with those observed. Unfortunately, not all cases are similar, as shown in the following section.

1.4.5 The case of Colima city, Mexico

It is not always possible to get good results. Where large heterogeneities occur, or where amplification is not due to a single, clear-cut impedance contrast between soil layers, microtremors are not useful. An example was met in the case of Colima city, western Mexico (Chávez-García et al., 2007).

The city of Colima is located near the Pacific coast of Mexico, and it is the capital of the federal state of the same name (Figure 1.4.6). Large earthquakes occur in this region, the northern section of the Pacific coast subduction zone in Mexico (Figure 1.4.6). However, the seismicity level is smaller than further South along the subduction zone making it difficult to record earthquakes. Previous studies (Gutiérrez et al., 1996) had shown that local amplification (measured using earthquake spectral ratios) is significant in this city but were unable to analyse its distribution within the city. Colima is underlain by a thick column of volcanic sediments (geologists speculate it may attain 800 m), filling a North–South oriented valley surrounded by limestone. These volcanic sediments are characterised by a large irregularity, with a mixture of different kinds of avalanche, debris and lahar deposits. Figure 1.4.7 shows the surface geology in the city. Different volcanic formations have been identified by geologists but it is far from evident that those differences are related to changes in the mechanical properties that condition seismic response.

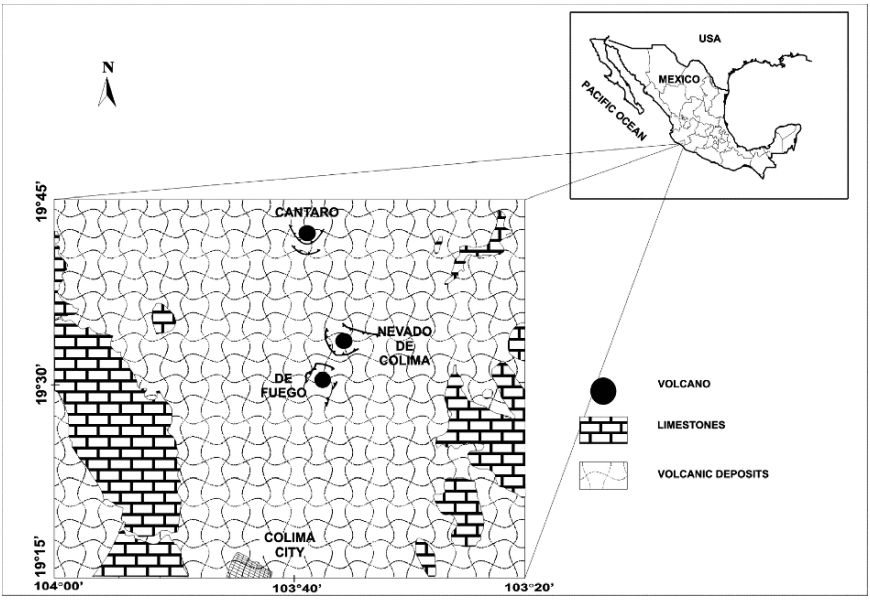

Fig. 1.4.6 Location of Colima city, Mexico in western Mexico. The regional geology is shown, consisting of a graben filled with volcanic deposits. Bedrock, consisting of limestone, outcrops East and West of the graben. (After Chávez-García et al., 2007.)

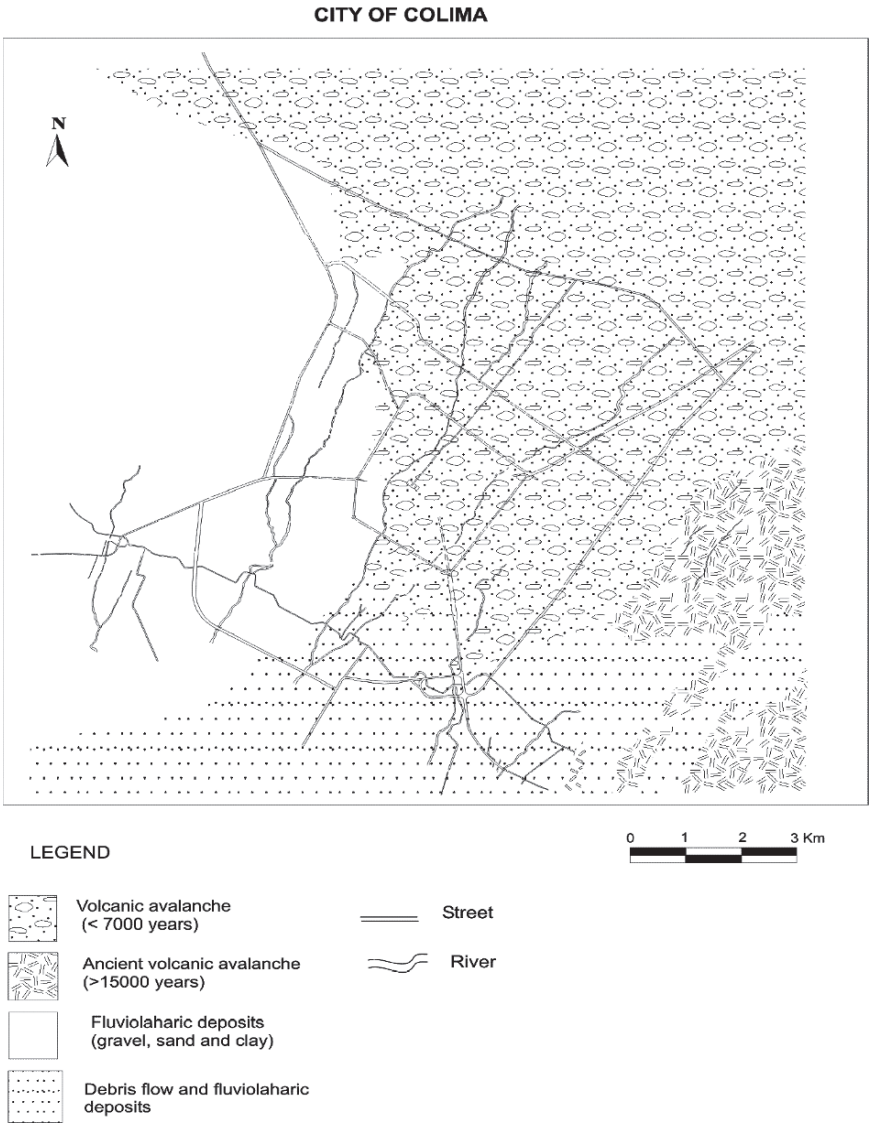

Fig. 1.4.7 Surface geology within Colima city. The main streets and rivers are shown with solid lines as reference. The urban zone is delimited by the rings formed by the main streets. (After Chávez-García et al., 2007)

A microtremor recording campaign was launched in the city of Colima. Although only one instrument could be used, plenty of student's time was available. Ambient noise was recorded at a total of 310 sites in an area roughly 10×10 km. H/V spectral ratios were computed. The results lead to the rejection of 185 sites; maximum amplitude of the H/V ratios was just too small, and no dominant period could be

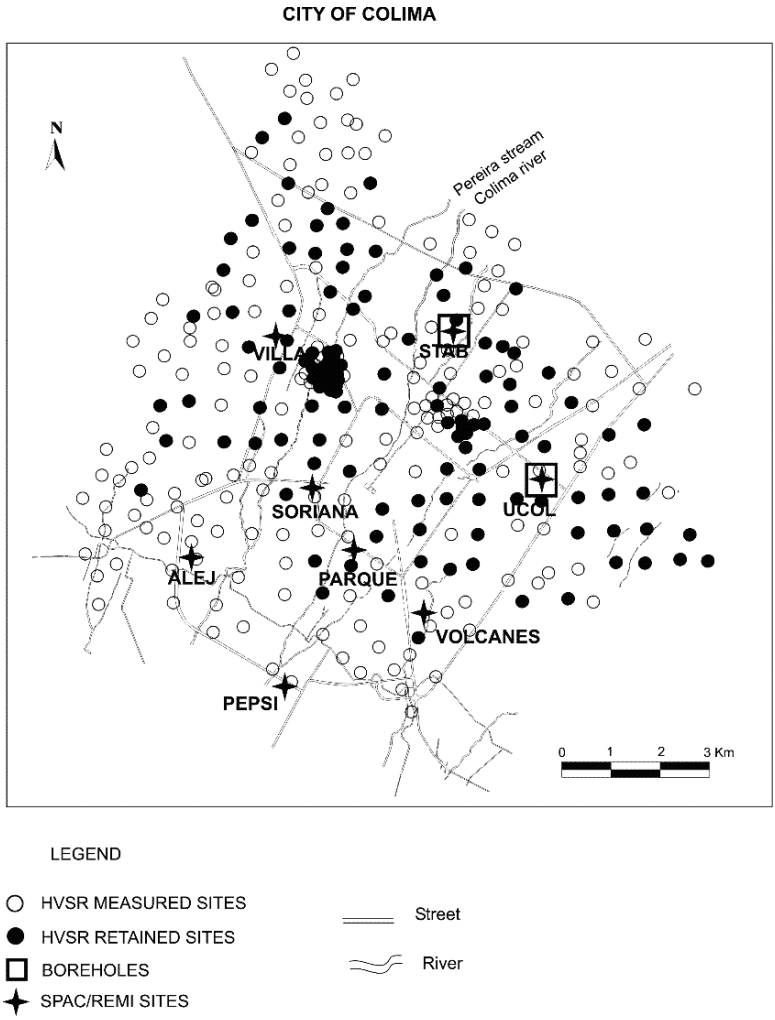

Fig. 1.4.8 Location of the points where measurements were carried out in Colima. Circles indicate the location of single station microtremors measurements. From the 310 total points, results from 125 (solid circles) were kept, while 185 (open circles) were discarded. Stars indicate the location of SPAC/ReMi measurements. The location of the two shallow boreholes is indicated with open squares. (After Chávez-García et al., 2007.)

identified. The results for the 125 sites whose information was retained were used to draw dominant period and maximum amplification maps for Colima (Figure 1.4.8). These maps are not very useful. There is no correlation with surface geology, amplification is extremely small, and the results are uncorrelated with previous dominant period maps (Chávez-García et al., 2007). These results indicate that, even when measurements are performed densely and carefully, if site effects are due to a complex structure, H/V of noise will not perform well.

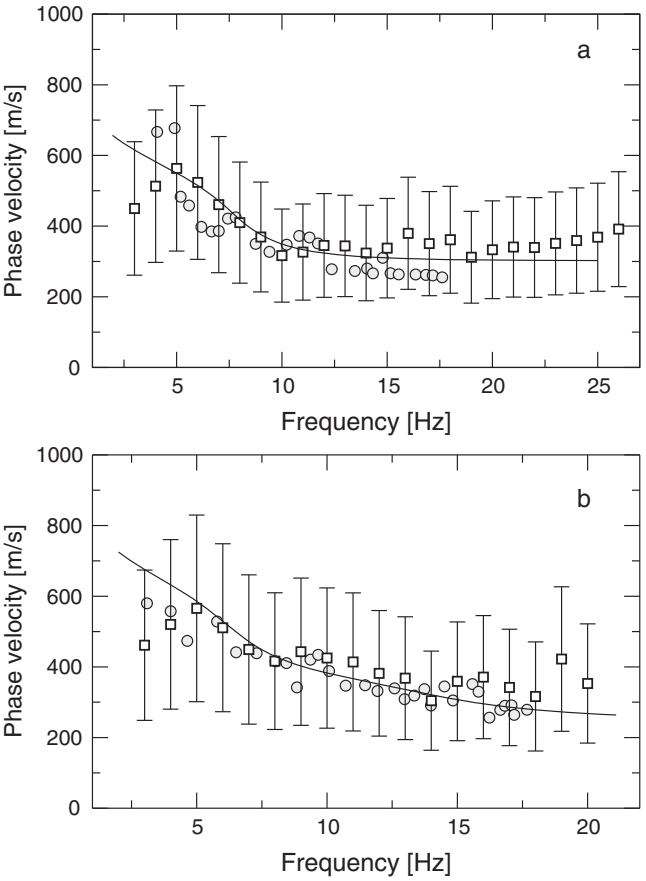

Fig. 1.4.9 Phase-velocity dispersion curves at locations UCOL (a) and STAB (b) (see Figure 1.4.8). The gray circles show the phase velocity determined with a manual picking from the ReMi images. Open squares with error bars show the mean values and the standard errors determined from the SPAC measurements. The solid line shows the phase velocity dispersion curve computed from the S-wave velocity profile inverted at the corresponding location using the open squares as input data. (After Chávez-García et al., 2007.)

The failure of H/V spectral ratios forced us to try array measurements in Colima. Two techniques were used: SPAC and ReMi. The data were recorded using an Oyo Geospace DAS-1 exploration seismograph with a 24-bit dynamic range and a line of 12, vertical-component, 4.5-Hz natural frequency geophones (see Chávez-García et al., 2007 for the details). Measurements were carried out at the 8 sites indicated with a star in Figure 1.4.8. One of the results is shown in Figure 1.4.9. This figure shows the final phase velocity dispersion curves estimated at sites UCOL and STAB for both SPAC and ReMi. Figure 1.4.8 also shows the dispersion curve computed from the inverted Vs profiles. Similar results were obtained at the other sites. Figure 1.4.10 shows the final Vs profiles at all the measured sites. We observe a steep

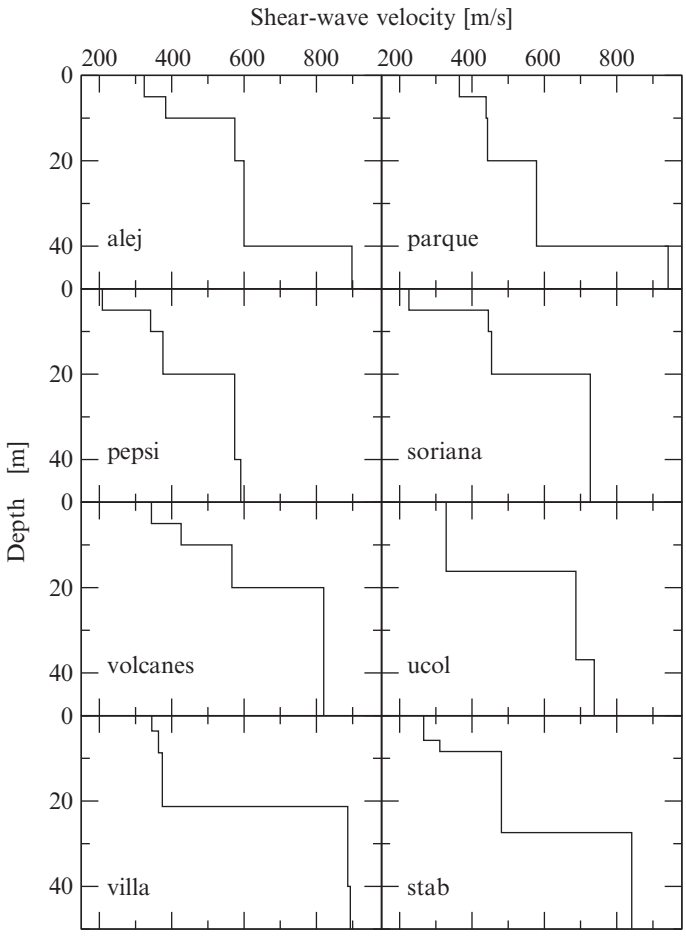

Fig. 1.4.10 Shear-wave velocity profiles inverted from phase-velocity dispersion curves observed using the SPAC method for the eight sites indicated with stars in Figure 1.4.8. Given the frequencies for which phase dispersion was observed, these profiles are reliable down to 40 m depth

Vs gradient in the topmost 40 m, where no single interface controls the impedance contrast. Amplification was computed assuming vertical shear-wave incidence on these profiles. The results were in good agreement with the amplification determined using earthquake data by Gutiérrez et al. (1996). Moreover, the results were validated at the two sites where shallow boreholes had been used to measure shear-wave velocities using a suspended logging tool. In the case of Colima, our results showed that a credible microzonation map was not a viable alternative. Due to the large heterogeneity of the subsoil and the poor control on its properties the more reasonable option was to propose a homogeneous amplification of a factor 6 throughout the city in the frequency band 0.2 to 5 Hz. This conclusion offers no details on the seismic response, but has the merit of being consistent with all available data.

1.4.6 Conclusions

I have discussed two possible paths to estimate site effects using microtremor measurements. The first one is direct measurement of the local amplification. Current practice uses single station ambient noise measurements analysed using the H/V spectral ratio. Most authors agree that H/V gives the dominant period of the soft soil layers. Of course the term dominant period may loose its meaning in many cases where site effects are still important. In those cases, H/V is not very useful. In addition to dominant period, the possibility of using H/V to estimate the level of amplification has been the subject of a large discussion. If the amplitude of H/V ratios is large, the results are usually dependable. However, when their amplitude is small it could indicate either that amplification is not significant (and then we need not worry about site effects) or that amplification is significant but not due to a single impedance contrast but resulting from a complex structure. This is a large problem and one that has no general solution at present. Clearly, the more reliable results are those that compare different techniques among them.

The second path to estimate site effects using microtremors is a very indirect one; determine subsoil structure and from there compute expected amplification. In this case, array measurements are required. Recently, the ReMi technique has been introduced. However, it has the disadvantage that it is not straightforward to pinpoint a dispersion curve in the resulting diagram. For this reason, most current studies make recourse to the SPAC method, more than 50 years old now. The result of using SPAC is a phase velocity dispersion curve, which can be inverted to recover a 1D Vs profile at the site. In addition to SPAC, the computation of cross-correlation of noise records in the time domain is currently a very dynamic field of research, where papers are being published in large numbers. Time domain correlations allow in theory to estimate the medium Green's function. However, most results have shown only the fundamental model of Rayleigh waves. The resulting seismic section may be analysed using the p-ω transformation that was mentioned before to estimate a phase velocity dispersion curve. Alternatively, group velocity dispersion may be estimated using, for example, the multiple filter technique (Herrmann, 1987). Again, the resulting dispersion curves must be then inverted to estimate a 1D Vs profile. In case of complex geological structures, 2D or 3D models may be built through the accumulation of 1D profiles.

These two paths were illustrated with the examples of Parkway basin and Colima city. In the first one, the interface between very soft alluvial deposits and a consistent graywacke formation leads to large amplification. The sediments behave as homogeneous, in face of the large contrast at their base. A clear resonance emerges in spectral ratios of earthquake data, a resonance that shows straight away in H/V spectral records of single station measurements. Both the resonant frequency and the amplification level are estimated quite well using ambient noise. The 1D Vs profiles derived from dispersion estimated using frequency or time domain correlations show a very good agreement with independent estimates and the computed amplification coincides with that observed. The case of Colima is a sharp contrast. Although amplification is not negligible, the subsoil structure is a complex mix-

ture of volcanic sediments. No single interface controls the subsoil impedance ratio and hence the amplification. In this case, H/V of single station microtremors were not useful. In the case of Colima, the concept of resonant frequency does not seem to apply and the effort invested in single station microtremor measurements was lost. However, the results of using SPAC and ReMi at Colima showed a good agreement between them and they could be validated at the location of two boreholes with a measured Vs profile. The final result although lacking details, is at least compatible with all available data. This example underscores the fact that, in experimental site effect studies, some validation of the results is necessary.

It is clear that no single approach is appropriate for all circumstances. An important consideration is that, in many cases, developing countries face a large seismic risk. The scientific challenges related to site effect estimation are the same as anywhere else. However, the resources available with which to cope with them are much smaller. This is an important consideration to make when developing techniques.

Acknowledgments I would like to thank the organizers of the NATO workshop, M. Mucciarelli and M. Herak, for their invitation to participate in the very interesting discussions during the workshop and for choosing a magnificent cadre. Signal processing benefited significantly from the availability of SAC (Goldstein et al., 1998). This research was supported by Conacyt, Mexico, through contract SEP-2003-C02-43880/A.

References

Aki K (1957) Space and time spectra of stationary stochastic waves, with special reference to microtremors. Bull. Earthq. Res. Inst. Univ. Tokyo 25:415–457

Aki K (1988) Local site effects on ground motion. In VonThun JL (ed) Earthquake Engineering and Soil Dynamics II – Recent Advances in Ground Motion Evaluation, Geotechnical Special Publication No. 20, Am. Soc. Civil Eng., New York, pp 103–155

Aki K, Richards PG (1980) Quantitative Seismology. W.H. Freeman, New York

Asten MW (1976) The use of microseisms in geophysical exploration. Ph.D. thesis, Macquarie University

Bard PY (1999) Microtremor measurements: a tool for site effect estimation? In Irikura K, Kudo K, Okada H, Sasatani T (eds) The Effects of Surface Geology on Seismic Motion, Balkema, Rotterdam, pp 1251–1279

Baskir E, Weller CE (1975) Sourceless reflection seismic exploration. Geophysics 40:158–159

Bettig B, Bard PY, Scherbaum F, Riepl J, Cotton F, Cornou C, Hatzfeld D (2001) Analysis of dense array noise measurements using the modified spatial auto-correlation method (SPAC): application to the Grenoble area. Boll. Geof. Teor. Appl. 42:281–304

Borcherdt RD (1970) Effects of local geology on ground motion near San Francisco Bay. Bull. Seism. Soc. Am. 60:29–61

Bouchon M, Schultz CA, Toksöz NM (1996) Effect of three-dimensional topography on seismic motion. J. Geophys. Res. 101:5835–5846

Campillo M (2006) Phase and correlation in 'random' seismic fields and the reconstruction of the Green's function. Pure Appl. Geophys. 163:475–502

Campillo M, Paul A (2003) Long range correlations in the diffuse seismic coda. Science 299:547–549

Chávez-García FJ, Rodríguez M (2007) The correlation of microtremors: empirical limits and relations between results in frequency and time domains. Geophys. J. Int. 171:657–664

Chávez-García FJ, Pedotti G, Hatzfeld D, Bard PY (1990) An experimental study of site effects near Thessaloniki (Northern Greece). Bull Seism. Soc. Am. 80:784–806
Chávez-García FJ, Stephenson WR, Rodríguez M (1999) Lateral propagation effects observed at Parkway, New Zealand. A case history to compare 1D vs 2D site effects. Bull. Seism. Soc. Am. 89:718–732
Chávez-García FJ, Castillo J, Stephenson WR (2002) 3D site effects. A thorough analysis of a high quality dataset. Bull. Seism. Soc. Am. 92:1941–1951
Chávez-García FJ, Rodríguez M, Stephenson WR (2005) An alternative to the SPAC analysis of microtremors: exploiting stationarity of noise. Bull. Seism. Soc. Am. 95:277–293
Chávez-García FJ, Rodríguez M, Stephenson WR (2006) Subsoil structure using SPAC measurements along a line. Bull. Seism. Soc. Am. 96:729–736
Chávez-García FJ, Domínguez T, Rodríguez M, Pérez F (2007) Site effects in a complex environment: a comparison between HVSR and array techniques. Bull. Seism. Soc. Am. 97:591–604
Chouet BC, DeLuca G, Milana P, Dawson M, Martin C, Scarpa R (1998) Shallow velocity structure of Stromboli volcano, Italy, derived from small-aperture array measurements of Strombolian tremor. Bull. Seism. Soc. Am. 88:653–666
Claerbout JF (1968) Synthesis of a layered medium from its acoustic transmission response. Geophysics 33:264–269
Cole S (1995) Passive seismic and drill-bit experiments using 2-D arrays. Ph.D. thesis, Stanford University
DeLuca G, Scarpa R, DelPezzo E, Simini M (1997) Shallow structure of Mt. Vesuvius volcano, Italy, from seismic array analysis. Geophys. Res. Lett. 24:481–484
Fäh D, Kind F, Giardini D (2001) A theoretical investigation of average H/V ratios. Geophys. J. Int. doi:10.1046/j.0956-540x.2001.01406.x, Volume 145, pp. 535–549
Ferrazzini V, Aki K, Chouet B (1991) Characteristics of seismic waves composing Hawaiian volcanic tremor and gas-piston events observed by a near-source array. J. Geophys. Res. 96:6199–6209
Field EH, Jacob KH (1995) A comparison and test of various site response estimation techniques, including three that are not reference site dependent. Bull. Seism. Soc. Am. 85:1127–1143
Field EH, Hough SE, Jacob KH (1990) Using microtremors to asses potential earthquake site response: a case study in Flushing Meadows, New York City. Bull. Seism. Soc. Am. 80:1456–1480
Goldstein P, Dodge D, Firpo M, Stan R (1998) Electronic seismologist: what's new in sac2000? Enhanced processing and database access. Seism. Res. Lett. 69:202–205
Gutiérrez C, Masaki K, Lermo J, Cuenca J (1996) Microzonificación sísmica de la ciudad de Colima. Cuadernos de Investigación 33, México (in Spanish)
Herrmann RB (1987) Computer Programs in Seismology. Saint Louis University, 8 vols.
Horike M (1985) Inversion of phase velocity of long period microtremors to the S-wave velocity structure down to the basement in urbanized areas. J. Phys. Earth 33:59–96
Horike M, Zhao B, Kawase H (2001) Comparison of site response characteristics inferred from microtremors and earthquake shear waves. Bull. Seism. Soc. Am. 91:1526–1536
Kagami H, Duke CM, Liang GC, Ohta Y (1982) Observation of 1 to 5 second microtremors and their application to earthquake engineering. Part II. Evaluation of site effect upon seismic wave amplification due to extremely deep soil deposits. Bull. Seism. Soc. Am. 72:987–998
Kagami H, Okada S, Shiono K, Oner M, Dravinski M, Mal AK (1986) Observation of 1 to 5 second microtremors and their application to earthquake engineering. Part III. A two-dimensional study of site effects in S. Fernando valley. Bull. Seism. Soc. Am. 76:1801–1812
Kagawa T (1996) Estimation of velocity structures beneath Mexico City using microtremor array data. Proceedings of the 11th World Conference on Earthquake Engineering, Soc. Mexicana de Ing. Sismica, Acapulco, Mexico
Kanai K, Tanaka T (1954) Measurement of the microtremor. Bull. Earthquake Res. Inst. Tokyo Univ. 32:199–209
Katz LJ (1976) Microtremor analysis of local geological conditions. Bull. Seism. Soc. Am. 66:45–60

Katz LJ, Bellon RS (1978) Microtremor site analysis study at Beatty, Nevada. Bull. Seism. Soc. Am. 68:757–765
Lermo J, Chávez-García FJ (1993) Site effect evaluation using spectral ratios with only one station. Bull. Seism. Soc. Am. 83:1574–1594
Lermo J, Chávez-García FJ (1994) Are microtremors useful in site response evaluation? Bull. Seism. Soc. Am. 84:1350–1364
Lobkis OI, Weaver RL (2001) On the emergence of the Green's function in the correlations of a diffuse field. J. Acoust. Soc. Am. 110:3011–3017
Louie JN (2001) Faster, better: shear-wave velocity to 100 meters depth from refraction microtremor arrays. Bull. Seism. Soc. Am. 91:347–364
Malcolm AE, Scales JA, vanTiggelen BA (2004) Retrieving the Green's function from diffuse, equipartitioned waves. Phys. Rev. E 70, 015601
McMechan GA, Yedlin MJ (1981) Analysis of dispersive waves by wave field transformation. Geophysics 46:869–874
Nakamura Y (1989) A method for dynamic characteristics estimation of subsurface using microtremor on the ground surface. QR of RTRI 30:25–33
Nikolaev AV, Troitskiy PA (1987) Lithospheric studies based on array analysis of P-coda and microseisms. Tectonophysics 140:103–113
Ohori M, Nobata A, Wakamatsu K (2002) A comparison of ESAC and FK methods of estimating phase velocity using arbitrarily shaped microtremor arrays. Bull. Seism. Soc. Am. 92: 2323–2332
Ohta Y, Kagami H, Goto N, Kudo K (1978) Observation of 1- to 5-second microtremors and their application to earthquake engineering. Part I: comparison with long-period accelerations at the Tokachi-Oki earthquake of 1968. Bull. Seism. Soc. Am. 68:767–779
Paul A, Campillo M, Margerin L, Larose E, Derode A (2005) Empirical synthesis of time-asymmetrical Green's functions from the correlation of coda waves. J. Geophys. Res. doi:10.1029/2004JB003521, Volume 110, B08302, pp. 1–13
Raptakis D, ChávezGarcía FJ, Makra K, Pitilakis K (2000) Site effects at Euroseistest – I. Determination of the valley structure and confrontation of observations with 1D analysis. Soil Dyn. Earthq. Eng. 19:1–22
Rickett JE (2001) Spectral factorization of wavefields and wave operators. Ph.D. thesis, Stanford University
Roux P, Sabra KG, Kuperman WA, Roux A (2005) Ambient noise correlations in free space: theoretical approach. J. Acoust. Soc. Am. 117:79–84
Sabra KG, Roux P, Kuperman WA (2005a) Arrival-time structure of the time-averaged ambient noise cross-correlation function in an oceanic guide. J. Acoust. Soc. Am. 117:164–174
Sabra KG, Roux P, Kuperman WA (2005b) Emergence rate of the time-domain Green's function from the ambient noise cross-correlation function. J. Acoust. Soc. Am. 118:3524–3531
Sabra KG, Gerstoft P, Roux P, Kuperman WA, Fehler MC (2005c) Extracting time-domain Green's function estimates from ambient seismic noise, Geophys. Res. Lett. doi:10.1029/2004GL021862, Volume 32, L03310, pp. 1–5
Shapiro NM, Campillo M, Stehly L, Ritzwoller M (2005) High resolution surface wave tomography from ambient seismic noise. Science 307:1615–1618
Snieder R (2004) Extracting the Green's function from the correlation of coda waves: a derivation based on stationary phase. Phys. Rev. E doi:10.1103/PhysRevE.69.046610, Volume 69, 046610, pp. 1–8
Stephenson WR, Barker PR (2000) Seismic CPT in strong soils. Earthquake Commission Research Project 99/380, Client Report 2000/47, Institute of Geological and Nuclear Sciences, Lower Hutt, New Zealand
Wapenaar K (2004) Retrieving the elastodynamic Green's function of an arbitrary inhomogeneous medium by cross correlation. Phys. Rev. Lett. 93, 254301
Weaver RL, Lobkis OI (2001) Ultrasonics without a source: thermal fluctuation correlations at MHz. Phys. Rev. Lett. 87, 134301
Weaver RL, Lobkis OI (2005) The mean and variance of diffuse field correlations in finite bodies. J. Acoust. Soc. Am. 118:3447–3456

Chapter 1.5
In-Situ Estimates of Material Damping from Environmental Noise Measurements

Dario Albarello and Francesco Baliva

Abstract Experimental results at two test sites are described, which support the idea that the cross-correlation of noise recordings allows the retrieval of the local Green's function also including subsoil attenuation properties. In particular, the analysis of field measurements of environmental noise carried on with arrays of common vertical geophones suggests that passive in-situ estimates of the attenuation exponent are possible and that the values provided in this way are comparable with those obtained with alternative active techniques. These results open new interesting perspectives for engineering and geotechnical application of environmental noise surveys.

Keywords In situ estimates · Damping · Seismic noise · Seismic interferometry · Passive seismic survey

1.5.1 Introduction

The ground motion generated at a site on the Earth surface by any radiating energy source can be represented as the convolution of a source function of any suitable distribution of volume forces and the Green's function, that represents the response of the Earth to a sudden point load (Aki and Richards, 2002). The form of the Green's function is determined by the elastic properties of the subsoil (in terms of seismic waves velocities) and the energy dissipation due to the anelastic properties of the subsoil materials and waves scattering.

For very low strain levels (typical of seismic waves) the absorption can be represented by a single parameter D (material damping). This non dimensional parameter is related to the energy loss ΔE from a total amount E available during each loading cycle, by the equation

$$D = \frac{\Delta E}{4\pi E} = \frac{1}{2Q} \tag{1.5.1}$$

D. Albarello (✉) and F. Baliva
Dip. Di Scienze della Terra – Università di Siena – Via Laterina, 8 – 53100 Siena – Italy
e-mail: albarello@unisi.it

M. Mucciarelli et al., (eds.), *Increasing Seismic Safety by Combining Engineering Technologies and Seismological Data,* NATO Science for Peace and Security Series C: Environmental Security,

where Q is the seismological quality factor, widely used in seismology in spite of D (e.g., Lai and Rix, 2002). The material damping plays an important role both in the field of the reconstruction of Earth structure (e.g. Lay and Wallace, 1995) and in small scale geotechnical applications. In particular, this parameter is of great importance when the analysis of the local seismic response is of concern (e.g. Kramer, 1986).

Damping is usually measured on laboratory specimens, but the effect of sample disturbance is uncertain and the frequencies used in laboratory tests are usually one to two orders of magnitude higher than those of interest in earthquake engineering. An alternative approach is to use field measurements to provide in-situ estimates. Some attempts in this direction have been performed by the direct measurement of body waves attenuation in the frame of cross-hole or down-hole configurations (e.g. Tonn, 1989). In alternative, to overcome the drawbacks of this approach, it has been proposed to measure attenuation of surface waves generated by artificial sources (Athanasopoulos et al., 2000; Rix et al., 2000; Xia et al., 2002; Lai et al., 2002). A severe limitation of the last ones is the difficulty to produce low frequency surface waves ($<10\,\mathrm{Hz}$) necessary to sample the deeper portions of the subsoil, and the difficulty in operating these approaches in anthropized areas characterised by strong environmental noise.

A possible alternative is the use of the environmental noise itself to measure damping. An attempt in this direction is described here. The theoretical background will be shortly outlined first. An experimental procedure is then discussed and applied at two test sites in Italy where independent in-situ estimates of material damping are available.

1.5.2 The Green's function from environmental noise measurements

Since the second half of the last century, seismologists have been aware that the Green's function relative to a portion of the crust can be retrieved by cross correlating seismographic registrations of the same event at two sites located along the direction of wave propagation (e.g. Dziewonski and Hales, 1972). This can be considered as the reminiscence of the input-output cross-correlation theorem relative to general linear systems (e.g. Lee, 1960).

After the pioneering work by Aki (1957), the possibility of extracting information about subsoil structure from cross correlation measurements has been extended to ground noise recordings and has been extensively studied (see Okada, 2003 and references therein). In the assumption that seismic noise can be considered as a linear combination of random independent plane waves moving along the Earth surface, phase velocities relative the most coherent and statistically persistent part of noise (in general surface waves) can be effectively determined from the analysis of noise recordings at arrays of geophones (e.g. SESAME, 2002).

More recently, these results have been generalized to include the complete retrieval of the Green's function (see Larose et al., 2006 and references therein) from

cross correlation (CC) measurements of seismic noise in the assumption that it can be considered as a random diffuse wave field generated by a number of independent stochastic sources or by the presence of a scattering medium. In this case, theoretical and experimental results indicate that the Green's function corresponds to the time derivative of the average cross correlation (DCC) of contemporaneous noise recordings at different positions. Actually, the difference between cross correlation function and its time derivative is immaterial (Roux et al., 2005) when real experimental signals are of concern. Thus, many Authors simply estimate the Green's function directly from CC measurements of seismic noise (e.g. Shapiro et al., 2005).

It is worth noting that the hypothesis of a purely diffuse wave-field is not strictly necessary. In fact, Louie (2001) demonstrated that the largest contribution to the CC function relative to seismic signals at two stations mostly comes from ray-paths nearly aligned along the direction connecting the two sites (see also Roux et al., 2005). This implies that, the possibility to measure the Green's function only requires the presence of at least some wavelet traveling along the direction nearly parallel to the one connecting the relevant sensors during the measuring interval.

1.5.3 Damping from noise cross-correlation measurements

Despite of the fact that this aspect has been so far overlooked in seismological applications of cross correlation analysis (e.g. Shapiro et al., 2005), a possibility exists to retrieve the Green's function from CC measurements of the noise wave field including attenuation properties (Roux et al., 2005). Thus, new perspectives open for the characterization of mechanical properties of a subsoil from passive seismic measurements at the geotechnical-engineering scale.

A simple model relative to the propagation a unitary pulse within a viscoelastic vertically heterogeneous medium (e.g. Rix et al., 2000) provides the relationship for the Green's function G relative to a single mode of propagation

$$G(r,\omega) = R(r,\omega)\, e^{-\alpha(\omega) r} \tag{1.5.2}$$

where r is distance along the ray-path from to the source to the site and ω is the angular frequency. The form of R represents the effect of geometrical spreading and depends on the specific seismic phase and source-receiver path considered. The attenuation exponent α represents the effect of material damping. When $D < 5\%$, the attenuation exponent can be expressed by the approximate relationship

$$\alpha \approx \frac{D\omega}{V} \tag{1.5.3}$$

where V is the velocity of the seismic phase of concern. In the range of frequency of seismological interest (0.1–10 Hz) D is considered to be nearly frequency independent (Lai, 1998). In this position, it has been also assumed that material damping dominates attenuation: otherwise, one has to interpret α as the combination of material damping and scattering.

By the results provided by Roux et al. (2005), the Fourier spectrum of the cross-correlation time derivative (TDCC) of noise recordings at a couple of sites located at a distance r one from the other can provide an experimental estimate of the Green's function. In particular, in the case of a single mode of propagation, one has

$$TDCC \cong A^2(\omega)\, G(r,\omega) = A^2(\omega)\, R(r,\omega)\, e^{-\alpha r} \tag{1.5.4}$$

where $A(\omega)$ is the average spectral magnitude of environmental noise at the relevant angular frequency ω. In general one has

$$\ln\left[\frac{TDCC}{R(r,\omega)}\right] \cong \ln\left(A^2(\omega)\right) - \alpha(\omega)\, r. \tag{1.5.5}$$

Thus, one could expect that natural logarithm of TDCC corrected for the geometrical spreading linearly depends on the inter-station distances.

In the simple case of a noise wave-field mainly constituted by fundamental mode surface waves (e.g. Shapiro et al., 2005), the term R in Equation (1.5.2) becomes

$$R(r,\omega) = \frac{b}{\sqrt{r}} \tag{1.5.6}$$

and b is a real constant (Rix et al., 2000). Thus, one has

$$\ln\left[TDCC\sqrt{r}\right] \cong \ln\left(bA^2(\omega)\right) - \alpha(\omega)\, r. \tag{1.5.7}$$

Equations (1.5.7) provides a tools for estimating α. In fact, if a number of DCC estimates is available for different inter-station distances r_i, linear regression could allow to compute α from (1.5.5) at each frequency of interest. To determine the form of R, the preliminary identification of the seismic phases present in the monitored noise is mandatory.

1.5.4 Experimental setting and data processing

To evaluate the possibility to use the above approach to estimate damping effect in a real situation, environmental noise has been monitored at the two test sites by using an array of standard vertical vertical geophones. Digital acquisition has been performed by using a system (24-bit equivalent) produced by Micromed S.p.A. (http://micromed-it.com/brainspy1.htm). No instrumental correction has been performed.

Each noise record has been subdivided into non overlapping 20 s time windows. The time series relative to each time window for each geophone has been cross-correlated with the ones relative to all the other geophones: relative time lags varies between -5 and 5 s. The cross-correlograms relative to the same couple of sensors and obtained for the different time windows have been averaged. In this way, a number of average cross-correlograms is made available corresponding to the set of

intergeophonic distances considered. The time derivative is evaluated numerically for each average cross correlogram. The resulting time series are assumed to be an image of the Green's functions relative to each inter-geophonic distance. Both negative and positive time lags have been considered to evaluate the isotropy of the monitored wave-field: the values corresponding to negative and positive time lags are considered as the causal and anti-causal Green's function respectively. In the case that a good correspondence exists between the causal and anti-causal parts of the, these two images are stacked to reduce their random variability. In this way, a set of time series has been obtained, each corresponding to a specific inter-geophonic distance.

Spectral amplitudes in (1.5.4) have been estimated from the spectrogram of the time series described above. In particular, each time series has been scanned by a moving window of 32 time units. For each window, after the tapering by an Hamming window, a discrete FFT is performed to determine spectral amplitudes. After that the time series has been scanned, the window characterized by the maximum spectral amplitude for each frequency is selected. It is worth noting that, due to the finite dimension of the scanning window, wavelets relative to very short arrival times cannot be analyzed and have to be discarded.

This procedure is iterated for each inter-geophonic distance. In this way, at each time series and frequency is associated one arrival time (the central location of the selected time window) and one spectral amplitude. This information allows the empirical estimate of the *TDCC* function in Equation (1.5.4).

The representation of arrival times as a function of the inter-geophonic distance allows a rough estimate of the relevant phase velocity. If Equation (1.5.5) holds, strong linear correlation should exist between the logarithm of *TDCC* and inter-geophonic distances r. The Pearson correlation coefficient has been used to evaluate reliability of the reference model for the considered frequency. In the case that correlation is high (>0.5 to say), a least squares regression analysis has been used to estimate α of Equation (1.5.5).

1.5.5 Test site 1: Pisa (Northern Tuscany, Italy)

The site is located nearby the famous Leaning Tower, one of the most important monuments of Italy. The considered site has been extensively studied in the past and noticeable efforts have been devoted for the geotechnical characterization of the Tower foundations (Jamiolkowski and Pepe, 2001 and references therein). The subsoil is mainly constituted by succession of clayey and sandy silts at least up to 70 m from the ground level (Figure 1.5.1A). Seismic measurements carried on by using a cross-hole configuration indicate V_s values of the order of 200 m/s, nearly constant with depth at least up the bottom of the well.

At this site, laboratory and *in situ* measurements have been used to characterize attenuation properties of the shallow subsoil. As concerns the laboratory test (Lo Presti et al., 1997), many high quality samples from the clayey layers in the depth

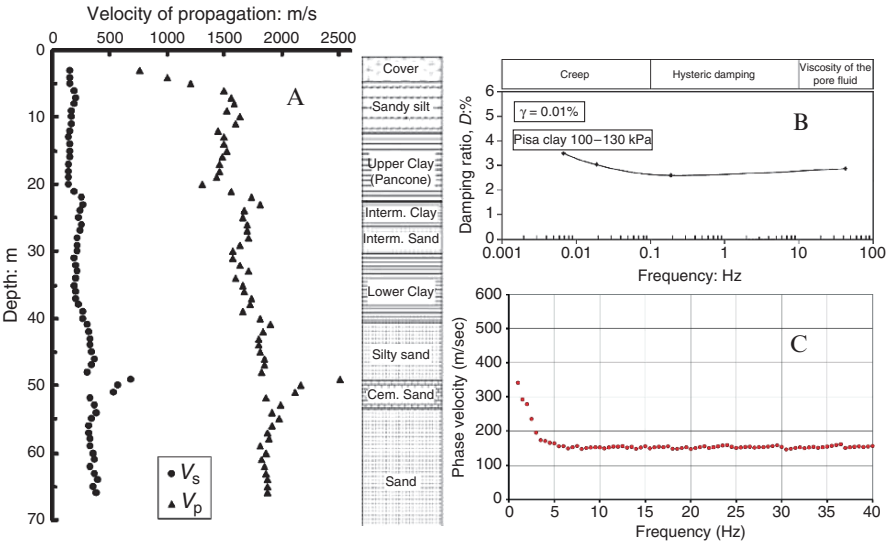

Fig. 1.5.1 Geotechnical data at the Pisa test site. A: Cross hole measurements of the Vp and Vs profiles at the Pisa site (Foti, 2003); B: laboratory estimates of the damping ratio in the local Clays (Lo Presti et al., 1997); C: dispersion curve from array noise measurements (this study)

range 12–17 m have been retrieved and tested. The damping ratio was evaluated during a series of cyclic torsional shear tests identifying values ranging between 2% and 3% in the very small strain range ($\varepsilon_s < 0.01\%$). These values remains nearly constant with frequency (Figure 1.5.1B).

Independent estimates of the attenuation exponent a have been also obtained by a surface wave test (Foti, 2003). The results relative to the frequency range 0–10 Hz are reported in Figure 1.5.3.

The seismic array used for the present study was located nearby (100 apart) the Leaning Tower, at the center of the city in a very crowded area. Tourists were walking near the sensors (not more than 10 m apart) and an intense vehicular traffic took place all around the measurement area.

Measurements have been carried on by using 16 vertical geophones (4.5 Hz) distributed along two perpendicular arms respectively 61 and 36 m long. Environmental noise has been measured in the late morning for 60 min at a sampling rate of 128 cps.

At first, recorded noise has been analyzed by using the ESAC approach (e.g., Okada, 2003) to evaluate dispersion curve of Rayleigh waves (Figure 1.5.1C). Results indicate that Rayleigh waves phase velocities are relatively constant (about 150 m/s) in the range 5–40 Hz.

In Figure 1.5.2, the average DCC traces relative to all the couples of geophones in the array are reported. One traveling wavelet can be easily individuated both in its causal and anti-causal form (respectively corresponding to positive and negative time lags).

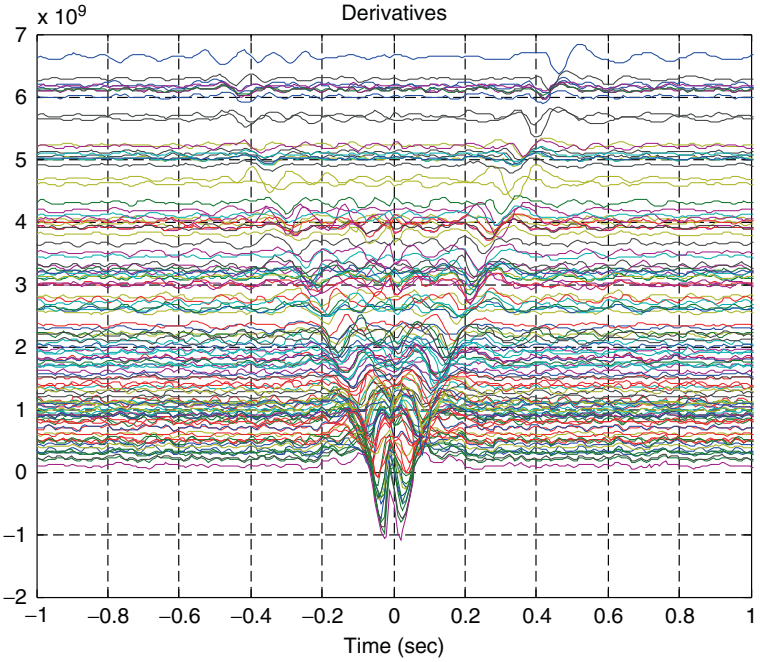

Fig. 1.5.2 Cross correlation functions as function of the considered time lag (in seconds), relative to all the pairs of geophones at the Pisa test site. Each trace corresponds to a couple of geophones located at the distance reported in the corresponding ordinate (in units of 10^{-8} m). The range of distances spans between 1 to 70 m

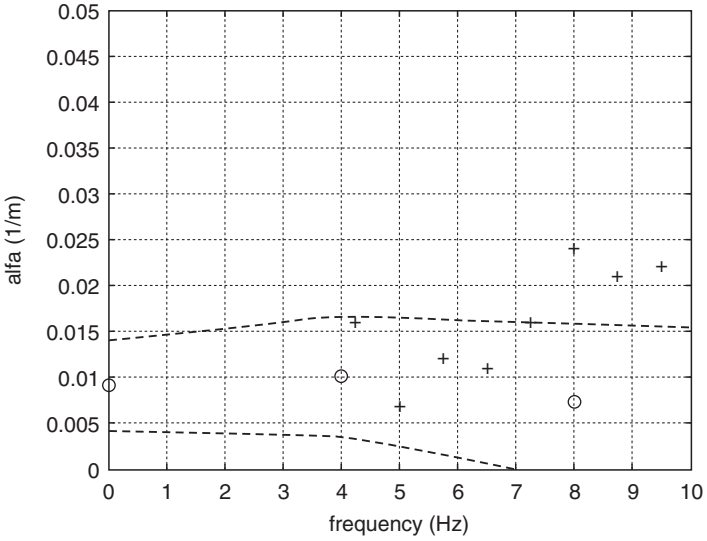

Fig. 1.5.3 Estimates of the attenuation exponent as a function of frequency at the Pisa test site. Empty circles and dashed lines respectively indicate the estimates of α and 95% confidence interval provided by the present analysis of environmental noise measurements. Crosses indicate the corresponding estimates provided by a surface wave test (Foti, 2003)

The wavelet travels at an approximate velocity of 150 m/s as expected in the hypothesis that the pulse corresponds to the Rayleigh phase in the fundamental mode. It results also evident the progressive attenuation of the pulses. No instrumental correction has been considered.

The application of the numerical procedure described above allows spectral characterization of the running wavelet. On this basis, Equation (1.5.7) has been used to parameterize attenuation. Regression analysis indicates that the most energetic part of the signal is in the frequency band (0–10 Hz). The empirical values of the attenuation exponent obtained in this way are reported in Figure 1.5.3 along with the relevant 95% confidence interval. The comparison with *in situ* estimates obtained by Foti (2003) indicates that results here obtained are fully compatible with the ones deduced with active methods.

1.5.6 Test site 2: Fucino (Central Apennines, Italy)

The Fucino basin is a wide intra-mountain depression (about 1,000 km^2) within the Central Apennines, surrounded by high mountains of Mesozoic-Cenozoic carbonatic rocks. Once the basin hosted a wide lake, which was artificially drained in the last century for land declamation. Fine lacustrine and coarse alluvial deposits fill the basin with a thickness that locally is larger than 1,000 m. At the test site, the sediments are lacustrine clays without any significant variation in grading up to the 40 m of depths explored by drilling. V_s values are low ($<100\,m/s$) up to 20 m of depth and gently increase up to 150 m/s (probably as an effect of the increase of calcium carbonate fraction) at the bottom of the drill (Burghignoli et al., 1991).

Damping ratio has been determined from laboratory measurements (cyclic torsional shear tests) carried on undisturbed 12 specimens sampled at depths ranging between 3 and 37 m (Pane and Burghignoli, 1988). Damping values corresponding to shear strain of 0.01% range between 4% and 5%.

Independent estimates of the attenuation exponent at the test site have been also obtained in this study by using a surface wave test following the approach proposed by Athanasopoulos et al. (2000). The results obtained in the frequency band 0–15 Hz (where most of the signal is concentrated) are reported in Figure 1.5.6. Noise measurements have been carried on in a very quite country area by using 16 vertical geophones (4.5 Hz) distributed along two perpendicular arms respectively 110 and 70 m long. Environmental noise has been measured in the late afternoon for 30 min at a sampling rate of 128 cps.

ESAC analysis of noise measurements indicate a Rayleigh waves dispersion curve (Figure 1.5.4C) characterized by very low velocity values (of the order of about 70 m/s) in the frequency band 5–30 Hz. These values are compatible with the very low Vs values determined by the cross-hole test (Figures 1.5.4A and B).

In Figure 1.5.5, the average DCC traces relative to all the couples of geophones in the array are reported. One travelling wavelet can be easily individuated both in its causal and anti-causal form (respectively corresponding to positive and negative time lags).

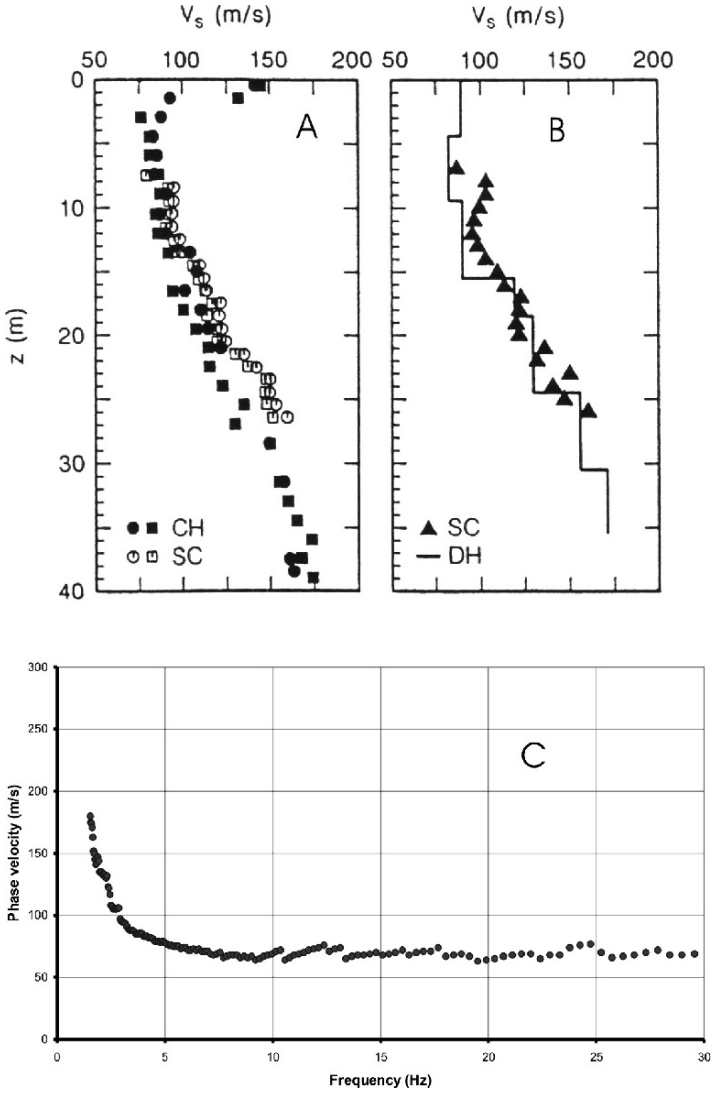

Fig. 1.5.4 Seismic velocity data at the Fucino test site. A: V_s velocity profile by using the Cross-Hole (CH) and seismic cone (SC) tests (Burghignoli et al., 1991); B: V_s velocity profile by using the Down-Hole (DH) and seismic cone (SC) tests (Burghignoli et al., 1991); C: Rayleigh waves dispersion curve at the Fucino test site obtained from seismic noise measurements by using the ESAC approach

The wavelet travels at an approximate velocity of 70 m/s as expected in the hypothesis that the pulse corresponds to the Rayleigh phase in the fundamental mode. Again it results also evident the progressive attenuation of the pulses.

The spectral characterization of the running wavelet and Equation (1.5.7) have been used to parameterize attenuation. Regression analysis carried on in each

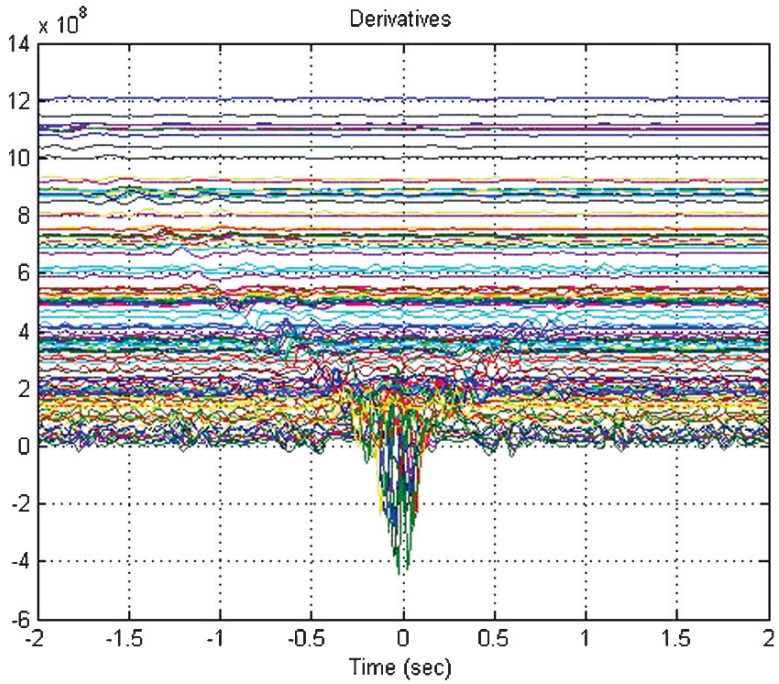

Fig. 1.5.5 Cross correlation functions as function of the considered time lag (in seconds), relative to all the pairs of geophones at the Fucino test site. Each trace corresponds to a couple of geophones located at the distance reported in the corresponding ordinate (in units of 10^{-7} m). The range of distances spans between 1 to 120 m

frequency band indicates that most of the signal is in the frequency band (0–15 Hz). The empirical values of the attenuation exponent obtained in this way are reported in Figure 1.5.6 along with the relevant 95% confidence interval. The results indicates that the α values deduced from noise measurements are fully compatible with the ones deduced with active methods.

The comparison of the results obtained at the Pisa test site, shows that a quite different α pattern has been obtained an effect of genuine differences in the dynamical characteristics of the soil in the two cases.

1.5.7 Conclusions

In this paper, an attempt is described to evaluate the possibility that material damping estimates can be obtained from environmental noise measurements carried on by using seismic arrays. The basic hypothesis is that time derivative of average cross-correlations of noise registered at couples of geophones allows the retrieval of the Green's function, also including attenuation effects. In this way, if the

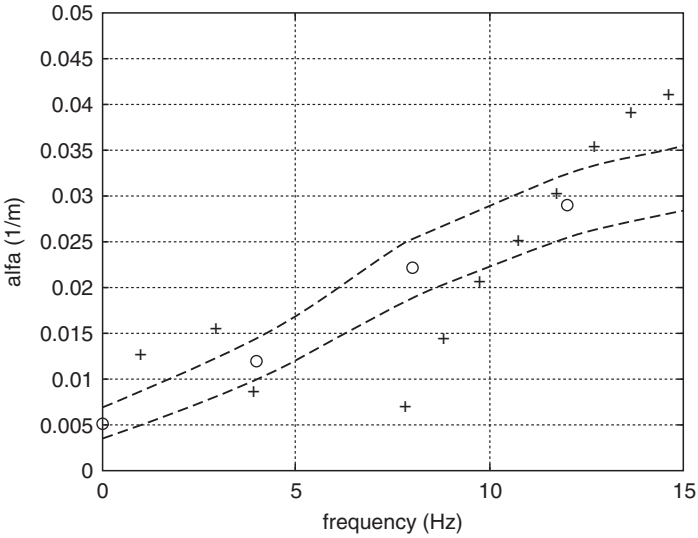

Fig. 1.5.6 Estimates of the attenuation exponent as a function of frequency at the Fucino test site. Empty circles and dashed lines respectively indicate the estimates of α and 95% confidence interval provided by the present analysis of environmental noise measurements. Crosses indicate the corresponding estimates provided by a surface wave test

identification of the relevant seismic phase is possible, geometric spreading effects can be separated from true attenuation effects and these can be determined with good approximation.

This approach has been applied at two test sites where independent estimates of damping were available along with direct estimates of the V_s profile. In both the test sites, the Green's function deduced from noise measurements is the one relative to Rayleigh waves propagating in the fundamental mode. This allows a simple modelization of the wave-field and the estimate of the relevant attenuation exponent. The attenuation estimates deduced from noise measurements are compatible with the corresponding values deduced from active in-situ seismic tests.

The basic limitations of the present results concerns the extremely narrow frequency bandwidth of the results obtained (0–15 Hz). This probably could depend on the fact that body waves contaminate the noise at higher frequencies making much more difficult the characterization of the seismic phases present in the signal. Another problem could also arise due to the very rough numerical procedure used to determine α values. Possibly more effective numerical procedures could be used both to detect and model the expected signal (e.g., wavelet analysis). Furthermore, in this first experiments, no optimization has been carried on about the experimental setting (duration, sampling rate, etc.). Anyway the results appear encouraging and open new possibilities in the exploitation of seismic noise for the mechanical characterization of the subsoil.

References

Aki K., 1957. Space and time spectra of stationary stochastic waves, with special reference to microtremor. Bull. Earthq. Res. Inst., 35, 415–456

Aki K., Richards P.G., 2002. Quantitative seismology. Univ.Sci. Book, Sausalito, CA, USA, 700 pp

Athanasopoulos G.A., Pelekis P.C., Anagnostopoulos G.A., 2000. Effect of soil stiffness in the attenuation of Rayleigh-wave motions from field measurements. Soil Dyn. Earthq. Engng., 19, 277–288

Burghignoli A., Cavalera V., Chieppa V., Jamiolkovski M., Mancuso C., Marchetti V., Pane V., Paoliani P., Silvestri F., Vinale F., 1991. Geotechnical characterization of Fucino clay. Proceedings of the Xth European Conference of Soil Mechanics and Foundation Engineering, Firenze, Italy, Balkema, Rotterdam, Brookfield, 27–40

Dziewonski A.M., Hales A.L., 1972. Numerical analysis of dispersed seismic waves. In *Method in Computational Physics*, Volume 11, edited by B.A. Bolt, Academic, pp. 39–85

Foti S., 2003. Small strain stiffness and damping ratio of Pisa clay from surface wave test. Geotechnique, 53, 455–461

Jamiolowski M., Pepe M.C., 2001. Vertical yield stress for Pisa clay from piezocone tests. J. Geothech. Geoenv. Engng., ASCE, 127, 893–897

Kramer S.L., 1996. Geotechnical earthquake engineering. Prentice-Hall, New Jersey, 653 pp

Lai C.G., 1998. Simultaneous inversion of Rayleigh phase velocity and attenuation for near-surface site characterization, Ph.D. dissertation, Georgia Institute of Technology, Atlanta.

Lai C.G., Rix G.J., Foti S., Roma V., 2002. Simultaneous measurements and inversion of surface waves dispersion and attenuation curves. Soil Dyn. Earthq. Engng., 22, 923–930

Lai C.G., Rix G.J., 2002. Solution of the Rayleigh eigenproblem in viscoelastic media. Bull. Seism. Soc. Am., 92(6), 2297–2309

Larose E., Margerin L., Derode A., Van Taggelen B., Campillo M., Shapiro N., Paul A., Stehly L., Tanter M., 2006. Correlation from randomn wave-field. Geophys., 71(4), SI11–SI21

Lay T., Wallace T.C., 1995. Modern Global Seismology. Academic, San Diego, CA, 521 pp

Lee Y.W., 1960. Statistical Theory of Communication. WileyNew York, 509 pp

Lo Presti D.C.F., Pallaro O., Cavallaro A., 1997. Damping ratio of soils from laboratory and in-situ tests. Proceedings of the 14th International Conference on Soil Mech. Fund. Engng., pp. 391–400

Louie J.N., 2001. Faster, better: shear-wave velocity to 100 meters depth from refraction microtremor arrays. Bull. Seism. Soc. America, 91(2), 347–364

Okada H., 2003. The microtremor survey method. Gephys. Monogr. Series, 12, Society of Exploration Geophysicists, 129 pp

Pane V., Burghignoli A., 1988. Determinazione in laboratorio delle caratteristiche dinamiche dell'argilla del Fucino (in Italian). Proc. Of the Meeting "Deformazioni dei terreni ed interazione terreno-struttura in condizioni di esercizio". Monselice, Padova, 5–6 october. 1, pp. 115–139

Rix G.J., Lai C.G., Spang Jr A.W., 2000. In situ measurements of damping ratio using surface waves. J.Geotech. Geoenv. Engng., 126(5), 472–480

Roux P., Sabra K.G., Kuperman W.A., Roux A., 2005. Ambient noise cross correlation in free space: theoretical approach. J. Acoust. Soc. Am., 117(1), 79–84

SESAME European project (2002). Optimum deployment strategy and quality measure for array layout in view of obtaining surface wave. Report WP05. http://sesame-fp5.obs.ujf-grenoble.fr/Delivrables/D07-05_Texte.pdf

Shapiro N.M., Campillo M., Stehly L., Ritzwoller M.H., 2005. High resolution surface wave tomography from ambient seismic noise. Science, 307, 1615–1618

Tonn R., 1989. Comparison of seven methods for the computation of Q. Phys. Earth. Planet. Int., 55, 259–268

Xia J., Miller R.D., Park C.B., Tian G., 2002. Determining Q of near surface materials from Rayleigh waves. J. Appl. Geophys., 51, 121–129

Chapter 1.6
Estimates of Vs30 Based on Constrained H/V Ratio Measurements Alone

Silvia Castellaro and Francesco Mulargia

Most seismic codes adopt as a key quantitative parameter the average shear wave velocity in the first 30 m of subsoil, commonly calling it Vs30. Estimates of Vs30 are therefore required in most countries for microzonation both at large-scale as well as at the scale of the single buildings. We propose a fast and inexpensive technique to measure the Vs30 based on the horizontal to vertical spectral ratio (H/V) of microtremor recorded at a single station. The experimental H/V is fitted with a synthetic curve using as a constraint the thickness of the most superficial layer of the subsoil, which is always independently known in the geotechnical practice for building design approval. The fitting procedure consists of three steps: (1) identify the depth of the first shallow stratigraphic horizon from geotechnical data, (2) identify its corresponding H/V marker and (3) use it as a constraint to fit the experimental H/V with the synthetic one. The synthetic H/V curve is calculated by assuming a tremor wavefield with Rayleigh and Love waves in the fundamental mode in a stratified 1-D soil model. A validity check of this technique has been performed on a variety of geological settings in Northern Italy. The validity check compares: (1) the theoretical Rayleigh wave phase velocity dispersion curves calculated for the models derived from the H/V fits with the experimental curves measured with ESAC and ReMi array surveys, (2) the Vs30 estimates obtained with the proposed technique with those obtained at the same sites by using the latter array techniques. The inferred stratigraphy has been also compared with the geological knowledge. The proposed technique is found capable to provide, at a small fraction of the costs and survey times, Vs30 estimates coherent with those measured by ESAC and ReMi. Furthermore, the proposed technique is also found to be more informative than array techniques, allowing to detect deviations from 1-D subsoil geometry over lengths of a few meters, the correctness of which was confirmed by direct drilling.

S. Castellaro (✉) and F. Mulargia
Dipartimento di Fisica, Università di Bologna, Viale Berti Pichat 8, 40127 Bologna, Italy

M. Mucciarelli et al., (eds.), *Increasing Seismic Safety by Combining Engineering Technologies and Seismological Data,* NATO Science for Peace and Security Series C: Environmental Security,

1.6.1 Introduction

Traditionally, the geophysical approach to seismic risk has given the highest priority to the estimate of seismic hazard, i.e. the probability that an earthquake of a given magnitude may occur in a given area within a given period of time. However, in spite of the importance of hazard estimates, it is another factor that has prevented reliable seismic risk estimates. This factor is the comparatively inaccurate mapping of site effects. An attempt to combine the two approaches has been recently presented by Parolai et al. (2007).

There is not full consensus on what is the most effective procedure to estimate potential site effects beforehand. Different countries have different protocols, although the relevant parameters are common to all and regard soil instability, soil rigidity and the principal soil resonance frequency. In all countries, the procedure leads eventually to a site classification which relies on compositional, static and dynamic properties. In particular, the Eurocode 8, which constitutes the standard for seismic design in Europe, where it inspires all the national codes, has its roots in the procedure for site classification of the U.S. National Earthquake Reduction Program (NEHRP). The site classification is generally based on the following steps: (1) dynamic classification of subsoil through the average velocity of S-waves in the first 30 m of depth (the so called Vs30), which can be measured through classical seismic active (refraction, downhole, crosshole, SASW, MASW, FTAN etc.) or seismic passive (e.g. ReMi, SPAC, ESAC etc.) methods, or derived from other geotechnical parameters such as N_{SPT} (number of blows in a static penetration test), undrained cohesion c_u, etc., (2) estimate of site effects (seismic amplification and soil response spectrum), (3) estimate of topographical effects.

The Vs30 parameter is then used to classify subsoil into classes, e.g. for the Italian territory, $V_s < 180,\ 180 \leq V_s < 360,\ 360 \leq V_s < 800,\ V_s \geq 800\,\mathrm{m/s}$.

The fact that the estimate of Vs30 for subsoil is required not only at large scale for regional microzonation, but also at the scale of the single building for designing its foundations, creates a number of practical problems. These are related to the fact that the measure of the S-wave velocity profile using seismic methods requires specific apparatuses and, for some active methods, also drilling, all factors which concur in establishing comparatively long survey times and high operative costs. The goal of the present paper is to propose a fast and inexpensive technique to estimate the Vs30, based on the horizontal to vertical spectral ratio (H/V) of microtremor recorded at a single station.

1.6.2 The proposed technique

There is general consensus on the fact that, in a single layer 1-D stratigraphy, the analysis of the H/V spectral ratio of microtremor allows to estimate with reasonable accuracy the principal S-wave resonance frequency f of the sedimentary cover overlying an infinite bedrock as well as its thickness h (Lermo and Chavez-Garcia, 1993,

1994; Lachet and Bard, 1994; Bard, 1998; Ibs-von Seht and Wohlenberg, 1999; Fah et al., 2001) simply by

$$f = V_s/4h \tag{1}$$

where V_s is the average S-wave velocity in the sediment layer.

One could attempt to refine Equation 1 by accounting for the gravitational compaction of sediments in order to extend its validity to greater depths than a few meters (cf. Ibs-von Seht and Wohlenberg, 1999). However, the existence of a single layer of sediments is almost never encountered in practice over substantial depths. In general, there are several alternated layers of different lithology and these produce a H/V curve with several peaks and humps and troughs. Assuming an appropriate model for the wavefield and for the medium, a theoretical H/V curve can be fitted to the experimental one to infer a subsoil model. We propose to use as constraint in the fit the thickness of the most superficial layer, which is usually independently known in the geotechnical practice.

1.6.2.1 Procedure

Let us first of all say that an independent knowledge of the very shallow subsoil stratigraphy is needed. Stratigraphy does *not* need to be known down to 30 m. Only the first discontinuity depth $h1$ suffices, which can also be the depth of the interface between vegetal soil/debris and the natural subsoil.

The thickness/depth of the first layers is generally available in the geotechnical practice from penetration tests, drillings, pits, trenches. Alternatively, the V_s of the first layer (when available from independent methods) can be used as starting point.

The proposed procedure consists of the following steps:

1. Measure the H/V. This requires 15 to 20 min with appropriate portable instruments and can be effected everywhere (no need for cable deployment, diggings, etc.).
2. Identify the H/V marker corresponding to a known superficial stratigraphic horizon which has depth $h1$.
3. Use $h1$ to constrain the fit of the synthetic H/V curve to the measured one.
4. Fit a synthetic H/V curve to the experimental one.

The H/V analyses were performed as described in Castellaro et al. (2005). We used 20 s windows to obtain the average H/V and its subintervals. Attention was paid to the cleaning of the H/V curve as in Castellaro and Mulargia (2008b, c).

The H/V peak of the shallow stratigraphic horizon. It may be argued that sometimes no H/V peak can be associated to a shallow stratigraphic horizon. In our experience, no marker can be recognized in a H/V curve when the recording is performed on perfectly homogeneous rock without any cover/alteration layer. The latter gives a truly flat H/V curve and is of little interest, since no particular amplification exists. Nevertheless, it is worth noting that in this particular case the procedure proposed in the present work cannot estimate the V_s of the rock.

In general, it should also be emphasized the importance of performing the H/V acquisition on natural soil and to absolutely avoid stiff artificial soils (pavments, asphalts and similar) since these can induce velocity inversions which force the H/V curve to amplitudes below 1 even down to 1 Hz. This is an important point which is generally disregarded or ignored since traditional seismometers are much easier to level on artificial soils rather than on natural ones. A paper dedicated to the problem is Castellaro and Mulargia (2008c). This problem is discussed also in case II (natural velocity inversion) below.

1.6.2.2 Fitting the synthetic H/V curve

In light of the coherence emerging from array measurements (see SESAME 2005, and references therein), the usual assumption is that the wavefield is composed of surface waves. However, if there is little doubt on the surface wave predominance, the relative importance of Rayleigh and Love waves and of the various modes appears still open to question. The presence of Love waves has been often experimentally suggested in tremor (e.g. SESAME 2005). Their relative weight seems largely variable: for example Kohler et al. (2007) suggest a composition of 90% Love waves and 10% Rayleigh waves, while Bonnefoy-Claudet et al. (2007) suggest at least 50% Love waves. At the same time, theoretical arguments suggest that Love waves should play a minor role with respect to Rayleigh ones (Campillo and Paul, 2003; Roux et al., 2004; Shapiro and Campillo, 2004) since they are not sufficiently excited from the scatterers in the crust. Similarly controversial is the discussion on the importance of higher modes. In light of this, Ockham's razor imposes to adopt the most simple model option compatible with the data. In this case the model is that noise is composed of Rayleigh waves and 30% of love waves and only in the fundamental mode (cf. Fah et al., 2001).

We assumed a 1-D stratigraphy, and adopted the 1-D coupling coefficients of Ben-Menahem and Singh (1981). A Dunkin (1965) stability correction was used in the propagators.

1.6.2.3 Validation

We compared the results of our procedure with those provided by a well-established array technique to infer V_s, that is ESAC (Extended Spatial AutoCorrelation, as defined by Ohori et al., 2002 and Chavez-Garcia et al., 2006), and an array technique very popular in the geotechnical practice, that is ReMi (Refraction Microtremor, as defined by Louie, 2001). We used 2D arrays for the ESAC analysis and the linear legs of the same arrays for the ReMi analyses. Ambient noise was sampled for 20–30 min and the final dispersion curves is the average computed on 10–15 s windows, after the removal of non-informative time-windows. The validity check

was twofold and compared (1) the theoretical dispersion curves calculated for the models derived from the H/V fits with the experimental Rayleigh wave phase dispersion curves from array measurements, (2) the Vs30 estimates from the H/V fits with those obtained at the same sites by using established array techniques. Finally, the inferred stratigraphy was also compared for geological coherence with surface geology and direct drilling.

We have always kept the arrays as short as possible in order to avoid strong 2D effects. The maximum array length used in this study was 43 m but in the majority of cases arrays were only 30 m long. In spite of this (see below) we had evidence of deviations from 1-D geometry in nearly all cases.

1.6.2.4 Differences with other techniques

Joint inversions of passive seismic array data and H/V curves in order to get V_s profiles has been successfully used by a number of authors (Arai and Tokimatsu, 2005; Parolai et al., 2005; Picozzi et al., 2005; Picozzi and Albarello, 2007). Note how the proposed procedure has nothing to do with these since it is *not* a joint H/V-array approach. It is just a single station H/V approach, and does not require any ancillary array measurements for its practical application. The use of array techniques in the present work is only to validate the single station procedure.

1.6.3 Instrumentation

All the single station tremor measurements in this work were performed with the Micromed Tromino tromograph, a very compact (1 kg in weight), 3 component, high sensitivity and resolution (2,200 V/m/s, 24 dB, 0.1250 Hz) tremor recorder.

The ESAC and ReMi surveys were performed through synthetic aperture (GPS synchronized) 2D arrays of Trominos using up to nine elements with prime number monotonically increasing inter-instrument spacing, from 0 to 43 m. Alternatively, when a sufficient number of Trominos was not available (the instruments were mostly borrowed) a more conventional (but digital, see below) array was used. Whenever available, Tromino arrays were preferred, since they allowed also to record simultaneously the H/V curves at each single point along the array. This allowed in turn to interpret any variation in the H/V curves along the array as the effect of true differences linked to the sites of measure, since differences in source/radiation could be excluded.

When a sufficient number of Trominos to deploy 2D arrays was not available, a Micromed Rosina digital array was used. The latter is a wired array with 16 vertical digital 4 Hz geophones, that guarantees a superior signal to noise ratio than the traditional arrays, in which the analog signal is only digitized at the end of a

10^2 m long cable. Indeed, thanks to the larger number of sensors, this array provided clearer dispersion curves (see case IV e V below) than Tromino arrays but lacked the advantage of simultaneous H/V acquisition at different points.

1.6.4 Results

We present a short selection of cases from Northern Italy, that represent a variety of geological conditions. More cases can be found in Castellaro and Mulargia (2008b).

For each site we will show:

(A) The H/V points of measure and the nodes of the arrays used for the validation step.
(B) The H/V curves recorded at the same time at different points. This allows to check the 1-D assumption for stratigraphy.
(C) The experimental H/V curve chosen to be representative for the site and the fitted synthetic one. The H/V marker which corresponds to the stratigraphic horizon identified from shallow penetration tests/drillings is indicated by an arrow.
(D) As a first validation, the theoretical Rayleigh wave phase dispersion curves calculated for the model derived from the H/V fits together with the experimental dispersion curves derived from ESAC and ReMi array surveys.
(E) A geological picture of the site.
(F) The V_s profile obtained from the H/V fit.

The second validation step, that is the comparison between the Vs30 values estimated through the H/V fitting with those obtained at the same sites by using ESAC and ReMi techniques, is given in the text. Figures in panel (E) and (F) allow a comparison for geological coherence of the inferred stratigraphy with surface geology and direct drilling.

1.6.4.1 Case I

This case is relative to a plane area in the N-E of Italy, located in the river Po Plain. The stratigraphy at this site is constituted of a first (about 5 m) layer of silts overlaying a large palaeochannel constituted of cemented sands. Below this palaeochannel, stiff clays are present. The direct knowledge of the subsoil here comes from a number of penetration tests (stopped at 8 m depth) and a nearby drilling stopped at 28 m depth.

Since the paleaochannel is large, 2D effects are presumably small.

The H/V curves recorded at different points (later used as arrays nodes for the arrays deployed in the validation test, Figure 1.6.1A) are very similar (Figure 1.6.1B), implying that the 1D assumption in this case holds. The experimental H/V curve selected for the fitting (indicated by the arrow in Figure 1.6.1A)

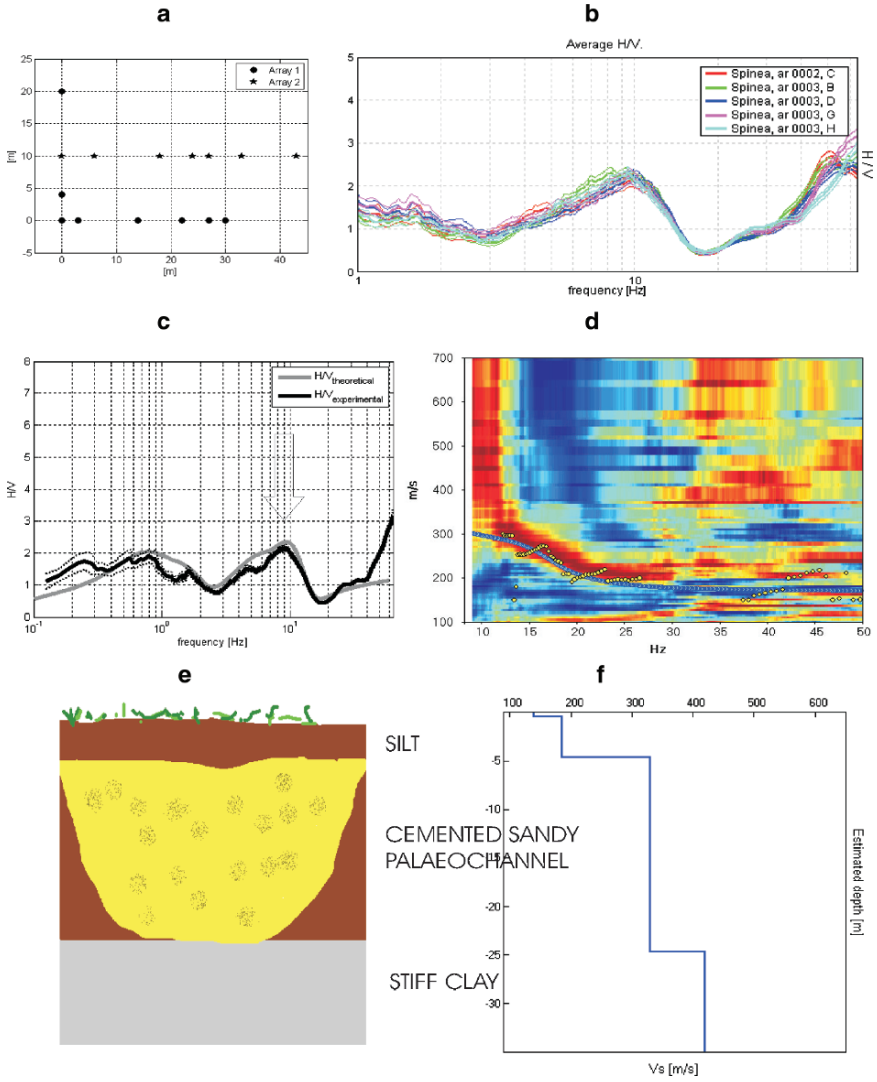

Fig. 1.6.1 Site I. (**a**) H/V location and array geometry, (**b**) comparison of the H/V at the nodes of the array. Thick lines are the average H/V, thin lines are the 2σ intervals, (**c**) synthetic vs. experimental H/V. The thick black line is the average experimental H/V, dotted lines are the 2σ intervals, (**d**) Dispersion curves from H/V fit (blue circles) and arrays (yellow circle for ESAC, contour map for ReMi, (**e**) geological model, (**f**) Vs profile

is shown in Figure 1.6.1C, together with the synthetic one. The stratigraphic horizon used to constrain the H/V fit is the contact between the shallow silts and the cemented palaeochannel located at 5–6 m depth (strong increase in the N_{SPT}). This is responsible for the H/V peak at 9–10 Hz well visible in Figure 1.6.1B and therefore provides for the first layer, according to Equation 1, a starting value $V_s \approx 180\,\mathrm{m/s}$, which is iteratively refined in the fitting process.

In the first validation step, the Rayleigh wave phase velocity dispersion curve resulting from the model used to fit the experimental H/V is shown in Figure 1.6.3D and superimposed to the dispersion curve resulting from ESAC and the contour map resulting from ReMi. Reminding that according to the ReMi procedure the picking of the dispersion curve should be performed on the lower margin of the maximum energy band, the visual observation shows a good match of the three curves in the range above 10 Hz.

In the second validation step, The Vs30 value provided by the H/V fit is 348 m/s while the Vs30 value provided by an automatic inversion (maximum likelihood method) of the dispersion curve deriving from a combined picking of ESAC curve and the ReMi contour map gives 364 m/s.

The difference between our Vs30 estimate and that of the array techniques is within 5%. The model obtained from the H/V fit is compared to the stratigraphy known from the drilling in Figure 1.6.3E, F, giving a good geological coherence.

1.6.4.2 Case II

This case is also relative to the river Po Plain but here only fine-grained sediments are present (alternations of clay and silt or silty-sands). The peculiarity of this example is the natural surface velocity inversion due to the presence of the uppermost 2.5–3 m of overconsolidated clays overlying clays, which sets the H/V amplitude below 1 from about 15 Hz downwards (Di Giacomo, 2004; Castellaro et al., 2008a; Castellaro and Mulargia, 2008c).

The H/V curves acquired at different points later used as array nodes (Figure 1.6.2A) show a modest variability (Figure 1.6.2B). The stratigraphy was known from five penetration tests reaching depths from 10 to 17 m. We constrained the fit to the depth of the velocity inversion (2.5 m, about 15 Hz at the selected point, Figure 1.6.2C). This provides for the first layer, according to Equation 1, a first iteration $V_s = 150\,\mathrm{m/s}$.

The comparison between the theoretical dispersion curve for the model derived from H/V fit and the experimental ones derived through ESAC and ReMi is shown in Figure 2.6.2D.

The Vs30 value provided by the H/V fit alone is 180 m/s while the Vs30 value provided by an automatic inversion of the dispersion curve deriving from a combined picking of ESAC curve and the ReMi contour map is 201 m/s.

1.6.4.3 Case III

This example comes from a gravel quarry in the Dolomites and has been selected because it deals with a different type of lithology and impedance contrast between layers. Gravel is naturally present at this site as slope debris.

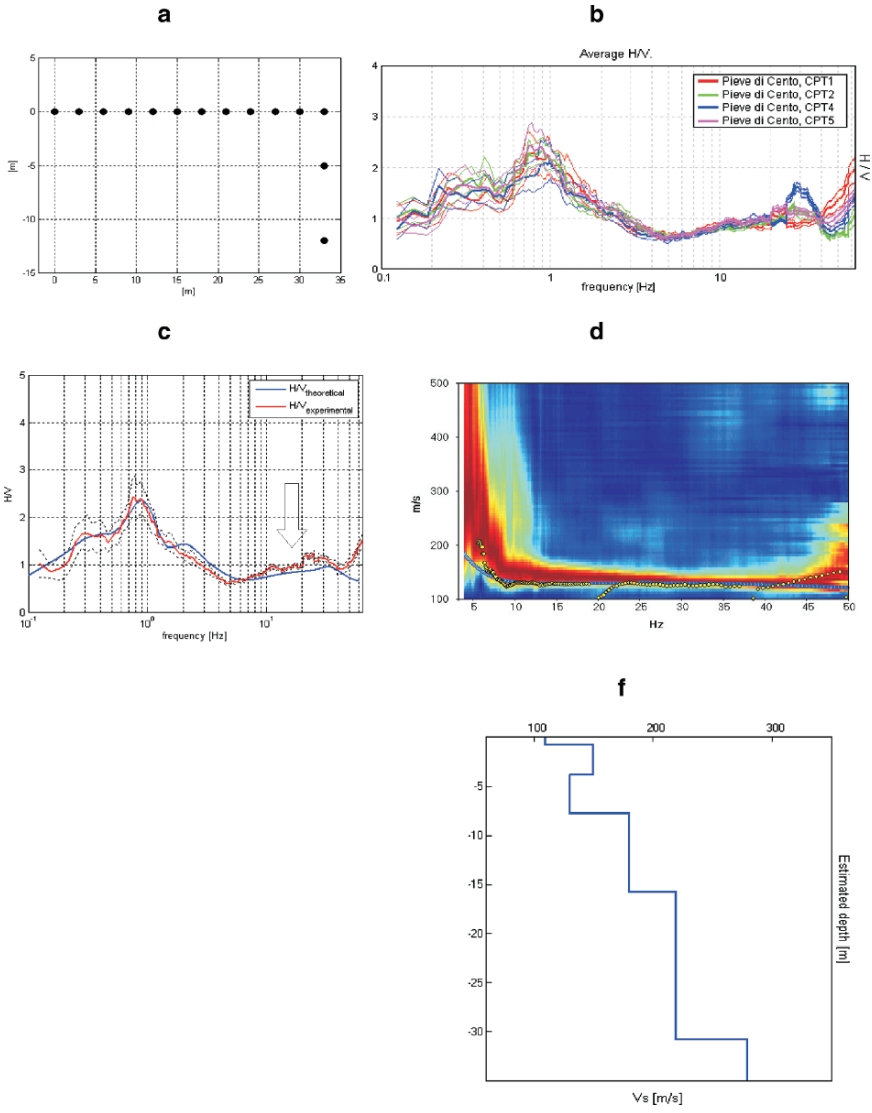

Fig. 1.6.2 As in Figure 1.6.1, for Site II

The H/V curves recorded at different points (later used as arrays nodes for the two arrays we deployed in the validation test, Figure 1.6.3A) show the dolomitic bedrock at a fixed 'depth' of 4 Hz and a clear layer which appears at about 9 Hz (10 m) only in the Eastern sites (Figure 1.6.3B), implying that the 1D assumption is not fulfilled. We have constrained the H/V inversion to this layer, for which Equation 1 provides a starting $V_s = 360\,\mathrm{m/s}$.

In order to limit unavoidable 2D effects, the passive array was set parallel to the slope and the independent knowledge of the shallow stratigraphy in this case

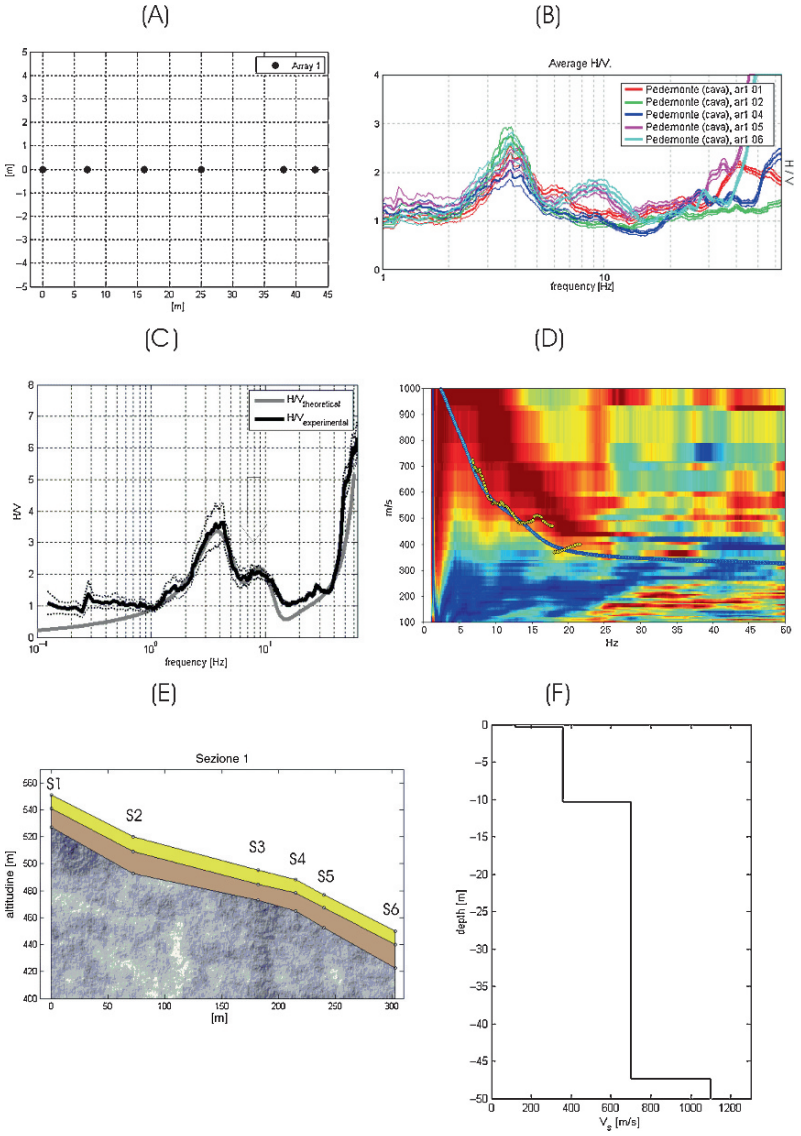

Fig. 1.6.3 As in Figure 1.6.1, for Site III

comes from the refraction surveys used to define the volumes of gravel which can be extracted. The comparison between the theoretical dispersion curve for the model derived from H/V fit and the experimental ones derived through ESAC and ReMi is shown in Figure 1.6.3D and shows a good match between the curves, despite the non 1D condition.

The Vs30 value provided by the H/V fit alone is 509 m/s while the Vs30 value provided by an automatic inversion of the dispersion curve deriving from a combined picking of ESAC curve and the ReMi contour map is 511 m/s.

1.6.5 Practical limitations of the proposed procedure

After the pros, let us analyze the cons of the proposed method.

1. As any model fitting technique, it relies on a fixed predetermined composition of seismic noise.
2. As any model technique of practical use, it relies on a 1D subsoil model, however we found that in the wide majority of cases the subsoil stratigraphy is not 1D.
3. Since the H/V amplitude at low frequency (approximately below 0.5 Hz) is weather dependent (Mulargia and Castellaro, 2007), the H/V fitting technique adopted in this study is only aimed at shallow subsoil analysis and should not be considered applicable below 1 Hz.
4. The presence of shallow velocity inversions can be easily recognized in the H/V Castellaro and Mulargia (2008c) curve but it can mask minor stratigraphic discontinuities. Note how shallow velocity inversions make also array dispersion curves difficult to interpret since higher modes usually make the curve picking, and inversion, difficult and unstable.

1.6.6 Discussion and conclusion

Seismic codes in most countries require an estimate of the Vs30 parameter for microzonation not only at the regional scale but also at the scale of the single building. In this paper we propose a procedure to estimate the Vs30 parameter based on the fitting of single station H/V curves using as a constraint the independent knowledge of the thickness of the most superficial layer (first 5–10 m), which is always available in the geotechnical practice.

The cases presented in this study cover a variety of geological conditions and show that the technique is capable, at a small fraction of the costs and survey times, of Vs30 estimates coherent with those provided at the same sites by ESAC and ReMi array techniques. The H/V single station measurements has also the bonus of providing a measure of the main resonance frequency of the sedimentary layer.

Our analysis raised an additional important point. Simultaneous H/V measurements at sites distant a few (less than 5) meters, even in plane areas showed nearly always differences which appear incompatible with 1-D subsurface geometry. This should be considered particularly on the use of array (or psuedo-array) techniques (SPAC, ESAC, SASW, MASW, FTAN, ReMi, etc.), which require linear spans of more than 100 m beneath which a 1-D subsurface geometry must be perforce assumed.

References

Arai, H. and K. Tokimatsu: S-wave velocity profiling by joint inversion of microtremor dispersion curve and horizontal-to-vertical (H/V) spectrum, *Bull. Seism. Soc. Am.*, **95**, 1766–1778 (2005).

Bard, P. -Y.: Microtremor measurements: a tool for site effect estimation? *Second International Symposium on the Effects of the Surface Geology on Seismic Motion-ESG98*, Japan (1998).

Ben-Menahem, A. and S. J. Singh: *Seismic Waves and Sources*, Springer, New York (1981).

Bonnefoy-Claudet, S., A. Kohler, C. Cornou, M. Wathelet, F. Cotton, P.-Y. Bard: Effects of love waves on microtremor H/V ratio amplitude, *IUGG XXIV General Assembly*, Perugia (Italy) (2007).

Campillo, M., and A. Paul: Long range correlations in the diffuse seismic coda, *Science*, **299**, 547–549 (2003).

Castellaro, S., F. Mulargia and L. Bianconi: Passive Seismic Stratigraphy: a new efficient, fast and economic technique, *J. Geotech. Environ. Geol.*, **3**, 51–77 (2005).

Castellaro, S., S. Imposa, F. Barone, F. Chiavetta, S. Gresta and F. Mulargia: Georadar and passive seismic survey in the Roman amphitheatre of Catania (Sicily), *J. Cult. Herit.*, in press (2008a).

Castellaro, S., and F. Mulargia. Constrained H/V only estimates of Vs30, *Bull. Seismol. Soc. Am.*, in press (2008b).

Castellaro, S., and F. Mulargia. The effect of velocity inversions on H/V: Pure Appl. Geophys., submitted (2008c).

Chavez-Garcia, F. J., M. Rodriguez and R. Stephenson: Subsoil structure using SPAC measurements along a line, *Bull. Seismol. Soc. Am.*, **96**, 729–736 (2006).

Di Giacomo, D., M.R. Gallipoli, M. Mucciarelli, S. Parolai and S.M. Richwalski: Analysis and Modeling of HVSR in the Presence of a Velocity Inversion: the case of Venosa, Italy, *Bull. Seism. Soc. Am.*, **135**, 91–106 (2005).

Dunkin, J. W.: Computation of modal solutions in layered, elastic media at high frequencies, *Bull. Seism. Soc. Am.*, **55**, 335–358 (1965).

Fah, D., F. Kind and D. Giardini: A theoretical investigation of average H/V ratios, *Geophys. J. Int.*, **145**, 535–549 (2001).

Ibs-von Seht, M. and J. Wohlenberg: Microtremors measurement used to map thickness of softsoils sediments, *Bull. Seism. Soc. Am.*, **89**, 250–259 (1999).

Kohler, A., M. Ohrnberger, F. Scherbaum, M. Wathelet, C. Cornou Assessing the reliability of the modified three-component spatial autocorrelation technique, *Geophys. J. Int.*, **168**, 779–796, doi: 10.1111/j.1365–246X.2006.03253 (2007).

Lachet, C. and P. -Y. Bard: Numerical and theoretical investigations on the possibilities and limitation of Nakamura technique, *J. Phys. Earth*, **42**, 377–397 (1994).

Lermo, J. and F. J. Chavez-Garcia: Site effect evaluation using spectral ratios with only one station, *Bull. Seism. Soc. Am.*, **83**, 1574–1594 (1993).

Lermo, J. and F. J. Chavez-Garcia: Are microtremors useful in site response evaluation?, *Bull. Seism. Soc. Am.*, **84**, 1350–1364 (1994).

Louie, J.: Faster, better: shear-wave velocity to 100 meters depth from refraction microtremor arrays, *Bull. Seismol. Soc. Am.*, **91**, 347–364 (2001).

Mulargia, F. and S. Castellaro: Single-Station Passive Seismic Stratigraphy to nearly 2 km depth in sedimentary basins *IUGG XXIV General Assembly*, Perugia (Italy) (2007).

Ohori, M., A. Nobata and K. Wakamatsu: A comparison of ESAC and FK methods of estimating phase velocity using arbitrarily shaped microtremor arrays, *Bull. Seismol. Soc. Am.*, **92**, 2323–2332 (2002).

Parolai, S., M. Picozzi, S. M. Richwalski and C. Milkereit: Joint inversion of phase velocity dispersion and H/V curves from seismic noise recordings using a genetic algorithm, considering higher modes, *Geophys. Res. Lett.*, **32**, L01301, doi: 10.1029/2004GL021115 (2005).

Parolai, S., G. Grunthal and R. Wahlstrom: Site-specific response spectra from the combination of microzonation with probabilistic seismic hazard assessment – An example for the Cologne (Germany) area, *Soil Dyn. Earthq. Eng.*, **27**, 49–59 (2007).

Picozzi, M., S. Parolai and S. M. Richwalski: Joint inversion of H/V ratios and dispersion curves from seismic noise: Estimating the S-wave velocity of bedrock, *Geophys. Res. Lett*., **32**, L11308, doi:10.1029/2005GL022878 (2005).

Picozzi, M., D. Albarello: Combining genetic and linearized algorithms for a two-step joint inversion of Rayleigh wave dispersion and H/V spectral ratio curves, *Geophys. J. Int*., **169**, 189–200 (2007).

Roux, P., W.A. Kuperman and the NPAL group: Extracting coherent wave fronts from acoustic ambient noise in the ocean, *J. Am. Acoust. Soc*., **116**, 1995–2003 (2004).

SESAME: http:sesame-fp5.obs.ujf-grenoble.fr (2005).

Shapiro, N. M. and M. Campillo: Emergence of broad band Rayleigh waves from correlations of the ambient seismic noise, *Geopys. Res. Lett*., **31**, L07614 (2004).

Chapter 1.7
Comparison of Recorded Dynamic Characteristics of Structures and Ground During Strong and Weak Shaking

Mehmet Çelebi

Abstract Variation of dynamic characteristics of undamaged structures, and free-field sites identified from strong motions as compared to those identified from weak motions has been the subject matter of numerous studies. Recently, this topic is rekindled with the premise but repeat of the well known conclusion that fundamental period (frequency) varies with amplitude of strong and weak shaking. Some researchers appropriately called this variation of dynamic characteristics as "wandering" of the natural frequencies of a structure. Although due to various sources of excitation and time-varying environmental conditions, variation of the fundamental period (frequency) of even an undamaged structure should not be a surprise to many, it is important to understand why such variation is important for practical purposes. It is important that, if such variation is significant, then, in practice, the dynamic characteristics identified from weak motions should be carefully considered before generalizing these characteristics as representative of strong shaking as well.

In this paper, we investigate the fundamental frequencies of an undamaged case study building for which there are numerous studies of several sets of vibration data, including forced vibration testing, strong shaking due to a distant large earthquake, and low-amplitude shaking due to ambient excitations as well as several small nearby earthquakes. It is shown that the fundamental frequency "wanders" in a consistent way with the level of shaking, and that the significant difference between low-amplitude and strong shaking is attributed to soil-structure interaction during stronger shaking. Furthermore, variation of dynamic characteristics for strong and weak motions are summarized for four additional buildings. The variations are too significant to ignore; thus leading to the conclusion that dynamic characteristics of buildings identified from weak motions cannot be generally used in lieu of those identified from strong shaking.

In addition, also for the free-field site associated with this building, using several approaches including strong and weak motions, site frequency is clearly

M. Çelebi
Earthquake Hazards Team, USGS, Menlo Park, CA. 94025, US gov. Licence
e-mail: celebi@usgs.gov

M. Mucciarelli et al., (eds.), *Increasing Seismic Safety by Combining Engineering Technologies and Seismological Data,* NATO Science for Peace and Security Series C: Environmental Security, © US Government License

identified for strong and weak motions. However, the variation of site frequency is insignificant.

Keywords Strong-motion · Weak-motion · Dynamic characteristics · Frequency · Period · Damping · Structure · Site · Acceleration

1.7.1 Introduction

Reasonably accurate assessment of dynamic characteristics [fundamental period (frequency) and damping] of a structure is an essential part of engineering design and analysis processes. In this paper, dynamic characteristics for a specific case building and its nearby free-field site are identified for strong and weak motions. Furthermore, variation of dynamic characteristics for strong and weak motions are summarized for four additional buildings.

It is known that variation of fundamental period (frequency) of undamaged structures has been subject matter of numerous studies – too long to cite herein. Recently, with advanced technologies and methods to acquire and analyze vibration data from structures excited by natural and man-made sources, study of the subject matter is rekindled with the premise that fundamental period (frequency) varies with the amplitude of shaking (e.g. Calvi et al., 2006; Dunand et al., 2006; Todorovska et al., 2006). Clinton et al. (2006) appropriately called this "wandering" of the natural frequencies of a structure. Due to various sources of excitation and time-varying environmental conditions, variation of the fundamental period (frequency) of even an undamaged structure should not be a surprise to many. Nonetheless it is important to understand and evaluate the implications as to such variation is important for practical purposes. It is also important to mention that accurate assessment of fundamental frequency is important to establish a baseline linear elastic behavior of a structure in order to interpret its nonlinear elastic or nonlinear inelastic behavior that may be observed in future events. The ultimate question is whether dynamic characteristics determined from low-amplitude motions can be used in lieu of those from strong shaking.

In this paper, the case study building is the undamaged Pacific Park Plaza [PPP] Building in Emeryville, CA, for which there are numerous studies of numerous sets of vibration data, including forced vibration testing, strong shaking due to a far distance large earthquake, and low-amplitude shaking due to ambient excitations as well as several small nearby earthquakes. It is shown in this study that the fundamental period (frequency) of PPP is observed to "wander" in a consistent way with the level of shaking. The scope of the paper is based on findings using actual data and does not include mathematical modeling of the building (except in reference to existing analyses by others). In the case of this building, the significant change in the value of fundamental period (frequency) between low-amplitude and strong shaking is attributed to soil-structure interaction (SSI) during stronger shaking. However, detailed SSI investigation of the building is beyond the scope of this paper but has been reported elsewhere (Kagawa and Al-Khatib 1993; Kagawa et al., 1993;

Aktan et al., 1992; Kambhatla et al., 1992; Çelebi, 1992, 1998). This paper introduces additional results from new data that reinforces this argument.

Also for this building, using different approaches and recorded strong and weak motion, site frequency is clearly identified to provide comparatively similar values.

1.7.2 The case study building and its site

1.7.2.1 The building, design spectra and instrumentation

The Pacific Park Plaza (PPP) Building is an equally-spaced three-winged, cast in place, 30-story, 312 ft (95.1 m) tall, ductile reinforced concrete moment-resisting frame building. The three wings of the building are constructed monolithically and are equally spaced at angles of 120° around a central core. Shear walls in the center core and wings extend to the second floor level only, but column lines are continuous from the foundation to the roof. The foundation is a 5-ft-thick concrete mat supported by 828 (14-in.-square) pre-stressed concrete friction piles, each 20–25 m in length, in a primarily soft-soil environment that has an average shear-wave velocity between 250 and 300 m/s and a depth of approximately 150 ft (∼50 m) to harder soil. A three-dimensional schematic of the building and its seismic instrumentation is shown in Figure 1.7.1. The instrumentation integrates arrays for the structure, surface, and downhole, and comprises a 30-channel accelerometer deployment uniquely designed to capture (a) the translational motions of the wings of the building relative to its core, (b) the vertical motions of the mat foundation slab at the ground floor level, and (c) free-field motions at the surface and at a downhole depth of 200 ft (61 m). The South Free-field (SFF) station is often referred to as the Emeryville (EMV) ground site. This building is selected for this study because there is a variety of old and new data and because there is no evidence that it experienced any damage during the various levels of shaking described in this paper.

1.7.2.2 Site conditions

Based on a relatively recent geologic log and shear-wave velocity profile (Gibbs et al., 1994), the soils at the site consist of artificial fill, soft silty clay (Holocene Bay Mud), and stiff to very stiff, undifferentiated deposits composed of numerous layers of clay, loam, sand, and gravel. The layer of Holocene Bay Mud, clearly evident on the shear-wave velocity profile shown in Figure 1.7.2, begins at about 16 ft (5 m) depth and is approximately 10 ft (3 m) thick. Stiff deposits with shear-wave velocity (V_s) of approximately 820 ft/s (0.25 km/s) extend from below the Holocene Bay Mud to a depth of approximately 80 ft (24 m). Very stiff Pleistocene deposits with V_s approximately equal to 1,300 ft/s (0.4 km/s) extend to a depth of about 155 ft (48 m).

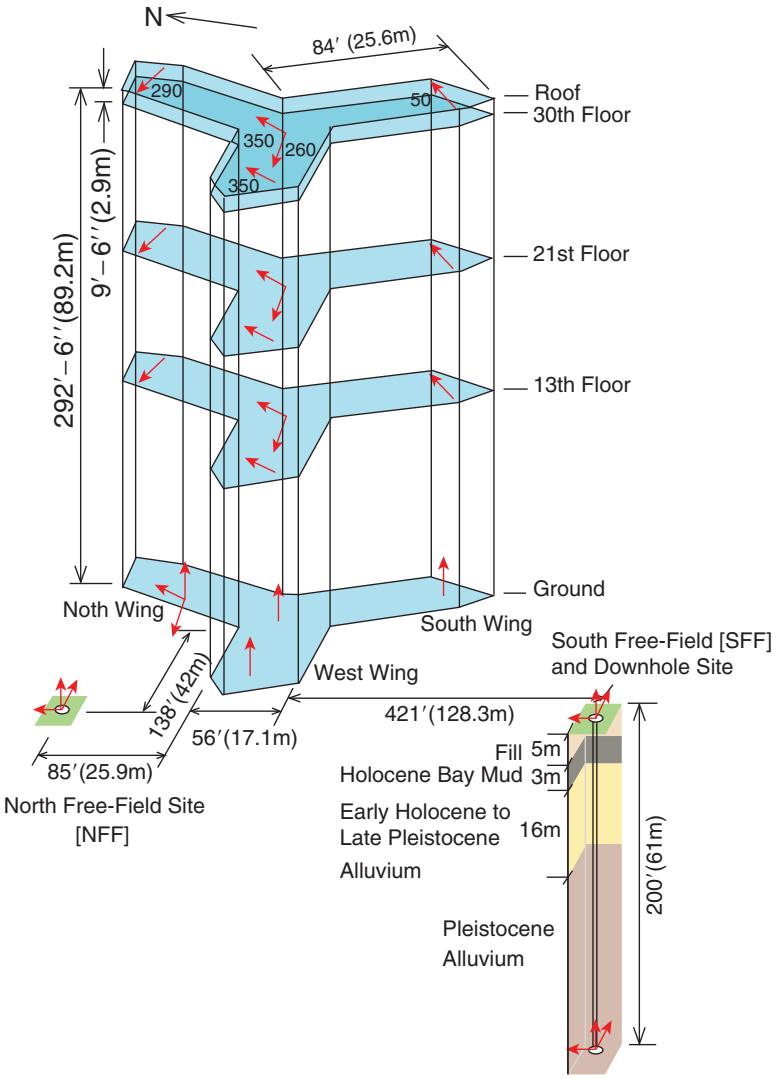

Fig. 1.7.1 A three-dimensional schematic of the building array with integrated surface and downhole array. Red arrows indicate sensor locations and orientations. The tri-axial downhole accelerograph was added after the 1989 Loma Prieta earthquake

The computed site transfer function, corresponding to the shear-wave velocity profile in Figure 1.7.2, using Haskell's shear-wave propagation method (Haskell, 1953, 1960) and coded by C. Mueller (2002, personal communication) is also provided in Figure 1.7.2, and indicates a site frequency at approximately 0.7 Hz. A detailed approach to identification of site frequency from site geotechnical logs as well as building response records are presented elsewhere (Çelebi, 2003).

1.7.2.3 Design spectra and significant shaking experienced

To date, the most significant shaking recorded by the building arrays was during the 1989 Loma Prieta (LPE), CA earthquake ($M_s = 7.1$). The data set from LPE is extensively used in several studies as well as in this investigation that specifically dwells upon the variation of fundamental period with level of shaking. As previously mentioned, the building was not damaged.

Responses of the building and the surface free-field recorded during the strong shaking caused by the LPE earthquake exhibit distinct amplification of motions (Figure 1.7.3a) at the site of the building as compared to the motions at Yerba Buena Island, both approximately 100 km (and at similar azimuths) from the epicenter of the LPE. The east-west components of acceleration recorded at the roof and the ground floor of the structure and at the associated free-field station (SFF in Figure 1.7.1) are shown in Figure 1.7.3a. The motion at Yerba Buena Island (YBI), the closest rock site, had a peak acceleration of 0.06 g, and is also shown for comparison. The response spectra (Figure 1.7.3b) clearly demonstrate that the motions at Emeryville (SFF) were amplified by as much as five times when compared with YBI. This is also inferred by the amplitude of the peak accelerations (0.26 g for SFF and 0.06 g for YBI). Furthermore, the differences in peak acceleration at SFF

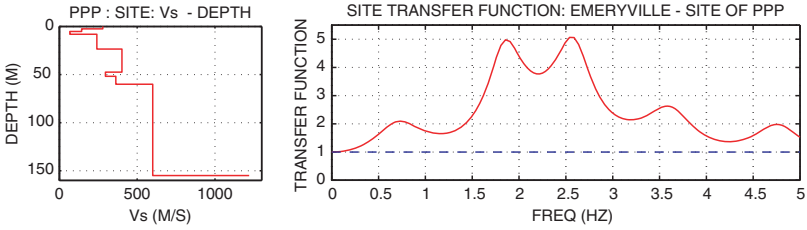

Fig. 1.7.2 Shear-wave velocity profile and the computed site transfer function. 0.7 Hz is the fundamental frequency and other peaks belong to higher modes

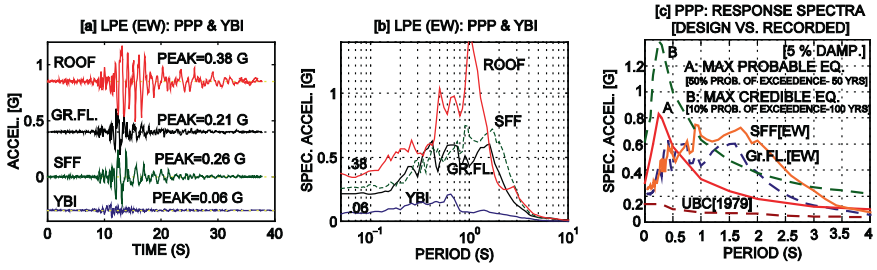

Fig. 1.7.3 (a,b) Amplified (EW) motions and their corresponding response spectra (5% damped) at the South Free-Field (SFF), ground floor and roof of the Pacific Park Plaza array as compared to the motions at Yerba Buena Island (YBI) at approximately the same epicentral distance as PPP. (c) Design response spectra and response spectra of recorded motions at the ground floor and SFF of Pacific Park Plaza. Also shown is the 1979 UBC response spectrum for comparison. [Note: Curve B is for 10% damping]

(0.26 g) and at the ground floor of the building (0.21 g) (Figure 1.7.3a) suggest the possibility of significant soil-structure interaction. Figure 1.7.3c shows a comparison of actual response spectra with site-specific design response spectra (based on the probabilistic earthquakes related to levels of performance) used in the design of the building: (a) the maximum probable earthquake (50% probability of being exceeded in 50 years with 5% damping) anchored at zero period acceleration (ZPA) of 0.32 g. [curve A in Figure 1.7.3c], and two maximum credible earthquakes both with 10% damping but 10% probability of being exceeded in (b) 100 years (ZPA of 0.63 g) [Curve B in Figure 1.7.3c] and (c) 50 years [ZPA of 0.53 g][1]. The spectra of the EW components of recorded motions at the ground floor and SFF are also shown in Figure 1.7.3c. At 100 km from the epicenter, even though the recorded EW peak acceleration at SFF (0.26 g) is smaller than the ZPA of the postulated maximum probable earthquake (0.32 g), the spectral accelerations of the EW component of SFF is considerably higher than the maximum probable earthquake for periods >0.6 s – that is, practically the first three modes of the building. This implies that, when large earthquakes occur closer to the structure, the level of shaking and the response spectra of motions are likely to be higher (for some period bands) than the design response spectra, and, in many cases, the code design response spectrum (e.g. the 1979 Uniform Building Code).

1.7.3 Summary of studies related to the building

1.7.3.1 Data sets

Extensive data sets from this building include not only the Loma Prieta earthquake response data but also those from smaller earthquakes and from forced and ambient vibration tests (Stephen et al., 1985; Çelebi et al., 1993). Table 1.7.1 summarizes the events (including LPE) that have been recorded by the building array and are used in this study. Those related to LPE and test data are summarized in Table 1.7.2.

1.7.3.2 Pre-1991 data sets including LPE and studies

The building has been studied in detail or as part of a larger investigation by several researchers (Çelebi and Safak, 1992; Safak and Çelebi, 1992; Anderson et al., 1991; Bertero et al., 1992; Kagawa and Al-Khatib, 1993; Kagawa et al., 1993; Aktan et al., 1992; Kambhatla et al., 1992; Çelebi, 1992, 1998). Using different methods, including spectral analyses, system identification techniques (Çelebi, 1998), and mathematical models, the majority of the investigators are in agreement that, for the 1989

[1] Not shown in the figure.

Table 1.7.1 Events that have been recorded by the PPP arrays

Event/Date	UTC	Lat. (N)/Long. (E)	Dist. (km)	Azim. (deg)	Depth (km)	Mag.
Loma Prieta 10/18/1989	04:15	37.036 −121.883	96	157	18.0	M_s 6.9
El Cerrito 12/04/1998	12:16	37.920 −122.290	9	4	6.8	M_w 4.0
Yountville 09/03/2000	08:36	38.379 −122.413	61	350	10.1	M_w 5.0
Piedmont 09/05/2003	01:39	37.845 −122.222	7	85	12.4	M_w 3.9
Berkeley 03/02/2006	06:08	37.863 −122.245	5	96	11.4	M_d 2.8

Table 1.7.2 Peak accelerations and system identification results for (Pre-1991) PPP data

	Peak accelerations (A[g]))			
	Loma Prieta Eq. (1989) [see refs]		Low-Amp. tests & analyses [see refs]	
	NS	EW	NS	EW
Roof	0.24	0.38	<0.01	<0.01
Gr. Fl.	0.17	0.21	<0.01	<0.01
FF	0.21	0.26	–	–
Dynamic characteristics (system identification)				
f_o (Hz)	0.38	0.38	0.48–0.59	
T_o (s)	2.63	2.63	1.69–2.08	
$\xi(\%)$	11.6	15.5	0.6–3.4	

Loma Prieta earthquake data, the predominant three response modes of the building and the associated frequencies (periods) are 0.38 Hz (2.63 s), 0.95 Hz (1.05 s), and 1.95 Hz (0.51 s).

The available free-field strong motion recording is pertinent to the convincing identification of the site frequency. Figures 1.7.4a and b depict building accelerations recorded at the core of the top instrumented level, at the core of the ground floor and the associated south free-field of the three-winged building. Corresponding amplitude spectra are provided in Figures 1.7.4c and d. The first three modal structural frequencies (periods) clearly identified from the recordings are 0.38, 0.95 and 1.95 Hz (2.63, 1.05, 0.34 s). The peak at 0.7 Hz that appears in the amplitude spectra of the roof also appear as the dominant peak in the amplitude spectra of the ground floor and the south free-field (SFF). However, this peak at 0.7 Hz disappears in the spectral ratios calculated from the amplitude spectra of the roof and ground floor as depicted in Figures 1.7.4e and f. This indicates that 0.7 is the site frequency as, although it appears in the roof spectra, it cancels out when ratios are calculated.

These three modes of the building are torsionally-translationally coupled (Çelebi, 1998) and are also depicted in the cross-spectra (S_{xy}) of the orthogonal records obtained from the roof, ground floor and SFF (the south free-field site) and the normalized cross-spectra of the orthogonal records (Figure 1.7.5). The site frequency

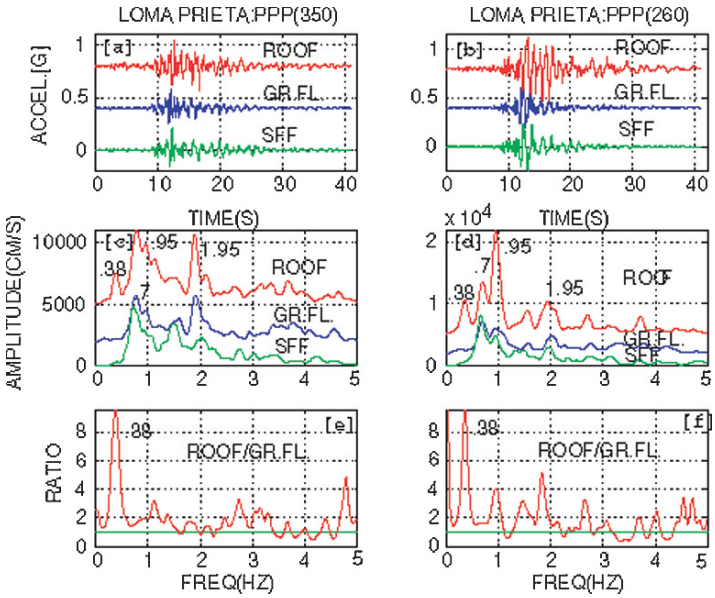

Fig. 1.7.4 (a,b) Recorded orthogonal accelerations at the roof, ground floor and south free-field of Pacifica Park Plaza, (c,d) corresponding amplitude spectra and (e,f) ratios of amplitude spectra

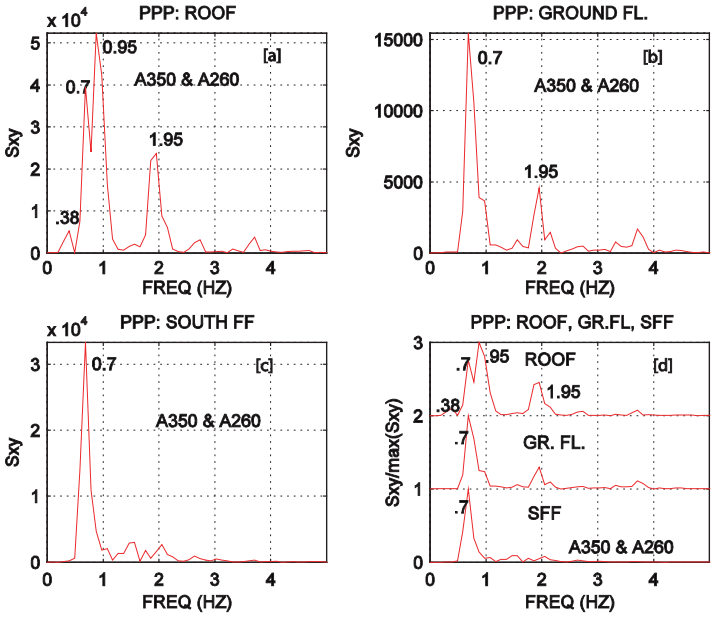

Fig. 1.7.5 Cross-spectra of orthogonal motions at the [a] roof, [b] ground floor, [c] free-field of PPP, and [d] the normalized cross-spectra depicting structural and site frequency peaks

at 0.7 Hz (1.43 s) observed in the cross-spectrum of the roof (Figure 1.7.5a) appears as the dominant peak in the cross-spectra of the ground floor and the south free-field (SFF) (Figure 1.7.5b and c). Figure 1.7.5d shows a summary of Figures 1.7.5a–c. The site frequency of 0.7 Hz has been also confirmed by the wave propagation method using site borehole data by Gibbs and others (1994) as shown in Figure 1.7.2. Detailed justifications of the site frequency as determined from this set of records are reported in Çelebi (2003).

Dynamic characteristics of the building extracted from the data sets are summarized in Table 1.7.2 and show considerable differences in the fundamental frequency determined from strong shaking versus low-amplitude shaking and analyses. The differences are attributed to SSI effects during strong shaking (Çelebi, 1998; Kagawa and Al-Khatib, 1993; Kagawa et al., 1993, Aktan et al., 1992; Kambhatla et al., 1992), and frequencies from recorded motions can be matched when SSI is incorporated into the mathematical models (Kagawa et al., 1993; Kagawa et al., 1993). Furthermore, a study of the building for dynamic-pile-group interaction (Aktan et al., 1992; Kambhatla et al., 1992) indicates that there is significant interaction. The study shows that computed responses of the building using state-of-the-art techniques for dynamic-pile-group interaction compares well with the recorded responses. Clearly, the mathematical models developed at that time needed improvements (Stephen et al., 1985). This conclusion could only be reached because we have recorded on-scale motions.

In addition, system identification techniques, when applied to the records of this building, yielded very large damping ratios corresponding to the 0.38-Hz first-mode frequency. These are 11.6% (north-south) and 15.5% (east-west) [Table 1.7.2] (Çelebi, 1996, 1998). Such unusually high damping ratios have been attributed to radiation damping that commonly occurs for buildings with large mat foundations in relatively soft geotechnical environment (Çelebi, 1996).

Anderson and others (1991) compared the design criteria, code requirements, and the elastic and nonlinear dynamic response of this building due to the earthquake. They also found the fundamental frequency of the building to be ∼0.37–0.39 Hz. However, contrary to others, but based only on comparison of ground level motions with those at the free-field, they concluded that soil-structure interaction was insignificant for this building during this earthquake.

1.7.3.3 Recent data, analyses and discussion

Analyses of subsequent data sets listed in Table 1.7.1 show that for shaking much lower than caused by LPE, the fundamental frequency (period) is significantly lower (longer) than that determined using the LPE record. In Figure 1.7.6, for each of the 1998, 2000, 2003 and 2006 earthquakes (Table 1.7.1), plots of acceleration time history and corresponding amplitude spectra are shown for the 30th floor and ground floor of the building. Consistently, a structural fundamental frequency (period) of ∼0.48 Hz (∼2.08 s) is identified. This identified frequency is

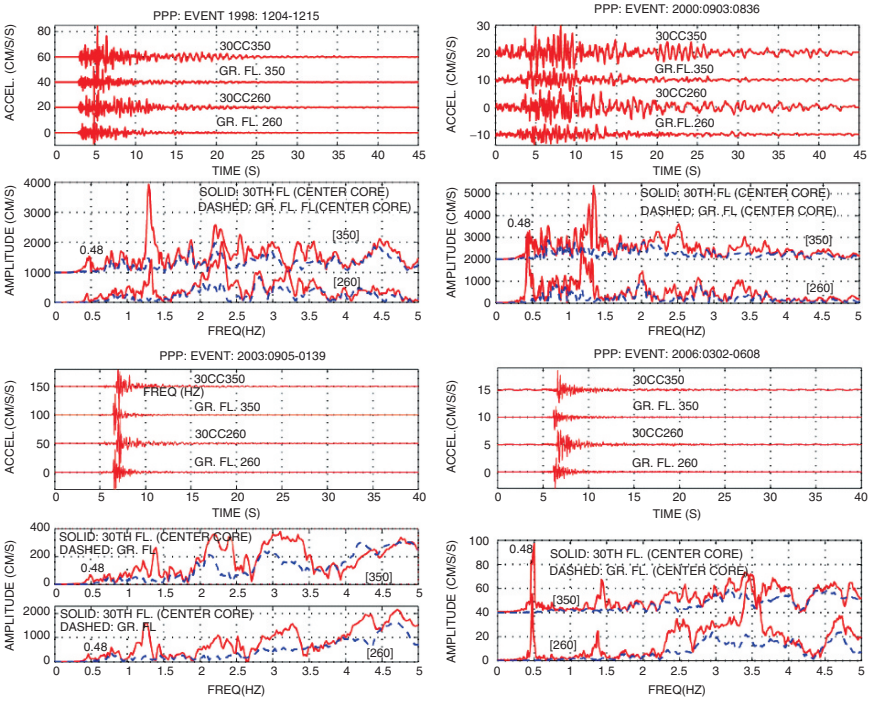

Fig. 1.7.6 Recorded accelerations at 30th and ground floors and corresponding amplitude spectra

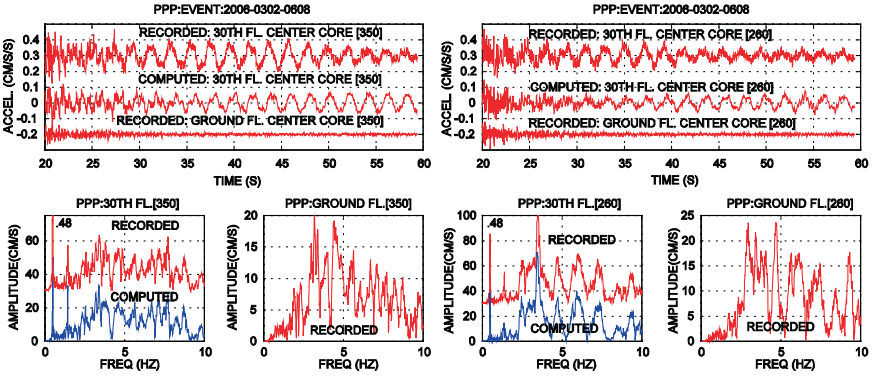

Fig. 1.7.7 System identification for 2006 event using 40-s window of acceleration data. Ground level motions are used as input and 30th floor motions are used as output

also confirmed by system identification method. For the sake of brevity, only a sample system identification plot is presented for the 2006 event (Figure 1.7.7) which clearly shows the fundamental frequency at 0.48 Hz. For all events and tests to date, Table 1.7.3 summarizes the level of shaking (acceleration in g's) and identified

Table 1.7.3 Summary – Events, levels of shaking (in g's) and identified dynamic characteristics

	Tests, analyses or events											
	1985		1989	1990	1998 EQ.		2000 EQ.		2003 EQ.		2006 EQ.	
	Tests/analyses		LPE	Tests	(1204_ 1216)		(0903-0836)		(0905_0139)		(0302_0608)	
	Peak accelerations (A[g]) [NS & EW represents 350° and 260° respectively]											
	NS/EW	*NS*	*EW*	NS/EW	NS	EW	NS	EW	NS	EW	NS	EW
Roof	<0.01	0.24	0.38	<0.01	0.025	0.016	0.01	0.007	0.056	0.067	0.004	0.003
Gr.Fl.	<0.01	0.17	0.21	<0.01	0.016	0.037	0.005	0.004	0.037	0.041	0.003	0.003
SFF	–	0.21	0.26	–	0.022	0.028	–	–	0.039	0.031	0.003	0.006
	Dynamic characteristics (system identification & spectral analyses)											
f_o(Hz)	0.59	0.38	0.38	0.48	0.48	0.48	0.48	0.48	0.48	0.48	0.48	0.48
T_o (s)	1.69	2.63	2.63	2.08	2.08	2.08	2.08	2.08	2.08	2.08	2.08	2.08
ξ(%)	0.6–3.4	11.6	15.5	0.6–3.4	–	–	–	–	0.5–2.	0.5–2.	0.5–2.	0.5–2.

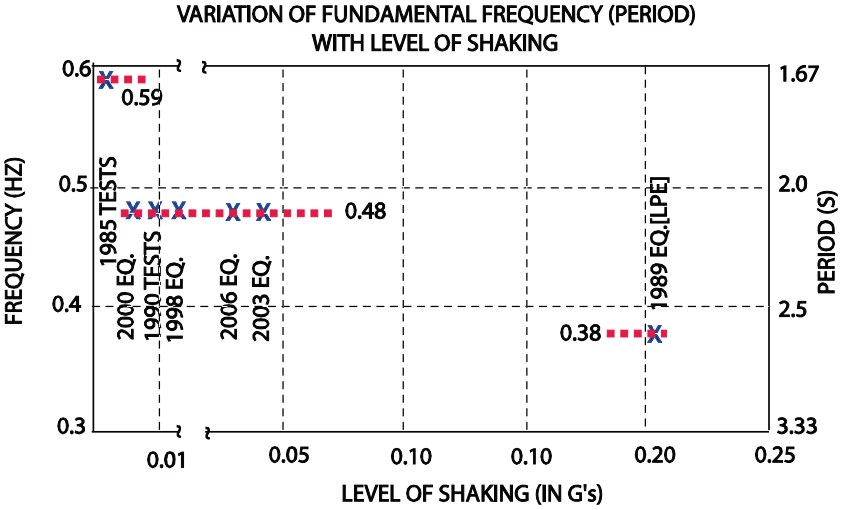

Fig. 1.7.8 Plot showing variation of fundamental frequency with level of shaking (in g's)

dynamic characteristics (frequencies and damping ratios). These results are also graphically depicted in Figure 1.7.8. Both Table 1.7.3 and Figure 1.7.8 complements and reinforces the argument that the fundamental frequency varies significantly with the level of shaking even if the building may not be damaged. In the case of Pacific Park Plaza Building, the variation is attributable to SSI.

As noted in this paper, there is significant difference between the 0.38 and 0.48 Hz frequencies (approximately 20% less for LPE if 0.48 Hz is considered as the baseline and even more if 0.59 Hz is considered). In many studies, establishment of baseline frequency can be an issue and therefore ought to be carefully assessed to prevent erroneous interpretation. Another point to be made is that, in reaching the conclusions in this paper, most of the data analyses were made with data with time

increments of 0.005 s. It was observed during the data analyses that overdecimating and oversmoothing the data can lead to significant differences in the assignments of values to the fundamental frequencies.

1.7.4 Summary of site characteristics

In addition to the site dynamic characteristics computed from geotechnical logs (Figure 1.7.2) and also identified from building records for LPE only (Figures 1.7.5c–d), site dynamic characteristics are herein comparatively presented for strong and weak shaking and computed using Nakamura's Method (1989, 2000). In absence of reference rock sites, this method facilitates computing transfer function as the ratio of amplitude spectra of horizontal to vertical components of motion at a station [R = A(horizontal)/A(vertical)]. Figures 1.7.9 and 1.7.10 respectively shows transfer function for the LPE and 1998 events. The figures also show the amplitude spectra used in computing these transfer functions. Both events indicate fundamental site frequencies that are similar and around 0.7 Hz. Furthermore, for both the strong shaking record of LPE, the weak motion record of 1998 event, second (1.2–1.4 Hz) and third frequencies (2.0 Hz) are also similar. It can be qualitatively stated that for these two (strong and weak) motions, the site frequencies are quite similar. It can be added that possibly due to absence of any significant non-linearity of the site conditions, the frequency does not vary significantly.

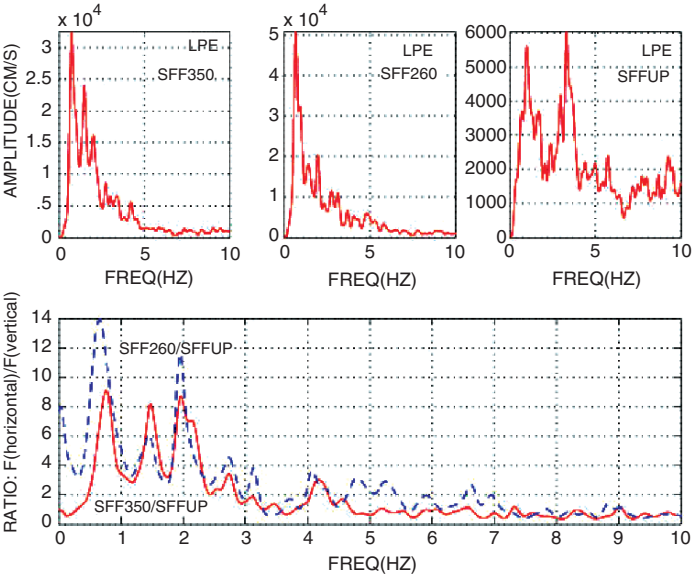

Fig. 1.7.9 (top frames) Amplitude spectra for horizontal and vertical motions for the LPE record. (bottom) Transfer function using Nakamura's method

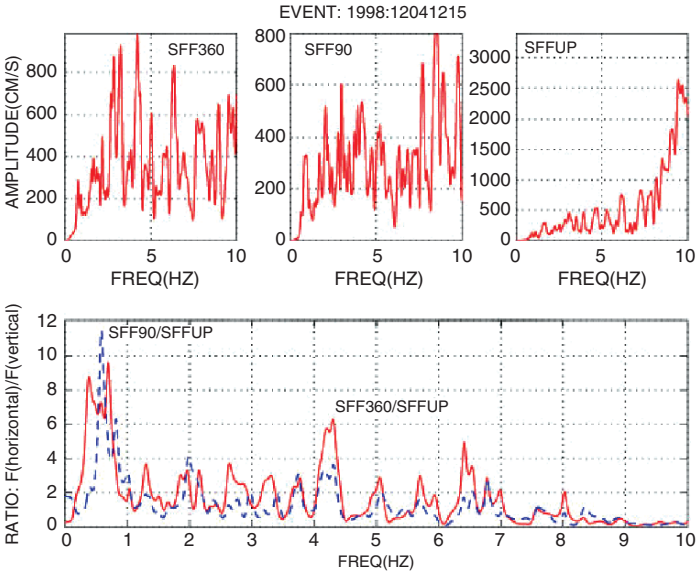

Fig. 1.7.10 (top frames) Amplitude spectra for horizontal and vertical motions for the 1998 event. (bottom) Transfer function using Nakamura's method

1.7.4.1 Summary characteristics for five building

In order to further postulate that variation of structural frequencies with amplitude of shaking is a consistent and important phenomenon that has wide applicability implications, identified dynamic characteristics are presented for five building (including PPP) comparatively for strong and weak motions. Table 1.7.4 provides general descriptive information about the buildings as well as the recorded LPE peak accelerations for the ground floor and roof of each building.

Table 1.7.5 provides summary information that shows comparative dynamic characteristics for strong motion (LPE) and weak motion (ambient) data that was acquired post-LPE (Marshall et al., 1992). Table 1.7.5 also included for two of the buildings, dynamic characteristics determined from tests or analyses prior to LPE. Two distinctive results (or conclusions) are cited herein:

1. There are significant differences in identified fundamental frequencies from strong shaking data s compared to those from ambient data. These differences are too large to ignore and leads to conclusive statement that fundamental frequencies (periods) identified low-amplitude shaking cannot be used in lieu of those identified from strong shaking.
2. Similarly, there are significant differences in critical damping percentages determined from strong shaking data as compared to those determined from ambient data. Naturally, higher damping percentages are identified from strong shaking data.

Table 1.7.4 Building characteristics and Loma Prieta peak accelerations (Data from Marshall et al., 1992 and Çelebi 1996)

Building (instrumentation administrator in paranthesis)	Comments	N_A/N_B [H] (m)	D (m)	n	LPE Peak accel. (g)		
					Nom. Dir.	Gr. Flr.	Roof
Pacific Park Plaza – PPP (USGS) N = 350°	Reinforced concrete moment resisting frame (1.5 m thick oncrete mat on piles)	30/1 [94]	97	21	NS EW UP	0.17 0.31 0.06	0.24 0.38
Transamerica Bldg – TRA (USGS) N = 351°	Steel frame, 48th floor is the top occupied floor (2.75 m thick concrete mat – no piles)	60/3 [257]	97	22	NS EW UP	0.11 0.12 0.07	0.29 0.31
Santa Clara County Office Bldg. – (SCOB) (CSMIP), N = 337°	Moment resisting steel frame (concrete mat – no piles)	12/1 [57]	35	22	NS EW UP	0.10 0.09 0.10	0.34 0.34
San Bruno Office Bldg. – SBR (CSMIP) N = 335°	Reinforced concrete moment resisting frame (individual spread footing)	6/0 [24]	81	13	NS EW UP	0.14 0.11 0.12	0.25 0.32
California State University Hayward Admin. Bldg – CSUH (CSMIP) N = 320°	Steel Moment-frame core; exterior reinforced concrete moment frame (0.45 m thick slab on grade and bearing piles)	13/0 [61]	70	16	NS EW UP	0.07 0.09 0.05	0.15 0.24

The reference building orientation in degrees clockwise from true north is different from adopted nominal north-south and east-west directions. Number of floors (N_A, above ground level; N_B below ground level).
H = height of building, D = Distance to epicenter, number of channels of accelerometers (during this study), N = orientation of reference north (clockwise from true north).

1.7.5 Conclusions

Recorded responses of structures and free-field sites serve to expose unusual and unexpected response characteristics that require detailed analyses in order to improve or validate analytical models and design processes and to identify possible methods for retrofit of the structure if necessary. Significant findings, although not limited by the list below, are summarized as:

1. It is shown that there are significant differences in the fundamental frequencies of Pacific Park Plaza Building determined from strong shaking as compared to low-amplitude shaking. Thus, the variation of fundamental frequency (period) is dependent on the amplitude of shaking.

Table 1.7.5 Dynamic characteristics of five buildings (Data from Marshall et al., 1992; Çelebi, 1996)

Building	Nominal direction	Pre-LPE test & analyses		LPE Data		Post-LPE Ambient	
		f/T	ξ	f/T	ξ	f/T	ξ
Pacific Park Plaza [PPP]	NS	0.59 (1.70)	2.6	0.38 (2.63)	11.6	0.48 (2.08)	0.6
	EW	0.59 (1.70)	2.6	0.38 (2.63)	15.5	0.48 (2.08)	3.4
Transamerica Building [TRA]	NS	0.34 (2.94)	0.9	0.28 (3.57)	4.9	0.34 (2.94)	0.8
	EW	0.34 (2.94)	1.4	0.28 (3.57)	2.2	0.32 (3.12)	1.4
Santa Clara County Office Building [SCCOB]	NS			0.45 (2.22)	2.7	0.52 (1.92)	–
	EW			0.45 (2.22)	2.7	0.52 (1.92)	–
San Brunp Office Building [SBR]	NS			1.17 (0.85)	7.2	1.72 (0.58)	2.2
	EW			0.98 (1.02)	4.1	1.41 (0.71)	2.3
California State Univ. (Hayward) Administration Building [CSUH]	NS			0.76 (1.32)	3.4	0.92 (1.09)	0.6
	EW			0.76 (1.32)	2.3	0.86 (1.16)	0.6

f = frequency (Hz), T = Period (s), ξ = damping (%). LPE = Loma Prieta Earthquake.

2. Also, the modal damping ratios (for the defined level of shaking) which otherwise are difficult to determine as they are not constant and increase with the level of shaking.
3. Soil-structure interaction, although neglected in the design-analysis process of this building and as is also neglected for most non-critical buildings, plays a significant role in altering dynamic characteristics and therefore the response of buildings. For this building, the variation of the fundamental period (frequency) is quite substantial.
4. In addition, also for this building, using several approaches including strong and weak motions, site frequency is clearly identified for strong and weak motions. However, the variation of site frequency is insignificant.
5. Finally, particularly in areas of high seismicity, deployment of seismic monitoring systems particularly for complex and irregular buildings and other types of structures are strongly encouraged since records obtained during future events reveal response characteristics that are not always envisioned or taken into account during design and analysis processes.

The fundamental frequencies of the study building (PPP) and additional four other buildings, as determined from strong and low-amplitude shaking exhibit significant variations that are dependent on the amplitude of shaking. Therefore, frequencies determined from weak motions cannot/should not be used in lieu of that from strong shaking. In case of PPP, soil-structure interaction (SSI), although neglected

in the design-analysis process of PPP, plays a significant role in altering the apparent dynamic characteristics.

The modal damping ratios increase with the level of shaking.

For PPP associated site, using several approaches including strong and weak motions, site frequency is clearly identified from strong and weak motions. The variation of site frequency is insignificant.

Finally, deployment of seismic monitoring systems particularly for complex and irregular buildings and other types of structures are strongly encouraged.

References

Aktan, H., Kagawa, T., Kambhatla, A., and Çelebi, M. (1992). "Measured and analytical response of a pile supported building," in Proceedings of the Tenth World Conference on Earthquake Engineering: A.A. Balkema, Rotterdam, v. 3, pp. 1791–1796.

Anderson, J.C., Miranda, E., Bertero, V.V., and Kajima Project Research Team. (1991). "Evaluation of the seismic performance of a thirty-story RC building", Earthquake Engineering Research Center, University of California, Berkeley, Report: UCB/EERC-91/16, 254 p.

Bertero, V.V., Miranda, E., and Anderson, J.C. (1992). "Evaluation of seismic response of two RC buildings," in Structures Congress '92 compact papers: American Society of Civil Engineers, New York, pp. 408–411.

Calvi, G.M., Pinho, R., and Crowley, H. (2006). "State-of-the-knowledge on the period elongation of RC buildings during strong ground shaking", PROC (CD) First European Conference on Earthquake Engineering and seismology, Geneva, Switzerland, 3–8 Sept. 2006.

Çelebi, M. (1992). "Highlights of Loma Prieta responses for four tall buildings", in Proceedings of the Tenth World Conference on Earthquake Engineering, A.A. Balkema, Rotterdam, v. 7, pp. 4039–4044.

Çelebi, M. (1996). "Comparison of damping in buildings under low-amplitude and strong motions", Journal of Wind Engineering and Industrial Aerodynamics, 59, 309–323.

Çelebi, M. (1998)."Performance of Building structures – A Summary", in The Loma Prieta, California, Earthquake of October 17, 1989 – Building Structures (M. Çelebi, editor), USGS Prof. Paper 1552-C, pp. c5–c76.

Çelebi, M. (2003). "Identification of Site Frequencies from Building Records", Journal of EERI, *Earthquake Spectra*, 19(1), 1–23.

Çelebi, M., and Safak, E. (1992). "Recorded Seismic Response of Pacific Park Plaza: Part I – Data and Preliminary Analysis." ASCE Journal of Structural Engineering, June 1992.

Çelebi, M., Phan, L.T., and Marshall, R.D. (1993). "Dynamic characteristics of five tall buildings during strong and low-amplitude motions," Journal of the Structural Design of Tall Buildings (Wiley), 2, 1–15.

Clinton, J.F., Bradford, S.C., Heaton, T.H., and Favela, J. (2006). "The Observed Wander of the Natural Frequencies in a Structure", Bulletin of the Seismological Society of America, 96(1), 237–257, Feb. 2006.

Dunand, F., Guegen, P., Bard, P.-Y., Rodgers, J., and Celebi, M. (2006). "Comparison of the dynamic parameters extracted from weak, moderate and strong motion recorded in buildings", PROC (CD) First European Conference on Earthquake Engineering and seismology, Geneva, Switzerland, 3–8 Sept. 2006.

Gibbs, J.F., Fumal, T.E., and Powers, T.J. (1994). Seismic velocities and geologic logs from borehole measurements at seven strong motion stations that recorded the 1989 Loma Prieta, California, earthquake: U.S. Geological Survey Open-File Report 94–222, 104 p.

Haskell, N.A. (1953). "The dispersion of surface waves on multilayered media", Bulletin of the Seismological Society of America, 43(1), 17–34.

Haskell, N.A. (1960). "Crustal reflection of plane SH waves", Journal of Geophysical Research, 65(12), 4147–4150.

International Conference of building Officials (1979). Uniform Building Code [1979 Edition]: Whittier, California.

Kagawa, T. and Al-Khatib, M.A. (1993). "Earthquake response of a 30-story building during the Loma Prieta earthquake", in Third Int'l Conf. On Case Histories of Geotechnical Engineering, Univ. of Missourin-Rolla, pp. 547–553.

Kagawa, T., Aktan, H., and Çelebi, M. (1993). "Evaluation of soil and structure model using measured building response during the Loma Prieta earthquake": Report of the Dept. of Civil Engineering, Wayne State University, Detroit, Michigan, 169 p.

Kambhatla, A., Aktan, H.M., Kagawa, T., and Çelebi, M. (1992). "Verification of simple soil-pile foundation-structure models," in Structures Congress'92, ASCE, NY, pp. 721–724.

Marshall, R.D., Phan, L.T., and Çelebi, M. (1992). "Measurement of Structural Response Characteristics of Full-Scale Buildings: Comparison of Results from Strong-Motion and Ambient Vibration Records" (Interagency Report – NIST, Gaithersburg, MD), NISTIR 4884, October 1992.

Nakamura, Y. (1989). "A Method for Dynamic Characteristics Estimation of Subsurface using Microtremor on the Ground Surface", QR of RTRI, February 1989, vol. 30, no. 1, 25–33.

Nakamura, Y. (2000). "Clear Identification of Fundamental Idea of Nakamura's Technique and its Applications", CD-ROM Proceedings of the 12th World Conference on Earthquake Engineering, Auckland, New Zealand.

Safak, E. and Çelebi, M. (1992). "Recorded Seismic Response of Pacific Park Plaza: Part II – System Identification." ASCE Journal of Structural Engineering, June 1992.

Stephen, R.M., Wilson, E.L., and Stander, N. (1985). "Dynamic properties of a thirty-story condominium tower building", Univ. of California, Berkeley, EERC Report 85-03, 100 p.

Todorovska, M., Trifunac, M., and Hao, T.-Y. (2006). "Variation of apparent Building Frequencies – Lessons from Full-Scale Earthquake Observation," PROC (CD) First European Conference on Earthquake Engineering and seismology, Geneva, Switzerland, 3–8 Sept.

Chapter 1.8
HVSR Technique Improvement Using Redundant Wavelet Transform

Filippos Vallianatos and George Hloupis

Abstract In this study we demonstrate the use of Wavelet Transform (WT) as an improvement tool for the horizontal to vertical spectral ratio (HVSR) technique. Since the use of non-stationary transients in microtremor signals remains an open question we investigate the effect of long duration undetectable (by amplitude thresholding methods) transients in HVSR estimation. For the urban areas, where the existence of these types of transients is intense, we used the WT in order to isolate undetectable transients. A number of examples with HVSR improvement are also presented.

Keywords HVSR · Reduntant Wavelet Transform · Non-stationarities

1.8.1 Introduction

During the last two decades Horizontal-to-Vertical-Spectral-Ratio (HVSR) has proved an invaluable tool for estimating a site's fundamental (f_0) frequency using cheap, rapid and fair accurate method. Since its first proposal by Nogoshi & Igarashi (1970, 1971) and latest revision by Nakamura (1989) the HVSR method widely used by many researchers but without following a de-facto standard for the stationarity of the selected microtremor signal. Successful efforts have been made (Bard, 1999; SESAME, 2004) under the frame of providing guides and rules for signal acquisition and processing. An open question that remains unanswered is that if a study must use only the stationary part or the whole microtremor signal. The problem arises since the main part of HVSR method is the spectral ratio which by default

F. Vallianatos (✉)
Department of Natural Resources and Environment, Technological Educational Institute of Crete, Romanou 3, 73133, Chania, Greece
e-mail: fvallian@chania.teicrete.gr

G. Hloupis
Department of Electronic and Computer Engineering, Brunel University, Uxbridge, Middlesex, UB83PH, United Kingdom

M. Mucciarelli et al., (eds.), *Increasing Seismic Safety by Combining Engineering Technologies and Seismological Data,* NATO Science for Peace and Security Series C: Environmental Security,

assumes stationarity. Some studies (Mucciarelli, 1998; Mucciarelli et al., 2003) showed that HVSR could not affected by using non-stationary noise to analyzed microtremor signals since others (Horike et al., 2001) reject the non-stationary part. There is no doubt that a method with less restriction is more attractive to a researcher but until today there are not enough proofs to use the whole microtremor signal. A step ahead to this direction was done by a recent study by Parolai and Merino (2006) who concluded that high amplitude, short duration, transients can be included in HVSR calculation without strongly affected the calculated f_0.

The use of HVSR method in urban areas and especially in densely populated areas seems to be the most demanding case since there will be artificial non-stationary signals from unknown sources which cannot be predicted. It's not unusual, even at late hours, these signals to have low amplitude (more or less than regular microtremors) and for this reason could not appear as common transients at a first view. This phenomenon identified in microtremor measurements that took place in several cities at Crete Island, Greece (Figure 1.8.1) and there were cases where these low amplitude but long duration non-stationary signals alter the f_0 at measured site.

Inspired by this idea, in the current study, we investigate if and how the low amplitude and long duration non-stationary signals affect the HVSR method and moreover we propose the wavelet transform (WT) to identify these transients. First, by using synthetic non-stationary signals added to real mictrotremor recordings,

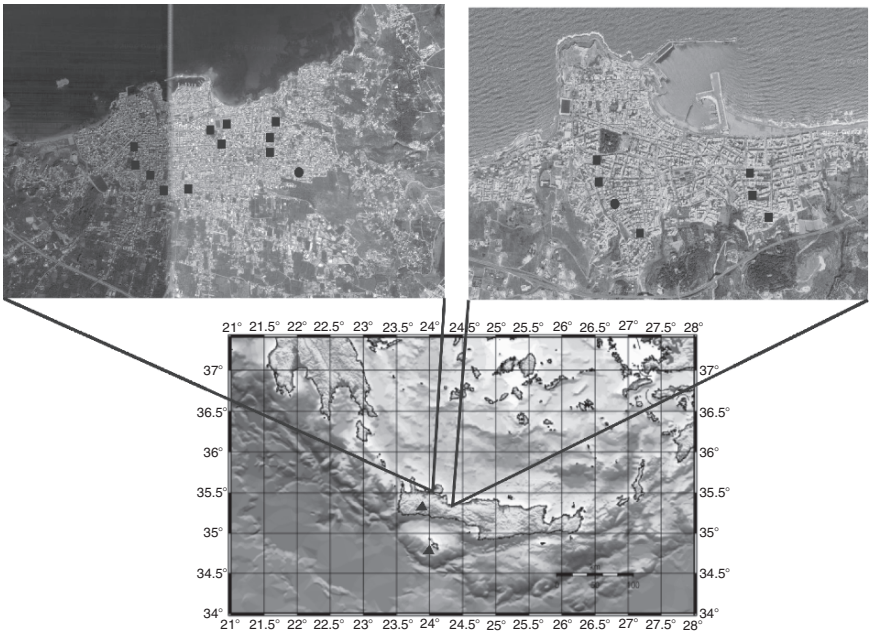

Fig. 1.8.1 Study areas: Chania (top left) and Rethymno (top right) at Crete Island (bottom). Triangles indicate RX sites, circles X sites and squares KRX sites

we investigate the detection capabilities of well known STA/LTA (Stewart, 1977) algorithm. Then we investigate the quantitative impact of non-stationarity in HVSR results. Next we propose the use of a specific WT as a non-stationary detection tool. Finally we present sites where the HVSR results differ from results derived by other methods and apply the WT in order to reveal undetectable non-stationarites.

1.8.2 Fundamentals of wavelet transform

A WT involves the decomposition of a signal function or vector into simpler, fixed building blocks at different scales and positions. Grossman and Morlet (1984) proposed the continuous WT which allows the decomposition of a signal into contributions from both the space and scale domains based on the invariance under the affine group, namely, translation and dilation. In 1989, Mallat (1989) introduced the multi-resolution signal decomposition (MRSD) algorithm. Daubechies (1990) adopted this approach to construct families of compact supported wavelets and coupled it to quadrature mirror filtering. This provides a general way for constructing orthogonal wavelet bases and leads to the implementation of the fast wavelet transform_(FWT) algorithm. Coifman and Wickerhauser (1992) developed the automatic decomposition method which had a very strong influence on the development of wavelet theory.

Like Fourier transform (FT), WT operates on a signal $f(\lambda)$ and transforms it linearly from its domain (i.e. time domain) to a different one. In Fourier analysis, only the sine and cosine functions which are localized in frequency domain can be applied to a function. It has difficulty to process a function having components that are localized in the time domain. As a result, a small frequency change in FT produces changes everywhere in this domain. On the other hand, wavelet functions are localized both in frequency or scale and in time via dilations and translations of the mother wavelet, respectively. This leads to compact representation of large classes of functions and operators in the wavelet domain. Spectra with sharp spikes may well be approximated by substantially fewer wavelet basis functions compared to the sine and cosine functions adopted in Fourier analysis.

In a WT terminology, all basis functions $\Psi_{\alpha,b}(\lambda)$ can be derived from a mother wavelet $\Psi(\lambda)$ through the following dilation and translation processes Chui (1992):

$$\psi_{\alpha,b}(\lambda) = \alpha^{-1/2}\Psi\left(\frac{\lambda - b}{a}\right) \alpha, b \in \Re \text{ and } a \neq 0 \tag{1.8.1}$$

where a and b are, respectively, the scale and position parameters expressed in real number R. The basic idea of the WT is to represent any arbitrary function $f(\lambda)$ as a superposition of wavelets. The continuous wavelet transform of $f(\lambda)$ is given by

$$W_f(\alpha, b) = \int_{-\infty}^{+\infty} \psi_{\alpha,b}(\lambda) f(\lambda) d\lambda \tag{1.8.2}$$

with $a > 0$ and b having arbitrary values. The inverse continuous wavelet transform can be obtained through the following formula

$$f(\lambda) = \frac{1}{C_\psi} \int_0^{+\infty} \frac{da}{a^2} \int_{-\infty}^{+\infty} W_f(\alpha, b) \psi_{\alpha,b}(\lambda) db \tag{1.8.3}$$

where C_ψ is a constant depending only on ψ. In general, the representation in Equation (1.8.3) is redundant by using the continuous wavelet transform $W f_{a,b}$ Chui (1992). A particularly well studied topic is the construction of orthogonal wavelets for discrete signals to obtain a relevant compact non-redundant multi-scale representation. Like FT, decomposition of $f(\lambda)$ with respect to the wavelet function series $\{\Psi_{j,k}(\lambda)\}$ described by the following formula:

$$f(\lambda) = \sum_{j=-\infty}^{+\infty} \sum_{k=-\infty}^{+\infty} c_k^{'(j)} \psi_{j,\kappa}(\lambda) \tag{1.8.4}$$

Therefore, the signal is represented by a set of coefficients $\{c_k^{'(j)}\}$ in the wavelet domain $\{\Psi_{j,k}(\lambda)\}$ is defined by Equation (1.8.1) with $a = 2^j$, $b = 2^j k$ and j being the resolution level. The fast implementation method as developed by Mallat and Hwang (1992) for the discrete wavelet transform (DWT) has made the wavelet method as an effective tool for signal processing.

The DWT can be considered as a filtering technique under the terminology of signal processing. A wavelet basis is characterized by a particular set of numbers, called wavelet filter coefficients. The DWT treatment is to perform two related convolutions on the signal with one being a low-pass filter $H(=\{h_k\})$ and the other a high-pass filter $G(=\{g_k\})$. Then, the signal is converted into two bases with equal size, that is

$$c_k^{(j)} = \sqrt{2} \sum_n c_n^{(j-1)} h_{n-2k} \tag{1.8.5}$$

And

$$d_k^{(j)} = \sqrt{2} \sum_n c_n^{(j-1)} g_{n-2k} \tag{1.8.6}$$

The variables h_k and g_k in these equations denote the coefficients of the low-pass and high-pass filters.

In practice, DWT is commonly implemented using dyadic multirate filter banks (consisting of H and G filters mentioned earlier) which divide the signal frequency band into sub bands as shown in Figure 1.8.2.

At each scale, detail coefficients are generated from the output of high-pass filter since approximation coefficients are outputs from low-pass filters. In other words at each scale approximation captures low frequency trends since detail captures high frequency components. So the connection between wavelets and filter banks is that high-pass filter leads to wavelet function and low-pass to scaling function. A typical structure for signal decomposition is depicted in Figure 1.8.3 where a three scale DWT is performed using octave-band filter bank.

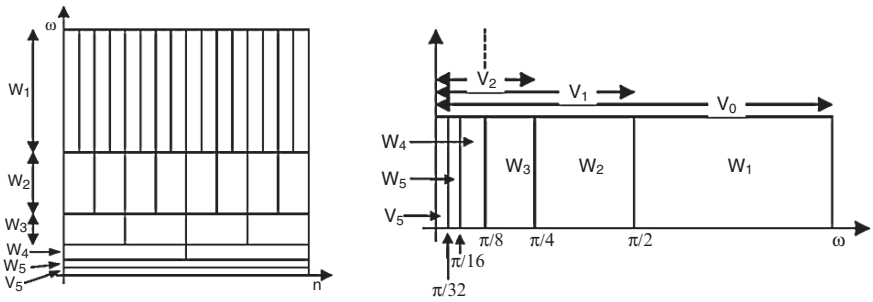

Fig. 1.8.2 DWT for $j = 5$ scales. Division of index-spectrum plane (left) and division of frequency spectrum using filter banks (right) (Provaznic, 2001)

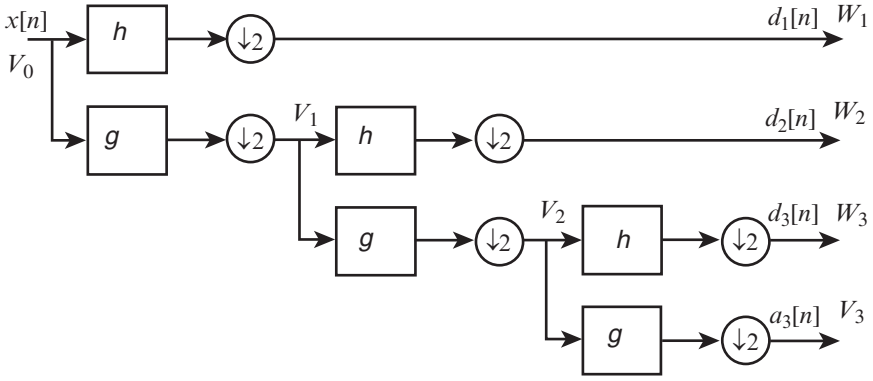

Fig. 1.8.3 A three scale DWT decomposition (Provaznic, 2001)

1.8.3 Practical considerations for DWT

When one begins a DWT analysis several issues arises since there is no "blind rule" that must be followed in order to get the results. Depending on the application and the nature of examined signal some consideration must be addressed. The boundary conditions, the number of levels, the choice of wavelet filter and sample size that is not power of two are some of them. In this section we give only the basic ideas behind these problems in order to prove the essence of a specific WT for the recording microtremor signals. For more details the reader is guided to Percival and Walden (2000).

1.8.3.1 Boundary effects

As already mentioned, DWT implemented by using filters. A filtering operation close the boundaries (the beginning and the end) of the time series $\{X_n : n = 0, 1, \ldots N-1\}$ assumes that is a periodic sequence with period N. This means that

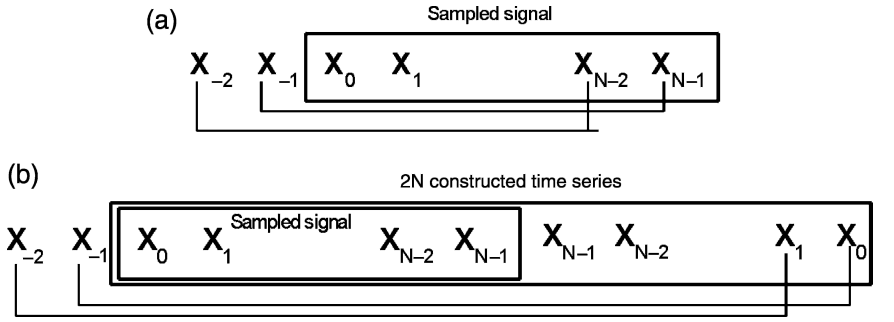

Fig. 1.8.4 (a): Corresponding surrogates for unobserved (X_{-1}, X_{-2}) and sampled $(X_0, \ldots X_{N-1}, X_{N-2})$ signal (top) and (b) Corresponding surrogates for unobserved (X_{-1}, X_{-2}) and 2N constructed time series $(X_0, \ldots X_{N-1}, X_{N-2}, X_{N-1} \ldots . X_0)$

is expected for X_{N-1}, $X_{N-2.} \ldots$ to be successful surrogates for unsampled values of process X_{-1}, X_{-2} that described by X as depicted in Figure 1.8.4a. This assumption holds only when the sample size is chosen appropriately otherwise is problematic especially when there is discontinuity between X_{N-1} and X_0. For example, a sampled signal with f_0 at 0.5 and 2 Hz would not affected by boundary conditions only if the sample size is equal to an integer multiple of 2. Percival and Walden (2000) found that boundary effects increased as the number of scales of WT increases but not in a proportional way. An effective technique to reduce boundary effects is to replace the time series X with a time series with length $2N$ consists of X along with the time reversed version of X as shown:

$$X^{[2N]} = X_0, X_1, \ldots, X_{N-2}, X_{N-1}, X_{N-1}, X_{N-2}, \ldots, X_1, X_0 \tag{1.8.7}$$

Using $X^{[2N]}$ constructed time series instead of X has the effect that the surrogates of unobserved signal's samples X_{-1}, X_{-2}.. are now the X_1, $X_2, \ldots$ of sampled signal, which is obvious that they present a lower mismatch possibility than before. A graphic representation of this fact is depicted in Figure 1.8.4b.

1.8.3.2 Number of levels

For a time series $\{X_n : n = 0, 1, \ldots N-1\}$ with sample size $N = 2^j$ the implementation algorithm for DWT will completed after j levels. Depending on the application, there is also a great possibility that the algorithm stop at level $J_0 < j$. In this case the DWT is called *partial DWT at level j*. Partial DWT are commonly used in practice because they provide the flexibility to specify a scale J_0 beyond which wavelet analysis of larger scales has no real interest. A reasonable selection of level J_0 is highly dependent from the application. Main idea under successful picking of J_0 is to set it in a way that scaling coefficients could have a meaningful association with phys-

ical scales. Setting J_0 too high will lead to large scales that will not provide useful information. On the other hand, setting J_0 too low will produce approximations that could not promote interesting features.

Another factor that will impact the choice of J_0 is the width L of the wavelet filter. This is because large L produces large filter widths for the higher level of $\overline{h}$ and $\overline{g}$ filters. For this reason an upper bound is $L_{J_0} \leq N \leq L_{J_0+1}$. This upper bound also ensures that details and approximation will decrease their influence by boundary conditions.

1.8.3.3 Choice of wavelet filter

The choice of wavelet filter is not a direct procedure and is always dependable from the application in use. A main factor for the selection of the wavelet filter is to define the aim of the analysis and then choose the appropriate wavelet filter. Although there are many studies using wavelets there are only few studies that provide step-by-step procedures (Torrence and Compo, 1998; Breiman, 1995).

In practice, two main considerations must be taken into account. First, there are many cases where wavelet filters with short widths ($L = 2, 4$ or 6) introduce artefacts in results producing unrealistic coefficients. On the other hand, wavelet filters with $L > 6$ has two main disadvantages:

- As L increases the number of coefficients that influenced from boundary conditions also increases.
- Computational requirement increase also.

The happy medium is the choice of the wavelet filter with smallest L that produces the most reasonable results. In other words there must be a pre-analysis procedure where the selection begins with quite small L and increases until an artefact free coefficient set is produced.

1.8.3.4 Handling non 2^J sample sizes

DWT (full or partial) designed to work with sample sizes of specific length. More specific, full DWT needs sample size N to be a power of two $\{N = 2^J\}$. Similarly, partial DWT of level J_0, needs sample size to be an integer multiple to 2^{J_0}. Of course these requirements usually not hold in practice. To overcome these limitations two approaches used in general: First approach based on padding which is a usual technique at FFT algorithms. The idea is to create a new time series, say X'_n, from original one X_n with new length $N' > N$ and then take the DWT of the. Padded values are equal to the sample mean $\overline{X}$ of X_n. Second approach based on truncation of X_n to shorter series whose lengths are a multiple of 2^{J_0}. Let $N'' < N$ an integer multiple of 2^{J_0} then two subseries of X_n can be defined: $X^{[1]} \equiv [X_0, \ldots . X_{N''-1}]$ and

$X^{[2]} \equiv [X_{N-N''}, \ldots X_{N''-1}]$ both of length N''. It is proved (Coifman and Donoho, 1995) that this scheme leads to scale based decomposition of weighted sum of squares with half weights being attached to the $N - N''$ samples at the beginning and end of X_n.

1.8.4 Maximal overlap DWT

Since the above limitations obviously hold for the case of microtremor signals the use of DWT for the current study is not the most successful choice. The use of a WT transform that focus on the elimination of DWT shortcomings that discuss earlier is more appropriate. This transform is the so called *maximum overlap DWT* (MODWT) and which belongs to the group of redundant and non-orthogonal wavelet transforms that met in the literature under names "undecimated DWT" (Shensea, 1992), "shift invariant DWT" (Beylkin, 1992), "translation invariant DWT" (Coifman and Donoho, 1995), "Stationary DWT" (Nason and Silverman, 1995) and "non-decimated DWT" (Bruce and Gao, 1996).

The MODWT differs from the DWT in that it is a highly redundant, nonorthogonal transform (Percival and Walden, 2000). The MODWT retains downsampled values at each level of the decomposition that would be otherwise discarded by the DWT. The MODWT is well-defined for all sample sizes N, whereas for a complete decomposition of J levels the DWT requires N to be a multiple of 2^J. It also offers several advantages over the DWT. The redundancy of the MODWT facilitates alignment of the decomposed wavelet and scaling coefficients at each level with the original time series, thus enabling a ready comparison between the series and its decomposition. Coefficients derived using the MODWT are not influenced by circular shifting of the input time series, whereas values derived using the DWT depend upon the starting point of the series.

1.8.4.1 Practical considerations for MODWT

Since MODWT uses circular filters for its implementation, Percival and Walden (2000) showed that boundary regions of MODWT are larger than DWT. This is not a serious shortcoming of MODWT since, on one hand, the difference is quit small and on the other hand the advantages from using MODWT against DWT are more important.

MODWT is defined for all sample sizes so (unlike the DWT) there is no need for special adaptation to handle certain sample sizes. This is one of the main differences between DWT and MODWT. Compared to DWT, MODWT is less dependant upon choice of wavelet filter but not so much so that a particular filter proposed for every wavelet analysis. A preliminary study of the investigated features of examined signal is still needed.

A time series can be completely or partially decomposed into a number of levels. For complete decomposition of a series of length $N = 2^J$ using the DWT, the maximum number of levels in the decomposition is J. In practice, a partial decomposition of level $J_0 < J$ suffices for many applications. A J_0 level DWT decomposition requires that N be an integral multiple of 2^{J_0}. The MODWT can accommodate any sample size N and, in theory, any J_0. In practice, the largest level is commonly selected such that J_0 preclude decomposition at levels heavily influenced by boundary conditions. In particular, for alignment of wavelet coefficients with the original series, the condition L_{J_0}, i.e. the width of the equivalent filter at the J_0-th level is less than the sample size, should be satisfied to prevent multiple wrappings of the time series at level J_0. Selection of J_0 determines the number of octave bands and thus the number of scales of resolution in the decomposition. In relevant literature the J_0

$$J_0 < \log_2\left(\frac{N}{L-1}+1\right) \tag{1.8.8}$$

if Equation (1.8.8) seems too tight, alternative upper bounds are

$$J_0 < \log_2(N) \tag{1.8.9}$$

1.8.5 Evaluation of STA/LTA algorithm using synthetic disturbances

The purpose of this section is to investigate the limits of the widely used STA/LTA algorithm. STA/LTA used in microtremor studies in order to automatically detect the non-stationary parts of the signal and thus to exclude them. This is done by using the algorithm in an antitrigger way: when it finds windows that fulfill the STA/LTA criteria, these are excluded from the processing stream of data (SESAME, 2004). By selecting appropriate parameters one can avoid the non-stationary parts of the signal that can possibly alter the frequency content.

The STA/LTA is, in principle, an amplitude comparison algorithm. In other words it produces results only when differences in amplitudes can identified; it usually has no ability over small differences. To illustrate this fact we run some test cases using artificial (hereafter SX) signals (Figure 1.8.5 – details at Table 1.8.1) added to real mictrotremors recordings (hereafter RX).

All recordings acquired using Reftek DAS-130 as data logger equipped with Guralp GMT-40T seismometer and with LGIT CityShark equipped with Lenartz 3D 5 s sensor. Sampling rate was 125 Hz and recording duration was 20 min. In order to avoid as much as possible the urban area disturbances that will be examined later, RX collection sites were located in countryside locations, far away from any human-involved activities. In addition, these recordings are analyzed thoroughly using he method that will be described later in order to verify the absence of important long duration transients.

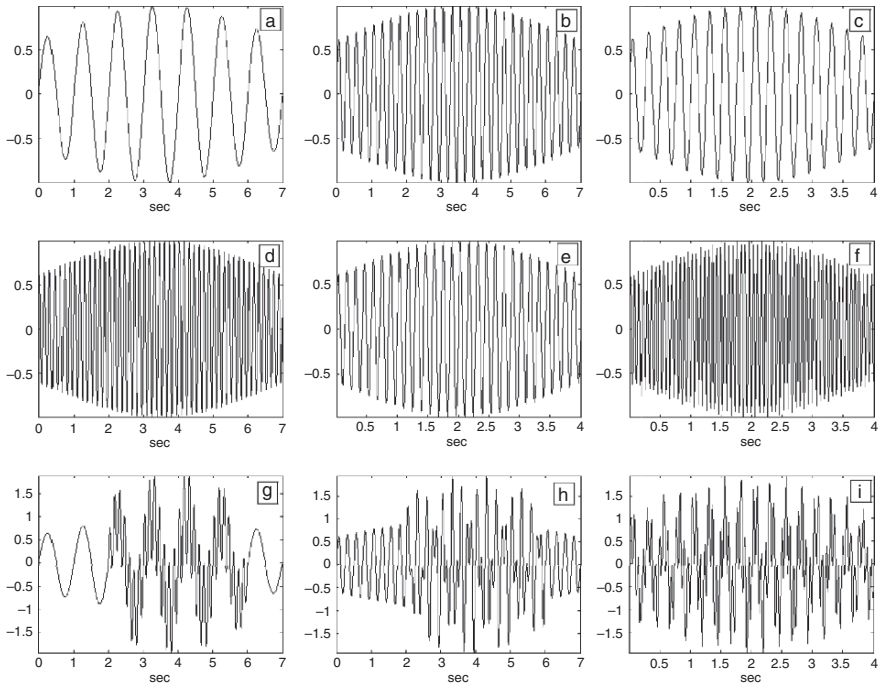

Fig. 1.8.5 Test signals used as artificial disturbances to microtremor recordings. Details of their attributes can be found in Table 1.8.1

Table 1.8.1 Specifications of used test signals

Signal name	Duration (s)	Frequency (Hz)
S1	7	1
S2	7	4
S3	4	4
S4	7	7
S5	4	7
S6	4	15
S7	7 (1st), 4 (2nd)	1 (1st), 7 (2nd)
S8	7 (1st), 4 (2nd)	4 (1st), 7 (2nd)
S9	7 (1st and 2nd)	4 (1st), 15 (2nd)

We used as detection threshold the value $\gamma = \overline{|X_n|}$ which is defined as the average of absolute values of microtremor time series X_n (for n samples). Typical examples of thresholds calculated using γ value are depicted in Figure 1.8.6, for different recordings.

Data are collected at locations as shown in Figure 1.8.1. As one can easily identify the proposed value of γ is rather conservative because we want to illustrate the transients with low amplitude (comparable to γ which is by definition

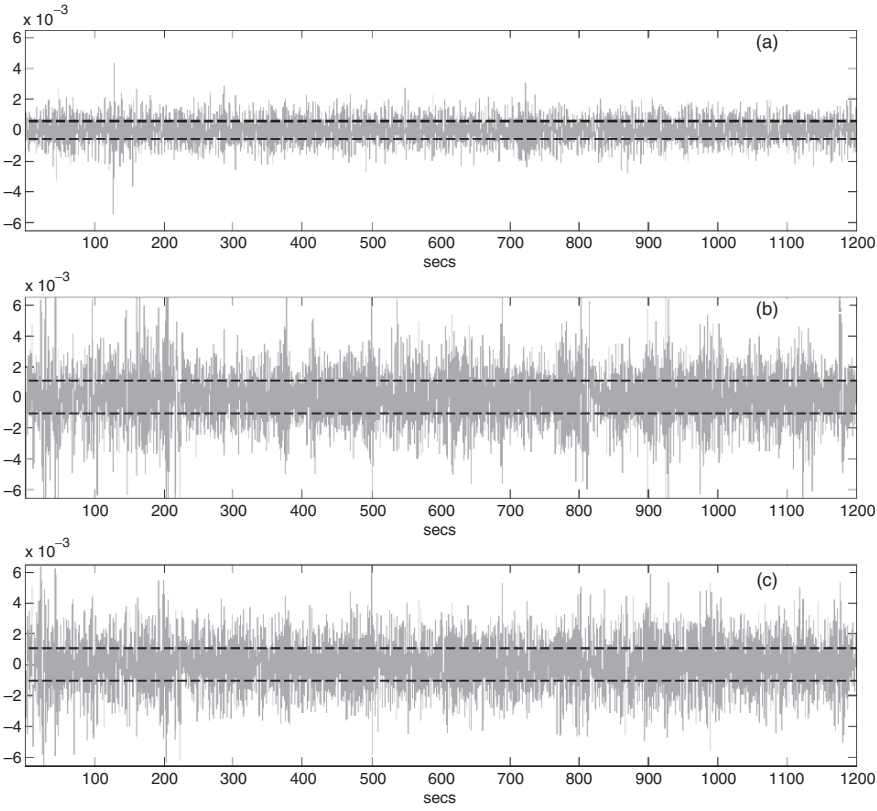

Fig. 1.8.6 Thresholds calculated from γ value (a): Vertical component, (b): N-S component, (c): E-W component for RX recordings

a low value attribute). The window selection procedure is tested using the corresponding modules from well known, public available, software packages GEOPSY (www.geopsy.org) and J-SESAME (http://www.geo.uib.no/seismo/software/jsesame/jsesame.html). Typical window selections from several recordings with and without added artificial disturbances are shown in Figure 1.8.7.

Initially we used the window selection procedure to raw recordings in order to determine the windows that will be accepted for the HVSR calculation. Next we contaminate the recordings by adding SX $(X : 1 \rightarrow 9)$ signal to every recording and reprocess them with the window module. Each artificial disturbance is added independently to each recording and repeated 20 times (starting from 50th s and repeated every 50 s). The value of γ remains stable for each recording. We tested γ values from 0.5 to 2.5 with 0.1 resolution. The performance (P_r) of "antitriggering" is calculated using the relation:

$$P_r = \frac{n_{dd}}{n_{ad}} \tag{1.8.10}$$

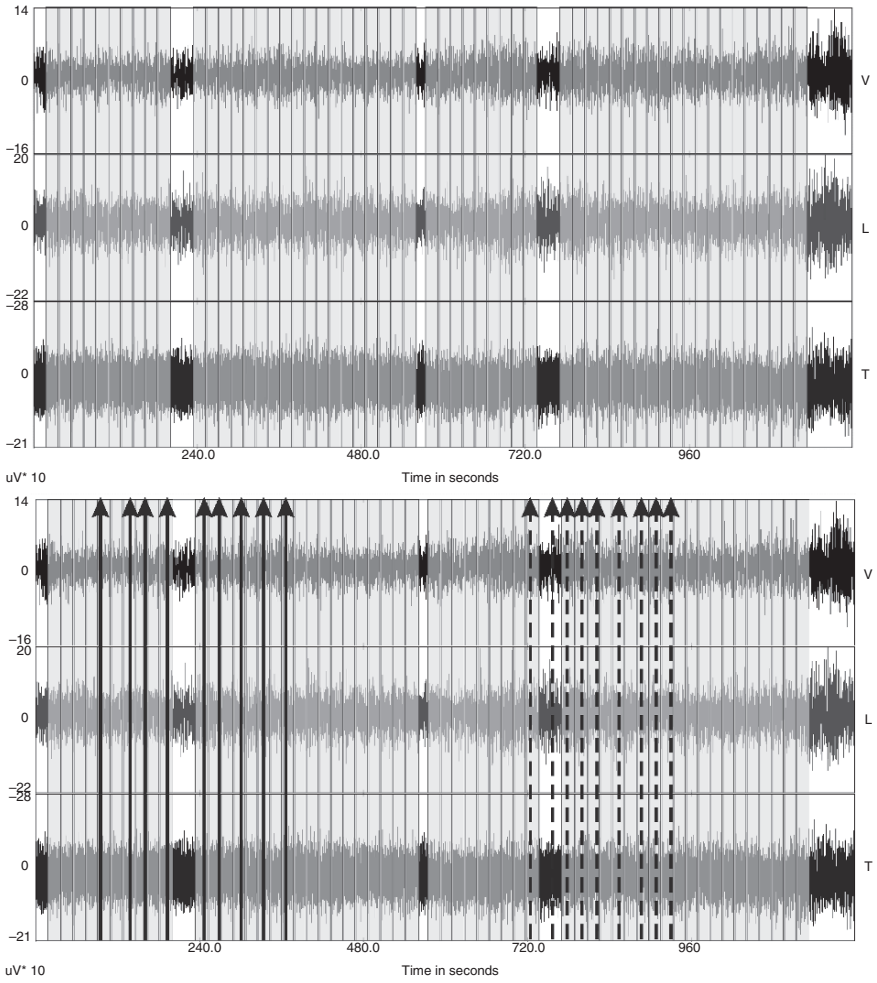

Fig. 1.8.7 Window selections (grey zones) using STA/LTA algorithm for raw microtremor recordings without artificial disturbances (top plot) and with disturbances (bottom plot) starting at points indicated by arrows. All signal (S1-S9) added consequently two times as indicated by arrow groups (first set – solid arrows, second set dashed arrows). Each individual arrow indicates the starting sample of artificial signal

Where n_{dd}: number of detected (and excluded) disturbances

n_{ad}: total number of disturbances, here 20

At Figure 1.8.8 we summarize the performance of "antitriggering" for STA/LTA by plotting the results of P_r in relation of γ.

We can conclude that if the amplitude of the transients is at least 1.5 times the value of γ it's rather impossible for the STAL/LTA algorithm to detect these transients. Between 1.5 and 1.85 there are some cases where the detection is achieved but these detections achieved to transients with higher frequencies (signals S4,

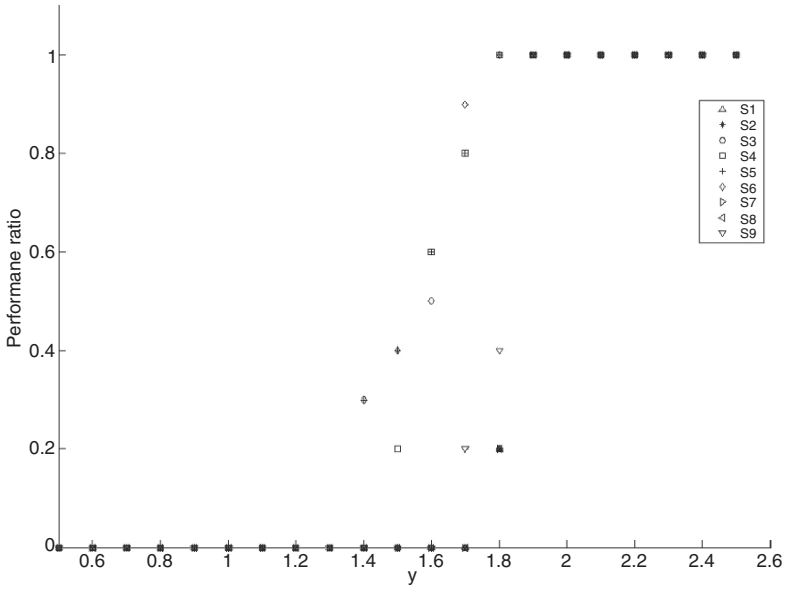

Fig. 1.8.8 Average results of STA/LTA performance according to γ value for all the artificial signals

S5, S6). In addition, the artificial signals that are monochromatic can be detected easier. Of course, this event cannot act as a rule because it can easily be inverted if one selects appropriate STA/LTA window lengths. For $\gamma > 1.85$ the STA/LTA performs as expected.

1.8.6 Impact of low amplitude transients to HVSR

The purpose of this section is to investigate if and how, undetectable transients from STA/LTA algorithm can affect the results of HVSR method. In order to facilitate this we use microtremor recordings (hereafter KRX) from 17 sites with known attributes. These are derived from results of previous studies (boreholes, array techniques) or we calculated 1D models using EERA code (Barder et al., 2000) based on V_s profiles derived from previous studies also (EMERIC/I-CRINNO, 2005; SE-RISK, 2008). We used the recordings with $\gamma < 1.85$ as described in the previous section and we prepared our dataset by adding the artificial disturbances in a progressive way: we begun by adding each one of nine SX signals in 50th s of each KRX thus creating $17 \times 9 = 153$ cases. We performed the HVSR calculation and then we add one more instance of each SX at 100th s (thus creating 153 more cases with recordings that included two parts of the same SX – at 50th and 100th s) and repeat the calculation. This procedure repeated 25 times. HVSR calculation performed as ordinary with

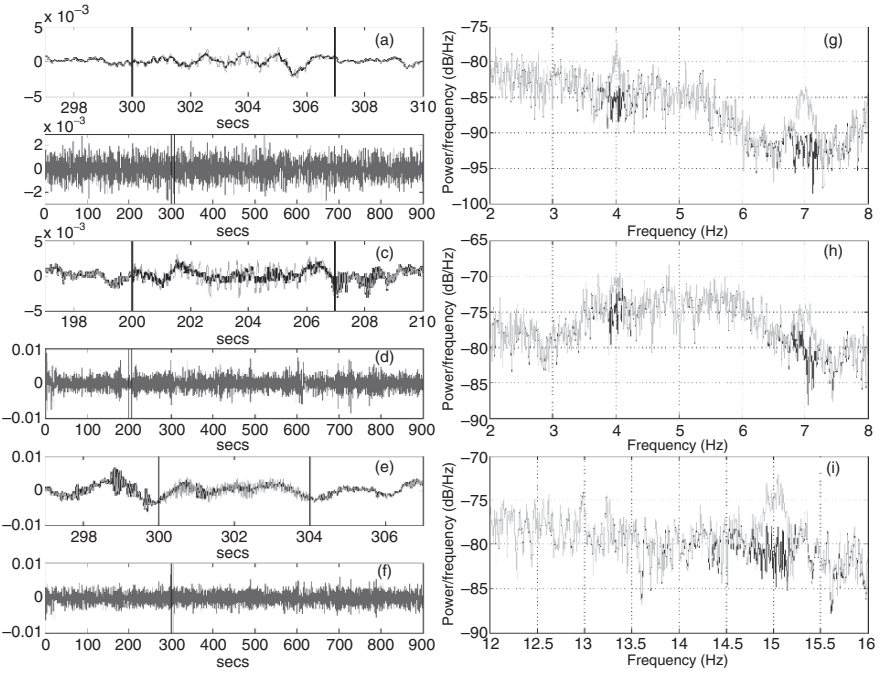

Fig. 1.8.9 Typical example of spectrum contamination when one part of artificial signal is added. (a,b) S8 signal ($\gamma = 1$) added from 300 until 307 s at raw recording. (c,d) S8 signal ($\gamma = 1.2$) added from 200 until 207s at raw recording. (e,f) S6 signal ($\gamma = 1$) added from 300 until 304 s at raw recording. (g) Spectrum of (b) recording without artificial signal (black line) and with it (grey line). (h) Spectrum of (d) recording without artificial signal (black line) and with it (grey line). (i) Spectrum of (f) recording without artificial signal (black line) and with it (grey line)

recordings that bandpass filtered (0.2 to 20 Hz), detrended and baseline corrected, 5% cosine tapered, smoothed using Kohno & Ohmachi window with b = 25.

A typical example of how a single undetectable transient can affect the calculated spectrum is illustrated in Figure 1.8.9. Since the FT provides excellent localization in frequency domain it is expected that the (undetectable by STA/LTA) added disturbance will produce a peak in frequency domain. Of course, it is not expected that a single peak could significant affect site's f_0 since HVSR is an averaging result method. The question that arises is if there is a limit, over which, HVSR could be affected.

In Figure 1.8.10 we present results from a site with good agreement between HVSR results and results obtained when parts of artificial disturbance (here S1) is added. It is obvious that as the number of undetectable disturbances increases the estimated f_0 is not depicted by a clear peak. At Figure 1.8.11 we illustrate the HVSR results using recordings (from different known sites) where 20 parts of artificial disturbances, added. We can identify three general cases: First, when f_0 and artificial disturbances appeared individual then it's difficult to identify which is real and which not. These are the case with 1 and 4 Hz signals and some of 7 Hz (only

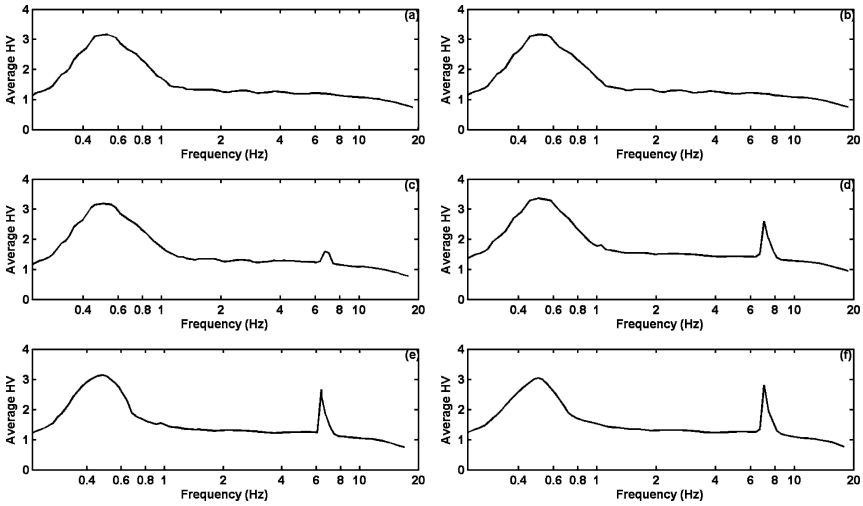

Fig. 1.8.10 HVSR results from a single site with increasing parts of S1 signal added to raw recordings. (a) raw recording, (b) 1 part, (c) 7 parts, (d) 14 parts, (e) 20 parts, (f) 25 parts

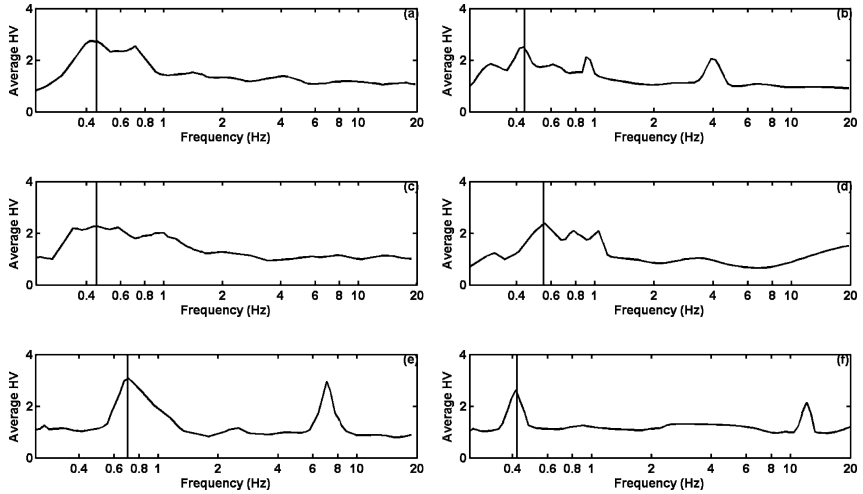

Fig. 1.8.11 HVSR results from different sites using recordings with artificial (non-detected) disturbances added. Vertical line in each plot indicates the calculated f_0 from same raw recordings. Signals used to contaminate the corresponding recordings are: S1 at (a), S7 at (b), S1 at (c), S1 at (d), S5 at (e), S6 at (f)

when f_0 is quite high). Second when f_0 and artificial disturbances are quite close, the f_0 seems shifted or more dispersed. This is the case with 1 Hz signals. Finally, with high frequency artificial disturbances (15 and some 7 Hz) an individual peak appeared at those values.

An experienced analyst, as far there is some knowledge of the local geology, could reject these values but here we seek a more "computational" way to reject it.

From the above it is obvious that there are enough cases where the undetectable transients could produce problems to estimation of f_0. At this point we must mention that the values of artificial disturbances are carefully selected to represent non-stationary disturbances that recorded during the big number of measurements that took place the last four years around big cities at Crete Island. These values are representable only for the urban areas that we investigate and no further extension should be made for other areas without prior acquisition of possible local singularities.

1.8.7 Application of MODWT for identification of low amplitude transients

In this section the application of MODWT in raw recordings will be discussed along with its application to experimental ones. From what we present so far it is obvious that, in case that we want to detect low amplitude non-stationary components to microtremor recording, we need a more efficient detector than traditional STA/LTA. Our proposal is to transfer the amplitude detection from 1D time domain to 2D time-frequency domain using wavelets. Briefly speaking, by using time-frequency representation we are able to detect the frequency of non-stationary part as well as its time attribute (i.e. position) inside recordings. For this transformation we used MODWT and not DWT because we don't want to make any prior assumptions about the nature of recordings as explained in previous section.

The MODWT performed using Least Asymmetric (LA) filters with length 8 using the WMTSA software (public available at www.atmos.washington.edu/~wmtsa). The number of levels used for decomposition was $J_0 = 8$ which corresponds to physical period up to 4.098 s. Using the MODWT transform we calculate wavelet and scaling coefficients for consecutive windows with length each recording. We propose the use of MODWT not to whole recording but to subsections of it. The smaller window that a decomposition can be achieved dictated by the number of samples as already mentioned by Equations (1.8.8) and (1.8.9). Figure 1.8.12 illustrates such a decomposition from a recording where we select $n = 20,000$ (160 s). It contains one S2 disturbance at 8th s, one S6 at 50th s and one S8 at 120th s. Lower panel illustrates the recording. The top panel shows the wavelet coefficients $\tilde{W}_{j,t}$ for levels $j = 1$–8 and the $\tilde{V}_8$ scaling coefficients plotted on the same vertical scale as the lower panel. For each level solid vertical lines near end points demarcate the boundaries outside of which the coefficients are influenced by boundary conditions.

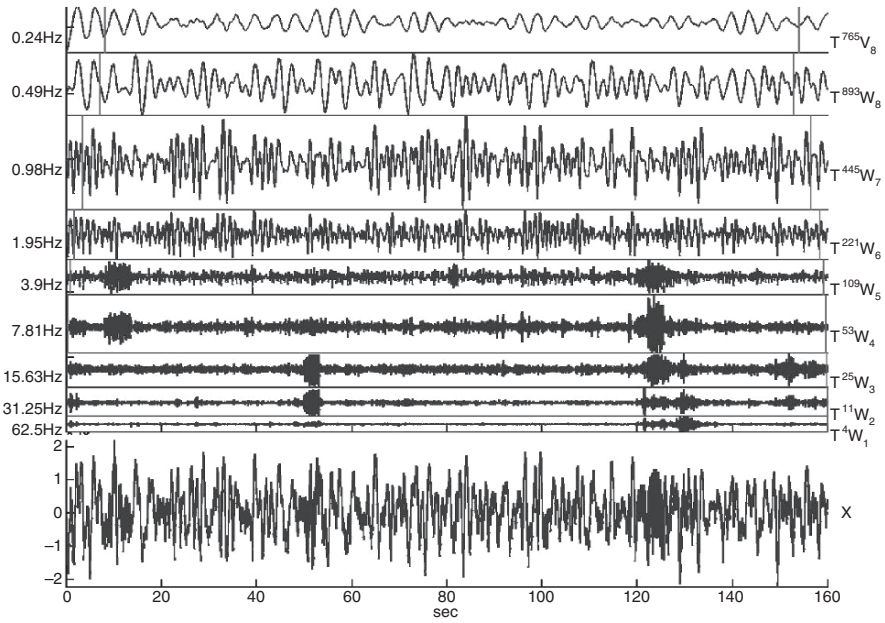

Fig. 1.8.12 MODWT wavelet (levels 1–8) and scaling ($J_0 = 8$) coefficients (top panel) and microtremor recording (bottom panel). Solid vertical lines (top panel) indicate the boundaries outside of which coefficients are influenced by circular shifting

The coefficients are plotted after circular shifting of wavelet coefficients $\tilde{W}_{j,t}$ in order to be properly aligned with original recording. The shifted vector is marked at the right of each subplot in the form of $T^{-v_j}\tilde{W}_j$ where v_j indicates the number of samples the coefficients have been shifted.

Without any prior experience the reader can easily identify the nature and position of S2, S6 and S8 signals at different scales which, as already mentioned, corresponds to different frequency bands. At this stage the analyst can select manually the portions of the recording that like to exclude or by using an automated procedure. The authors are preparing a MATLAB toolbox for automatic detection and rejection of these non-stationarites before the beginning of HVSR processing (Vallianatos and Hloupis, in preparation).

At final stage we apply the MODWT to recordings from sites with calculated f_0 is not agree with those than calculated from other methods. We present representative results from two sites (X01 and X02) with known differences between f_0 from HVSR and 1D linear equivalent model using EERA code (Figure 1.8.13).

The MODWT transformed recordings are shown in Figures 1.8.14 to 1.8.15. After detection and rejection of possible disturbed non-stationarities the HVSR results that we produced are illustrated in Figure 1.8.16.

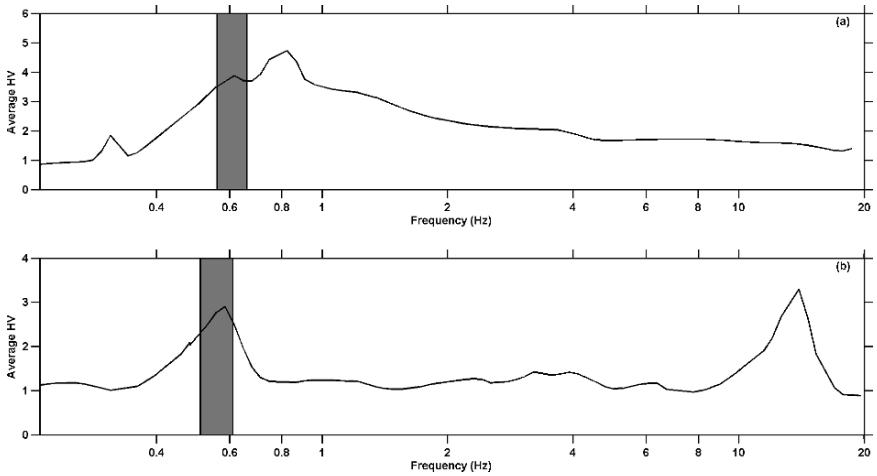

Fig. 1.8.13 Results from sites X01(top) and X02(bottom) where there is no good agreement between f_0 from HVSR and 1D model calculated from inverted V_s profile (EERA model) as indicated at grey zones

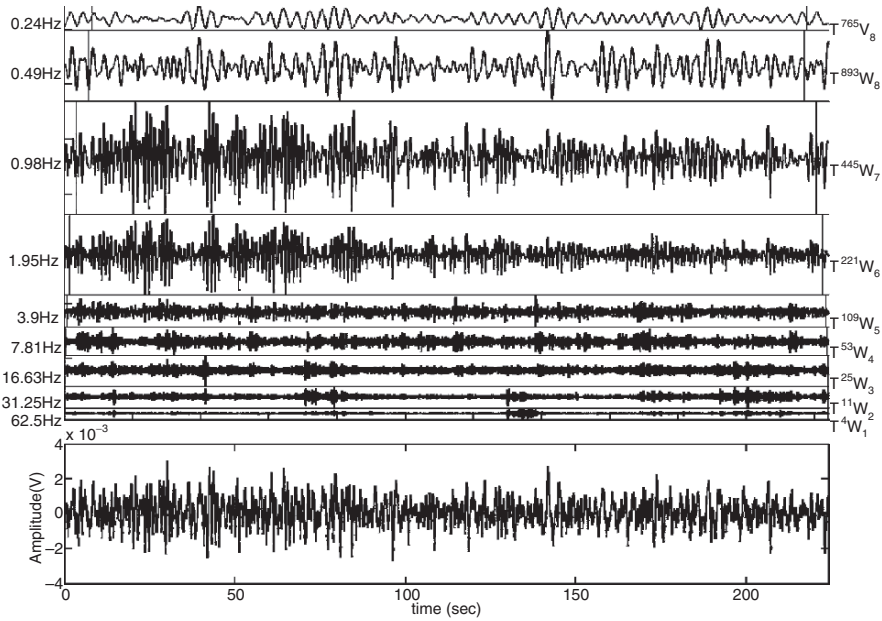

Fig. 1.8.14 MODWT for recording from site X01. Significant non-stationary signal detected between 10th and 95th s at around 1 Hz

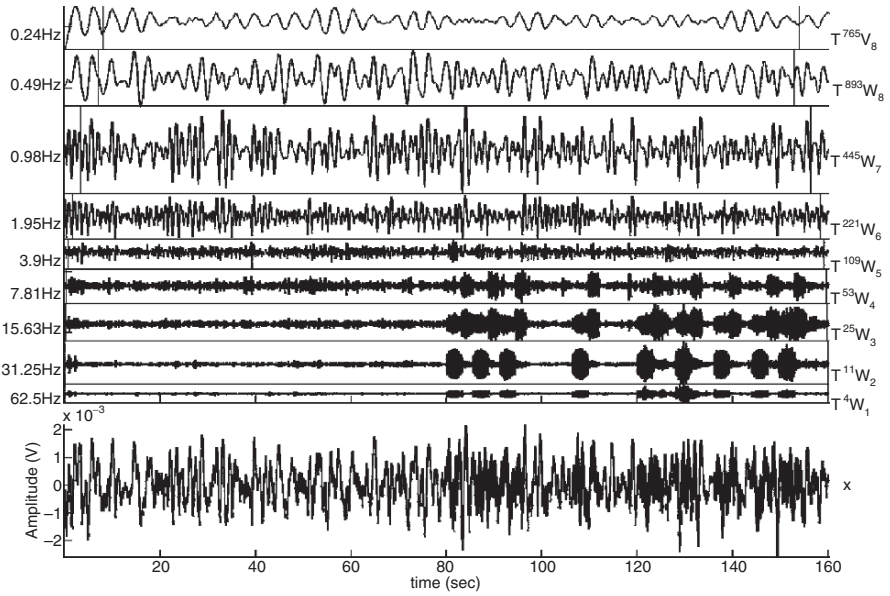

Fig. 1.8.15 MODWT for recordings from site X02. Significant non-stationary signal detected at 80th, 85th, 87th, 110th, 120th, 128th, 138th, 145th and 150th s

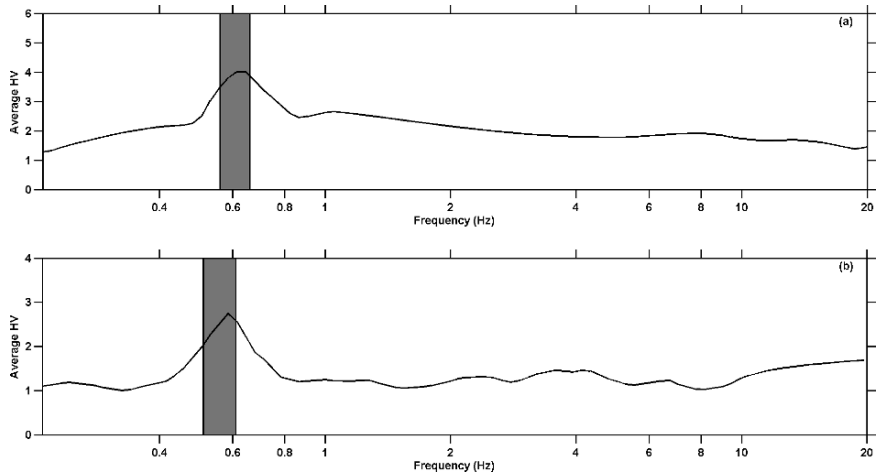

Fig. 1.8.16 Results from sites X01(top) and X02(bottom) after rejection of non-stationarities that detected from MODWT. Grey zones point out the f_0 from EERA model

1.8.8 Conclusions

Non-stationary, artificial disturbances are a usual situation in urban places where industrial and anthropogenic activities run continuously. At these locations, microtremor recordings collected even at late hours could suffer from transients with amplitudes comparable to those of microtremors. Based on analysis described in the previous sections we may conclude that these transients remain undetectable by the STA/LTA algorithm. In case these transients have long duration there is a strong possibility to contaminate the calculation of f_0. An experienced analyst could probably identify the non-stationarities by examining the FT in each window but our intension is to focus on an automated signal selection procedure. The use of a WT in order to localise a signal in time-frequency domain and especially the use of a redundant one, such as the MODWT, can solve the problem of accurate automatic determination of the above transients. If the amount of transients is significant, they can be excluded since the MODWT is able to provide their time position in the recording. The whole procedure can run as a preliminary test to microtremor recordings in order to provide a clear view of the existence of transients in such records.

References

Bard P (1999). Microtremor measurement: a tool for site effect estimation. in The Effects of Surface Geology on Seismic Motion. Irikura K, Kudo K, Okada H and Sasatami T (Editors), Balkema, Rotterdam, 1251–1279.

Bardet JP, Ichii K and Lin C (2000). EERA: a computer program for equivalent-linear earthquake site response analyses of layered soil deposits. University of Southern California, 40 pp.

Beylkin G (1992). On the representation of operators in bases of compactly supported wavelets. SIAM Journal of Numerical analysis, 29, 1716–1740.

Breiman L (1995). Better subset regression using the nonnegative. Technometrics 37, 373–384.

Bruce AG and Gao HY (1996). Applied Wavelet Analysis with S-Plus. Springer, New York.

Chui CK (1992). Wavelets: A tutorial in theory and applications. Academic, New York.

Coifman R. and Donoho DL. (1995). Translation invariant de-noising. In Wavelets and Statistics (Lecture Notes in Statistics, Vol 103) edited by Antoniadis A and Openheim G, New York, Springer,125–150.

Coifman R and Wickerhauser MV (1992). Entropy based algorithms for best basis selection. IEEE Trans. Inf. Theory, 32, 712–718.

Daubechies I (1990). The wavelet transform: time-frequency localization and signal analysis. IEEE Trans. Inf. Theory, 36(5), 961–1005.

EMERIC I – CRINNO Project (2006). http://www.crete-region.gr/greek/programs/CRINNO/EMERICI/emericI_pres_en.htm

Grossman A and Morlet J (1984). Decomposition of Hardy function into square integrable wavelets of constant shape. SIAM J. Appl. Math., 723–773.

Horike M, Zhao B and Kawase H (2001). Comparison of site response characteristics inferred from microtremors and earthquake shear waves. Bull. Seism. Soc. Am., 81, 1526–1536.

Mallat S (1989). A theory for multiresolution decomposition – the wavelet representation. IEEE Trans. Patt. Anal. Machine Intell., II(7), 674–692.

Mallat A and Hwang L (1992). Singularity detection and processing with wavelets, IEEE Trans. Inf. Theory, 38(2), 617–643.

Mucciarelli M (1998). Reliability and applicability of Nakamura's technique using microtremors: an experimental approach, J. Earthq. Eng., 2, 625–638.

Mucciarelli M, Gallipoli MR, and Arcieri M (2003). The stability of the horizontal-to-vertical spectral ratio of triggered noise and earthquake recordings. Bull. Seism. Soc. Am., 93, 1407–1412.

Nakamura Y. (1989). A method for dynamic characteristics estimations of subsurface using microtremors on the ground surface, Q. Rept. Railway Technical Research Institute Japan 30, 25–33.

Nason G and Silverman B (1995) The stationary wavelet transform and some statistical applications. In Wavelets and Statistics (Lecture Notes in Statistics, Vol 103) edited by Antoniadis A and Openheim G, Springer, New York, pp. 281–99.

Nogoshi M and Igarashi T (1970). On the propagation characteristics estimations of subsurface using microtremors on the ground surface, J. Seism. Soc. Jpn., 23, 264–280.

Nogoshi M. and Igarashi T (1971). On the amplitude characteristics of microtremor (part 2), J. Seism. Soc. Jpn., 24, 26–40.

Parolai S and Galliana-Merino J (2006). Effects of transient seismic noise of H/V spectral ratio, Bull. Seism. Soc. Am., 96, 228–236.

Percival D. and Walden A. (2000), Wavelet methods for time series analysis, Cambridge University Press, Cambridge, UK.

Provaznic I (2001) Wavelet analysis for signal detection-applications to experimental cardiology research. Ph.D. thesis, Brno University of Technology.

SE-RISK (Advanced techniques for SEismic RISK reduction in Mediterranean Archipelago Regions) project (2008). http://www.ims.forth.gr/joint_projects/se_risk/se_risk.html.

SESAME (Site EffectS assessment using AMbient Excitations) project (2004), EVG1-CT-2000–00026. http://sesame-fp5.obs.ujf-grenoble.fr/

Shensea J (1992), The discrete wavelet transform: wedding the a trous and mallat algorithms, IEEE Trans. Signal Processing, 40, 2464–2482.

Stewart SW (1977). Real time detection and location of local seismic events in central California, Bull. Seism. Soc. Am., 67, 433–452.

Torrence C and Compo G (1998). A practical guide to wavelet analysis, Bull. Am. Met. Soc., 79, 61–78.

Chapter 2
Effect of Buildings on Free-Field Ground Motion

Marco Mucciarelli

Introduction

The idea that during an earthquake the vibration of buildings may transmit back to the soil a quantity of energy able to modify the ground motion was theoretically postulated by Wong and Trifunac (1975) and Wirgin and Bard (1996). During an earthquake it is difficult to measure and to separate the source and site effects from that of the oscillating building (Chavez Garcia and Cardenas-Soto, 2002). Again, it is most difficult to separate the quantity of energy related by a single vibrating building from the effects of the others and to separate them from the energy of incident wave train. To estimate the quantity of energy that building can release back to the soil controlled conditions experiments have been carried out. The first experiment has been performed by Jennings (1970), during forced vibration of buildings, while Kanamori et al. (1991) studied the effects of high-rise buildings in Los Angeles, whose vibration was caused by the sonic boom of the Space Shuttle. Recent active experiments have been carried out by Guéguen et al. (2000) and Guéguen and Bard (2005) on a five-story RC-building model (1:3) located in the EuroSeisTest site at Volvi (GR), by Mucciarelli et al. (2003) on a base isolated building during a release test and by Gallipoli et al. (2006) taking advantage of a controlled demolition experiment at Bagnoli (IT). Recent passive tests using ambient noise are described in Gallipoli et al. (2004) and Cornou et al. (2004). The conclusions of all these experiments confirm the importance that buildings may have as seismic sources. On the other hand, numerical simulation were made on idealised models of city-soil interaction: see, e.g., Tsogka and Wirgin (2003), Kham et al. (2006), Ditommaso et al. (2007).

M. Mucciarelli
DiSGG – Università della Basilicata, Potenza, Italy
e-mail: marco.mucciarelli@unibas.it

M. Mucciarelli et al., (eds.), *Increasing Seismic Safety by Combining Engineering Technologies and Seismological Data,* NATO Science for Peace and Security Series C: Environmental Security,

Both experimental and numerical results agree on the fact that the presence of building is able to modify significantly the free-field motion, and thus inside a densely populated city the same notion of free-field is meaningless.

The main debatable point is if the presence of building is increasing or decreasing the free-field motion. Kham et al. (2006) suggest that the global energy is decreased (mainly due to added damping) while Ditommaso et al. (2007) note that more engineering parameters such as PGA or spectral ordinates, are likely increased by the presence of building.

References

Chavez-Garcia, F.J. and M. Cardenas-Soto (2002). The contribution of the built environment to the free-field ground motion in Mexico City, Soil Dyn. Earthq. Eng., 22, 773–780.

Cornou, C., Guéguen, P., Bard, P.-Y., and E. Haghshenas (2004). Ambient noise energy bursts observation and modeling: Trapping of harmonic structure-soil induced–waves in a topmost sedimentary layer, J. Seismol., 8(4), 507–524.

Ditommaso, R., Gallipoli, M.R., Mucciarelli, M., and F.C. Ponzo (2007). Effect of vibrating building on "free field" ground motion: from the Bagnoli experiment to many-buildings simulation, Proc. 4th Int. Conf. Earthq. Geotech. Eng., CD-ROM edition, Paper No. 1388. Springer, ISBN 978-1-4020-5893-6.

Gallipoli, M.R., Mucciarelli, M., Castro, R.R., Monachesi, G., and P. Contri (2004). Structure, soil-structure response and effects of damage based on observations of horizontal-to-vertical spectral ratios of microtremors, Soil Dyn. Earthq. Eng., 24, 487–495.

Gallipoli, M.R., Mucciarelli, M., Ponzo, F., Dolce, M., D'Alema, E., and M. Maistrello (2006). Buildings as a seismic source: analysis of a release test at Bagnoli, Italy, Bull. Seismol. Soc. Am., 96, 2457–2464.

Guéguen, P. and P.-Y. Bard (2005). Soil-structure and soil-structure-soil interaction: experimental evidence at the Volvi test site, J. Earthq. Eng., 9(5), 657–693.

Guéguen, P., Bard, P.-Y., and C.S. Oliveira (2000). Experimental and numerical analysis of soil motion caused by free vibration of a building model, Bull. Seismol. Soc. Am., 90(6), 1464–1479.

Jennings, P.C. (1970). Distant motion from a building vibration test, Bull. Seismol. Soc. Am., 60, 2037–2043.

Kanamori, H., Mori, J., Anderson, D.L., and T.H. Heaton (1991). Seismic excitation by the space shuttle Columbia, Nature, 349, 781–782.

Kham, M., Semblat, J.-F., Bard, P.-Y., and P. Dangla (2006). Seismic site–city interaction: main governing phenomena through simplified numerical models, Bull. Seismol. Soc. Am., 96, 1934–1951.

Mucciarelli, M., Gallipoli, M.R., Ponzo, C.F., and M. Dolce (2003). Seismic waves generated by oscillating building, Soil Dyn. Earthq. Eng., 23, 255–262.

Tsogka, C. and A. Wirgin (2003). Simulation of seismic response in an idealized city, Soil Dyn. Earthq. Eng., 23, 391–402.

Wirgin, A. and P.-Y. Bard (1996). Effects of building on the duration and amplitude of ground motion in Mexico City, Bull. Seismol. Soc. Am., 86, 914–920.

Wong, H.L. and M.D. Trifunac (1975). Two dimensional antiplane building-soil-building interaction for two or more buildings and for incident plane SH waves, Bull. Seismol. Soc. Am., 65, 1863–1885.

Chapter 2.1
Effect of Building-Building Interaction on "Free-Field" Ground Motion

Marco Mucciarelli, Rocco Ditommaso, Maria Rosaria Gallipoli, and Felice Ponzo

Abstract We investigate the effect induced on free-field ground motion by the interaction among buildings set in vibration by an earthquake. This is a refinement of a previous model where the building interacted with the soil, but not among each others. The waves are propagated in a multi-layered 1-d model that includes soil and a layer for each floor of the structure. We implemented numerical models in Simulink, a toolbox of MatLab, that easily allows solving the differential equations of the case. The final model is a chain of SDOF oscillators, whose dynamic behaviour depends on mass, stiffness and damping. Comparing the results with the non-interacting case, there is a reduction of the mean and median of the ground motion enhancement and an increase of the dispersion.

Keywords Free-Field · City-soil interaction · Numerical modeling of seismic waves

2.1.1 Introduction

Ditommaso et al. (2007) reproduced with a numerical model the ground motion observed by Gallipoli et al. (2006) during a 7 cm top-floor displacement test of a real two-stories building. This displacement is representative of the maximum excitation that this kind of building might withstand during an earthquake. The highest PGA (Peak Ground Acceleration) observed on the soil is 5% g with a 7 cm displacement of a structure whose frequency was in the range 1–2 Hz. If we consider the standard 5% damping response spectra provided by the Italian Seismic Code, a top-floor 6 cm displacement at 1 Hz is obtained for the Zone 2 – Soil A spectrum, whose PGA is 0.25 g. Thus the observed PGA is about 20% of the hypothetical unmodified

M. Mucciarelli (✉), R. Ditommaso, M.R. Gallipoli, and F. Ponzo
DiSGG – Università della Basilicata, Potenza, Italy
e-mail: macro.mucciarelli@unibas.it

M. Mucciarelli et al., (eds.), *Increasing Seismic Safety by Combining Engineering Technologies and Seismological Data,* NATO Science for Peace and Security Series C: Environmental Security,

free-field PGA. After reproducing this result, Ditommaso et al. (2007) modelled a "virtual village" made of three structures of different height to study their effect on an accelerometer located among them, varying the azimuth of incident waves and the coupling between building and soil, obtaining a statistical distribution of the influence of vibrating structures on "free-field" ground motion. The distribution of the output PGA is centred on the input value, with minimum and maximum variation of the order of 50% and with most of the values in the range $\pm 25\%$ input. The analysis of the ratios of response spectra (Out/In) showed that the values above unity are concentrated around the periods of buildings fundamental mode, while the ratio tends to be lower for longer period. In this paper we want to put a step forward the model of Ditommaso et al. (2007), including the feedback of each building on the others.

2.1.2 The model

We followed the approach of Şafak (1998), where the building and the foundation soil are idealised as propagators of up- and down-going S-waves. The whole system was modelled using Matlab Simulink. The advantage of this approach is that one can work with subsystems (i.e., soil strata or building floors), adding as many as it is necessary. The only unchanged sub-systems are the bedrock (half-space with inelastic attenuation) and the building's roof. To estimate the three parameters needed for each subsystem (mass, stiffness and damping), three buildings of different mass and height were designed using SAP2000 and following the rules for anti-seismic design provided by the new Italian code (largely similar to EuroCode8) (Table 2.1.1).

To take into account the variability of the position of the buildings among them and with respect to the accelerometer, a random delay time was included in the model. The output of each building was summed to the input ground motion with a variable delay, uniformly distributed from 0 to 0.1 s. The velocity in the soil layer was set to 150 m/s, thus leading to simulated change in position in the range -15 to 15 m depending on the direction. The signals coming from the buildings were propagated in an inelastic medium. The distances were calculated from the centre of mass of the structures projected on the ground to the accelerometer, with the attenuation given by:

$$A(r) = \frac{A_0}{r} . e^{-\frac{f \cdot r}{Q \cdot v}}$$

Table 2.1.1 Parameter of the three buildings

Structure	Mass (kg)	Stiffness (N/m)	Damping factor (%)
1	149,696	75,920,931	5
2	1,847,000	409,450,806	5
3	3,053,940	225,008,060	5

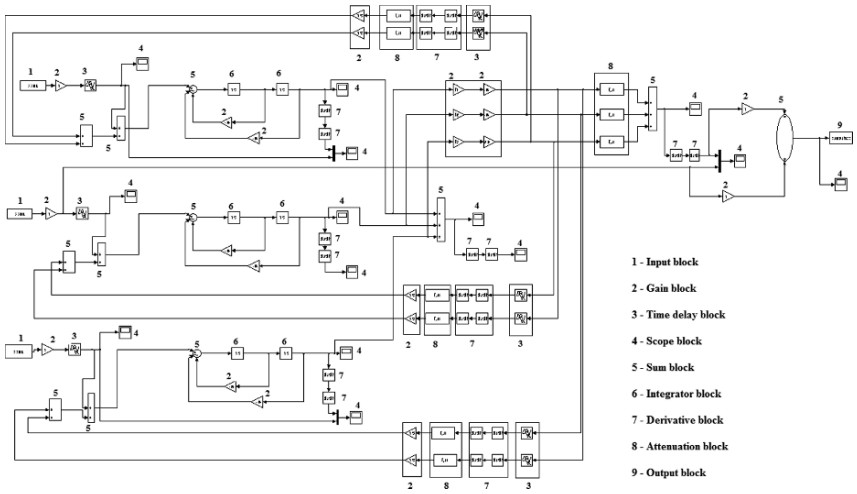

Fig. 2.1.1 Matlab simulink model used for the simulation

where A is the signal amplitude as a function of the distance r, A0 is the initial amplitude, f is its frequency, v is the shear wave velocity and Q is the quality factor (taken equal to 18). To account for the variability in the dynamic coupling between building foundation and the soil, and thus to represent the different quantity of energy transferred back to the soil by the vibrating structure, a random coefficient was included in the simulation, with uniformly distributed values in the range from 1% to 90%. The model is reported in Figure 2.1.1.

The input was provided by 11 real accelerograms with PGA ranging from 0.15 to 0.35 g.

2.1.3 Results

A Monte Carlo simulation was then performed, with 300 runs of the Simulink model for each input. We then obtained 3,300 possible combination of different position of the buildings with respect to the incoming wave, soil/foundations coupling and input. From each simulated output accelerogram, we extracted the PGA, the Housner Intensity (H) and the maximum value of the acceleration response spectra (Sa).

Figure 2.1.2 reports the histograms and the Empirical Cumulative Distribution Functions (ECDFs) for the ratio between output and input values. The distribution are asymmetrical and well described by a log-normal model. The main point to consider is the percentage of results below 1, that means the output is diminished by the presence of the vibrating building. This kind of destructive interference is present in 30% of the cases for PGA, 10% for H and never for Sa. The output is larger than 1.5 times the input in less than 10% of the cases for PGA, never for H and in half the cases for Sa. This is in agreement with the theoretical expectations: the

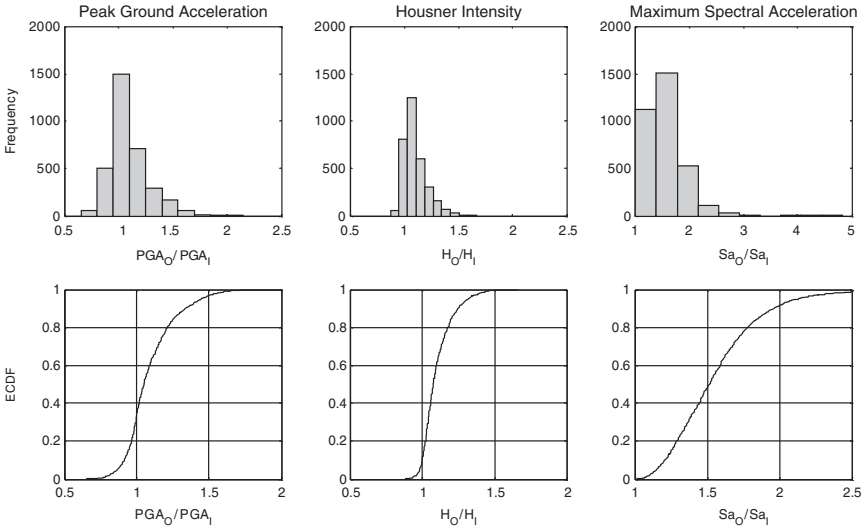

Fig. 2.1.2 ECDFs of 3,300 Monte-Carlo simulation

energy is partly absorbed by the damping of the buildings, but in the range of frequency corresponding to the buildings fundamental modes, the spectral amplitude is enhanced.

2.1.4 Discussion and conclusions

We compared the result obtained with the one given by the model without feedback among the buildings (Ditommaso et al., 2007). Figure 2.1.3 reports the match between PGA, while Figure 2.1.4 shows the comparison between Sa. For the previous model, the variation of the Housner intensity was not given.

It is possible to note that the general pattern of the curve for PGA remains the same, with a small decrease of the median value and an increase of the dispersion with a larger probability of greater motion amplification due to the presence of buildings. The trend is the same also for Spectral Amplification.

In conclusion this more refined model does not change the conclusion of previous works, but given the larger number of simulation allows for a more precise insight on the role that vibrating building may have in modifying the "free field" ground motion. The energy back-radiated in the range of building fundamental periods leads to the conclusion that inside an urban area it is difficult to record a real free field motion. The presence of buildings strongly affects the response spectra and, to a lesser extent, the PGA. The variation is always positive for the maximum spectral values, while for PGA it can be either positive or negative. The Housner Intensity tends to be increased rather than decreased, but the range of variation is smaller

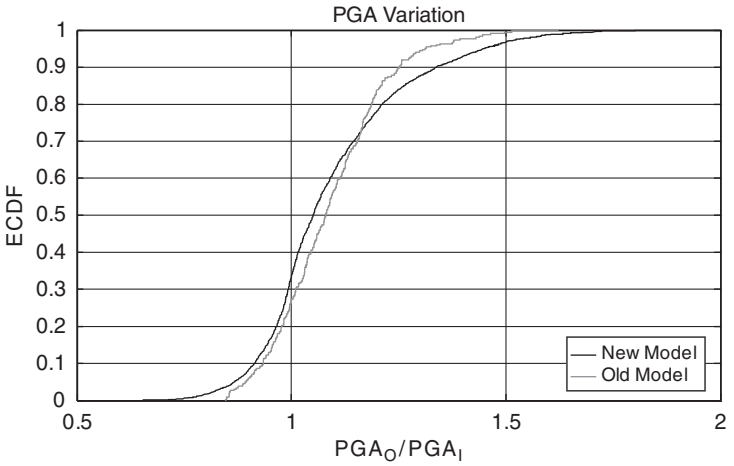

Fig. 2.1.3 Comparison between this work and Ditommaso et al. (2007) for PGA

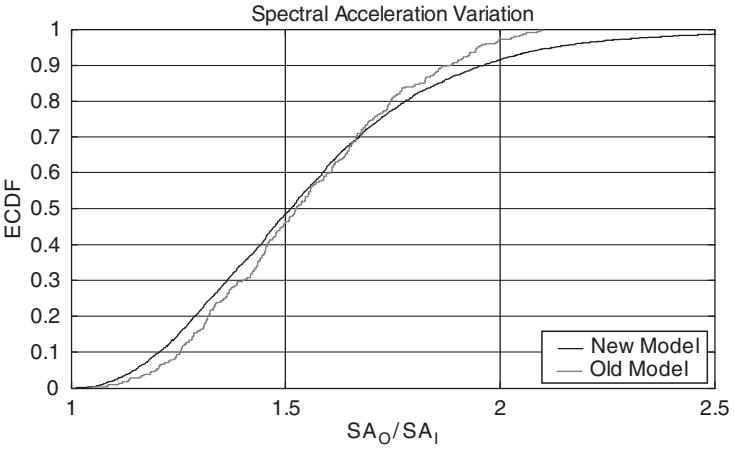

Fig. 2.1.4 Comparison between this work and Ditommaso et al. (2007) for Sa

that the one observed for PGA and Sa. This result is obtained without selecting soil properties that may induce resonance between soil and buildings, and thus can be regarded as a lower limit of the modeled phenomenon.

References

Ditommaso, R., M. R. Gallipoli, M. Mucciarelli, F. C. Ponzo (2007) Effect of vibrating building on "free field" ground motion: from the Bagnoli experiment to many-buildings simulation, Proc. 4th Int. Conf. Earthq. Geotech. Eng., CD-ROM edition, Paper No. 1388. Springer, ISBN 978-1-4020-5893-6.

Gallipoli, M. R., M. Mucciarelli, F. Ponzo, M. Dolce, E. D'Alema, M. Maistrello (2006) Buildings as a seismic source: analysis of a release test at Bagnoli, Italy, Bull. Seismol. Soc. Am., 96, 2457–2464.

Şafak, E. (1998) New approach to analyzing soil-building systems, Soil Dyn. Earthq. Eng., 17, 509–517.

Chapter 3
Role of Dynamic Properties on Building Vulnerability

Angelo Masi

Introduction

Dynamic properties have a major role on the seismic behavior and vulnerability of building structures. Particularly, fundamental periods of vibration are needed, both in design of new buildings and in assessment of existing ones, so that their seismic response can be evaluated.

Several codes (e.g. CEN, 2003; NZSEE, 2006) recommend empirical simplified expressions between the height of a building type and its fundamental period. Such expressions were calibrated keeping in mind a force-based design (Goel and Chopra, 1997), thus intentionally aim at underestimating period values. For this reason they usually provide rather low values when compared to those ones obtained keeping in mind a displacement-based design (see e.g. Chopra and Goel, 2000), also when the latter were obtained from numerical simulations performed on carefully set up models (see e.g. Crowley and Pinho, 2004; Priestley et al., 2007). Even larger differences appear when numerical estimates are compared to experimental results based on ambient vibration measurements, that provide very low period values (see e.g. Navarro et al., 2004). An overview of the different approaches together with a comparison of the relevant results is reported in Masi and Vona (2008); further, period-height expressions for some reinforced concrete building types are given, where the role of important structural characteristics (building height, cracking, masonry infills, elevation irregularities, etc.) is carefully taken into account.

Coupling between soil and building fundamental periods of vibration may cause resonance effects. For this reason also their variation, as a consequence of possible building damage and/or soil non linear behavior during the motion, needs to be considered. Typically, structural and geotechnical engineers have different points of

A. Masi
DiSGG – University of Basilicata, Campus Macchia Romania, Potenza, Italy
e-mail: angelo.masi@unibas.it

M. Mucciarelli et al., (eds.), *Increasing Seismic Safety by Combining Engineering Technologies and Seismological Data,* NATO Science for Peace and Security Series C: Environmental Security,

view about resonance effect and its variation during a seismic motion. Structural engineers say that whereas building and soil have initially close periods and an earthquake occurs, the building period, as a result of structural and non structural damage, is expected to increase during the motion, so that the building "hides" itself reducing the heaviest effects of resonance. Geotechnical engineers do not completely agree with this opinion saying that also the soil period can shift towards higher values, that is in the same direction of the building one, thus the resonance condition could arise again. The question to be dealt with is: how much is the relative amount of that increase? A general answer is not possible, as it depends on building and soil type. For example, in case of reinforced concrete buildings with masonry infills, a very large increase of the building period can be expected with the level of shaking due to cracking of structural members and, particularly, of brittle masonry infills, see e.g. Mucciarelli et al. (2004), Calvi et al. (2006).

Finally, estimating the variation of the dynamic characteristics after retrofitting or strengthening interventions, by computing the modified values of fundamental periods, damping factors and mode shapes, can be a practical tool to evaluate the effectiveness of the intervention (Farsi et al., 2008). To this purpose and also as a diagnosis tool, ambient vibration measurements can be very helpful (Boutin and Hans, 2008).

All the above questions strongly require that further studies as well wide in-situ and laboratory experimental campaigns are carried out to set up procedures able to evaluate, in a reliable as well not expensive way, building dynamic properties.

References

Boutin, C. and Hans, S., 2008. How far ambient noise may help to assess building vulnerability? Proc. of Workshop Increasing Seismic Safety by Combining Engineering Technologies and Seismological Data (this volume), Springer Ed., The Netherlands.

Calvi, G.M., Pinho, R., and Crowley, H., 2006. State-of-the-knowledge on the period elongation of RC buildings during strong ground shaking, Proc. of 1st European Conference on Earthquake Engineering and Seismology, CD-ROM edition, Paper No. 1535.

CEN, 2003. Eurocode 8: Design of structures for earthquake resistance, Part 1: General rules, seismic actions and rules for buildings, Final Draft, Comite Europeen de Normalisation, Brussels, December 2003.

Chopra, A.K. and Goel, R.K., 2000. Building period formulas for estimating seismic displacements, Earthquake Spectra, 16(2), 533–536.

Crowley, H. and Pinho, R., 2004. Period-height relationship for existing European reinforced concrete buildings, Journal of Earthquake Engineering, 8(1), 93–119.

Farsi, M.N., Guillier, B., Chatelain, J., and Zermout, S., 2008. Retrofitting and strengthening evaluation from stiffness variations of a damaged building from ambient vibration recordings, Proc. of Workshop Increasing Seismic Safety by Combining Engineering Technologies and Seismological Data (this volume), Springer Ed., The Netherlands.

Goel, R.K. and Chopra, A.K., 1997. Period formulas for moment resisting frame buildings, Journal of Structural Engineering, ASCE, 123(11), 1454–1461.

Masi, A. and Vona, M., 2008. Estimation of the period of vibration of existing RC building types based on experimental data and numerical results, Proc. of Workshop Increasing Seismic Safety

by Combining Engineering Technologies and Seismological Data (this volume), Springer Ed., The Netherlands.

Mucciarelli, M., Masi, A., Gallipoli, M.R., Harabaglia, P., Vona, M., Ponzo, F., and Dolce, M., 2004. Analysis of RC building dynamic response and soil-building resonance based on data recorded during a damaging earthquake (Molise, Italy, 2002), Bulletin of the Seismological Society of America, Vol. 94, N. 5, pp. 1943–1953.

Navarro, M., Vidal, F., Feriche, M., Enomoto, T., Sánchez, F.J., and Matsuda, I., 2004. Expected ground-RC building structures resonance phenomena in Granada city (Southern Spain), Proc. 13th World Conf. on Earthq. Engin., Vancouver, B.C., Canada, August 1–6, 2004, Paper No. 3308.

NZSEE, 2006. Assessment and improvement of the structural performance of buildings in earthquakes, Recommendations of a NZSEE Study Group on Earthquake Risk Buildings, June 2006.

Priestley, M.J.N., Calvi, G.M., and Kowalsky, M.J., 2007. Displacement-Based Seismic Design of Structures. IUSS Press, Pavia, Italy.

Chapter 3.1
How Far Ambient Noise Measurement May Help to Assess Building Vulnerability?

Claude Boutin and Stéphane Hans

Abstract The use of noise data in seismic diagnosis of buildings is analyzed. From the responses to ambient noise, harmonic excitation and shocks, the dynamic behavior of usual buildings is identified in the range of $10^{-5} - 10^{-2}\,g$. Taking advantage of the demolition, the influence of the light work elements, full precast facade panels, bearing masonry walls and the presence of neighboring joined buildings is determined. These experiments show that noise measurements efficiently provide reliable data of real interest for understanding the actual building behavior.

Then, the integration of these data in a vulnerability diagnosis is presented. It is shown that regular concrete structures are described by suited beam modeling. Thus for a given structure, taking into account the noise data, the adequate beam model, and taking the maximum tensile and compression strains of concrete and steel as damage criteria, two levels of ground acceleration can be determined, namely the Seismic Thresholds of Elasticity and of Yielding. Quantify the levels that onset the structural damages and the plastic hinge may be a useful tool for vulnerability diagnosis.

Keywords Ambient noise · Structural dynamics · Generalized beams for buildings · Vulnerability · Seismic thresholds of integrity and yielding

3.1.1 Introduction

The macroseismic intensity scale, based on observed damages after earthquakes, constitutes the first frame of statistical analysis of vulnerability, according to the typology of structures. Introducing qualitative factors known to increase the

C. Boutin (✉) and S. Hans
Université de Lyon, Laborataire Géomateriaux, Département Génic Civil et Bâtiment,
URA CNRS 1652
and
Ecole Nationale des Travaux Publics de l'Etat, rue Maurice Audin, 69518 Vaulx-en-Velin, France
e-mail: claude.boutin@entpe.fr; stephane.hans@entpe.fr

M. Mucciarelli et al., (eds.), *Increasing Seismic Safety by Combining Engineering Technologies and Seismological Data,* NATO Science for Peace and Security Series C: Environmental Security,

vulnerability (transparency, asymmetry) leads to a finer frame of analysis than the solely typology. Such statistical information are relevant at large scale – for instance when assessing the seismic vulnerability of a city (Benedetti et al., 1988; Spence et al., 1992) – despite the large standard deviations reported by every post earthquake survey. In fact, because of the large number of structures, the random errors vanish by summation and the mean value is reached.

The question is more complex when the vulnerability of given structure(s) have to be assessed. Obviously, the statistical information attached to the category of the studied structure is of first importance. However, the knowledge of the category's mean value is not sufficient, because of the possible unknown deviation for this particular building. For instance, a structure belonging to the category "60% of chance of moderate damages" can actually be severely or weakly damaged.

To reduce the uncertainty, data specific to the studied structure have to be integrated. However, the number of buildings to be evaluated avoid sophisticated but very time-consuming methods, and argue in favour of procedures as simple and reliable as possible. These obligations introduce two mains questions:

- How to reduce the deficiency of information on a given building by going from qualitative to relevant quantitative information?
- How to exploit efficiently this complementary specific information in terms of vulnerability for the considered building?

This work attempts to answer these two questions. At the light of experiments on real buildings, and on the basis of realistic, tough simple modeling, the aim is to propose a protocol giving practical criteria of interest for a vulnerability diagnosis.

The first part of this chapter focus on the first question by investigating in detail the interest of in situ dynamic monitoring tests (Hudson, 1970) and particularly the ambient noise measurements. This latter auscultation method, that records vibrations at a level much smaller than that induced by seismic events, is frequently criticized. Trough experiments realized with ambient noise, shaker and shocks, on intact and modified buildings (Boutin and Hans, 1998; Boutin et al., 2005; Hans, 2002; Hans et al., 2005), it will be shown that – for practical applications and with sufficient care in the use of the data – the critics are not founded in most cases.

The Section 3.1.2 is devoted to the experimental procedure and data processing. The Section 3.1.3 focus on the identification of the behavior of usual buildings – built according to the design rules of common practice – from a weak level of acceleration (ambient noise $\approx 10^{-5}\,g$) to a medium level (shock $\approx 10^{-2}\,g$), with and without soil structure interaction. The modal characteristics gathered during progressive demolitions are exposed in Section 3.1.4 and show:

– A significant influence of full precast facade panels and bearing masonry walls
– The weak influence the light work elements like secondary dividing walls,...
– The weak influence of the presence of neighboring joined buildings

Section 3.1.5 synthesises the main lessons drawn from this experimental program.

The second part is dedicated to the second point, i.e., the links between the experimental data and a draft diagnosis. This purpose is achieved in two steps:

- First – in the framework of generalized beam theory describing the behaviour of regular buildings – the identification of criteria enabling to relate the modal characteristics extracted from the measurements to the mechanical functioning of the structure (Section 3.1.6)
- Second, the definition and calculation of the so called Seismic Thresholds of Elasticity and Yielding suited to a given structure (Section 3.1.7)

This procedure highlights the actual interest of coupling both experimental data and relevant beam modelling of the building for establishing a vulnerability diagnosis.

3.1.2 Monitoring methods and tested structures

3.1.2.1 In situ monitoring methods

Testing real structures enable identifying some phenomena otherwise difficult to reproduce or identify in idealized laboratory experiments. In addition, these experiments avoid the sensitive questions of the scale similarities which interfere with the interpretation of tests at reduced scale or enlarged time. In counter part, the tested structures are only partially known and the range of loading is limited.

The in situ testing method consisted in recording the accelerometer responses of the structure. Three types of excitations were used to identify frequencies, modal shapes and non-dimensional damping ratios: ambient loads, harmonic excitation (using a mechanical shaker constituted by two counter-rotating masses) and shock loading (induced by a mechanical shovel). Whatever the excitation is, the acceleration is small enough not to move the structure's response beyond its elastic domain.

The measurement device is composed of:

- Twelve ICP 1D accelerometers of sensibility of $10^{-5}\,g$, linear in the range 0–80 Hz
- A 12-channel HP3566A synchronized analogical recorder
- A PC with HP software driving the hardware storage and the signal processing

A sampling frequency of 128 Hz and a time-recording of 64 s were retained to avoid problems of spectrum folding and cut-off frequency, permitting to analyze a 0–50 Hz frequency bandwidth sufficient to capture the modes of interest in the seismic range. The accelerometers were located in the center of the structural cross-section, one at the first floor, one at the top floor, the others in the intermediate levels. Longitudinal (lengthwise) or transverse (in the direction of the width) oscillations may be recorded independently when changing the accelerometers orientation. In this study, the attention is focused on horizontal vibrations, more critical for the seismic risk than vertical vibrations.

Ambient vibrations

This method, initiated in the 1970s, (Stubbs and MacLamore, 1973; Trifunac, 1972), knows actually large developments due to its simplicity, (Farsi, 1996; Ivanovic et al., 2000). Ambient vibrations result from a mechanical noise (earth and urban activity) transmitted to the structure through the soil. Wind and internal activity could also contribute, however, in this study, the measurements were made by calm weather in buildings free of inhabitants. It has been verified that on the ground the density of probability of the signals is Gaussian, enabling to consider that the building responds to a white noise imposed motion. The horizontal acceleration is of the order of 10^{-5} g at the bottom and 10^{-4} g at the top.

Harmonic forcing

Harmonic oscillator was used for instance by Englekisk and Matthiesen (1967), Jennings and Kuroiwa (1968) or Petrovski et al. (1973) as device to identify the dynamic behavior of structures. Here a shaker (CEBTP) constituted by two counter-rotative masses was used. This device delivers in a given horizontal direction a sinusoidal horizontal force controlled in amplitude (maximum 7,000 N) and frequency (in the range 1–10 Hz), (Paquet, 1976).

Tests consist in fixing the oscillator at the center of the top floor with two orientations corresponding to the main directions of the building. Accelerations are recorded in harmonic steady state regime and in free oscillation regime (after the shaker is switched off). The horizontal accelerations reaches 10^{-4} g at the basis and 10^{-3} g at the top, i.e. about ten times the level induced by the ambient vibrations.

Shocks

Shocks tests were realized by impacting the building in the two main directions (generally at an high storey and at the center of the facade) by means of an heavy mechanical shovel (usually used for demolition). It should be mentioned that the damage (when it appears) is localized in the very vicinity of the impact and outside this zone the structure remains entirely intact. The accelerometers triggered before the shock records the entire free oscillations response.

Compared to ambient vibrations and harmonic oscillations, the short impulsive record is of larger magnitude, giving a pick acceleration of about 10^{-2} g even on the ground floor, i.e. 1,000 times greater than the ambient level.

3.1.2.2 Tested structures

The tested building – located in Vaulx-en-Velin, suburbs of Lyon, France – were all in good condition, their demolition was subsequent to an new urban designed

planning policy. They are representative, from both engineering and architectural points of view, of number of urban buildings erected between 1970 and 1975. Some common characteristics are:

- Structural regularity in plan (with transverse and longitudinal symmetry)
- Structural regularity in elevation (all levels identical, no transparency on the ground floor)
- Weak amount of steel reinforcement bars in the concrete elements (of standard thickness of 15 cm) and very poor steel reinforcement in the precast panels

The soil is mixed gravel and consolidated clay deposits with good mechanical properties; a surface wave measurement indicates a shear wave velocity around 300 m/s at 5 m depth. All the tested buildings are founded on shallow foundations.

Features of buildings

The cross-sectional plans of typical floor and a picture of the tested structures are presented in the Figure 3.1.1. Their main characteristics are described below:

- Building C of eight storeys was constructed using the industrial "tunnel casing" technique; the floors and transverse shear walls are made by reinforced concrete; the lengthwise bracing is mainly provided by the two full precast facade panels and the shaft walls of the lift.
- Buildings D, E, F, of five storeys, have floors of reinforced concrete associated, external shear bearing walls in light parpen (masonry bricks) and internal shear bearing walls in heavy parpen (bricks); they were roughly placed on an axe parallel to one of their diagonal and separated by 5 cm gaps filled with polystyrene that run only over a small part of the longitudinal facade.

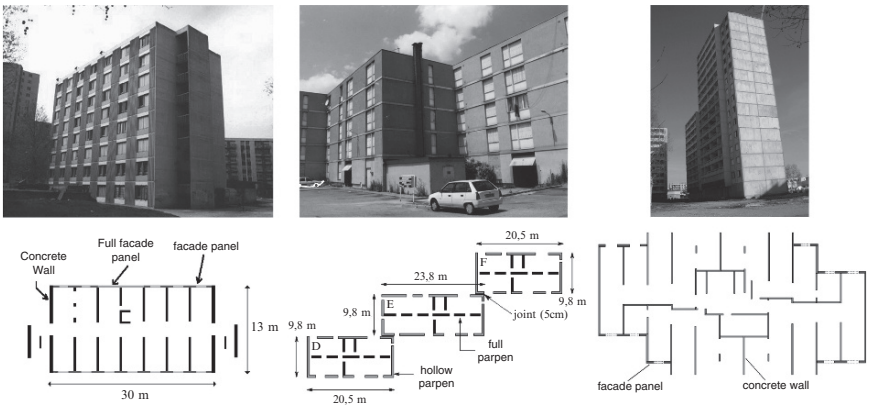

Fig. 3.1.1 The tested buildings and their typical floor plan view

Table 3.1.1 Dimensions and masses of tested buildings

Building	C	D	E	F	G
Length L (m)	30.0	20.5	23.8	20.5	31.4
Width W (m)	14.0	9.8	9.8	9.8	13.4
Height H (m)	21.6	14.1	14.1	14.1	43.2
H/W ratio	1.54	1.45	1.45	1.45	3.22
H/L ratio	0.72	0.69	0.59	0.69	1.38
L/W ratio	2.14	2.1	2.44	2.1	2.33
Story specific mass (t/m^3)	0.27	0.23	0.23	0.23	0.25
Linear mass (t/m)	114	46	53	46	110

– Building G of 16 storeys presents floors and longitudinal and transversal shear walls in reinforced concrete; the facades are made by precast panels.; close to this building, separated by a 5 cm gap, a similar building of 11 storeys is located.

Table 3.1.1 shows the dimensions and slender parameters of these buildings, together with their storey density and lineic mass, both deduced from the plans and the usual density value of materials.

3.1.2.3 Analysis of the records

The classical framework of modal analysis is used to extract information from the records. This is well supported by the experimental facts among them:

– The presence of sharp peaks in the response spectra which indicates a notable response amplification at those frequencies.
– The fact that those frequencies are identical in any point of the structure which proves that, actually, the whole structure is affected by the same oscillation.
– The good agreement of the results derived from multi-type loadings (random, harmonic, shock) and very different levels of amplitudes (ranging over four decades) which illustrates the characteristic feature of (quasi-)linear systems.
– Systematically, the nth modal shape has n fix nodes.

Theoretically, all the modes appear simultaneously in the response. Nevertheless as the eigenfrequencies of studied buildings were well separated and the damping weak (see Table 3.1.2), the contribution of the other modes at the frequency of a given mode can reasonably be neglected, at least for the few first modes.

Processing technics

The signals are processed either in spectral or in time domain.

Spectra of ambient vibrations (with smoothing), free oscillations and shocks have been calculated by Fast Fourier Transform (FFT). The modal frequencies and shapes

Table 3.1.2 Modal characteristics of buildings C and G

Building		Building C		Building G			
Direction		Longitudinal		Longitudinal		Transversal	
Mode number	Monitoring method	Freq (Hz)	$\zeta(\%)$	Freq (Hz)	ζg(%)	Freq (Hz)	$\zeta(\%)$
Mode 1	Ambient	4.3	2.85	2.08	2.5	1.56	1.3
	Free osc.	4.25	2.4	1.96	2.6	1.49	1.5
	Harmonic	4.19	2.6	1.94	2.3	1.48	1.5
	Shock	4.18	4	–	–	–	–
Mode 2	Ambient	13.4	3.5	7	2.5	6.6	4
	Free osc.	–	–	6.75	2.6	6.26	2.2
	Harmonic	–	–	6.73	2.4	6.17	2.3
	Shock	12.8	4	–	–	–	–
Mode 3	Ambient	23	4	12.8	12	13.5	5
	Shock	22.5	3.8	–	–	–	–
Mode 4	Ambient	–	–	20	4	–	–

of the coupled soil-structure system are simply deduced by peak-picking. The damping ratio is assessed from the pass-band width. A similar procedure applies for the calculation of the modal transfer functions of the structure on fixed base (see below).

The process in the time domain are specific for each kind of signal. Random signals are firstly filtered around each modal frequency, then the autocorrelation functions are determined. From these, the mode shape is deduced by extracting the extrema and the modal damping ratio is derived very accurately from the logarithmic decrement. Harmonic responses are exploited classically. Eigenfrequencies are identified from the maximum sweep response, mode shapes from the amplitudes at the eigenfrequencies and damping ratio from the sweep response bandwidth. Finally some impulse responses under shocks were processed using Cauchy wavelet (Argoul et al., 2000). The amplitude patterns of the wavelet transforms enable a refined determination of the modal characteristics and even reveal the weak non-linearity effects when occur.

Structure-soil system and structure on fixed basement

The in-situ measurements naturally lead to the modal characteristics of the structure coupled with the soil. However, when the soil presents good characteristics, as in the present case, a weak contribution of the soil-structure interaction might be expected and therefore, the modal parameters of the structure coupled with the soil (SS) to be close to those of the structure lying on a rigid basis (SB), at least for the first modes. When possible, it is interesting to derive the own modal characteristics of the structure on fixed base, corresponding to the intrinsic properties of the structure.

Assuming that the building base is infinitely rigid, the soil-structure system is composed of two coupled sub-systems, (i) the soil, and (ii) the structure on rigid

basement (SB). In the case of ambient vibrations due to soil motions, a weak soil-structure interaction means that the base motion is almost identical to the incident motion. Thus, it can be considered that the structure motions, observed in the non-galilean frame attached to the base, define the SB transfer functions. Consequently the intrinsic behavior of SB structure is deduced by suppressing the rigid body motion induced by the base motion.

Conversely, for shaker excitation and shocks, since the level of vibration is much higher than the level of the ambient soil motion, it is expected that the base motion be mainly due to the soil-structure interaction; therefore, the identification of the SB behavior from the SS behavior would require more sophisticated derivations.

3.1.3 Results concerning intact structures

3.1.3.1 Identification of modal characteristics

Modal frequencies and damping ratio for buildings C et G are gathered in Table 3.1.2 and the corresponding modal shapes are presented in Figures 3.1.2 and 3.1.3. A very good agreement is observed between the results given by different vibration methods. This result was systematically observed for all the tested buildings.

These experimental findings confirm that from small amplitudes of ambient vibrations to significantly larger amplitudes (shocks), the structures respond systematically by following the same quasi-elastic behavior (Trifunac, 1972). An important conclusion is that *ambient measurements are sufficient to identify the structure's behavior for the whole quasi-elastic domain*.

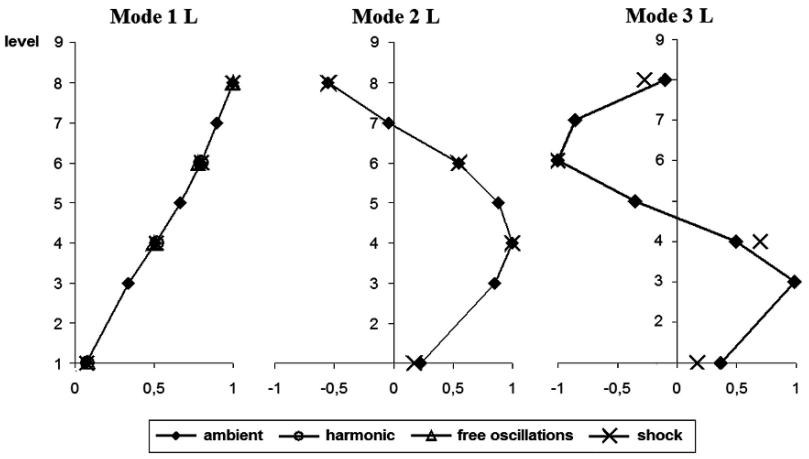

Fig. 3.1.2 Mode shapes of building C in longitudinal direction identified from the several types of excitation

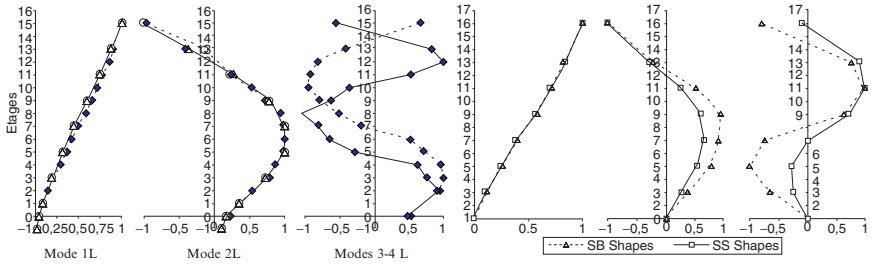

Fig. 3.1.3 Modal shapes of building G. Left, modal shapes of the system soil-structure (SS). Right, comparison between SB modal shapes (obtained by extracting the soil-structure interaction) and SS modal shapes (whose base motions were nullified)

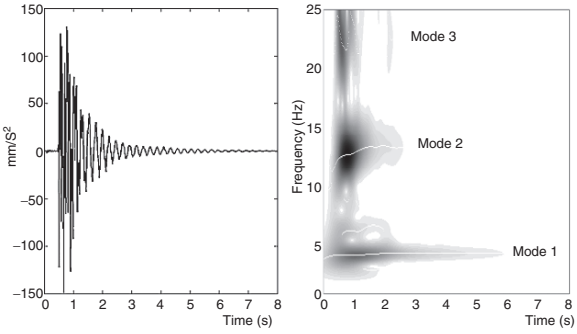

Fig. 3.1.4 Shock on building C (longitudinal direction). Left, temporal record. Right, wavelet analysis. Note the presence of three modes and the slight migration of eigenfrequencies corresponding to a weak non-linear effect when amplitude varies from 10^{-2} to 10^{-5} g

3.1.3.2 Weak non-linear effects

The tests bring to the fore a weak non-linearity of the buildings, function of the motion amplitude. Systematically, the eigenfrequencies tends to decrease from ambient to shocks tests (Table 3.1.2). Nevertheless, this fall is of order of 2–5% while amplitude wins a factor 1,000 (from about 10^{-5} to $10^{-2}\,g$). The variations on damping are not so clear and any modification of modal shapes seems occur. This phenomena has already been observed in the past by different authors (e.g. Ellis (1996), Jennings and Kuroiwa (1968)).

To investigate this non-linear effect, a wavelet analysis has been realized on shocks tests. This provides the instantaneous characteristics of a transient signal, i.e., in function of the time, the modal frequencies and modal amplitudes from which the associated damping or shapes can be deduced. As a shock response ranges from high level at the beginning to ambient level at the end, a good overview can be obtained (Figure 3.1.4). In time-frequency domain, the first three vibration modes (respectively between 4.1 and 4.3 Hz, 12.8 and 13.5 Hz and around 22.5 Hz) appear with a clear temporal localization, the third mode being quickly damped, followed by the

second and finally the first. This analysis shows a light decrease of the eigenfrequencies and a light increase of the modal damping with the increase of amplitude response. This softening behavior is very similar to soil behavior. It seems hence reasonable to localize the origin of this non-linearity in the soil foundation through soil-structure interaction phenomena. It has nevertheless to be underlined that the modal shapes do not present any variation. The observed variations are sufficiently limited (never more than 7%) to be neglected in first approximation in case of good soils.

3.1.3.3 Soil-structure interaction

The modal shapes of building G, presented on Figure 3.1.3, are related to the real system (SS) – that includes the soil participation in the dynamics – and the structures on fixed base (SB) (cf. "Structure-soil system and structure on fixed basement"). Clearly a (SS) displacement of the base is visible, increasing from the first to the higher modes. According to the procedure given in the section "Structure-soil system and structure on fixed basement", the characteristics of the structures on fixed base (SB) are deduced and compared in Table 3.1.3 and Figure 3.1.3 with SS modal characteristics. As expected, the SS eigenfrequencies are smaller than SB ones, because of the softness induced by the soil. Moreover, the differences grow for higher modes. This is consistent with the increase of the modal stiffness of the structure with modal number, leading in turn to increase the soil-structure interaction:

– For the first and second modes, the modal stiffness is too low to initiate significant interaction with the soil, and, de facto, there is small differences between SB and SS modal characteristics.
– For higher modes, the modal structure stiffness grow quickly and larger modification of the modal characteristics appears.

It is worth to mention that, for studied buildings, this effect is limited (less than 5% for the eigenfrequencies), so that, for a seismic vulnerability point of view, soil-structure interaction does not modify significantly the seismic behavior.

Table 3.1.3 Soil-structure interaction – comparison between soil-structure (SS) and structure-on-fixed-base modal frequencies (SB) for buildings C and G

Building		Building C		Building G	
Direction	Mode	SS (Hz)	SB (Hz)	SS (Hz)	SB (Hz)
Longitudinal	1	4.32	4.45	2.08	2.15
	2	13.5	14.1	7	7.25
	3	23	23.6	12.8	14
Transversal	1	4.5	4.66	1.56	1.56
	2	–	–	6.6	6.65
	3	–	–	13.5	14

3.1.4 Experiments on modified buildings

Measurements on real buildings may be actually of interest for seismic assessment, provided that they represent the effective dynamic behavior before significant structural damages. This question is nevertheless difficult to address theoretically because of the lack of reliable information for modelling parasite phenomena that may modify the modal characteristics. Thus experiments dedicated to the analysis of these perturbation effects (presence of light work elements, ...) provide qualitative, or when possible, quantitative estimates. In this aim, tests were also performed after modifying the buildings or their immediate vicinity. If general conclusions can not be drawn from the particular studied cases, the trends will nevertheless be useful for number of buildings presenting similar configurations.

3.1.4.1 Effect of light work elements

How large extent can the presence of light work elements influence the modal characteristics? The additional mass of these elements can reasonably be estimated to about 5% (or less) of the mass of the structure. The difficulty lies in the additional stiffness brought by the light elements well connected to the structure. A direct quantification is unrealistic because of the large number of unknowns.

The demolition of the building G gave the possibility to investigate on this aspect. As the concrete was intended to be recycled after demolition, any contamination with the other construction materials was avoid. For this reason, the light elements as the secondary dividing walls in plaster or bricks (thickness of 5–7 cm), the windows and their aluminium frames, the doors and doorways in wood and steel, were taken off before beginning the demolition of the 'naked' concrete structure.

Ambient vibrations measurements were performed on the cleared structure. The comparison with the spectra of the intact building is given in Figure 3.1.5. It appears that removing the whole non structural elements induces a slight (but clearly measurable) decrease of eigenfrequencies of about 3–4%. This means that, in the considered case, the stiffness effect is more significant than the mass effect.

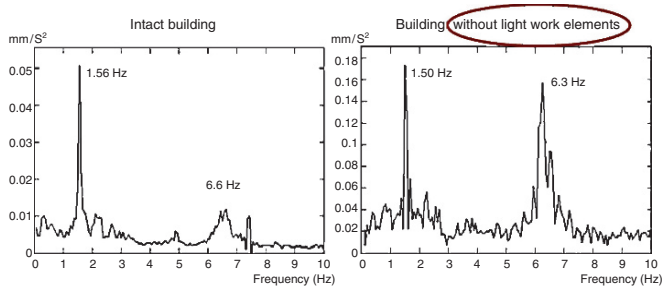

Fig. 3.1.5 Examples of Fourier transforms of ambient vibrations measurements realized on building G before and after the removal of light work elements (transverse direction)

It can be also deduced that, for this kind of very common buildings equipments, the presence of these non-structural elements increases the shear and bending stiffness by about 6–8%. This effect can therefore be neglected in a first analysis.

3.1.4.2 Importance of masonry parpen walls

The role of the masonry parpen wall in the modal behavior is not always clear, essentially because the material properties are not very well known, and the quality of the connections with the other structural elements is questionable.

In building F, the influence of walls made of light parpen was investigated in the following way. The entire wall (i.e. for the four storeys) constituting the south facade was demolished, leaving unmodified the rest of the building (Figure 3.1.6). Then free oscillations after impacts in the North-South and East-West directions were recorded. Note that the destruction of the wall broke the quasi-symmetry of the intact building, so that a pure E-W translation mode is no more possible. The Figure 3.1.6 shows the comparison of the responses spectra for the intact and modified building.

In the E-W direction (shear direction of the destroyed wall), a drastic reduction of the eigenfrequency from 5.15 to 4.5 Hz is observed. This leads to a roughly assessment of the wall contribution about a quarter of the storey stiffness. This estimate is consistent with the reduction of the total length of the E-W shear walls.

In the N-S direction (out of plane bending of the destroyed wall), the frequency of the main peak remains the same, meaning that the out of plane stiffness is negligible in regard to the shear stiffness of the N-S walls (the secondary peak at the same frequency [4.5 Hz] than in the E-W direction may result either from the coupling between both directions or from an imperfect direction of the impact).

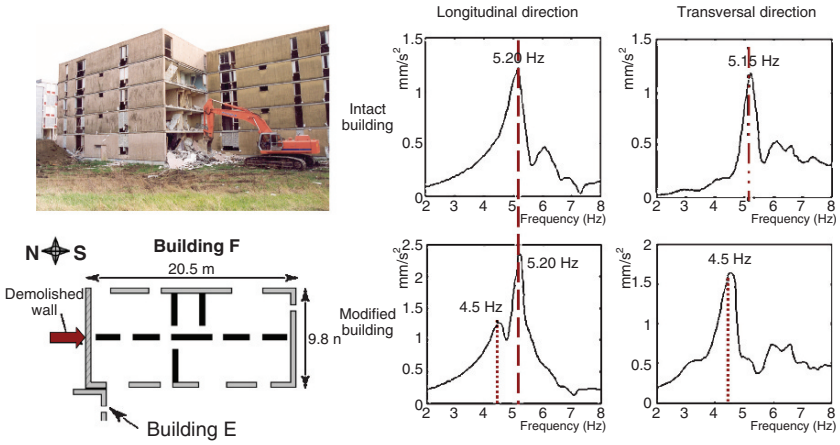

Fig. 3.1.6 Modification of building F – the wall has been demolished from the base to the top of the building and comparison of the spectrum responses for the intact and modified building

Additionally, those experiment enables, from a simple discrete shear beam model, to assess the equivalent modulus of the heavy and light parpen respectively to $E_{FP} \approx 2.7\,\text{GPa}$ and $E_{HP} \approx 1.5\,\text{GPa}$. These values, which are ten times smaller than for a concrete, are consistent with those given in the literature.

To conclude, despite the presence of internal walls of heavy parpen, the contribution of the light parpen walls (in their shear direction) is very significant and cannot be neglected. This result is of first importance for framed building with masonry infill. This conclusion is supported by number of post earthquake reports, mentioning that the absence of infills at the ground level creates a critical 'transparent' storey.

3.1.4.3 Role of plain precast facade panels

Precast facade panels are widely used in recent buildings. It is generally assumed that their connection with the concrete structure is sufficiently good to consider that the full panels (i.e. without large opening for windows) may participate to the horizontal strength of the building. This point was checked by means of a step by step demolition realized on the building C which included two full panels by storey. At first, at the ground level, a panel of the longitudinal North-West facade was removed. Then a shock were applied in the N-W direction (shear direction of the removed panel) and the free oscillations recorded. The same procedure were reproduced twice for the two plain panels at the second level.

The spectra recorded in the four states (intact and 1, 2, 3 removed panels) are presented in Figure 3.1.7 where a zoom around the first longitudinal eigenfrequency is plotted. A slight but measurable regular decrease of the frequency clearly appears, although the modifications only affect two of the eight storeys. By a simple

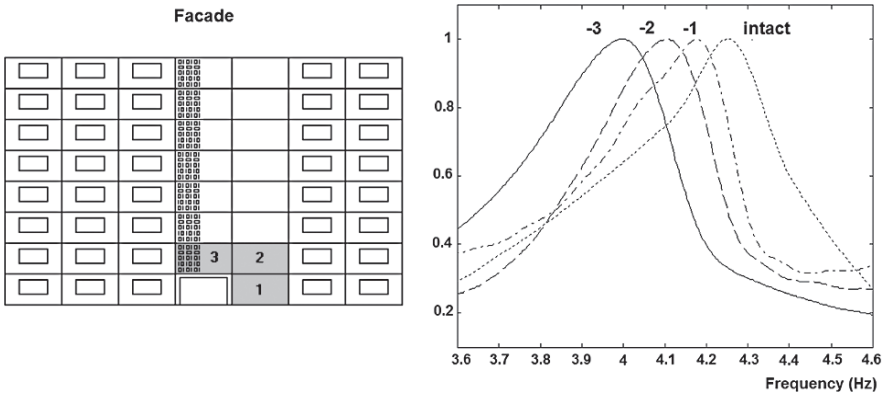

Fig. 3.1.7 Evolution of first longitudinal eigenfrequency during the successive removals of full precast panels on the building C

modelling based on discrete shear beam, one deduces that the contribution of the two panels to the storey shear stiffness lies in between 20% and 25%.

This confirms that full panels in their shear direction can not be neglected for interpreting the modal behavior. Let us mention that, as the parpen walls, the panels are almost unreinforced and would not present any ductility.

3.1.4.4 Influence of neighboring joined buildings

The possible mutual influences of close building are generally disregarded. This point was investigated in the group of the three similar buildings D, E, F: the ambient vibrations of the intact building D was recorded in presence of buildings F and E, then again after demolishing F, and finally after both F and E were destroyed.

The resulting modifications of the first eigenfrequency are given in Table 3.1.4. In both directions, the successive demolitions induced a systematic decreasing of the frequencies. The differences are not negligible and can reach 10% in the more significant case. As the ambient motion is very small compared to the thickness of the structural joints (which concerns only a small part of the facade), this latter do not play any role in the dynamics. Thus, the origin of the buildings coupling has to be found in the transmission of motions and stresses throughout the soil.

Modeling this dynamic structure-soil-structure interaction would require numerical approaches. Nevertheless an explanation consistent with the measurements can be proposed. Consider two identical joined buildings. The soil stiffness imposes the differential motion of their rigid foundation to be negligible. Therefore both buildings should respond almost as if they were lying on an unique common foundation. Comparing with the same single isolated building, the only difference lies in the fact that, proportionally, the rocking impedance is smaller. Consequently, the eigenfrequency of single building should be smaller than that of the two joined buildings.

This experiment tends to show that the mutual influence, namely the structure-soil-structure interaction, may play a role, especially for close buildings presenting almost the same features (and eigenfrequency). Further experimentations should be carried on before generalizing this conclusion.

Table 3.1.4 Structure-soil-structure interaction – decreasing of fundamental frequency of building D during the demolition of neighboring buildings E and F

Building(s) in presence	D-E-F intact	D-E intact F demolished	D intact E-F demolished	Total decreasing
Longitudinal first frequency of D (Hz)	5.6	5.4	5.08	9%
Transversal first frequency of D (Hz)	5.65	5.47	5.35	5%

3.1.5 Synthesis of lessons drawn from experiments

The main lessons drawn from these experiments are that (i) the lack of information on existing buildings may be overcomed by means of ambient vibration measurements, and (ii) that these later do provide data directly linked with the key elements actually participating to the structural behavior.

The very good agreement observed on real buildings when using ambient, harmonic and shock excitation deserve to be emphasized for two main reasons. First, the stability and the consistency of the results prove the robustness and the reliability of information collected through those methods. Second, it demonstrates that almost the same quasi-elastic behaviour remains valid on a wide range of acceleration levels covering the ambient level (around 10^{-5} g) up to the shock level (10^{-2} g for the tested buildings). It is worth mentioning that this result has been somehow extended to earthquakes by Dunand (2005) who performed ambient tests on instrumented Californian buildings. The records of both strong motions and ambient noise show that when buildings suffer *a weak level of damage*, the shift of eigen frequency is temporary and no more than 20%. Moreover, the top motion in the building under earthquake can be fairly well reproduced from the first mode identification – deduced from ambient noise – and the strong motion recorded on the basis.

The tests performed on intact and modified structures enables to identify and quantify the leading and negligible phenomena that may influence the actual quasi-elastic behaviour. It is shown that:

- Full precast facade panels or masonry shear walls do have a significant role, and consequently they have to be considered in the analysis of the building behavior.
- On the contrary, the influence of light work elements or the effect of neighbouring structure may exist as perturbation that can neglected in a first approximation.

As these effects are weakly documented, their quantification in some particular cases should be useful in a number of similar situations. Moreover, these investigations point out the elements of the structure that have actually to be considered in the building behaviour before significant damage. This is a key point before to intend integrating in situ data in a diagnosis procedure.

Now, the question is to establish a link between the experimental data and a draft diagnosis. The idea is to exploit the fact that the quasi-elastic behavior:

- Is well defined by ambient noise vibrations
- Coincides with that of the real structure during earthquakes until the onset of structural damages in the concrete
- Might be extended up to the onset of yielding of concrete in compression and of steel bars (in first approximation)

Thus provided that criteria for the onset of tension cracks in concrete and of yielding of steel bars and of concrete in compression are given, two thresholds of damage can be derived from the quasi-elastic vibration modes. This purpose is achieved in two steps.

The first step consists in relating the modal characteristics extracted from the measurements to the mechanical functioning of the structure. This is developed in Section 3.1.6, in the frame work of the generalized beam theory. In the second step, Section 3.1.7, these results are used to deduce the internal strains associated to the modal deformations. Thus, using as damage criteria for the key structural elements, the strains that onset, (i) cracks in tension within concrete, and (ii) yielding of concrete in compression and of steel bars, the Seismic Thresholds of Elasticity (STE) and of Yielding (STY), suited to a given structure, are derived. These normalized acceleration amplitudes (according to the seismic codes) are directly related to the onset of structural damages and plastic hinges.

This approach is illustrated on the building C. This study case shows how the STE value and the gap between the STE and the acceleration level required by the codes could be of interest for diagnosis of vulnerability.

3.1.6 Relevant beam model for regular buildings

It was established that ambient vibration measurements give the modal characteristics of a building with a good reliability in the whole quasi-elastic domain (despite the presence of slight perturbations induced by a few 'parasite' effects). Moreover experiments on modified buildings indicate that this data are directly linked with the response of the key structural elements. But the link between the modal deformation at the global building scale and the internal strain at the structural element scale, where the damages may occur, is not explicitly given by the experimental data.

The aim of this section is to fill this gap by determining relevant though simple beam modelling whose the conformity with the data could by easily checked. In addition, a clear mechanical understanding at both global and local scales, is given by these beam models that condense in a very synthetic way the essential parameters of the dynamic behavior.

3.1.6.1 The framework of generalized beams

The analysis is here focused on regular buildings of height H made of a sufficient number N of identical storey of height $\ell (H = N\ell)$. The building material is assumed to be elastic of Young's modulus E. Provided that the scale ratio $\varepsilon = \frac{\pi}{2}\frac{\ell}{H} = \frac{\pi}{2N}$ is sufficiently small (say $N > 5$), the homogenization method of discrete structures can be applied to derive the equivalent beam modeling. The theoretical developments, exposed in Boutin and Hans (2003) and Hans and Boutin (2008), show that the dynamic behavior is that of generalized beams controlled by a combination of three mechanisms, namely a shear storey deformation, a global storey bending and an inner storey bending. These mechanisms, illustrated in the Figure 3.1.8, are related to three elastic parameters – the shear stiffness (K), the global bending stiffness (EI)

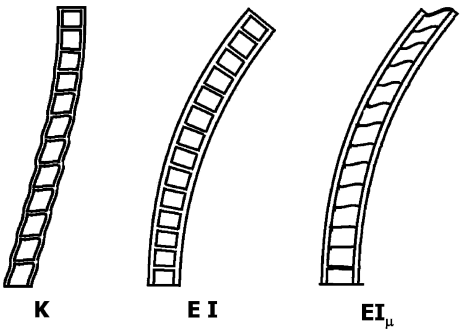

Fig. 3.1.8 Illustration of the three mechanisms driving the transverse dynamic behaviour of periodic hollow structures as buildings

and the inner bending stiffness (EI_μ) – which are derived from elastic properties of the generic storey under static shear or bending deformations. In the general case where all mechanisms are of the same order, the behaviour is described by the non-classical beam equation of the sixth degree:

$$\frac{EI_\mu EI}{K}U^{(6)} - (EI_\mu + EI)\,U^{(4)} - \frac{EI}{K}\Lambda\omega^2 U^{(2)} + \Lambda\omega^2 U = 0 \tag{3.1.1}$$

where $U(x)$ is the horizontal displacement of the floors of the structure. When one mechanisms becomes negligible compared to the others, the general model degenerates into more simple behaviours, namely a slender Timoshenko beam (characterized by EI and K) – Stephen (1999) – or an inner bending-shear beam (EI_μ and K) and when only one mechanism is predominant, a pure shear beam (K), a global bending beam (EI) or an inner bending beam (EI_μ) is obtained.

Two dimensionless parameters are introduced to estimate the weight of each mechanism relatively to the others, namely:

$$C = \frac{EI}{KL^2} \qquad \gamma = \frac{EI_\mu}{EI} \tag{3.1.2}$$

where $L = 2H/\pi$. The parameter C evaluates the global bending effect compared to the shear effect and γ the inner bending effect compared to the global bending effect. The change of variable $\mathrm{x} = x/L$ and $\omega^{*2} = \Lambda\omega^2 L^2/K$ transforms Equation (3.1.1) to its dimensionless form:

$$C\gamma U^{*(6)} - (1+\gamma)U^{*(4)} - \omega^{*2}U^{*(2)} + \frac{\omega^{*2}}{C}U^* = 0 \tag{3.1.3}$$

By comparing the values of C, γ and $C\gamma$ with powers of ε, i.e. writing:

$$C = \varepsilon^\alpha \qquad \gamma = \varepsilon^\beta \qquad \varepsilon = \frac{\pi}{2N} \tag{3.1.4}$$

seven possible behaviours are identified according the value of α and β. The domain of validity of each model is represented on Figure 3.1.9.

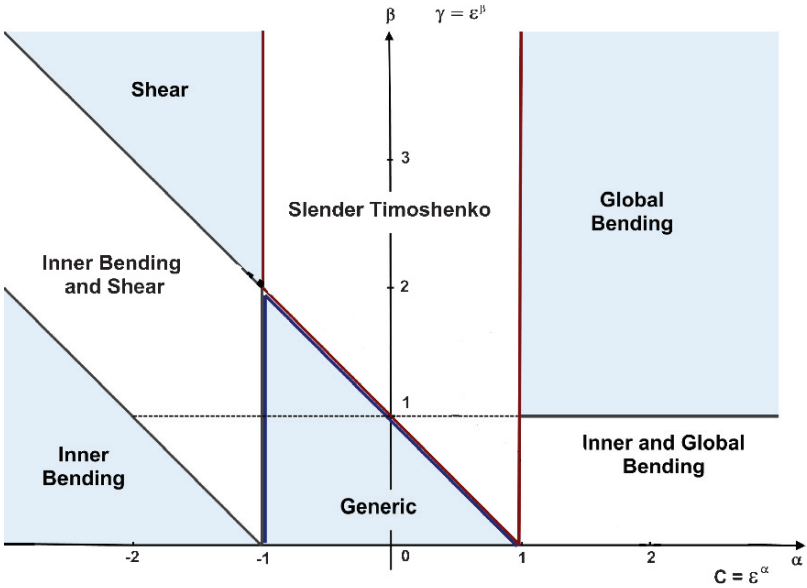

Fig. 3.1.9 Domains of validity of the equivalent beam according to values α and β defined by $C = \varepsilon^{\alpha}$ and $\gamma = \varepsilon^{\beta}$

For instance, when $C = O(1)$ and γg $O(\varepsilon)$, Equation (3.1.3) degenerates into:

$$U^{*(4)} - \omega^{*2} U^{*(2)} + \frac{\omega^{*2}}{C} U^{*} = 0 \tag{3.1.5}$$

which corresponds to a slender Timoshenko beam.

Note that the inner bending effect can participate only if a gap in the bracing of the generic storey exists, like a corridor going through the entire building (e.g. building C in the transverse direction). Consequently, in absence of such a gap (see building G for instance), regular buildings behave as a slender Timoshenko beam.

3.1.6.2 An example: The slender Timoshenko beam

We focus in this section on the slender Timoshenko beam model, whose equation is:

$$EI\, U^{(4)}(x) + \frac{EI}{K} \Lambda \omega^2 U^{(2)}(x) = \Lambda \omega^2 U(x) \tag{3.1.6}$$

that will be used to describe the behaviour of the building G in the following. The feature of such a beam are characterized by the single parameter C. The beam degenerates into an usual Euler-Bernoulli beam when $C = 0$ and into a pure shear beam

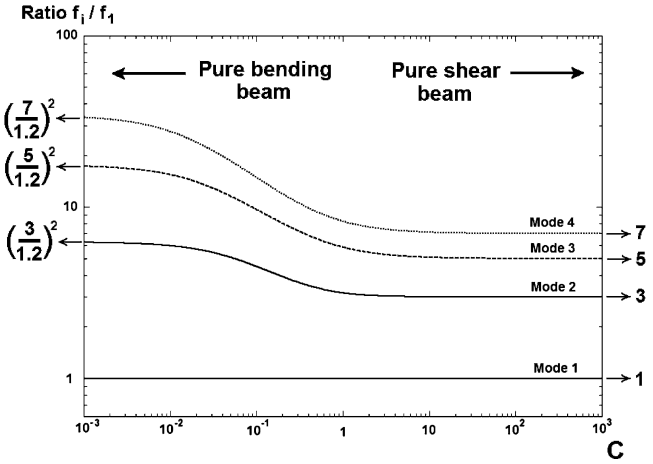

Fig. 3.1.10 Evolution of frequencies ratio f_i/f_1 in function of parameter C

when $C = +\infty$. The usual modal analysis applied to this Timoshenko beam clamped at the base and free at the top, gives the kth eigen frequency:

$$f_k = \frac{1}{2\pi L}\frac{\delta_{1k}^2}{\sqrt{\frac{\Lambda L^2}{EI} + \delta_{1k}^2 \frac{\Lambda}{K}}} \qquad \text{with} \quad \delta_{1k} \qquad \text{closeto} \quad 2k+1$$

The distribution of the eigenfrequencies strongly depends on the nature of beam: the sequence is almost homothetic to the odd integer sequence for beam where the shear dominates (say $C > 5$), whereas, for beams where the bending dominates (say $C < 0.05$), the sequence is almost homothetic to the square odd integer sequence $(2k+1)^2$. Moreover the ratio between two eigenfrequencies depends on the parameter C only. For instance, as illustrated in Figure 3.1.10, the ratio of the two first frequencies monotonically decreases when C increases. Therefore there is a bi-univoque relationship between this ratio and the beam parameter C. *It is worth mentioning that this observation provide a very simple way to identify the nature of the beam from the sequence of the measured eigenfrequencies or even from the* f_2/f_1 *ratio.*

3.1.6.3 Basic assessment of the beam parameters

To go further in the identification of the building with a slender Timoshenko beam, we have to specify how the shear (K) and bending (EI) stiffness (in a given main horizontal direction) and lineic density (Λ) can be determined.

The lineic density Λ is estimated accurately from the plans, and the density of materials (a mean value of 2.3 t/m^3 is adopted for the reinforced concrete). The elastic beam constants are estimated using the following assumptions:

- Perfectly rigid connections are assumed between the structural elements.
- The elastic modulus and Poisson ratio of the material are estimated from usual values (E $\approx$ 20 GPa $\nu \approx 0.2$ for reinforced concrete).
- The floors are assumed infinitely rigid (this assumption is only partially justified and considered in a first level of analysis).

The storey shear stiffness is derived by imposing a differential horizontal drift to two successive rigid floors. This drift applies to the columns and bearing walls whose extremities are clamped on the floors. The elements stiffness is given by usual static formulae that include bending (dominating for columns and out of plane wall motions) and shear (dominating for in plane wall motions). According to these stiffnesses, a global horizontal force is obtained by summing up the contributions of all the elements. This force divided the shear strain (i.e. the differential drift divided by the height of the storey) defines the storey shear stiffness in the studied direction.

The storey bending stiffness is obtained in a similar way. Imposing to two successive floors a differential rotation around a given horizontal axis lead to a linear distribution of positive and negative vertical tensile strains in columns and bearing walls. According to their normal stiffness, this results in a distribution of traction and compression forces giving a global momentum (the position of rotation axis corresponds to a zero global compressive force). The coefficient relating the momentum to the curvature (i.e. the differential rotation divided by the height ℓ of the storey) defines the global bending stiffness in the considered direction.

The Table 3.1.5 gives the numerical results obtained for the building C (longitudinal direction) and building G in both longitudinal and transversal directions. Clearly the C value indicates a dominating shear beam behavior for building C ($C \approx 20$), and a Timoshenko beam behavior in both directions for building G ($0.1 < C < 2$). The three first frequencies calculated from these estimations show an acceptable accordance with the experimental values (at least for these modes), meaning that this model provides a reasonably good description of the building behavior.

Table 3.1.5 Basic estimations on tested buildings with E = 20 GPa

Building	C	G	
Direction	Longitudinal	Longitudinal	Transversal
Lineic mass (t/m)	114	110	110
Shear parameter K (MN)	11,895	27,830	115,600
Bending inertia I (m^4)	2,140	1,836	354
Estimated frequencies (f_1; f_2; f_3)	3.63–11.5–17.8	2.58–7.91–14.12	2.24–10.54–23.07
Experimental frequencies	4.45–14.1–23.5	2.15–7.24–13.97	1.56–6.64–14

3.1.6.4 Experimental derivation of the beam parameters

To complement the a priori assessments, the beam parameters can also be estimated independently from the experimental sequence of eigenfrequencies.

Building C

According to the previous result, building C can be modeled, in its longitudinal direction, by a pure shear beam characterized by its shear stiffness $K = E \cdot S_s$, where S_s reflects the geometry of the structure. Then, the lineic density and the geometry being known, the identification of the beam parameter reduces to determine the Young's modulus E. It is therefore possible to adjust the modulus of the material. In the present case, the fit of the first eigenfrequency of the model with the experimental value (4.45 Hz) yields the realistic value $E = 31\,GPa$. Moreover, with this modulus, the three first model eigenfrequencies are respectively 4.45–13.3–21.8 Hz very close to the experimental ones 4.45–14.1–23.6 Hz.

Building G

For building G, Timoshenko beams were found in the direct procedure to explain the dynamic behavior in both directions. Now, as seen above, the ratio of the two first eigenfrequencies $f_{2/}f_1$ yielding to a unique value of C, two experimental values of C – one for each direction – are given from the experimental ratio $f_{2/}f_1$. The experimental C values – respectively 0.51 and 0.134 in the longitudinal and transverse directions – confirm the Timoshenko behaviour – see Figure 3.1.10. Then, using the first frequencies, the stiffness parameters (EI and K) can be determined for each direction. The Table 3.1.6 gives the results obtained by this procedure. Observing that the longitudinal value (29,288 MN) of K is very close to that (27,830 MN) derived by the direct procedure (Table 3.1.5), it can be conclude that, for this direction, the assumption of rigid floors is satisfactory. Then, the fitting with experimental value leads to evaluate the concrete modulus to 21 GPa.

Table 3.1.6 Experimental refitting on Building G. The Young's modulus (21 GPa) is found by fitting the first longitudinal frequency

Direction	Longitudinal	Transversal
Experimental frequencies (Hz)	2.15–7.24–13.97–20.5	1.56–6.64–14
Experimental ratio f_2/f_1	3.37	4.26
Experimental C	0.510	0.134
Fitted beam model frequencies (Hz)	2.15–7.24–13.97–20.1	1.56–6.64–14
Shear parameter K (MN)	29,288	36,808
Global bending stiffness El $(\mathrm{MN} \cdot \mathrm{m}^2)$	1.13×10^7	3.74×10^6

3.1.6.5 Checking the relevancy of the continuous beam modelling

The beam parameters in accordance with experimental data being now available, the reliability of the modelling can be checked by complementary comparisons. For this purpose, the mode shapes and eigenfrequencies of higher modes have been calculated and compared to the experimental data.

The eigenfrequencies are well described by the beam models, up to the third frequency for building C – though only the first was fitted – and up to the fourth for building G, tough only the two first frequencies were fitted (Table 3.1.6).

The Figure 3.1.11 presents the comparison of mode shapes for building G. Despite the mode shapes were not involved in the fitting process, there is a very good agreement between experiments and modelling, even for the modes whose frequencies were not fitted. Note also that the first mode curvature is consistent with the beam model: negative for beam with dominating bending effect (transversal direction); with an inflexion for Timoshenko beam (longitudinal direction).

Let us also mention that the modulus E experimentally determined ($20 < E < 30\,GPa$) are realistic, and argue in favour of the reliability of this approach. Finally, the consistency of the results (also observed for building C) lead to think that even moderately tall buildings can actually be considered as beams, whose parameters can be determined rather simply from basic information and in-situ measurements.

3.1.7 Seismic thresholds of damage

The question addressed here is: how these experimental data, consistently described by a beam modelling suited to the structure, could contribute to a seismic

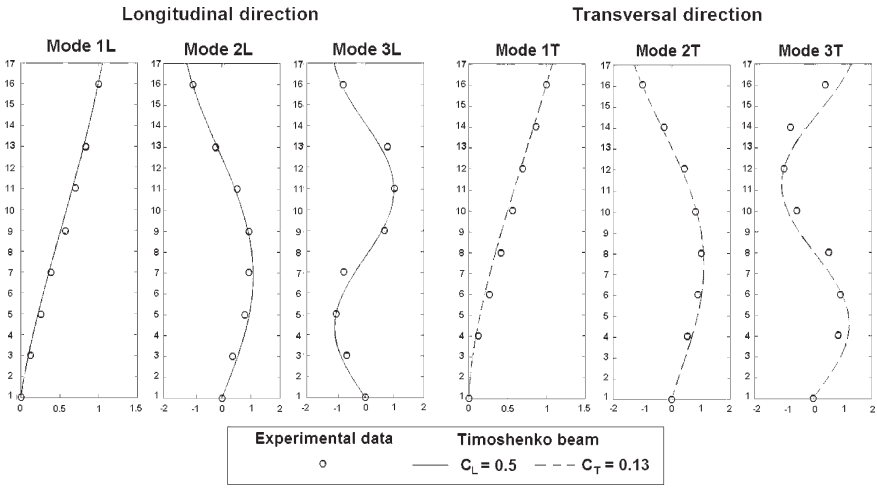

Fig. 3.1.11 Modelling-experiment comparison of modal shapes for the building G

vulnerability diagnosis? It should be emphasized that one focus here on reinforced concrete structures (but the same principle can be adapted to other types of structures).

3.1.7.1 Principle

Since a reliable description of the (quasi) elastic building behavior (including all the mechanically active elements) is available, the first idea consists in determining the limit of this elastic domain. More precisely, it is intended to estimate the seismic acceleration level – related to the normalized spectra given by the code – which generates the onset of structural damages. Beneath this level, called Seismic Threshold of Elasticity (STE), the structure remains elastic, i.e. undamaged. In the same spirit, the second idea is to estimate the level corresponding the onset of plastic hinge, called Seismic Threshold of Yielding (STY).

For determining these thresholds, *strain* criteria for concrete and steel will be adopted. It is worth mentioning that, in addition to simplicity, this choice overcome the lack of information on the amount and position of steel bars. In fact, this deficiency avoid the use of stress criteria that should necessarily include the reinforcements. Note also that strain criteria are consistent with the displacement-based vulnerability assessment methods, Priestley (1997), or the concept of maximum story drift (Gulkan et al., 1996).

Criterion for the onset of structural damages

As for the onset of structural damage, a criterion of maximum tensile strain of concrete is taken. In fact, whatever the amount of reinforcements, the concrete matrix can not sustain tensile strains greater than $10^{-4}\,(\mathrm{m/m})$ (for usual concretes). Below this limit, the concrete (and thus the reinforced concrete) remains intact; above, the cracking of the concrete begins and weakens the reinforced concrete elements. Note that the maximum tensile strain can be adapted for other material (e.g. parpen).

Criterion for the onset of plastic hinge in reinforced concrete columns

As for the onset of plastic hinge, a criterion of maximum elastic tensile strain of steel and compression strain of concrete is taken. Indeed, the failure by compression of the concrete matrix and the yielding of usual steel bars begin for tensile strains greater than $10^{-3}\,(\mathrm{m/m})$. Note that up to this strain level, the damage of the concrete in the columns remains limited: typically, the unconfined concrete cover is ejected at the extremities of the columns. This localized reduction of the effective section and inertia acts as a softening of the connections. This effect being limited, its impact is weak on the global stiffness of the structure. For these reasons, one may admit – in first approximation – that after the onset of concrete damages and before the onset

of plastic hinges, the first modal frequency and shape are almost unaffected (say a decrease of about 10%), at least for framed structures (remind that for buildings of five storeys and more, if the stiffness of the ground floor is divided by 2 [resp. 5], the frequency is only reduced of 20% [resp. 40%]). This might not apply to walls, whose shear cracks affect the whole element.

Seismic thresholds of damage

The Seismic Threshold of Elasticity (STE) is deduced from:

- The quasi-elastic behavior identified from ambient vibration tests
- The beam model deduced from experiments suited to the building structure
- The damage criterion of concrete

It is clear that, if the structure was purely elastic, its temporal response to any seismic shaking could be fully determined. Obviously, this response will coincide with that of the real structure until the onset of damage, afterwards 'elastic' and 'damaged' response begin to diverge. Consider now signals respecting the normalized earthquake spectra, whose amplitudes are characterized by the normalized accelerations. In the quasi-elastic domain, the response of the building increases proportionally to the amplitude of the signal, i.e. the normalized acceleration. This will be true until a first damage appears in concrete somewhere in the structure. At this moment, the corresponding normalized acceleration will be called the Seismic Threshold of Elasticity (STE). Note that the localization of the first structural damages can be achieved from the deformed structural shape defined according to its quasi-elastic vibration modes.

The Seismic Threshold of Yielding (STY) is defined in a similar way. However the additional assumption of weak non linear effect before steel yielding must be introduced. The threshold expressed in terms of normalized acceleration is reached when somewhere in the structure the *strain in the vertical direction* (of the steel bars) reaches the elastic strain limit of steel in tension and concrete in compression.

Calculation of the thresholds using the first mode approximation

In the frame of these assumptions, the calculation of the thresholds could be performed through common linear dynamic numerical methods, the model being fitted by the experimental data. In order to give a better insight of the method, the calculation are performed using the first mode approximation. This latter consider that the first mode is mainly responsible for the structural deformations. This simplification can be partially justified:

- The distribution of seismic energy is such that for buildings with well separated eigenfrequencies (e.g. 4.45 and 14.1 Hz for building C), the maximum of energy is concentrated on the first mode.
- The participation factor, then the effective amplitude, is smaller for higher modes.

It is then possible to straight estimate the amplitudes of the first mode displacements which would lead to the onset (i) of structural damages and (ii) of plastic hinges. Using the normalized elastic response spectra provided by the codes, these modal amplitudes can be converted into the corresponding acceleration levels, i.e. the STE and STY.

Practical interest of the threshold values

The Seismic Threshold of Elasticity corresponds to a seismic elastic limit, whereas the safety strategy against earthquake is based on ductility. In these conditions, it is important to clarify why the knowledge of the STE could be of interest for the assessment of the vulnerability:

- As the STE value is based on measured data and does not require any supplementary assumptions on the post elastic behavior, the uncertainty is minimized.
- The fact that the STE is associated with normalized elastic response spectra should mean a real benefit for earthquake engineering practitioners. Moreover, site effects could be easily integrated by using specific spectra suited to the site.
- The comparison of the STE value with the level of acceleration required by the seismic code gives an assessment of the ductility that the structure should be able to develop; this can be a useful tool to identify the more critical cases, or to define a strategy of reinforcement.
- For the large number of buildings made of materials of low (slightly reinforced concrete) or very low (masonry) ductility, the STE value can be a close indicator of the acceleration level leading to severe damages (nevertheless the reserves of stability brought by hyperstatism may preserve from collapse).
- Finally, for specific buildings that should be kept in service, the STE value should help to estimate whether the damage level remains acceptable.

Beyond the Seismic Threshold of Elasticity, for framed reinforced concrete buildings, the post-elastic behavior is expected to induce limited damages in the columns up to the STY level. Beyond STY, significant damages can be expected depending on the ductility potential and its effective use during earthquake:

- If the quasi-elastic mode shape clearly shows a level which concentrates the deformation (for instance in presence of a ‘transparent’ level), the strength will essentially depends on the local ductility at this level, the ductility of other parts of the building remaining almost unemployed.
- If the design ends up in a regular mode shape, the ductility will be activated in the whole building, and after the onset of plastic hinge (STY), the strength can be estimated using a push-over analysis, (Priestley, 1997) (assuming or knowing the amount and disposition of steel reinforcement).

To sum up, if the STE is lower than the acceleration required by the seismic code, it is believed that first damages would be induced by the reference earthquake. The gap between the Thresholds values and the reference acceleration of the seismic

zone provides an indication of the ductility needed by the building to resist to the reference earthquake. The larger this gap is, the more attention should be paid to the structure.

As an example, the calculation of STE is illustrated in the next section on building C, using the first mode approximation.

3.1.7.2 Case study: STE of building C in the longitudinal direction

Internal strain limits of the structural elements

As presented in Section 3.1.6.3, the building C behaves longitudinally as a pure shear beam. Then, at a given floor level i, in each structural element e, the strain tensor $[\varepsilon]_{i,e}$ (non uniform) results from:

- The strains $[\varepsilon^d]_{i,e}$ given by the dead loads (including the own load and for the carrier elements, the load of higher levels)
- The strains $[\varepsilon]_e(\Delta u_i)$ imposed by the inter-storey displacement Δu_i and composed by the linear functions $[\varepsilon^s]_e$ given by the shear and $[\varepsilon^b]_e$ by the bending

$$[\varepsilon]_{i,e} = [\varepsilon^d]_{i,e} + [\varepsilon^s + \varepsilon^b]_e(\Delta u_i) \tag{3.1.7}$$

The strain tensor $[\varepsilon^d]_{i,e}$ is fully identified assuming a normal and uniform stress distribution in the cross-section (with the values E = 30 GPa, $\nu = 0.2$). The strain tensors under unit inter-storey displacement $[\varepsilon^s]$ and $[\varepsilon^b]$ are classically derived. Then, the diagonalization of $[\varepsilon]_{i,e}$, leads to an analytic expression of the maximum tensile strain parameterized by inter-storey displacement $\Delta \mathrm{u}_i$.

For each structural element e of each floor level i, one may deduce the relative displacement $\Delta u_{i,e}^{lim}$ for which the limit tensile strain of 10^{-4} is reached. At the floor level i, the inter-storey displacement Δu_i^{lim} which triggers off the damage is the minimum of the $\Delta u_{i,e}^{lim}$ values of the whole elements of the storey. Because of the dead load force, these values vary with the floor levels.

For longitudinal vibrations of building C, the critical elements are the full precast panels, on ground floor and the three first levels; the walls of the lifts cage, above.

For calculating the STY, it is sufficient to consider *the tensile strain in the vertical direction* (instead of the maximal tensile strain) and to replace the limit tensile strain of concrete by the elastic strain limit of steel. This leads to the inter-storey displacement Δv_i^{lim} that would onset the yielding of a steel bar on the floor level i.

Seismic threshold of elasticity of Building C

Let's introduce $[U_1^*]$ and $[\Delta U_1^*]$, the normalized first mode eigenvector ($|U_1^*| = 1$) and the corresponding differential displacement vector, respectively. If A is the amplitude of the first mode, then the displacement and differential displacement are:

$$[u_1] = A \cdot [U_1^*] \qquad \text{and} \qquad [\Delta u_1] = A \cdot [\Delta U_1^*] \tag{3.1.8}$$

The amplitude A_i, that would trigger off the structural damages at the floor i, reads:

$$\Delta u_i^{lim} = A_i \cdot [\Delta U_1^*]_i \tag{3.1.9}$$

The minimum of $\{A_i\}$ is the amplitude A_{lim} triggering off the damage in the building.

It remains now to transform the value of A_{lim} into an acceleration level. Conveniently, the seismic codes give the normalized elastic response spectra, i.e. the maximum displacement d^* (f) of single-degree of freedom oscillators (SDOF) of eigen frequency f, submitted to signals conform to the seismic spectra, with a reference acceleration of $a^* = 1\ m/s^2$. For a standardized acceleration $S.a^*$, according to the modal analysis, the amplitude of the modal response of the structure of first mode frequency f_1 is:

$$A(S) = S.p_1.d^*(f_1) \tag{3.1.10}$$

where $p_1 = \frac{{}^t[U^*][M][1]}{{}^t[U^*][M][U^*]}$ is the first modal participation factor ($p_1 = \pi/4$ for pure shear beam). The STE is reached for a standardized acceleration $STE \cdot a^*$ such that $A(STE) = A_{lim}$, i.e.,

$$STE = \frac{A_{lim}}{p_1.d^*(f_1)} \tag{3.1.11}$$

Therefore, the STE, i.e. the level of ground acceleration corresponding to seismic elastic limit of the building can be derived according to the code recommendations. The STY could be deduced similarly by replacing Δu_i^{lim} by Δv_i^{lim}.

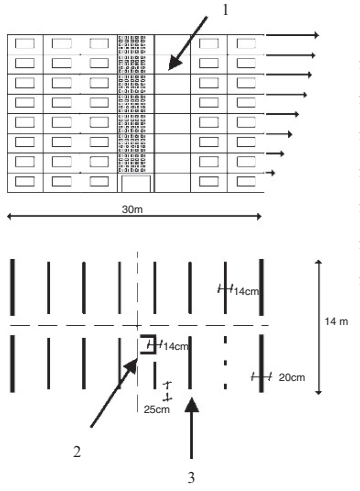

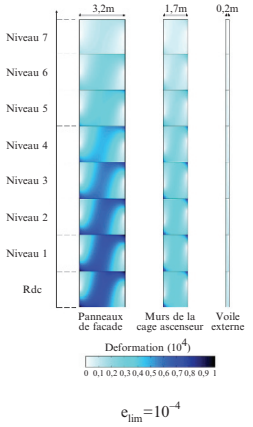

Norme PS 92

Zone	Accélération réglementaire (m/s²)
Ia	1
Ib	1,5
II	2,5
III	3,5

Site	Critère d'intégrité (m/s²)	
	8 niveaux	4 niveaux
S0	0,45	0,92
S1	0,45	1,07 > Ia
S2	0,57	1,42 > Ia
S3	0,78	1,84 > Ia,Ib

Fig. 3.1.12 Strain limits of the main structural elements of the building C

Considering a damping ratio of 5%, the STE values of building C in the longitudinal direction are presented in Figure 3.1.12, considering that the structure is settled on different site conditions, from S_0 (very good soil) to S_3 (soft soil). To investigate the sensibility of the STE, the same calculations were developed for a fictitious building C' identical to C but with a number of storey reduced to 4 (therefore more rigid with an higher first frequency). It can be seen that, according to the site conditions, the STE values of the building C range between 0.05 and 0.08 g. This order of magnitude is in agreement with the post-earthquake observations which showed that below 0.1 g, there are very limited structural disorders in common concrete buildings. The STE values of building C', less solicited because of its higher frequency, take higher values (0.09–0.18 g).

3.1.8 Conclusions

This study shows the interest of the ambient noise vibration in the seismic diagnosis of existing structures. The experiments prove the robustness and the reliability of information collected through ambient vibrations which enable to identify the leading and negligible phenomena. Even if the data are limited to the quasi-elastic domain, their knowledge is of very first importance: the quasi-elastic behavior is known to play an essential part specially for the dynamic amplification near eigenfrequencies, this phenomenon being one of the main reason of the structural damages.

Keeping in mind the necessity of draft analysis for number of buildings, simple approaches have been favored, based on few elementary though physically based assumptions, that give descriptions sufficiently realistic for engineering purposes. On this point, the interest of identifying experimentally several eigenfrequencies, instead of the only fundamental frequency, is underlined.

The concept of equivalent beam yields a drastic simplification in the modelling of dynamic behaviour of regular buildings: the complete dynamic calculation can be achieved in two much more simple independent steps; first the calculation of the beam parameters determined on a *single storey in statics*; second, the analytic calculation of unidirectional generalized beam in dynamic regime.

In the same spirit, the concept of Seismic Thresholds of damage presents the practical advantages to be based on real data, to minimize the introduction of uncertain assumptions on the non linear post-elastic behavior (at the three scales of the material, the structural elements and the structure) and to provide an acceleration level that can be easily compared with the reference acceleration given by the codes. By comparing reference acceleration and threshold values, the extend of the ductility needed by the structure can be evaluated. The confrontation with the usual ductility of the material could provide a good criterion to identify the most vulnerable structures. Although the results could be regarded as coherent, further improvements should be done, for instance considering the simultaneous presence of several

modes (in two directions), and extending the applications to buildings made of different materials.

It should be also emphasized that, if the limits of service must be evaluated or a retrofitting is needed, experimental data allow a good fitting of the numerical modelling. Indeed whatever the complexity of the linear and non-linear numerical method, the results depend on the chosen assumptions. The knowledge of the quasi-elastic behavior help to reduce the uncertainty of the modelling and as well to define an adequate reinforcement owing to a better understanding of the structure.

As a conclusion, the association of experimental and simple models can be a good complement of the existing methods.

Acknowledgements This research was supported by the French Ministry of Environment and the French Association of Earthquake Engineering (AFPS).

References

Argoul P, Hans S, Conti F, Boutin C, Time-frequency analysis of free oscillations of mechanical structures. Application to the identification of the mechanical behaviour of buildings under shocks, *Proceedings of the System Identification and Structural Health Monitoring – COST F3 Conference,* Madrid, Spain, 2000, pp. 283–292.

Benedetti D, Benzoni G, Parisi MA, Seismic vulnerability and risk evaluation for old urban nuclei, *Earthquake Engineering and Structural Dynamic,* 1988, 16, 183–201.

Boutin C, Hans S, Using buildings to be demolished for vulnerability assessment, *Acts of the Eleventh European Conference on Earthquake Engineering*, Paris, 1998.

Boutin C, Hans S, Dynamics of periodic framed structures – Continuum modelling by homogenisation, *Computer and Geotechnics, Special Number: Homogenisation in Geomechanics*, 2003, 30(4), 303–320.

Boutin C, Hans S, Ibraim E, Roussillon P, In situ experiments and seismic analysis of existing buildings – II seismic integrity threshold, *Earthquake Engineering and Structural Dynamics,* 2005, 34, 1531–1546.

Dunand F, Pertinence du bruit de fond sismique pour la caracterisation dynamique et l'aide au diagnostic sismique des structures de Gnie Civil, Ph.D. thesis, Universite Joseph Fourier I, Grenoble, 2005.

Ellis BR, Full-scale measurements of the dynamic characteristics of buildings in the UK, *Journal of Wind Engineering and Industrial Aerodynamics,* 1996, 59, 365–382.

Englekirk RE, Matthiesen RB, Forced vibration of an eight-story reinforced concrete building, *Bulletin of the Seismological Society of America*, June 1967, 57(3), 421–436.

Farsi MN, Identification des structures de Genie Civil a partir de leur reponse vibratoire. Vulnerabilite du bati existant. *These Universite Joseph Fournier*, Grenoble, December 1996.

Gulkan P, Sozen MA, Demir S, Ersoy U, An alternative evaluation for determining seismic vulnerability of building structures, *Acts of the Eleventh World Conference on Earthquake Engineering*, Acapalco, Mexico, 1996.

Hans S, Auscultation des batiments existants, Ph.D. thesis, ENTPE- INSA, Lyon, 2002.

Hans S, Boutin C, Dynamics of discrete framed structures – Unified homogenized description, submitted, 2008.

Hans S, Boutin C, Ibraim E, Roussillon P, In situ experiments and seismic analysis of existing buildings – I Experimental investigations, *Earthquake Engineering and Structural Dynamics*, 2005, 34, 1513–1529.

Hudson DE, Dynamic tests of full-scale structures, Earthquake Engineering, Prentice-Hall, 1970, 127–149.

Ivanovic SS, Trifunac MD, Todorovska MI, Ambient vibration tests of structures – A review, *Bulletin of Indian Society of Earthquake Technology*: *Special Issue on experimental methods*, December 2000, 1–49.

Jennings PC, Kuroiwa JH, Vibration and soil-structure interaction tests of a nine-story reinforced concrete building, *Bulletin of the Seismological Society of America*, June 1968, 58(3), 891–916.

Paquet J, Etude experimentale du comportement dynamique des structures, *Annales de ITBTP*, December 1976, n200, 129–151.

Petrovski J, Jurukovski D, Paskalov T, Dynamic properties of fourteen-story reinforced concrete building from full-scale forced vibration study and formulation of mathematical model, *Proceeding of Fifth World Conference on Earthquake Engineering*, Rome, Italy, 1973.

Priestley MJN, Displacement-based seismic assessment of reinforced concrete buildings, *Journal of Earthquake Engineering*, 1997, 1(1), 157–192.

Spence RJS, Coburn AW, Pomonis A, Correlation of ground motion with building damage: The definition of a new damage-based seismic intensity scale, *Acts of the Tenth World Conference on Earthquake Engineering*, Madrid, Spain, 1992.

Stephen NG, On the vibration of one-dimensional periodic structures, *Journal of Sound and Vibration*, 1999, 227(5), 1133–1142.

Stubbs IR, MacLamore VR, The ambient vibration survey, *Proceedings of Fifth World Conference on Earthquake Engineering*, Rome, Italy, 1973.

Trifunac MD, Comparisons between ambient and forced vibrations experiments, *Earthquake Engineering and Structural Dynamics*, 1972, 1, 133–150.

Chapter 3.2
Assessment of Seismic Capacity of Existing Buildings – Effects of Uncertainties

Dimitrios Baros, Miltiadis Kyrkos, Andreas Maravas, and Stavros Anagnostopoulos

Abstract The seismic capacity of three buildings used as telecommunication centers in Greece is assessed based on design drawings that do not reflect accurately the "as built structure" and on limited information about the soil conditions. The buildings were designed under the old Greek codes for Earthquake Resistant Reinforced Concrete structures, already known to be quite inadequate both in the characterization of the seismic action and in providing sufficient strength and ductility to the structural members and the building as a whole. Steel telecommunication towers with several disk antennas had been added to the building roofs at later times. With limited knowledge about the type of soil at the building sites, the effect of soil flexibility was first examined in a parametric way and subsequently the assessment of the buildings' capacities was made on the basis of both elastic dynamic and inelastic static (pushover) analyses. For the latter analyses, the main uncertainty that was hereby addressed was the selection of a suitable horizontal load distribution. It was observed that different distribution may lead to different results regarding the buildings' capacity. However, in all cases examined, it was found that a drastic intervention would be needed to bring all three buildings up to current standards of increased seismic safety required by the new code for high importance telecommunication buildings that should stay operational during a strong, design level, earthquake.

Keywords Existing buildings · Seismic capacity assessment · Elastic modal analysis · Soil conditions · Pushover analysis · Load patterns

3.2.1 Introduction

In the past few decades very strong, catastrophic earthquakes have hit major cities worldwide, causing death, injury and extensive destruction to buildings and other structures. These events accelerated research in earthquake engineering and seismic

D. Baros, M. Kyrkos, A. Maravas, and S. Anagnostopoulos (✉)
Department of Civil Engineering, University of Patras, 26500, Patras, Greece
e-mail: saa@upatras.gr

M. Mucciarelli et al., (eds.), *Increasing Seismic Safety by Combining Engineering Technologies and Seismological Data,* NATO Science for Peace and Security Series C: Environmental Security,

hazard assessment and were also the reason to target new research towards capacity assessment of existing structures and buildings in particular, as well as towards new techniques and materials for repair and strengthening. As a consequence, new improved codes for earthquake resistant design have been developed and applied, supported by updated seismic hazard maps for seismically prone regions throughout the world. In addition to the new codes that are applicable to new construction, substantial effort has also been put into codifying capacity assessment methods of existing structures as well as repair and strengthening techniques. The result is a series of documents published in the form of model codes, pre-standards or simply recommendations, available now to engineers for use and guidance (FEMA 356, FEMA, 2000; ATC-40, ATC, 1996; Part 3 of Eurocode 8, CEN, 2004b; Greek Retrofitting Code Drafts, OASP, 2004, 2006).

The high activity for repair and strengthening after a damaging earthquake is followed by a less intense, yet substantial, activity for capacity assessment and strengthening of older buildings, to increase their seismic strength and even bring them to current safety standards. Of course, the key motivation for such activity stems from the raised awareness about the shortcomings of older design and construction practices, due in large part to inadequate codes, and the consequent lower seismic safety of older structures, compared to present day standards.

Seismic capacity assessment is the first step required to decide whether an existing building needs strengthening or not or whether should be targeted for eventual demolition. The need for such assessment usually arises when a new usage for the building is sought or simply when the owner becomes aware that his building may not be safe enough compared to new buildings, if hit by an earthquake.

The aforementioned regulatory documents include detailed numerical procedures of varying complexity, ranging from simplified elastic static computations to detailed inelastic static or dynamic analyses for assessing the seismic strength of an existing building. In carrying out such assessments, however, one should realize that the reliability of assessment depends more on the quality of the available data for the examined structure than on the sophistication of the analysis method to be used. A number of uncertainties are typical in such problems and unless they are properly dealt with, the final strength or seismic capacity assessment may be unreliable and questionable. In the worst of cases, which can be encountered if the building is very old, there may be no drawings available and all the information would need to be obtained from detailed geometrical and structural surveys, including, in the case of reinforced concrete buildings, extraction of concrete cores for strength tests, use of reinforcement detection devices to spot-check for diameter and location of steel bars, digging at selected locations along the building exterior to get some idea about the type and dimensions of foundation, etc. Some of the required testing may be difficult or even impossible to carry out, e.g. when the building occupancy or functioning must not be disrupted, or when the location for a required digging is not easily accessible. On the other hand, design drawings of the building may be available but not reflecting – usual case – the “as built” conditions; hence there still exists a need for checking their reliability using spot-checks.

Whatever the structural documentation of an existing building might be, the engineer charged with the seismic capacity assessment should try to verify the existing information and/or obtain whatever additional data he deems necessary. In any case, it is important to realize that even under the best of circumstances there will be uncertainties in the data that the engineer must cope with. Therefore sensitivity checks in the form of analyses with lower and upper bound values of various properties will normally be necessary, before arriving at specific recommendations for intervention.

In the present paper the capacity assessment of three existing buildings, carried out by applying the aforementioned considerations, is discussed and presented. The buildings are used in a telecommunications network and should remain functional during a design level earthquake. Since detailed design drawings were made available by the buildings' owner, who assured us about their accuracy, no systematic verification of structural data was attempted but their values were taken directly from the drawings. Thus, the only uncertainty considered was in the local soil and foundation conditions and this was dealt with through a parameter variation. Initially, elastic response spectrum analyses were performed, to be followed by non-linear, static pushover analyses for a presumably more refined assessment. The results from the two types of analyses are discussed and conclusions are drawn.

3.2.2 Building description

The three buildings considered are typical reinforced concrete structures with heavy external masonry infills. The internal infills consist of either lighter (thinner) masonry or light panels. All buildings are currently used as telecommunication centers, thus they store sensitive equipment which should remain operational during a design level earthquake. Steel telecommunication towers with several disk antennas have been added to the building roofs at later times. Although the steel towers have been included in the building models that were analyzed, their seismic performance is not assessed herein.

The first building will be referred to as SPR building. According to the available detailed drawings, it was designed and constructed during 1967–1968 following design regulations issued in the 1950s. It consists of one basement, and four storeys of unequal height (Table 3.2.1). All storeys except the last one are irregular in plan, consisting of two rectangular "wings" (Figure 3.2.1). The steel antenna tower is placed on the roof on the second storey. The total height of the building is 17.71 m and the covered area is about 350.00 m^2. The structural system consists of typical moment resisting frames, with relatively strong beams, while columns in the upper two storeys seem to be rather weak. This is attributed to the decrease of the column sections and reinforcement along the height of the building, which was common during the period it was constructed. These weak stories are expected to be critical for the overall performance of the building. As for the foundation system, contrary to what was "common practice" during the period when the building was constructed,

Table 3.2.1 Building storey heights (m)

	SPR	AGR	NPT
Basement	2.98	4.70	–
Ground storey	3.98	3.70	3.88
First storey	4.23	4.40	4.22
Second storey	4.45	4.10	–
Third storey	4.45	–	–
Total	17.71	16.90	9.50

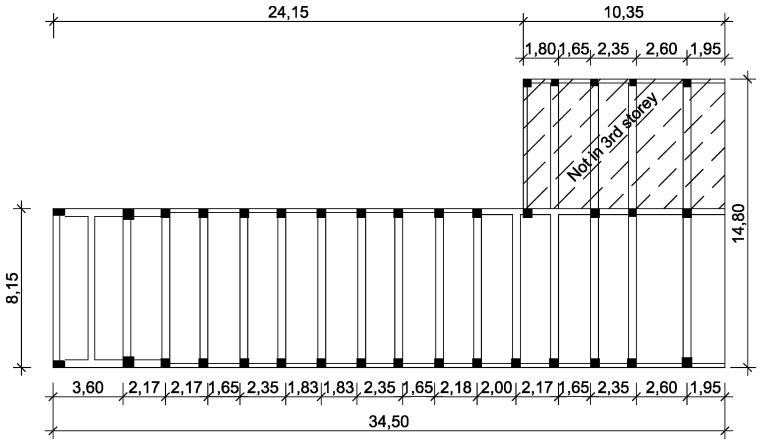

Fig. 3.2.1 Layout of the SPR building

it consists of continuous footings, connected with a 0.25 m wide concrete perimeter wall at the basement that appears to comply with current foundation standards. Thus, the approximation of fixed supports either at the level of the basement or the ground storey is expected to lead to acceptable results.

The second building examined is referred as the AGR building. It was designed and constructed in 1962 following the same design principles with the SPR building. It consists of one basement and three storeys of unequal height (Table 3.2.1). All storeys are generally rectangular in plan and cover an area of about 325.00 m^2 (Figure 3.2.2). The total height of the building is 16.90 m. The steel tower with the communication antennas is located on the roof of the last storey. The structural system in this case comprises a combination of moment resisting frames and shear walls. The latter are mostly lightly reinforced walls with typical sections, 1.00–1.40 m long and 0.20 m wide, with the exception of the "stairway core", which has significantly longer wall sections (more than 4.00 m long). These elements constitute the main lateral force resisting system of the structure. Their main shortcoming is that they are greatly under-reinforced compared with current standards. Moreover, the strong beam versus weak column configuration and the gradual weakening of the columns along the height, which were also observed in the SPR building, are expected to negatively affect the seismic behavior of both buildings.

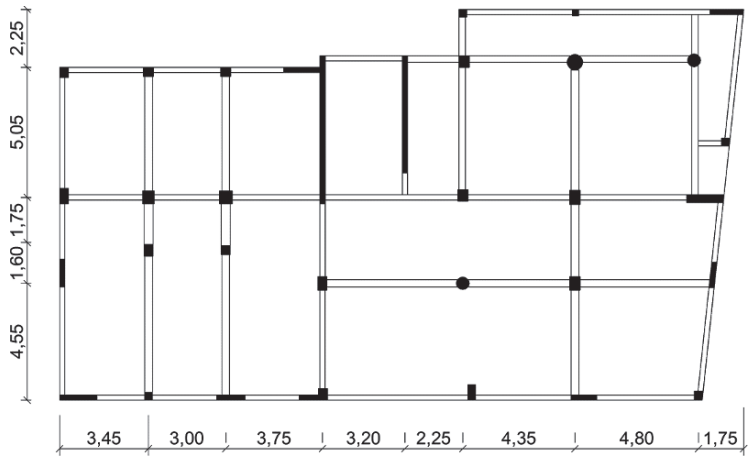

Fig. 3.2.2 Layout of the AGR building

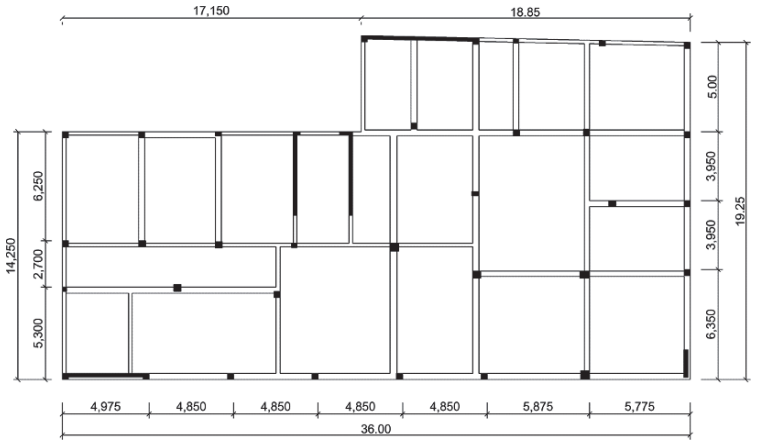

Fig. 3.2.3 Layout of the NPT building

Finally, the foundation system, differently than that of the SPR building, consists of separate footings for small groups of columns and for each shear wall, connected with light tie beams.

The third building examined will be referred as the NPT building. It is a two storey building designed and built in 1972 according to the same codes as the other two buildings. It is non symmetric in plan (Figure 3.2.3) and its structural system consists of a combination of moment resisting frames and lightly reinforced shear walls, with section lengths exceeding 4.00 m (Figure 3.2.3). These elements are the primary lateral force resisting members of the structure and, since they are lightly reinforced, they are expected to be inadequate according to current requirements. As for the moment resisting frames, the weak column – strong beam design, typical

of buildings of that period, is a shortcoming, although the existence of large shear walls makes it less important. The foundation is similar to that of the AGR building, consisting of separate, isolated, footings for each column or wall.

Summarizing, it should be noted that the drawbacks of the three buildings discussed above, namely the relatively strong beam – weak column configuration, the decrease of column sections along the height for the buildings SPR and AGR, the light reinforcement of the shear walls in the cases of AGR and NPT and, finally, the lack of closely spaced stirrups in the columns (only one Φ6 hoop every 300 mm according to the drawings) are common for buildings designed and constructed in Greece prior to the introduction of the new Codes. These shortcomings are partly attributed to the code provisions of the time the buildings were designed and to the lower estimates of seismic hazard applicable then.

For all three buildings the only information about the soil conditions provided by the owner was that the soil is soft and should be classified as Category C, in the classification scheme of the new Greek Code (OASP, 2000).

Due to the lack of other information, it was decided to carry out a parametric investigation of the effects of soil stiffness on the response of all three buildings, before performing the detailed capacity assessment.

3.2.3 Models used for the analyses

Linear dynamic (response spectrum) analyses and non-linear static analyses have been performed in order to assess the seismic capacity of the three buildings. The SAP 2000 (CSi, 2007) analysis software has been used for the needs of these evaluations.

Structural members were modeled using typical beam – column frame elements. For member properties the FEMA 356 (FEMA, 2000) provisions were followed. Thus, the effective slab width for all beams was calculated as the minimum of eight times the slab thickness, one fifth the beam span and half the distance to the next parallel beam. As for the effective rigidities, FEMA suggests $0.50EI_g$ for beams and columns with compression due to design gravity loads less than $0.30A_gf_c$ or $0.70EI_g$ for columns with more than $0.50A_gf_c$ compression, with A_g and I_g the area and moment of inertia of the gross concrete section and E the concrete modulus of elasticity. The above approximation was considered acceptable for the beams. However for the shear walls and columns, slightly higher effective stiffness values were adopted, as suggested by the Greek Seismic Design Code (OASP, 2000), namely $EI_{ef} = 0.60EI_g$, for shear walls and columns at the perimeter of the building and $EI_{ef} = 0.80EI_g$, for columns at the interior of the building.

Perimeter walls at the basement were modelled by a combination of high stiffness beams and columns that reproduced the box type action of the basement structure.

As it has already been discussed, no material samples were taken to verify through testing the material properties, namely concrete strength f_c and steel strength f_y. Thus, values from the design drawings were used. In all cases, normal

concrete of grade C12 and steel of grade S220 were specified. The respective nominal strengths, used for the strength based checks of the linear analyses, are $f_{ck} = 12\,\text{MPa}$ and $f_{yk} = 220\,\text{MPa}$. For non-linear procedures, median values were used for material strengths. Concrete median strength can be calculated from its nominal value using the following expression provided in Eurocode 2 (EC 2, CEN, 2004a):

$$f_{cm} = f_{ck} + 8(\text{MPa}) \tag{3.2.1}$$

whereas for reinforcing steel the following approximation was adopted:

$$f_{ym} = 1.15 f_{yk} \tag{3.2.2}$$

considering that according to the EC 2 provisions (CEN, 2004a), the maximum actual yield stress may not exceed its nominal value by more than 30%. The modulus of elasticity for concrete was calculated using EC 2 (CEN, 2004a), which gave the value $E_{cm} = 27.1\,\text{GPa}$.

In all three buildings the usual assumption of floors acting as diaphragms in their planes was made. Vertical loads were calculated and distributed to the beams using tributary floor areas. Dead loads consisted of the weight of the structural components, infill walls and slab overlays. Live loads were taken equal to $3.00\,\text{kN/m}^2$ for interior areas, which is the value for Group B specified by Eurocode 1 (EC 1, CEN, 2001), except for areas where a higher loading value was specified on the design drawings, due to the installation of heavy equipment. Floor masses for seismic analyses include dead loads and 30% of live loads.

3.2.4 Effects of soil flexibility

When assessing the seismic capacity of existing buildings, it is conservative for the superstructure to consider it fixed at the base, because typically fixed base buildings are subjected to higher seismic forces than buildings on flexible supports. Nevertheless, in the framework of the present investigation, it was decided for the linear analysis to carry out limited parametric investigation and to include the flexibility of the foundation using soil springs at the supports. This was dictated, in part, from the fact that the only information supplied to the investigators by the owner about the soil was that for all three buildings the soil consists of soft deposits classified as category C according to the new Greek Seismic Design Code (OASP, 2000).

To estimate the soil spring stiffnesses the following equations were used, taken from the Greek Retrofitting Code Draft (OASP, 2004) with the corresponding correction factors for embedment.

$$K_z = \frac{GB}{(1-\nu)}\left[1.55\left(\frac{L}{B}\right)^{0.75} + 0.8\right] \tag{3.2.3}$$

$$\beta_z = \left[1+\frac{1}{21}\frac{D}{B}\left(2+2.6\frac{B}{L}\right)\right]\left[1+0.32\left(\frac{d\,(B+L)}{BL}\right)^{2/3}\right] \tag{3.2.4}$$

$$K_{rx} = \frac{GB^3}{(1-\nu)}\left[0.4\frac{L}{B}+0.1\right] \tag{3.2.5}$$

$$\beta_{rx} = 1+2.5\frac{d}{B}\left[1+\frac{2d}{B}\left(\frac{d}{D}\right)^{-0.2}\sqrt{\frac{B}{L}}\right] \tag{3.2.6}$$

$$K_{ry} = \frac{GB^3}{(1-\nu)}\left[0.47\left(\frac{L}{B}\right)^{2.4}+0.034\right] \tag{3.2.7}$$

$$\beta_{rx} = 1+1.4\left(\frac{d}{L}\right)^{0.6}\left[1.5+3.7\left(\frac{d}{L}\right)^{1.9}\left(\frac{d}{D}\right)^{-0.6}\right] \tag{3.2.8}$$

where k_z, k_{rx}, k_{ry} are spring stiffnesses for vertical translation and for rocking in the xz and yz planes, respectively, β the corresponding correction factors for embedment, G the shear modulus and ν Poisson's ratio of the soil ($\nu = 0.4$ was assumed for the present study). B, L, d, D and h are footing and embedment dimensions as shown in Figure 3.2.4.

The basic uncertainty is in the value of the shear modulus G. Based on wave propagation measurements the shear modulus is typically estimated from the equation:

$$G_0 = \rho V_s^2 \tag{3.2.9}$$

where ρ = density of the soil and V_s shear wave velocity. The Greek Retroffiting Draft Code (OASP, 2004) provides that for soils classified as category C and for design peak ground acceleration equal to 0.24 g, the effective G value to use in the previous equations should be taken equal to $0.65G_0$. Moreover, it is estimated that for soils in category C a reasonable value of the shear wave velocity could be in the range of 200–300 m/s. Then, assuming a typical value for soil density of $\rho \cong 1.9\,t/m^3$, leads to the range of values for $G \cong 49.0 \div 110.0$ MPa.

These values, however correspond to the small strains in the free field soil, developed during measured shear wave propagation velocities. In a strong earthquake, the soil material surrounding the foundation will undergo substantially greater

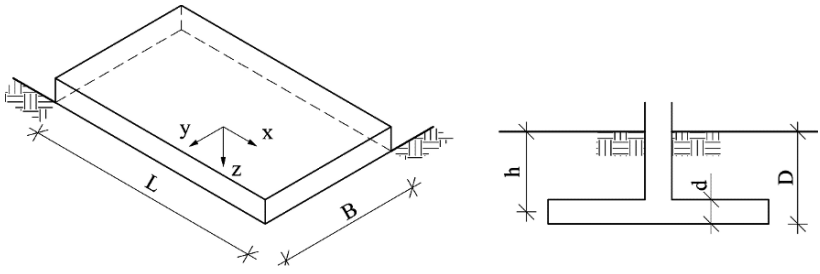

Fig. 3.2.4 Footing and embedment dimensions

deformations and the values of G to be used for estimating soil spring properties should be compatible with them. Under such circumstances, an estimate of G for soil category C may be obtained from the relation:

$$\frac{G}{S_u} \cong 400 \tag{3.2.10}$$

where S_u is the shear strength of the soil. Considering that for category C soil, $S_u \cong 30 \div 60$ kPa, with 50 kPa being a typical value, the above relationship gives $G \sim 20$ MPa, a value substantially lower than those obtained from the shear wave propagation velocity formula.

In view of such differences and given the lack of other information for the three building sites, elastic dynamic response spectrum analyses were carried out with soil springs computed for the following values of G: (a) $G_H = 110$ MPa (high value) (b) $G_L = 49$ MPa (low value) and (c) $G_{ST} = 20$ MPa (static value). The first two values come from Equation (3.2.9) with the code correction, and the third value comes from Equation (3.2.10), applicable for static problems. In addition the fixed base case $(G = \infty)$ was included. These four cases and their symbols are listed in Table 3.2.2.

The analyses were carried out using the design spectrum of the Greek code for soil category C with PGA = 0.24 g, corresponding to seismic zone II (OASP, 2000). This spectrum is shown in Figure 3.2.5. This is an elastic design spectrum and its use for capacity assessment must be combined with an appropriate behavior factor q.

A value of q = 2.0 was used in the analyses herein, which comes from rounding the value q = 1.80, recommended by the Greek Retrofitting Draft Code (OASP, 2006). Results for the three buildings and the four values of G are summarized in Tables 3.2.3–3.2.5.

Table 3.2.3, gives the effect of soil flexibility on the periods of the three buildings SPR, AGR and NPT. The second column lists the mode number (periods for the first three modes are only examined) and the third column lists the Fixed Base periods. The last three columns give the percent change in the fixed period for the flexible soil, each column corresponding to a G value as explained earlier. As expected, the lower the value of G, the higher the increases of the buildings' lower three periods. We also observe that the influence on periods is very little on the SPR building, more on the AGR building and highest for the NPT building.

Table 3.2.2 Cases analyzed for soil properties variation

Case description	Case symbol	Soil properties	
		V_s (m/s)	G (MPa)
Fixed base	FB	–	∞
$V_{s,high}$	G_H	300	110
$V_{s,low}$	G_L	200	49
G from S_u (static)	G_{ST}	–	20

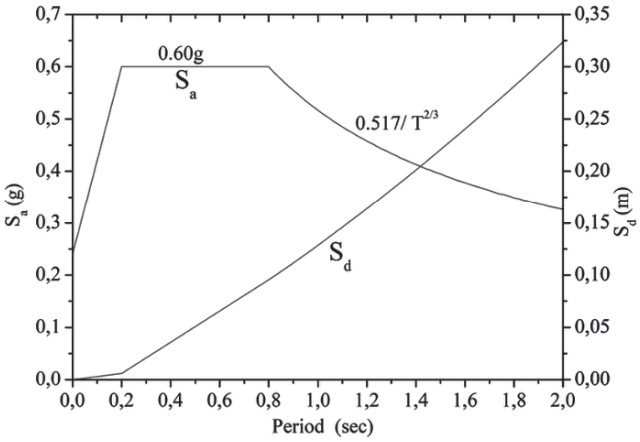

Fig. 3.2.5 Elastic design acceleration spectrum and displacement spectrum

Table 3.2.3 Effects of soil flexibility on building periods

Building	Mode	Period fixed base (s)	Percentage change in period		
			$G_H = 110\,MPa$	$G_L = 49\,MPa$	$G_{ST} = 20\,MPa$
	1	1.028	−0.1	1.2	3.9
SPR	2	0.840	0.6	0.9	1.6
	3	0.726	0.9	1.4	2.2
	1	0.736	2.4	6.5	12.2
AGR	2	0.632	2.5	7.1	15.0
	3	0.470	11.3	21.3	34.9
	1	0.368	27.7	40.8	58.5
NPT	2	0.305	22.7	32.3	45.3
	3	0.224	23.2	33.9	49.8

Table 3.2.4 Effects of soil flexibility on building base shear

Building	Loading case $(G + 0.3Q\pm)$	V_x fixed base (kN)	Percentage change in V_x			V_y Fixed base (kN)	Percentage change in V_y		
			G_H	G_L	G_{ST}		G_H	G_L	G_{ST}
SPR	$E_x \pm 0.3E_y$	4,284.6	−0.2	−0.1	0.2	1,607.9	1.3	1.2	1.4
	$0.3E_x \pm E_y$	1,441.6	2.9	3.4	4.5	4,839.0	−1.6	−2.0	−2.7
AGR	$E_x \pm 0.3E_y$	4,418.6	1.6	3.2	4.6	2,725.3	8.7	16.3	29.8
	$0.3E_x \pm E_y$	1,983.0	8.2	18.2	39.6	4,890.4	1.1	0.9	1.7
NPT	$E_x \pm 0.3E_y$	4,023.7	5.4	10.3	23.2	2,049.7	−11.3	−5.9	−22.9
	$0.3E_x \pm E_y$	2,203.2	−2.8	−0.5	−11.2	3,858.9	−2.2	−2.9	−4.3

This is as expected, because it is easy to see that the effect of soil flexibility becomes greater as the building becomes stiffer. The soil flexibility may be viewed as a spring connected in series to the spring representing the building. It is for the same reason that soil flexibility affects more the higher modes, which correspond to

Table 3.2.5 Effects of soil flexibility on building top displacements

Building	Loading case $(G + 0.3Q\pm)$	u_x Fixed Base (cm)	Percentage change in u_x			u_y Fixed Base (cm)	Percentage change in u_y		
			G_H	G_L	G_{ST}		G_H	G_L	G_{ST}
SPR	$E_x \pm 0.3E_y$	8.4	2.4	3.6	5.9	4.9	10.2	4.1	20.4
	$0.3E_x \pm E_y$	3.1	6.5	9.7	16.1	13.7	2.2	5.8	13.9
AGR	$E_x \pm 0.3E_y$	6.9	4.4	11.6	18.8	5.5	10.9	25.5	45.5
	$0.3E_x \pm E_y$	3.6	19.4	38.9	69.4	5.0	18.0	38.0	58.0
NPT	$E_x \pm 0.3E_y$	2.3	61.0	87.0	113.0	0.5	38.0	42.0	52.6
	$0.3E_x \pm E_y$	1.2	58.3	91.6	133.3	0.8	37.5	87.5	62.5

stiffer building deformation shapes. The coupling of the listed first three modes is the reason that the influence, as seen in Table 3.2.3 is not regular and explains the small decrease in period for the SPR building, mode 1, $G_H = 110\,\text{MPa}$ case.

Table 3.2.4 shows the percentage changes in base shear in directions x and y of the three buildings for four loading conditions. These percentage changes, are for the three values of soil springs corresponding to the three values of G, where again the basis for comparison are the values of corresponding base shears given for the fixed base. Again as expected, the largest differences are in the buildings AGR and NPT. However, the changes now are either increases or decreases, depending upon the values of the fundamental periods along the x and y axes, in relation to the design spectrum shown in Figure 3.2.5 and the loading combination considered. The changes in the second and third period of each building also play a role, again depending upon their contribution to the modal summation and their location on the horizontal axis in Figure 3.2.5 showing the design spectrum. Obviously, if the period changes, for any mode, do not move the period outside the range $0.20 \leq T \leq 0.80\,\text{s}$, which corresponds to the plateau of the design spectrum, the corresponding modal contribution to the base shear remains unchanged.

Table 3.2.5 shows the effects of soil flexibility on top displacements. Here we see the greatest influence of soil flexibility, which increases as the period of the building decreases. However, contrary to what happens with the base shears, here we see only increases in displacements, as one would expect by looking into the displacement design spectrum, Figure 3.2.5, which increases monotonically with increasing periods.

The presented comparisons suggest that the soil flexibility can affect results of an elastic dynamic analysis and hence the corresponding seismic capacity assessment of a given building considerably and thus should be included in such assessments. The stiffer the building the larger this influence becomes and hence it should be taken into account, at least when elastic analyses are employed.

In view of these results and the uncertainties in soil properties discussed earlier, it was decided to use soil spring properties based on the value of $G = 49\,\text{MPa}$, which corresponds to the low shear wave propagation velocity $V_s = 200\,\text{m/s}$. This value is considered as a reasonable estimate for the elastic dynamic analysis assessments, perhaps on the conservative side, which is appropriate for engineering purposes.

3.2.5 Seismic capacity assessment based on elastic modal analyses of the buildings

The capacity assessment of the three buildings is made for two levels of seismic demand: the first is when the buildings are considered as regular and the second, which is the most appropriate, when they are considered of vital importance. The second level corresponds to the highest importance category, in which telecommunication buildings are classified according to the Greek Seismic Design Code (OASP, 2000). For such buildings, the seismic demand is set for a more rare earthquake, compared to the design earthquake for regular buildings calculated for a mean return period of ∼475 years. This more rare earthquake has a design spectrum 1.3 times higher the design spectrum of Figure 3.2.5 for regular buildings.

The elastic dynamic analyses for capacity assessment were carried out using the models with the flexible soil springs corresponding to $G = 49\,\text{MPa}$, i.e. to a surrounding soft soil with shear wave propagation velocity of $V_s = 200\,\text{m/s}$. These analyses were carried out with SAP 2000 computer code, using a sufficient number of modes to include at least 90% of the effective modal mass in each direction. 3-D models were used for each building and were subjected to two-component earthquake actions, specified by the design spectra according to the combinations $\pm E_x \pm 0.3E_y$ and $\pm E_y \pm 0.3E_x$, for two levels of importance.

Results are presented in the following graphs, Figures 3.2.6 to 3.2.10. They include only vertical elements, i.e. columns and shear walls because these are the critical elements usually leading to structural failure in a strong earthquake, compared to beams. The Figures show the distribution of the member flexural capacity index λ_f, which is equal to the flexural demand over the flexural capacity ratio of a column or shear wall, computed according to the EC 2 (CEN, 2004a). A similar index for shear capacity is not presented because for most members the flexural capacity index was more critical.

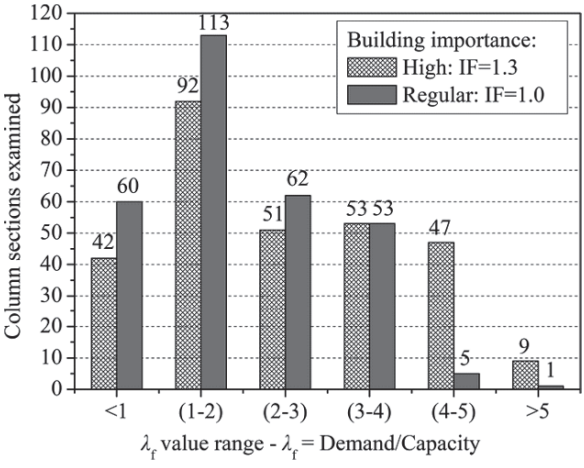

Fig. 3.2.6 Assessment of column capacity for the SPR building based on linear analysis results

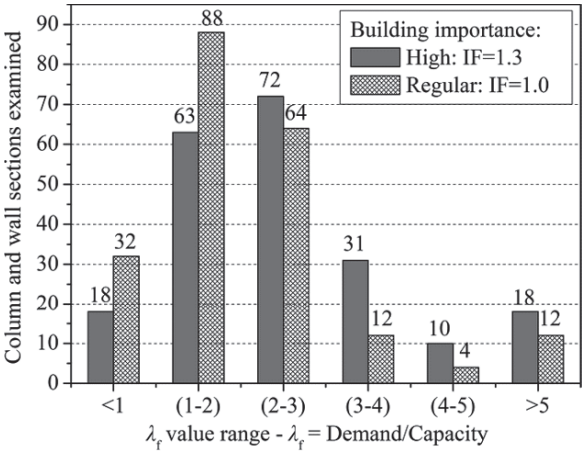

Fig. 3.2.7 Assessment of column and shear wall capacity for the AGR building based on linear analysis results

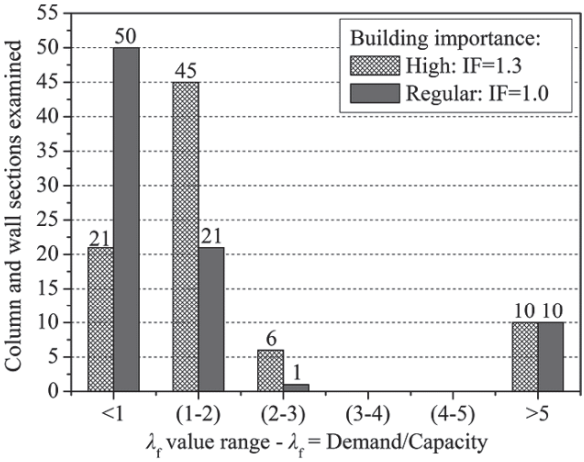

Fig. 3.2.8 Assessment of column and shear wall capacity for the NPT building based on linear analysis results

Among the three buildings, the one-story NPT building appears to be in a somewhat better condition than the other two. In any case, all three buildings require strengthening, if they are to meet current standards.

Figure 3.2.9 shows the distribution of the column λ_f index between the lower and the upper stories for the SPR. We see that the SPR building has a large distribution of weaker columns in the upper two stories. Similar results were obtained from the analysis of AGR building. However, the distribution of weak columns and shear walls is more uniform compared to SPR building.

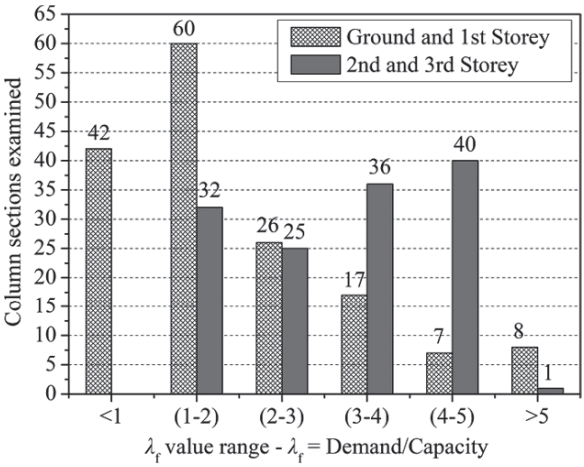

Fig. 3.2.9 Storey distribution of λ_f values of the SPR building

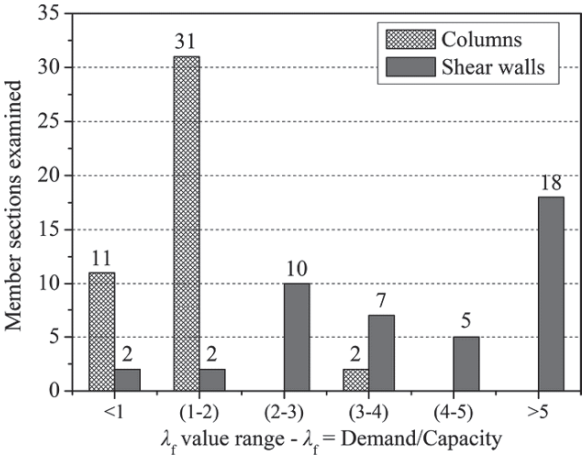

Fig. 3.2.10 Comparison of the seismic performance of columns and shear walls in the basement of the AGR building

Finally, Figure 3.2.10 compares the seismic performance of columns and shear walls for the AGR building, indicating that the shear walls appear to present a larger problem than the columns. Results from NPT building lead to the same observation. We remind here that the reliability of these predictions is directly related to the value of the behaviour factor q (R factor in American terminology), which for our analyses was assumed equal to 2.0.

The inelastic analyses in the following section will provide more reliable estimates than the elastic solutions of the present section, which, nevertheless give us a good picture of the anticipated behaviour under design level events.

3.2.6 Capacity assessment using inelastic pushover analysis

In resent years, inelastic static, push-over type, of analyses have been suggested for capacity assessments aimed at retrofitting existing buildings. (FEMA 356, FEMA, 2000; ATC-40, ATC, 1996; Part 3 of Eurocode 8, CEN, 2004b; Greek Retrofitting Draft Code, 2004, 2006). This method has been used in the past for assessing design weaknesses in fixed offshore structures (Kallaby and Millman, 1975; Gates et al., 1977), whose final design was checked by conventional static or dynamic methods as prescribed in the pertinent regulatory document (API-RP2A, 1975). Several variations of the push-over method, all having to do with the load distribution used, have been suggested as preferable alternatives to the typical method based on a triangular distribution of the lateral loads. All these variations give reasonable results when applied to symmetric buildings, i.e. when no torsion is present. Application to irregular buildings which will be subject to torsion during an earthquake, although permitted by the FEMA documents (FEMA 356, 2000) and the Greek Retrofitting Draft Code (OASP, 2006), is an open issue because its relevance to realistic extreme earthquake loadings is highly questionable. Results from inelastic pushover analyses will be hereby presented, without, however, suggesting that the findings are better than those from the elastic analyses. It should be noted that the most reliable procedure is to use multiple inelastic dynamic analyses for a number of real earthquake motions, selected to be realistic for the site of each building. Such analyses have not been included in this paper.

The push-over analysis method consists in using a certain distribution of lateral forces on the structural joints, whose magnitude is gradually increased, keeping the distribution constant, or changing it (adaptive pushover methods), until the structure collapses. Ideally, the distribution of lateral forces to be used should correspond to the inertia forces on the joint masses for a design level earthquake the instant the peak response occurs. However, for a different design level, real earthquake this distribution will be different. The structure is analyzed statically at every value of the loading vector and its deformations and member forces are monitored. The members can exhibit a prescribed inelastic behavior. The total lateral force (base shear) plotted against the lateral displacement of a "control point" of the structure, typically a joint at the top level, constitutes the "push-over" or strength diagram of the structure. An estimate of the peak displacement that a design level earthquake will impose provides the limited or "target" displacement δ_t for the push-over diagram. Such an estimate is obtained based on the displacement response spectrum of the design earthquake, modified to reflect the approximation of an inelastic multistory building with an elastic SDOF system.

For the present application, the procedure as described in FEMA 356 (FEMA, 2000) was used. Thus, the target displacements were computed from Equations (3–15) of FEMA 356 which is:

$$\delta_t = C_0 C_1 C_2 C_3 S_a \frac{T_e^2}{4\pi^2} g \tag{3.2.11}$$

where:

S_a = acceleration design spectral ordinate at the fundamental period T_e of the equivalent SDOF, g=acceleration of gravity and C_0, C_1, C_2, C_3 are modification factors given in FEMA 356 (FEMA, 2000).

We note that for the push-over analyses the buildings were assumed fixed at the ground level, an assumption that is very close to reality if the building has a basement encased with shear walls all around its perimeter. This is the case with the SPR building, while for the other two it is only an approximation. By fixing the buildings at the ground level, their natural periods change (decrease) in comparison to the actual periods, based on the flexible soil. The fixed base periods, with base assumed at the ground level, are given in Table 3.2.6. The limiting target displacements for the three buildings are summarized in Table 3.2.7 for the two axes x and y and for two directions, + and −, along each axis.

Results from inelastic analyses are presented in terms of member performance (deformation or damage) at the limiting target displacement of each building provided that such a displacement could be reached. The performance levels of a flexural member, in our case column or shear wall, are shown schematically in Figure 3.2.11, where the symbols indicate the following performance: B = Incipient of yield, IO = Immediate Occupancy, LS = Life Safety, CP = Collapse Prevention and C = Collapse.

The limiting inelastic rotations at each column's end corresponding to these performance levels are provided in FEMA 356 (FEMA, 2000). For shear walls, however, these deformation levels and the secant stiffness at yield, were estimated in accordance to the Greek Retrofitting Draft Code (OASP, 2006), considered to give better approximations for these walls than FEMA. The results that are subsequently presented give numbers of columns and shear walls in the performance ranges indicated by the arrows on the deformation axis in Figure 3.2.11.

Table 3.2.6 Periods of the fixed base building models used for the push-over analyses

Mode	Period (s)		
	SPR	AGR	NPT
1	0.960	0.770	0.419
2	0.823	0.651	0.340
3	0.722	0.448	0.268

Table 3.2.7 Target displacements for the analyzed buildings

Building	Target displacement δ_t (cm)							
	High importance				Normal importance			
	$+x$	$-x$	$+y$	$-y$	$+x$	$-x$	$+y$	$-y$
SPR	17.4	17.1	23.4	23.2	13.3	13.2	17.9	18.5
AGR	16.8	16.8	9.6	10.5	12.8	12.8	7.2	7.8
NPT	13.8	12.5	15.2	14.3	10.4	9.4	11.3	10.5

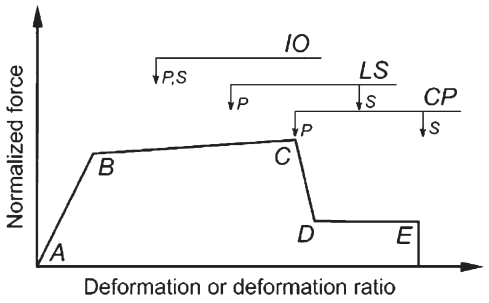

Fig. 3.2.11 Performance levels for structural members (FEMA 356, FEMA, 2000)

(a) SPR Building

For the SPR building three different load distributions were assumed and for each distribution four push-over analyses were carried out with "push" directions: +x, −x, +y, −y. Thus a total of 12 analyses were performed. The three types of load distribution are suggested in FEMA 356 (FEMA, 2000). The first, called modal distribution, has lateral forces that are products of the floor masses times the corresponding first mode acceleration, the second, called uniform distribution, uses a uniform acceleration over the height to multiply the floor masses and the third, called storey shear distribution, uses forces in proportion to the elastic floor loads determined from a response spectrum analysis, where 90% of the effective modal mass has been captured. The three distributions for the ±x directions along with the resulting pushover curves are shown in Figure 3.2.12. The great differences are obvious and indicative of the uncertainties associated with such analyses. Similar results were obtained for the ±y direction but are not shown here. It is noted that the following discussion concerning the effect of different horizontal load patterns on the results of pushover analysis, as well as the applicability of this method for the assessment of irregular buildings is based on results regarding the ±x direction of loading. The detailed assessment of any building requires that analyses for loading parallel to ±y axis are also performed. Results of these analyses were not included in the present paper, since, in all cases, they led to similar conclusions as the analyses along the x axis.

Figure 3.2.13 shows the deformed shapes and the location of the plastic hinges of the SPR building during the last step of the pushover analyses along the +x axis direction, for the cases of storey shear and uniform load distribution. The most interesting observations, here, which justify the use of pushover analyses, in spite all its shortcomings in their application to irregular buildings, are: (a) the large deformations of the top story, revealing its weakness relative to the other stories and (b) the large plastic deformations in many columns (light dark grayed hinges, indicating plastic hinge rotations beyond what corresponds to point C of Figure 3.2.11), that exceed those of the perimeter beams (dark grayed hinges, Figure 3.2.13), which are lightly reinforced and so their yield moments are low.

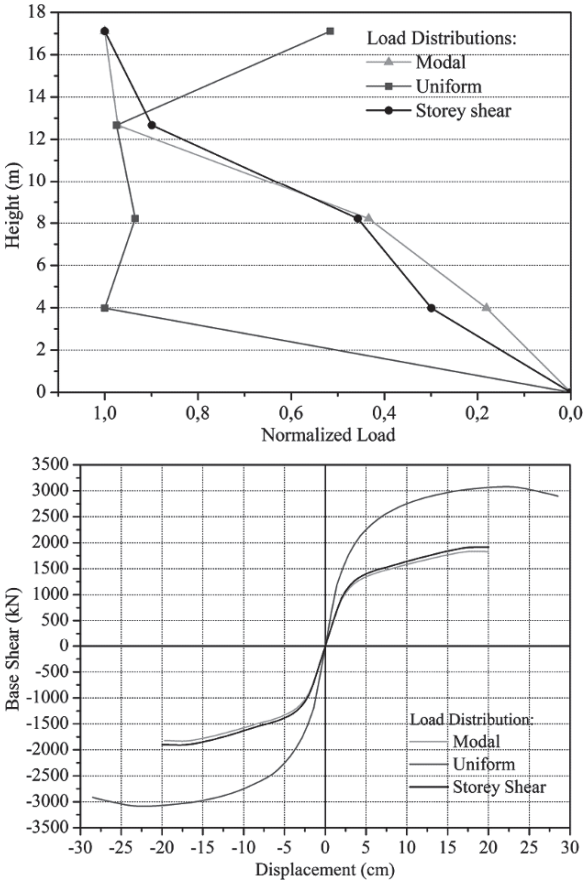

Fig. 3.2.12 Load patterns parallel to the ±x axis and resultant pushover curves of the SPR building

Thus, the analysis properly identifies the weak column-strong beam design of the building's frames, as was the practice when the structure was designed and built. It should also be noted that different load patterns lead to different results in terms of plastic hinge formation and inelastic deformation, once again indicating the effect of the uncertainties associated with such analyses on the result of the assessment procedure. As expected, the similarity of the modal and storey shear distributions (Figure 3.2.12), led to very similar results and for this reason only the results from the shear distribution have been presented.

The push-over curves for the ±x axis for the storey shear load pattern are shown again in Figure 3.2.14. They are the thick continuous curves, while the thinner, dashed curves are bilinear fits to them. On these curves the limiting target displacements δ_t according to Equation (3.2.11) are shown for the two levels of building importance: high and normal. We note that the graph on the negative side is for forces acting in the direction of −x. The points where the continuous curves stop are points where the analysis could not be continued because

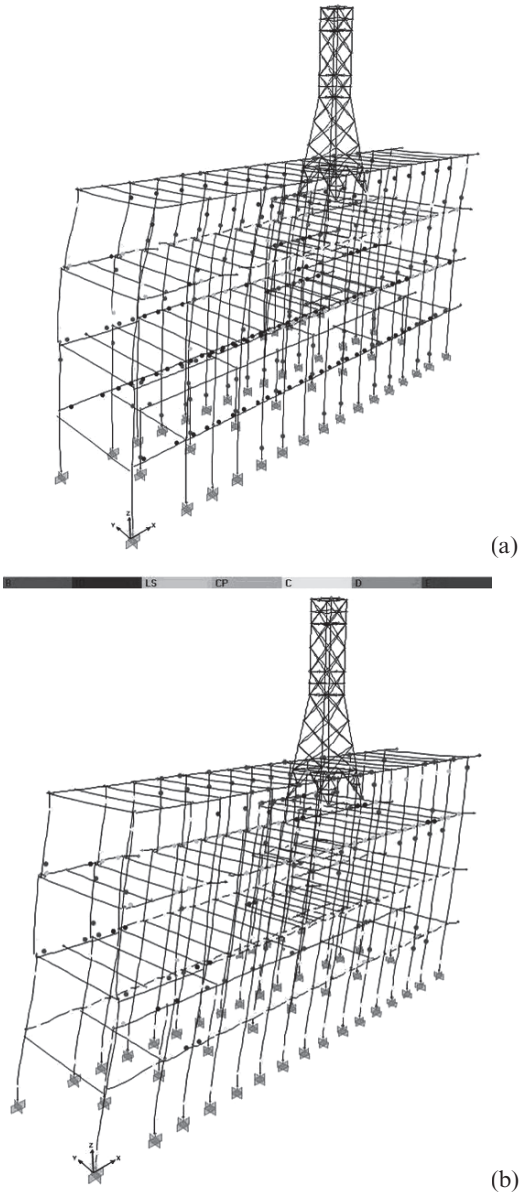

Fig. 3.2.13 Plastic hinge locations and states at the last step of the pushover analysis of the SPR building for the +x direction of loading and two load distributions (a) storey shear (b) uniform

of stability problems. The other points on the curve indicate the displacements at which the corresponding performance level has been reached by at least one member. In both curves, target displacements lie well after the point at which the building complies even with the "CP" performance objective. Thus, it can

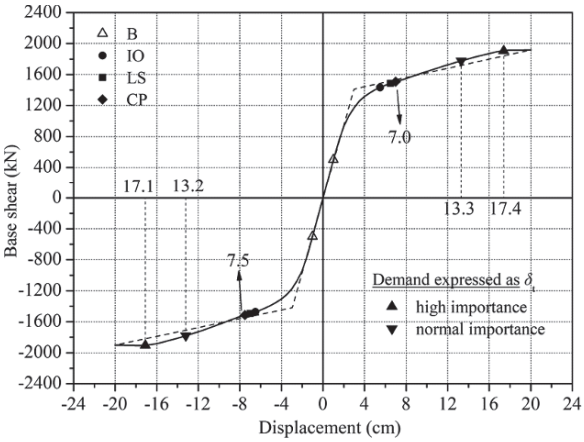

Fig. 3.2.14 Pushover curves and target displacements of the SPR building for loading parallel to ±x axis

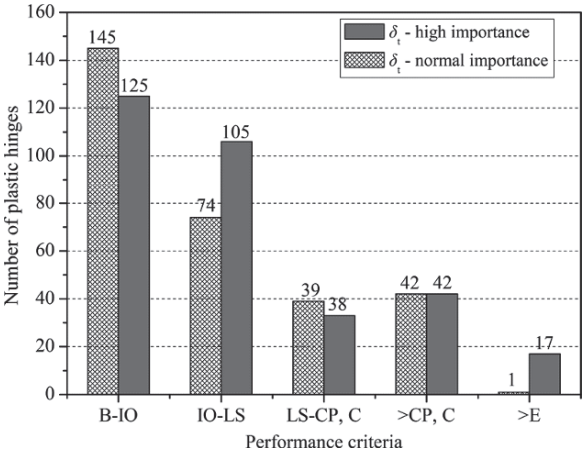

Fig. 3.2.15 Member performance of the SPR building based on pushover analysis for loading parallel to +x direction

be concluded that analysis indicates that the building is susceptible even to premature failure, should a design earthquake in accordance to present standards hit it.

Figure 3.2.15 shows the number of columns in the various performance groups, as defined in Figure 3.2.11 for push-over analyses along the +x axis. The presented results correspond to the limiting target displacement for regular importance and high building importance. It can be seen that analysis indicates a large number of members, mostly columns, in the performance range CP-C (Collapse Prevention – Collapse) and, in the case of high building importance, 17 members in the range beyond collapse. It is apparent that the seismic capacity

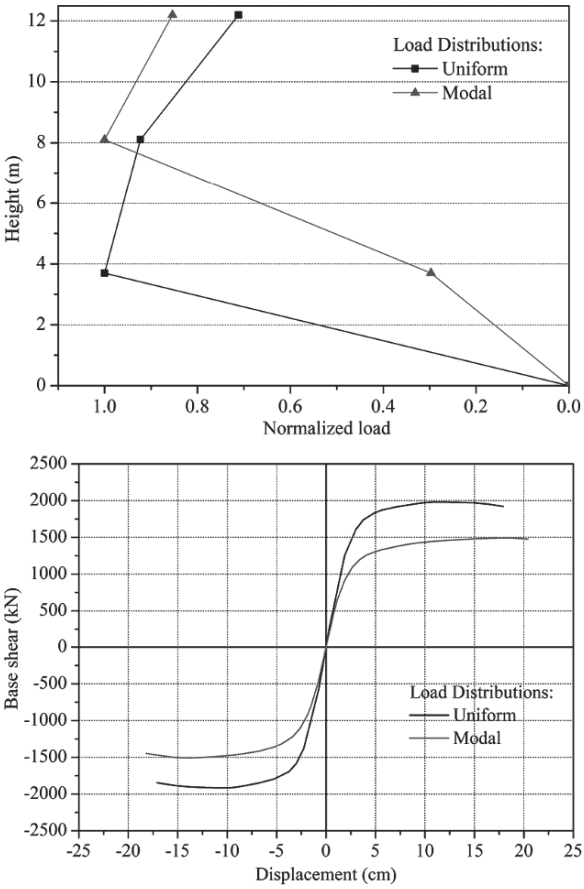

Fig. 3.2.16 Load patterns parallel to the ±x axis and resultant pushover curves of the AGR building

of this building, even if we consider it as a building of regular importance, is inadequate, result that is in agreement with the findings from the elastic modal analyses.

(b) AGR Building

For the AGR building two different load distributions were assumed, the modal and uniform distribution (FEMA, 2000), and again for each distribution four push-over analyses were carried out with "push" directions: +x, −x, +y, −y, leading to a total of eight analyses. The two distributions for the ±x directions along with the resulting pushover curves are presented in Figure 3.2.16. Once again, the effect of the uncertainties concerning the distribution of the lateral loads in push-over type analyses is obvious.

It should be noted that the AGR building is susceptible to torsion, thus, the modal load pattern was rather irregular in plan, leading to a premature failure due to a concentration of large deformations in one side of the building.

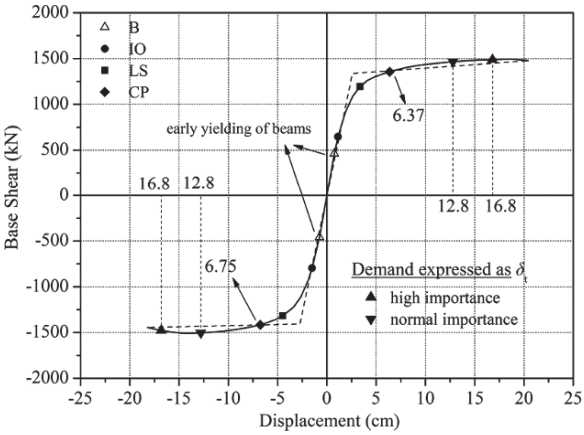

Fig. 3.2.17 Pushover curves and target displacements of the AGR building for loading parallel to ±x axis – modal load pattern

Defining a load pattern that properly represents the distribution of inertial forces for buildings with torsional behavior is a matter of current research and since the drawbacks of the conventional push-over algorithm are well known, it is suggested that for such cases of buildings more accurate nonlinear dynamic analyses should be performed. Otherwise, the results of pushover analysis should be complemented with linear modal analyses.

The push-over curves for the modal loading pattern of the AGR building parallel to the ±x axis are given in Figure 3.2.17 along with bilinear fits to each one of them, represented by dashed lines, and the calculated target displacements. It is observed that in both directions of loading along the x axis, the target displacement (demand) is greater than the available capacity as related to performance objectives. Thus the observed performance is inadequate and not acceptable according to modern seismic standards. This observation agrees with the results of the assessment based on elastic analyses presented previously in this paper. The poor behavior of this building is mostly attributed to the premature failure of the shear walls which are very lightly reinforced, in accordance with the design practice of the time. Of course we must note that modeling of shear walls with a low height to width ratio as prismatic beam column elements is a rather gross approximation that may be inappropriate. This is a well recognized problem that is not addressed herein.

The distribution of member performance for the pushover analysis of the AGR building along the +x axis is presented in Figure 3.2.18. This distribution is given for the limiting target displacements corresponding to the two levels of importance (regular and high). The results indicate again that the building is far from meeting current standards, as a significant number of members lie in the CP-C performance category.

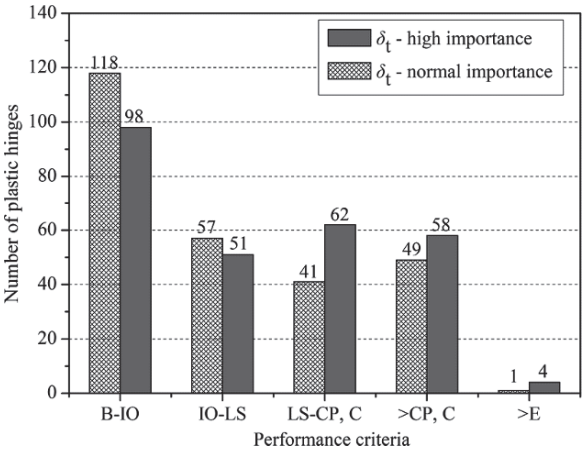

Fig. 3.2.18 Member performance of the AGR building based on pushover analysis for loading parallel to +x direction

(c) NPT Building

The NPT building was analyzed assuming modal and uniform load distribution (FEMA, 2000). Again for each distribution four push-over analyses were carried out with "push" directions: +x, −x, +y, −y. The load distributions for the ±x directions along with the resulting pushover curves are presented in Figure 3.2.19. Since the building has only two storeys, the load patterns are in this case similar. However, the differences between the obtained curves indicate the uncertainties associated with such analyses. The most interesting observation here is the premature failure of the major shear walls in each direction leading to the termination of the analysis due to stability problems, while most of the deformation capacity of the columns has not yet been exceeded.

The push-over curves for the modal loading pattern of the NPT building parallel to the ±x axis direction are given in Figure 3.2.20, along with bilinear fits to each one of them, shown by dashed lines, and the calculated target displacements. In most cases the target displacement even for the normal building importance level could not be reached, whereas the δ_t for the high importance level lies beyond the displacement range displayed in the graphs. The curves are indicative that the building may be subject to premature failure, should a design level earthquake hit it. Here again it is noted that the behaviour of the NPT building is greatly affected by the poor performance of the lightly reinforced shear walls, whose capacity was exceeded, while most column hinges lied on the B-IO performance range. Similar results concerning the behaviour of shear walls were obtained from the elastic analyses. This suggests that upgrading these shear walls should be the first measure to apply when the building is strengthened to meet the current standards.

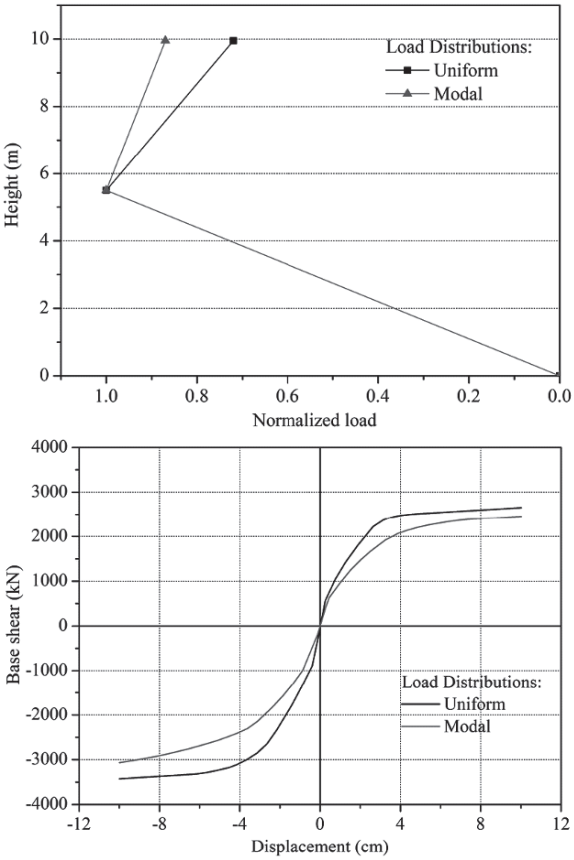

Fig. 3.2.19 Load patterns parallel to the ±x axis that were used for the non linear static analysis of the NPT building and resultant pushover curves

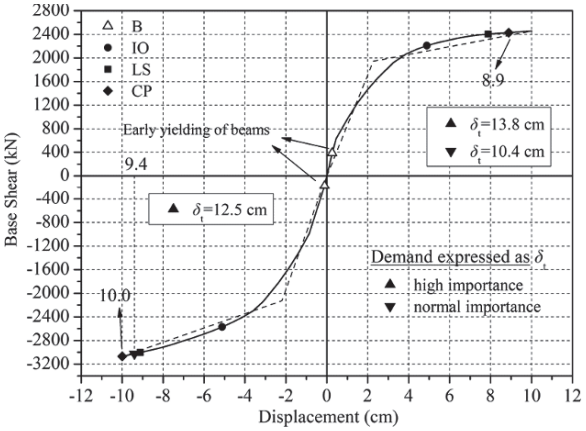

Fig. 3.2.20 Pushover curves and target displacements of the NPT building for loading parallel to x-axis – modal load pattern

3.2.7 Concluding remarks

The results of the present study indicate that the problem of capacity assessment of existing buildings can be dealt with either elastic or inelastic analyses. Both procedures involve major approximations and uncertainties associated with the seismic input, the models used, and the actual properties of the structure, as well as the soil. These uncertainties and approximations are present in the seismic design of new structures, except from those associated with structural properties, which in a new structure are accurately known.

Uncertainties in the soil and in member properties could be drastically reduced by applying extensive experimental campaigns, which however can be quite costly for usual, regular buildings. The same is true with analysis sophistication which is limited by cost considerations. Thus, the engineer faced with such problems must deal with them by checking his answers using a reasonable parameter variation. In the present study, this was done with the soil properties and the obtained results were properly assessed and considered.

In terms of modeling approximations, our models did not include the masonry infill walls, which typically increase the capacity of the building, provided they are well encased in the frame bays, are of good quality and are strengthened with concrete belts. Omitting such infill walls is normally on the safe side, although not always so. Modeling of shear walls having a low height to length (or width) ratio, with prismatic beam-column elements and plastic hinges, is another major approximation, especially for inelastic analyses, that casts significant doubts on the credibility of the results. All the uncertainties must be considered by the engineer-analyst who must always keep in mind the modeling limitations imposed by the available software.

Finally, another important issue concerning the nonlinear static analyses is the effect of the horizontal load pattern that is applied. This problem was hereby addressed by assuming alternative load distribution and evaluating the obtained results. However, in cases of buildings susceptible to torsion and when the effect of higher modes in the behavior of the building is not negligible, the accuracy of the results of such procedures can be questionable. In such cases the engineer should verify the results using elastic modal analysis or, better, resort to more accurate nonlinear dynamic analysis.

All the above were kept in mind while carrying the analyses and the assessment of the three buildings presented herein. For these buildings the conclusion that they cannot meet current standards of seismic safety, was obvious and came out of both types of analyses, elastic and inelastic, with full consideration of all the pertinent uncertainties. The great differences between the old (when the buildings were designed) and the new standards, makes such an assessment much easier.

Acknowledgements The present work has been supported by the Greek Secretariat for Research and Technology. The data for the buildings were provided by Mr. Yannis Hatzinikolis.

References

API-RP2A (1975) "API recommended practice for planning, designing and constructing fixed offshore platforms", 10th Edition, American Petroleum Institute, Washington, DC.

ATC (Applied Technology Council) (1996) "Seismic Evaluation and Retrofit of Concrete Buildings," ATC (Report N^{o} ATC-40), Redwood City, California.

CSi (Computers and Structures Inc.) (2007) SAP 2000 Advanced Structural Analysis Program, CSi, California.

CEN (European Committee for Standardisation) (2001) "European Standard EN 1991-1-1: Eurocode 1 – Actions on structure – Part 1-1: General actions – Densities, self weight, imposed loads for buildings," CEN, Brussels.

CEN (European Committee for Standardisation) (2004a) "European Standard EN 1992-1-1: Eurocode 2 – Design of concrete structures – Part 1-1: General rules and rules for buildings," CEN, Brussels.

CEN (European Committee for Standardisation) (2004b) "European (draft) Standard EN 1998-1: Eurocode 8 – Design of structures for earthquake resistance – Part 3: Assessment and retrofitting of buildings – Stage 49," CEN, Brussels.

FEMA (Federal Emergency Management Agency) (2000) "FEMA 356: Pre-standard and commentary for the seismic rehabilitation of buildings," FEMA, Washington, DC.

Gates W. E., Marshall P. W. and Mahin S. A. (1977) "Analytical methods for determining the ultimate earthquake resistance for fixed offshore structures," Proceedings of the 9th Annual Offshore Technology Conference, Houston, TX.

Kallaby J. and Millman D. (1975) "Inelastic analysis of fixed offshore platforms for earthquake loadings". OTC #2357, Proceedings of the 7th Annual Offshore Technology Conference, Houston, TX.

OASP (Greek Organization for Seismic Planning and Protection) (2000) "Greek seismic design code," OASP, Greek Ministry for Environmental Planning and Public Works, Athens, Greece (in Greek).

OASP (Greek Organization for Seismic Planning and Protection) (2004) "Greek retrofitting code – First draft version," OASP, Greek Ministry for Environmental Planning and Public Works, Athens, Greece (in Greek).

OASP (Greek Organization for Seismic Planning and Protection) (2006) "Greek retrofitting code – second draft version," OASP, Greek Ministry for Environmental Planning and Public Works, Athens, Greece (in Greek).

Chapter 3.3
Estimation of the Period of Vibration of Existing RC Building Types Based on Experimental Data and Numerical Results

Angelo Masi and Marco Vona

Abstract In the present paper the fundamental period of Reinforced Concrete (RC) frames of varying structural characteristics (number of stories, irregularity in elevation, presence and position of masonry infills, etc.) has been evaluated with the main objective of deriving period-height expressions for classes of European RC buildings. To this purpose, relationships from design codes and reported in the literature have been examined and their results have been compared to those ones obtained from numerical simulations (eigenvalue analyses) and experimental measurements (ambient vibration analyses). A wide parametric analysis has been carried out on several structural types selected and detailed (simulated design) to represent typical European RC buildings without earthquake RC design. As for the experimental evaluation of T values, ambient vibration analyses based on measurements carried out using quick survey techniques have been used. High differences between the values obtained from code relationships and numerical and experimental results have been found and discussed in the paper. Finally, future developments of the study have been outlined.

Keywords Existing buildings · Reinforced Concrete · Seismic vulnerability · Period of vibration · Eigenvalue analyses · Ambient vibration tests

3.3.1 Introduction

In the last years many experimental and numerical studies as well as many research projects have been carried out in order to define in a simplified way the fundamental period of Reinforced Concrete (RC) buildings. Particularly, empirical relationships

A. Masi (✉) and M. Vona
DiSGG, University of Basilicata, Campus Macchia Romana, Potenza, Italy
e-mail: angelo.masi@unibas.it

M. Mucciarelli et al., (eds.), *Increasing Seismic Safety by Combining Engineering Technologies and Seismological Data,* NATO Science for Peace and Security Series C: Environmental Security,

between the height of a building type and its fundamental period of vibration have been sought, as they can be very useful in many applications.

Simplified expressions are mandatory in large scale applications, where the period of a building (or of a class of buildings) needs to be estimated in assessing the seismic vulnerability at urban scale. Modern technology allows to perform a detailed assessment of the dynamic properties of a building in a very short time, thus an empirical relationship between a building's main characteristics (structural typology, shape, dimensions, age, etc.) and its dynamic behaviour can be obtained. On the basis of a classification scheme, the relationship can be applied to similar buildings over a large spatial extent, where building characteristics are obtained from quick field survey or from remote sensing.

A reliable evaluation of the fundamental period T is important both in classic (Force Based Design) as well as more recent (e.g. Push Over analysis, Displacement Based Design) design procedures. Different values of the fundamental period should be used according to the adopted design procedure. When using Force Based Design (FBD) procedures the elastic value of the period T is required. On the contrary, in Push Over (PO) analysis and Displacement Based Design (DBD) an effective value of the period is usually considered, where the post-elastic behaviour of the structure is taken into account.

In FBD procedures the effects of seismic actions on buildings can be determined using various methods of analysis. Assuming a linear elastic behaviour of the structure, two methods can be used:

- The Lateral Force Method of Analysis (LFMA), for "simple" buildings
- The Modal Response Spectrum Analysis (MRSA), applicable to all types of buildings

Both methods make use of an elastic ground acceleration response spectrum (elastic response spectrum) in the evaluation of the seismic response, where the calculation of the fundamental period (LFMA) or periods (MRSA) of the structure has a main role. LFMA may be applied to buildings whose response is not significantly affected by contributions from higher modes of vibration. This condition is deemed to be satisfied in buildings regular in elevation and having limited values of the fundamental period of vibration T; e.g. in EC8 (CEN, 2003): $T < 2.0\,\mathrm{s}$.

Based on the estimation of T, base shear F_b can be determined as follows:

$$F_d = S_d(T) \cdot m \cdot \lambda$$

where:

$S_d(T)$ is the ordinate of the design spectrum at period T.
m is the total mass of the building.
λ is the correction factor, the value of which is equal to: $\lambda = 0.85$ if $T < 2T_C$ and the building has more than two storeys, or $\lambda = 1.0$ otherwise.
T_C is the upper limit of the period of the constant spectral acceleration branch in the adopted horizontal elastic response spectrum.

For the determination of T, expressions based on methods of structural dynamics (for example the Rayleigh method) may be used. For example, the commentary to the NEHRP design provisions (BSSC, 2003) provides the formula:

$$T = 2\pi \left[\sum_{i=1}^{N} W_i u_i^2 \Big/ g \sum_{i=1}^{N} F_i u_i \right]^{1/2}$$

where W_i is the weight at the *i-th* floor and u_i are the floor displacements due to static applications of a set of lateral forces F_i at floor level i = (1, 2, …, N) in an N-story building. F_i may be any reasonable distribution over the building height.

Similar expressions are given also in the National Building Code of Canada and the Mexico Federal District Code (IAEE, 1996). Alternatively, many design codes (e.g. ATC3-06, 1978; CEN, 2003; NZSEE, 2006) provide simple relationships to calculate T that depend on building material (concrete, steel, masonry, etc.), building type (frame, shear wall, etc.), and overall dimensions.

In the DBD (Priestley et al., 2007) displacements are used for seismic design and assessment of structures as they, as opposed to forces, are better correlated to the damage level that a structure can suffer under seismic actions. Displacement values are dependent on the fundamental period of the structure as they can be obtained from response spectra. However, for RC frame buildings, displacements, contrary to forces, typically increase with period, thus underestimating periods (that is using elastic values of T) can lead to an unconservative design.

Finally, the fundamental period has a main role also in the determination of the target displacement for nonlinear static analysis (PO), where the analysis is carried out under conditions of constant gravity loads and monotonically increasing horizontal loads. PO analysis may be applied to verify the structural performance of newly designed and of existing buildings.

In the present study relationships from design codes and reported in the literature have been examined and their results have been compared to those ones obtained from eigenvalue analyses and ambient vibration analyses. It is worth noting that empirical relationship currently available were obtained from measurements carried out on buildings constructed in certain regions, thus are dependent on local design and construction practice. For this reason, main objective of the study is the derivation of period-height expressions for classes of European RC buildings.

3.3.2 Simplified period-height expressions

As already said, in the past years, empirical relationships between the height of a building type and its fundamental period of vibration have been usually set up keeping in mind an elastic force-based design.

The typical form of the expression reported in literature or codes is as follows:

$$T = C \cdot H^{\alpha}$$

where C and α are coefficients theoretically or experimentally derived. It was obtained applying the Rayleigh method assuming that the equivalent static lateral forces are distributed linearly along the height of the building and the distribution of stiffness with height produces a uniform storey drift under the adopted distribution of lateral forces.

The first semi-empirical formula employed in seismic codes is provided in (ATC 3-06, 1978):

$$T = C \cdot H^{0.75} \tag{3.3.1}$$

where C is 0.03 for RC moment resistant frames and H is the height of the building in feet. The value of C was obtained from the measured periods of buildings during the 1971 San Fernando earthquake.

In EC8 (CEN, 2003), an analogue form is proposed. For buildings with heights up to 40 m the value of T (in second) may be approximated by the same expression (1) of ATC 3-06, where C is 0.075 for moment resistant space concrete frames, 0.085 for moment resistant space steel frames and 0.050 for all other structures. H, in meter, is the height of the building from the foundation level. It has to be noted that the coefficient C for concrete frames has the same value provided in ATC 3-06 taking into account the adaptation of H from feet to metres (see Table 3.3.1).

In NZSEE (2006) T may be computed through the expression (1), where C is 0.09 for moment resistant concrete frames, 0.14 for moment resistant steel frames and 0.06 for all other structures.

Table 3.3.1 Different values of coefficients of period-height relationship for concrete moment resistant frames

Code/author	C (m)	α	Comments
ATC 3-06 (1978), CEN (2003)	0.075	0.75	C has been obtained from the measured periods of buildings during the 1971 San Fernando earthquake
NZSEE (2006)	0.09	0.75	
NEHRP, Goel and Chopra (1997)	0.0466	0.90	Periods measured in some US earthquakes (from San Fernando, 1971 to Northridge, 1994), coefficients obtained by subtracting one standard deviation from the best-fit curve
Hong and Hwang (2000)	0.0294	0.804	Periods measured on 21 Taiwanese buildings as subjected to moderate intensity earthquakes
Chopra and Goel (2000)	0.067	0.90	Same data of Goel and Chopra (1997) but coefficients obtained by adding one standard deviation from the best-fit curve, expression proposed for displacement base design and assessment (DBD)
Crowley and Pinho (2004)	0.10	1	Expression obtained from numerical simulations and bibliographic data proposed for displacement base design and assessment (DBD) in Europe, effect of cracking on member stiffness is considered

In the NEHRP 2003 Provisions (Goel and Chopra, 1997) T for moment resistant concrete frames is defined as:

$$T = 0.0466 \cdot H^{0.9}$$

Finally, another expression for concrete moment resistant frames to be used in force-based design is reported in (Hong and Hwang, 2000):

$$T = 0.0294 \cdot H^{0.804}$$

Period-height formulas for displacement-based design are proposed in (Chopra and Goel, 2000) and in (Crowley and Pinho, 2004). The former was obtained by adding one standard deviation to the best-fit curve derived in the work by Goel and Chopra (1997), thus providing:

$$T = 0.067 \cdot H^{0.9}$$

Crowley and Pinho (2004) proposed a relationship based on analytical methods aimed at providing reasonable estimates of the yield period of vibration of European RC frame buildings. Based on the results of eigenvalue, PO and nonlinear dynamic analyses carried out on 17 RC frames representative of European building stock, a very simple period-height relationship was obtained, as follows:

$$T = 0.1 \cdot H$$

A summary of the different values of coefficients of period-height relationship for concrete moment resistant frames proposed by codes and in literature are reported in Table 3.3.1, while the relevant curves are shown in Figure 3.3.1.

In Figure 3.3.1 strong differences can be observed among the values obtained using different formulas. Beyond the highest values provided by the Crowley and

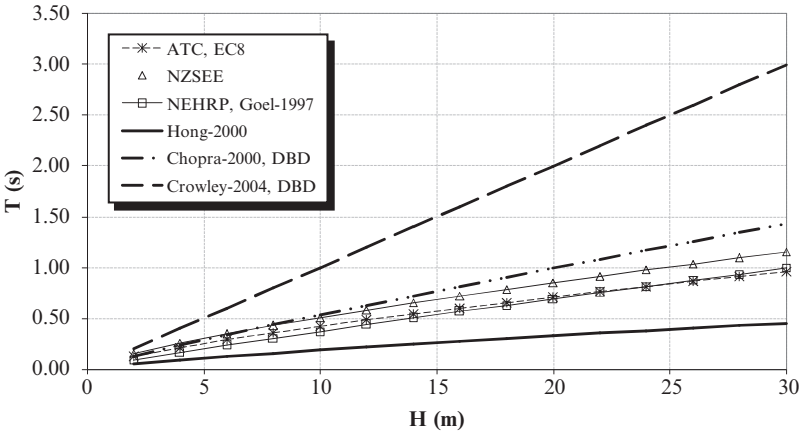

Fig. 3.3.1 Simplified period – height relationships for concrete moment resistant frames

Pinho formula for DBD, very large differences can be obtained also comparing the results provided by the various formulas for FBD (for example a ratio up to about three comparing T values from NZSEE and Hong and Hwang).

3.3.3 Description of the study

Empirical period-height relationships, currently available, are typically provided dependent only on the structural type (concrete frames, steel frames, masonry, etc.), but do not take into account other important structural characteristics such as:

- Structural regularity in plan and in elevation
- Member stiffness (dimensions, extent of concrete cracking)
- Axial load level
- Reinforcement ratio
- Geometry, presence and position of masonry infills

Further, as already said, these relationships have been usually developed keeping in mind force-based design. For this reason, they provide low estimates of period such that the lateral shear force is conservatively predicted from an acceleration spectrum. On the contrary, in displacement-based assessment, the displacement demand is required, being better correlated to the expected damage. This displacement would be underestimated using the aforementioned period-height formulae (Crowley and Pinho, 2004).

In the present work the fundamental period of RC frames of varying structural characteristics (number of stories, irregularity in elevation, presence and position of masonry infills, etc.) is evaluated. In particular, the strong influence of masonry infills on dynamic behaviour of RC frames (specifically on fundamental period values) is highlighted and simplified period-height expressions for classes of existing European RC buildings are provided.

Relationships from design codes and reported in the literature have been examined and their results have been compared to those ones obtained from numerical simulations (eigenvalue analyses) and experimental measurements (ambient vibration analyses).

As for numerical simulations, a wide parametric analysis on structural types representative of typical RC buildings has been carried out. Further, ambient vibration analyses based on measurements carried out using quick survey techniques have been used and compared with numerical analyses and design code provisions.

3.3.4 Parametric analysis

A wide parametric analysis has been carried out on several structural types purposely selected and detailed (simulated design) to represent typical European RC

buildings without earthquake resistant design. For the selection and the simulated design of the structures a procedure, described in detail in (Masi, 2003), has been used. A flow-chart of the procedure is shown in Figure 3.3.2.

As for the selection of structural types, the review of the technical original documentation of typical existing residential buildings has pointed out some important characteristics influencing their global seismic behaviour. In RC buildings designed only to vertical loads internal beams are present in one direction only, generally the longitudinal one. In the orthogonal direction the frames are present on the external sides only. Stiffness distribution is generally symmetric in both principal directions. Based on these observations, several 3D building types symmetric in plan (Figure 3.3.3) have been defined on the basis of the number of story, plan

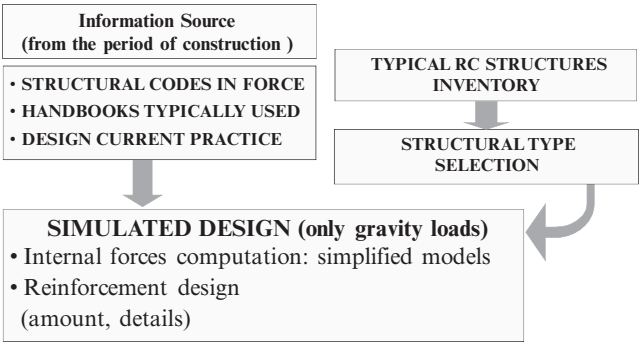

Fig. 3.3.2 Flow-chart of the procedure for the simulated design of existing RC buildings

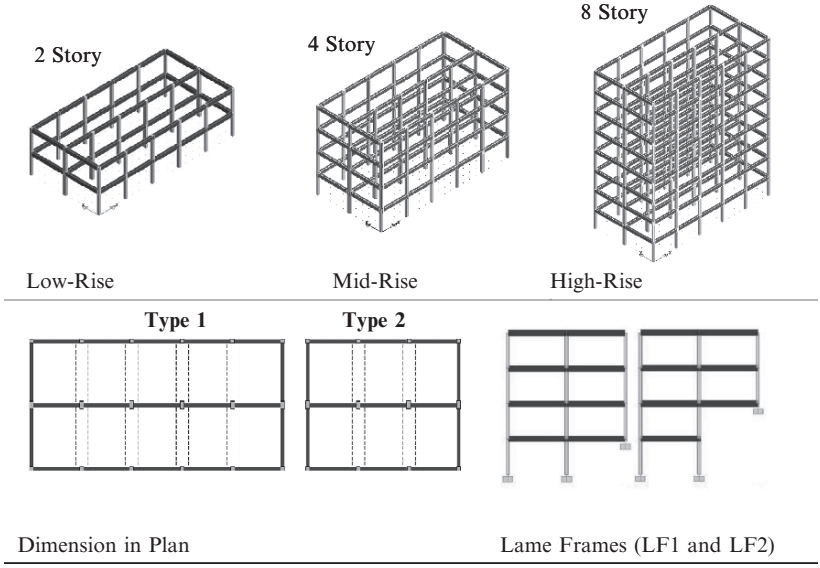

Fig. 3.3.3 Number of story, plan dimensions and elevation irregularities considered in the building types under examination

dimensions, irregularity in elevation, presence and position of masonry infills, stiffness of structural members. In all the types interstory height is equal to 3.0 m and bay length is equal to 5.0 m.

As for the simulated design of the selected structural types, procedures typically adopted for RC framed buildings have been considered, making reference to codes in force, handbooks and typical technical documents of the period (simulated design, Masi, 2003). Safety verifications have been performed according to the allowable stress method, assuming mechanical properties of materials relevant to post-1970 standards (medium quality concrete C 20/25 and steel with grade close to S400 type). The columns have been designed taking into account only axial load and adopting the minimum requirements provided in the Italian code of the period regarding reinforcement. The beams have been designed on the basis of the simplified model of continuous beam resting on simple supports. Where the dimensions of structural elements and the reinforcement amounts could not be inferred by code prescriptions or by internal force values, reference has been made to the most prominent handbooks and to the current practice of the period.

As for presence and position of masonry infills, some typical situations have been considered, thus obtaining the following types (Figure 3.3.4):

- Exterior frames without infills (BF, Bare Frame)
- Exterior frames with regularly arranged masonry infills (IF, Infilled Frame)
- Exterior frames without masonry infills at the ground floor (PF, Pilotis Frame) or partially infilled at the ground floor (PPF, Partial Pilotis Frame)

As regards BF type, it is worth noting that while infills are generally present in exterior frames, they sometimes have many and/or very large openings or they are badly connected to the structure and thus their contribution to the strength and stiffness of the structure can be neglected.

Stiffness variation of structural members has been taken into account in two different ways. In the first one, variation in member stiffness is dependent on transverse beam dimensions (Rigid Beams, Flexible Beams and No Beams, Figure 3.3.5); in the second one effect of cracking on stiffness, both of beams and columns, has been considered.

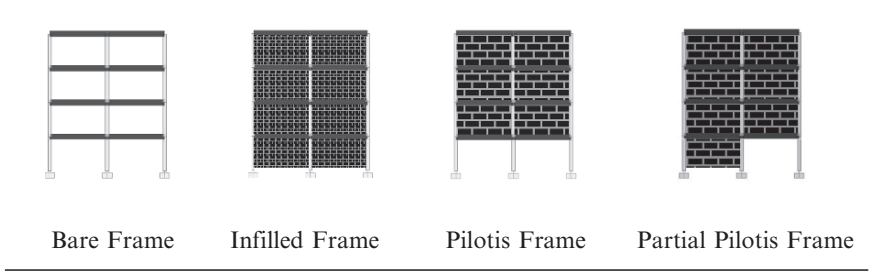

Fig. 3.3.4 Masonry infill distributions considered in the building types under examination

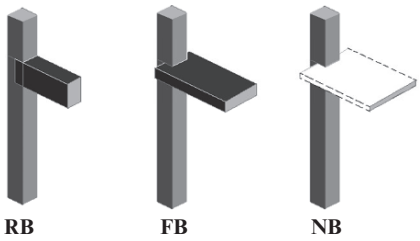

Fig. 3.3.5 Stiffness of transverse beams: Rigid Beams (RB), Flexible Beams (FB), No Beams (NB)

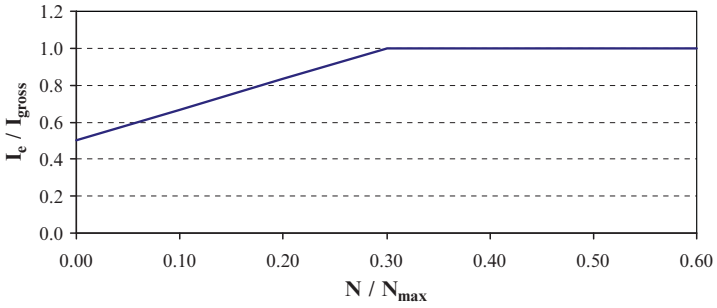

Fig. 3.3.6 Stiffness reduction dependent on the axial load value

Experimental results (e.g. Kunnath et al., 1995) show that the elastic stiffness properties of concrete members is reduced by cracking due to non-seismic actions. Different values of the ratio I_e/I_{gross} between the reduced inertia I_e and the gross inertia I_{gross} can be adopted to take into account the different effect of cracking on columns and beams (role of the axial load value). The European seismic code (CEN, 2003) in the modelling of the structures allows a stiffness reduction of the load bearing elements due to cracking suggesting that

> In concrete buildings the stiffness of the load bearing elements should, in general, be evaluated taking into account the effect of cracking. … Unless a more accurate analysis of the cracked elements is performed, the elastic stiffness properties of concrete elements may be taken to be equal to one-half of the corresponding stiffness of the uncracked elements.

Three cases have been considered in the parametric analysis as regards the values of the ratio I_e/I_{gross}:

1. $I_e = I_{gross}$
2. $I_e = 0.7\ I_{gross}$ for Columns and Rigid Beams
   $I_e = 0.5\ I_{gross}$ for Flexible Beams
3. $I_e = \mathrm{k}\ (\mathrm{N})\ I_{gross}$ dependent on the axial load value for Columns
   $I_e = 0.5\text{–}0.7\ I_{gross}$ for Flexible and Rigid Beams

In the third case reduction of column stiffness is dependent on the axial load value due to vertical loads normalized to the ultimate axial load N_{max}, as shown in Figure 3.3.6. Stiffness reduction value is variable in the 0.50–0.70 range for two stories building, and in 0.50–0.90 range for four and eight stories building.

In conclusion, in the parametric analysis the following parameters and the relevant number of cases have been considered:

- Number of story: 3 cases
- Dimensions in plan: 2 cases
- Irregularity in elevation: 3 cases
- Presence and position of masonry infills: 4 cases
- Member stiffness: 3 + 3 cases

3.3.4.1 Results of numerical analyses

The eigenvalue analyses reported in this study have been carried out using the Finite Element code SAP 2000 (SAP2000, 1999). Models able to represent the selected structural types in a sufficient reliable way have been implemented. According to (CEN, 2003) only a limited share of the live loads has been considered in the evaluation of the seismic response.

As regards infills, in RC existing buildings they are usually made of two layers of hollow brick masonry with a total thickness equal to about 200 mm and scarce mechanical characteristics. Taking into account the modeling capabilities of the program used in the analyses, each masonry panel has been modelled by using an equivalent diagonal strut, whose area has been determined by multiplying the panel thickness t_w by an equivalent width b_w. The following expression due to Mainstone (1974), relevant to rectangular masonry panels, has been used to compute b_w:

$$\frac{b_w}{d_w} = 0.20 \cdot \sin(2\theta) \left(\frac{E_w \cdot t_w \cdot h_w^3 \cdot \sin(2\theta)}{E_c \cdot I_p} \right) \tag{3.3.2}$$

where h_w = panel height, d_w = diagonal length, θ = angle of the diagonal with the horizontal, E_w = modulus of elasticity of masonry, E_c = modulus of elasticity of concrete and I_p = moment of inertia of columns. The characteristics of the equivalent strut are the area $A_s = b_w \cdot t_w$, and the stiffness $K_s = (E_w A_s / d_w)$.

The main results obtained from eigenvalue analyses have been represented in period-height plots together with the regression curve obtained assuming a linear relationship having the form $T = C\,H$ to make the comparison among the different expressions easier. Specifically, the role of stiffness reduction due to cracking, of masonry infill distribution, and of elevation irregularity has been pointed out in Figures 3.3.7–3.3.9.

Figure 3.3.7 shows that the member stiffness reduction in regular Bare Frames has a significant effect on the H-T relationship with increased values of T up to about 30% when cracking due to non-seismic actions is taken into account. On the contrary, it has to be noted that the different methods adopted to compute the stiffness reduction have a negligible influence on results. For this reason, in the following reduced inertia will be computed using the simplified formula $I_e = 0.5\text{–}0.7\, I_{gross}$.

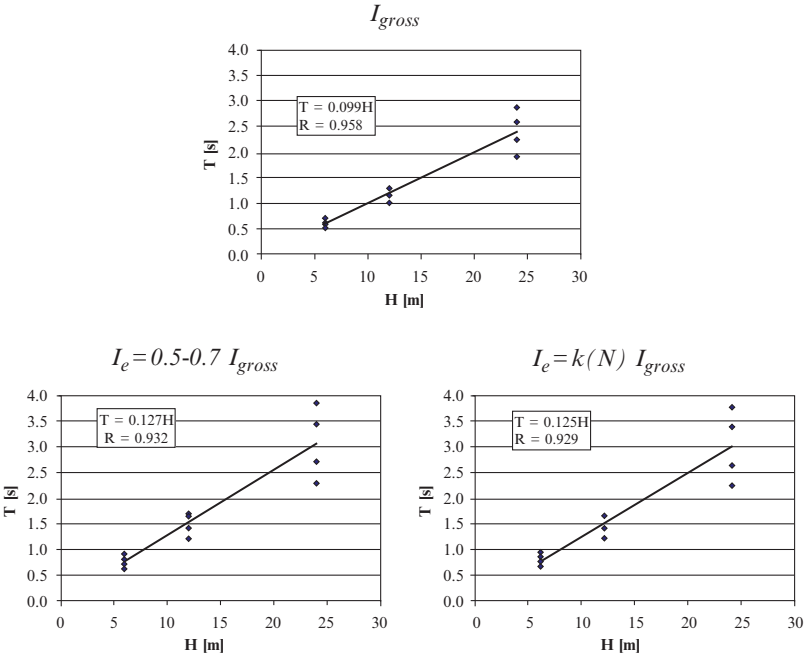

Fig. 3.3.7 Period-height relationships obtained using different stiffness values of structural members (Bare Frame type, regular in elevation)

As for the role of the infill distribution, the results of the numerical simulations are summarized in Figure 3.3.8. Considering the cracked stiffness of members (plots on the right) the curves for Bare Frame types show values far higher than the curves for Infilled Frame types: the value of C coefficient decreases from 0.110 (BF type) to 0.057 (IF type). Together with a general decrease, also a reduction of scatter of T values for each H value considered in the analyses can be observed in IF type, to confirm the major role of infills. Results for Pilotis Frame are substantially coincident to those ones for IF type, providing C = 0.058, thus the absence of infills at the ground floor can be neglected in the computation of T. Similar trends can be observed in the plots obtained for BF, IF and PF types, when the uncracked inertia is considered (Figure 3.3.8, plots on the left).

The role of elevation irregularities is analysed in Figure 3.3.9, showing a decrease of T values both for Bare and Infilled Frames. In Bare Frames the coefficient C decreases from 0.127 to 0.101 when the irregularities are taken into account, whereas in the Infilled Frames the reduction is from 0.062 to 0.055. This comparison confirms the major role of infills on T values when compared to other structural characteristics of RC buildings. However, it is worth noting that in this study elevation irregularities have been considered as shown in Figure 3.3.3, that is making reference only to Lame Frame types, where one or two floors are partially absent.

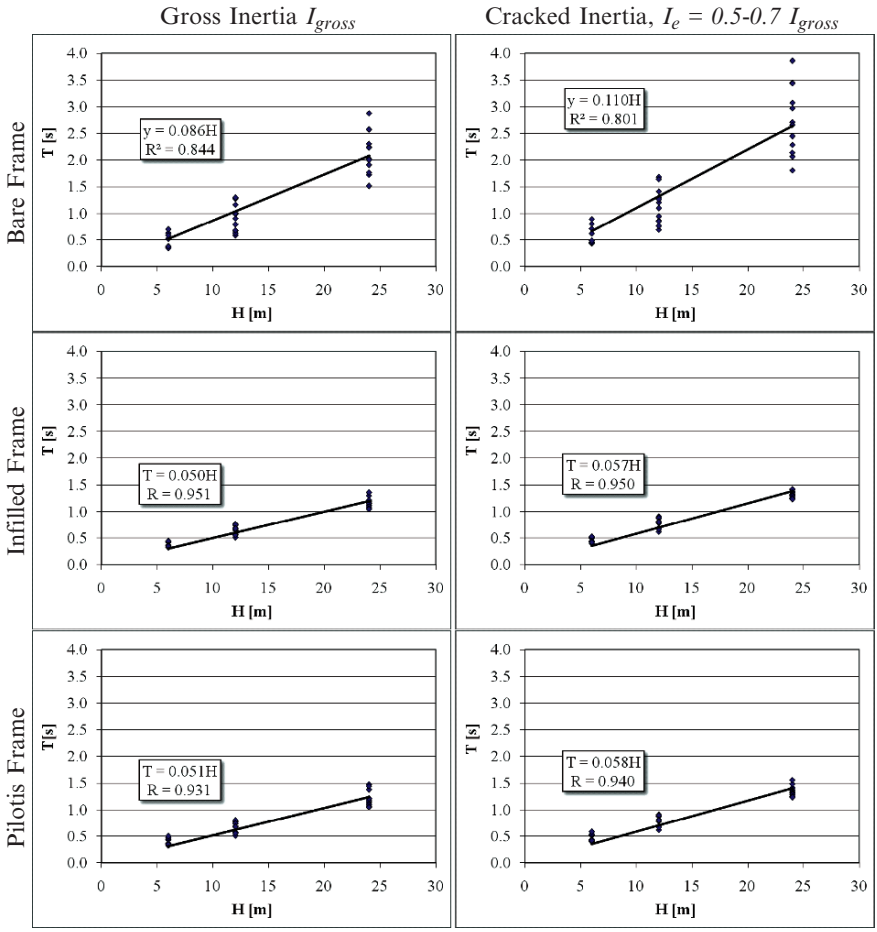

Fig. 3.3.8 Period-height relationships obtained with different infill distributions

3.3.5 Experimental measurements

In this section, some experimental results are reported and analysed. The results of a wide campaign of structural vibration measurements on Italian building structures (Gallipoli et al., 2006) are initially described and, after, a comparison with other measurements reported recently in the technical literature is performed.

Microtremor measurements on 50 RC Italian buildings have been performed mainly in Potenza town (Southern Italy). Some measurements were carried out also in Senigallia town (Central Italy). As for Potenza, building sample has been selected to be representative of the building stock, taking into account structure height and period of construction. Most of measurements were carried out on RC buildings designed and constructed in the period 1950s–1970s (structure without earthquake

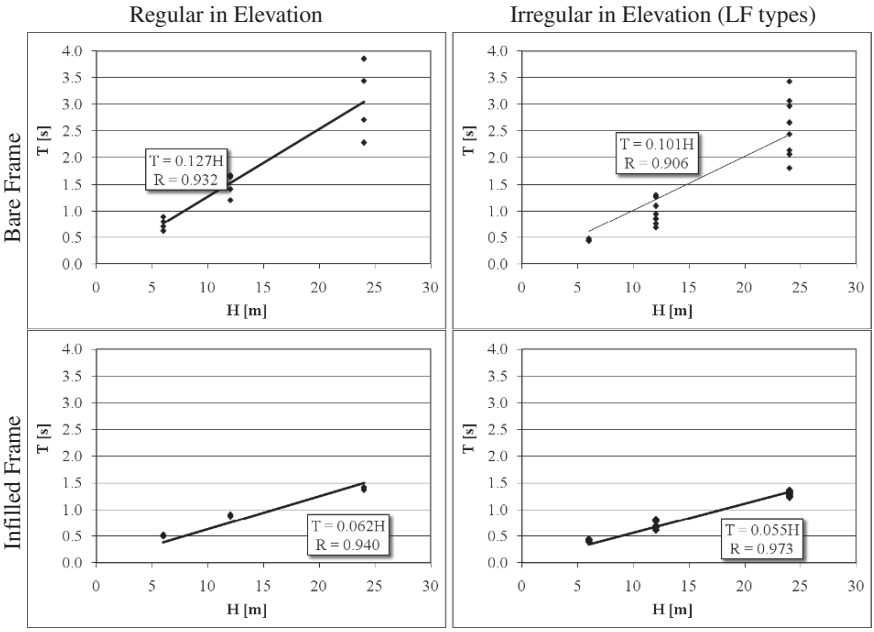

Fig. 3.3.9 Period-height relationships obtained without or with elevation irregularities

resistant design), but in a few cases buildings designed in the 1990s (with earthquake resistant design) have been considered. The buildings under examination exhibit strongly different characteristics both in plan and in elevation (Figure 3.3.10). Masonry infills are generally present, often not at the ground floor.

Ambient vibration measurements have been carried out using quick survey techniques. Using a three component data acquisition system, the horizontal and vertical components of microtremors at the base and at the top of the buildings have been recorded. A simple as well as reliable time-domain non-parametric methodology has been used to estimate the fundamental period of buildings (Gallipoli et al., 2006).

T values are in the range 0.074–0.588 s as a result of measurements carried out on buildings whose height varies from 3 m (1 story) to over 27 m (12 stories). In Table 3.3.2 the mean values of T and the relevant values of standard deviation SD and coefficient of variation CV, considering different sub sets referred to different heights (number of stories) of the buildings, are reported. SD relevant to the entire dataset is equal to 0.116 s, with a coefficient of variation CV equal to 0.39.

The measured periods in function of the relevant building height are shown in Figure 3.3.11 together with the best-fit linear regression $T = 0.016H$, having a correlation coefficient R = 0.789. In Figure 3.3.11 also the curves obtained by adding and by subtracting one standard deviation are reported.

The measurements carried out in Italy have been compared with other similar measurements reported in the literature. In particular, reference has been made to a wide experimental campaign carried out in Granada City (Spain) on 89 RC buildings

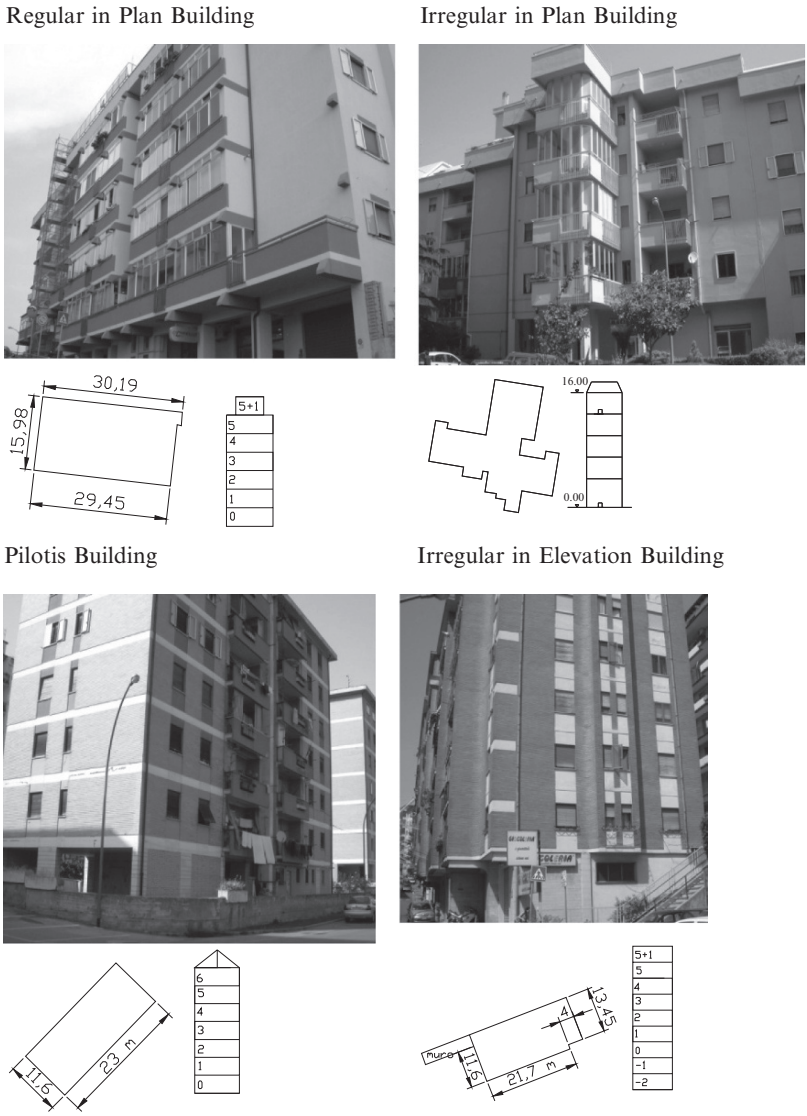

Fig. 3.3.10 Examples of RC buildings studied in Potenza town

(Navarro et al., 2004). The typical structural system in Granada City is similar to that one in Potenza, as it consists in RC frames without earthquake resistant design, having unidirectional floors, exterior brick walls, RC foundation formed by clamped footings. Buildings regular both in plan and in elevation were considered. The structural vibration measurements were performed at the centre of plan at the roof floor or at the last story of buildings. The displacement of the structure was measured, and Fast Fourier Transformation was applied to every record in order to compute

Table 3.3.2 Mean, SD and CV values of the measurements carried out for different building heights in Potenza and Senigallia (Italy)

Building height (m)	No. of cases	T (mean) (s)	SD (s)	CV
3	2	0.160	–	–
6	2	0.200	–	–
9	1	0.190	–	–
12	3	0.277	0.045	0.163
15	4	0.248	0.022	0.090
18	9	0.302	0.037	0.122
21	10	0.338	0.030	0.088
24	11	0.411	0.064	0.155
>27	8	0.484	0.043	0.090

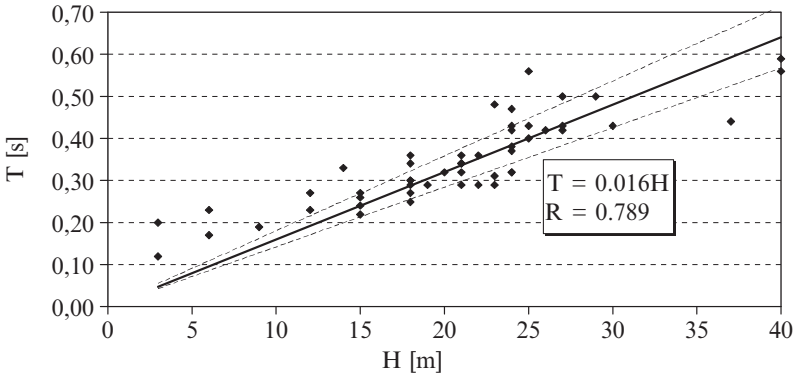

Fig. 3.3.11 Period-height relationship for Italian buildings derived from experimental measurements

Fourier spectrum. As a result of the measurements the same period-height relationship obtained for the Italian RC buildings was derived, that is: $T = 0.016\,H$ (Spanish RC buildings).

It has to be noted that the results obtained for Italian and Spanish Buildings are consistent with those provided by several authors using microtremor measurements (Kobayashi et al., 1986; Kobayashi et al., 1996; Midorikawa, 1990; Enomoto et al., 2000).

3.3.6 Analysis of results

Analysing the results obtained from the numerical simulations some general remarks can be drawn:

– Cracking due to non-seismic actions, generally present in RC structures, significantly influences the fundamental period.
– The presence of regularly arranged masonry panels (IF types) strongly reduce both T values and their scatter.
– T values computed for IF and PF types are practically coincident.
– Elevation irregularities (LF types) cause a reduction in T values even though lower than this one due to masonry infills.

As a result of the above remarks it appears that the role of cracking and masonry infills cannot be neglected in the evaluation of the fundamental period of RC framed buildings, particularly when they are designed only to gravity loads.

For these reasons in Figure 3.3.12 the proposed period-height relationships for some classes of existing European RC buildings are shown, distinguishing only Bare and Infilled Frame types. The proposed relationships are as follows:

Bare Frame types: $T = 0.110H$
Infilled Frame types: $T = 0.055H$

Together with the mean curves an estimation of the maximum and minimum predictable values has also been shown in Figure 3.3.12, based on the variability of the results.

To compare the main results provided by the numerical simulations and experimental measurements described in this study some period – height relationships, together with the expression provided in the EC8, are shown in Figure 3.3.13.

The curves in Figure 3.3.13 show that there are very high differences when comparing the T values provided by the numerical simulations to those ones obtained from the experimental measurements. As an example, for a mid-rise building (six story, H = 18 m) T value increases from 0.288 s (experimental results) to 1.98 s

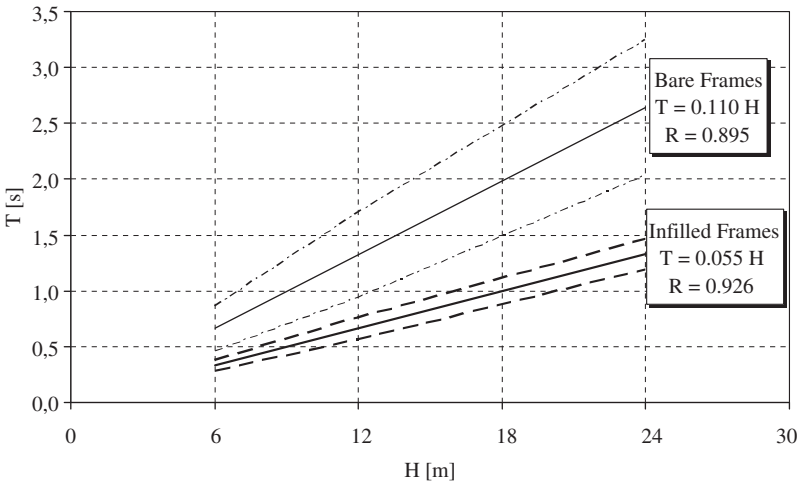

Fig. 3.3.12 Proposed period-height relationships for existing RC framed buildings

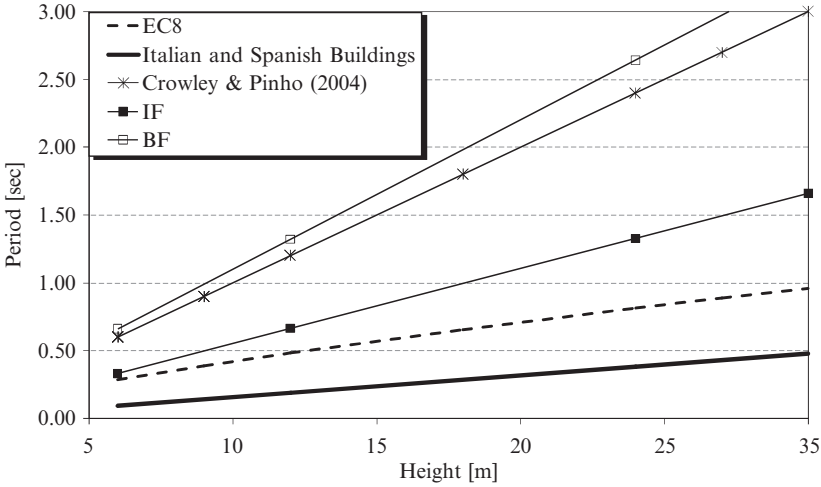

Fig. 3.3.13 Comparison among some period-height relationships for existing RC buildings

(eigenvalue analyses, Bare Frame types), with the latter value about seven times larger the former one. Really, the ambient vibration measurements were carried out mostly on Infilled Frame types. However, also making reference to the expression provided for IF types, T equal to 0.99 s is computed for H = 18 m, that is over three times larger than the experimental value.

Intermediate values but closer to the experimental ones can be computed by using the EC8 simplified expression provided for Force Based Design of earthquake resistant buildings.

Results very close can be seen between the expression obtained for the Bare Frame types and that one provided by Crowley and Pinho (2004) for Displacement Based Design, thus pointing out that the latter should not be used in case of RC buildings with masonry infills.

3.3.7 Conclusions and future developments

The effects of seismic actions on building structures are strongly dependent on their dynamic characteristics and, especially, on their fundamental period of vibration. For this reason, many experimental and numerical studies have been performed to define in a simplified way the fundamental period of RC buildings.

Typically, empirical relationships between period and building height have been provided, whose results may be conditioned by the design and construction practices currently used in the examined region. Further, empirical period-height relationships dependent only on the material and structural system (concrete or steel frames, shear walls, masonry, etc.) have been obtained, do not taking into account

other important structural characteristics such as regularity in plan and in elevation, member stiffness, presence and position of masonry infills, etc.

In the present paper the fundamental period of RC frames of varying structural characteristics (number of stories, irregularity in elevation, presence and position of masonry infills, etc.) is evaluated with the main objective of deriving period-height expressions for classes of European RC buildings. To this purpose, relationships from design codes and reported in the literature have been examined and their results have been compared to those ones obtained from numerical simulations (eigenvalue analyses) and experimental measurements (ambient vibration analyses).

A wide parametric analysis has been carried out on several structural types selected and detailed (simulated design) to represent typical European RC buildings without earthquake resistant design. For the selection and the simulated design of the structures a purposely set procedure has been used. The strong influence of masonry infills and of cracking on the fundamental period values of RC buildings has been highlighted. Simplified period-height expressions have been provided relevant to some structural types widely present in the European built environment.

As for the experimental evaluation of T values, ambient vibration analyses based on measurements carried out using quick survey techniques have been used.

The comparison between numerical and experimental results shows very large differences. It has to be noted that numerical simulations have been carried out on carefully set up models where the role of cracking, masonry infills, elevation irregularities was taken into account, but other structural characteristics as stairs and plan irregularities have to be considered. On the other hand, the results obtained from experimental measurements on existing Italian and Spanish Buildings are consistent with those ones provided by other authors using microtremor measurements.

Further studies and in-situ or laboratory tests are needed to set up procedures able to reliably evaluate the fundamental period of a building, particularly to better understand the large differences between numerical and experimental values.

References

ATC, 1978. Tentative provisions for the development of seismic regulations for buildings, Report No. ATC3-06, Applied Technology Council, California.

BSSC, 2003. NEHRP recommended provisions for seismic regulations for new buildings and other structures (FEMA 450), 2003 Edition, Building Seismic Safety Council, Washington, DC.

CEN, 2003. Eurocode 8: Design of structures for earthquake resistance, Part 1: General rules, seismic actions and rules for buildings, Final Draft, Comite Europeen de Normalisation, Brussels, December 2003.

Chopra, A.K. and Goel, R.K., 2000. Building period formulas for estimating seismic displacements, Earthquake Spectra, 16(2), 533–536.

Crowley, H. and Pinho, R., 2004. Period-height relationship for existing European reinforced concrete buildings, Journal of Earthquake Engineering, 8(1), 93–119.

Enomoto, T., Schmitz, M., Abeki, N., Masaki, K., Navarro, M., Rocavado, V., and Sanchez, A., 2000. Seismic risk assessment using soil dynamics in Caracas, Venezuela, 12WCEE, CDROM.

Gallipoli, M., Mucciarelli, M., and Vona, M., 2006, Stima di alcuni parametri principali degli edifici con metodi speditivi, GNGTS – 25° Convegno Nazionale, Roma 28–30 novembre 2006 (in Italian).

Goel, R.K. and Chopra, A.K., 1997. Period formulas for moment resisting frame buildings, Journal of Structural Engineering, ASCE, 123(11), 1454–1461.

Hong, L. and Hwang, W., 2000. Empirical formula for fundamental vibration periods of reinforced concrete buildings in Taiwan, Earthquake Engineering and Structural Dynamics, 29, 327–337.

IAEE, 1996. Earthquake resistant regulations, a world list, International Association of Earthquake Engineering, Tokyo.

Kobayashi, H., Seo, K., and Midorikawa, S., 1986. Estimated strong ground motions in México City. The México Earthquake-1985, Factors involved and lessons learned, ASCE, 55–69.

Kobayashi, H., Vidal, F., Feriche, D. Samano, T., and Alguacil, G., 1996. Evaluation of dynamic behaviour of building structures with microtremors for seismic microzonation mapping. The 11th World Conference on Earthquake Engineering, Acapulco, México, June 23–28.

Kunnath, K.S., Hoffmann, G., Reinhorn, A.M., and Mander, J.B., 1995. Gravity load designed reinforced concrete buildings – part I: seismic evaluation of existing construction, ACI Structural Journal, May–June.

Mainstone, R.J., 1974. Supplementary note on the stiffness and strength of infilled frames, Current Paper CP13/74, Building Research Establishment, London.

Masi, A., 2003. Seismic vulnerability assessment of gravity load designed R/C frames, Bulletin of Earthquake Engineering, 1(3), 371–395.

Midorikawa, S., 1990. Ambient vibration tests of buildings in Santiago and Viña del Mar. A report on the Chile-Japan Joint Study Project on Seismic Design of Structures. The Japan International Cooperation Agency.

Navarro, M., Vidal, F., Feriche, M., Enomoto, T., Sánchez, F.J., and Matsuda, I., 2004. Expected ground–RC building structures resonance phenomena in Granada city (Southern Spain), Proc. 13th World Conf. Earthq. Eng.,Vancouver, BC, Canada, August 1–6, 2004, Paper No. 3308.

NZSEE, 2006. Assessment and improvement of the structural performance of buildings in earthquakes, Recommendations of a NZSEE Study Group on Earthquake Risk Buildings, June.

Priestley, M.J.N., Calvi, G.M., and Kowalsky, M.J., 2007. Displacement-Based Seismic Design of Structures. IUSS Press, Pavia, Italy.

SAP2000, 1999. Three dimensional static and dynamic finite element analysis and design of structures, Computers and Structures Inc. Berkeley, CA.

Chapter 3.4
Retrofitting and Strengthening Evaluation from Stiffness Variations of a Damaged Building from Ambient Vibration Recordings

Mohammed N. Farsi, Bertrand Guillier, Jean-Luc Chatelain, and Sid-Ahmed Zermout

Abstract The rigidity of a six-story shear-wall building, damaged by the May 21, 2003 Boumerdes earthquake (Algeria) has been evaluated before the event, in its damaged state, and after retrofitting, by estimating its natural frequency, damping factor, and modal shape. Pre-event parameters are estimated through a numerical analysis, based on the structure drawings, complemented by an ambient vibration investigation of an identical non-damaged building located on the same site. Parameters of the damaged and retrofitted states were obtained from ambient vibration recordings. Variations of the modal parameters, for the three states of the building, allow evaluating rigidity changes, and thus checking of both the retrofitting and strengthening of the building.

Keywords Building · Earthquake · Stiffness · Modal characteristics · Retrofitting · Ambient Vibrations

3.4.1 Introduction

The building under investigation, damaged by the May 21, 2003 Boumerdes earthquake (Mw 6.8), is located in the COSIDER neighborhood at Bordj-El-Bahri (Figure 3.4.1), 20 km East of Algiers and about 40 km West of the 2003 epicenter (36.83N–3.65E, 10 km depth; Bounif et al., 2004). Bordj-El-Bahri is located in the Mitidja basin, characterized by tertio-quaternary alluviums that reach locally

M.N. Farsi, B. Guillier, J.-L. Chatelain, and S.-A. Zermout
Centre National de Recherche Appliquée en Génie Parasismique (CGS), Algiers, Algeria
e-mail: mnfarsi@cgs-dz.org; sazermou@cgs-dz.org

B. Guillier and J.-L. Chatelain
Laboratoire de Géophysique Interne et de Tectonophysique, IRD, CNRS, Université Joseph Fourier, Grenoble, France
e-mail: Bertrand.Guillier@bondy.ird.fr; jlchatel@obs.ujf-grenoble.fr

M. Mucciarelli et al., (eds.), *Increasing Seismic Safety by Combining Engineering Technologies and Seismological Data,* NATO Science for Peace and Security Series C: Environmental Security,

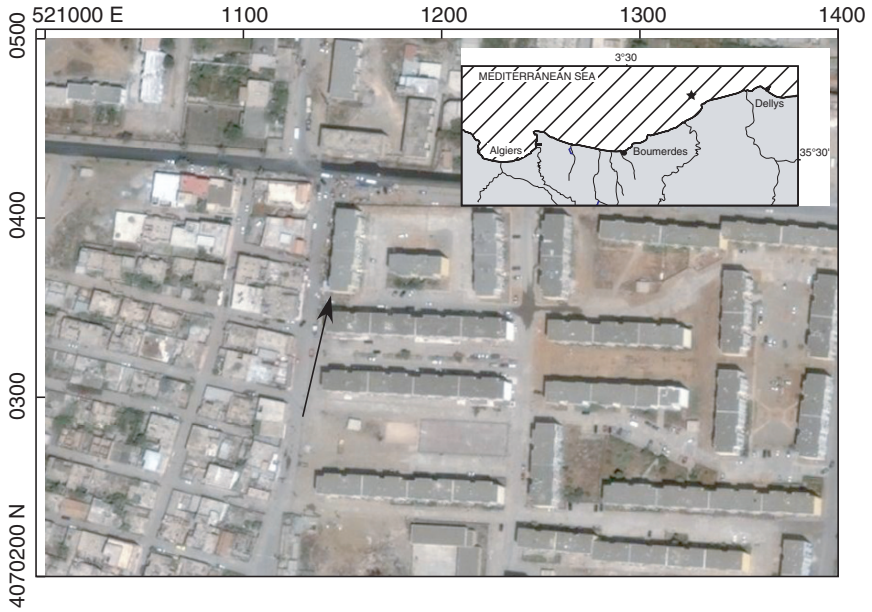

Fig. 3.4.1 Location of the studied building (black arrow) in its urban setting. The building is located in Bordj El Bahri, in the North-East Algiers suburbs. The upper inset shows the location of the satellite view and the USGS location of the Boumerdes earthquake (black star)

close to 1 km depth, with a very low shear wave velocity in the surficial layer $(V_{s30} = 300\,m/s)$ indicating a soft soil (Guillier et al., 2005). Strong motion studies of the 2003 earthquake show that E-W accelerations were greater than the N-S ones, demonstrating a fault related directional effect of the earthquake (Laouami et al., 2004, 2006). The accelerometer closest to the epicenter installed at Dar-El-Beida (6 km South from the studied building) show accelerations of 0.46 and 0.52 g in the E-W and N-S directions respectively, with a maximum peak ground acceleration in the 2–6 Hz frequency range (Laouami et al., 2006). Three ambient vibrations campaigns of in-situ measurements were performed to study the dynamical parameters of the building (before and after the earthquake, and after retrofitting), as well as a numerical modeling. In this paper, we describe the results from numerical model and experimental data, and investigate the reliability of both the different methods used and the retrofitting.

Since few years, damage assessment of a building having experienced a strong earthquake is of high interest for researchers and structural engineers. In some cases, the building damages are probably unrecoverable or may lead progressively to total collapse. Nowadays, the most used and developed methodologies to evaluate the post-seismic state of a building the nondestructive tests (NDT) such as, the story damage index (SDI) and the approximate story damage index (ASDI), forming the basis of any decision to repair, rehabilitate or destroy a building. Generally, NDT implies to collect earthquake (aftershocks) signal recordings in the building after the occurrence of a strong earthquake (main shock). Nevertheless, this phase of

data collection is aleatory and requires a lot of material and specialists to conduct the recordings. In this paper, we used ambient vibration recordings to evaluate the dynamic response characteristics of a building under very low levels of excitation, i.e. without any earthquake shaking. The natural frequencies, modal damping and modal shapes were studied for three states of the COSIDER building: before the 2003 earthquake, the damaged state after the 2003 earthquake, and after retrofitting of the building.

The main interest of using ambient vibrations is the possibility to conduct extensive recording campaigns, with the opportunity to evaluate a large amount of structures, not only after the earthquake occurrence, but also, before and after retrofitting. This study is part of a joint research venture between the Laboratory of Internal Geophysics and Tectonophysics (LGIT) of Grenoble, France and the National Center of Research Applied in paraSeismic (CGS) of Algiers, Algeria. The goal of this project is to statistically establish the dynamic response characteristics of various types of buildings (masonry, concrete, reinforced concrete…) in the entire Algiers level, to have an image of the "pre-event" state, to evaluate the post-strong earthquake state of the building, by a simple determination of the natural frequencies, allowing theoretically to help for a building diagnosis without any human influence. Moreover, the determination of modal characteristics gives inputs for finite elements calculus.

3.4.2 Structure, damages and retrofitting

The COSIDER building (Figure 3.4.2) is a five-storey building with the following heights: underground floor, 2.56 m; first to fifth floors, 2.88 m. The resistant structure is made of eight transversal RC 15 cm-thick shear-walls of and one eccentric longitudinal 20 cm-thick RC shear-wall. The floors are 15 cm-thick RC slabs. The building is founded on a 40 cm-thick RC mat foundation. The principal and lateral facades are constituted by pre-cast RC elements as shown on the photo of Figure 3.4.2.

In its longitudinal direction, the building is oriented N-S, when the direction of the fault that originated the 2003 earthquake is ENE. The longitudinal orientation of the studied building, related to the fault, is consistent with the observations in Boumerdes, where, in the "1200 Logements" housing lot, the most impacted structures have a N-S longitudinal direction (Dunand et al., 2004). Thus, as in the Boumerdes case, visual damages were located on the longitudinal (N-S) shear-wall, at the underground and first levels, and consisted in shearing cracks that reached over 10-cm opening at places (Figure 3.4.3, left and center). As the building is located at the western end of the housing lot (see Figure 3.4.1), it is likely that part of the train wave has been modified by the transmission back to the soil by identical neighboring buildings (Wong and Trifunac, 1975, Wirgin and Bard, 1996), increasing locally the energy in a frequency band around the natural frequency of the building.

Fig. 3.4.2 Plan (upper), elevation (lower left) and view (lower right) of the studied COSIDER building. Values are given in meters

Fig. 3.4.3 Details of the structure. Crack on the longitudinal shear-wall at first floor (left), horizontal crack on the longitudinal shear-wall at first floor (center) and steel reinforcement of longitudinal shear-wall jacket (right)

The jacketing technique was used to repair and to strengthen the damaged shear-wall (Figure 3.4.3, right). These retrofitting operations concerned only the underground and the levels where cracks were visible. The reinforcement of the longitudinal shear-wall consists in two tablecloths of 12-mm diameter steel bars constituting a mesh of 20×20 cm, and four to six 14 or 16 mm diameter steel bars,

forming a 20×20 cm cross section column installed at the building end to rigidify the openings (Figure 3.4.3, right). The more seismic loaded lintels were also reinforced by two sets of four diagonal steel bars.

3.4.3 Experimental data

3.4.3.1 Instrumentation

Ambient vibration recordings, were collected at three different times in different ways:

- Initial measurements, part of a global building seismic brittleness survey in the Algiers area, only modal frequencies and damping were evaluated, without taking into account the modal shape. A single 15-min recording (at 200 sps) has been performed at the top of the building, using a 5-s Lennartz LE3D seismometer connected to a CityShark station (Chatelain et al., 2000), equipment considered as pertinent for this type of study (Guillier et al., 2007).
- Post-seismic measurements were focused on evaluation of modal frequencies and damping. The same protocol as for initial recordings has been used.
- Post-retrofitting measurements included not only fundamental frequencies and damping evaluation, but that of modal shape too. A CityShark II-6 recording synchronously six 5-s Lennartz LE3D seismometers was used with 30-min recordings, at 200 sps, with one seismometer per level, installed in the stairwell.

For the three experiments:

- The gain was adjusted to minimize signal clamping for the 3 components (initial and post-seismic measurements) or the 18 components (post-retrofitting measurements).
- The N-S component of the seismometers was oriented along the longitudinal direction and the E-W component in the transversal direction.

3.4.3.2 Data processing

Data have been processed using the Geopsy software (www.geopsy.org), following as much as possible seismic noise processing SESAME recommendations (SESAME, 2004). Modal frequencies were determined with the "Peak Picking" method (Bendat and Piersol, 1993). No sensor nor station correction were used, and the following procedure has been used:

- Removal of the offset by subtracting for each sample the average of the whole recording.

– Window selection using an anti-trigger to eliminate transients (1-s STA, 30-s LTA, STA/LTA ratio thresholds of 0.3 and 2.0).
– A cosine taper (5%) has been applied on both sides of each window of all components.
– Spectral amplitudes are obtained through a FFT applied to each window of the three components. Then, a Konno and Ohmachi smoothing (1998) is applied with a bandwidth of 40.
– Frequency peak pickings, using the automatic recognition Geopsy facility.

For damping analysis, we applied the Randomdec method, which to the ambient vibration recordings which allows to individualize the Impulse Response Function (IRF) from a random solicitation (Dunand, 2005). This method consists in a stack of numerous signal windows with the same initial conditions (in this case, null velocity with positive displacement) and the same time length. Thus, the random part of the signal is canceled because its mathematical hope is null and then we deduce the impulsive response.

For modal shape determination, we evaluate the amplitude of each studied frequency at each level, and the amplitude of each studied frequency, obtained at each storey is normalized to the upper level amplitude (Dunand, 2005).

3.4.3.3 Frequency and damping experimental results

The modal frequencies and damping obtained are shown on Figure 3.4.4 and resumed in Table 3.4.1.

From initial to post-earthquake state. The stronger change occurred in the longitudinal direction, with a 48% decrease of the first modal frequency (3.9 down to 2.06 Hz), while in the transversal direction the first modal frequency downfall was only 14% (3.56 down to 3.06 Hz). From these frequency variations, a strong impact of the earthquake is suspected on the longitudinal direction, whereas in the transversal direction only a marginal impact is expected. Moreover, the longitudinal damping demonstrated a very deep effect of the earthquake, with a 70% crumbling of the damping factor, showing in the post-earthquake state a very small possibility to dissipate energy in the longitudinal direction. Finally, no changes are observed for the transversal damping factor (stable at 2.77%), confirming the very marginal impact of the earthquake in this direction. It should be noticed that the damping is stable, even though the transversal first modal frequency slightly decreased.

From post-earthquake to post-retrofitting state. Again, major changes occurred in the longitudinal direction where the first modal frequency increased from 2.06 to 4.43 Hz, a 115% jump, and a 14% increase from initial to retrofitted state. The longitudinal direction damping increased of 450%, to reach a greater value than in the pre-earthquake state $(+70\%)$. In the transversal direction, the retrofit produced a 0.45 Hz (14%) of the first modal frequency f, a frequency very close to the pre-earthquake frequency, and a 7% damping increase.

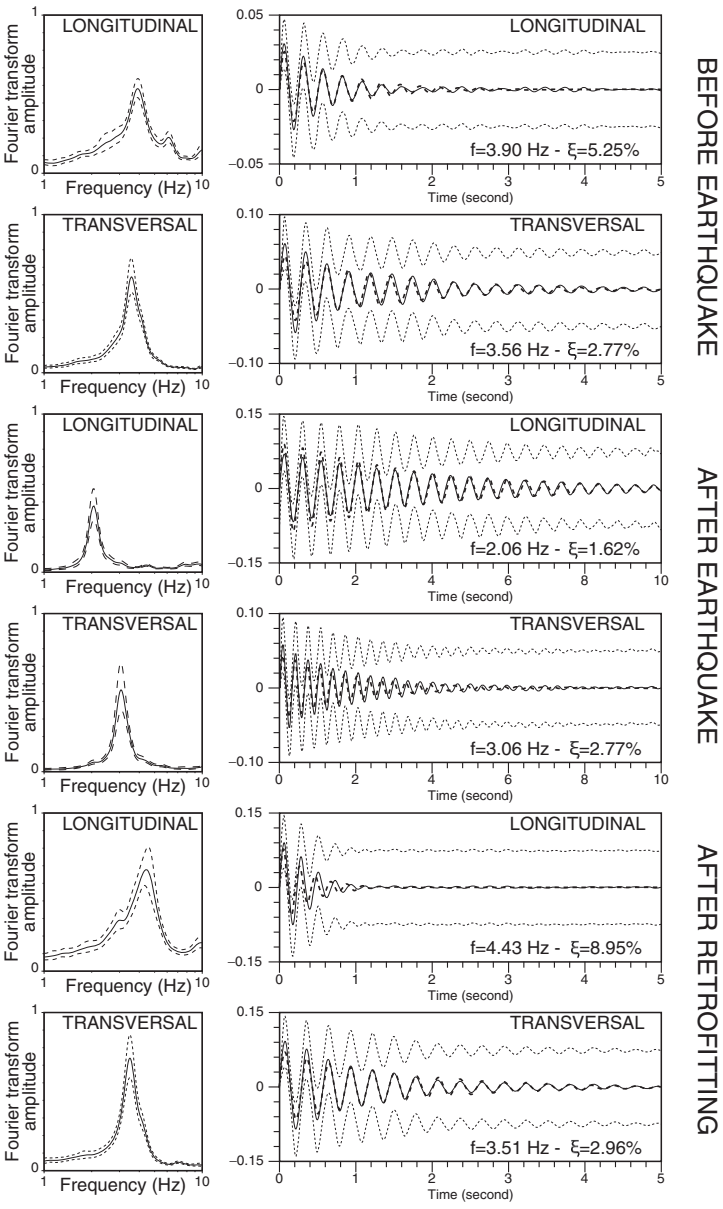

Fig. 3.4.4 Fundamental frequencies and damping curves obtained from in-situ seismic noise measurements on COSIDER building in Bordj-El-Bahri (Algeria) for longitudinal and transversal directions. Measurements have been done before and after the Boumerdes earthquake and the after retrofitting. The left column shows the average (plain line) and the standard deviation (dashed lines) of spectra, derived from selected time windows. The right column displays the averaged damping curve (thin plain line), its standard deviation (thin dashed line) and the modeled theoretical damping curve (thick dashed line) obtained by the Randomdec method (null displacement and positive velocity; Dunand, 2005)

Table 3.4.1 First modal frequencies and damping obtained from seismic noise

	Longitudinal direction		Transversal direction	
	Frequency (Hz)	Damping (%)	Frequency (Hz)	Damping (%)
Before earthquake	3.90	5.25	3.56	2.77
After earthquake	2.06	1.62	3.06	2.77
After retrofitting	4.43	8.95	3.51	2.96

3.4.3.4 Experimental results for modal shape

Modal shapes have been calculated only before the earthquake and after retrofitting (Figure 3.4.5). Due to a lack of time, it has not been possible to perform recordings in the time interval after the earthquake occurrence and before the retrofitting. Normally, at the ground level, the energy released by the building is very low (2–4% of the energy released at the top), representing the soil-structure interaction (SSI). The left curves on Figure 3.4.5 display a very different pattern, as the energy at ground level is very high, letting to suspect a very intense interaction in-between soil and structure (14–22%). Moreover, at the first and second levels, the energy release is lower that it should be assuming a linear decrease of the energy with the height of the building.

The longitudinal first modal shape (Figure 3.4.5, upper right) demonstrates that the retrofitting has strongly stiffened the structure. However, stiffening has been done only at the bottom of the building (breaking point on the curve observed at the first floor). A second breaking point shows up on the longitudinal curve after retrofitting at the third level, which let strongly suspect non-apparent damages at the third and fourth floor (Clinton et al., 2006).

In the transversal direction, the mode shapes (Figure 3.4.5, lower right) are very strongly homogeneous. As the post-earthquake mode shape is not available, it is not possible to ensure that the retrofitting do not improve the stiffness of the structure, but the stability in that direction of both modal frequency and damping sustains this assumption.

3.4.4 Discussion

In its pre-earthquake state, the building displays natural frequencies in the 3–4 Hz frequency range (Table 3.4.1), right in the frequency band with the maximum peak ground acceleration at this distance of the main shock (2–6 Hz, Laouami et al., 2006). The earthquake has mainly impacted the building in the longitudinal direction (N-S oriented), which according to Laouami et al. (2006), is the most solicited direction (0.52 g acceleration), producing a reduction of the stiffness evidenced by a modal frequency decrease (close to 50%). In transversal direction, the lower accel-

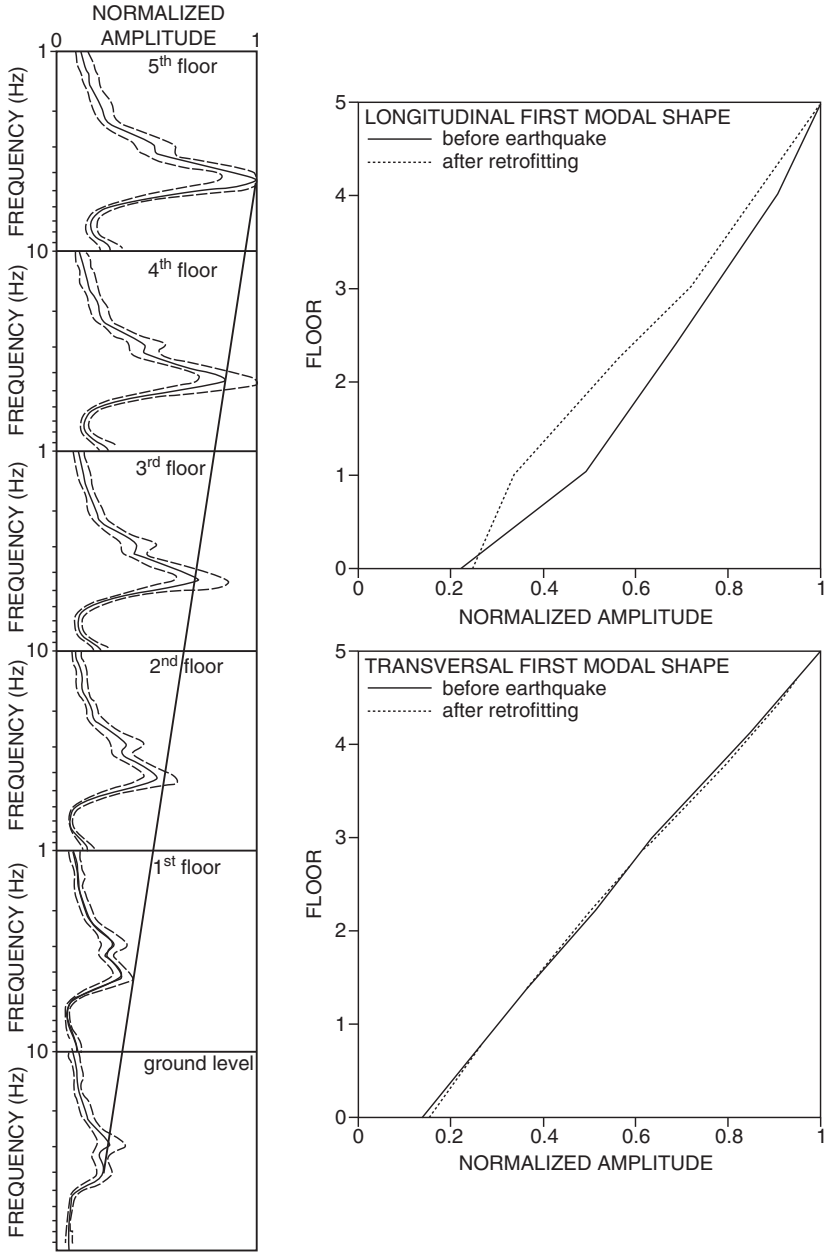

Fig. 3.4.5 Modal shapes coming from seismic noise data on COSIDER building. The left column graphics the average (plain line) and the standard deviation (dashed lines) of spectra (longitudinal direction, after retrofitting) on each level of the building (top: fifth floor, and bottom: ground floor), the black line shows the modal shape in-between the fifth floor and the ground floor. Graphs on right display the calculated modal shapes on longitudinal (top) and transversal (bottom) directions. Graphs (before earthquake and after retrofitting) have been normalized to the fifth floor results

Table 3.4.2 Structural characteristics used for modeling

Concrete density	Elastic concrete modulus	Roof mass	Current story mass	Soil rigidity	Damping
2.5	$2.3\ 10^7$ KPa	$7.3\,\mathrm{KN/m^2}$	$6.75\,\mathrm{KN/m^2}$	$50\,\mathrm{MN/m^3}$	10%

eration (0.46 g, Laouami et al., 2006) induced marginal changes in modal characteristics, without strong impact on the structure stiffness and modal frequency (Table 3.4.1). The building rehabilitations have generated a return of the structure to its initial natural frequency band, demonstrating the legitimacy of the rehabilitation when considering the frequency domain. However, the modal shape, especially in the longitudinal direction, displays an abnormal pattern with a strong stiffening at the bottom of the building, probably generating a strong localization of the shear at the second floor, thus increasing the vulnerability of the building in case of a future strong shake (Michel, 2007). The longitudinal mode shape shows a second abnormality at the fourth floor, certainly reflecting hidden earthquake damages, and has not been corrected during the rehabilitation, adding another vulnerability factor to the building. It is noticeable that the building stiffness is mainly given by single eccentric shear-wall, increasing the impact of torsional modes.

Finally, from modal shapes, it is clear that there is a strong interaction between soil and structure (Dunand et al., 2002). This interaction is probably due to rocking movement that is very difficult to demonstrate, especially with ambient vibrations. A finite element modeling has been performed in order to estimate the different building modes (see Table 3.4.2 for parameter description). Concrete data are coming from in-situ sampling and soil rigidity evaluation comes from local studies. Following the Algerian seismic code (RPA99/2003), the shear-wall damping value has been fixed to 10%. The numerical process has been done using the original pre-earthquake plans, as drawn by the architect, and the final plans made during the retrofitting phase. The pre-earthquake state finite element dynamic calculus gives, a first transversal mode at 3.71 Hz and a second longitudinal mode at 4.13 Hz. Post-retrofitting state calculus give a first transversal mode at 3.76 Hz and a second longitudinal mode at 4.30 Hz. These results are in agreement with the results from in-situ ambient vibration recordings. However, a rocking component had to be integrated in the numerical process to obtain this good fit.

The Algerian seismic code 10% shear-wall damping factor (RPA99/2003) is quite far from the ambient vibration damping factors. The experimental values (3–9%) are very low, probably because of (1) a bad quality of the materials (concrete…) and (2) the soil-structure interaction. It is necessary to recognize also that the damping parameter, especially deduced from seismic noise (i.e. low level excitation), is more difficult to estimate that the modal frequency. Whatever the origin of the difference between theoretical and real damping values, it appears as very important to give more realistic data for numerical modeling.

3.4.5 Conclusion

Ambient vibration techniques are very robust to define building dynamic response characteristics (natural frequency, modal damping and modal shape), allowing evaluating the stiffness changes of a structure, as a decrease of a building natural frequencies is always linked to a loss of stiffness. However, the simple definition of the natural frequencies seems to be insufficient to thoroughly evaluate a building behavior. In the COSIDER case natural frequencies by themselves give good results, accrediting the rehabilitation robustness, while the modal shape analysis raises serious doubts on the rehabilitation reliability. Thus, for more thorough building diagnosis, it is mandatory to study not only natural frequencies, but also modal shapes. If damage in different locations and components leads to different changes in different modes, it is actually quite simply impossible to locate the damages using modal frequency parameters only. Currently, it seems that modal shape is the only effective damage location related parameter, even if its precision is not so good.

As seismic noise recordings in buildings are very easy and not time consuming, it could be useful to undertake systematic recordings in earthquake prone areas (Farsi, 1996; Farsi et al., 2006) to evaluate the behavior of any building as to optimize post-earthquake diagnosis, with much better results than any visual inspection. At the same time, frequent measurements for dynamic modal characteristics of a building will allow to follow its health over time. Of course, as noted by numerous authors, the ambient vibration technique is also very interesting to get input data for finite element methods, as there is generally way too many assumptions for the values of essential parameters.

Finally, ambient vibration recordings might be an alternative method for repairing and retrofitting evaluations, as generally rehabilitations are not very well evaluated and may lead to catastrophic consequences because of poor vulnerability parameter assessment.

Acknowledgement The authors gratefully acknowledge Mr Saichi, Technical Director and Mrs Bensalem, Civil Engineer at COSIDER Enterprise who have provided us drawings of the buildings and facilitated to us the access in the building to get recordings.

References

Bendat J S and Piersol A G (1993) *Engineering Application of Correlation and Spectral Analysis* (2nd edition). Wiley, New York.

Bounif A et al. (2004) The 21 May, 2003, Zemmouri, (Algeria) earthquake Mw = 6.8: Relocation and aftershock sequence analysis. *Geophys. Res. Lett.*, 31, L19606, doi: 10.1029/2004GL020586.

Chatelain J-L et al. (2000) CityShark: A user-friendly instrument dedicated to ambient noise (microtremor) recording for site and building response studies. *Seismol. Res. Lett.*, 71(6), 698–703.

Clinton J F et al. (2006). The observed wander of the natural frequencies in a structure. *Bull. Seismol. Soc. Am*., 96(1), 237–257.

Dunand F (2005) Pertinence du bruit de fond sismique pour la caractérisation dynamique et l'aide au diagnostic sismique. *Thèse de doctorat de l'Université Joseph Fourier*, Grenoble, France.

Dunand F et al. (2002) Damping and frequency from Randomdec method applied to in situ measurements of ambient vibrations. Evidence for effective soil structure interaction. *Proceedings of the 12th European Conference on Earthquake Engineering*, paper no. 869, Londres.

Dunand F et al. (2004) Utilisation du bruit de fond pour l'analyse des dommages des bâtiments de Boumerdes suite au séisme du 21 mai 2003. *Mém. Serv. Géol. Algérie*, 12, 177–191.

Farsi M N (1996) Identification des structures de génie civil à partir de leurs réponses vibratoires. *Thèse de doctorat de l'Université Joseph Fourier*, Grenoble, France.

Farsi M N et al. (2006) Dynamic characteristics of common buildings under strong shaking: A statistical study trough system identification from CSMIP data. *Eur. Earthq. Eng*., XX-3, 22–36.

Guillier B et al. (2005) Smooth bumps in H/V curves over a broad area from single-station ambient noise recordings are meaningful and reveal the importance of Q in array processing: The Boumerdes (Algeria) case. *Geophys. Res. Lett*., 32, L24306, doi: 10.1029/2005GL023726.

Guillier B et al. (2007) Influence of instruments on the H/V spectral ratios of ambient vibrations. *Bull. Earthq. Eng*., Online 3 July 2007, doi: 10.1007/s10518-007-9039-0.

Konno K and Ohmachi T (1998). Ground-motion characteristics estimated from spectral ratio between horizontal and vertical components of microtremor. *Bull. Seismol. Soc. Am*., 88, 228–241.

Laouami N et al. (2004) Analysis of strong ground motions registered by the Algerian accelerograph network during the Boumerdes, Algeria, earthquake. *Mém. Serv. Géol. Algérie*, 12, 93–102.

Laouami N et al. (2006) Evidence for fault-related directionality and localized site effects from strong motion recordings of the 2003 Boumerdes (Algeria) earthquake: Consequences on damage distribution and the Algerian seismic code. *Soil Dyn. Earthq. Eng. J*., 26, 991–1003.

Michel C (2007) Vulnérabilité sismique de l'échelle du bâtiment à celle de la ville. Apport des techniques expérimentales in situ. Application à Grenoble. *Thèse de doctorat de l'Université Joseph Fourier*, Grenoble, France.

RPA99/2003 (2003) Règles Parasismiques Algériennes, *Ministère de l'Habitat et de l'Urbanisme, Document technique réglementaire*, CGS, 89 p.

SESAME (2004) Guidelines for the implementation of the H/V spectral ratio technique on ambient vibrations. Measurements, processing and interpretation. *European Commission – Research General Directorate Project No. EVG1-CT-2000-00026 SESAME*, report D23.12, http://SESAME-FP5.obs.ujf-grenoble.fr.

Wirgin A and Bard P-Y (1996) Effects of building on the duration and amplitude of ground motion in Mexico city. *Bull. Seismol. Soc. Am*., 86, 914–920.

Wong H L and Trifunac M D (1975) Two dimensional antiplane building – soil –building interaction for two or more buildings and for incident plane SH waves. *Bull. Seismol. Soc. Am*., 65, 1863–1885.

Chapter 4
State-of-the-Art – Recent Advances and Applications

John F. Cassidy

Introduction

Earthquake site response studies are rapidly gaining popularity worldwide. There are many reasons for this, including: the development of a new-generation of low-cost, portable recording instruments; improvements in software and analysis methods; and recent results (many of which are documented in this publication) showing that ambient noise measurements can successfully be used for hazard and vulnerability assessments in a wide range of geologic and tectonic environments, and for a variety of purposes.

This chapter summarises some recent applications of earthquake site response studies, from Canada to Croatia to Tunisia, and many points in between. Diverse applications, from evaluating the site response of thick sedimentary basins, to assessing the vulnerability of world heritage sites are presented in this chapter.

While there are still important questions regarding the validity of amplification factors derived from ambient noise measurements, there is a general consensus that the fundamental period of the site response is a robust measurement, and a key parameter that can be compared with the fundamental period of buildings, to assess vulnerability.

In Slovenia, A. Gosar conducted a detailed site response study in the Bovek Basin – a region that suffered extensive damage during moderate (Mw = 5.2–5.6) earthquakes in 1998 and 2004. The observed fundamental frequencies could not be related to the thickness of the Quaternary sediments, but could be explained by the presence of shallow conglomerate or lithified moraine. A key result of this study was that the damage distribution can largely be explained by soil-structure resonance. The hardest hit areas were those where the fundamental frequency of the soil (generally 7–11 Hz) matched that of the buildings (typically 5–13 Hz).

J.F. Cassidy
Natural Resources Canada, Sidney, BC, Canada, and University of Victoria, Victoria, BC, Canada
e-mail: JCassidy@NRCan.gc.ca

M. Mucciarelli et al., (eds.), *Increasing Seismic Safety by Combining Engineering Technologies and Seismological Data,* NATO Science for Peace and Security Series C: Environmental Security,

In Canada, site response studies are underway in a variety of tectonic settings, including the Fraser River Delta of greater Vancouver (comprised of some of the youngest soils on earth) to Ottawa and Montreal, where marine clays overlay some of the oldest rocks on earth. J. Cassidy describes a variety of methods (including using earthquake recordings, ambient noise, geological and geotechnical) that provide valuable new results in the major urban centres in western Canada. The clay layers in eastern Canada show very large amplification factors (on the order of 50–100 times) that may be attributed to very strong impedance contrasts. More detailed work is currently underway to examine this.

Ambient vibration measurements were conducted in Croatia, by M. Herak, in both the free field and in structures. It was demonstrated that the free field measurements provided valuable constraints on geotechnical properties of the soil, especially the fundamental frequency of sedimentary deposits. In buildings, spectral methods were shown to be more robust than time domain analysis, and the ambient noise measurements led to reliable estimates of frequencies and damping of the buildings' vibrational modes.

Ambient noise measurements were used by Saita for vulnerability assessments of important heritage sites around the world, including the leaning tower of Pisa, structures within the old walled city of Manila, and ancient buildings in Istanbul, Turkey. The use of ambient noise is an ideal, non-invasive method to look at the vulnerability of old structures – particularly those that may have already been weakened by historic earthquakes.

Applications of the H/V spectral ratios to cultural heritage and historic masonry by Liberatore, Mucciarelli, Gallipoli, and Masini, highlight methods of using ambient noise data to evaluate the effectiveness of retrofitting and strengthening techniques for historic structures in Italy.

In Tunisia, Bouden-Romdhane, Mechler, Duval, and Anibi conducted a detailed study to evaluate seismic site-response and liquefaction potential in the densely populated Tunis City area. This region is dominated by a thick sedimentary basin of loose Quaternary sediments over Eocene bedrock. Results using the H/V method with ambient noise were compared to those from the Standard Spectral Ratio method and found to be in good agreement – especially the fundamental period. Numerical modelling was used to confirm the natural site frequencies observed in the microtremor data, and to estimate the effects for stronger ground motions.

One of the applications of detailed ambient noise measurements is for seismic microzonation mapping. Rodriguez-Marek and his colleagues demonstrate that soil depth is an important parameter in estimating earthquake site response. As an alternative to existing geologic-based and S-wave velocity-based schemes, they propose a new site classification scheme that includes measures of the dynamic stiffness of the surficial materials and depth to bedrock.

Over the next few years a wealth of new data – geological, geophysical and seismological (both ambient noise data and strong ground motion data), will allow for greatly improved estimates and understanding of local earthquake site effects. This, in turn, will result in improved codes and standards, and reduced losses from future earthquakes around the world.

Chapter 4.1
Microtremor Soil-Structure Resonance Study in the Bovec Basin (NW Slovenia) Related to 1998 and 2004 Damaging Earthquakes

Andrej Gosar

Abstract The Bovec basin, which is filled with glaciofluvial sediments, has recently been struck by two strong earthquakes (1998 and 2004) which caused extensive damage (VII–VIII EMS-98). Strong site effects resulted in large variations in damage to buildings in the area, which could not be explained by the surface variations in Quaternary sediments. The microtremor horizontal-to-vertical-spectral ratio (HVRS) method was therefore applied to a 200 m dense grid of free-field measurements to assess the fundamental frequency of the sediments. Large variations in the sediments frequency (3–22 Hz) were obtained, with most of the observed values in the range 6–12 Hz. The observed frequencies cannot be related to the total thickness of Quaternary sediments (sand, gravel), but can be explained by the presence of conglomerate or lithified moraine at shallow depths. Microtremor measurements performed in 20 two, three and four storey houses (masonry with RC floors), which prevail in the Bovec basin, have shown that the main building frequencies in the area are in the range 7–11 Hz. This indicates that damage to houses in both earthquakes in some parts of the basin was enhanced by site amplification. Areas of possible soil-structure resonance were identified which correspond good to the distribution of damage in both earthquakes.

Keywords Ambient vibrations · Microtremors · Horizontal-to-vertical spectral ratio (HVSR) · Site effects · Soil-structure resonance

4.1.1 Introduction

The Bovec basin is located in the Upper Soča valley in NW Slovenia (Figure 4.1.1), a region undergoing a recent increase in seismic activity. Two strong earthquakes struck the area in 1998 and 2004. Both earthquakes occurred on the NW-SE

A. Gosar
Environmental Agency of Slovenia, Seismology and Geology Office, Dunajska 47, SI-1000 Ljubljana, Slovenia and University of Ljubljana, Faculty of Natural Sciences and Engineering
e-mail: andrej.gosar@gov.si

M. Mucciarelli et al., (eds.), *Increasing Seismic Safety by Combining Engineering Technologies and Seismological Data,* NATO Science for Peace and Security Series C: Environmental Security,

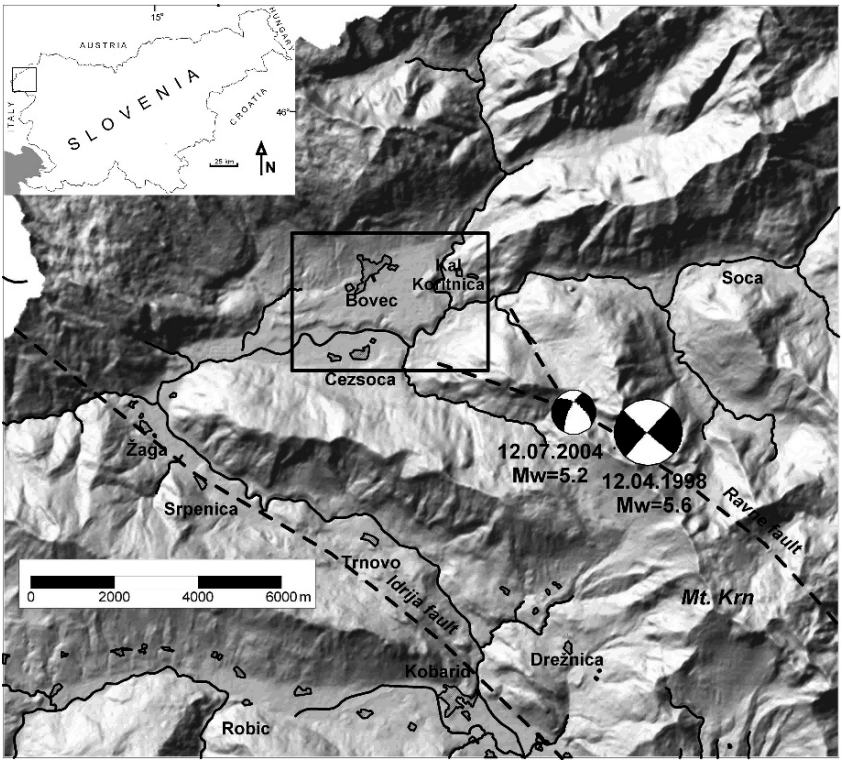

Fig. 4.1.1 Shaded relief map of the Upper Soča valley with the Bovec basin and epicentres of two recent strong earthquakes in Krn mountains. Fault plane solution for 12/04/1998 event is from Zupančič et al. (2001) and for 12/07/2004 event from Kastelic et al. (2006). Boxed area indicates the maps shown in Figures 4.1.2–4.1.4

trending near-vertical Ravne fault in the Krn mountains at 7–9 km depth. The focal mechanisms show almost pure dextral strike-slip. The epicentral distance to the town of Bovec was 6–7 km. The 12 April 1998 earthquake ($M_w = 5.6$) had a maximum intensity of VII–VIII EMS-98 (Zupančič et al., 2001) and the 12 July 2004 ($M_w = 5.2$) earthquake VI–VII EMS-98 (Živčić et al., 2006). Both earthquakes caused extensive damage to buildings in the area, but strong variations in damage were observed within short distances in the whole Bovec basin. They can only be attributed in part to differences in building vulnerability, since the building typology is similar throughout the area. The influence of site effects was therefore very prominent (Gosar, 2007).

The study area is located in a transition zone between E-W striking thrust faults of the Alpine system and NW-SE striking faults of the Dinarides system. In the seismic hazard map for a return period of 475 years, the Bovec basin is located in a region with a design ground acceleration 0.225–0.250 g (Lapajne et al., 2001). Relatively high seismic hazard is caused mainly by high seismic activity in the Friuli area where the $M_w = 6.4$ earthquake occurred in 1976 (Perniola et al., 2004). The

strongest earthquake ever recorded in the Alps-Dinarides junction was the 1511 western Slovenia M = 6.8 earthquake (Fitzko et al., 2005).

Seismic microzonation of the Bovec basin based on surface geological data and data from shallow geotechnical boreholes (Ribičič et al., 2000) has shown that it is not possible to explain with these data most of the observed variations in the distribution of damage. More promising results have been obtained by combined application of microtremors and 1D modelling of ground motion based on the results of shallow geophysical investigations (Gosar et al., 2001).

To study in more detail the site effects, we performed free-field microtremor measurements at 124 points in the Bovec basin. In addition, 20 buildings were surveyed in order to determine their main resonance frequencies. By overlying the frequency map of the sediments with the frequencies of buildings, the areas of potential soil-structure resonance were identified. Results were compared to the distribution of damage caused by the 1998 and 2004 earthquakes and to available geological, geotechnical and geophysical data. The soil-structure resonance was in our opinion the main reason for the relatively high damage to buildings in different parts of the Bovec basin.

4.1.2 Geological setting

The Bovec basin, which is located in the Soča river valley is 6 km long and 2 km wide (Figure 4.1.1). The basement consists of Mesozoic platform carbonates (Figure 4.1.2). They are overlain by a succession of deep-water flysch or by marly limestone (scaglia) with intercalated calcarenites, shales, marls and conglomerates of Cretaceous age (Buser, 1986; Jurkovšek, 1986). Quaternary sediments are represented from bottom to top by partly lithified glaciofluvial sediments, overlain by lacustrine chalk (Kuščer et al., 1974; Bavec et al., 2004). During the Holocene, the chalk was partly eroded and covered by glaciofluvial sand and gravel (Bavec, 2002) which are weakly cemented in some parts into conglomerate and by moraine (till).

A 2D cross-section (Figure 4.1.5) was prepared based on general geological knowledge of the area and sparse geophysical data, because no deep boreholes have been drilled in the basin. The thickness of glaciofluvial sediments was determined by electrical sounding, but it did not distinguish between flysch and lacustrine chalk (Gosar et al., 2001). In the vicinity of the cross-section, according to the geological data, the chalk is found mainly in the Čezsoča area under younger sand and gravel, while under the Bovec terrace only flysch is expected.

4.1.3 Microtremor measurements in the Bovec basin

The microtremor HVSR method is in the last decade widely used for microzonation and site effects studies. Reviews on the method can be found in Bard (1999) or Mucciarelli and Gallipoli (2001). However, the theoretical basis of HVSR method

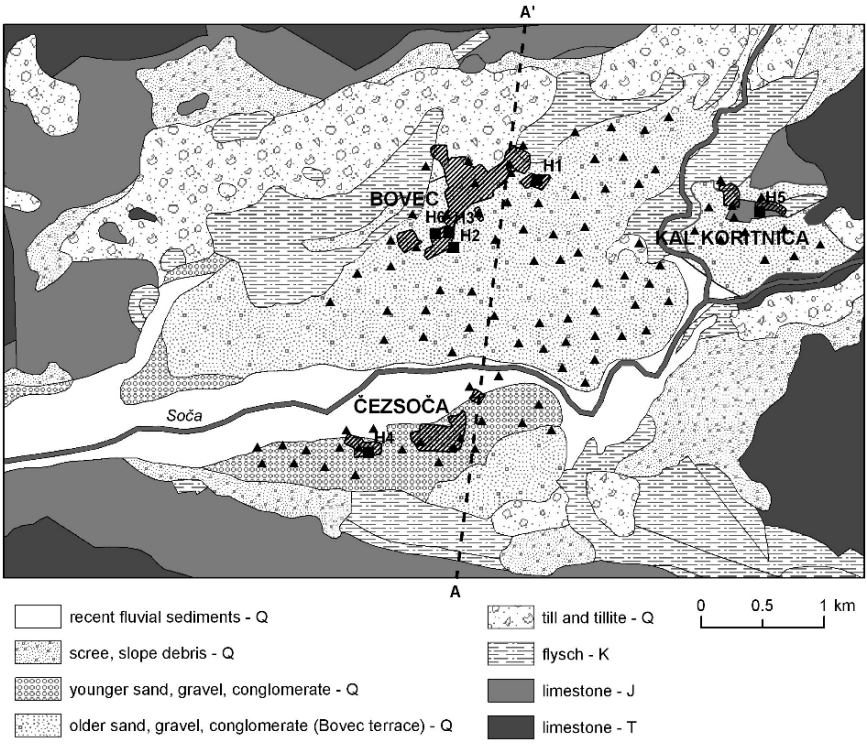

Fig. 4.1.2 Simplified geological map of the Bovec basin after Buser (1986), Jurkovšek (1986) and Bavec et al. (2004). Transfer to GIS was done by Geological Survey of Slovenia. Triangles indicate points of free-field measurements. Squares (H1–H6) indicate measurements in houses shown in Figure 4.1.7. A-A′ indicates cross-section shown in Figure 4.1.5

is still debated and different explanations have been given (Nakamura, 2000; Bard, 1999; Bonnefoy-Claudet et al., 2006). Attempts to provide standards for data acquisition and processing were only recently been made (SESAME, 2004). It is widely accepted today that the frequency of the HVSR peak reflects the fundamental frequency of the sediments. Its amplitude depends mainly on the impedance contrast with the bedrock and cannot be used as a site amplification. However, comparisons with results of standard spectral ratio method has shown that the HVSR peak amplitude underestimates the actual site amplification (Bard, 1999; SESAME, 2004; Gosar, 2008). HVSR also does not provide any estimate of the actual bandwidth over which the ground motion is amplified. The main advantages of HVSR method are therefore simple and low cost measurements and direct estimates of the resonance frequency of sediments without knowing the geological and S-velocity structure of the underground. Any knowledge about the thickness or/and velocity of sediments and the comparison of HVSR results with other methods and with the observed earthquake damage can significantly improve the reliability of the results (Bard, 1999).

The use of microtremors was later extended to identifying the main resonance frequencies of the buildings, their vulnerability and soil-structure resonance (Mucciarelli et al., 2001; Gallipoli et al., 2004a). Damage enhancement and soil-structure resonance was recently studied using microtremors for Umbria-Marche earthquake (Mucciarelli and Monachesi, 1998; Natale and Nunziata, 2004), for Thessaloniki earthquake (Panou et al., 2005) and for Molise earthquake (Gallipoli et al., 2004b).

4.1.3.1 Free-field measurements

In the Bovec basin, a 7 km^2 large area was surveyed in an approximate 200×200 m grid of free-field measurements (Figures 4.1.2–4.1.4). This area covers almost the whole extent of Quaternary sediments in the central part of the basin and includes Bovec, Čezsoča and Kal-Koritnica (Figure 4.1.2), the three settlements which suffered extensive damage in the 1998 and 2004 earthquakes. Altogether, 124 free-field measurements were performed. Their locations were carefully selected to avoid the influence of trees, rivers and strong topographic features. Measurements were performed only on no-wind days, because the noise introduced by strong wind can severely affects the reliability of HVSR analysis (Mucciarelli et al., 2005; SESAME, 2004). The noisiest conditions were in the Čezsoča area, because of retrofitting construction activities following the 2004 earthquake. Coherent noise in the vicinity of the industrial area in the easternmost part of Bovec was found to be less problematic, because its dominant frequency was seldom below 20 Hz.

Measurements were performed by using six portable seismographs Tromino (Micromed) composed of three orthogonal electrodynamic velocity sensors, GPS

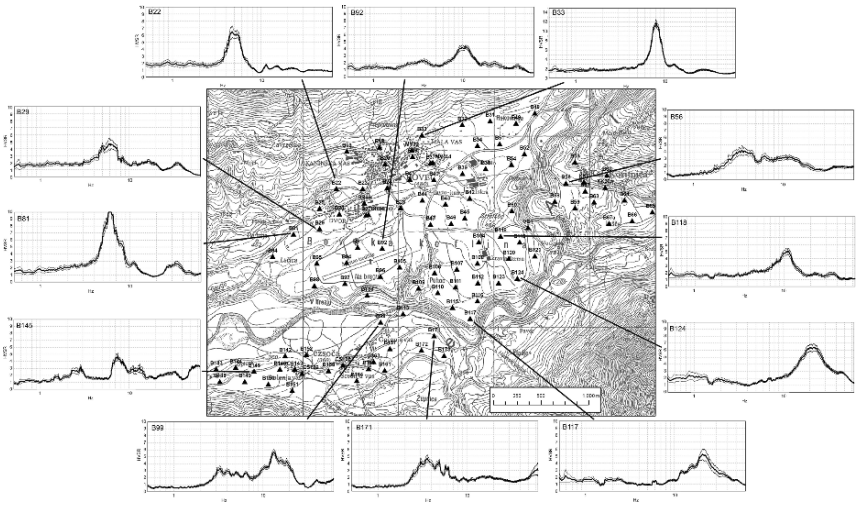

Fig. 4.1.3 Some examples of microtremor HVSR curves from the Bovec basin. Thin lines represent 95% confidence interval

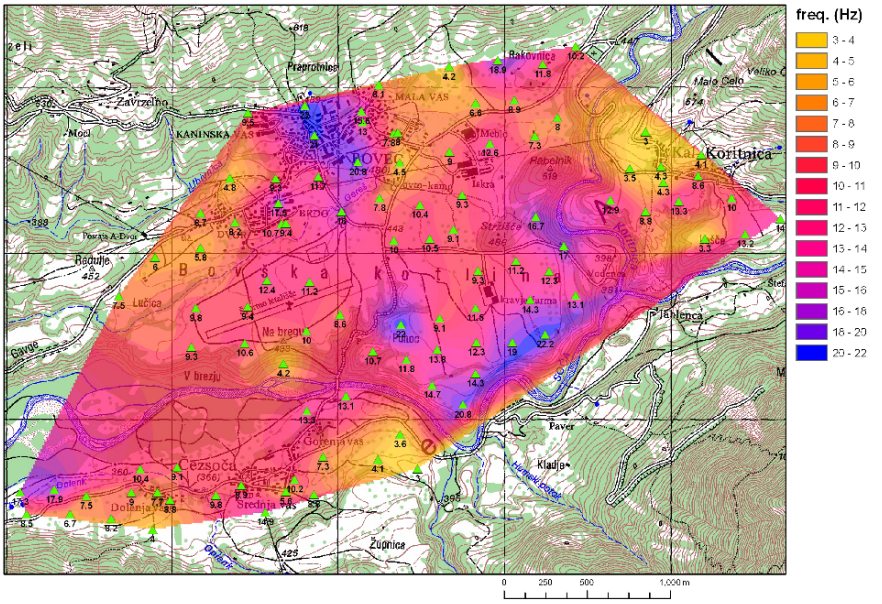

Fig. 4.1.4 Map of the fundamental frequency peak derived from HVSR analysis of microtremor data. Triangles indicate points of free-field measurements; label indicates the frequency of the peak

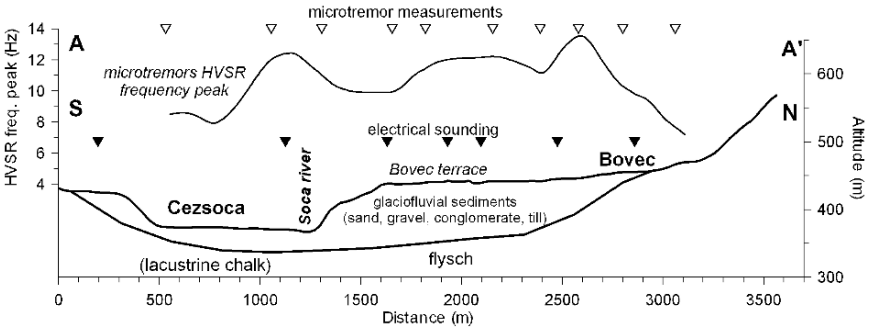

Fig. 4.1.5 Cross-section of Quaternary sediments across the Bovec basin interpreted from vertical electrical soundings and microtremor HVRS curve derived from the map in Figure 4.1.4. The position of the cross-section is shown in Figure 4.1.2

receiver, digitizer and recording unit with flash memory card. All parts are integrated in a common case to avoid electronic and mechanical noise that can be introduced by wiring between equipment parts. Good ground coupling on soft soils was obtained by using long spikes mounted at the base of the seismograph. The recording length was 20 min, which allows spectral analysis down to 0.5 Hz.

HVSR analysis was performed in the following way. Recorded time series were visually inspected to identify possible errorneous measurements and stronger transient noise. Each record was then split into 30 s long non-overlapping windows for

which amplitude spectra in a range 0.5–64 Hz were computed using a triangular window with 5% smoothing and corrected for sensor transfer function. HVSR was computed as the average of both horizontal component spectra divided by the vertical spectrum for each window. From the colour coded plot of HVSR functions for all 40 windows, the windows including strong transient noise were identified in order to be excluded from further computation. The effect of transient seismic noise on HVSR analysis is still debated (Parolai and Galiana-Merino, 2006). In our measurements transient noise occurs mostly in a frequency range lower than is the value of the peak. At the end, the average HVSR function with a 95% confidence interval was computed.

4.1.3.2 Measurements inside buildings

For measurements inside buildings the recording length was 10 min, because frequencies below 1 Hz were not of interest. Two storey residential houses prevail in the area, with some multi-flat three or four-storey buildings. Older houses are mainly of simple and massive stone, while newer houses are mainly masonry with RC floors. Measurements were performed on all floors of the building. Two horizontal components were oriented in the longitudinal and transverse directions of the building. The instrument was placed as close as possible to the mass centre of the building and close to a wall. Outside each building, but far enough to avoid its influence, a free-field measurement was also performed.

Each record was split into 10 s long non-overlapping windows for which amplitude spectra were computed using a triangular window with 3% smoothing. Windows including strong transient noise were excluded from further computation, although some investigations indicate that influence of transients is small (Yuen et al., 2002). Average amplitude spectra for each component were computed from selected windows. For each floor, a separate HVSR of each horizontal component to the vertical component was also computed, as proposed by Gallipoli et al. (2004a). Directional analysis was performed in 10° angular steps for easier recognition of the two main resonance frequencies in longitudinal and transverse directions. In addition, ratios of amplitude spectra for records taken on higher floors to the spectra of a reference record taken at ground floor were computed.

4.1.4 Results and interpretation

4.1.4.1 The map of fundamental frequency of sediments

HVSR analyses of 124 free-field microtremor measurements in the Bovec basin showed that most of them (80%) fulfil the criteria defined by European SESAME project for reliable measurements (SESAME, 2004). Three of these criteria for a

reliable HVSR curve are based on the relation of a peak frequency to the window length, number of significant cycles and standard deviation of a peak amplitude. Six criteria for a clear peak are based on the relation of the peak amplitude to the level of the HVSR curve elsewhere, and standard deviations of the peak frequency and of its amplitude (the amplitude should decrease rapidly on each side). If all three criteria for reliable curve and at least five criteria for a clear peak are fulfilled, the frequency of the peak is considered to be the fundamental frequency of sediments down to the first strong contrast in shear-wave velocity. In the Bovec basin the main reasons for 20% of measurements which do not fulfill these criteria were: (a) artificial noise, (b) two or more peaks in a spectrum or (c) too small amplitude of the peak. In cases in which the small amplitude of the HVSR peak caused failure to the criteria for a clear peak, we compared the results with adjacent measurements. If the frequencies of questionable peaks were comparable with the frequencies obtained at adjacent points, we kept them in the database. Finally, the frequencies of peaks determined at 104 points were used for contouring a map of the fundamental frequency of sediments (Figure 4.1.4).

The frequencies of the observed HVSR peaks are distributed in the wide range of 3–22 Hz (Figure 4.1.6), but most of them are in the range 7–11 Hz. Since two storey residential houses prevail in the area, their vulnerability can be expected in the frequency range 6–12 Hz. This range is shown on the map with red colours (Figure 4.1.4). The danger of soil-structure resonance in the Bovec basin therefore seems to be considerable. This is discussed further in the section describing the results of measurements in buildings.

The amplitudes of the HVSR peaks are distributed in a range of 2–12, but most of them (80%) are in the range 3–6. No correlation between the frequency of the peak and its amplitude was established (Figure 4.1.6).

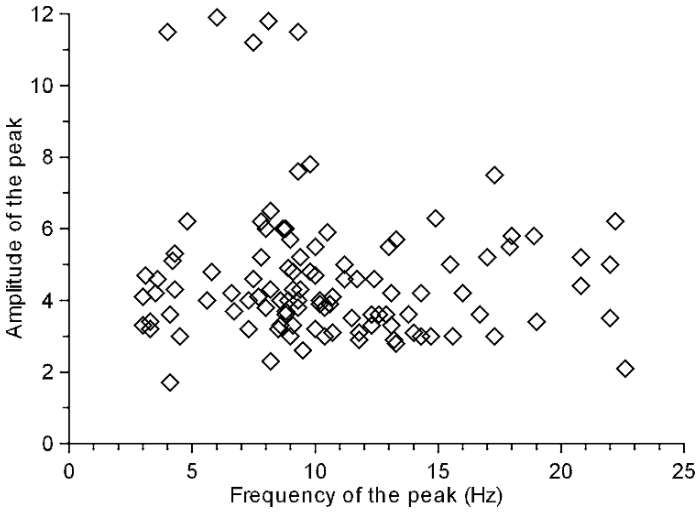

Fig. 4.1.6 Amplitude vs. frequency graph of HVSR peaks

Next section describes some examples of HVSR analyses shown in Figure 4.1.3 and the main features of the map of HVSR fundamental frequencies of the Bovec basin (Figure 4.1.4).

- Frequencies in the range 7–11 Hz prevail (B33, B92, B118) in the largest part of the map (Bovec terrace, Čezsoča, Kal-Koritnica). Although some measurements were disturbed by monochromatic noise (B145), it was possible to determine the fundamental frequency in the majority of spectral ratios.
- Lower frequencies (3–6 Hz) were obtained at the margins of the basin (B22, B171, B56), where flysch and deep sea clastic rocks outcrop.
- Very high frequencies (18–22 Hz) were obtained in two areas. In the central part of Bovec they are related to a very thin layer of till or sand-gravel overlying flysch bedrock. At the SE margin of the map (B117, B124), they are related to very shallow conglomerate visible in a nearby cliff.

Comparison of several adjacent measurements has shown that the amplitudes of the HVSR peaks are also highly variable within short distances. For example, points B29 and B81, which were measured only 200 m away, show almost the same fundamental frequency (6 and 6.2 Hz), but have considerably different peak amplitudes (4.5 and 11).

Comparison of the HVSR iso-frequency map (Figure 4.1.4) with the geological map (Figure 4.1.2) and the cross-section (Figure 4.1.5) showed that large variations in fundamental frequencies cannot be explained by known variations in surface geology or related to the total thickness of the Quaternary sediments which is up to 100 m. They must be related to shallow geological structures. If a mid S-wave velocity for glaciofluvial sediments of 350 m/s is taken for sediments, the rough estimate of the corresponding thickness of assumed single layer for observed frequencies (3–22 Hz) would give a range of 4–30 m.

The curve of fundamental frequencies derived from the map (Figure 4.1.4) shown at the top of the cross-section A-A′ (Figure 4.1.5) also shows great variability. Although the structure of Quaternary deposits in the basin is poorly known we try to interpret the observed variations of fundamental frequencies in terms of expected lithological units:

- Frequencies of 8–10 Hz in the southern part (Čezsoča) correspond to a 15–25 m thick layer of younger sand and gravel overlaying lacustrine chalk and flysch.
- The 12.5 Hz peak close to the Soča river is most probably related to shallow lacustrine chalk.
- Frequencies of 10–14 Hz observed in the northern part of the profile are probably related to the layer of conglomerate inside the Bovec terrace. The extent of this weakly cemented layer was not known before, because it was not detected by electrical sounding due to the small resistivity contrast.
- The largest variations in frequency (6–14 Hz) on this profile were observed in the Bovec area. The town is located at the margin of the Bovec terrace, partly on it (sand, gravel), partly on glacial till and tillite overlying flysch rocks. In any case, the thickness of Quaternary sediments is in general small, but due to fluvial relief the variations can be considerable.

4.1.4.2 Main building frequencies and soil-structure resonance

Measurements performed in buildings confirmed that microtremors are an effective tool to identify the main building frequencies. For all measured houses (Figure 4.1.7), it was possible to identify the longitudinal and transverse frequencies.

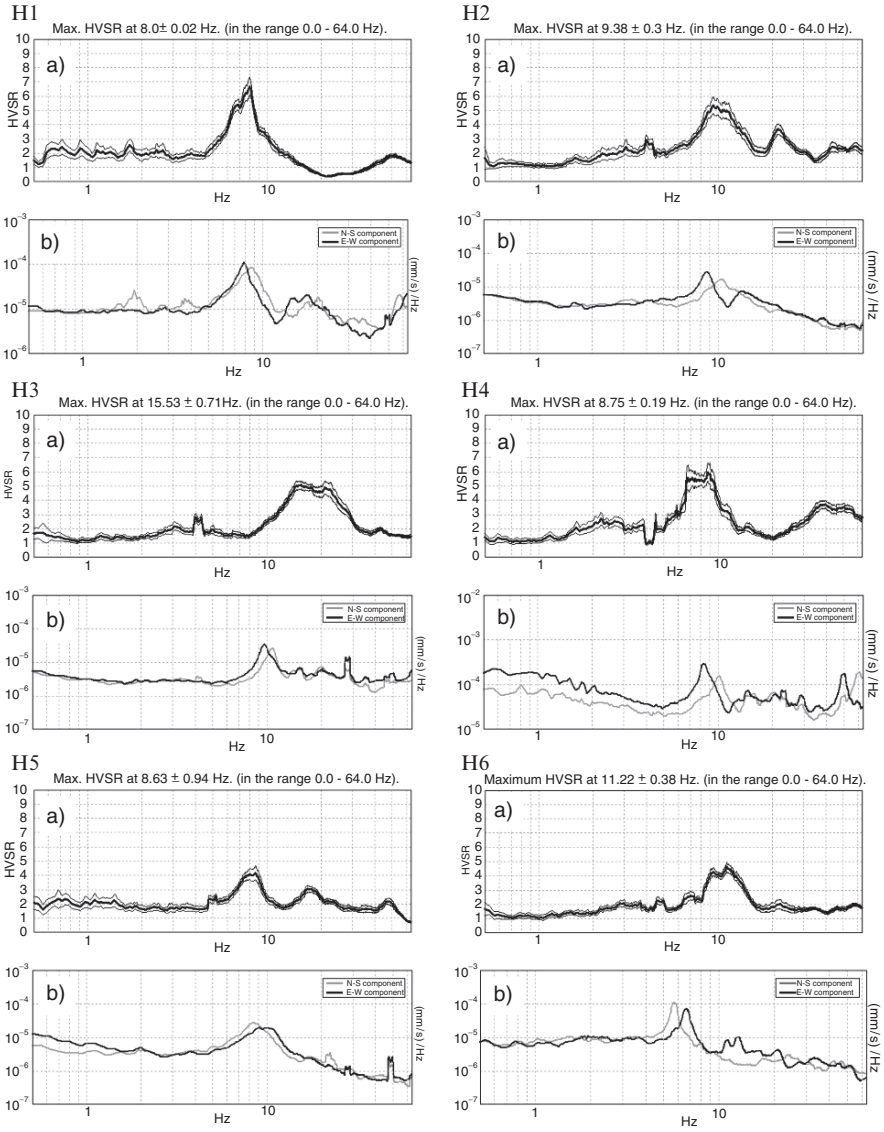

Fig. 4.1.7 Results of microtremor measurements in six houses (H1–H6) in the Bovec basin. Their locations are shown in Figure 4.1.2. For each building: (a) free-field HVSR, (b) amplitude spectra of horizontal components for microtremor measurements at highest floor

We have found a good correspondence in the frequency of the peaks from measurements taken on different floors in the same building, showing an increasing amplitude response at higher levels. Since it is not the purpose of this paper to discuss the dynamic behaviour of buildings, but to identify possible soil-structure resonance, only the results from the highest floor of each building are presented below.

Two-storey residential houses (masonry with RC floors) prevail in the Bovec basin, but there are also some higher multi-flat buildings. Examples of five two-storey and one three-storey buildings from different parts of the basin are discussed in this section. The locations of houses are shown in Figure 4.1.2. Two graphs are shown for each building (Figure 4.1.7): (a) the result of HVSR analysis for free-field measurement performed in the vicinity of the building, (b) amplitude spectra of both horizontal components for measurements taken on the highest floor of the building. In buildings "N-S" component corresponds to its longitudinal and "E-W" component to its transverse direction. For each house, damage caused by the 1998 and 2004 earthquakes, assessed according to the classification of damage for masonry buildings in European Macroseismic Scale (ESM-98), is also given. The main results of microtremor measurements inside building are summarised in Table 4.1.1, together with nearby free-field data and an indication whether soil-structure resonance is probable.

House H1 is located in Bovec-Mala vas district on the Bovec terrace, where a clear peak at frequency 8 Hz with amplitude of 6.5 was obtained in free-field measurements. The old house at this location was very heavily damaged in the 1998 earthquake. It was therefore demolished and a new house of similar size was built at the same location. In the 2004 earthquake, the new house suffered slight to moderate damage. From microtremor measurements in the house, it was possible to identify the main building longitudinal (8.7 Hz) and transverse (7.6 Hz) frequencies. Soil-structure resonance is therefore a probable reason for the very high damage to the previous house in the 1998 earthquake, as well as for the relatively high damage in 2004 to the new house constructed according to the latest building codes. In general, the damage caused by 1998 earthquake was considerably higher in Mala vas (VII EMS-98) than in other districts of Bovec (VI EMS-98) (Gosar et al., 2001).

House H2 is located in Bovec-Brdo district on the Bovec terrace, where a wide peak centred around 9.3 Hz with amplitude of 5.0 was obtained in free-field measurements. The main building longitudinal (8.5 Hz) and transverse (9.7 Hz)

Table 4.1.1 Main results of microtremor measurements inside buildings

Building	Number of storeys	Longitudinal freq. (Hz)	Transverse freq. (Hz)	Free-field freq. (Hz)	Soil-structure resonance
H1	2	8.7	7.6	8.0	Yes
H2	2	8.5	9.7	9.3	Yes
H3	2	10.7	9.6	17.5	No
H4	2	10.2	8.5	8.0	Yes
H5	2	8.3	8.8	8.6	Yes
H6	3	5.8	6.6	11.2	No

frequencies were identified. Soil-structure resonance is therefore very likely. The house was moderately damaged in the 1998 and 2004 earthquakes.

House H3 is also located in Bovec-Brdo on the Bovec terrace, 100 m to the north of house H2. A wide peak centred around 17.5 Hz with HVSR amplitude of 5.0 was obtained in free-field measurements. The main building longitudinal (10.7 Hz) and transverse (9.6 Hz) frequency were identified. Since both frequencies of the building are considerably lower than the frequency of sediments, soil-structure resonance is not expected. In fact, the house was only slightly damaged in both earthquakes.

House H4 is located in Čezsoča on younger Quaternary gravel, where a wide peak (6.5–10 Hz) centred around 8 Hz was obtained in free-field, which were partly disturbed by monochromatic noise (4–4.5 Hz). The main building longitudinal (10.2 Hz) and transverse (8.5 Hz) frequencies were identified. Soil-structure resonance is therefore very likely. The house was moderately damaged in the 1998 earthquake, later retrofitted, and then substantially damaged in the 2004 earthquake. In general, the damage in Čezsoča was slightly higher in the 2004 event than in 1988 event. The reason for this can be sought in slightly different mechanism of the Ravne fault rupture from the 2004 event close to the structural barrier of the Bovec basin (Kastelic et al., 2006), but is not yet adequately explained.

House H5 is located in Kal-Koritnica on the Bovec terrace, where a wide peak centred around 8.6 Hz was obtained in free-field. The main longitudinal (8.3 Hz) and transverse (8.8 Hz) frequencies of the building were identified. The house was moderately damaged in the 1998 earthquake, later retrofitted, and again moderately damaged in the 2004 earthquake. Soil-structure resonance is therefore very likely, especially because the damage to other buildings in Kal-Koritnica was considerably smaller during the 2004 event than in 1998.

Three storey multi-flat house H6 is located in Bovec-Brdo. A wide peak centred around 11.2 Hz with amplitude of 4.5 was obtained in the free-field and the main building longitudinal (5.8 Hz) and transverse (6.6 Hz) frequency were identified. Since both frequencies of the building are considerably lower than the frequency of sediments, soil-structure resonance would not be expected. In fact, the house was only slightly damaged in both earthquakes.

The graph of the building main frequency vs. height (no. of storeys) for all 20 examined buildings is shown in Figure 4.1.8. The main building frequency for two-storey houses is considerably higher (7–13 Hz) than for three and four-storey houses (5–9 Hz). The difference between the later two categories is not significant. The difference in the building main frequency in longitudinal and transverse direction is in the range of 0.5–2 Hz.

4.1.5 Conclusions

Microtremor measurements performed in the Bovec basin showed considerable variations in the fundamental frequency (3–22 Hz) of sediments within short distances. Because most observed frequencies were in the range 7–11 Hz, they overlap with

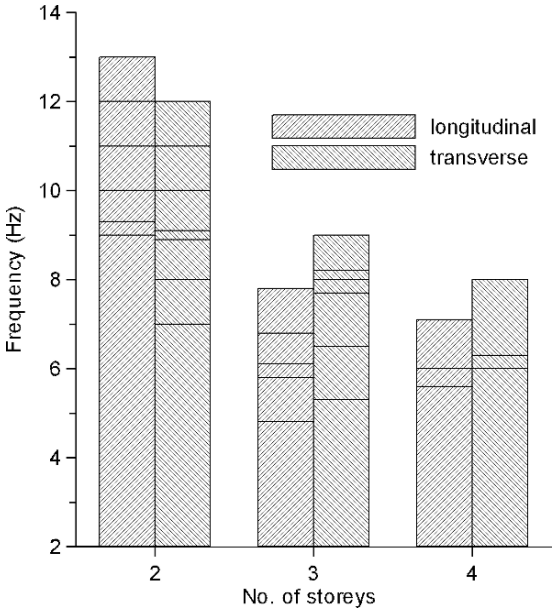

Fig. 4.1.8 Plot of the building main frequency vs. height (no. of storeys) for 20 examined buildings: 11 two-storey, 6 three-storey and 3 four-storey buildings

the range of building frequencies (5–13 Hz). This indicated that the danger of soil-structure resonance is considerable in the area. Observed frequencies cannot be related to the total thickness of Quaternary sediments, but can be explained by shallow layers of lithified sand-gravel (conglomerate) or glacial moraine (tillite). Additional site effect studies of the Bovec basin which enclosed also spectral ratios from earthquake data (H/V and SSR) also shows broad frequency range of ground motion amplification related to the complex geological structure (Gosar, 2008).

Microtremors were used also to identify the main frequencies of the buildings in the area and to establish possible soil-structure resonance. The results are promising and indicated that the major variations in the distribution of damage in the Bovec basin can be explained by soil-structure resonance. Measurements in two storey houses which prevail and in some higher buildings showed that the main building frequencies in the area are in the range of 7–11 Hz. Areas of possible soil-structure resonance were therefore identified in the settlements of Bovec-Brdo, Bovec-Mala vas, Čezsoča and in Kal-Koritnica. In the whole surveyed area of the Bovec basin, the area with fundamental frequencies of sediments in the range 6–12 Hz, in which soil-structure resonance is possible, occupies more than 60%. Nevertheless, before more general conclusions can be made, microtremor measurements in a larger number of houses should be performed, including analyses of their dynamic behaviour and of available information on the construction of individual buildings.

Microtremor method has proved to be an effective tool for assessment of site effects in the case of complex geological structures commonly encountered in young

Alpine basins filled with glacial and fluvial sediments that are partly cemented. Cemented layers (conglomerate and tillite) can considerably change the fundamental frequency. For several reasons: the irregular shape of layers, weak contrast in electrical resistivity, layers are frequently thin, it is very difficult to detect these layers by geophysical methods. The cost of geophysical investigations usually also precludes performing measurements in a grid dense enough to reveal the detailed stratigraphy. In such geological conditions, the microtremor method is very useful for quantitative seismic microzonation and assessment of possible soil-structure resonance.

Acknowledgments The study was realised with the support of NATO SfP project 980857: Assessment of seismic site amplification and seismic building vulnerability in FYR of Macedonia, Croatia and Slovenia and Interreg IIIB Alpine Space project SISMOVALP: Seismic hazard and Alpine valley response analysis. The help of Miha Lubi in the realization of the study is gratefully acknowledged.

References

Bard PY (1999) Microtremor measurements: a tool for site effect estimation? In: Irikura K, Kudo K, Okada H, Sasatami T (Eds.), The Effects of Surface Geology on Seismic Motion, pp. 1251–1279, Rotterdam: Balkema

Bavec M (2002) New temporal, and genetic determination of some Late Quaternary sediments in Bovec basin and its surroundings (NW Slovenia). Geologija 45:291–298

Bavec M, Tulaczyk SM, Mahan SM, Stock GM (2004) Late Quaternary glaciation of the Upper Soča River Region (Southern Julian Alps, NW Slovenia). Sediment Geol 165:265–283

Bonnefoy-Claudet S, Cornou C, Bard PY, Cotton F, Moczo P, Kristek J, Fäh D (2006) H/V ratio: a tool for site effects evaluation. Results from 1-D noise simulations. Geophys J Int 167:827–837

Buser S (1986) Basic geological map of Yugoslavia 1:100.000 – sheet Tolmin and Videm. Geological Survey of Slovenia

Fitzko F, Suhadolc P, Aoudia A, Panza GF (2005) Constraints on the location and mechanism of the 1511 Western Slovenia earthquake from active tectonics and modeling of macroseismic data. Tectonophysics 404:77–90

Gallipoli MR, Mucciarelli M, Castro RR, Mochavesi G, Contri P (2004a) Structure, soil-structure response and effects of damage based on observations of horizontal-to-vertical spectral ratios of microtremors. Soil Dyn Earth Eng 24:487–495

Gallipoli MR, Mucciarelli M, Eeri M, Gallicchio S, Tropeano M, Lizza C (2004b) Horizontal to vertical spectral ratio (HVSR) measurements in the area damaged by the 2002 Molise, Italy, earthquake. Earthq Spect 20/1:81–93

Gosar A (2007) Microtremor HVSR study for assessing site effects in the Bovec basin (NW Slovenia) related to 1998 Mw5.6 and 2004 Mw5.2 earthquakes. Eng Geol 91:178–193

Gosar A (2008) Site effects study in shallow glaciofluvial basin using H/V spectral ratios from ambient noise and earthquake data; the case of Bovec basin (NW Slovenia). J Earth Eng 12:17–35

Gosar A, Stopar R, Car M, Mucciarelli M (2001) The earthquake on 12 April, 1998 in Krn mountains (Slovenia): ground motion amplification study using microtremors and modelling based on geophysical data. J Appl Geophys 47/2:153–167

Jurkovšek B (1986) Basic geological map of Yugoslavia 1:100.000 – sheet Beljak and Ponteba. Geological Survey of Slovenia

Kastelic V, Živčić M, Pahor J, Gosar A (2006) Seismotectonic characteristics of the 2004 earthquake in Krn mountains. Potresi v letu 2004 78–87, EARS

Kuščer D, Grad K, Nosan A, Ogorelec B (1974) Geology of the Soča valley between Bovec and Kobarid. Geologija 17:425–476

Lapajne J, Šket Motnikar B, Zupančič P (2001) Design ground acceleration map of Slovenia. Potresi v letu 1999 40–49, EARS

Mucciarelli M, Gallipoli MR (2001) A critical review of 10 years of microtremor HVSR technique. Boll Geof Teor Appl 42:255–266

Mucciarelli M, Monachesi G (1998) A quick survey of local amplifications and their correlation with damage observed during the Umbro-Marchesan (Italy) earthquake of September 26, 1997. J Earth Eng 2:325–337

Mucciarelli M, Contri P, Mochavesi G, Calvano G, Gallipoli MR (2001) An empirical method to assess the seismic vulnerability of existing buildings using the HVSR technique. Pure Appl Geophys 158:2635–2647

Mucciarelli M, Gallipoli MR, Di Giacomo D, Di Nota F, Nino E (2005) The influence of wind on measurements of seismic noise. Geophys J Int 161:303–308

Nakamura Y (2000) Clear identification of fundamental idea of Nakamura's technique and its applications. 12WCEE, pp. 1–8

Natale M, Nunziata C (2004) Spectral amplification effects at Selllano, Central Italy, for the 1997–98 Umbria seismic sequence. Nat Hazards 33:365–378

Panou AA, Theodulidis N, Hatzidimitriou P, Stylianidis K, Papazachos CB (2005) Ambient noise horizontal-to-vertical spectral ratio for assessing site effects estimation and correlation with seismic damage distribution in urban environment: the case of city of Thessaloniki (Northern Greece). Soil Dyn Earth Eng 25:261–274

Parolai S, Galiana-Merino JJ (2006) Effects of transient seismic noise on estimates of H/V spectral ratios. Bull Seism Soc Am 96/1:228–236

Perniola B, Bressan G, Pondrelli S (2004) Changes in failure stress and stress transfer during the 1976–77 Friuli earthquake sequence. Geophys J Int 156:297–306

Ribičič M, Vidrih R, Godec M (2000) Seismogeological and geotechnical conditions of buildings in Upper Soča territory, Slovenia. Geologija 43:115–143

SESAME (2004) Guidelines for the implementation of the H/V spectral ratio technique on ambient vibrations: measurements, processing and interpretation. http://sesame-fp5.obs.ujf-grenoble.fr/Delivrables/Del-D23-HV_User_Guidelines.pdf. Accessed 14 Feb 2008

Yuen KV, Beck JL, Katafygiotis LS (2002) Probabilistic approach for modal identification using non-stationary noisy response measurements only. Earth Eng Struct Dyn 31/4:1007–1023

Živčić M, Krn-2004 team (2006) The Krn mountains (Slovenia) M_W 5.2 earthquake: data acquisition and preliminary results. Geoph Res Abstr 8:06439

Zupančič P, Cecić I, Gosar A, Placer L, Poljak M, Živčić M (2001) The earthquake of 12 April 1998 in the Krn mountains (Upper Soča valley, Slovenia) and its seismotectonic characteristics. Geologija 44:169–192

Chapter 4.2
Recent Earthquake Site Response Studies in Canada

John F. Cassidy and Sheri Molnar

Abstract Earthquake site response studies are becoming increasingly common across Canada – particularly in large, urban centres. This is due, in part, to new instrumentation that can be easily used to collect recordings of ground shaking, and new geotechnical methods to map out shear-wave velocity and subsurface geometry. Since 2003, nearly 1,000 microtremor recordings have been collected in southwestern British Columbia. Coverage includes numerous sites on Vancouver Island, greater Victoria, greater Vancouver, and a 10-km stretch of the Sea-to-Sky Highway that links Vancouver to Whistler (site of the 2010 Winter Olympic Games). Single-instrument microtremor recordings were collected to evaluate earthquake site response using the horizontal-to-vertical (H/V) spectral ratio method. These results were used for: (1) comparison at strong-motion instrument sites with earthquake spectral ratios, (2) comparison at sites with macroseismic (earthquake intensity and damage) information, (3) comparison at sites with measured shear-wave velocities (12 seismic cone penetration tests and four spectral analysis of surface wave technique), (4) hazard mapping projects, and (5) investigating soil-structure interaction. Results obtained from these various methods in Victoria are in good agreement. In eastern Canada, where most earthquake damage has been associated with the soft Leda clay layer that overlies the hard Precambrian rocks of the Canadian Shield, studies have focussed on the urban centres of Montreal, Ottawa, and Quebec City. Here, NEHRP (National Earthquake Hazards Reduction Program) classification maps are being produced, and significant resonant amplification factors are observed (greater than 50 in some cases). This paper documents earthquake site response studies currently underway in urban centres of Canada, and some of the applications of those studies.

Keywords Earthquake site response · Microtremor method · Earthquake risk · Canada · Ambient noise

J.F. Cassidy (✉) and S. Molnar
Natural Resources Canada, Sidney, BC, Canada, and University of Victoria, Victoria, BC, Canada
e-mail: JCassidy@NRCan.gc.ca

M. Mucciarelli et al., (eds.), *Increasing Seismic Safety by Combining Engineering Technologies and Seismological Data,* NATO Science for Peace and Security Series C: Environmental Security,

4.2.1 Introduction

Earthquake site response studies are becoming increasingly common across Canada. There are several reasons for this, including:

1. Recent large urban earthquakes around the world have clearly shown a significant variation in ground shaking (amplitude, duration, and frequency) across urban centres. Examples include, 1995 Kobe (Kawase, 1996); 1996 Northridge (Hartzell et al., 1996), and 2001 Nisqually (Booth et al., 2004).
2. Some of Canada's largest cities and critical infrastructure are built on soft soils (e.g., clay layers, or thick delta sediments).
3. The seismic provisions in the 2005 National Building Code of Canada utilize an adaptation of the site factors in NEHRP 2001 (Building Seismic Safety Council, 2001).

Given that large $(M > 7)$ earthquakes occur in many areas of Canada, and some of the world's largest earthquakes have occurred along Canada's west coast (Figure 4.2.1), understanding local site conditions, soil profiles, and the variation in ground shaking is becoming more important. More than 75% of Canada's population lives in urban areas, with most of the large urban centres located in areas of high seismic hazard (Figure 4.2.2). In terms of risk (hazard multiplied by population), Vancouver, Montreal, Ottawa, Victoria, and Quebec City top the list. It is in these cities (and along the 2010 Winter Olympic corridor between Vancouver and

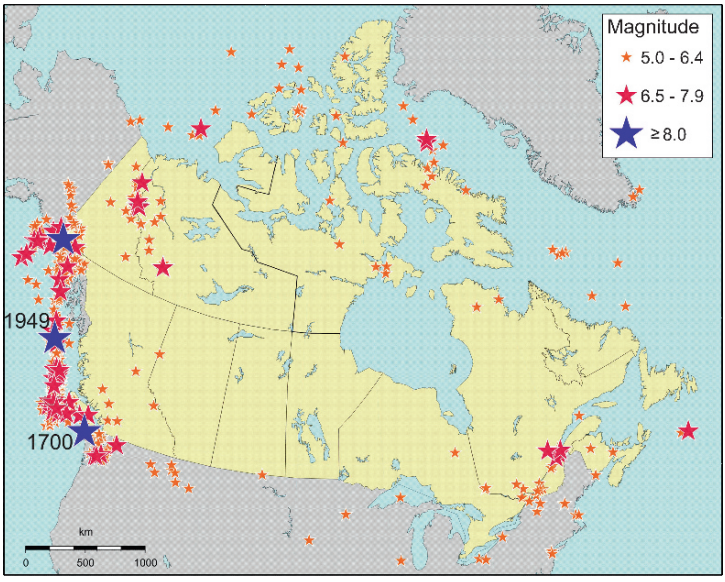

Fig. 4.2.1 Location of the largest earthquakes recorded in, and adjacent to, Canada. With few exceptions (e.g., the M = 9.0 Cascadia earthquake of 1700) these earthquakes have occurred during the past 150 years

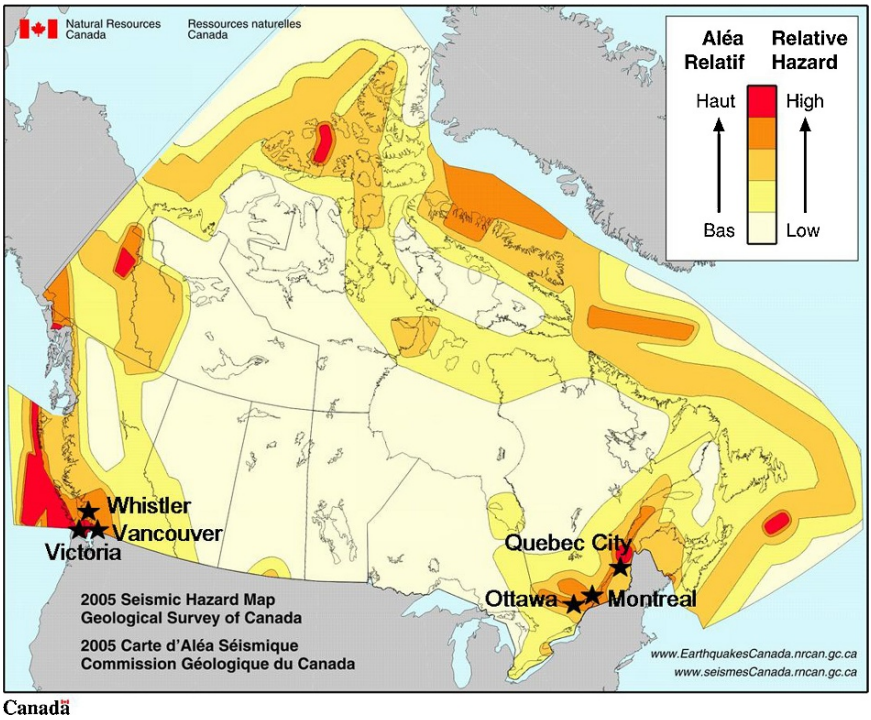

Fig. 4.2.2 Seismic hazard map (peak acceleration) of Canada. Study areas discussed in this manuscript are shown by stars

Whistler, BC) that much of the site response research effort in Canada is currently being focused.

Other recent developments that are providing new opportunities for site response studies are:

1. The deployment of strong motion "Internet Accelerometers" (IA's) in urban centres of Canada (Cassidy et al., 2007)
2. The development of portable, lightweight, and easy-to-use instruments (there are several on the market – complete with analyses packages) for quickly recording and analyzing seismic ambient noise

Some examples of the applications of site response studies include: development of detailed seismic hazard maps; integration with building response information to identify structures at risk; risk and loss estimations (e.g., Ventura et al., 2005; Onur et al., 2005).

In this article, we summarise a number of site response studies recently conducted or underway in Canada. These studies incorporate not only seismic data, but also data and results from geophysical and geological studies (including near-surface S-wave velocity from seismic reflection and refraction, boreholes, cone penetrometers and surface wave methods).

4.2.2 Recent advances – Data, methods, and comparisons of techniques

Recent advances in instrumentation and methodologies are providing new opportunities for earthquake site response studies in Canada. Here we briefly describe some of the new datasets available, and outline some of the methodologies being used. More details, including (where available) a comparison of site-response results using different methodologies, are given in the following sections of this manuscript.

Some methods used to help evaluate earthquake site response in Canada include measuring ground shaking (recordings of earthquakes and ambient noise measurements), earthquake felt intensity reports, detailed geological information, mapping shear-wave velocity using seismic reflection and refraction, seismic cone penetrometer (SCPT) and surface wave methods.

4.2.2.1 Recording of ground shaking

The development of portable, easy-to-use, instruments (often complete with analysis software) for ambient noise measurements has greatly facilitated site response studies. A number of studies are described in this article that make use of noise measurements in Victoria, Vancouver, Ottawa, Montreal, and Quebec City.

The deployment of the new "Internet Accelerometer" (IA) strong motion network in Canada is also advancing our understanding of ground shaking variations. Beginning in 2001, the Geological Survey of Canada's (GSC) strong motion network has been modernized as described by Rosenberger et al. (2007). As of 2007, the GSC operates more than 100 IA's in Canada, with nearly half deployed across greater Vancouver (Figure 4.2.3). For details on this network, and available data, see Cassidy et al. (2007). Additional IA's have been deployed in Ottawa (six instruments), and up to 25 are expected to be deployed in greater Montreal in the near future. These instruments are not useful for ambient noise measurements, but provide recordings of small earthquakes (weak shaking) as well as large earthquakes (strong shaking).

4.2.2.2 Detailed geological, geotechnical, and shear-wave velocity information

In recent years there has been increased efforts to compile geological and geotechnical datasets in urban areas of Canada. For example, in greater Victoria, a detailed geologic map (1:25,000) was compiled (Monahan et al., 2000) using over 5,000 geotechnical borehole logs obtained from a variety of public and private agencies; several hundred water well logs; and nearly 3,000 engineering drawings for municipal sewer and water lines, that commonly show where bedrock was encountered.

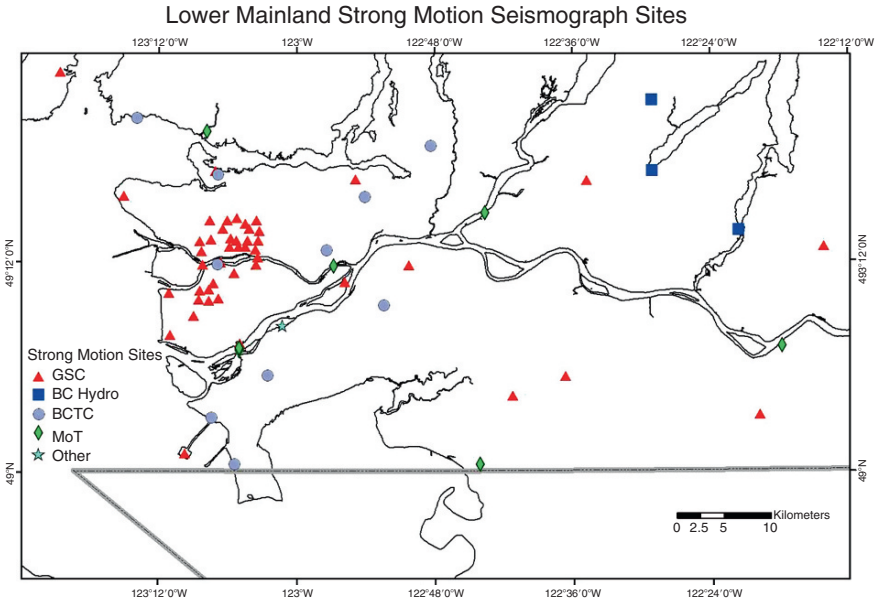

Fig. 4.2.3 Location of strong motion instruments across greater Vancouver. GSC IA's are shown as red triangles

In greater Vancouver, seismic reflection data, borehole logs, seismic cone penetrometer measurements, and seismic refraction data have been used to estimate shear-wave velocities and geotechnical properties of the deltaic sediments and underlying bedrock and to map the depth to bedrock (for details see Hunter et al., 1999; Britton et al., 1995; Hunter, 1995).

In Ottawa, detailed surficial geological maps (GSC, 1977, 2006) combined with geotechnical data (based on more than 28,000 boreholes in the greater Ottawa area – see Hunter and Motazedian, 2006) and new measurements of S-wave velocity, and subsurface imaging provide a valuable database for site response studies (as documented in following sections of this article). In recent years, seismic reflection and refraction methods have been used to map the surficial geology beneath greater Ottawa (see Hunter and Motazedian, 2006). This includes a land-streamer shear wave reflection technique that was used to map shear wave velocity in both rural and urban settings. Most recently, a Minivibe swept-frequency source has proven very useful to map out the subsurface structure (see Pugin et al., 2007).

4.2.2.3 Site response methodologies

The primary methods to evaluate site response in Canada are: (1) use of weak-motion earthquake recordings using both the Standard Spectral Ratio (SSR) method

and the Horizontal-to-Vertical (H/V) ratio method; (2) use of Ambient Noise measurements with the H/V ratio method (Nakamura, 1989); (3) measurement of Vs_{30} using shear-wave refraction and reflection techniques to generate NEHRP classification maps (e.g., Hunter and Motazedian, 2006).

The microtremor method has been used most extensively by studies across southwestern British Columbia (Molnar et al., 2006; Molnar and Cassidy, 2006; Onur et al., 2004; Ventura et al., 2004), along with a study of the seismic microzonation for Montreal, Quebec (Chouinard et al., 2004), and at seismic instrument sites across Ontario (Read and Eaton, 2005; Sneider et al., 2005).

The horizontal-to-vertical spectral ratio determined from microtremors has shown a clear peak that is well correlated with the fundamental resonance frequency at "soft" soil sites (Bard, 2004; Horike et al., 2001; Lachet et al., 1996; Field and Jacob, 1995; Lachet and Bard, 1994; Lermo and Chavez-Garcia, 1994). Numerical analysis suggests that microtremor site response is most effectively generated when the impedance contrast is greater than 3.5 (Malischewsky and Scherbaum, 2004), thus the good correlation at "soft" soil sites. Most studies have shown that the peak amplitude of the microtremor ratio tends to underestimate the peak amplitude of earthquake spectral ratios with respect to a reference (bedrock) site (Bard, 1999 lists 14 studies with this conclusion). Only a few studies claim rough agreement between the peak amplitude of the microtremor ratio and earthquake site-to-reference spectral ratios (Molnar and Cassidy, 2006; Mucciarelli et al., 2003; Horike et al., 2001; Lermo and Chavez-Garcia, 1994). In general, the site response shown by the earthquake site-to-reference spectral ratio method is regarded as the best approximation for engineering use, whereas H/V spectral ratios from earthquakes and/or microtremors are regarded as providing the fundamental peak and lower bound estimate of amplification for a soil site. This paper highlights some of those applications across Canada.

4.2.3 Earthquake site response studies – Some examples

4.2.3.1 Fraser River Delta – Greater Vancouver, British Columbia

Greater Vancouver has a population of more than 2 million people and is the economic hub of British Columbia. Many critical facilities, including Canada's most important port and second busiest airport, are built on the thick, young (less than 11,000 years) unconsolidated soils of the Fraser River delta. Geology across the region varies from Tertiary bedrock outcrops, Pleistocene glacial till, and Holocene soils (up to 300 m thick) on the Fraser River Delta. A simplified cross-section of the delta, showing location of strong motion recording sites, is given in Figure 4.2.4. Detailed geological, geophysical and geotechnical data from boreholes, seismic reflection and seismic refraction studies (e.g., see Hunter et al., 1999; Britton et al., 1995; Hunter, 1995) and recordings of moderate to large earthquakes (shaking levels of up to about 5–6% g) provide an opportunity to evaluate the variation in local site response.

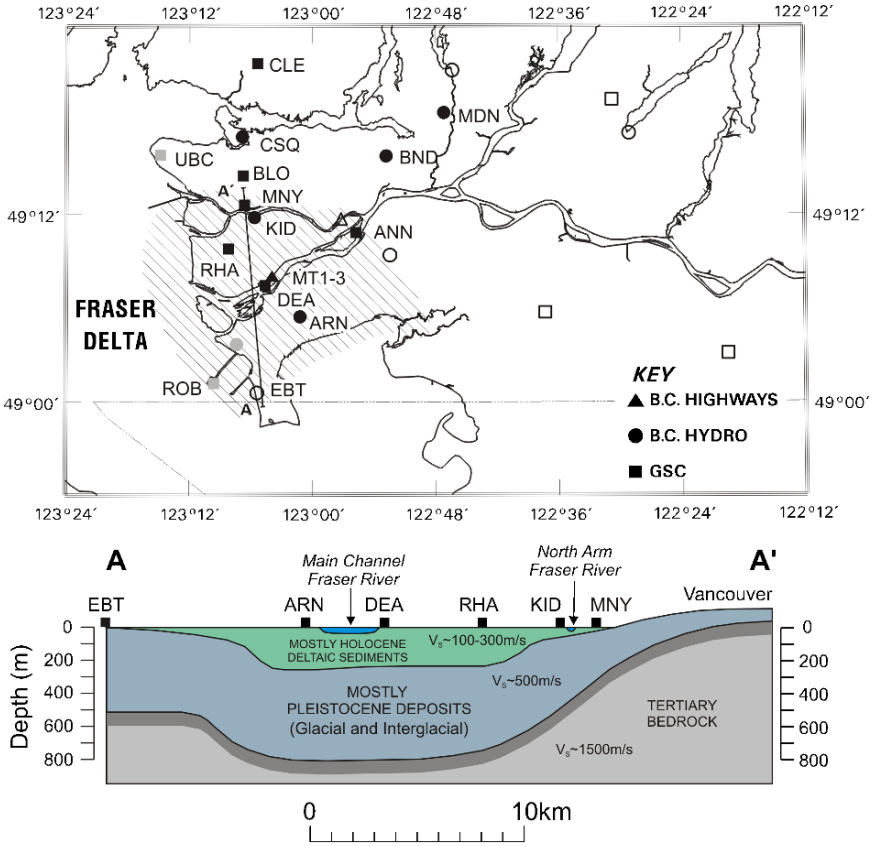

Fig. 4.2.4 Simplified cross section (bottom) of the Fraser River delta (hatched area – top) and location of strong motion instrument (pre-2001) recording sites discussed in this article. The current strong motion network is shown in Figure 4.2.3

Results

In the vicinity of the Fraser River Delta of greater Vancouver, a clear variation in site response has been observed. Amplification factors of up to about ten times (Figure 4.2.5) were observed and significant variations in both amplification and duration of shaking were observed, in some cases, over just a few kilometres (Cassidy et al., 1997; Cassidy and Rogers, 1999). A grid of microtremor measurements and a new dense urban strong motion array (Figure 4.2.3) show a variation in the fundamental period across the Delta (Molnar et al., 2006). However, the strongest shaking appears to be at the edge of the delta, where the soft, Holocene sediments thin (Figure 4.2.4). Research is currently underway to examine the effect of the deeper 3D basin structure on the local site response, and to incorporate that with the response of the upper 30 m.

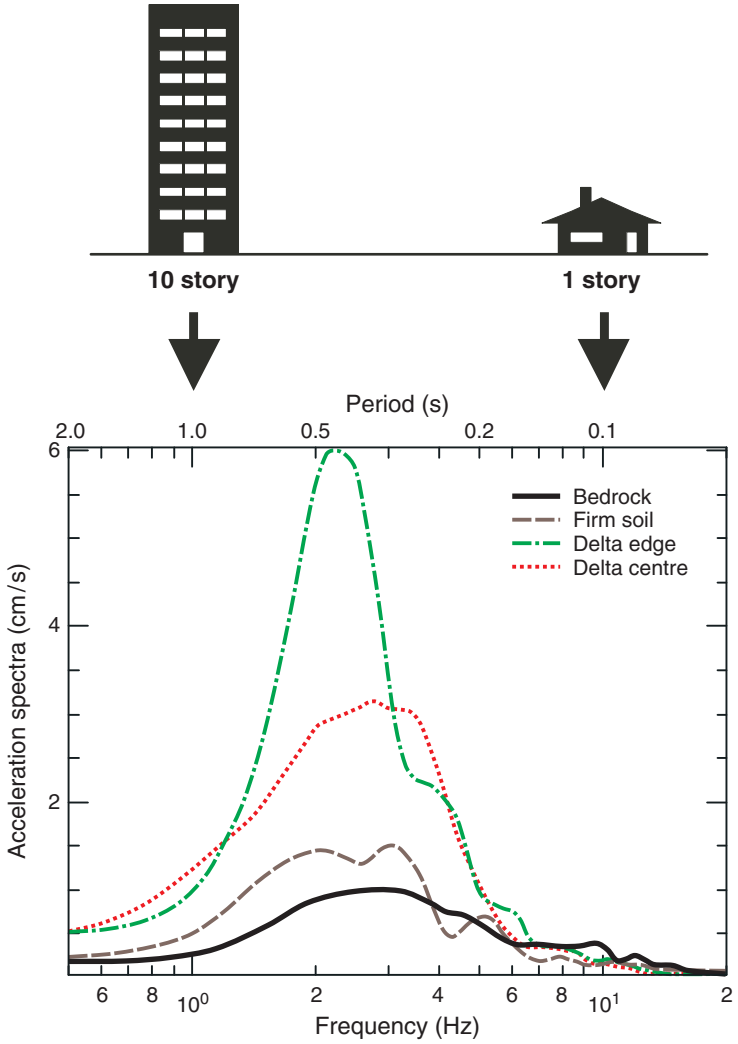

Fig. 4.2.5 Variation in ground shaking in greater Vancouver (From Cassidy et al., 1997). The black trace is a bedrock recording, the brown dashed line is a firm soil (glacial till) site (BND), the red dotted line is a site (RHA) in the middle of the delta, and the green line is a site (MNY) at the edge of the delta. Shaking near 10 Hz would impact small structures, whereas shaking near 1 Hz would impact larger structures

A soil-structure interaction study on the delta was conducted near a 14-storey concrete highrise (Molnar et al., 2006). Measurements made from the edge of the building to 160 m distance showed little influence to the free-field response except for within the footprint of the building.

4.2.3.2 Greater Victoria, British Columbia

Greater Victoria, with a population of 350,000, is the capital city of British Columbia and is situated in the highest seismic hazard zone in Canada. In this region crustal earthquakes (up to M = 7.5), subcrustal earthquakes (up to M = 7), and subduction zone earthquakes (as large as M = 9) can occur (Hyndman et al., 1996).

A wide variety of detailed site-response studies have been conducted in Victoria. This is the result of the availability of detailed geological maps, a wealth of geotechnical information, ground shaking recordings of ten moderate to large (M_W 4.0–6.8) earthquakes, several hundred ambient noise measurements, detailed felt intensity and damage reports associated with larger earthquakes (that can be compared to the other datasets and modelling), and detailed SHAKE modeling (Molnar et al., 2004b). Here we summarise some results of those studies.

Geology and geotechnical data

The geology of greater Victoria is highly variable with bedrock, glacial till, glaciomarine clays, and Holocene organic soils (see the detailed geological maps of Monahan and Levson, 2000). Three glaciations and rapid changes in sea level have created this complex environment. The typical geologic profile in the city consists of pockets of glaciomarine clay over competent bedrock – resulting in large impedance contrasts. Subsurface geological and geotechnical data that are available across the city (as documented by Monahan and Levson, 2000) include: over 5,000 geotechnical borehole logs; several hundred water well logs; nearly 3,000 engineering drawings for sewer and water lines; and shear-wave velocity data from 15 seismic cone penetrometer test (SCPT) sites and four spectral analysis of surface wave (SASW) sites.

Results

The first study of site response in greater Victoria utilizing earthquake recordings is documented in Molnar et al. (2004b). This study used weak-motion (<3.5% g) recordings of the M = 6.8 Nisqually earthquake (150 km epicentral distance) at eight sites across the city. Using both H/V ratios and standard spectral ratios (SSR) with a bedrock reference site, significant variations in ground shaking (up to six times amplification) were observed and a good correlation was found with local soil conditions. These two methods (H/V and SSR) yielded similar site response curves – for both fundamental period, and, notably, for peak amplification factors (Molnar et al., 2004b). Numerical modeling (SHAKE) indicated that the observed site response can be attributed to the known geologic profiles. The results of this study were expanded to incorporate recordings of additional earthquakes (sampling different distances and directions), and also ambient noise data, as discussed in the following section.

Comparison of microtremor and earthquake spectral ratios

The Molnar et al. (2004b) study was subsequently expanded to include recordings of ten earthquakes, ranging in magnitude from M_W 4.0 to M_W 6.8, made on digital strong-motion instruments. In addition, noise measurements were collected at each of the strong-motion instrument sites.

All the recordings can be considered "weak" strong-motion with a maximum peak ground acceleration of 5.5% g. Figure 4.2.6 shows a comparison of the M_W 6.8 2001 Nisqually, Washington, earthquake site-to-reference spectral ratio (quartz diorite bedrock reference site PGC), with the average earthquake h/v spectral ratio of up to five weak-motion earthquakes, and with the average microtremor h/v spectral ratio for sites in greater Victoria. Regardless of excitation source (weak-motion earthquakes or microtremors) and spectral ratio method, similar peak amplitudes and fundamental frequencies are found. This suggests that microtremor recordings are valid for estimation of linear earthquake response at sites in greater Victoria.

Comparison of microtremor recordings with macroseismic information and shear-wave velocity measurements

The significant variation in surface geology over short distances in greater Victoria, combined with the most frequent seismicity in Canada, make it an ideal location to incorporate macroseismic data (felt reports of shaking and damage reports) for the study of local site effects. Three detailed microzonation studies have examined the macroseismic (earthquake intensity and damage) information for the city of Victoria from the 1946 M_S 7.2 Vancouver Island earthquake (Wuorinen, 1974), the 1996 M_W 5.0 Duvall (Levson et al., 1998), and the 2001 M_W 6.8 Nisqually, Washington earthquakes (Molnar et al., 2004a). Measured shear-wave velocity information (12 seismic cone penetration tests [SCPT] and four spectral analysis of surface wave technique) is available at 16 locations in greater Victoria. Molnar and Cassidy (2006) present the comparison of microtremor recordings with these datasets. An example of the good agreement between the various methods is given in Figure 4.2.7.

A residential area in southern Victoria, where all three macroseismic investigations and three SCPT sites are located, provides an ideal case study for local site effects as there is a large variation in the geology from competent bedrock to glaciated material to marine silty clay with the presence of peat at surface. This provides a relatively high and shallow (within 30 m of surface) impedance contrast, an ideal setting for application of the single-instrument microtremor method.

Chimney damage from the 1946 M_S 7.3 Vancouver Island earthquake, roughly 200 km distant, occurred only in this area of Victoria. During the 1996 M_W 5.0 and 2001 Mw 6.8 Washington earthquakes, residents felt little to no vibration on bedrock (MMI I–II), but those living on marine silty clay soils reported the movement of some heavy furniture (MMI VI). Figure 4.2.8 shows microtremor site response at 22 sites that sample the different geological conditions (Monahan et al., 2000). The

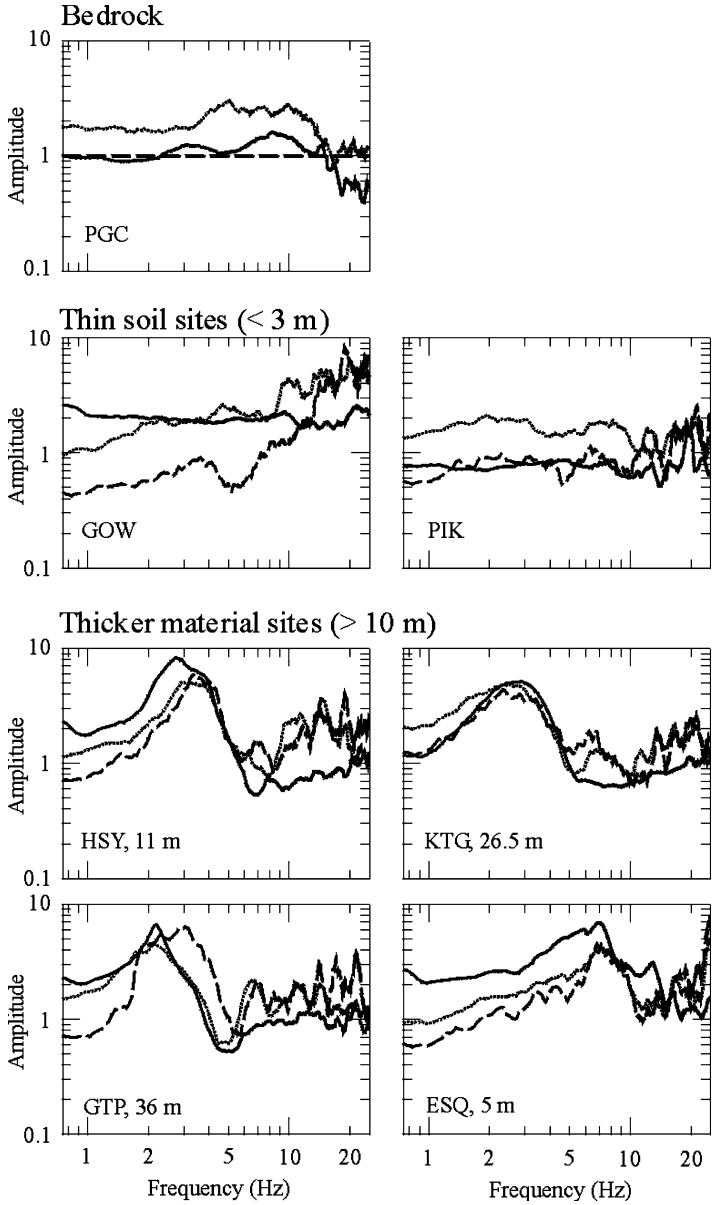

Fig. 4.2.6 Comparison of results from three different site response techniques for strong motion sites in greater Victoria (From Molnar and Cassidy, 2006). Shown are the average microtremor H/V spectral ratios (solid lines), the average H/V spectral ratio for up to five weak-motion earthquakes (dotted lines) and estimates from the standard spectral ratio (dashed lines) for the 2001 Nisqually earthquake

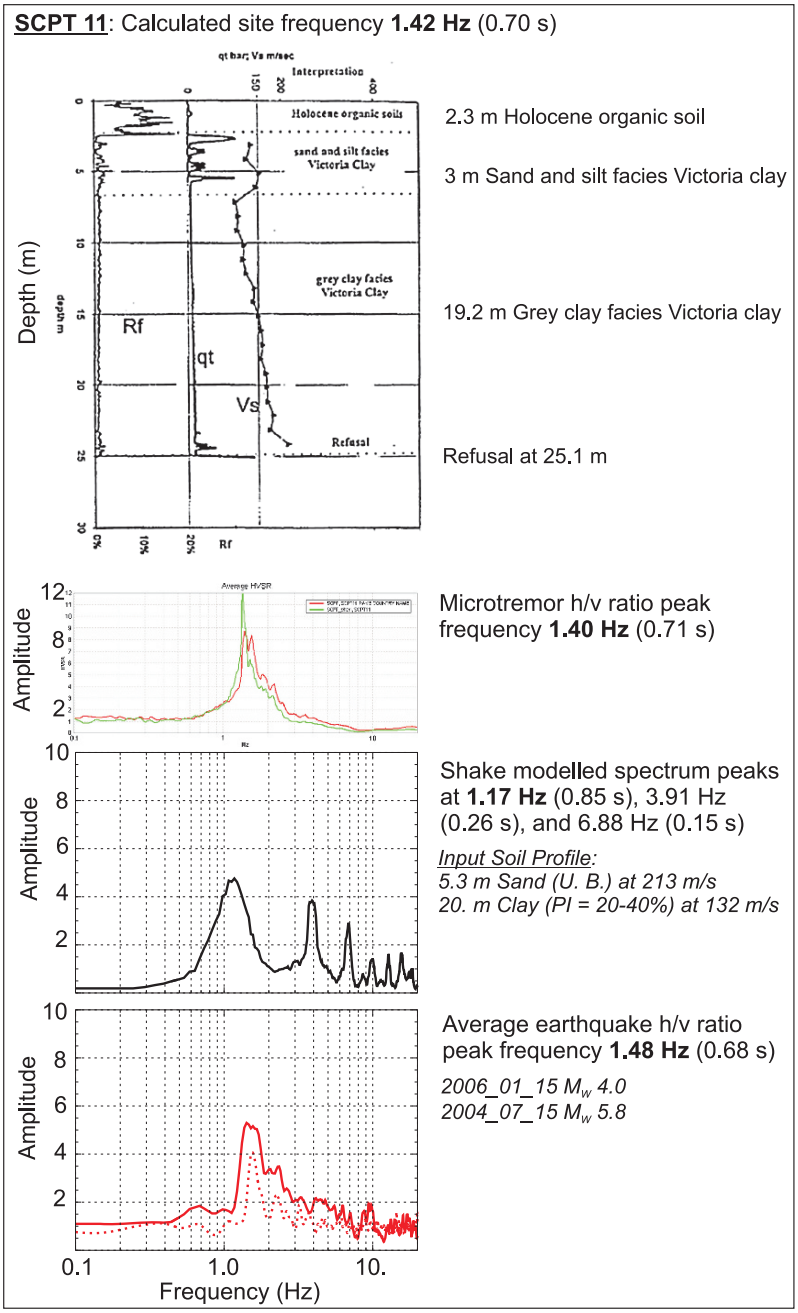

Fig. 4.2.7 Similar peak frequency demonstrated by three methods (microtremor recordings, SHAKE modelling based on SCPT results, and weak earthquake motion) for a firm soil site (25 m depth to bedrock) in downtown Victoria. Both microtremor and earthquake peak frequency determined by horizontal-to-vertical spectral ratio method. SCPT parameters: Vs = shear-wave velocity, qt = tip resistance, and Rf = friction ratio (From Molnar et al., 2007)

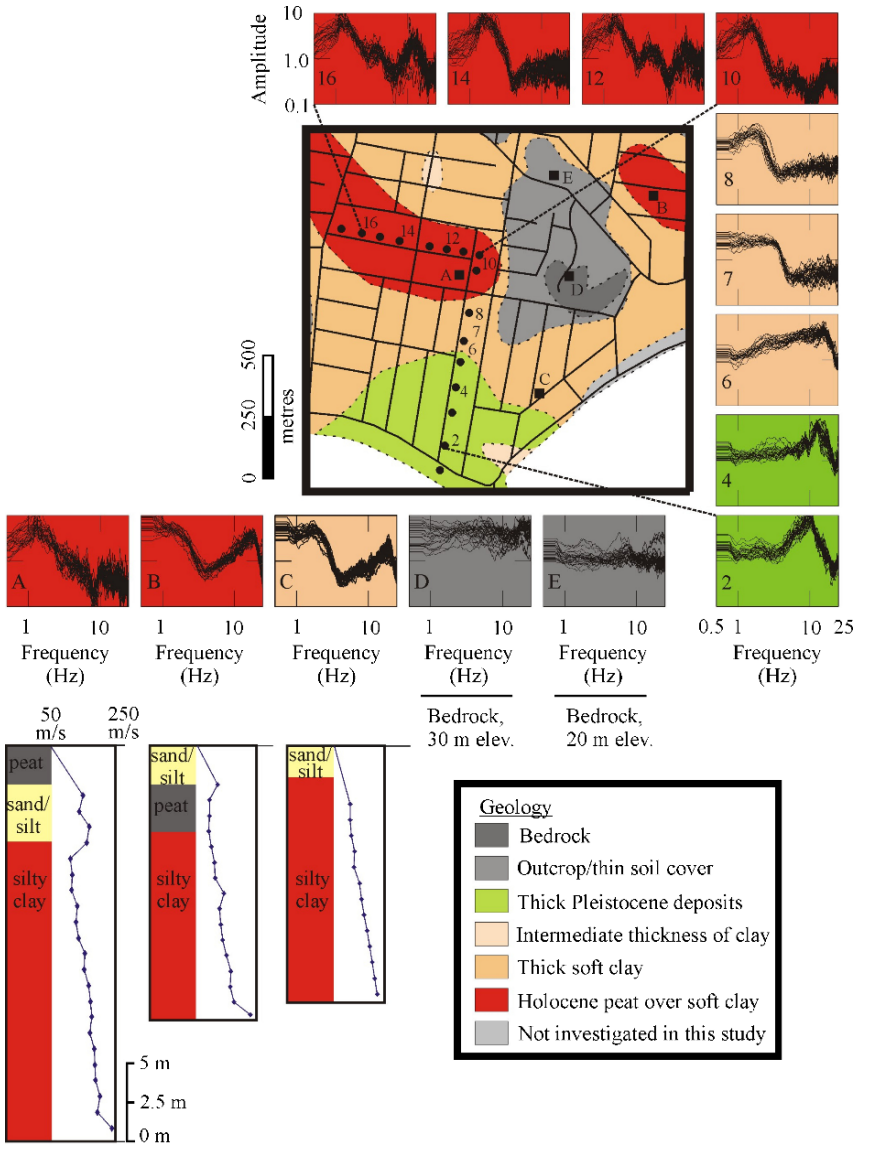

Fig. 4.2.8 Microtremor site response of 22 sites in southern Victoria. There is a large difference of fundamental frequency from 1 to 10 Hz between ground conditions (colour-coded), consistent with macroseismic (earthquake intensity and damage) information. Shear-wave velocity profiles for three sites (A, B, and C) are shown (lower left)

fundamental frequency at sites 1 to 5 on dense glacial material is at or above 10 Hz (0.1 s) and decreases within a city block to 1 Hz (1 s) at site 10 as the glacial material tapers out into an old bog area filled with marine silty clay and peat. Low-level earthquake recordings available from five strong-motion instrument locations

in the area show a similar variation of site response (not shown). The microtremor site response is consistent with macroseismic intensity information demonstrating lower frequency response in marine silty clay areas compared to higher frequency response on dense glacial material and bedrock.

Summary

As documented above, the very good agreement (for both fundamental period and amplification level) found between earthquake methods (standard spectral ratio and H/V methods) and microtremor H/V analysis (Molnar and Cassidy, 2006) has encouraged the application of ambient noise measurements for site response analysis across greater Victoria. Subsequently, microtremor analysis has been used in a number of studies in greater Victoria including a School Seismic Retrofit Project – where 193 microtremor recordings were made at 18 greater Victoria schools as part of a seismic hazard assessment project. This campaign provided several locations with known borehole geology to confirm and/or validate the microtremor site response. Microtremors were used to identify those schools that have a similar resonant period to that of the local site conditions.

4.2.3.3 2010 Winter olympic corridor, British Columbia

More than 100 microtremor recordings were collected along the Sea-to-Sky highway that links Vancouver to Whistler (site of the 2010 Winter Olympic Games) as part of an all-encompassing seismic hazard assessment for the area. Figure 4.2.9 shows the locations of 50 microtremor recordings in the Squamish, BC area and selected spectral ratios using microtremors. These data show a clear variation in site response. Sites beside the Squamish River sample Holocene floodplain deposits (S2 and B2) and consistently show peak amplification at relatively low frequencies around 0.3–0.5 Hz. Site response of the stiffer gravel fan deposits (C9) show peak amplification at higher frequencies between 1 to 2 Hz. Sites in the rocky Garibaldi Heights (G7) were among the stiffest with relatively flat site response below 10 Hz (for details see Molnar et al., 2006). Results from the Whistler Village area show a similar pattern; areas on thick (up to about 30 m), soft deposits showed peak amplification at frequencies of 0.5–4 Hz, whereas recordings from nearby bedrock sites had peaks at 10–13 Hz. In Pemberton, where the sediments are up to 90 m thick, peak amplification occurred at 0.3–0.5 Hz (Internal GSC Report).

4.2.3.4 Greater Ottawa, Ontario

Ottawa, the capital city of Canada, with a population of just over 1 million people, is situated in the moderately active Eastern Quebec Seismic Zone (Adams

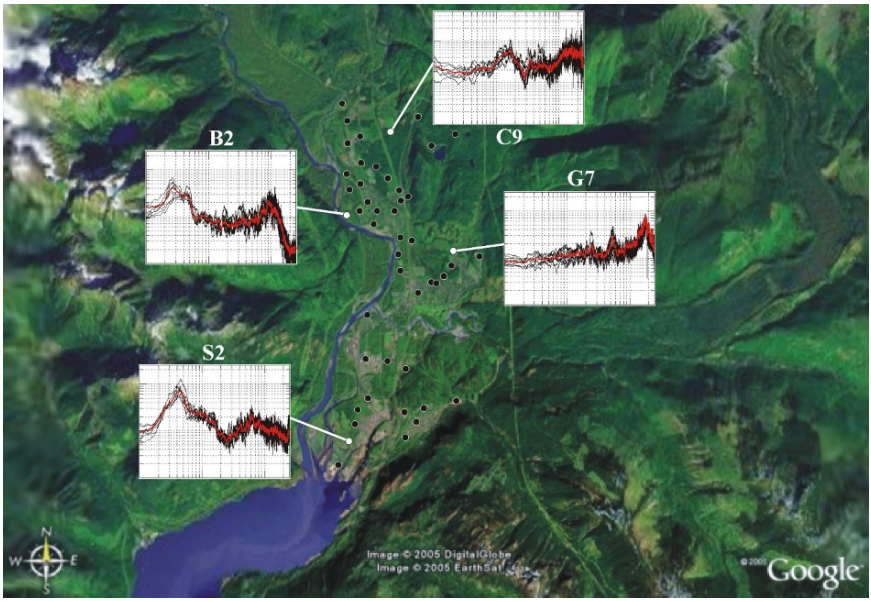

Fig. 4.2.9 Google Earth aerial image of the 50 microtremor recording sites along a 10-km stretch of the Sea-to-Sky Highway near Squamish (between Vancouver and Whistler, British Columbia). Microtremor site response shown ranges from 0.1 to 20 Hz on a log-log plot (From Molnar et al., 2007)

and Basham, 1991; Adams and Atkinson, 2003). The geology of greater Ottawa is complex, ranging from rock outcrops (Precambrian and Paleozioc), to glacial till over bedrock, to thin (and thick) Holocene clays and silts overlying till and bedrock (Figure 4.2.10). For details on the urban geology, see Bélanger (1998), or http://gsc.nrcan.gc.ca/urbgeo/natcap/surf_introduction_e.php.

Studies – Methods

A number of geophysical, geological and geotechnical mapping studies are underway in the greater Ottawa region. These are focussed on mapping the shear-wave velocity in the uppermost 30 m (e.g., Hunter and Motazedian, 2006) and mapping the 3-D subsurface geology using seismic reflection and refraction techniques (e.g., Pugin et al., 2007). The results of these studies are being used to map the NEHRP zones throughout the Ottawa area. Other datasets that are being incorporated with these studies include geological/geotechnical data from more than 33,000 boreholes in the area, recordings of weak-motion earthquakes (e.g., Adams, 2007) and recordings of ambient noise (J. Hunter and G. Brooks, personal communication, 2008).

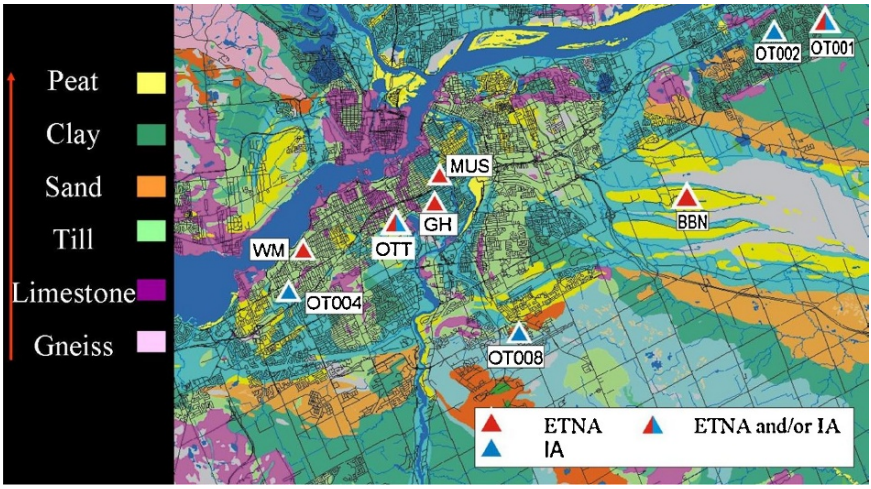

Fig. 4.2.10 Surface geology of the greater Ottawa area. Triangles denote the locations of strong motion seismographs (both ETNA's and Internet Accelerometers [IA's])

Results

Preliminary NEHRP classification zone maps for greater Ottawa are currently being produced, based on Vs_{30} (e.g., Figure 4.2.11) from seismic reflection, refraction, and borehole measurements. In addition, mapping the depth to bedrock has revealed a significant buried bedrock valley filled with soft sediments in the eastern part of the city. This area will be targeted for future 3D resonance studies. Fundamental site period maps, based on these new measurements are being produced (e.g. Figure 4.2.12).

A comparison of weak-motion recordings of three earthquakes (H/V ratios and standard spectral ratios) show very significant amplification (up to 50 times or more) and sharp resonance (Figure 4.2.13) at thick, soft soil sites (Al-Khoubbi and Adams, 2004; Adams, 2007). This strong amplification/resonance is unusual, and may be attributed to the strong impedance contrast between very hard Precambrian rock, and very soft Holocene soils, or perhaps other causes. Further investigations are required to understand this.

4.2.3.5 Montreal, Quebec

Montreal, with a population of nearly 3 million people, is the largest city in Quebec, and the second largest city in Canada. It has critical port facilities, and is an economic and industrial centre. It is also situated in a moderately active seismic zone (Adams and Basham, 1991; Adams and Atkinson, 2003) and is particularly vulnerable to earthquake damage as many of the structures were built prior to modern

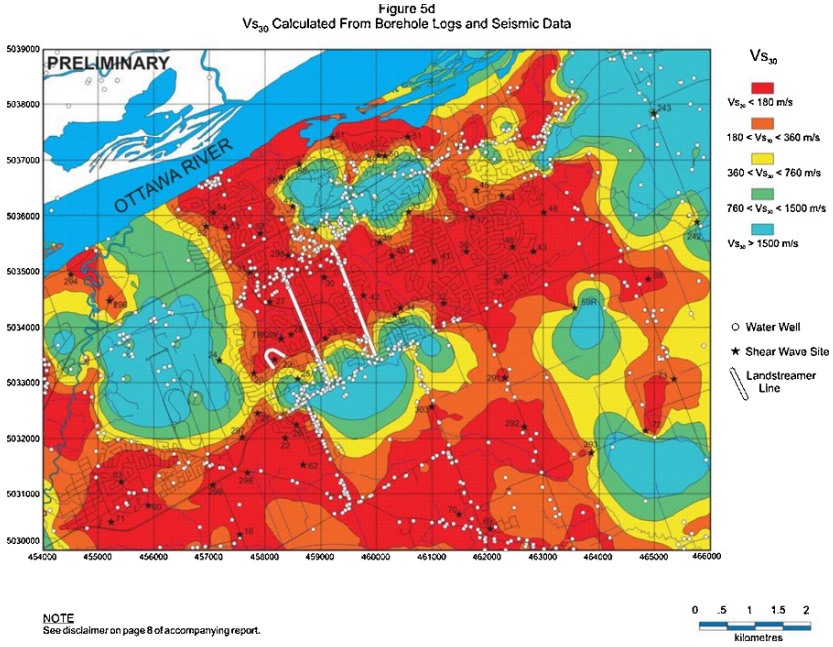

Fig. 4.2.11 Preliminary Vs_{30} map of the Ottawa suburb of Orleans (From G. Brooks and J. Hunter, personal communication, 2008)

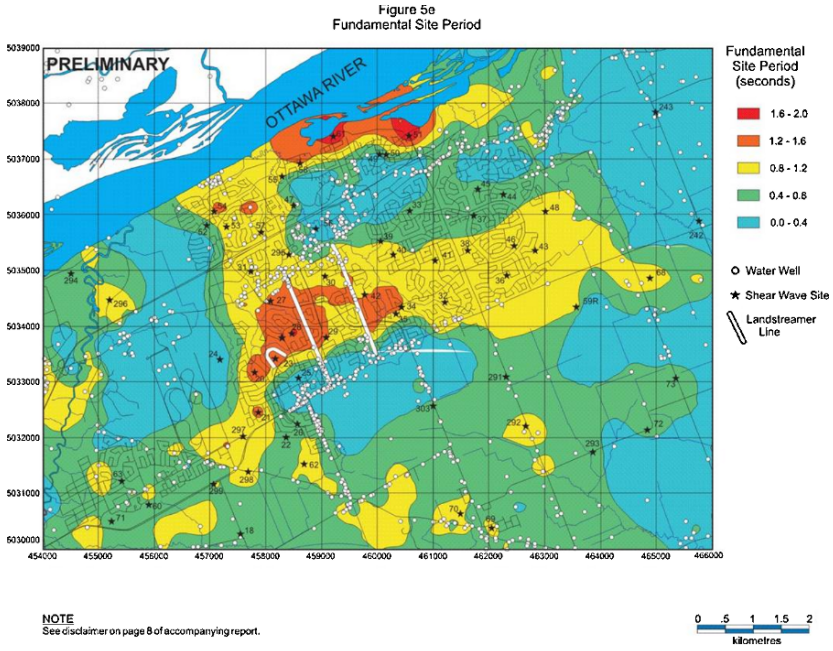

Fig. 4.2.12 Fundamental site period estimates for the Ottawa suburb of Orleans. Estimates are based on soil thickness from water wells and seismic refraction/reflection data combined with shear-wave velocities (J. Hunter and G. Brooks, personal communication, 2008)

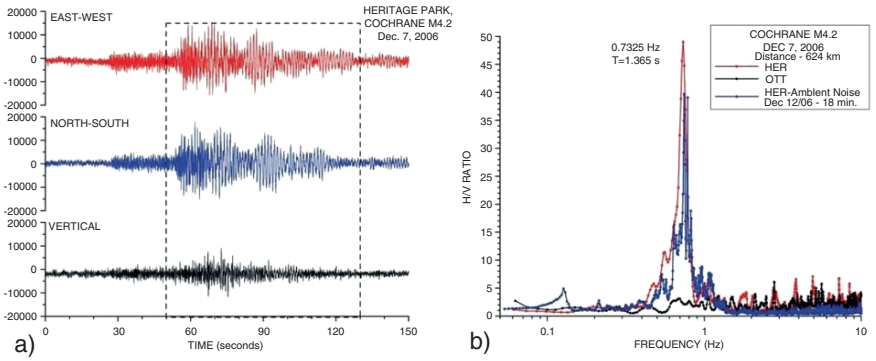

Fig. 4.2.13 Recordings (left) of a magnitude 4.2 earthquake (distance of 624 km) made on thick (80–90 m) soft ($Vs < 200\,m/s$) soil in Ottawa. Spectral H/V ratios (right) for this earthquake (red line) are compared to H/V ratios for a nearby rock site (black line) and H/V using ambient noise (blue line)

building codes, and much of the area is blanketed by a thick layer of marine clay overlying tills and Precambrian rock (Prest and Hode-Keyser, 1977). Seismic site effects and seismic risk have been studied by combining field investigations (using ambient noise measurements with the H/V method) and numerical simulations of seismic wave propagation. This work is documented in Chouinard and Rosset (2007) and Chouinard et al. (2004).

Results

Measurements of ambient noise were made at more than 700 locations across greater Montreal (Chouinard and Rosset, 2007). The H/V method was used to obtain detailed maps of fundamental frequency (Figure 4.2.14). Numerical modeling was used to estimate amplification factors (see Chouinard and Rosset, 2007). A compilation of 2,000 boreholes were used to constrain bedrock depth and to compute transfer functions used in the 1D modeling. By combining these approaches Chouinard and Rosset (2007) produced a preliminary seismic microzonation map for Montreal. Additional studies are planned, and will be facilitated by the deployment of up to 25 GSC IA's across greater Montreal in the near future.

4.2.3.6 Quebec City, Quebec

Quebec City, with a population of more than 700,000 people, is the capital city of Quebec. The complex geology of this region, like that of Montreal and Ottawa, includes significant deposits of Leda clay, and Champlain Sea sediments. Currently, ambient noise data are being collected and analysed (D. Perret, personal

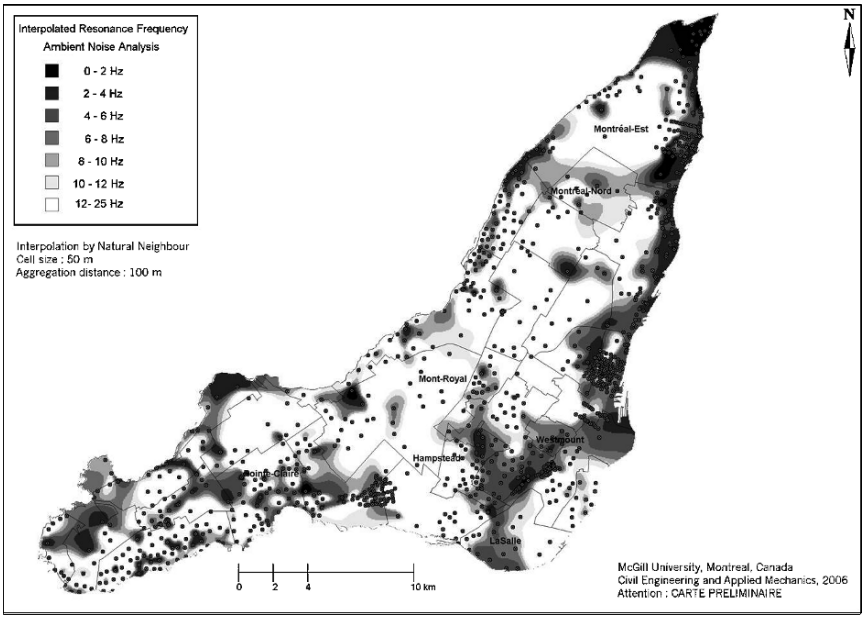

Fig. 4.2.14 Interpolated map of the fundamental site frequency from ambient noise measurements. Black dots indicate measurement sites (From Chouinard and Rosset, 2007)

communication, 2008) to examine the variation in earthquake site response across greater Quebec City. Seismic motions on bedrock in the Quebec City area are documented by Nastev et al. (2007).

4.2.4 Summary

Earthquake site response studies are becoming increasing common across Canada. There are a number of reasons for this, including the ease with which ambient noise measurements can be collected and processed, the availability of new data from urban strong motion instruments, improved seismic reflection and refraction methodologies that provide shear-wave velocity measurements and images of the subsurface geology in urban areas, and a wealth of geological and geotechnical data that has been compiled in a number of cities. Currently, efforts are focussed in the major urban centres with the greatest seismic risk, including Vancouver, Victoria, Ottawa, Montreal, and Quebec City.

Since 2003, approximately 1,000 microtremor recordings have been made in southwestern British Columbia. These data have been analyzed using the horizontal-to-vertical spectral ratio method. Comparison of microtremor and earthquake spectral ratios at strong-motion instrument sites in greater Victoria showed similar amplitudes and fundamental frequencies, validating the use of the method for linear

earthquake site response. Macroseismic information compared with microtremor H/V spectral ratios confirmed a rapid change in fundamental frequency related to a change in the geologic properties of the subsurface. The microtremor method has provided a quick and efficient first estimate as part of seismic hazard assessment projects for greater Victoria schools, the Fraser River delta, and a 10-km stretch of the Sea-to-Sky Highway that links Vancouver to Whistler. In eastern Canada, site response studies are well underway in Ottawa, Montreal, and Quebec City. The combination of soft soils over very hard Precambrian rock yields very high impedance contrasts that result in resonant amplification factors of 50 or more in some cases. Vs measurements from seismic reflection and refraction studies are being used to produce detailed NEHRP classifications maps. The deployment of additional strong motion instruments in urban centres, and the collection of ambient noise data provide key information, in combination with the existing geological and geotechnical data. Results from earthquake site response studies, when combined with information on building response from engineering studies, are critical to mitigate losses from future earthquakes in urban centres.

Acknowledgments We gratefully acknowledge those who have provided data and shared results, including Jim Hunter, Didier Perret, Dariush Motazedian, Greg Brooks, Philipe Rosset, Luc Chouinard, Pat Monahan, Carlos Ventura, Tuna Onur, and John Adams (Figure 4.2.13). This article was reviewed, and improved by Garry Rogers and Ralph Currie. This is ESS/GSC Contribution Number 20070614.

References

Adams, J. (2007). Soil amplification in Ottawa from urban strong ground motion records, Proceedings of the 9th Canadian Conference on Earthquake Engineering, Ottawa, Canada, 10pp.

Adams, J., and Atkinson, G.M. (2003). Development of seismic hazard maps for the 2003 National Building Code of Canada, Canadian Journal of Civil Engineering, 30, 255–271.

Adams, J., and Basham, P.W. (1991). The seismicity and seismotectonics of eastern Canada. In: Neotectonics of North America, D.B. Slemmons, E.R. Engdhal, M.D. Zoback, and D.D. Blackwell (eds), Geological Society of America. Boulder, CO: Decade Map Volume 1.

Al-Khoubbi, I., and Adams, J. (2004). Local site effects in Ottawa, Canada – First results from a strong motion, Proceedings of the 13th World Conference on Earthquake Engineering, Ottawa, Canada, Paper 2504 on CD-ROM.

Bard, P.-Y. (1999). Microtremor measurements: A tool for site effect estimation? Proceedings of the Second International Symposium on the Effects of Surface Geology on Seismic Motion, Yokohama, Japan, December 1998, pp. 1251–1279.

Bard, P.-Y. (2004). Effects of surface geology on ground motion: Recent results and remaining issues, Proceedings of the 10th European Conference on Earthquake Engineering, Vienna, Austria, August 28–September 2, 1994, pp. 305–325.

Bélanger, J.R. (1998). Urban Geology of Canada's National Capital Area, in Karrow, P.F. and White O.L., Urban Geology of Canadian Cities; Geological Association of Canada, Special Paper 42, pp. 365–384.

Booth, D.B., Wells, R.E., and Givler, R.W. (2004). Chimney damage in the greater Seattle area from the Nisqually earthquake of 28 February, 2001, Bulletin of the Seismological Society of America, 94, 1143–1158.

Britton, J.R., Harris, J.B., Hunter, J.A., and Luternauer, J.W. (1995). The bedrock surface beneath the Fraser River delta in British Columbia based on seismic measurements, in Current Research 1995-E, Geological Survey of Canada, pp. 83–89.

Building Seismic Safety Council (BSSC) (2001). NEHRP (National Earthquake Hazards Reduction Program) Recommended Provisions for Seismic Regulations for New Buildings and Other Structures, Part 1: Provisions and Part2: Commentary, Federal Emergency Management Agency, FEMA-368 and FEMA-369, Washington, DC.

Cassidy, J.F., and Rogers, G.C. (1999). Seismic site response in the greater Vancouver, British Columbia, area: Spectral ratios from moderate earthquakes, Canadian Geotechnical Journal, 36, 195–209.

Cassidy, J.F., Rogers, G.C., and Weichert, D.H. (1997). Soil response on the Fraser Delta to the Mw = 5.1 Duvall, Washington, earthquake, Bulletin of the Seismological Society of America, 87, 1354–1361.

Cassidy, J.F., Rosenberger, A., Rogers, G.C., Little, T.E., Toth, J., Adams, J., Munro, P., Huffmann, S., Pierre, J.-R., Asmis, H., and Pernika, G. (2007). Strong motion seismograph networks in Canada, Proceedings of the 9th Canadian Conference on Earthquake Engineering, Ottawa, Canada, June 26–29, 2007, 10pp.

Chouinard, L., and Rosset, P. (2007). Seismic site effects and seismic risk in the Montreal area – The influence of marine clays, Proceedings of the 9th Canadian Conference on Earthquake Engineering, Ottawa, Canada, June 26–29, 2007, 10pp.

Chouinard, L., Rosset, P., de la Puente, A., Madriz, R., Mitchell, D., and Adams, J. (2004). Seismic hazard analysis for Montreal, Proceedings of the 13th World Conference of Earthquake Engineering, Vancouver, BC, Paper 7010.

Field, E.H., and Jacob, K.H. (1995). A comparison and test of various site-response estimation techniques, including three that are not reference-site dependent, Bulletin of the Seismological Society of America, 85, 1127–1143.

GSC (1977). Surficial materials and terrain features Ottawa-Hull Ontario-Quebec, scale 1:125,000, Geological Survey of Canada 1977: Map 1425A.

GSC (2006). Subsurface database of the National Capital area, Geological Survey of Canada. Website: http://gsc.nrcan.gc.ca/urbgeo/natcap/sub_introduction_e.php

Hartzell, S., Leeds, A., Frankel, A., and Michael, J. (1996). Site response for urban Los Angeles using aftershocks of the Northridge earthquakes, Bulletin of the Seismological Society of America, 86, S168–S192.

Horike, M., Zhao, B., and Kawase, H. (2001). Comparison of site response characteristics inferred from microtremors and earthquake shear waves, Bulletin of the Seismological Society of America, 91, 1526–1536.

Hunter, J.A. (1995). Shear wave velocities of Holocene sediments, Fraser River delta, British Columbia, in Current Research 1995-A, Geological Survey of Canada, pp. 29–32.

Hunter, J.A., and Motazedian, D. (2006). Shear wave velocity measurements for soft soil earthquake response evaluation in the Eastern Ontario region, Ontario, Canada, Proceedings of a Symposium on the Application of Geophysics to Engineering and Environmental Problems (SAGEEP), Seattle, WA, April 1–5, 2006.

Hunter, J.A., Christian, H.A., Harris, J.B., Britton, J.R., and Luternauer, J.L. (1999). Mapping shear wave velocity structure beneath the Fraser River delta sediments – preliminary results, Proceedings of the 8th Canadian Conference on Earthquake Engineering, Vancouver, Canada, June 13–18, 1999, pp. 101–106.

Hyndman, R.D., Rogers, G.C., Dragert, H., Wang, K., Clague, J.J., Adams, J., and Bobrowsky, P.T. (1996). Giant earthquakes beneath Canada's west coast; Geoscience Canada, 23, 63–72.

Kawase, H. (1996). The cause of the damage belt in Kobe: "The basin-edge effect", constructive interference of the direct SD-wave with the basin-induced diffracted/Rayleigh waves, Seismological Research Letters, 67, 25–34.

Lachet, C., and Bard, P.-Y. (1994). Numerical and theoretical investigations on the possibilities and limitations of Nakamura's technique, Journal of the Physics of the Earth, 42, 377–397.

Lachet, C., Hatzfeld, D., Bard, P.-Y., Theodulidis, C.P., and Savvaidis, A. (1996). Site effects and microzonation in the city of Thessaloniki (Greece): Comparison of different approaches, Bulletin of the Seismological Society of America, 86, 1692–1703.

Lermo, J., and Chavez-Garcia, F.J. (1994). Are microtremors useful in site response evaluation? Bulletin of the Seismological Society of America, 84, 1350–1364.

Levson, V.M., Monahan, P.A., and Mate, D.J. (1998). Observed relationships between geology and liquefaction/amplification hazards, Proceedings of the 8th International Congress International Association for Engineering Geology and the Environment, Vancouver, Canada, September 21–25, 1998, pp. 849–855.

Malischewsky, P.G., and Scherbaum, F. (2004). Love's formula and H/V-ratio (ellipticity) of Rayleigh waves, Wave Motion, 40, 57–67.

Molnar, S., and Cassidy, J.F. (2006). A comparison of site response techniques using weak-motion earthquake and microtremors, Earthquake Spectra, 22, 169–188.

Molnar, S., Cassidy, J.F., and Dosso, S.E. (2004a). Comparing intensity variation of the 2001 Nisqually earthquake with geology in Victoria, British Columbia, Bulletin of the Seismological Society of America, 94(6), 2229–2238.

Molnar, S., Cassidy, J.F., and Dosso, S.E. (2004b). Site response in Victoria, British Columbia, from spectral ratios and 1D modeling, Bulletin of the Seismological Society of America, 94(3), 1109–1124.

Molnar, S., Cassidy, J.F., Monahan, P.A., and Dosso, S.E. (2007). Comparison of geophysical shear-wave velocity methods, 9CCEE, Ottawa, Ontario, June 26–29, Paper 1173.

Molnar, S., Cassidy, J.F., Monahan, P.A., Onur, T., Ventura, C.E., and Rosenberger, A. (2006). Application of microtremor measurements for earthquake site response studies in southwestern British Columbia, Proceedings of the 100th Anniversary Earthquake Conference, EERI/SSA, San Francisco, CA, April 18–22, 2006.

Monahan, P.A., and Levson V.M. (2000). Quaternary Geological Map of Greater Victoria, British Columbia Geological Survey, Ministry of Energy and Mines, Victoria, BC, Geoscience Map 2000-2.

Monahan, P.A., Levson, V.M., Henderson, P., and Sy, A. (2000). Relative amplification of ground motion hazard map of Greater Victoria, British Columbia Geological Survey, Ministry of Energy and Mines, Victoria, BC, Geoscience Map 2000-3, Sheet 3B.

Mucciarelli, M., Gallipoli, M.R., and Arcieri, M. (2003). The stability of the horizontal-to-vertical spectral ratio of triggered noise and earthquake recordings, Bulletin of the Seismological Society of America, 93, 1407–1412.

Nakamura, Y. (1989). A method for dynamic characteristics estimation of subsurface using microtremor on the ground surface, Quarterly Reports of the Railway Technical Research Institute, 30, 25–33.

Nastev, M., Lin, L., and Naumoski, N. (2007). Characteristics of seismic motions recorded on bedrock in the Quebec City region, Proceedings of Geo Ottawa 2007, Ottawa, ON, Oct. 21–24, 2007.

Onur, T., Molnar, S., Cassidy, J.F., Ventura, C.E., and Hao, K.X.-S. (2004). Estimating site periods in Vancouver and Victoria, British Columbia using microtremor measurements and "SHAKE" analyses, Proceedings of the 57th Canadian Geotechnical Conference, Québec City, Canada, October 24–27, 2004.

Onur, T., Ventura, C.E., and Finn, W.D.L. (2005). Regional seismic risk in British Columbia – Damage and loss distribution in Victoria and Vancouver, Canadian Journal of Civil Engineering (CJCE), 32(2), 361–371.

Prest, V.K., and Hode-Keyser, J. (1977). Geology and engineering characteristics of surficial deposits, Montreal island and vicinity, Quebec, Geological Survey Paper 75-27, 28pp.

Pugin, A., Hunter, J.A., Motazedian, D., and Khaheshi-Banab, K. (2007). An application of shear wave reflection landstreamer technology for soil response evaluation of earthquake shaking in an urban area, Ottawa, Ontario, Proceedings of a Symposium on the Application of Geophysics to Engineering and Environmental Problems (SAGEEP), Denver, CO, April 1–5, 2007.

Read, K., and Eaton, D. (2005). Investigation of local site effects using empirical methods, 1st Polaris-Polo Research Workshop, Queen's University, Kingston, January 6, 2005.

Rosenberger, A., Rogers, G.C., and Cassidy, J.F. (2007). The new real time reporting strong motion seismograph network in southwest BC: More strong motion instruments for less money, Proceedings of the 9th Canadian Conference on Earthquake Engineering, Ottawa, Canada, 10pp.

Sneider, A.J., Motazedian, D., and Atkinson, G.M. (2005). Seismic soil amplification studies for Ontario Polaris stations, 1st Polaris-Polo Research Workshop, Queen's University, Kingston, January 6, 2005.

Ventura, C.E., Onur, T., and Hao, K.X.-S. (2004). Site period estimations in the Fraser River delta using microtremor measurements – Experimental and analytical studies, Proceedings of the 13th World Conference of Earthquake Engineering, Vancouver, BC, Paper 1075.

Ventura, C.E., Finn, W.D.L., Onur, T., Blanquera, A., and Rezai, M. (2005). Regional seismic risk in British Columbia classification of buildings, Canadian Journal of Civil Engineering (CJCE), 32(2), 372–387.

Wuorinen, V. (1974). A preliminary microzonation of Victoria, British Columbia, M.A. thesis, University of Victoria, Victoria, British Columbia, 156pp.

Chapter 4.3
Recent Applications of Ambient Vibration Measurements in Croatia

Marijan Herak

Abstract The chapter describes recent applications of the measurements of ambient vibrations in Croatia. They include free-field measurements in Zagreb and Ston, as well as those done within buildings. Data obtained in the field at both localities are consistent with the properties of shallow geological structures known to exist there. In Zagreb, HVSR spectra indicate thick alluvial cover (over 100 m) that gradually gets thinner as one reaches the southernmost slopes of the Medvednica Mt. A similar situation, but on a smaller scale, is also encountered in Ston, where HVSR profiles reveal several tens of meters thick sedimentary cover over the bedrock which gets exposed at the Stoviš hill. Measurements in the buildings were analysed by FREDA – a suite of Matlab routines that permit several modes of data analyses. Based on tests on synthetic and real data we conclude that spectral methods are in general more robust and less dependent on parameters of the respective algorithm, than time-domain analyses. Spectral algorithms are also much better in resolving higher modes. The random decrement method is in most cases found to be inferior to spectral or band-pass procedures using original signals. Applications to real buildings proved that analyses of shaking induced by ambient vibrations in most cases leads to well constrained, reliable, and time independent estimates of frequencies and damping of the buildings' vibrational modes.

Keywords HVSR · Damping in buildings · Building frequency · Soil structure interaction

4.3.1 Introduction

The first studies of microseismic noise in Croatia date back to Marković (1948), who studied noise recorded at the Zagreb seismological station. Measurements of microtremors have been used in Croatia for assessing local site effects since 1960s.

M. Herak
University of Zagreb, Faculty of Science, Department of Geophysics, Horvatovac bb, 10000 Zagreb, Croatia
e-mail: herak@irb.hr

M. Mucciarelli et al., (eds.), *Increasing Seismic Safety by Combining Engineering Technologies and Seismological Data,* NATO Science for Peace and Security Series C: Environmental Security,

Based on works of Kanai (1957a, b), the measurements were used to constrain and verify available geotechnical models by assessing the fundamental soil period, but there have also been attempts to compare the spectrum of recorded noise with the theoretical amplification spectra. Limited mostly by the need to digitize analogue recordings by hand and by capabilities of the instruments of that time, such measurements gradually faded away. They have gained new impetus as the topic reappeared in literature (Nakamura, 1989) and digital instruments started to replace the old ones in the 1990s. However, only after acquisition of truly portable dedicated instruments for the measurements of ambient vibrations within the NATO SfP 980857 project (2005–2008), the quality and quantity of measurements increased to the level required by today's standards. This chapter presents a short overview of measurements done within the project in the free-field as well as in the buildings.

4.3.2 Free-field measurements

Although a large number of measurements were done all over Croatia, two cases will be presented here – the ones of Zagreb and Ston. Zagreb is the capital of Croatia, a city with population approaching 1 million, and a history of large earthquakes. The most important one that occurred in 1880 (epicentral intensity VIII–IX °MCS) beneath the NE flanks of the Medvednica Mt. damaged all of the houses in the city, and practically defines the seismic hazard in Zagreb. In spite of rich seismic history, Zagreb still does not have an official seismic microzonation, which prompted the city officials to launch a large, long-term project of comprehensive geotechnical, geological and seismological investigations. One of the goals of the project is to produce a map of seismic microzonation, and microtremor measurements are expected to provide important information.

The city of Ston is located about 50 km to the NW of Dubrovnik, in southern Dalmatia. It is a small town with rich history, know for the ancient salterns and the third longest fortification walls in the world. As a part of the Dubrovnik Republic, Ston was also one of the first townships in this part of the world that developed according to the strict urban code enforced from the 14th century. Earthquakes are frequent there. The most recent devastating one occurred in 1996 (M = 6.0, intensity VIII° MCS in Ston), and Ston needed almost a decade to recover. Detailed damage reports exist in the archives, so we hoped that they could be compared to the noise measurements.

4.3.2.1 Measurements in Zagreb

The Zagreb metropolitan area encompasses over 640 km^2. Geologically it consists of thick (100 m or more) alluvial sediments (clays, sands, gravel) in the Sava river valley, that gradually get thinner as we approach the Medvednica mountain to the

north which mainly consist of green slates, shales, and limestones. In order to asses the applicability of the horizontal-to-vertical spectral ratio (HVSR) technique to this terrain, we have made over 150 measurements most of them in the proluvial Podsljeme area where the Sava valley meets the mountain flanks.

The instrument used was the portable Tromino (produced by Micromed, Italy), a small all-in-one package with three-component geophones, digitizer, GPS-timing, batteries and 512 Mb flash memory for storage. Measurements were done in the first half of 2007. All of them lasted for 20 min, and were processed uniformly: each trace was divided into non-overlapping 30-s long segments, spectra for all three components were computed for each of them. The three spectra were then smoothed with a 5% triangular smoothing function, and HVSR was computed as the ratio of the geometrical mean of spectra of the two horizontal components and the spectrum of the vertical one.

Figure 4.3.1 presents typical HVSR spectra obtained in an approximately 3×3 km area in the Podsljeme zone. It is seen that in the south the spectra are characterized by relatively broad low-frequency peaks (ranging from 0.85 to 2 Hz), indicating presence of thick alluvial deposits. Moving towards the north, the HVSR peaks shift towards the higher frequencies (about 3–6 Hz), as the sedimentary cover gets thinner. Reaching the foothills of the Medvednica Mt., the bedrock gets very close to the surface, as indicated by HVSR peaks found at frequencies above 10–20 Hz.

The HVSR profile (as shown in the map in Figure 4.3.1) is 2,500 m long. This is a spatial spectrogram constructed of all HVSR spectra measured within 500 m from the profile trace. It clearly shows systematic increase of the fundamental frequency as one moves from left (south) to the right (north). Assuming an average S-wave velocity of 300 m/s in the whole sedimentary layer above bedrock, the observed variation of fundamental frequency maps into thickness variation from over 100 m in the south to only a few meters in the north, which is in agreement with (very few) available geotechnical data.

Podsljeme is today one the most prestigious residential areas in Zagreb, where houses are typically two to four storeys high, with expected fundamental frequencies of about 5 Hz or higher. According to our measurements so far, it is also the only place in Zagreb where such buildings are in danger due to soil-structure resonance during earthquake shaking.

4.3.2.2 Measurements in Ston

In Ston ambient noise measurements were done in 2005 and 2006. A total of 70 free-field points were measured, as shown in Figure 4.3.2. They were processed as described in the previous section. The town itself is situated between the Stoviš hill, and the shallow Ston channel. Limestones prevail here. According to a few boreholes, there is about 15–30 m of weathered weak material (mostly sands) above the bedrock beneath the town. Our measurements confirm this as the fundamental frequency all across the plane beneath Stoviš vary between 2 and 4 Hz. As we start

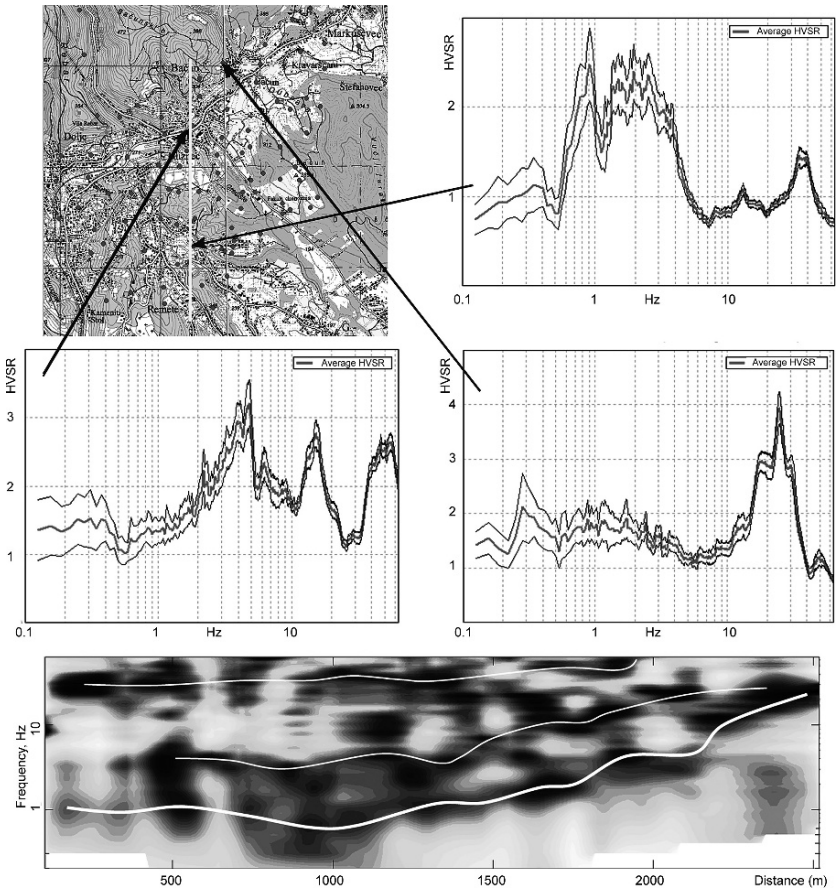

Fig. 4.3.1 *Top left*: Map view of the Podsljeme area in Zagreb which was chosen as a test neighbourhood for the HVSR measurements. Black dots show the locations of measurement points. The foothills of the Medvednica Mt. are in the northern and north-western part. The white AB-line shows the location of the profile in the bottom. *Top right and middle*: Examples of the measured HVSR spectra (mean ± 1 standard deviation), showing how the dominant frequency shifts towards higher values as we move along the profile from A to B. *Bottom*: HVSR profile AB (see the map on the top). Only measurements within 500 m from the profile line are considered. Dark shades correspond to high HVSR values. The lines are drawn to emphasize features, and have no direct geological interpretation, although clear systematic increase of the fundamental frequency with the thinning of the sedimentary cover close to B is evident

climbing up the hill, the layers' thickness rapidly decrease and the dominant frequency increases to over 20 Hz.

Fundamental frequencies of stone houses in Ston vary between about 3 and 6 Hz, depending on their height, shape and position. This frequency interval coincides well with the dominant soil frequencies beneath the town centre and especially at the Stoviš foothills, which, together with high amplification, may explain severity

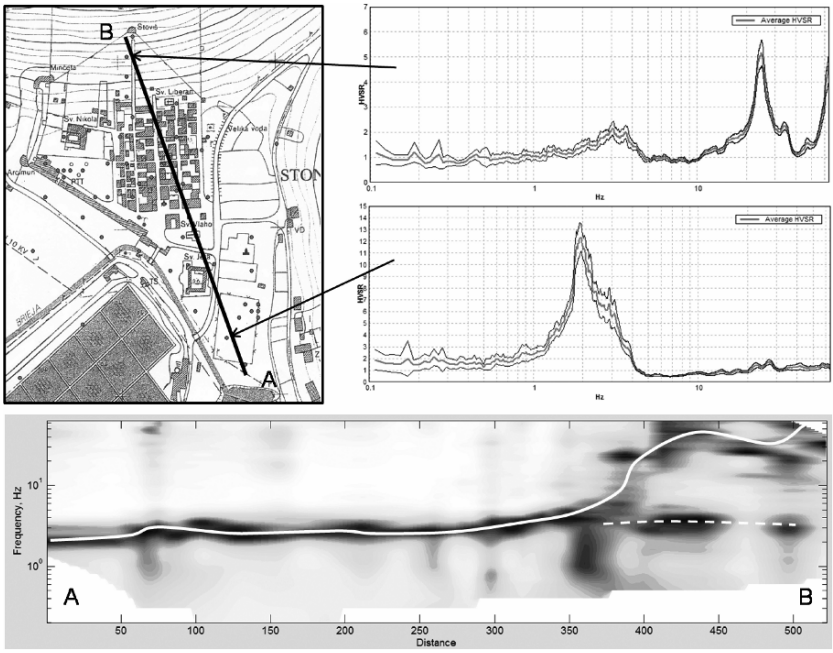

Fig. 4.3.2 *Top left*: Map view of the town of Ston (southern Dalmatia). Black dots show the locations of measurement points. The Stoviš hill is in the north. The AB-line shows the location of the profile in the bottom. *Right*: Examples of the measured HVSR spectra (mean ± 1 standard deviation), showing typical results obtained at the hill and in the plane beneath. HVSR spectra in the southern part are all characterized by a single pronounced peak in the range 2–4 Hz. The locations up the hill, situated practically on the bedrock are characterized by much higher dominant frequencies, well above 10 Hz. *Bottom*: HVSR profile AB. Only measurements within 80 m from the profile line are considered. Dark shades correspond to high HVSR values. The lines are drawn to emphasize features, and have no direct geological interpretation

of the damage (VIII° EMS) caused by the 1996 earthquake whose epicentre was 20 km away.

Results obtained in Zagreb and Ston clearly confirmed applicability of the HVSR technique in cases of both thick and thin sedimentary covers, especially in determining the soil fundamental frequency. Based on preliminary measurements described above, ambient noise measurements are officially adopted to be used in the course of microzonation of Zagreb.

4.3.3 Measurements in buildings

An important aspect of the NATO SfP 980857 project was estimation of buildings' free periods of oscillation in order to asses each construction's potential for resonance with the soil layers it is founded on. As resonance effects will depend

also on the damping of the structure, it was of interest to compile a program that will simultaneously estimate periods of free vibrations and their respective damping from the records of ambient vibrations in buildings and in the free field. These efforts resulted in a collection of Matlab routines, assembled together in a graphical user interface (GUI) FREDA (FREquency–Damping Analyses). The GUI is shown in Figure 4.3.3. Main features of FREDA include:

- Plain ASCII files of ambient vibration time-histories as input.
- Instrument corrections (for displacement and velocity).
- Correction for the reference spectrum (excitation signal).
- Five modes of analyses:

(A) *Time domain*:
  – Slightly modified nonparametric analyses (NonPaDAn, Mucciarelli and Gallipoli, 2007)
  – Bandpass NonPaDAn

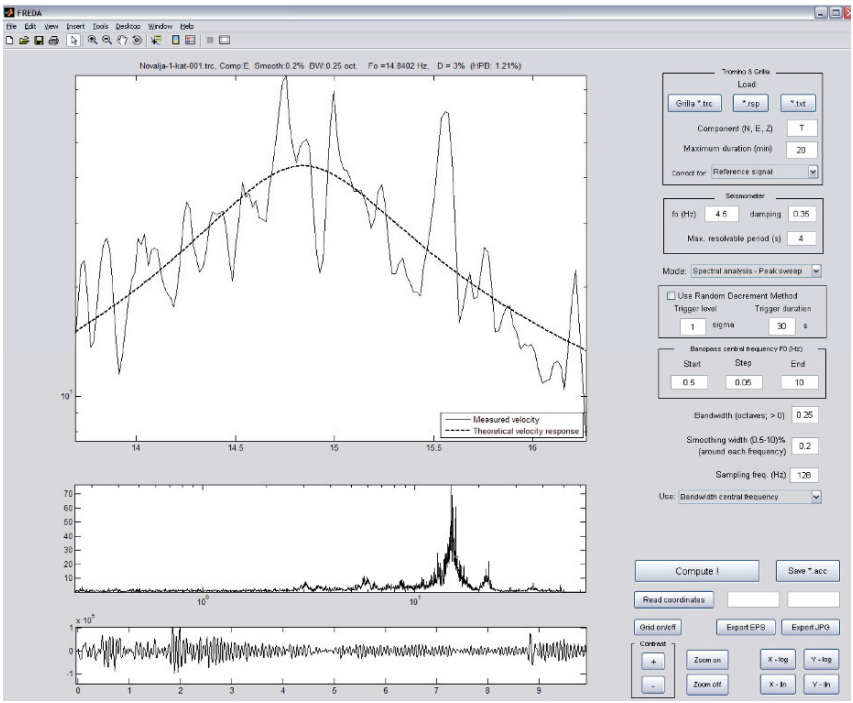

Fig. 4.3.3 FREDA graphical user interface (GUI), showing an example of the spectral single-peak transfer function analyses. The bottom subplot shows the first 10 s of the 20 min long measured noise time series of the transversal horizontal component of the building vibrations induced by ambient noise. Above it is its Fourier spectrum divided by the spectrum of the free-field noise. The main window shows the blow-up of the selected peak and the best fitting SDOF theoretical response. All controls for choosing the mode of analyses and various parameters are in the right part of the GUI

(B) *Frequency domain*:
- Spectral single-peak transfer function analyses
- Spectral sweep transfer function analyses
- HVSR

- Each analysis mode may also be used with the *random decrement* (Cole, 1971) signature of the signal as input.
- Uses real or synthetic signals.
- Output graphics (eps, jpg).

The program has been tested extensively using synthetic signals as well as measurements on many building types. As an example, Figure 4.3.4 presents spectral peak-sweep analyses of a synthetic signal generated by superimposing responses

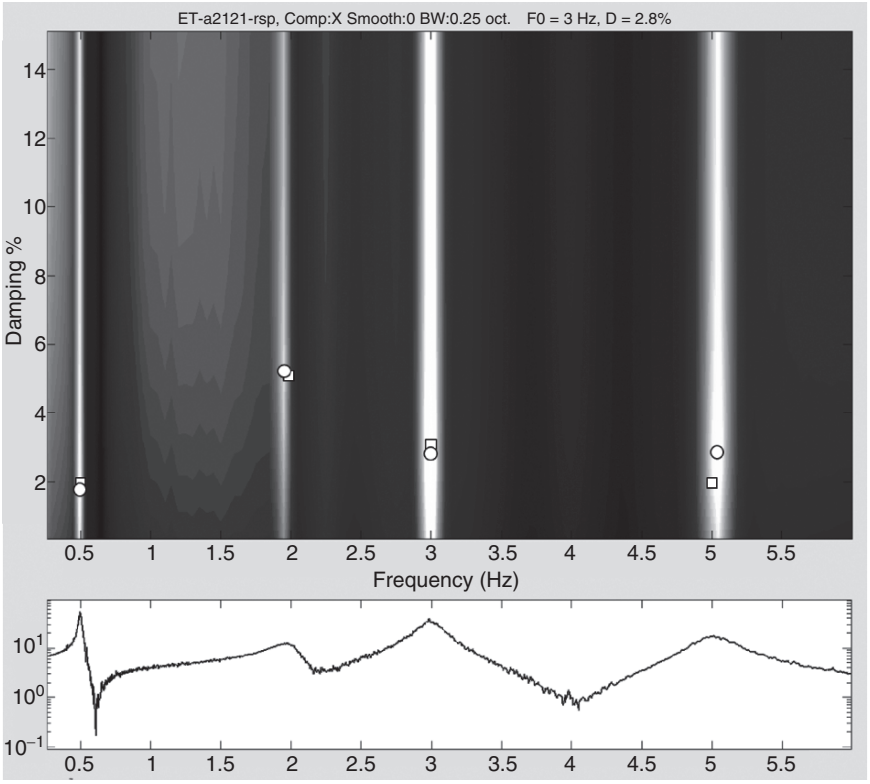

Fig. 4.3.4 Spectral sweep transfer function analyses of the synthetic signal simulated by superimposing time-domain responses of four SDOF systems excited by a real microseismic noise record. The method involves finding the best-fitting theoretical SDOF response for a number of frequency windows that are 'swept' along the observed spectrum (bottom graph). In the top subplot (frequency on the abscissa, damping on the ordinate), the light shades mark the best fits of theoretical responses. The local maxima of the frequency-damping surface are accentuated by white circles. White squares are the 'true' frequencies and damping of the four assumed SDOF oscillators

of four single-degree-of-freedom (SDOF) systems, driven by a real ambient noise time-series as recorded at a location in Zagreb. As can be seen, the 'true' (squares) and measured (circles) frequencies and damping agree very well. Similar analyses have been done using other FREDA modes and different synthetic signals generated under assumption of white-noise or realistic excitation. The comparison of results reveals that estimates of frequencies and damping obtained by spectral methods are in general more robust and less dependent on parameters of the respective algorithm, than the results based on time-domain analyses. Spectral algorithms are also much better in resolving higher modes. The random decrement method is in most cases found to be inferior to spectral or band-pass procedures using original signal.

In particular, the use of HVSR is not recommended, although it may yield reasonable frequency estimates in some instances. However, there is no theoretical basis for its application as we can not safely assume that horizontal and vertical spectra do not differ at the ground level. This is especially dangerous if soil amplification is significant (with prominent HVSR peaks), in which case the free-field HVSR may contaminate building response, leading to false identification of possible resonance. All subsequent analyses were done using spectra of vibrations measured in the building, divided by the corresponding spectra of excitation signal (microtremors recorded in the vicinity of the building).

Application to a real building is illustrated by an example of one of the highest skyscrapers in Zagreb (26 floors). Figure 4.3.5 shows FREDA analyses of recordings of the ambient-noise induced vibrations in the centre of the terrace at the top

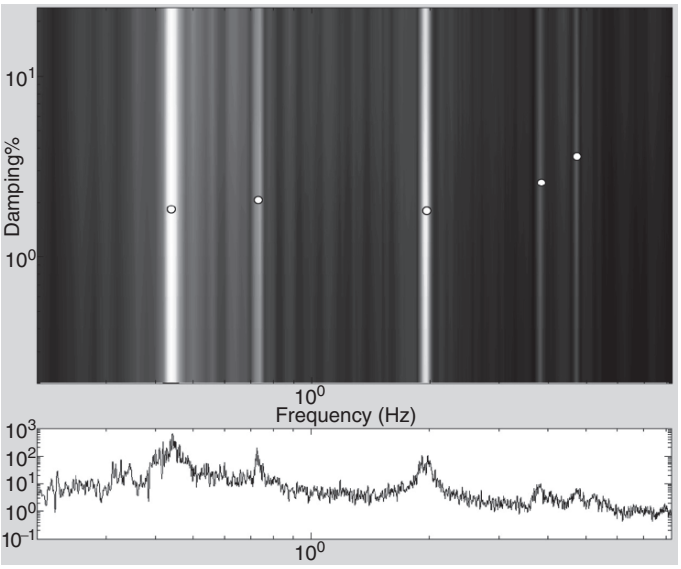

Fig. 4.3.5 Spectral sweep analyses of vibrations measured on top of the 26-storey skyscraper in Zagreb. The bottom plot is the amplitude spectrum of the horizontal component of recorded velocity. The top plot presents results, clearly marking at least five vibrational modes. See caption to Figure 4.3.4

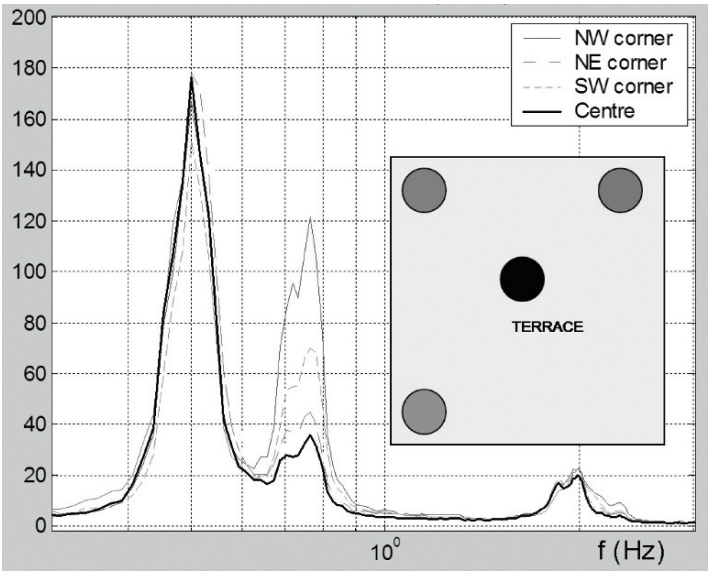

Fig. 4.3.6 Spectra of horizontal vibrations on top of the 26-storey building in Zagreb, measured simultaneously at three corners and in the middle of the terrace. Notice how the peak at 0.73 Hz is the only one whose amplitude varies with the location (and is the smallest in the centre), indicating a twisting mode

of the building. At least five modes are discernible, with the following frequencies (f) and damping (D, % of critical): $f_1 = 0.44\,\text{Hz}$, $D_1 = 1.0\%$; $f_2 = 0.73\,\text{Hz}$, $D_2 = 1.4\%$; $f_3 = 1.95\,\text{Hz}$, $D_3 = 1.6\%$; $f_4 = 3.83\,\text{Hz}$, $D_3 = 2.0\%$; $f_5 = 4.72\,\text{Hz}$, $D_3 = 3.0\%$. Comparing the spectra of vibrations simultaneously recorded at the corners and in the centre (Figure 4.3.6), suggests that frequency of 0.73 Hz corresponds to a predominantly torsional mode, as its amplitudes at corners are notably larger than in the centre.

Analyses as presented above were done on over 100 buildings in Croatia, most of them in Zagreb. We have checked the stability of measured spectra by repeated measurements during different times in a day, seasons, and weather conditions. Typical variation of estimated frequencies was found to be within a few percent. For damping the values varied not more than $\pm 1\%$ of the critical damping.

In order to gain more insight into the temporal variation of frequencies and damping, we are conducting continuous measurements in the building of the Department of Geophysics using two broad-band seismometers (Guralp CMG-40T), one in the ground floor, the other one on the second floor. The building has a simple, rectangular floorplan (Figure 4.3.7). Its skeleton is made of reinforced concrete (RC) beams lying on RC pillars, with only a few bearing walls. Most of the beams run in the transverse direction, thus making the building stiffer in the transverse (T) than in the longitudinal (L) direction. Consequently, the average fundamental frequency in the L-direction ($f_L = 4.34 \pm 0.05\,\text{Hz}$) is higher than in the T-direction ($f_T = 6.11 \pm 0.08\,\text{Hz}$), as clearly seen in the spectrograms presented in Figure 4.3.7.

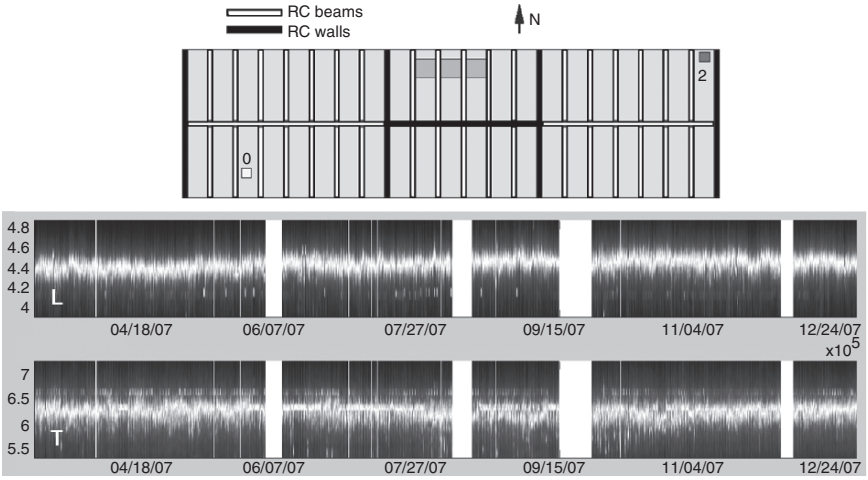

Fig. 4.3.7 *Top*: Simplified floor-plan of the building of Department of Geophysics in Zagreb. The two instruments are located in the ground floor (white square) and on the second floor (dark square). All internal walls, except the two bearing walls, are made of light infills. *Bottom*: The spectrograms showing temporal variation (300 days, 1 h resolution) of the spectra of building vibrations measured on the second floor in the longitudinal (E–W), and the transversal (N–S) direction, zoomed around the dominant frequency and normalized by the maximum in each hour

As we do not have continuous free-field measurements, all interpretations are done on spectra 'as measured', with no correction for the free-field input spectrum. Fortunately, this did not introduce serious errors, because free-field noise measurements indicate that both f_L and f_T lie far away from the characteristic soil frequencies, and excitation level of the ambient vibrations is nearly uniform in the bandwidth of interest around them.

Figure 4.3.8 shows observed variation of the fundamental frequencies with the rms velocity amplitude in the respective hour. For the L-component, behaviour is more-or-less as expected, showing slight frequency decrease with the increase of the level of excitation. For the T-component the variation is relatively smaller and more complicated, with no monotonic dependence on the amplitude. Damping values (Figure 4.3.9) are rather stable, with the averages of $D_L = 3.91\% \pm 0.66\%$ and $D_T = 8.24\% \pm 0.99\%$ of critical damping.

4.3.4 Conclusions

Recent measurements of the free-field microtremors in Croatia proved to be valuable in providing additional insight into the geotechnical properties of the soil, especially in constraining the fundamental frequency of sedimentary deposits. Measurements of ambient vibrations in buildings were shown to be efficient and quick, yielding reliable, accurate and temporally stable estimates of frequencies and damping of the

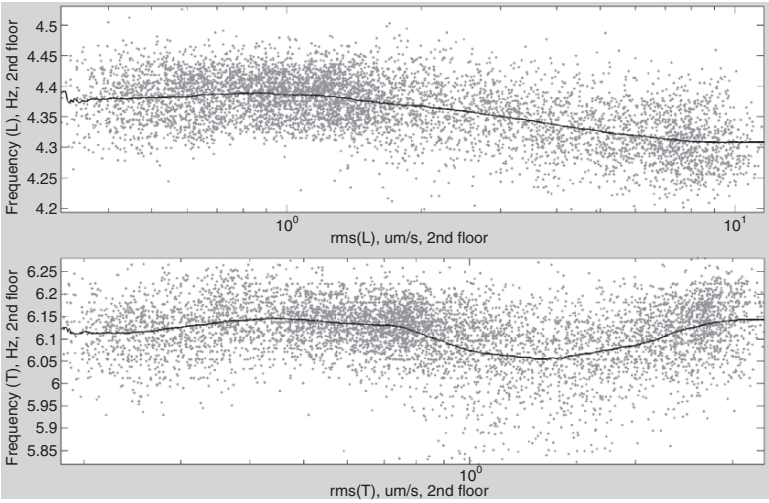

Fig. 4.3.8 Dependence of the fundamental frequency of the Department building on the rms level of vibrations due to ambient noise

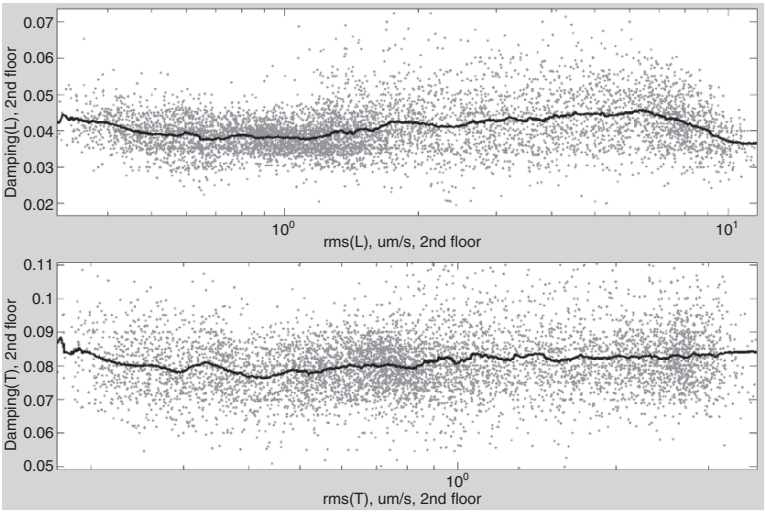

Fig. 4.3.9 Dependence of the damping (% of critical) of the Department building on the rms level of vibrations due to ambient noise

buildings' vibrational modes. Combining the free-field measurements with those within houses and other structures can point to constructions likely to exhibit soil-structure resonance. The measurements done so far form initial nucleus of the building inventory, a collection of fundamental periods, damping, spectral shapes, and other data which can prove important in documenting buildings' structural integrity and assessing the degree of possible damage in future earthquakes.

References

Cole H A (1971) Method and apparatus for measuring the damping characteristic of a structure. United State Patent No. 3,620,069.

Kanai K (1957a) Semiempirical formula for the seismic characteristics of the ground. Bull Earthq Res Inst 35:309–325.

Kanai K (1957b) The requisite conditions for predominant vibration of ground. Bull Earthq Res Inst 35:457–471.

Marković B (1948) Microseismic noise in Zagreb (Mikroseizmički nemir u Zagrebu). Rad Geofizičkog zavoda u Zagrebu II/l:87pp (in Croatian).

Mucciarelli M, Gallipoli R M (2007) Non-parametric analysis of a single seismometric recording to obtain building dynamic parameters. Ann Geophys 50:259–266.

Nakamura Y (1989) A method for dynamic characteristics estimation of subsurface using micro-tremor on the ground surface. Quart Rep Railway Tech Res Inst 30:25–33.

Chapter 4.4
Applications to World Heritage Sites

Yutaka Nakamura, Jun Saita, and Tsutomu Sato

It is important for the countermeasure against earthquake damage not only to learn the earthquake damage history, but also to grasp exactly the vulnerability of ground and structures.

Especially, the historical structures as the world heritages are usually exposed under the dangerousness of the damages caused by the earthquake motion because of the hidden weak points with long history. In general, it is difficult to inspect or understand the behavior of such kind of structure because of the complex structure, no design plan and so on. And also, it is impossible to get test pieces or oscillate the structure. So it is useful to use microtremor as a tool to inspect the structures and understand the dynamic characteristics.

The microtremor, ambient noise, exists anywhere and the microtremor measurement requires no long time and any vibrators so there is no possibility to injure the measuring objects. So it is useful and applicable for the inestimable facilities like the world heritages. Recently, the H/V spectral ratio is popular for the vulnerability investigation of both ground and structures because the H/V spectral ratio can show the predominant frequency and the amplification characteristics. And some indices as the K values are introduced for the vulnerability index.

Here shows some result of the vulnerability assessment of mainly the world heritages and the surrounding area using the microtremor. And some of them show the changes before and after the damaging earthquake and the stability of long time span.

Y. Nakamura
President, System and Data Research Co., Ltd., Tokyo, Japan
Visiting Professor, Department of Built Environment, Interdisciplinary Graduate School of Science and Engineering, Tokyo Institute of Technology, Japan

J. Saita (✉) and T. Sato
Senior Research Engineer, System and Data Research Co., Ltd., Tokyo, Japan

M. Mucciarelli et al., (eds.), *Increasing Seismic Safety by Combining Engineering Technologies and Seismological Data,* NATO Science for Peace and Security Series C: Environmental Security,

4.4.1 Old walled city of Manila, Philippines

4.4.1.1 Overview of the measurement

The study area Intramuros, the old walled city of Manila, frequently suffered earthquake damage in the past (Su, 1969; Omote et al., 1969). Although the 1990 Luzon earthquake occurred about 120 km away from Manila, it caused considerably damage to some 15 RC-buildings in the metropolis. After the earthquake, microtremor measurement was conducted to compare with the damage (Ohmachi and Nakamura, 1992). The results of the microtremor measurement in after the 1990 earthquake show that the low frequency values of around 1 Hz with the amplification factor as high as 3–8 predominated in the reclaimed area where the earthquake damages were also rather serious. Meanwhile, to verify stability of microtremor through time, a series of microtremor measurements were conducted by this study from 2002–2003.

Figure 4.4.1 shows the distribution of measurement points in the study area. In and around this area, there were ten points surveyed in 1990 (shown by red circles), 14 points in 2002 (shown by blue circles) and 30 points in 2003 (shown by green circles). Some points were resurveyed in 2002 and 2003 for the purpose of comparing results of the 1990 survey.

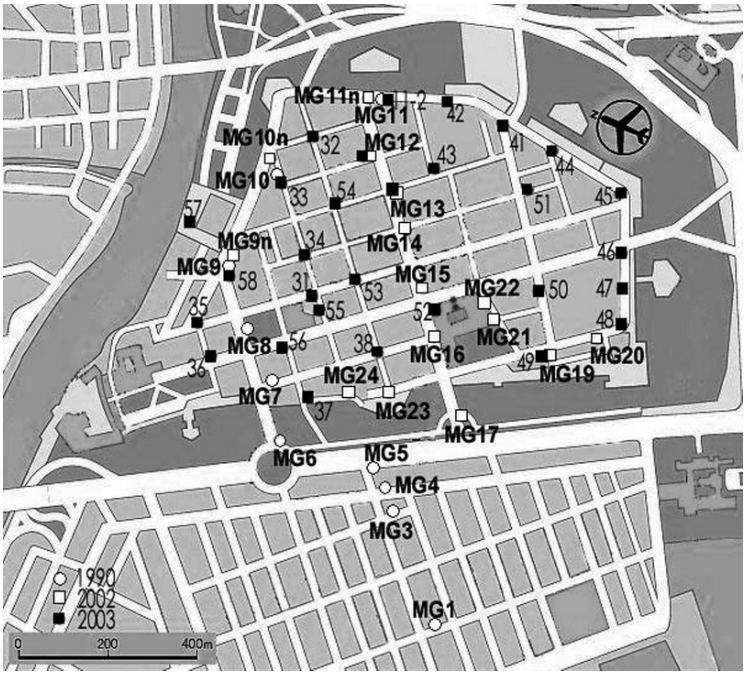

Fig. 4.4.1 Distribution of measurement points

At each site, microtremor was recorded for 4,096 samples in 100 Hz sampling. This procedure was repeated three times for each site. This methodology was also adopted for the 1990, 2002 and 2003 measurements. There were also five sites done during the 1990 measurements and one site during the 2002 measurement outside of the ancient wall.

4.4.1.2 The result of the microtremor measurement with long time span

Figures 4.4.2 and 4.4.3 shows the results of measurement in terms of the predominant frequency Fg (Hz) and the amplification factor Ag derived from the H/V spectral ratio of recorded microtremor.

The H/V spectral ratio was derived from the averaged horizontal to vertical Fourier spectral ratio. Smoothing was done using a Hanning window of 80 times (bandwidth is 0.4 Hz) for ground and 20 times (bandwidth is 0.2 Hz) for structures.

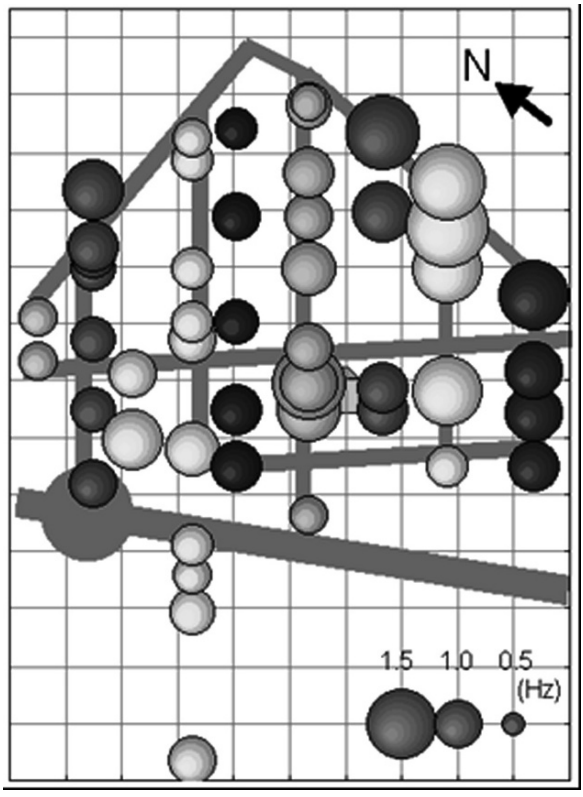

Fig. 4.4.2 Distribution of Fg

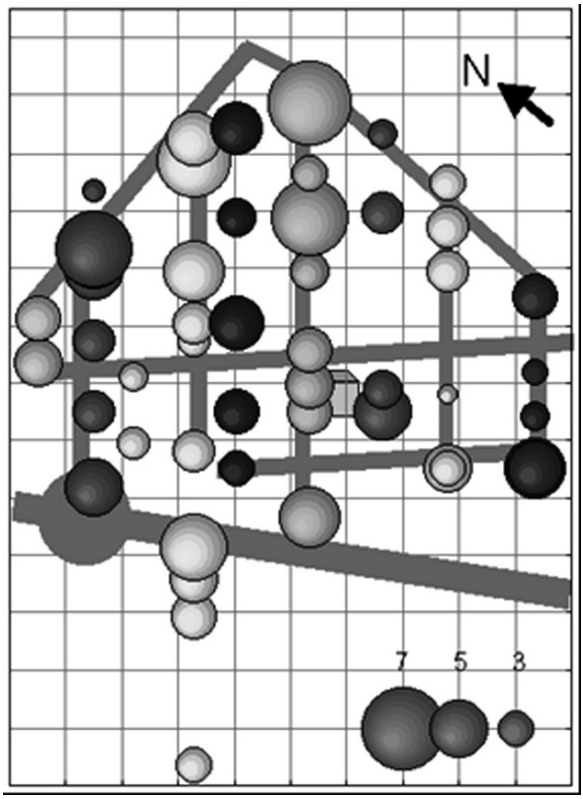

Fig. 4.4.3 Distribution of Ag

Figure 4.4.4 shows the comparison between Kg values and major damages of past earthquakes on detailed map. In Figures 4.4.2–4.4.4, the diameter of the circle indicates measurement point corresponds to Fg, Ag and Kg values.

When shear deformation at ground surface at the time of earthquake is set to δ_g, the strain of surface ground γ_g is expressed as follows (see Figure 4.4.5);

$$\begin{aligned}\gamma_g &= \delta_g/h \\ &= e \times a/(2\pi F_g)^2 \times 4F_g/V_s \\ &= e \times A_g \times a/(\pi^2 F_g V_b) \times V_b/V_s \\ &= \tfrac{A_g^2}{F_g} \times \tfrac{e \times a}{\pi^2 \times V_b} \\ &= K_g \times C \times a\end{aligned} \tag{4.4.1}$$

Where,

$$Kg = Ag^2/Fg \tag{4.4.2}$$

$$C = e/(\pi^2 \cdot Vb) \tag{4.4.3}$$

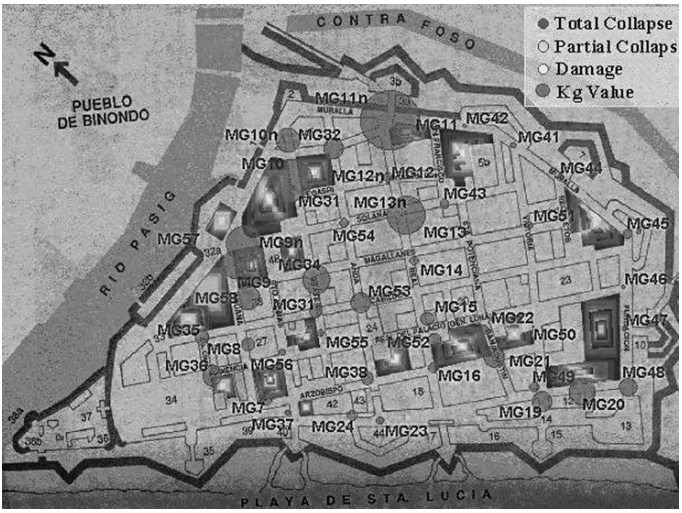

Fig. 4.4.4 Distribution of Kg value and damage history

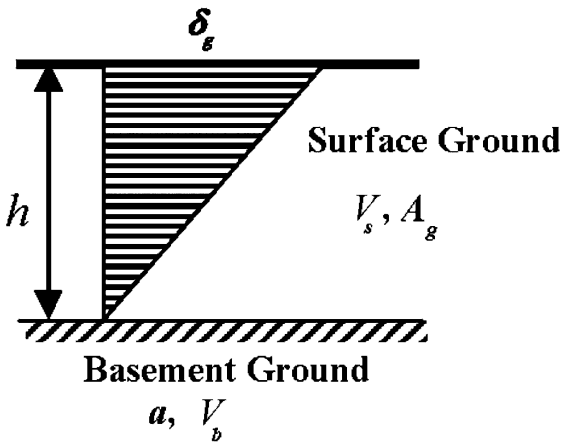

Fig. 4.4.5 Overview of Kg

A_g *and* F_g: Amplification factor $(=V_b/V_s)$ and Natural frequency $(=V_s/4h)$ of the surface

a and e: Maximum basement acceleration (Gal) and Efficiency of it
V_b and V_s: S-wave velocity (m/s) of basement and surface ground
h: thickness of surface ground

Although the predominant frequency is almost stable for the study area, amplification factors show variation. Three sites (MG5, MG6 and MG17) show high Kg values. These are located on the reclaimed land near the ditch. Meanwhile, MG1, MG3 and MG4 have relative low Kg value. It seems that it depends on the age of reclaimed area.

Three points MG9, MG10 and MG11 conducted in 1990 locate close to MG9n, MG10n and MG11n conducted in 2002, respectively. By comparing with the results, MG9 and MG10 give approximately similar frequency and amplification. However, in the case of MG11, the shapes of spectrum are almost similar, but the peak values differ from each other. We investigated the possible cause and we found out that a sewer has recently been constructed near this observation site. The operation of this structure may have caused the change of site condition.

4.4.1.3 Comparing with the detailed damage and microtremor

Figure 4.4.6 shows the overview and damage situation of San Agustin Church after the July 18, 1880 earthquake, located inside Intramuros and considered as one of the world heritage sites in the world. This church repeatedly suffered the earthquake damage. Figure 4.4.6b shows its picture in 1880 after this earthquake caused one of the bell towers to fall.

Around this church, microtremor was measured at points MG15, MG16, MG21 and MG22. Since depth of soil layer is another important criterion for determining earthquake damage, we tried to determine the estimated depth of soil layer using the same methodology for 2.3. Figure 4.4.7 shows the soil profile one block away from the church (Dy, 2000). By comparing the depth with the soil profile, it seems that the estimated depth of the surface layer corresponds to the fine-grained sand layer at 34 m depth.

Figure 4.4.8 shows that the base ground is leaning and the deepest site is MG15, close to the left (lost) tower of this church. The influence of the base ground inclination is considered to be a large factor for estimating the potential damage of this structure. However, considering that other building abuts on another surviving tower, it is supposed that the influence of an adjoining building is also large. In order to clarify such a damage factor, a thorough understanding of the dynamic characteristic of the ground and the characteristic of the structures are necessary.

To grasp the dynamic characteristics in detail, microtremor measurement was also conducted inside the church, both for the main building and the bell tower shown in Figure 4.4.6. Here the height of the main building and the bell tower assumed to 12 and 8 m, respectively. Measurement points were installed on the grand floor and the top for the main building and on the bottom, middle and top of the bell tower.

From the microtremor on the ground, the predominant frequency and amplification factor is a little higher than 1 Hz and 2–4, respectively, so Kg value is less than 20.

Figure 4.4.9 is the mode diagram for the main building, the tower and unified of the main building and the tower.

The predominant frequency of the main building is around 3 Hz in general for both HL and HT direction. Here HL and HT direction corresponds to the direction along the longitudinal and transverse axis of the main building, respectively. But in

(a) present condition

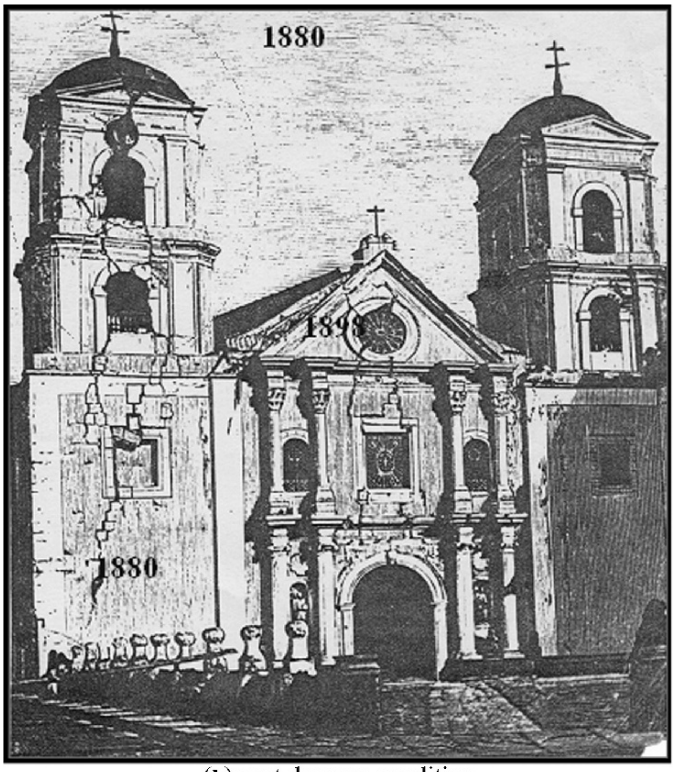

(b) past damage condition

Fig. 4.4.6 Overview of San Agustin Church (**a**) present condition (**b**) past damage condition

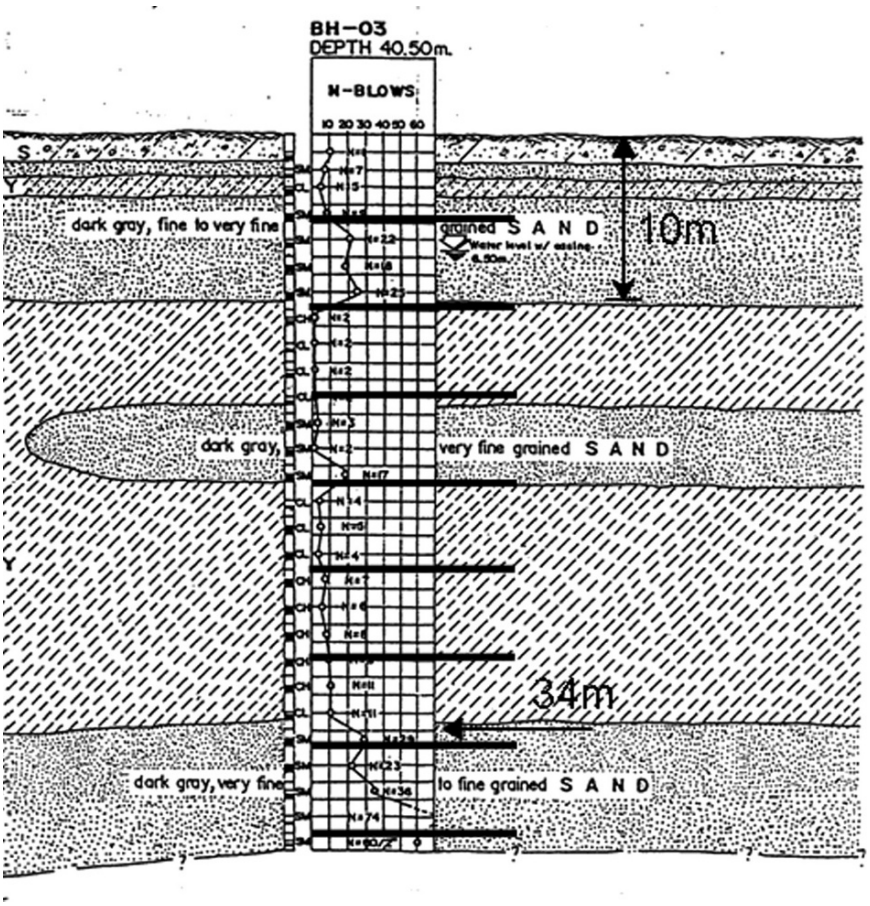

Fig. 4.4.7 Soil profile around San Agustin Church

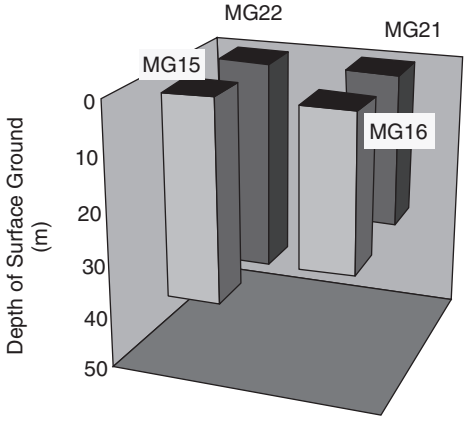

Fig. 4.4.8 Estimated depth of surface ground

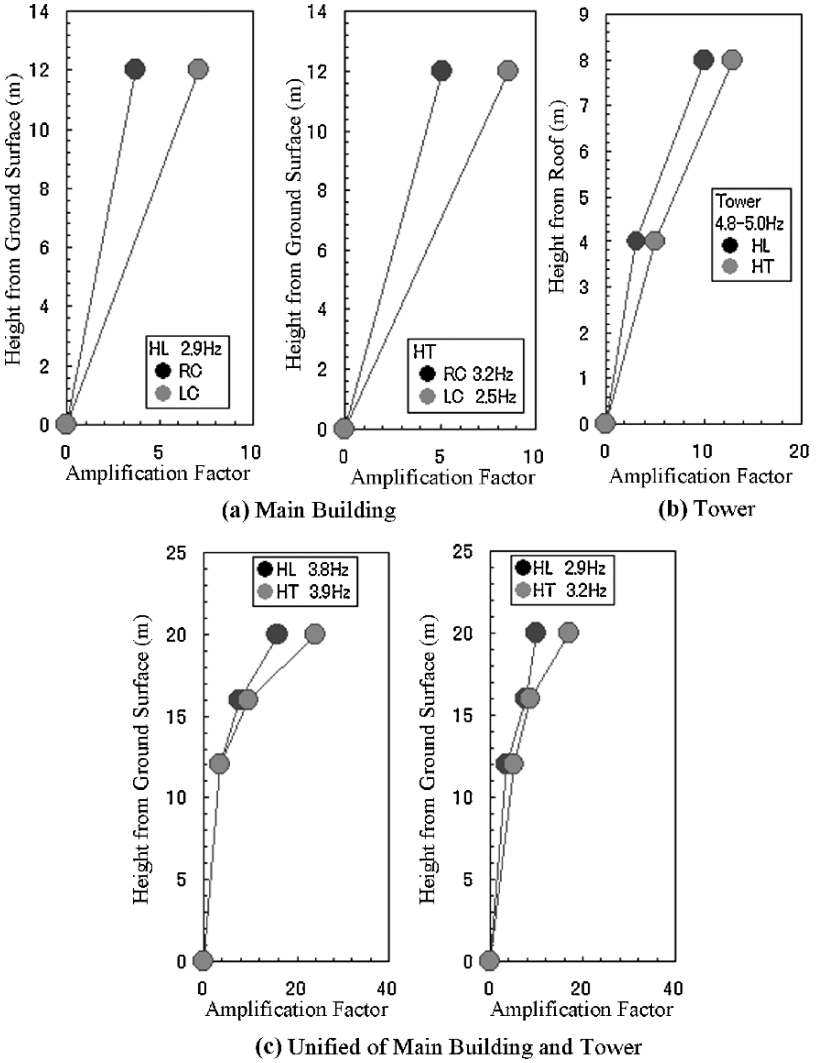

Fig. 4.4.9 Mode diagrams of San Agustin Church (**a**) main building (**b**) tower (**c**) unified of main building and tower

detail, in case of HL direction, predominant frequency is 2.9 Hz for both left and right side but the amplification factor of left side is several times more than that of right side. In case of HT direction, predominant frequency is 3.2 and 2.5 Hz for left and right side, respectively, and the amplification factor of left side is 5 or more than that of right side. Of course it is impossible to avoid the effect of the dead load to keep the balance for the lost left tower, it seems to be damaged on the left side. On the tower, there are two predominant frequencies, around 3 Hz and less than 4 Hz. Former seems to be the characteristics consist of the main building and the

tower. Latter is thought as the characteristics effected by the tower. For both cases, HT component has high amplitude two times or more than HL component, and the damage had been caused toward this direction.

4.4.1.4 Short summary

Here shows the microtremor measurement and vulnerability index can explain past earthquake damages. The results also show that microtremor measurements provide almost stable results with long time span. This technique can be used to identify possible areas or structures that may be damaged in the future by earthquakes. At the same time, the technique can be used for monitoring a structure's state of health through time.

4.4.2 Istanbul, Turkey

4.4.2.1 Overview of the measurement

Istanbul, Turkey has long history with many earthquake disasters. Considering the geotectonic environment and historical importance of Istanbul, it is necessary to investigate the dynamic characteristics of the historical constructions in the city and to work out rational and effective countermeasures to the earthquake disasters. Since autumn 1998, microtremor measurements have been started to investigate the dynamic characteristics of several structures in Istanbul.

In August 17, 1999 the Kocaeli Earthquake (Mw = 6.7) occurred and caused severe damage in the epicentral area. Although Istanbul is approximately 100 km away from the epicenter and was not suffered serious damage, this earthquake might affect some old structures. We have investigated some historical structures before and after the earthquake. Here, the influence of the Kocaeli earthquake is considered focusing on the shift of the natural frequency of structures. In Istanbul, although only 41 Gal in PGA was observed at YPK site (Yapi Kredi Plaza strong motion station of Kandilli observatory), comparison of the results of an investigation before and after the earthquake shows the natural frequency are shifted lower several percent for both old and new structures. This frequency shift corresponds to the vulnerability index against the earthquake disaster for structures (Nakamura, 1997).

Microtremor measurement was conducted for historical structures as Suleymaniye mosque, Hagia Sophia museum, Sehzade mosque, and newly constructed office building as a reference. Figures 4.4.10–4.4.13 show the overview, floor plan and elevation with measurement points, and Table 4.4.1 shows the details of the structures as height, structural type, established year and the date of measurement.

Measured historical structures have a main dome supported by four arches on four big piers. In case of Suleymaniye mosque and Hagia Sophia museum, a pair of

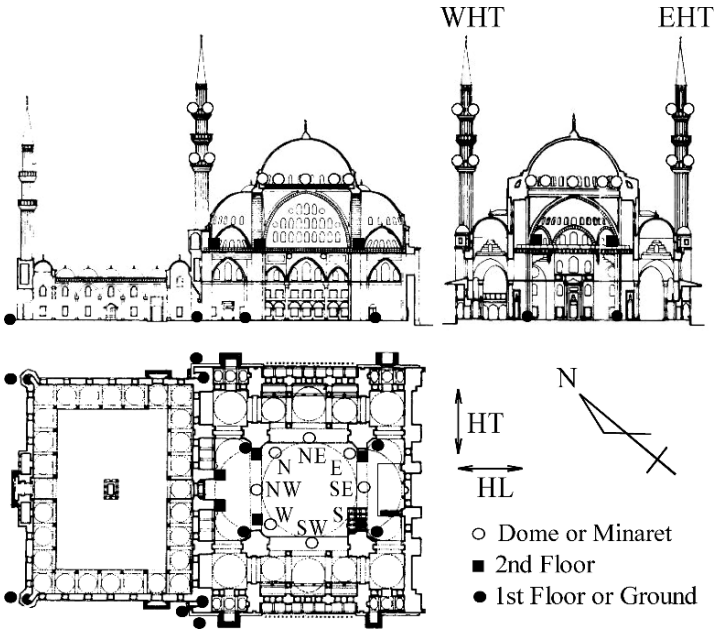

Fig. 4.4.10 Overview of measurement at Suleymaniye

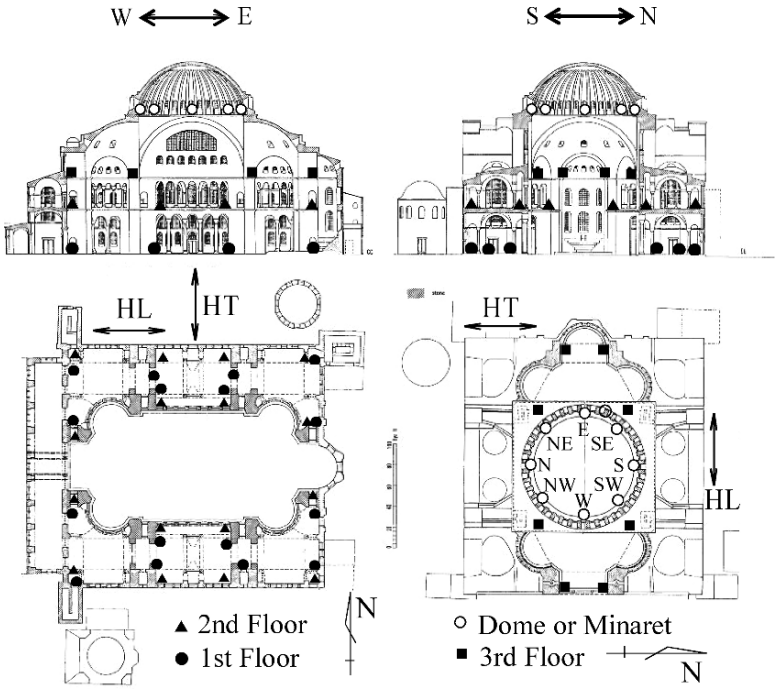

Fig. 4.4.11 Overview of measurement at Hagia Sophia

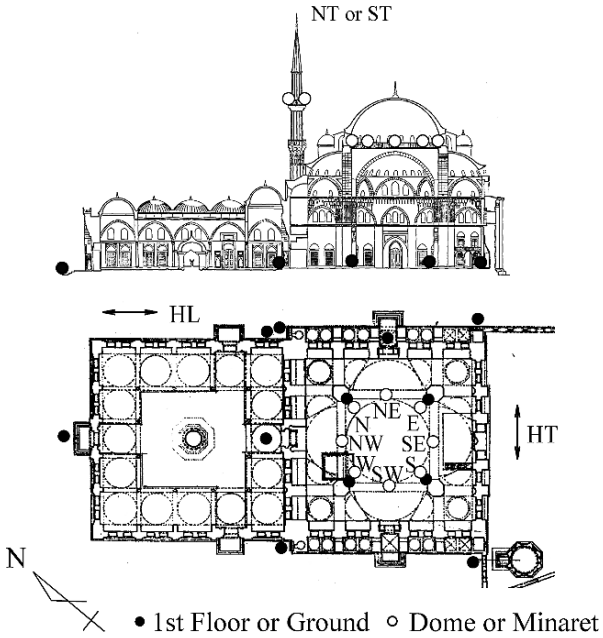

Fig. 4.4.12 Overview of measurement at Sehzade

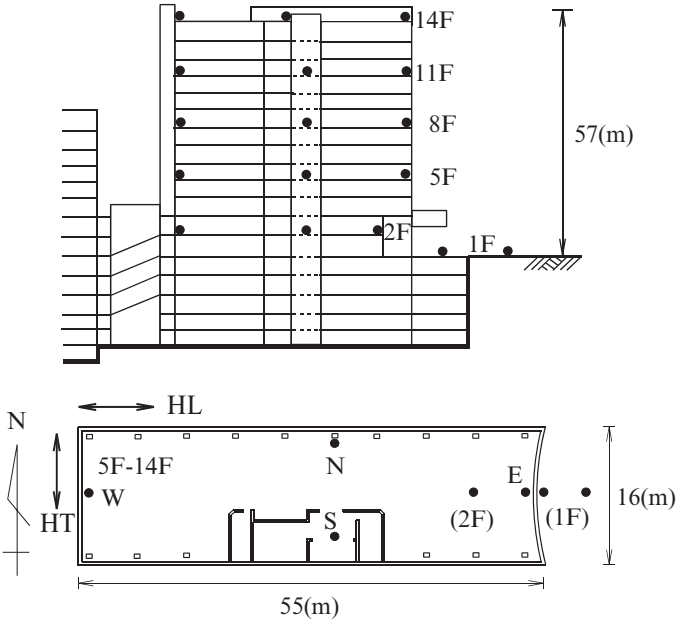

Fig. 4.4.13 Overview of measurement at an office building

Table 4.4.1 Dimensions, completion year and etc. of measured structures

Name of building	Suleymaniye Mosque	Hagia Sophia Museum	Sehzade Mosque	An office building
Height	53 m	56 m	37 m	57 m
Dimensions of a plane	68 × 63 m	95 × 70 m	50 × 43 m	57 × 16 m
Diameter of main dome	27 m	31 m	18 m	–
Structural type	Stone	Stone and brick	Stone	RC (14F + 5BF)
Completion year	1550 AD	512 AD	1543 AD	1999 AD
Date of measurement before the earthquake	19 and 21 October, 1998	8 and 9 June, 1999	6 June, 1999	11 June, 1999
Date of measurement after the earthquake	7 September, 1999	3 and 4 September, 1999	10 September, 1999	2 September, 1999
Measured floors	1F, 2F, DM	1F, 2F, 3F, DM	1F, DM	1F, 2F, 5F, 8F, 11F, 14F

opposite arches is reinforced by two semi domes. In case of Hagia Sophia museum with a main dome of diameter of 31 m, the spaces beneath the arches are filled as a wall and the dome looks like supported by the walls instead of arches. The internal space of Hagia Sophia museum is 30 m width and 80 m length. The main dome has been affected by earthquakes several times and restored each time. On the whole, the structure has deteriorated considerably and a certain countermeasure has been required.

The four arches of Sehzade mosque supporting main dome are supported by four semi domes. Sehzade mosque is an etude of an architect Sinan (1490–1588), and he adopted the structure for the main dome to be supported by four semi domes. And also the Suleymaniye mosque is one of the highest masterpieces of his maturity. The basement ground for historical structures mentioned above is hard and good conditions.

An office building made by Reinforced Concrete (RC) structure is 14 storied building with 5 underground levels. Each floor has the 55 and 16 m rectangular section, and in the central part of the north side, there are service facilities such as elevators, stairs and so on. This building was constructed on good base ground close to YPK station, which recorded maximum acceleration 41 Gal at the time of Kocaeli earthquake.

4.4.2.2 Measurement and analysis

Microtremor measurement was done either one or two point individually for each structure. At this time, some measurement points were set for every floor

to understand the behavior of the structure. Besides of the main building, two minarets of both Suleymaniye and Sehzade mosque were measured.

Suleymaniye mosque has two high minarets and two low minarets. High minarets (WHT and EHT) were measured at the highest and lowest balcony of three balconies. Every balcony has four measurement points and a pair of them was measured simultaneously. Measurement was conducted at four measurement points only on the upper balcony. Moreover, about the base ground, measurement points were situated around the structures.

At every measurement point, microtremor was recorded three times with 1/100 s sampling and 40.96 s data length. After measurements, Fourier spectrum for each component is calculated from the waveform of whole length and three records are averaged. Each Fourier spectrum is smoothed by Hanning spectral window repeated 20 times as bandwidth to be approximately 0.2 Hz before averaging.

For representative spectra of the historical structures, these calculated spectra related to the four supporting columns for each floor and these calculated spectra eight points on the corridor of main dome (DM) for every component are averaged. And these spectra of minarets are averaged for representative spectra. In case of the office building, every three floor has four measurement points at the center of the each side of the floor, and these spectra are averaged for representative spectra.

The transfer function of each floor shall be presumed by the ratio of a representation spectrum between the floor and the ground floor. In addition, the ground floor is set to the first floor (1F).

It is considered that the vulnerability of structures against earthquake disasters can be estimated by the drift angle, related to the worked earthquake accelerationα in $\mathrm{cm/s^2}$. Here, α is a portion which affects this structure among whole earthquake motion a, namely,

$$\alpha = e \times a \tag{4.4.4}$$

where e shows the efficiency of earthquake motion working for this structure.

A deformation performance and the degree of earthquake motion amplification can be estimated from the dynamic characteristic of structures. Here, primary natural frequency of the structure seemed to have influence on earthquake damage is considered. Displacement δi of i-th floor is estimated from this primary natural frequency F and amplitude Ai of i-th floor as followings.

$$\delta i = Ai \times \alpha/(2\pi F)^2 \tag{4.4.5}$$

So, the drift angle γi of i-th floor is shown as,

$$\gamma_i = (\delta_{i+1} - \delta_i)/h_i \tag{4.4.6}$$

$$= \Delta A_i \times \alpha/(2\pi F)^2/h_i \tag{4.4.7}$$

$$= e \times Kbi \times a \tag{4.4.8}$$

where,

$$Kbi = \Delta A_i/(2\pi F)^2/h_i \times 10000 \tag{4.4.9}$$

ΔAi: difference of amplification of the i-th floor, $(= A_{i+1} - A_i)$, and

hi: the height of i-th floor in m.

Thus, the drift angle γi for each floor is estimate from vulnerability index K_{bi} multiplied by the maximum acceleration on the surface ground a in $\mathrm{cm/s^2}$ and the efficiency of earthquake motion e.

Here, ${}_{av}K_b$ value is derived as averaged K_{bi} for each structure for the discussion followings.

$$ {}_{av}K_b = A/(2\pi F)^2/H \times 10000 \tag{4.4.10} $$

where,

A: amplitude of the top floor, and

H: height of the structure in m.

In addition, when ${}_{av}K_b$ is substituted for K_{bi} of formula 4.4.8, averaged drift angle γ_{av} will be calculated. K_{bi} and ${}_{av}K_b$ are expressed in unit of 10^{-6}, 10,000 in formulas (4.4.9) and (4.4.10) is multiplied for adjustment.

4.4.2.3 Result of the analysis

Figure 4.4.14 shows the locus of microtremor at every measurement point on Sehzade mosque. It shows the locus of microtremor for 5 s in the circle to the position corresponding to every measurement point, and the amplitude of velocity (in $10^{-6}\,\mathrm{m/s}$) equivalent to the radius of a circle is shown near the circle. This figure shows that minarets seem to be vibrating extremer than the other structures. Moreover, the outline of the vibration mode for main dome can be grasped by this figure.

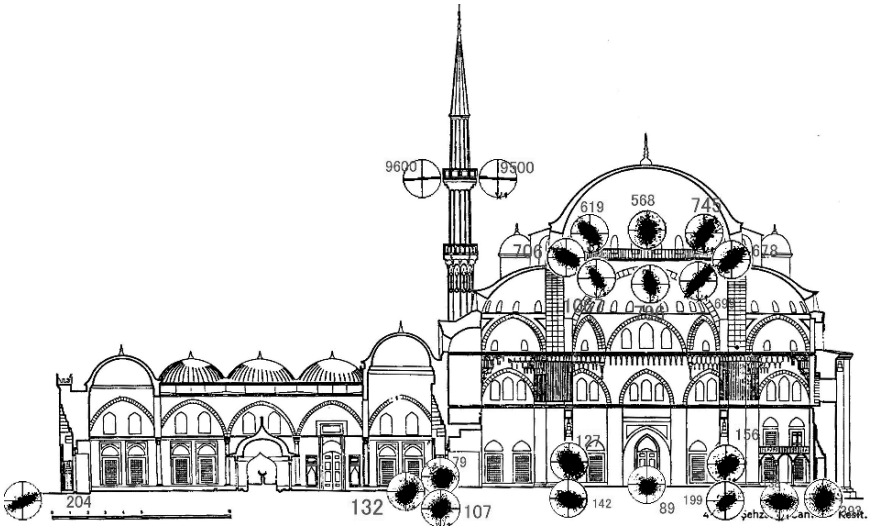

Fig. 4.4.14 Vibration locus of Sehzade

Figure 4.4.15 shows the transfer functions of the structure before and after the earthquake estimated from the result of microtremor measurement.

In case of Suleymaniye mosque, the peak near 0.8 Hz is significant on the corridor of the main dome (DM) only before the earthquake. And in case of Sehzade

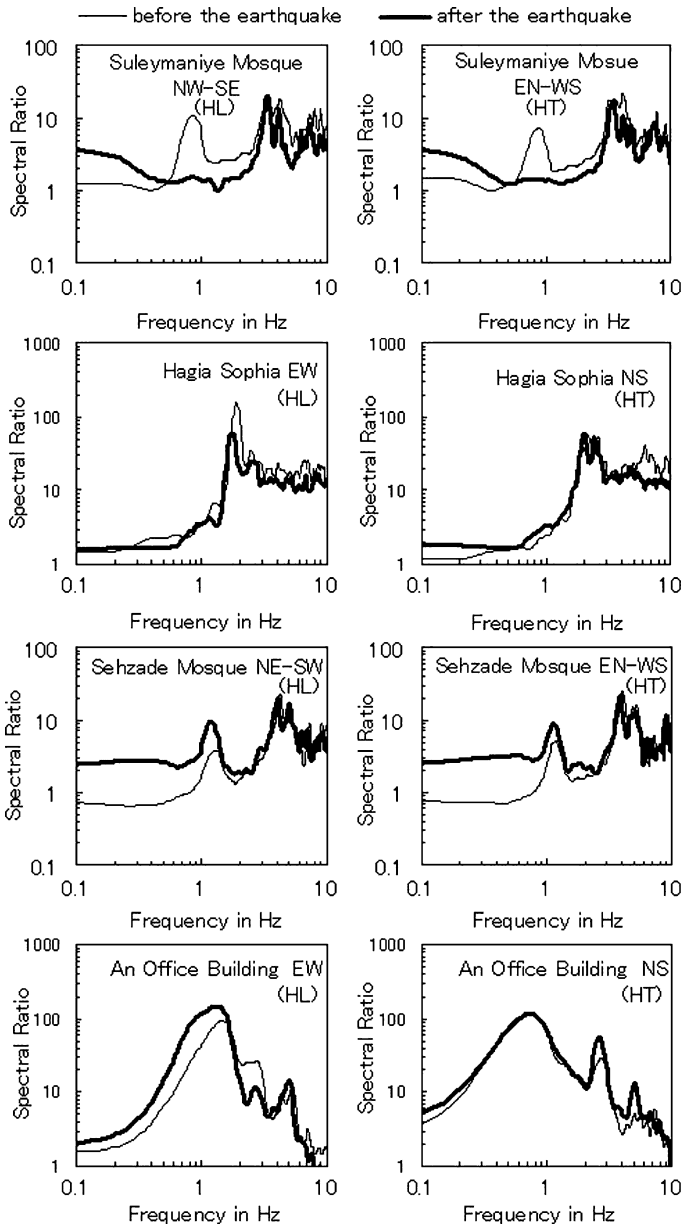

Fig. 4.4.15 Estimated transfer functions of the highest floor of structures

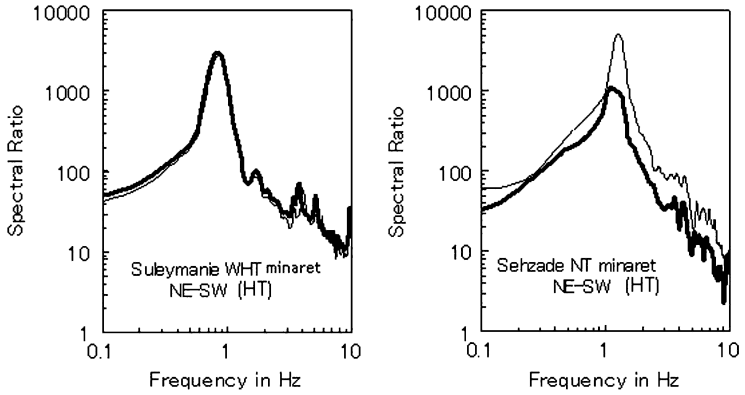

Fig. 4.4.16 Examples of estimated transfer function of Minaret

mosque, the peak value near 1.2 Hz increased after the earthquake. These peaks may correspond to the peak of minarets. Table 4.4.1 also shows the changes of the predominant frequencies and amplification factor of the estimated transfer functions before and after the earthquake for both horizontal components and torsion component, except the peak mentioned above. Measurement before the earthquake of a Suleymaniye mosque was performed in 2 days a total every other day. The day WHT minaret was measured was not windy and was a quiet day. However, the day DM and EHT minaret was measured was windy. So the amplitude of EHT minaret was the amplitude of ten times or more compared with it of WHT minaret (See Figure 4.4.16). From such a thing, neither 0.8 Hz vibration of Suleymaniye mosque nor 1.2 Hz vibration of Sehzade mosque transmitted from the foundation and it is guessed that the minarets were excited the influence of a wind and so on nor then was the vibration transmitted to the main dome.

Table 4.4.2 shows the natural frequency of transfer function at the top of the structure on each horizontal component and torsion vibration. In this table, the vibration seemed to be affected by the vibration of minarets are ignored. Additionally, this table includes the amplification factor. Furthermore, the change of natural frequency is also shown in a unit of the minimum frequency unit on analysis.

4.4.2.4 Discussion

Before and after the earthquake, the form of transfer functions shown in Figure 4.4.15 seldom change and the position of peak frequency has shifted, except the change of the lowest peak of the natural frequency seen in Suleymaniye and Sehzade mosque.

Minarets show the little change of the frequency and it is considered to be relatively healthier structure than the main body, except the NT minaret of Sehzade mosque.

Table 4.4.2 Change of the dynamic characteristics before and after the Kocaeli earthquake

(a) Suleymaniye

Main body		Before	After	dF/F (%)	dF
HL: NW-SE	F (Hz)	3.43	3.36	2.21	3.11
	A	20.5	20.2	–	–
	avKb (10^{-6})	11.0	11.4	–	–
HT: NE-SW	F (Hz)	3.55	3.46	2.78	4.04
	A	18.6	17.5	–	–
	avKb (10^{-6})	9.3	9.3	–	–
Torsion	F (Hz)	6.69	6.45	3.59	9.83
WHT Minaret		Before	After	dF/F (%)	dF
HL: NW-SE	F (Hz)	0.843	0.819	2.86	0.987
HT: NE-SW	F (Hz)	0.867	0.842	2.79	0.991
Torsion	F (Hz)	9.69	9.59	1.03	4.10
EWT Minaret		Before	After	dF/F (%)	dF
HL: NW-SE	F (Hz)	0.842	0.842	−0.01	−0.003
HT: NE-SW	F (Hz)	0.842	0.842	0.08	0.028
Torsion	F (Hz)	9.36	9.33	0.32	1.23

dF is frequency shift in unit ΔF, $\Delta F = 1/40.96\,\text{Hz}$.

(b) Hagia Sophia

Main body		Before	After	dF/F (%)	dF
HL: EW	F (Hz)	1.92	1.75	8.92	7.00
	A	156	60.5	–	–
	avKb (10^{-6})	261	122	–	–
HT: NS	F (Hz)	2.16	2.01	6.82	6.04
	A	54.6	59.6	–	–
	avKb (10^{-6})	72.0	90.5	–	–
Torsion	F (Hz)	3.32	3.10	6.63	9.01

dF is frequency shift in unit ΔF, $\Delta F = 1/40.96\,\text{Hz}$.

(c) Sehzade

Main body		Before	After	dF/F (%)	dF
HL: NW-SE	F (Hz)	4.06	3.87	4.78	7.96
	A	24.3	21.5	–	–
	avKb (10^{-6})	14.3	14.0	–	–
HT: NE-SW	F (Hz)	4.26	4.07	4.56	7.96
	A	23.0	20.2	–	–
	avKb (10^{-6})	12.3	11.9	–	–
Torsion	F (Hz)	5.25	5.00	4.76	10.2
ST Minaret		Before	After	dF/F (%)	dF
HL: NW-SE	F (Hz)	1.13	1.14	−0.12	−0.06
HT: NE-SW	F (Hz)	1.33	1.31	1.97	1.08
Torsion	F (Hz)	11.8	11.6	1.69	8.19
NT Minaret		Before	After	dF/F (%)	dF
HL: NW-SE	F (Hz)	1.15	1.10	4.26	2.00
HT: NE-SW	F (Hz)	1.27	1.12	11.5	6.00
Torsion	F (Hz)	11.4	11.0	3.51	16.4

dF is frequency shift in unit ΔF, $\Delta F = 1/40.96\,\text{Hz}$.

(continued)

Table 4.4.2 (continued)

(d) An office building

Main body		Before	After	dF/F (%)	dF
HL: EW	F (Hz)	1.45	1.33	8.38	4.99
	A	91.6	147	–	–
	avKb (10^{-6})	217	414	–	–
HT: NS	F (Hz)	0.720	0.745	−3.38	−0.999
	A	118	114	–	–
	avKb (10^{-6})	1,138	1,029	–	–
Torsion	F (Hz)	1.037	0.964	7.05	2.994

dF is frequency shift in unit ΔF, $\Delta F = 1/40.96$ Hz.

However, it is thought that the minarets themselves vibrated quite greatly. Especially in case of WHT minaret of Suleymaniye mosque, damage as shown in a Figure 4.4.17 has appeared in incidental facilities such as a roof. That is, buckling arises in the west side lower part of a cone-like roof, and the ornament at the top of the minaret is crooked on the east side.

Damaged WHT minaret is the one shows larger change of the natural frequency, and as a result, the change of the natural frequency and the damage grade of incidental facilities correspond.

Hereafter, a measurement result for every structure is examined.

1. Suleymaniye mosque
   As shown in Table 4.4.2, a natural frequency of horizontal NS-EW component of the main part was decreased to 3.36 Hz after the earthquake from 3.43 Hz before the earthquake. And that of EN-WS component was decreased to 3.46 from 3.55 Hz. These changes correspond to 3ΔF–4ΔF and are considered a significant change. These rates of the change are 2.21–2.78%, and are equivalent to about 5% of rigidity lowering generally. It is guessed that this is the reason of slight damage.

   The *avKb* value is also shown in Table 4.4.2. From the common relationship ship between an amplitude and RMS, it is possible to assume that the effective seismic motion is about 1/3 of the maximum acceleration. In this time it is assumed that the effective seismic motion is about 15 Gals and averaged drift angle will be presumed to be about 1/6,000. And it is considered that it was stand against this earthquake motion with the margin.
2. Hagia Sophia museum
   As shown in Table 4.4.2, a natural frequency of horizontal NS component was decreased to 1.75 Hz after the earthquake from 1.92 Hz before the earthquake. And that of EW component was decreased to 2.01 from 2.16 Hz. These changes correspond to 6ΔF–7ΔF and are considered a significant change. These rates of change are 8.92% (EW component) – 6.82% (NS component), and are equivalent to about 13–17% of rigidity lowering. As a result, this might be affected slightly. The *avKb* value is also shown in Table 4.4.2. As mentioned above, it is possible to assume that the effective seismic motion is about 15 Gals and the averaged

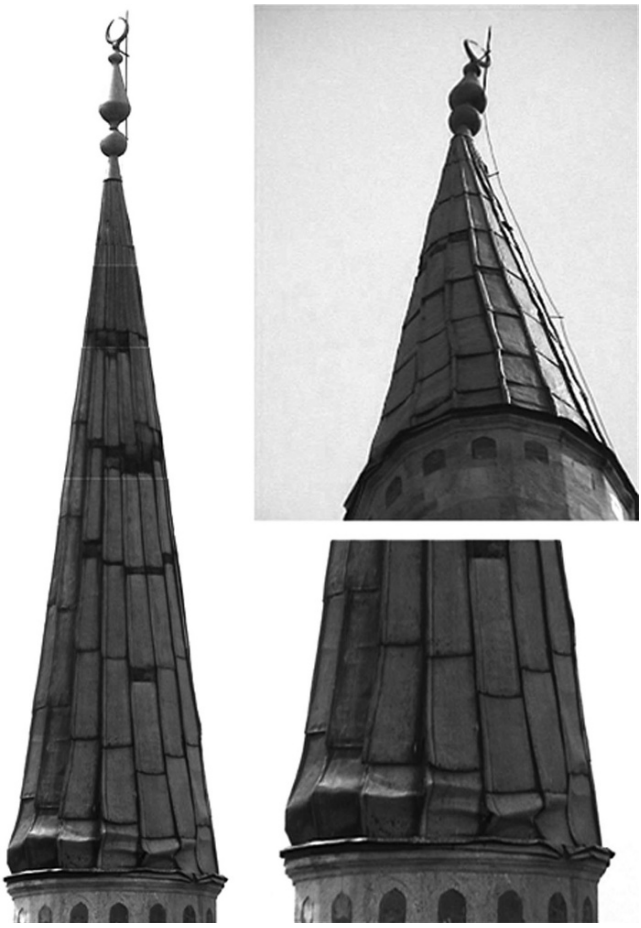

Fig. 4.4.17 Damage of WHT Minaret of Suleymaniye

drift angle will be presumed to be about 1/250. Generally it is thought that a structure begins to collapse on 1/100–1/200 of drift angle. It is considered that it was stand against this earthquake motion without so much margin, and for this reason, it is thought that the significant decrease of natural frequency occurred.

3. Sehzade mosque
   According to the result of the measurement at the base of the four main pillars and the dome corridor equivalent to the upper part, predominant frequencies change from 4.14 and 4.00 Hz before the earthquake to 3.93 and 3.80 Hz after the earthquake for NS and EW component, respectively. These changes correspond to 8ΔF–9ΔF and are considered a significant change. These rates of change are about 5%, and are equivalent to about 10% of rigidity lowering generally. As mentioned above, it is possible to assume that the effective seismic motion is about 15 Gals and the *avKb* value in Table 4.4.2 shows that averaged drift angle

will be presumed to be about 1/5,000. It is considered that it was stand against this earthquake motion with the margin.

Moreover, it is conformed that natural frequency changes quite remarkable in NT minaret of Sehzade mosque, and it is shown that damage by the earthquake was relatively larger than ST minaret. In addition, NT minaret is said to have been damaged before the earthquake.

4. An office building

In case of an office building, on the vibration of NS component and torsion, the changes of predominant frequency correspond to less than 1ΔF and are not considered a significant change. Considering that this building has a shape as extremely short flat form in the NS component, rocking vibration excels in vibration of the NS direction. And it is thought that the rigidity of the base is more strongly reflected rather than the rigidity of the building main part. The natural frequency of the NS component did not change before and after the earthquake and it suggests that the earthquake has not influenced the base at all.

On the other hand, it is supposed that the vibration of EW component reflects the rigidity of the building itself. The changes of predominant frequency correspond to 5ΔF and are considered a significant change. These rates of change are about 8.4%, and are equivalent to about 15% of rigidity lowering.

It seems that the damage of the frequency shift can be considered as the expression of the damage degree. Figure 4.4.18 shows the relationship between *avKb* value and the rate of frequency change. The relation between *avKb* and the frequency shift rate suggests *avKb* can be given as damage degree before the earthquake.

Figure 4.4.18 shows that large *avKb* correspond to larger damage in general. Both Suleymaniye and Sehzade mosque have same structure and Hagia Sophia museum is also same kind of structure. On the other hand, the office building has different characteristics as RC structure.

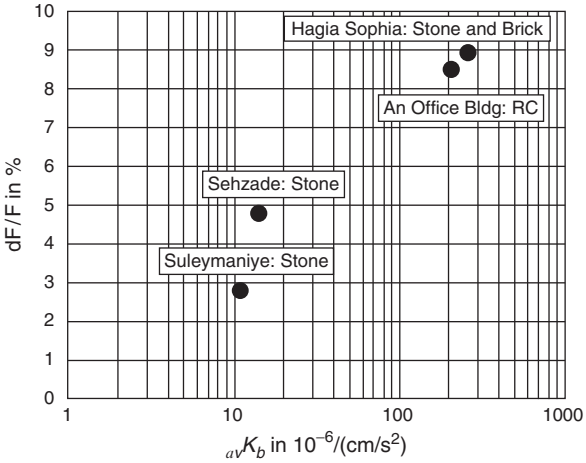

Fig. 4.4.18 Relationship between $_{av}K_b$ and dF/F for measured structures

4.4.2.5 Short summary

At the time of the Kocaeli earthquake, the seismic motion in Istanbul was small relatively because of the hard base ground. For some structures measured before the earthquake, it was able to measure after the earthquake again and to investigate the change of the natural frequency. As a result, the change of the natural frequency were 2.8%, 8.9%, 4.8% and 8.5% for Suleymaniye mosque built 500 years ago, Hagia Sophia museum built 1,500 years ago, for Sehzade mosque and 8.5% for an office building newly built. It seems that the influence by the earthquake is small, so that the change of the natural frequency is small. For the measured structures, they were affected by the Kocaeli earthquake as 7–16% of rigidity lowering. The change of the natural frequency also corresponds well to the vulnerability index against earthquake disasters for structures, and is shows that the proposed index is appropriate.

4.4.3 Leaning tower of Pisa

4.4.3.1 Outline of the measurement

The 14,000 t, 58 m high eight-story leaning tower of Pisa is one of the most original works of the art of the European Middle-Age and there are lots of uncertainties about the original architect. It was started building in the year 1173 and completed at 1530. After a short time of construction started, the tower started to incline toward the north. And nearly after 100 years, the building shifted again so that by 1272, it was visibly leaning to the south. It stands more than 800 years against the gravity and today the top of the tower is about 5.227 m off centers, tilting southward. The tower has 19.6 m diameter with a foundation depth little less than 3 m. Under the tower the ground structure consists of mainly soil, clay and mud. The area where Pisa is located had been a port in medieval times and the soil is a spongy mixture. The surface layer (about 10 m) which is an accumulated fluvium from River Arno has compacted unevenly making the tower tilted. Under this layer, there is a resistant band known as Pancone marine clay with fine sand and shells which is about 20 m deep. This is followed by a deep layer of sand boundary which is horizontal under most of Pisa, except where it is under the tower. Layers of clay and sand alternate down to roughly 70 m. The entire area where the tower is built is gradually sinking.

Figure 4.4.19 shows the area where the tower is located and position of the measurement points on the ground surface. Also the H/V spectrum for ground surface measurement is included in this figure. Figure 4.4.20 shows the cross section of the tower in NS direction, including measurement points on the structure and local geology under the tower. Rocking centers depth for each floor is pointed with x.

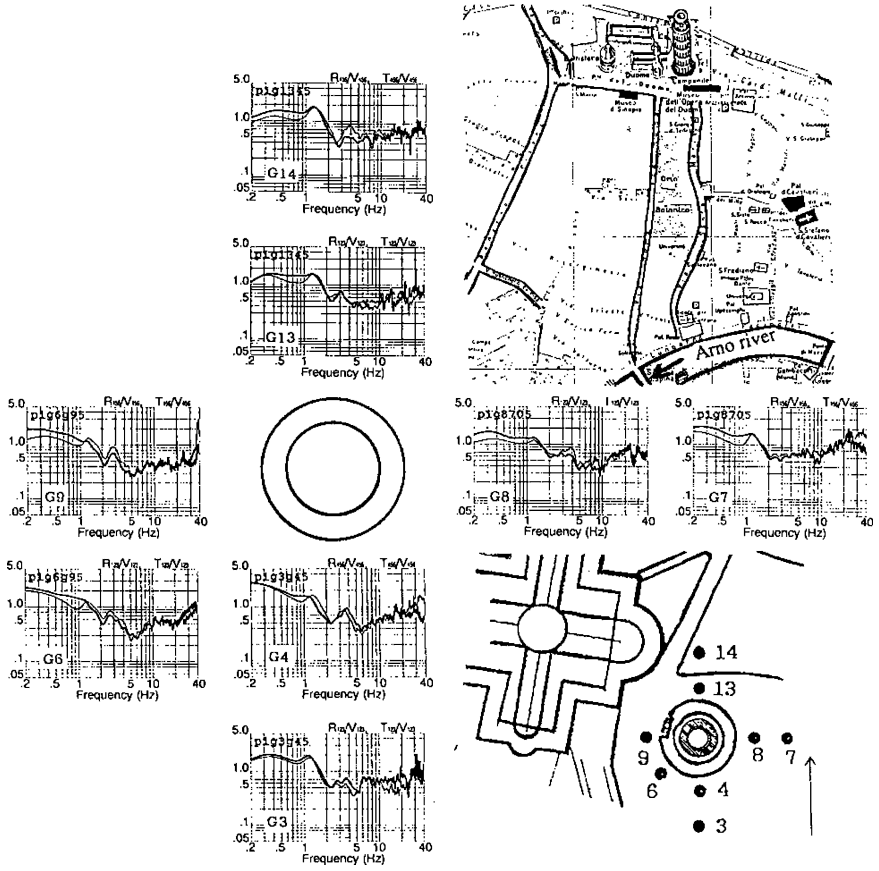

Fig. 4.4.19 Location of the tower and measurement points with H/V spectrum

The measurement was conducted with 1/100 s sampling and the length of each record is 40.96 s. Measurement was repeated three times at each observation point. Microtremor of the tower and ground were recorded at the same time. Measurements were performed at 1P, 2P, 3P, 4P, 5P and 6P levels of the tower shown in Figure 4.4.20.

After the measurements, Fourier spectrum for each components and H/V spectrum are calculated after Nakamura (1989). From a spectral ratio of horizontal to vertical components, predominant frequency F and amplification factor A which represents dynamic characteristic of the ground and spectral ratios between each floor and ground floor were calculated. This ratio provided the combined predominant frequency and amplification factor of the entire tower and ground. Using a methodology introduced by Nakamura et al. (1995), the rocking and other vibration frequencies, together with the rocking vibrations center depths were calculated for each floor.

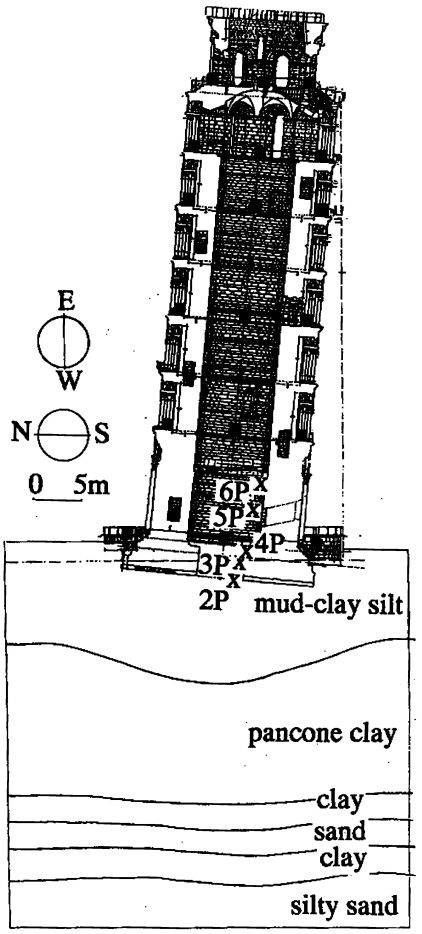

Fig. 4.4.20 Cross section of the tower in NS direction with measurement points

4.4.3.2 The result of the measurement on 1998

The H/V spectral ratios of ground are also given in Figure 4.4.19. It can be followed that having an amplification factor of 1.2. G6 and G8 have no clear peak probably because of the effects of the structure of the tower, as well as different ground characteristics at these points. Natural frequency is around 1.2 Hz at all the points. Amplification is rather high at G3, G4, G13 and G14 having a value of about 1.7 at longitudinal (NS) and transversal (EW) direction.

Figure 4.4.21 shows spectral ratios of 2P, 3P, 4P, 5P and 6P with 1P. This ratio provided the combined predominant frequency and amplification factor of the entire tower together with ground. There are several peaks showing the different modes of the structure in longitudinal and transversal components. First mode frequency is about 0.98 Hz in NS and 1.06 Hz for EW direction. These show the rocking vibration frequency of the tower. One reason of higher frequency in EW direction thought

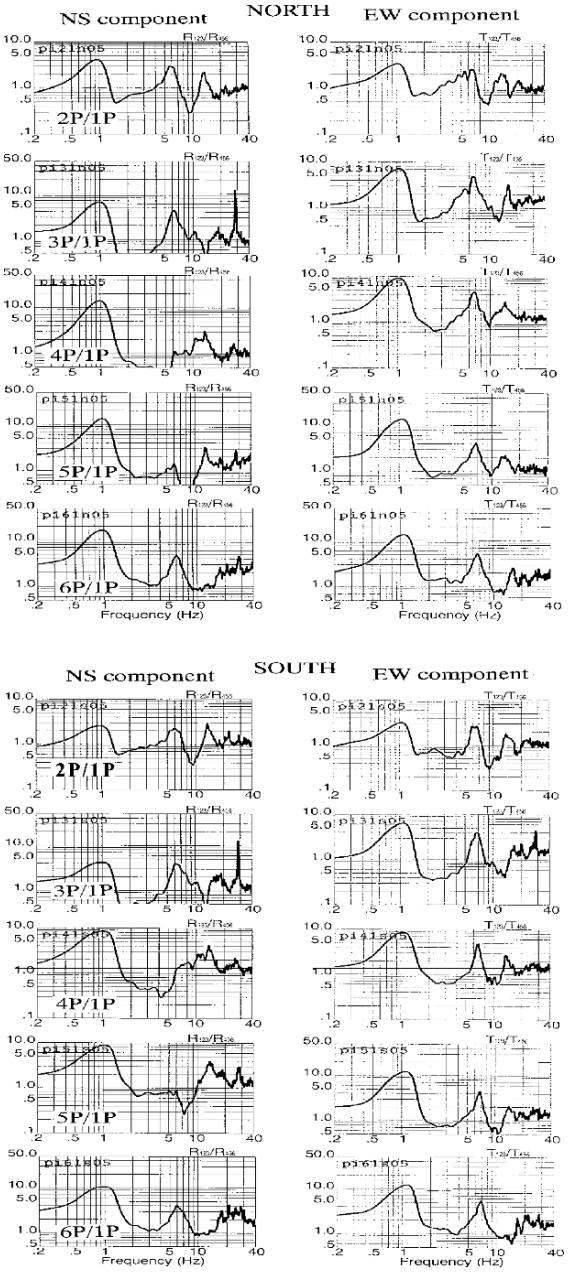

(a) NS direction

Fig. 4.4.21 Spectral ratios (**a**) NS direction (**b**) EW direction

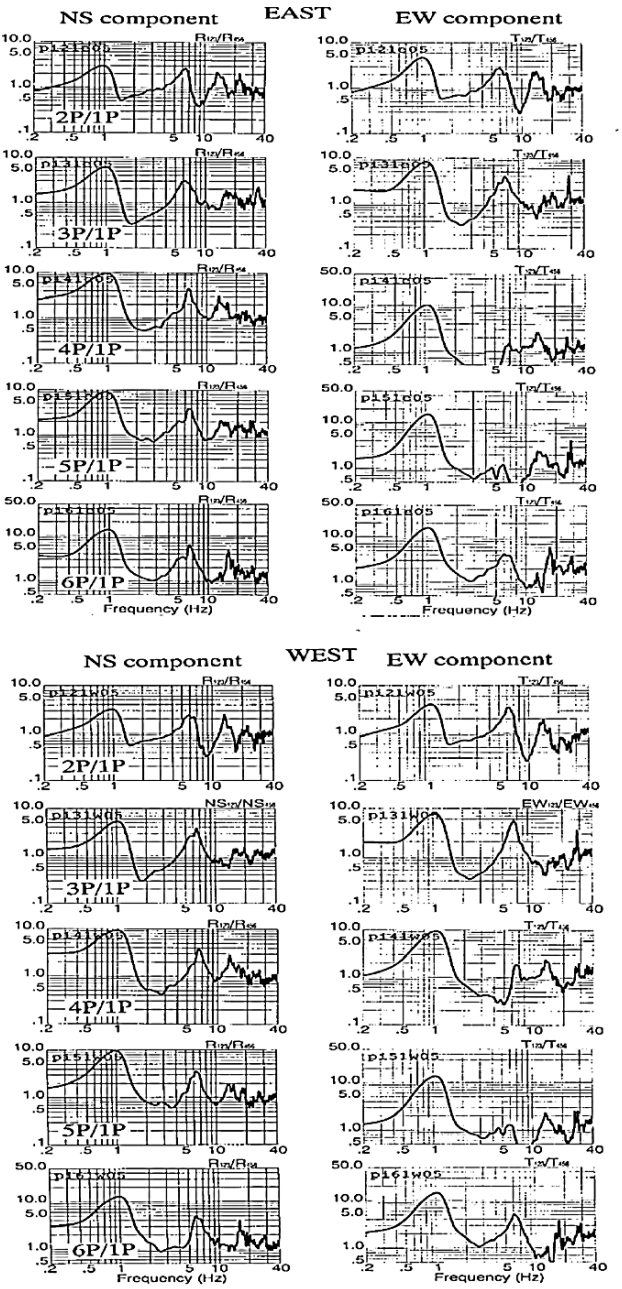

(b) EW direction

Fig. 4.4.21 (continued)

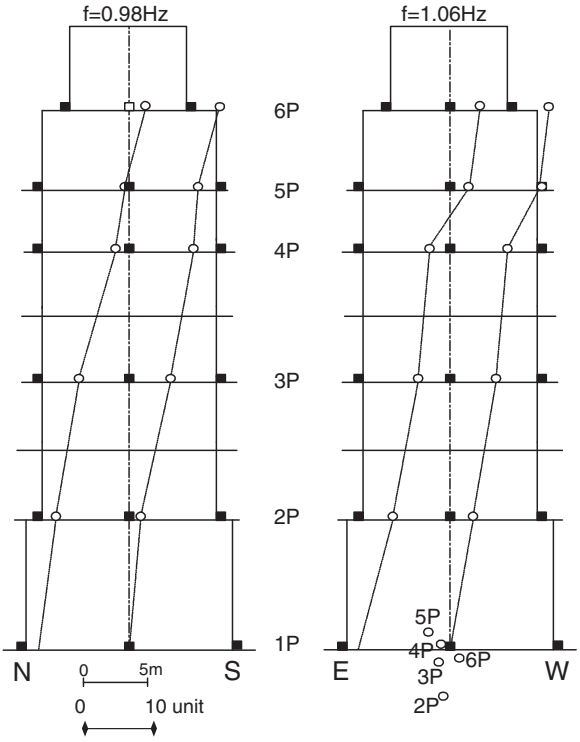

Fig. 4.4.22 Mode vibration characteristics and location of rocking center depth in EW direction

to be the weight of 830 t of lead that is placed on the south of the tower. This weight causes a small amount of difference in inertial force in NS direction that might cause just a negligible difference in momentums which will almost have no effect in frequencies. The only reason seems to be a softer ground characteristic in NS direction. Vibration frequencies of the structure for the second and third mode are 6.3 and 14 Hz, respectively. Figure 4.4.22 shows the first mode vibration characteristics in NS and EW directions. In EW direction, amplification is higher than NS direction, and this shows that the tower has a tendency to move in EW direction also. Especially from 5P level, this difference becomes bigger. This might be because of change of the floor characteristics starting from this floor. Rocking center depth for each floor was also obtained from the spectrum ratio of the horizontal movements measured by two fixed at the same floor.

Although having a deeper rocking center is better, the center of rocking vibration found from present measurement is quite shallow in NS direction (almost bottom of the foundation) located at the south of the central axis. In EW direction this center is about 1.5 m. Change of the location of the rocking depth in NS and EW direction is given on Figure 4.4.23.

Vertical vibration frequency for the entire tower is also checked from the ratio of vertical movement for the same floors. Figure 4.4.24 shows an example for

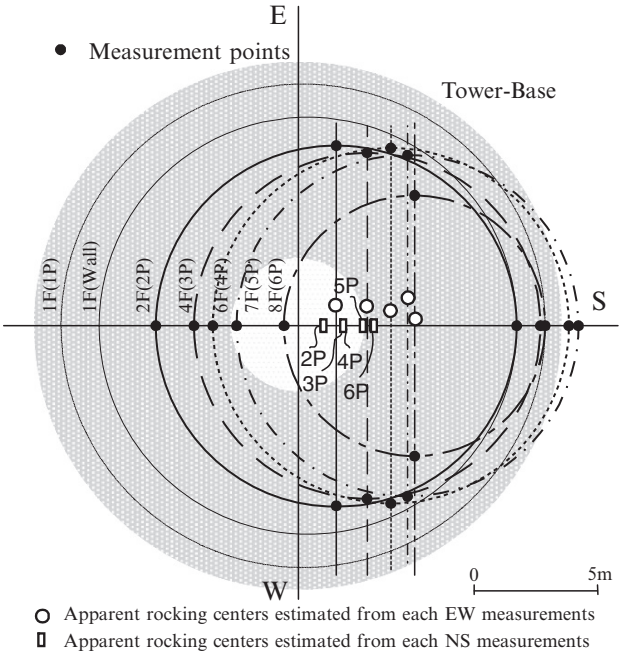

Fig. 4.4.23 Bird eye view of floors showing rocking center locations

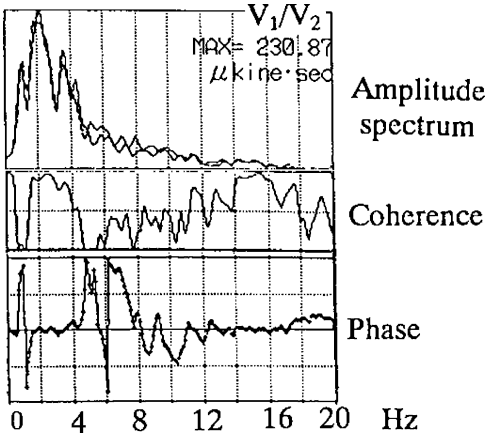

Fig. 4.4.24 Relation between vertical motions V1 and V2 for opposite sides on 5P level

5Peast/5Pwest ratio of the vertical movement at 5P level. Amplitude spectrum, coherency and phase of these records are given. A peak at 1 Hz represents rocking vibration. And a peak around 2 Hz appears at each floor shows a vertical vibration frequency for the entire tower. Clear identification of vertical vibration frequency is quite important since it gives an opportunity to calculate the spring coefficient

kv that will be helpful to calculate ground bearing capacity. Normally investigation of this coefficient needs time consuming and expensive experiments. On the other hand, with the investigation of vertical vibration frequency this can be easily calculated with the following formulation.

$$\frac{Kv \cdot g}{W} = w^2, \therefore Kv = \frac{W \cdot w^2}{g}$$
$$Kv = A \cdot kv, \therefore kv = \frac{W \cdot w^2}{g \cdot A} \tag{4.4.11}$$

Where Kv is ground bearing capacity, $w = 2\pi f$. Here, f is the vertical vibration frequency, W/g is the mass and g is gravity. By inserting the values for Pisa tower into this formulation which are, $W = 14{,}000 + 820$ (lead) t, $A = 294\,\mathrm{m}^2$, $g = 980\,\mathrm{m/s}^2$, $f = 2.2$–$2.5\,\mathrm{Hz}$, we can find the value of Kv changes between 1.0–$1.3\,\mathrm{kg/cm}^3$ for 2.2 and 2.5 Hz. Vertical vibration frequencies, respectively. This represents the bearing capacity of soft ground that Pisa locates.

The dynamic characteristics of the Pisa tower are investigated as follows;

1. Predominant frequency and amplification factor of the ground is $f = 1.2\,\mathrm{Hz}$ and $A = 1.7$.
2. Rocking vibration frequency is 0.98 Hz in NS direction and 1.06 Hz in EW direction. Center of this vibration locates at the south of the center line almost under the bottom of the foundation in NS direction. This depth is about 1.5 m in EW direction.
3. Vertical vibration frequency for the entire tower is 2 Hz.
4. Bearing capacity has been calculated as 1.0–$2.5\,\mathrm{kg/cm}^3$ for the area that the tower locates.
5. It has been shown that it is possible to investigate the response characteristics and structural damage of the structures through the analysis of microtremor records. In later analysis other vibration frequencies and ground bearing capacity are planned to be calculated from these information.

4.4.3.3 Comparing the result of the measurement in 1998 and 2004

After finishing the retrofitting of the tower, we measured microtremor again concentrating to understand the change of the behavior of the tower main body in 2004.

After the retrofitting, although the rocking center of the NS-component, the leaning direction, is no so differ from that before the retrofitting, the location of the rocking center of the EW-component moves to higher. The location after the retrofitting is around one third of the height of the tower and it is close to the theoretical location of that of a cantilever beam, so it shows that the retrofitting works as fixing the tower to the basement. Figure 4.4.25 shows the change of the location of the rocking center.

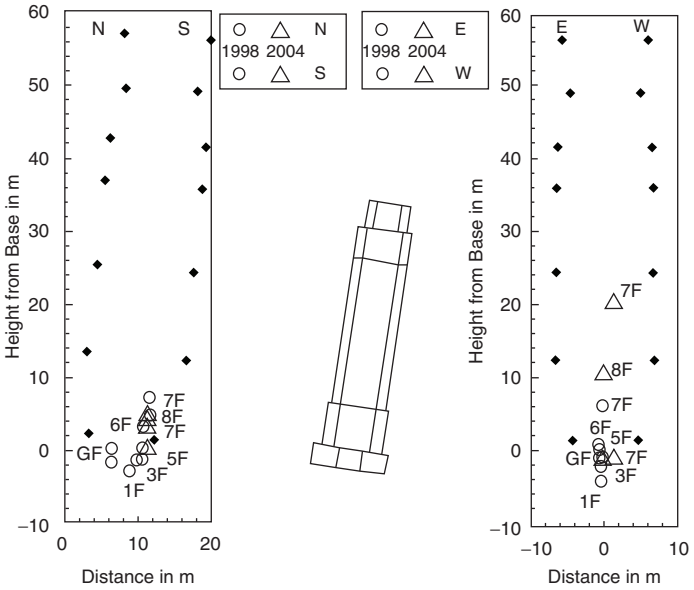

Fig. 4.4.25 Change of rocking center before and after retrofitting

The predominant frequencies for each floor shift to higher than that before the retrofitting, more than 1 Hz. The amplification factor of the seventh floor was measure both in 1998 and 2004, and the value decreased after the retrofitting. These result shows that the retrofitting made the tower stiffer to keep it safer. Figure 4.4.26 shows the predominant frequency and the amplification factor with the measurement points.

4.4.4 Conclusion

Here introduced the microtremor measurements for the world heritages including the surrounded area of them.

At first the stability of the microtremor with long time span is shown from the result of the measurement in Manila, Philippines. Then as the practical example of the microtremor measurement before and after the large earthquake, the measurement for the historical structures in Istanbul, Turkey shows the effect of the earthquake motion as the significant change of the predominant frequency. And also the vulnerability index can explain the estimate damage degree. It shows that the microtremor measurement beforehand for the important facilities is valuable to understand the behavior of the structures and the result must be useful to grasp the damage degree after the earthquakes. And the result of the measurement for the leaning tower of Pisa shows that the effect of the retrofitting can be explained by the change of the characteristics of the microtremor.

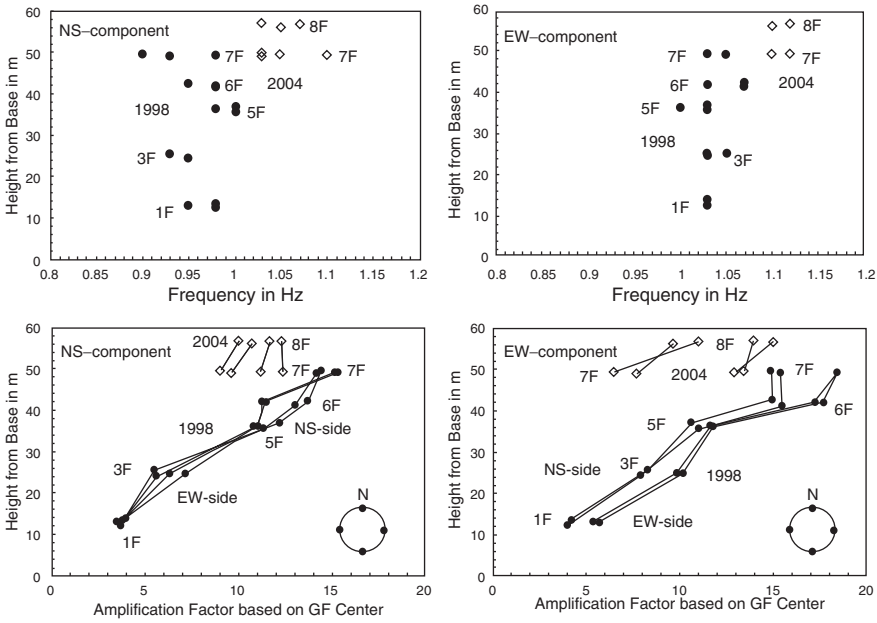

Fig. 4.4.26 Change of natural frequency and amplification factor before and after retrofitting

On the other hand, the earthquake damage relates to the site characteristics and it is important to know how the response of the ground against the earthquake is, but it is generally difficult to grasp the detailed site condition.

The authors would like to thank Dr. Bartolome C. Bautista, Dr. Ishmael C. Narag and Dr. Esmeralda L. Banganan of Philippine Institute of Volcanogy and Seismology (PHIVOLCS) for their coordination of measurement in Intramuros.

Thanks are due to Prof. Mustafa Erdik of Bogazici University, who guided us to measure the historical buildings such as Hagia Sophia museum and so on, and to Prof. Karadogan of Istanbul Technical University, who gave possibility to measure a newly completed office building.

And we would like to express our sincere gratitude to members of department of earth science, Genova University for their help ad accompany during our measurement. And also to Dr. Paolo Heiniger for his cooperation.

References

Dy, S.S. (2000). Seismic site response evaluation on surface ground of Western Manila, A thesis presented to the faculty of the college of Engineering, Tokyo Metropolitan University.

Ohmachi, T. and Y. Nakamura (1992). Local site effects detected by microtremor measurements on the damage due to the 1990 Philippine earthquake. Proceedings of the Tenth World Conference on Earthquake Engineering, pp. 997–1002.

Omote, S., Y. Osawa, I. Skinner, and Y. Yoshimi (1969). PHILIPPINES: Luzon Earthquake of 2 August 1968, UNESCO, Serial No. 977/BMS.RD/SCE.NR.

Nakamura, Y. (1997). Seismic vulnerability indices for ground and structures using microtremor. World Congress on Railway Research (CD-ROM).

Su, S.S. (1969). The Luzon earthquake of 1 August 1968: A preliminary report. Bulletin of the Seismological Society of America, 59(1):459–470.

Nakamura, Y. (1989): A Method for Dynamic Characteristics Estimation of Subsurface using Microtremor on the Ground Surface, Quarterly Report of RTRI, Vol. 30, No. 1, pp. 25–33.

Nakamura, Y., K. Hidaka, T. SATO, and M. Tachibana (1995): Proposition of a Method for Pier Inspecction Using Microtremor, QR of RTRI, Vol. 36, No. 2, pp. 65–70.

Chapter 4.5
Two Applications of the HVSR Technique to Cultural Heritage and Historical Masonry

Domenico Liberatore, Marco Mucciarelli, Maria Rosaria Gallipoli, and Nicola Masini

Abstract The application of the HVSR technique to cultural heritage and historical masonry is examined. The technique confirms the expected mechanisms, as the overturning of a church façade or of a masonry panel. In addition, the technique highlights the existence of a local mechanism of the rose-window, and the increase of frequency induced on a masonry panel by the temporary "reinforcement" of a test apparatus.

Keywords Masonry · Cultural heritage · Rose-Window · Adobe

4.5.1 Introduction

The damage of cultural heritage and historical masonry is often induced by local out-of-plane mechanisms. Examples of such mechanisms for a church façade are the overturning around a "hinge" at the base (Figure 4.5.1a), or at an intermediate height (Figure 4.5.1b), or around a set of inclined and vertical hinges (Figure 4.5.1c) (Giuffrè, 1991, 1993; Doglioni et al., 1994; Giuffrè and Carocci, 1997, 1999; Lagomarsino, 1998a, b; Doglioni, 1999; Lagomarsino and Podestà,

D. Liberatore (✉)
University of Basilicata, DiSGG, Potenza, Italy
e-mail: domenico.liberatore@unibas.it

M. Mucciarelli
University of Basilicata, DiSGG, Potenza, Italy
e-mail: marco.mucciarelli@unibas.it

M.R. Gallipoli
University of Basilicata, DiSGG, Potenza, Italy
e-mail: gallipoli@imaa.cnr.it

N. Masini
CNR, IBAM, Potenza, Italy
e-mail: masini@iisf.pz.cnr.it

M. Mucciarelli et al., (eds.), *Increasing Seismic Safety by Combining Engineering Technologies and Seismological Data,* NATO Science for Peace and Security Series C: Environmental Security,

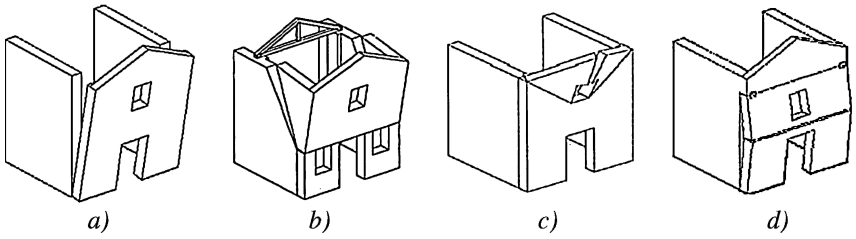

Fig. 4.5.1 Typical out-of-plane mechanisms of a church façade

1999; Sorrentino, 2003). These mechanisms are characterized by the transformation of masonry in a system of rigid bodies. The condition which allows the formation of such mechanisms is the lack of connection between the elements composing the structural set, for instance between the façade and the lateral walls.

The analysis of local out-of-plane mechanisms is an essential component in the assessment of masonry structures, as churches and buildings (OPCM 3431, 2005), for which abaci of expected mechanisms have been developed, based on the experience of past earthquakes. However, the identification of mechanisms may be problematic for complex geometries, as masonry aggregates in historical centres. In addition, the mechanisms activated during past earthquakes may be difficult to identify, when the cracks are closed and covered with plaster. Finally, the degree of connection between the façade and the orthogonal walls is often difficult to evaluate. For these reasons, developing an experimental technique capable of identifying the active mechanisms is of great interest.

In this study, the application of the Horizontal to Vertical Spectral Ratio (HVSR) technique (Mucciarelli and Gallipoli, 2002) to cultural heritage and historical masonry is examined, attaining to a preliminary evaluation of its reliability in identifying local out-of-plane mechanisms.

The HVSR technique is non destructive and can be applied to a large number of accessible points, as windows. The hypotheses at the basis of the method are generally satisfied: the amplification of the horizontal components of the motion is significant, especially for the out-of-plane component, whilst the amplification of the vertical component is negligible. When active mechanisms are present, the HVSR is expected to yield different H/V spectral ratios for the different rigid bodies composing the mechanism, e.g. the façade and the orthogonal walls. An essential pre-requisite for the HVSR technique is that the mechanism has been already activated. On the contrary, mechanisms which can be potentially activated, but are not yet active, cannot be identified. Moreover, the technique requires that the actives mechanisms involve a significant difference of the out-of-plane stiffness of the different rigid bodies, even at low level of excitation, which is typical of ambient vibrations. Another interesting issue is that the HVSR technique is expected to provide information about the effectiveness of those interventions which modify the mechanism, as tie rods (Figure 4.5.1d).

Two case studies of the applications of the HVSR technique are shown: the former on the façade and the rose-window of Troia Cathedral (Liberatore et al., 2006a), the latter on the historical adobe buildings of Aliano (Liberatore et al., 2006b).

4.5.2 The façade and the rose-window of Troia Cathedral

According to historical tradition, Troia Cathedral (Apulia, Italy) was founded in 1093 and consecrated in 1120. It is the masterpiece of the Romanesque architecture of the region of Capitanata, blending Byzantine and Muslim reminiscences with oriental elements.

The plan has the shape of Latin cross. The three naves are separated by 12 columns, divided in two rows of six. A 13th column is located at the side of the first column on the right.

The façade (Figure 4.5.2) is 18.28 m wide and 19.90 m high. It has a basement whose height ranges from 1.48 to 2.08 m. Over the basement, there is a sequence of seven blind arches, placed on pilaster strips, which frame rhombs and oeil-de-boeufs. The central arch surmounts the portal, consisting of two smooth posts, ending with two capitals bearing an architrave, richly adorned in bas-relief representing the theme of conversion, bearing in turn a lunette consisting of a smooth arch with moulded cornice. The blind arches and the rhombs are characterized by chiaroscuro effects. A moulded cornice, resting on corbels decorated with zoomorphous, phytomorphous and geometric shapes, separates the lower part from the upper part of the façade. The upper part is divided in three parts: the central part, consisting of the tympanum and corresponding to the section of the nave, and the lateral parts, with single pitch, recalling the section of the side aisles.

The central tympanum consists of a round arch, resting on two couples of columns in reused marble, each resting in turn on a stylophorus lion. Inside the arch of the tympanum, there is another arch with plastic elements, in tondo or bas-relief with anthropomorphous, zoomorphous and floral figures. Inside this arch, there is the rose-window. Over the imposts of the outer arch, there are two other lions keeping the head of a calf and a human head.

The rose-window has diameter 6 m and consists of 11 twin columns, outer and inner, in stone and reused marble, connected to a central oeil-de-boeuf and to a ring consisting of pre-fabricated elements, whose surface is decorated by arched ribworks forming ogives. There are 11 transennae between the twin columns, embroidered to openwork, each with a different and strongly symbolic pattern: the square, the rhomb, the cross, the circle.

The outer columns are in white marble, sandstone, limestone, breccia with elements of marble or limestone. Some inner columns are in white marble with grey bands.

The rose-window presents a wide set of constructive solutions aimed at providing equilibrium, not only in the final configuration, but also during the assemblage. Besides a particular care to stereotomy, the contact between the different elements is integrated by iron bolts and melted lead, especially between the columns and the capitals, and between the capitals and the arched ribworks.

The main damage of the façade consists of a rotation around a horizontal “hinge”, approximately 9.50 m above the base. The top of the façade is nearly 30 cm out of plomb.

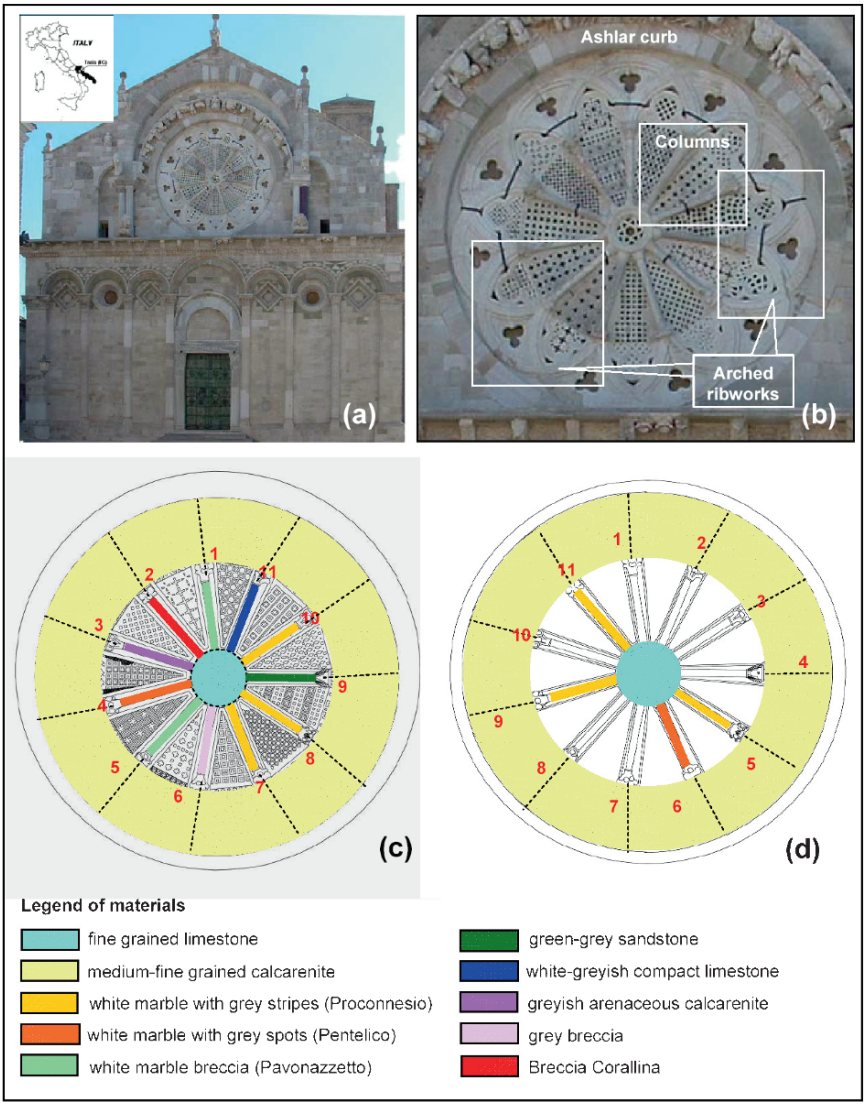

Fig. 4.5.2 Façade and rose-window of Troia Cathedral

The rotation is also confirmed by the displacement of the inner surface of the façade, with reference to the corbel which was originally located on the top of the longitudinal wall on the left of the central nave, with the aim to bear the first roof truss. That corbel was originally in contiguity with the inner surface of the façade wall, whilst now it is displaced of nearly 25 cm. The opening created by the rotation of the façade was closed in the past. It is also interesting to note that the longitudinal walls were superelevated, with the aim to position the new roof trusses, preventing

the interaction of the tie with the rose-window. The new corbel, which presently bears the first roof truss, is in contiguity with the façade, and is offset nearly 25 cm with reference to the original corbel below.

The damage of the façade is also confirmed by the damage of two couples of columns at the sides of the rose-window. The columns on the right appear splintered, with damage especially pronounced for the column in red porphyry, which has also conchoid fractures in the upper part and in the capital. Both columns are slightly tilted towards the right and inwards. The couple of columns on the left are tilted outwards and splintered at the base and at the top. Vertical cracks, indicating compression failure, can also be observed in their capitals.

The rotation of the façade is the presumable cause of a set of slidings and damages of the façade. The upper arch appears strongly ovalized, its keystone presents vertical fractures, and is displaced outwards and downwards. The lower arch presents a vertical fracture at the key, and some voussoirs are displaced outwards and downwards.

The rotation of the façade induced heavy deformations and damages in the rose-window, which is displaced outwards in the upper part, and inwards at the centre. Disconnections and rotations of the capitals, as well as compression failures of the columns are observed. Relative displacements, up to 1 cm, may also be observed at the joints between the arched ribworks. An out-of-plane restraint was set up, consisting of two horizontal tubes, anchored to the ashlar and connected to some columns and arched ribworks through metal elements.

The origin of the rotation of the façade is clearly seismic. The seismic history of Troia is summarized in Figure 4.5.3 (Stucchi et al., 2007). An earthquake of MCS intensity 8 occurred in 1456, two of intensity 7.5 in 1627 and 1731, two of intensity 7 in 1875 and 1930. The out-of-plane restraint of the rose-window is documented by paintings dating back to the early 20th century, permitting to exclude the last event (1930) as the main cause of the rotation of the façade. Among the others, it is not possible to associate the rotation to a single event. Since no ties have been found, aiming at restraining the façade, it is possible that the rotation increased progressively in consequence of several events.

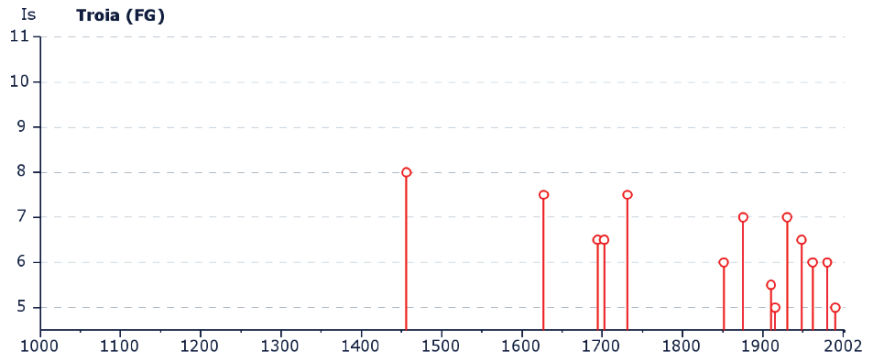

Fig. 4.5.3 Seismic history of Troia

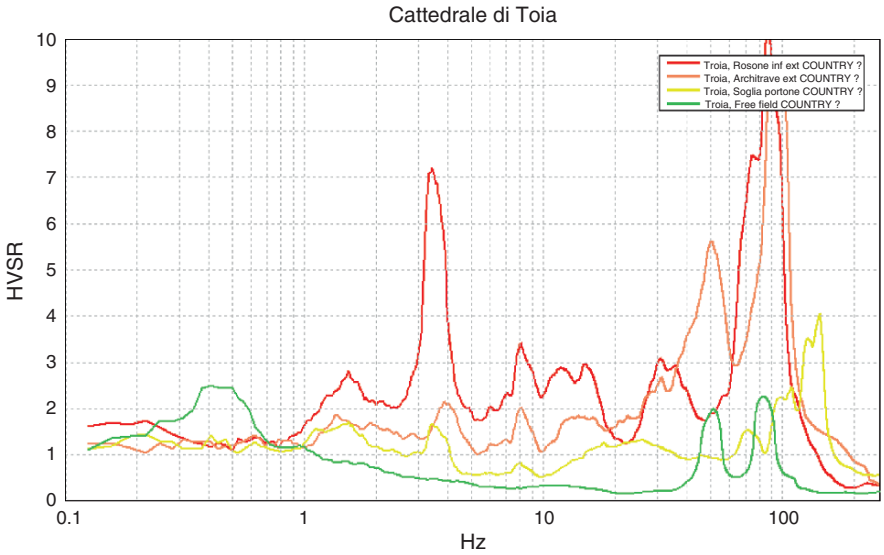

Fig. 4.5.4 HVSR of the façade at different heights

The HVSR is used to estimate the fundamental frequency of the façade and of the rose-window. The measurements were performed with a digital tromometer (Micromed Tromino), that hosts in a single, small case 3 seismometers, a 24-bit digitizer and the data storage unit. For all the measurement points, six recordings were acquired, lasting 1 min each, with sampling frequency 512 Hz. The signals were detrended and filtered in the range 0.1–256 Hz. After the transform in the frequency domain, the ratio between the horizontal and the vertical component was calculated in order to estimate the fundamental frequencies.

The HVSR analysis identifies separate fundamental frequency for the two orthogonal directions (in-plane and out-of-plane). On the façade, two frequencies were identified, at 3.2 and 8.0 Hz, with amplitude increasing with height, as expected for the fundamental in-plane and out-of-plane modes (Figure 4.5.4).

The measurements carried out on the rose-window are shown in Figure 4.5.5 (yellow: oeil-de-boeuf, orange: arched ribworks, red: connection with the façade). Whilst the frequencies of the façade are still visible, a separate frequency emerges at 22 Hz. This mode has greater amplitude at the centre of the rose-window and decreases towards the connection with the façade, identifying a local 2D plate fundamental mode of the rose-window.

4.5.3 The historical adobe buildings of Aliano

The historical heritage of the adobe buildings of Aliano (Basilicata, Italy) represents the witness of a vernacular constructive culture, closely related to the resources of the territory (Figure 4.5.6). In the past, the scarcity of stones and the availability of

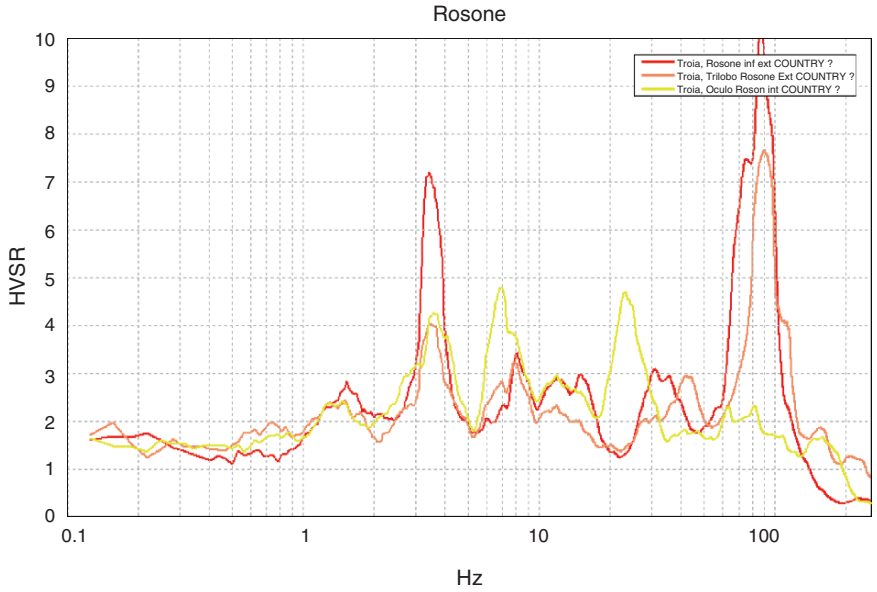

Fig. 4.5.5 HVSR of the rose-window

Fig. 4.5.6 Examples of adobe walls

clay from the badlands ("calanchi") encouraged the use of blocks made of clay and minced straw, dried in the sun.

The blocks ("ciuci") have modular size (length 380 mm, thickness 155 mm, height 165 mm) and are generally used in single storey buildings, or to build an additional storey to buildings made of ashlar. In both cases, the adobe bears a saddle roof made of timber beams and rafters, with lining in reed and mantle of bent tiles.

The outer surface of the walls is plastered only if exposed to dominant winds and rain water which could produce weathering of the material and loss of bearing capacity. In alternative to plaster, the walls are protected by an outer facing in ashlar, more or less connected to the adobe. The witnesses of this constructive technique are few, because of the extreme deterioration of the material.

A number of damage mechanisms has been observed: disaggregation of the fabric, out-of-plane separation between walls, out-of-plane collapse, separation cracks, loss of connection between horizontal structure and walls, damage of the upper part of the walls, bending damage of the walls at mid-height, diagonal cracks, corner cracks, localized compressive failure, cracks near the openings, weathering.

A number of laboratory and *in situ* tests have been accomplished on adobe blocks, adobe panels and structures. Adobe underwent chemical analysis and geotechnical investigations aimed at determining Atterberg limits and friction coefficient. Two adobe blocks have been tested in three-point bending. The four semi-blocks coming from the tests underwent compression test, together with two additional blocks. Sonic transmission tests have been carried out on adobe walls, adobe walls with facing in ashlar, ashlar with air-setting mortar. Penetration tests have been carried out through an instrument and a procedure purposely developed for masonry joints. An *in situ* diagonal compression test on an adobe panel has been carried out, resulting in the sliding of the upper part of the panel (Figure 4.5.7).

The ambient noise at the top of the panel subjected to diagonal compression was recorded for 10 min. The grey curve in Figure 4.5.8 is the average of HVSR function: the peak at about 4.5 Hz is identified as the main frequency of vibration of the building, whilst the peak at about 15 Hz is due to the local vibration of the panel. It is important to note that the HVSR function has its maximum amplitudes on the out-of-plane component (Figure 4.5.8, black line).

Other ambient noise measurements were carried out on the panel equipped for the *in situ* diagonal compression test. The HVSR average function shows the peak of the panel at about 20 Hz. The increase of the frequency is due to the stiffness provided by the test apparatus. Also in this case, the HVSR function of the out-of-plane component has the maximum amplitudes (Figure 4.5.9, black line).

Fig. 4.5.7 Diagonal compression test

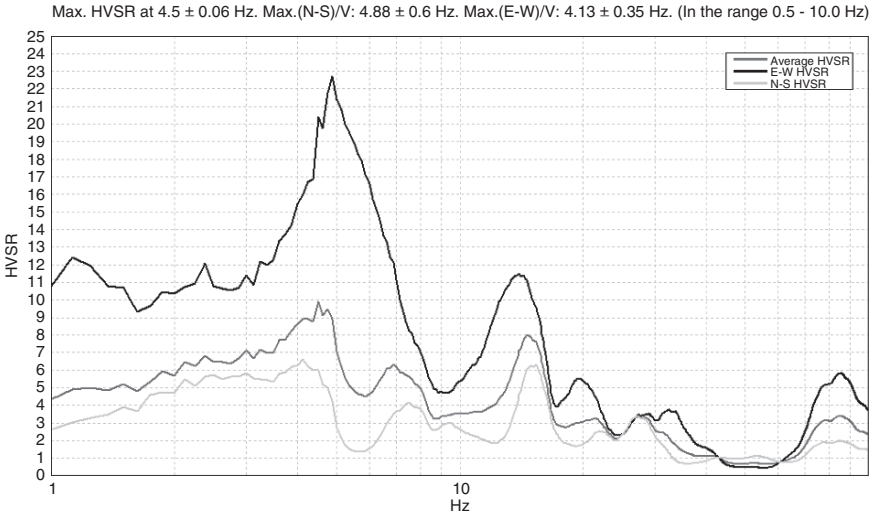

Fig. 4.5.8 Mean HVSR for the panel before the diagonal compression test

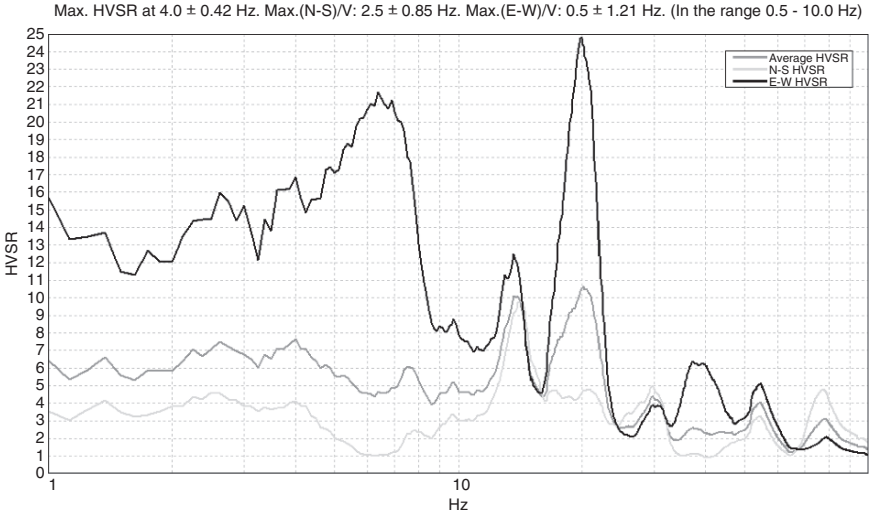

Fig. 4.5.9 Mean HVSR for the panel stiffened by the apparatus for diagonal compression test

A third measurement has been performed during the diagonal compression test when damage occurred. Figure 4.5.10 reports the comparison of HVSR functions: the light grey curve is the HVSR of the panel without any stiffening, the grey curve that of the stiffened panel and the black one that of the panel during the diagonal compression test.

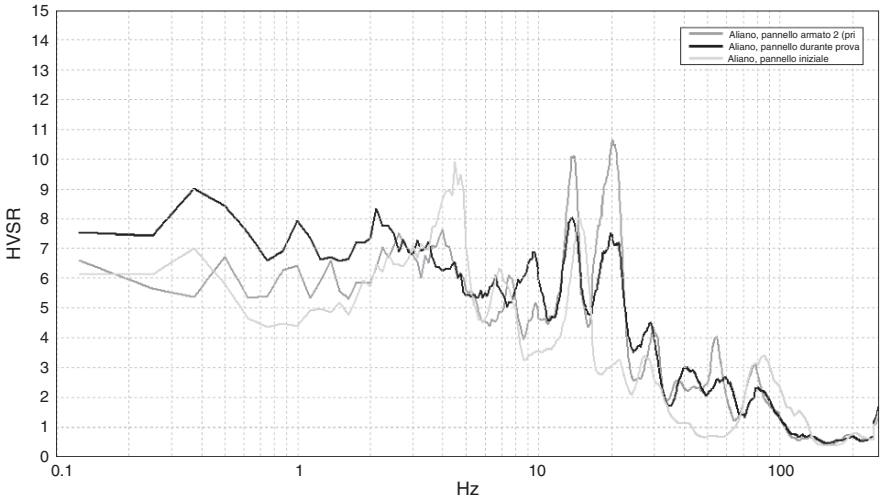

Fig. 4.5.10 Summary of average HVSR functions

4.5.4 Conclusions

In this study, the HVSR is applied with the aim of identifying the local out-of-plane mechanisms of cultural heritage and historical masonry.

The application to Troia Cathedral highlights the local mode of the rose-window, in the form of a 2D plate out-of-plane mode. The façade has H/V spectral ratios which increase with height. However, this is a very common behaviour for structures, and further investigations are required, involving measurements on the lateral walls – not accessible during the experimental campaign – in order to identify the disconnection between the façade and the lateral walls, and therefore the overturning mechanism of the façade.

The application of the HVSR technique to the adobe panel of Aliano highlights the frequency increase when the panel is "reinforced" through the test apparatus, and the decrease of frequency during the test, when damage occurs. This result shows that the HVSR technique could be used to assess the effectiveness of strengthening techinques which involve an increase of stiffness. Also in this case, this preliminary result has to be corroborated by further investigations on "real" intervention techniques.

Both applications are encouraging the use of the HVSR technique, which proves to be able to identify local mechanisms. Further and extensive investigations are necessary to validate the technique on a more systemic basis, in particular when the aim is to identify more complex mechanisms, not known *a priori*. Another related use of the technique will be that to identify masonry discontinuities, through measures at the two sides of the discontinuity itself, or to evaluate the degree of connection between orthogonal walls.

Acknowledgements Study funded by MIUR Grant COFIN 2004089719_003, Comune di Troia, Ente Diocesi di Lucera-Troia and Comune di Aliano. The authors are also grateful to Edoardo Beccia, Stefano Cibelli, Piero Guadagno and Giulio Tricarico for their help.

References

Doglioni, F., 1999. Code of practice (guidelines) for the design of the interventions of repair, seismic improvement and restoration of the architectural heritage damaged by the Umbria-Marche 1997 earthquake – Knowledge and preservation of architecture, Bollettino Ufficiale della Regione Marche (in Italian).

Doglioni, F., Moretti, A., Petrini, V., 1994. Churches and earthquake, LINT, Trieste (in Italian).

Giuffrè, A., 1991. Lectures on the mechanics of historical masonry, Kappa, Rome (in Italian).

Giuffrè, A. (Ed.), 1993. Safety and preservation of the historical centres: the case of Ortigia, Laterza, Rome-Bari (in Italian).

Giuffrè, A., Carocci, C., 1997. Code of practice for the safety and the preservation of the *Sassi di Matera*, La Bautta, Matera (in Italian).

Giuffrè, A., Carocci, C., 1999. Code of practice for the safety and the preservation of the historical centre of Palermo, Laterza, Rome-Bari (in Italian).

Lagomarsino, S., 1998a. A new methodology for the post-earthquake investigation of ancient churches, Proc. of the 11th European Conference on Earthquake Engineering, Paris, A.A. Balkema (Abstract Volume & CD-ROM), p. 67.

Lagomarsino, S., 1998b. Seismic damage survey of the churches in Umbria, Proc. of the Workshop on Seismic Performance of Monuments (Monument-98), Lisbon, pp. 167–176.

Lagomarsino, S., Podestà, S., 1999. Methods for the vulnerability analysis of churches, Proc. of the 9th National Conference on L'Ingegneria Sismica in Italia, Turin (in Italian).

Liberatore, D., Spera, G., Mucciarelli, M., Masini, N., Calia, A., Capriuoli, A., Racina, V., Nuzzo, L., Rizzo, E., Binda, L., Cantini, L., 2006a. The façade and the rose-window of Troia Cathedral (Apulia, Italy), Proc. of the 5th International Conference on Structural Analysis of Historical Constructions, New Delhi.

Liberatore, D., Spera, G., Mucciarelli, M., Gallipoli, M.R., Santarsiero, D., Tancredi, C., Masini, N., Racina, V., Capriuoli, A., Cividini, A., Tedeschi, C., 2006b. Typological and experimental investigation on the adobe buildings of Aliano (Basilicata, Italy), Proc. of the 5th International Conference on Structural Analysis of Historical Constructions, New Delhi.

Mucciarelli, M., Gallipoli, M.R., 2002. A critical review of ten years of HVSR technique, Bollettino di Geofisica Teorica e Applicata, 42, 255–266.

OPCM 3431, 2005. Technical regulations for the design, assessment and seismic retrofitting of buildings (in Italian).

Sorrentino, L., 2003. Dynamics of masonry walls under out-of-plane excitation as systems of rigid bodies, Ph.D. thesis, Rome (in Italian).

Stucchi, M., Camassi, R., Rovida, A., Locati, M., Ercolani, E., Meletti, C., Migliavacca, P., Bernardini, F., Azzaro, R., 2007. DBMI04, database of macroseismic observations on Italian earthquakes used for the compilation of the parametric catalogue CPTI04, http://emidius.mi.ingv.it/DBMI04.

Chapter 4.6
Overview of Seismic Hazard Studies in Tunis City

Najla Bouden-Romdhane, Pierre Mechler, Anne-Marie Duval, and Sameh Anibi

Abstract Tunis City (roughly 30,000 inhabitants per km^2) is developing in a subsiding sedimentary basin, 350 m deep, which is occupied by loose Quaternary deposits over a more rigid Eocene bedrock with a strong estimated impedance transition between the subsurface and the deep layers. Huge investment projects are initiated all around the edges of the Lac de Tunis and cover more than 25 millions square meters of buildings, towers, tourist complexes, bridges and yacht embankments. Due to this socio economic context, a comprehensive seismic risk analysis was conducted since a decade at the Tunis National School of Engineers with a special emphasis on site effects, liquefaction potential assessment and vulnerability studies of two pilot built areas located in the downtown zone and in the old Medina. All the collected and produced data are compiled in a geo-referenced database management system (GIS).

This chapter presents a broad coverage of the seismic site response analyses and liquefaction potential studies conducted in Tunis City by means of experimental techniques and numerical modelling.

Keywords Site effects · Transfer function · Signal-to-noise ratio · Optimum Wiener filter · 1D numerical modelling · Liquefaction potential

N. Bouden-Romdhane (✉)
Ecole Nationale d'Ingénieurs de Tunis, Department of Civil Engineering, Tunis, Tunisia

P. Mechler
Département de Géophysique Appliquée, Université Paris 6

A.-M. Duval
CETE méditerranée, Nice, France

S. Anibi
Ecole Nationale d'Ingénieurs de Tunis, Department of Civil Engineering, Tunis, Tunisia

M. Mucciarelli et al., (eds.), *Increasing Seismic Safety by Combining Engineering Technologies and Seismological Data,* NATO Science for Peace and Security Series C: Environmental Security,

4.6.1 Introduction

The H/V technique is widely used to estimate the site effect parameters. In order to investigate the reliability of this technique in Tunis City, we compared it to the Standard Spectral Ratio (SSR) technique. However, SSR technique suffers in Tunis City from a low regional seismicity and a high level of ambient vibrations. The use of an Optimum Wiener Filtering improved the signal-to-noise ratio and therefore the site response estimation. The results corroborate those of H/V Technique. The H/V technique was then pursued in a dense field survey across Tunis City and the edges of the Lac de Tunis. The main results are commented here.

During the both campaigns, the recorded accelerations remained very weak; in order to better approach the magnitude and predictability of site effects for various input expected shake levels, a 1D numerical modelling based on equivalent linear soil model and nonlinear hysteretic soil model was also carried out. This study led to the development of maps showing peak frequencies and corresponding amplication factors for increasing levels of input acceleration.

The assessment of liquefaction potential was carried out within the upper 20 m where the loose silty units are interrupted by saturated sandy interbeds. The implemented methodology is based on the French Agency of Seismic Protection (AFPS) recommendations and led to the development of liquefaction maps and cross sections which show the variation of the liquefaction potential with depth for various expected shake levels.

4.6.2 The site of Tunis

4.6.2.1 Seismotectonic context of Tunis

Tunisia is located in the western front of collision of the African and Eurasiatic plates (Figure 4.6.1). In this region, the convergence of plates generates an active compressive tectonic (Dlala and Rebaî, 1994) which is responsible of the great earthquakes in the Maghreb area: Orléanville (1954, M = 6.7), Agadir (1960, M = 6.7), El Asnam (1980, M = 7.3), Zemmouri-Boumerdes (2003, M = 6.7).

Moreover, Tunis and its surroundings are situated in a convergence zone of the main structural units of the country (Figure 4.6.1). The seismicity of the region is controlled mainly by three active faults: Mohamedia fault, Mornaguia-Tunis fault and Jebel Amar fault (Figure 4.6.2).

Mornaguia-Tunis and Essaîda Manoubia faults are sub parallel, cross the city of Tunis and delimit a subsiding alluvial basin (Tunis Valley) which opens towards the Lac de Tunis (El Bhira) eastward and is bounded by relief elsewhere (Figure 4.6.3). The western relief separate the Tunis Valley from the continental depression occupied by the salt lake, Sebkhet Essijoumi.

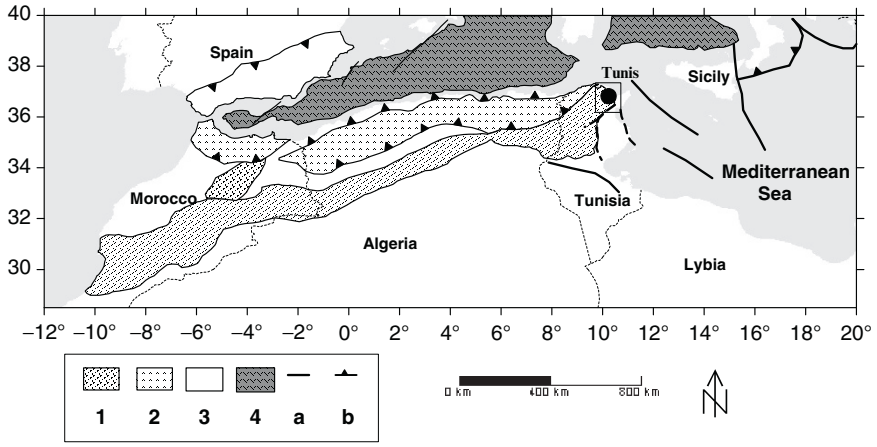

Fig. 4.6.1 Simplified tectonic map of the occidental part of Mediterranean Sea (Bousquet and Phillip, 1981). 1: Atlasic chain; 2: Maghrebide chain; 3: Betic cordillera; 4: oceanic crust; a: active fault; b: subduction

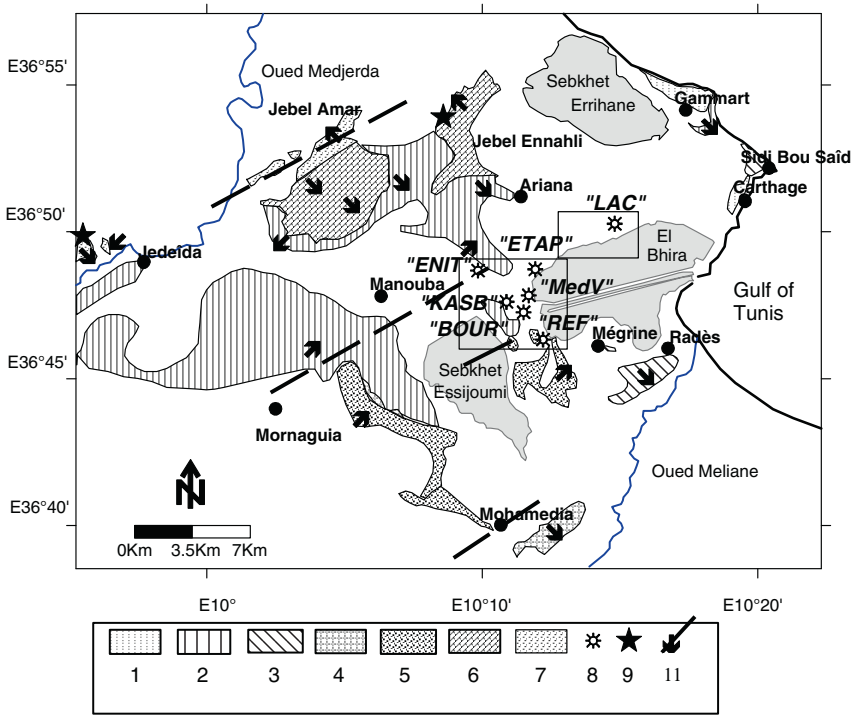

Fig. 4.6.2 Simplified seismo-tectonic map of Tunis and its surrounding area (Piementa, 1959, Ben Ayed and Viguier, 1978, Boutib, 1998). 1: recent and fossilized dunes; 2: continental Plio-Quaternary deposits; 3: Miocene: colored marls, marls with gypsum; 4: Oligocene; 5: Auversian marls and sandstones, Eocene limestones (Bou dabbous formation) and Danian marls (El haria formation); 6: Senonian marls and limestones; 7: Early Cretaceous marl, shale and limestone; 8: telemetric mobile network of CETE-Méditerranéen (Nice-France); 9: rock blasting; 10: layer dip, 11:fault

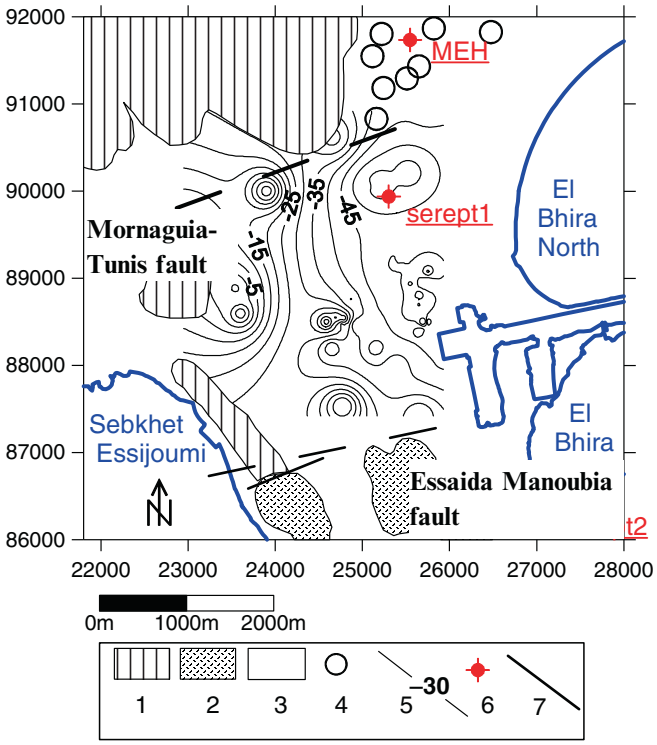

Fig. 4.6.3 Simplified geotechnical zoning map of Tunis City (Bouden-Romdhane, 2002). 1: succession of mio-pliocene-quaternary sandy beds, clays, sandstone lenses and beds; 2: Eocene limestone and marly limestones; 3: infill, succession of silty complex, plastic clayey-sandy formations and sandstone lenses over a more compact sandy-clayey layer; 4: sandstone bars, silt and plastic clays; 5: roof position of the compact sandy-clayey layer; 6: deep borehole; 7: observed and supposed faults

The Figure 4.6.4 shows a north to south cross section of the basin of Tunis achieved from the petroleum prospecting deep boreholes MEH, serept1 and serept2 (location in Figure 4.6.3). The alluvial layer is divided in two types. The basin is filled by Quaternary deposits, 360 m thick, overlying an Eocene limestone substratum which outcrops in the southern compartment of Essaîda Manoubia fault. The superficial part of the deposits (the first 10–70 m) is made of soft lagoonal infill. Below, the thickness of the clayey and sandy Quaternary deposits may reach 300 m.

4.6.2.2 Geotechnical zoning

The assessment of the site response requires detailed information on the subsurface layering, seismic velocities and complementary geotechnical properties of the formations. In a first step, all the recent geotechnical data including 150 pressiometric

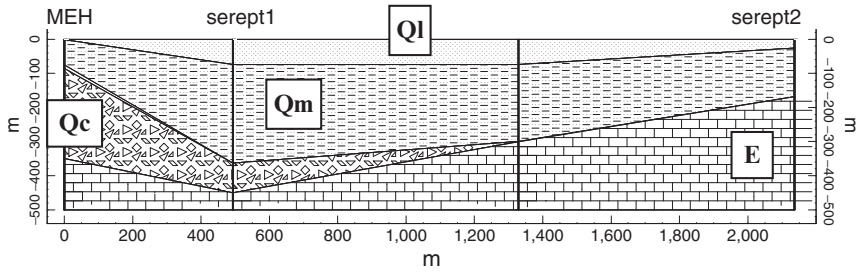

Fig. 4.6.4 North to South cross section of the basin of Tunis (Piementa, 1959); E: Eocene limestone, Qc: continental Pliocene and Quaternary deposits, Qm: clayey and sandy marine Quaternary sediments, Ql: soft lagoon Quaternary infill

and 500 penetrometric (SPT and CPT) data as well as 220 core sampling boreholes were collected and processed in a database (Bouden-Romdhane, 2002). A geotechnical zoning map was elaborated for this work (Figure 4.6.3); the main superficial lithology of the Tunis Valley (the first 10–70 m) is a succession of embanking and of a silty complex over a more compact sandy-clayey continental layer which constitutes the deepest soil of foundation of the modern buildings of the city. The muddy formation is interrupted, by plastic clayey-sandy interbeds, sandy soils or sandstone lenses.

4.6.3 Seismic site effect assessment

In order to estimate the seismic site effect, two experimental surveys have been conducted, as well as numerical modelling.

4.6.3.1 Experimental surveys

The most direct method to estimate the site effect compares the seismic activity recorded simultaneously on a horizontal outcropping rocky reference and on the site. Seven stations of the seismic mobile network of the CETE-Méditerranée were positioned on the main geotechnical features of Tunis (Figures 4.4.2 and 4.4.5); REF is the reference station sited over the Eocene outcropping limestone.

During the 4 months data acquisition period, only nine earthquakes have been recorded by the whole network. To remedy to this weak seismic activity, three rocks blasting have been organized in careers near Tunis (location in Figure 4.6.2).

The Figure 4.6.6 represents the Standard Spectral Ratio (SSR or SBSR) computed from the signals recorded at the central station "MedV" (mean level of ambient noise: $10\,\mu m/s$) taking into account a signal-to-noise ratio S/B up to 2. Beyond 2 Hz, it is difficult to estimate the transfer function SSR (or SBSR). This is awkward

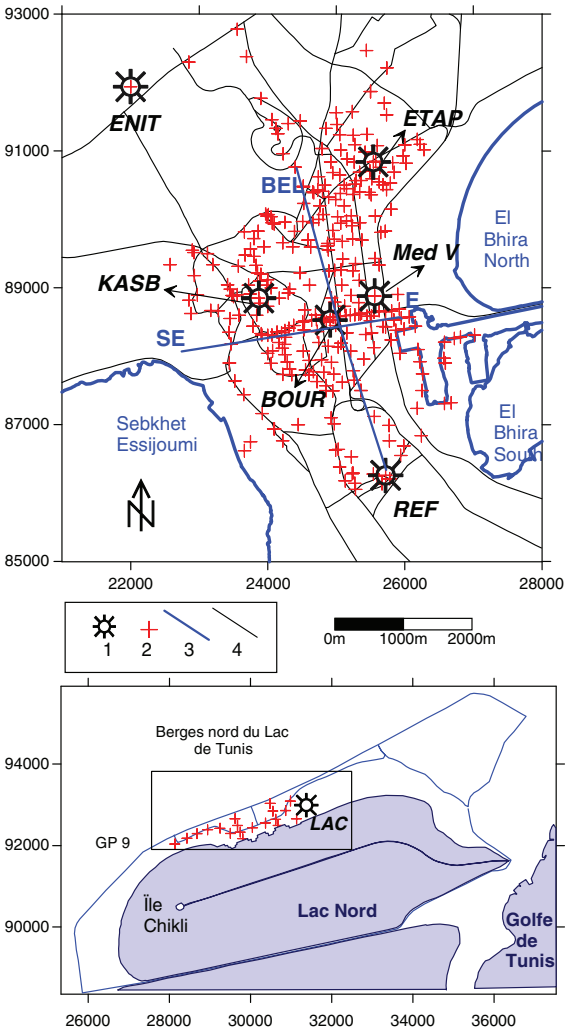

Fig. 4.6.5 Site location of the weak motion and microtremor measurements over Tunis: 1: telemetric mobile network of CETE-Méditerranéen (Nice-France); 2: microtremors measurements; 3: geotechnical cross-sections; 4: the main roads

knowing that the concerned range of frequencies (2–15 Hz) is significant in earthquake engineering and is lacking here. This illustrates the limit of the SSR method in the case of urban "noisy" zones characterised by a weak seismic activity.

To palliate this inconvenience, we used an Optimum Wiener Filtering. The Wiener filter is widely used in geophysical prospecting to improve the signal-to-noise ratio and to identify filtering relation between two traces. The Wiener filtering has been applied in seismology to highlight the coherent parts between seismic

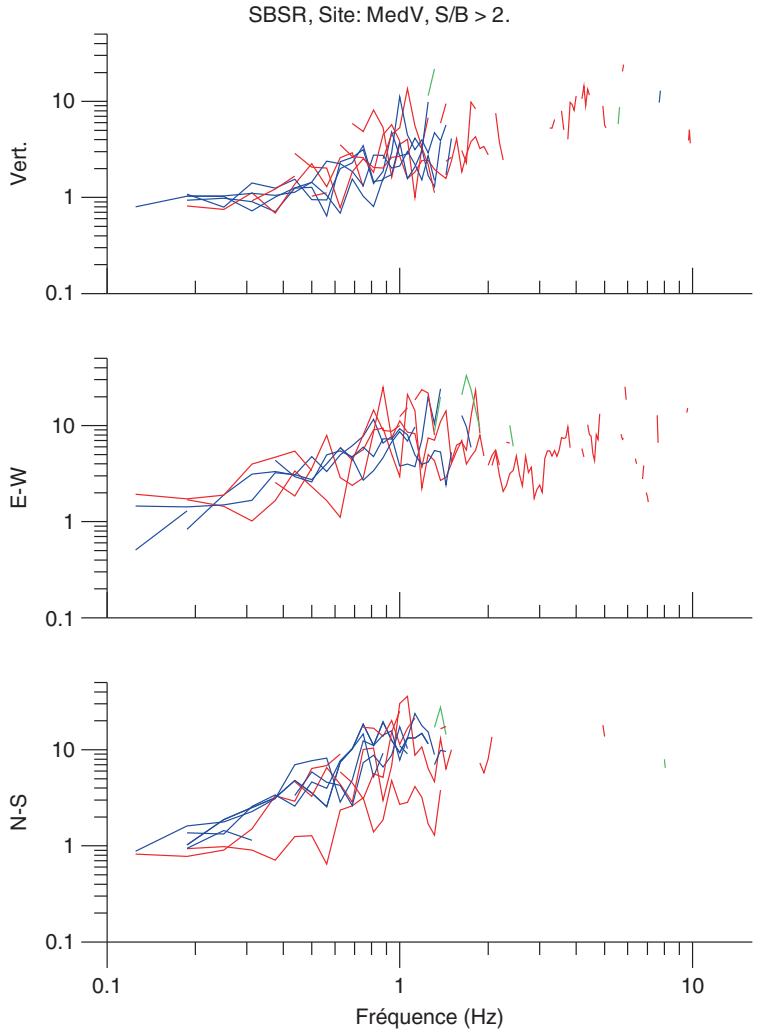

Fig. 4.6.6 Standard Spectral Ratio, SSR (or SBSR), estimated at site " MedV " with a signal-to-noise ratio S/B $>$ 2; local earthquakes are represented in red, rock blasting in green and teleseisms in blue

records carried out in Tibet, from part to part of lithospheric plates (Mari et al., 1997). This method is easy to implement and gives comparable results as SSR method's (amplified frequencies and corresponding amplitudes) as illustrated in Figure 4.6.7 where the signal-to-noise ratio of 2 corresponds to a coefficient of coherence of 0.9. The use of a Wiener filtering permits to extend the range of frequencies which is not covered by the Standard Spectral Ratio and hence, to identify new amplified frequencies around 10 Hz.

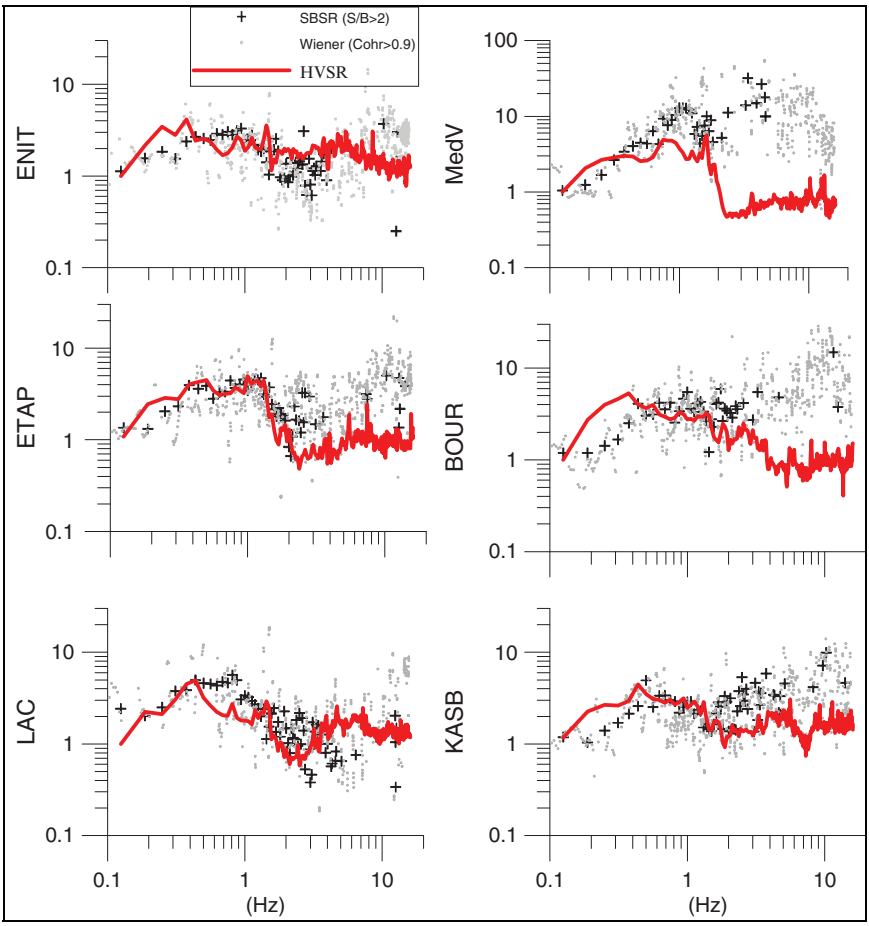

Fig. 4.6.7 Median values of Wiener filter (coherence modulus >0.9), SSR transfer function (S/B >2) and HVSR versus frequency obtained at each station of the network (north-south horizontal components) taking into account all the records

4.6.3.2 H/V technique

The Horizontal to Vertical Spectral Ratio (HVSR) was computed with microtremors selected in nocturnal records at each stations of the seismological network and superimposed to SSR and Wiener filter modulus in Figure 4.6.7. We can observe that the first amplified frequencies are comparable and that the corresponding amplitudes are very close. However, and as expected, amplitudes given by HVSR are lower than those of SSR method beyond 2 Hz.

Since the validity of H/V technique was checked on the principal geotechnical features, a dense microtremor measurement survey covered 330 points over the city and the edges of the Lac de Tunis (Figure 4.6.5). The stability in time and space of

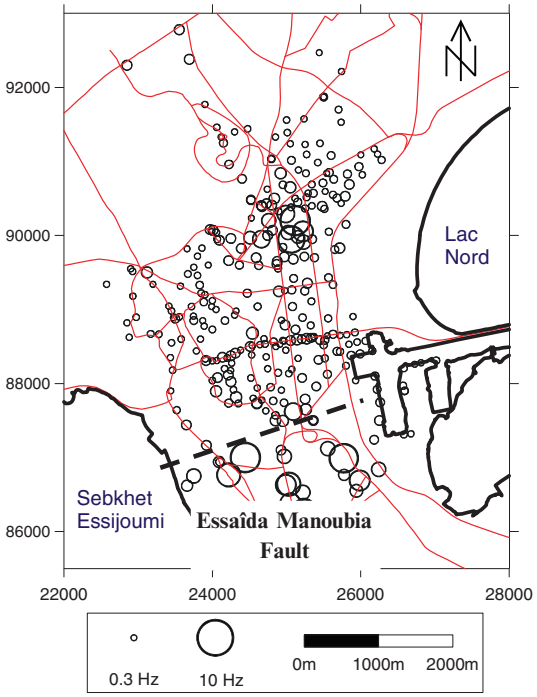

Fig. 4.6.8A HVNR frequency peaks map

HVSR was tested and it is important to emphasize the coherence between the values of HVSR and the geotechnical zoning (Bouden-Romdhane et al., 2000).

Figures 4.4.8A and 4.4.8B show the amplified frequencies and corresponding amplitudes maps. The highest amplified frequencies are estimated on the Eocene outcropping limestone in the southern compartment of Essaîda Manoubia fault. In the northern part of this fault, low to very low frequencies predominate: about 60% of these frequencies are below 1 Hz. On the other hand, strong site amplifications are expectable in silty infill areas. The amplification factor increases with the thickness of the soft fill especially in the vicinity of the banks of the Lac de Tunis (Bouden-Romdhane and Mechler, 2002).

4.6.4 Numerical modeling

One major objective of the seismic site response analysis is the comparison between the measured and the calculated natural site frequencies (and corresponding amplification factors).

The 1D site response analyses are based on the equivalent linear model, EERA (Bardet et al., 2000), and the nonlinear hysteretic model, NERA (Bardet and Tobita,

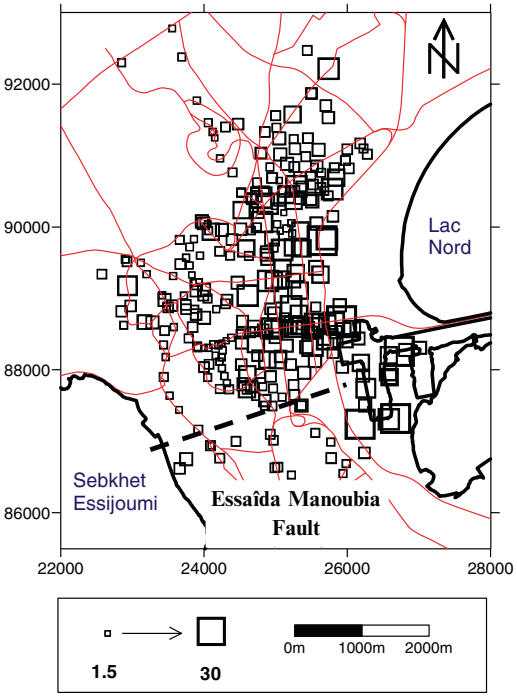

Fig. 4.6.8B HVNR amplitude factors map corresponding to frequency peaks represented in Figure 4.6.8A

2001). The deep borehole "serept1" is located in the central basin (Figure 4.6.3) in the vicinity of the Lac de Tunis where the layers have a tabular disposition due to the sedimentation in lagoonal conditions. A layer description, 400 m deep, is available at this site as well as weak motions and microtremors recordings. The site response models were constructed using shear wave velocities deduced from correlations between pressiometric parameters (E, Pl), SPT and shear strength available at the sites (Bouden-Romdhane, 2002; Sassi, 2004). The variation of shear modulus and damping ratio with shear strain amplitude are available for the first 20 m of the silty formations (Kanoun, 1981). For deeper silty and clayey layers, the strain dependencies on shear moduli and damping ratio were assumed to be described by the standardized G/Gmax and damping curves recommended for Japanese port areas soils (PHRIE, 1997) and Californian soils (Vucetic and Dobry, 1991) with similar confining pressures and geotechnical properties, such as OCR and plastic Index IP. Such analyses show that the amplified frequencies and the corresponding amplification are controlled by the upper deposits (Bouden-Romdhane and Mechler, 2002). The 1D modelling was hence generalised to all the area and the comparison of the results with those of the H/V Technique permitted to define the spatial limits of a 1D modeling.

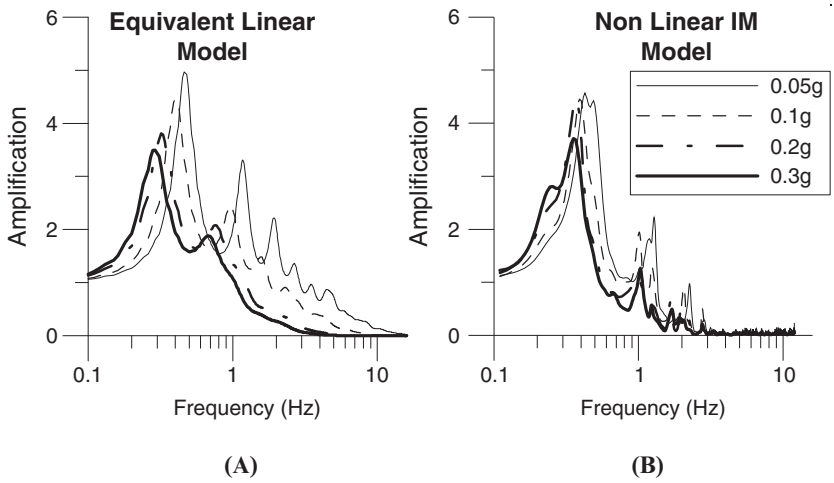

Fig. 4.6.9 Spectral amplification factor versus frequency computed using EERA (A) and NERA (B) for various input ground motions at site "serept1"

As the recorded accelerations (weak motions and microtremors) during the both campaigns did not exceed 0.001 g, we also analysed the seismic site response for increasing shaking levels ranging from 0.05g to 0.3 g according to the regional hazard studies (Ksentini, 2004). Figure 4.6.9A, B show the transfer functions computed at "serept1", using respectively EERA and NERA. Both soil models display a similar slip of amplified frequencies toward lower frequencies (about 40%) and a decrease of the corresponding amplification factors at the rate of 1.2 to 1.4.

All the results (peak of frequency and corresponding amplification factor for increasing levels of input acceleration) were implemented in a GIS environment (examples in Figure 4.6.10A, B).

4.6.5 Liquefaction potential assessment

As point out in Section 4.6.2.2, the superficial lithology (the last 70 m) of the Valley of Tunis and the edges of the Lac de Tunis includes a saturated silty unit which is interrupted, by plastic clayey-sandy interbeds, sandy soils or sandstone lenses. The liquefaction potential assessment of these features was conducted in three levels, following the recommendations of the French Agency of Seismic Protection (AFPS, 1993):

1. A detailed study of geological and hydro geological data of the site (geology and piezometric data as well as laboratory testing results). The formations are classified as susceptible to liquefaction or not according to the recommendations of Youd and Perkins (Youd and Perkins, 1978), the recommendations of Seed et al. (Seed et al., 2003) and the grading envelop of liquefiable sands (Pecker, 1984).

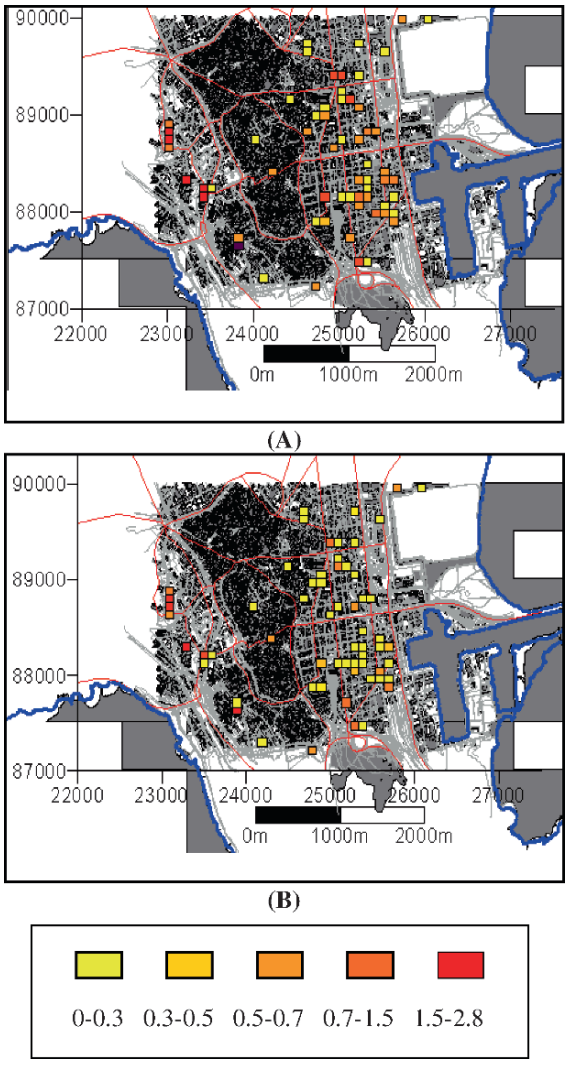

Fig. 4.6.10 Amplified frequency maps for 0.1 g (A) and 0.2 g (B) input ground acceleration (Sassi, 2004)

2. A comparison between the cyclic resistance ratio (CRR) expressed in terms of the prevailing soil stress characteristics taken out from the in situ tests results (SPT and CPT tests) and the cyclic intensity of loading, expressed by the equivalent uniform cyclic stress ratio (CSReq) according to the "simplified method" established by Seed and Idriss in 1971.
3. A one-dimensional seismic analysis, based on the computing of shear stress of the investigated soil considering a viscoelastic behaviour of the materials. The calculation was carried out by means of the computer code EERA® (2000)

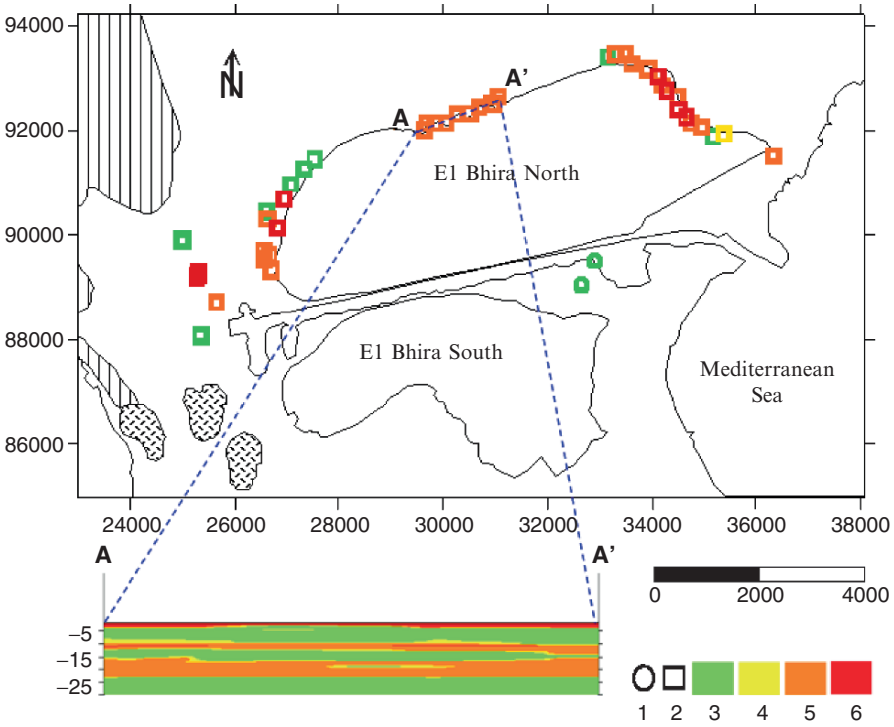

Fig. 4.6.11 Susceptibility to liquefaction for an expected PGA of 0.15 g, at a depth of −15 m; 1: SPT, 2: CPT, 3: no liquefaction, 4: low liquefaction potential, 5: moderate liquefaction potential, 6: high liquefaction potential (Anibi and Bouden-Romdhane, 2007)

which requires geophysics parameters of soil (Vs, Gmax, etc.); an original approach used a correlation between the needed parameters and the plentiful pressiometric data available in Tunis City and all around the edges of the Lac de Tunis (Sassi, 2004).

This study had led to the development of liquefaction maps and cross sections (an example is given in Figure 4.6.11) representing the variation of the liquefaction potential with the depth for different expected shake levels calculated according to a deterministic analysis of the regional and local risk (Ksentini, 2004).

4.6.6 Final remarks

Seismic hazard analysis is the major component of microzonation for seismic hazard and seismic risk. It can be an expensive and time consuming activity. The Standard Spectral Ratio method suffers in Tunis from major practical difficulties, particularly the long and costly data acquisition duration (because of the low regional seismic

activity) and the difficulty of undertaking seismic measurements due to the high level of the ambient background noise. The use of a Wiener filtering permits to ameliorate the accuracy of the site filter and hence, the Nakamura technique was compared and checked.

The microtremors measurement survey shows that the basin of Tunis is characterized by low natural frequencies and strong site amplifications are expected in zones with silty infill.

The 1D site response analysis confirmed the natural site frequencies obtained from microtremor measurements, mainly in zones with tabular lithology in the vicinity of the Lac de Tunis. For increasing ground motions, the numerical modeling shows a diminution of the dynamic site frequencies and the corresponding amplification factors.

Finally, the liquefaction potential assessment, based on AFPS recommendations, also shows that moderate liquefaction potential is expected on the edges of the Lac de Tunis. Further studies in progress are using detailed static and dynamic geotechnical properties of the subsurface loose layering.

Acknowledgment This overview chapter corresponds to studies developed during one decade in collaboration with two institutions: The Département de Géophysique Appliquée (Université Paris 6) and the CETE-Méditerranéen. Many colleagues and students have participated in the developments summarised here, to whom I would like to express my sincere acknowledgement: Sylvain Vidal, Christian Camerlynck, Faycal Rejiba, Anouar Romdhane, A.Sassi, A. Ksentini, and A. Dhmaied.

References

AFPS (1993) Guide méthodologique pour la réalisation d'études de microzonage sismique, Saint-Rémy-lès-Chevreuse.

Anibi S, Bouden-Romdhane N (2007) Contribution à l'estimation du risque de liquéfaction du sous sol de Tunis. Colloque international "Sols et matériaux à problèmes", 09–11 Février 2007, Tunisie.

Bardet J P, Tobita T (2001) NERA: A computer program for nonlinear earthquake site response analysis of layered soils deposits. University of South California, Department of Civil Engineering, 40p.

Bardet J P, Ichii K, Lin C H (2000) EERA: A computer program for equivalent-linear earthquake site response analysis of layered soils deposits. University of South California, Department of Civil Engineering, 38p.

Ben Ayed N, Viguier C (1978) Observations sur la tectonique récente du Néogène continental de Tunis. Bull. Soc. Sc. Naturelles de Tunisie, T13, 105–108.

Bouden-Romdhane N (2002) Contribution au Microzonage Sismique de Tunis, Evaluation de l'Effet de Site, Sc Thesis, Ecole Nationale d'Ingénieurs de Tunis, 320p.

Bouden-Romdhane N, Mechler P (2002) Seismic site effect, evaluation methods: application to the city of Tunis. Bull. Eng. Geol. Env., 61:269–281.

Bouden-Romdhane N, Mechler P, Duval A M, Menerould J P, Vidal S (2000) Microzoning the city of Tunis, using both background noise and weak motions. Proc.12th World Conf. Earthq. Eng., Auckland, New Zealand, 8p.

Bousquet J C, Philip H (1981) Les caractéristiques de la néotectonique en méditerranée occidentale- Sedimentary basins of mediterranean margins. F.C.Wezel, Ed., C.N.R., Italian Project of oceanography, Tecnoprint, Bologne, pp. 389–405.

Boutib L (1998) Tectonique de la région du Grand Tunis: évolution géométrique et cinématique des blocs structuraux du Mésozoîque à l'Actuel (Atlas nord oriental de Tunisie). Thèse de Doctorat de l'Université Tunis II, Faculté des Sciences de Tunis, 170p.

Dlala M, Rebaî S (1994) Relation compression-extension Miocène supérieur à Quaternaire en Tunisie: implication sismotectonique. C. R. Acad. Sci. Paris, 319, série II, 945–950.

Kanoun F (1981) Propriétés dynamiques de la vase de Tunis, Ph.D. thesis, Ecole Nationale d'Ingénieurs de Tunis, Tunisia.

Ksentini A (2004) Apport des systèmes d'information géographique dans l'analyse et la gestion du risque sismique. mémoire de mastère à l'ENIT, 91p.

Mari J L, Glangeaud F, Coppens F (1997) Traitement du signal pour géologues et géophysiciens. Editions Technip, Paris, 460p.

Pecker A (1984) Dynamique Des Sols. Edition de l'Ecole Des Ponts et Chaussées.

Piementa J (1959) Le cycle pliocène-actuelle dans les bassins paralyques de Tunis. Thèse de la Faculté des Sciences de Paris et Mémoire de la Société Géologique de France, 85, 180p.

PHRIE (Port and Harbour Research Institute, Editor) (1997) Handbook on liquefaction remediation, A.A.Balkema, Rotterdam, The Netherlands.

Sassi A (2004) Simulation numérique unidimensionnelle de l'effet de site sismique et son application au micro zonage de la ville de Tunis. mémoire de diplôme d'études approfondis, ENIT, 69p.

Seed R B, Cetin R E S, Moss A, Kammerer J, Wu J M, Pestana M F, Riemer R B, Sancio J D, Bray R E, Kayen R E, Faris A (2003) Recent advances in soil liquefaction engineering: A unified and consistent framework. 26th Annual ASCE Los Angeles Geotechnical Spring Seminar, Keynote Presentation, H.M.S. Queen Mary, Long Beach, California.

Vucetic M, Dobry R (1991) Effect of Soil Plasticity on Cyclic Response, Journal of the Geotechnical Division, ASCE, Vol. 111, No. 1, 89–107.

Youd T L, Perkins D M (1978) Mapping liquefaction-induced ground failure potential. Journal of the Geotechnical Engineering Division 104, 433–446.

Chapter 4.7
An Empirical Geotechnical Seismic Site Response Procedure*

Adrian Rodriguez-Marek, Jonathan D. Bray, and Norm A. Abrahamson

Abstract A simplified empirically based seismic site response evaluation procedure that includes measures of the dynamic stiffness of the surficial materials and the depth to bedrock as primary parameters is introduced. This geotechnical site classification scheme provides an alternative to geologic-based and shear wave velocity-based site classification schemes. The proposed scheme is used to analyze the ground motion data from the 1989 Loma Prieta and 1994 Northridge earthquakes. Period-dependent and intensity-dependent spectral acceleration amplification factors for different site conditions are presented. The proposed scheme results in a significant reduction in standard error when compared with a simpler "rock vs. soil" classification system. Moreover, results show that sites previously grouped as "rock" should be subdivided as competent rock sites and weathered soft rock/shallow stiff soil sites to reduce uncertainty in defining site-dependent ground motions. Results also show that soil depth is an important parameter in estimating seismic site response. The standard errors resulting from the proposed site classification system are comparable with those obtained using the more elaborate code-based average shear-wave velocity classification system.

Keywords Site Classification · Soils · Vs30

A. Rodriguez-Marek (✉)
Department of Civil and Environmental Engineering, Washington State University, Pullman, WA 99164-2910

J.D. Bray
Department of Civil and Environmental Engineering, University of California, Berkeley, CA 94720-1710

N.A. Abrahamson
Geosciences Department, Pacific Gas & Electric Company, San Francisco, CA 94177

* This article appeared first in the February 2001 issue of *Earthquake Spectra* and is reprinted here with permission of EERI.

M. Mucciarelli et al., (eds.), *Increasing Seismic Safety by Combining Engineering Technologies and Seismological Data,* NATO Science for Peace and Security Series C: Environmental Security,

4.7.1 Introduction

Significant damage and loss of life has been directly related to the effect of local site conditions in several recent earthquakes (e.g., 1985 Mexico City, 1989; Loma Prieta, 1994 Northridge, and 1995 Kobe earthquakes). While there are potentially other factors contributing to damage (such as topography, basin effects, liquefaction, and structural deficiencies), the amplification of ground motion due to local site conditions plays an important part in increasing seismic damage. The correlation between site effects and building damage is dramatically illustrated in Figure 4.7.1 by the work of Seed et al. (1972) for the 1967 Caracas earthquake. Significantly more damage occurred when the natural period of the building "matched" that of the soil deposit. Soils in the Caracas region are relatively uniform in stiffness, so that variations in soil depth led to the observed large levels of structural damage for buildings with natural periods close to that of the underlying soil deposit (Seed et al., 1972). These observations, as well as numerous others, indicate that quantification of site effects is a necessary component of a comprehensive assessment of seismic hazard. Moreover, the quantification of site effects should include a measure of uncertainty for its incorporation into a probabilistic seismic hazard assessment.

The importance of site effects in characterizing seismic ground motions has long been recognized (e.g., Seed and Idriss, 1982). Recently, Borcherdt (1994) developed

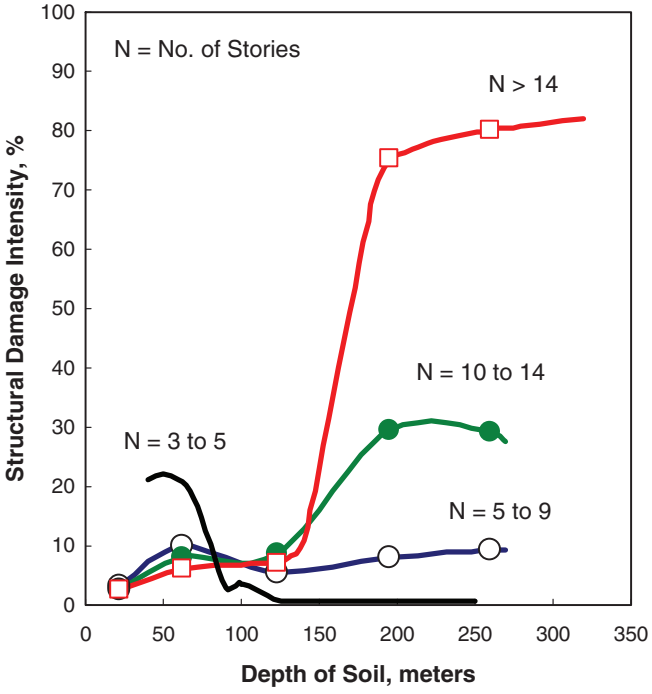

Fig. 4.7.1 Relationship between structural damage intensity and soil depth for the 1967 Caracas earthquake (From Seed et al., 1972)

intensity-dependent, short- and long-period amplification factors based on the average shear-wave velocity measured over the upper 30 m of a site. This work along with work by Seed et al. (1991) and Dobry et al. (1994) has been incorporated into the 1997 Uniform Building Code (UBC, ICBO, 1997). Using the average shear-wave velocity over a set 30 m depth to classify a site has the advantage of uniformity. Seismic site response, however, is also a function of soil depth as shown already in Figure 4.7.1. Thus, ignoring soil depth may introduce an undesirable level of uncertainty in ground motion prediction. Moreover, 1997 UBC/Borcherdt (1994) site amplification factors are based primarily on observations from the 1989 Loma Prieta earthquake, which shows significant nonlinear site response effects; whereas, observations from the 1994 Northridge earthquake indicate that site amplification factors should not decrease as rapidly with increasing ground motion intensity (e.g., Trifunac and Todorovska, 1996; Chang et al., 1997). Hence, the current code site factors may be unconservative, and this requires re-evaluation using the extensive Northridge ground motion database.

Site effects have also been introduced into most current ground motion attenuation relationships (e.g., Abrahamson and Silva, 1997; Campbell, 1997; Sadigh et al., 1997). However, most attenuation relationships account for site effects only through a broad site classification system that divides sites into either "rock" (actually, rock and shallow stiff soil) or "soil" (actually, intermediate to deep stiff soil), with the additional "soft soil" category for this special case (e.g., Abrahamson and Silva, 1997; Sadigh et al., 1997). Data from recent earthquakes suggest that a further refinement in this classification system is warranted to achieve improved predictions of ground motions.

This paper introduces a new "simplified" geotechnically based site classification system that includes both a measure of soil stiffness and depth. The site classification system is applied to ground motion sites from two recent earthquakes: the 1989 Loma Prieta and 1994 Northridge earthquakes. Ground motion estimates include quantification of the level of uncertainty associated with the prediction. Results are used to evaluate the validity of the proposed classification system and to compare its performance to a more simplified "rock vs. soil" attenuation relationship approach and to the more elaborate code shear-wave velocity classification system. Emphasis is placed on evaluating the importance of soil depth. Site-dependent, intensity-dependent spectral amplification factors with respect to a baseline site condition are presented. These factors can be incorporated into a probabilistic seismic hazard assessment to achieve an improved estimate of ground motions that includes the important effects of local site conditions.

4.7.2 Site classification system

The site classification system proposed herein is an attempt to capture the primary factors affecting seismic site response while minimizing the amount of data required for site characterization. It was developed to evaluate if significant reductions in

uncertainty could be achieved by employing a site classification scheme more sophisticated than the simple "rock vs. soil" scheme often used in probabilistic seismic hazard assessments. The reduction in uncertainty has to be sufficient to justify the additional effort required to implement the proposed site classification system.

The amplification of ground motions at a nearly level site is significantly affected by the natural period of a site ($T_n = 4H/V_s$; where T_n = natural period, H = soil depth, and V_s = average shear-wave velocity); both dynamic stiffness and soil depth are important. Although earlier codes made use of natural site period as a means to classify site conditions (e.g., 1976 UBC), recent codes such as the 1997 UBC use average shear-wave velocity over the upper 30 m of a site as the sole parameter for site classification. Such a parameter is only an indirect measure of the depth of soil deposit.

The seismic response characteristics of a site will also vary as a function of the intensity of the ground motion, due to the nonlinear stress-strain response of earth materials. The effect of soil nonlinearity is largely a function of soil type (e.g., Vucetic and Dobry, 1991). Factors such as geologic age and cementation may also affect the nonlinear response of soil and rock. The primary effects of material nonlinearity are twofold: (a) the site period increases and (b) material damping increases, as the intensity of ground motion increases. The larger damping levels result in lower spectral amplifications for all periods. The effect of damping, however, is more pronounced for high frequency motion. Hence, peak ground acceleration (PGA) is more significantly affected by soil damping. The consequences of the shift toward higher site periods depend on the soil type and input motion. For some sites, the site period may be shifted toward periods containing high-energy input motion, resulting in large spectral accelerations with an associated increase in PGA. Conversely, the site period may be shifted to periods where the energy of the input motion is low, resulting in a decrease of amplification over short periods. This may result in lower levels of PGA, and possibly even in attenuation of PGA.

The proposed site classification system is based on two primary parameters and two secondary ones. The primary parameters are as follows:

1. Type of deposit, i.e., hard rock, competent rock, weathered rock, stiff soil, soft soil, and potentially liquefiable sand. These general divisions introduce a measure of stiffness (i.e., average shear-wave velocity) to the classification system. However, a generic description of a site is sufficient for classification, without the need for measuring shear-wave velocity over the upper 30 m.
2. Depth to bedrock (defined by $V_s \geq 760$ m/s) or to a significant impedance contrast between surficial soil deposits and material with Vs ≈ 760 m/s.

The secondary classification parameters are depositional age and soil type. The former divides soil sites into Holocene or Pleistocene groups and the latter into primarily cohesive or cohesionless soils. These subdivisions are introduced to capture the anticipated different nonlinear responses of these soils. Table 4.7.1 summarizes the site classification scheme. This classification system (referred to as B&R-M) allows for an evaluation of the importance of soil depth on seismic site response.

Table 4.7.1 Simplified geotechnical site categories (Bray and Rodriguez-Marek, 1997)

Site	Description	Site period	Comments
A	Hard rock	$\leq$0.1 s	Hard, strong, intact rock; $V_s \geq 1,500$ m/s
B	Rock	$\leq$0.2 s	Most "unweathered" California rock cases ($V_s \geq 760$ m/s or $<$6 m of soil).
C-1	Weathered/soft rock	$\leq$0.4 s	Weathered zone $>$ 6 m and $<$30 m ($V_s > 360$ m/s increasing to $>$700 m/s)
-2	Shallow stiff soil	$\leq$0.5 s	Soil depth $>$6 m and $<$30 m
-3	Intermediate depth stiff soil	$\leq$0.8 s	Soil depth $>$30 m and $<$60 m
D-1	Deep stiff holocene soil, either S (sand) or C (clay)	$\leq$1.4 s	Soil depth $>$60 m and $<$200 m. Sand has low fines content ($<$15%) or non-plastic fines (PI $<$ 5). Clay has high fines content ($>$15%) and plastic fines (PI $>$ 5).
-2	Deep stiff pleistocene soil, S (sand) or C (clay)	$\leq$.4 s	Soil depth $>$60 m and $<$200 m. See D_1 for S or C sub-categorization.
-3	Very deep stiff soil	$\leq$2 s	Soil depth $>$200 m.
E-1	Medium depth soft clay	$\leq$0.7 s	Thickness of soft clay layer 3 m to 12 m
-2	Deep soft clay layer	$\leq$1.4 s	Thickness of soft clay layer $>$12 m.
F	Special, e.g., potentially liquefiable sand or peat	$\approx$ 1 s	Holocene loose sand with high water table ($z_w \leq 6$ m) or organic peat

4.7.3 Ground motion and site data

Ground motion data from two recent earthquakes (i.e., the 1989 Loma Prieta and 1994 Northridge earthquakes) were used in this study. Most ground motion recordings were obtained from a database provided by Dr. Walter Silva from Pacific Engineering and Analysis (W.J. Silva, 1998, personal communication). The database consists of computed elastic spectral acceleration values at 5% damping and peak ground accelerations. Details on the ground motion recordings used are given in Rodriguez-Marek et al. (1999). This report also includes detailed documentation of the site conditions of the recording stations used in this study. The B&R-M site designations for the recording stations are summarized in the appendix as Tables A1 and A2.

The distribution of ground motion data sites as a function of site type and distance is given in Figure 4.7.2. The response spectral values are only used if the frequency is greater than 1.25 times the high-pass-corner frequency and less than 1/1.25 times the low pass-corner frequency (Abrahamson and Silva, 1997). Consequently, the number of recordings is also a function of spectral period (Figure 4.7.3).

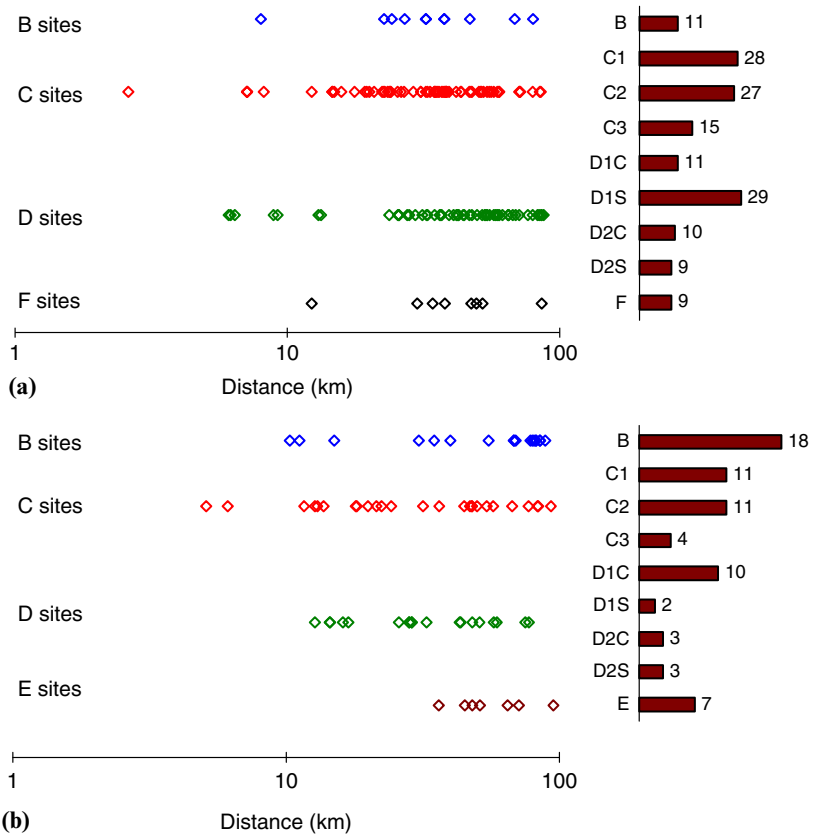

Fig. 4.7.2 Distribution of data by site type: **(a)** Northridge earthquake, and **(b)** Loma Prieta earthquake

4.7.4 Analysis

The ground motion data were used to develop earthquake-specific attenuation relationships for the elastic acceleration response spectra at 5% damping for each major site type. The earthquake-specific attenuation relationships were then used to develop site-dependent amplification factors with respect to a baseline site condition. Site condition B, "California Rock," was selected to be the baseline condition. This is in accordance with the *1997 UBC* and most attenuation relationships (e.g., Idriss, 1991; Abrahamson and Silva, 1997). The site-dependent amplification factors are a function of both spectral period and intensity of motion. Amplification factors estimated for both earthquakes are then combined to develop recommendations that can be generalized to other events.

A basic form of an attenuation relationship was selected for the event-specific attenuation relationships, that is,

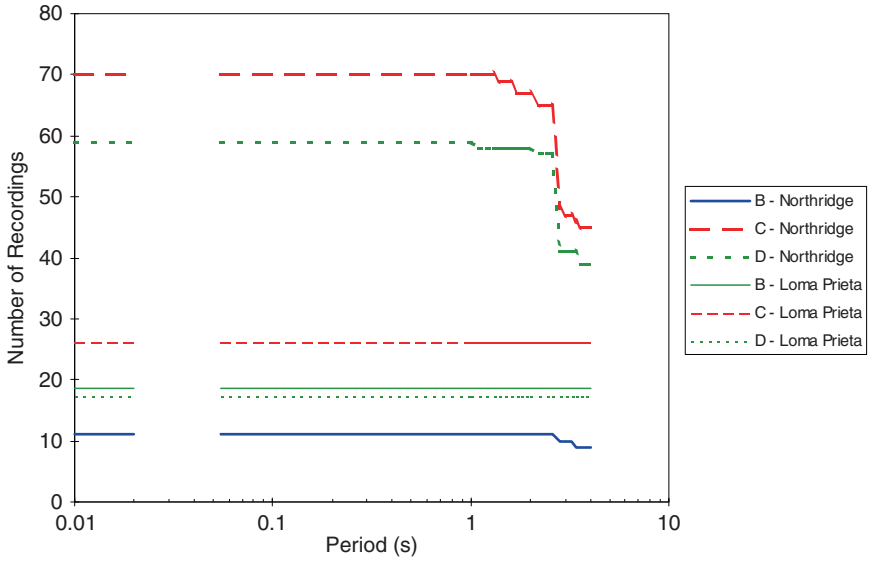

Fig. 4.7.3 Number of recordings as a function of period and site type (PGA values identified on this and other figures as the spectral ordinate at T = 0.01 s)

$$ln[S_a] = a + bln(R + c) + \varepsilon \tag{4.7.1}$$

where, *ln[Sa]* is the natural logarithm of the spectral acceleration at a specified period, T; R is the closest distance to the rupture zone (Sadigh et al., 1997); ε is an error term; and a, b, and c are regression coefficients. Equation (4.7.1) is used for various spectral periods, thus the regression coefficients a, b, and c, and the error term ε are functions of period. This functional form was previously used by Idriss (1991) and P.G. Somerville (1998, personal communication).

This functional form does not capture the effects of directivity (Somerville et al., 1997) and hanging-wall (Abrahamson and Somerville, 1996). Forward-directivity effects result in larger response spectral values at periods longer than 1 s for near-fault sites and for the component of motion perpendicular to the fault orientation. Directivity and hanging-wall effects introduce a systematic bias for the affected near-fault sites. This bias, however, affects all near-fault sites, so the effect on amplification factors should be relatively minor. A list of sites affected by these effects is given in Rodriguez-Marek et al. (1999).

The regression coefficients were estimated by means of a maximum likelihood estimate (Benjamin and Cornell, 1970). The error term ε in Equation (4.7.1) is assumed to be normally distributed with mean zero and standard deviation σ. With this assumption, maximum likelihood estimates are equivalent to ordinary least squares estimates (Benjamin and Cornell, 1970). The regression analysis was performed at selected periods separately for each earthquake and each major site condition. Soft soils (Site E) were excluded from the analysis because of the lack of soft soil data from the Northridge earthquake and their low number and poor distribution

with distance in the Loma Prieta earthquake (see Figure 4.7.2). Potentially liquefiable sand deposits (Site F) were also excluded from the analysis because response at these sites is mainly a function of whether or not liquefaction is triggered or partially triggered (i.e., significant pore pressure generation develops) at the site. Triggering of liquefaction is a function of the intensity and duration of ground motion, the relative density of the soil, the fines content of the soil, as well as other factors. If liquefaction is triggered or nearly triggered, ground motion is a function of a number of parameters including rate of excess pore pressure generation, dissipation of pore pressure, shear modulus degradation, duration of motion, site geometry, as well as other factors. The analysis of these sites is beyond the scope of this "simplified" site classification scheme.

Some of the coefficients in Equation (4.7.1) were constrained to render reasonable relationships. The coefficient c was assumed to be non-negative for all periods. Moreover, the coefficient c was held constant across site conditions to avoid the coupling of uncertainty in the coefficient c with the uncertainty in amplification factors. This is consistent with a number of previous studies (e.g., P.G. Somerville, 1998, personal communication; Abrahamson and Silva, 1997). The coefficient a in the Northridge earthquake was constrained such that it is equal for sites B and C. This constraint was necessary because of the poor sampling of Site B across all distances in the Northridge earthquake.

Most of the ground motion sites are concentrated between 20 and 70 km of the zone of energy release (Figure 4.7.2). Accordingly, the resulting attenuation relationships are judged to be appropriate for sites located within this distance range from a fault. Only three rock sites (Site B) in the Northridge earthquake, and one in the Loma Prieta earthquake are located closer than 20 km from the rupture plane. This is especially important, because Site B is the baseline site for developing amplification factors.

4.7.5 Results and discussion

The coefficients a, b, c, and σ found in the regression analyses of each earthquake were smoothed across period. The resulting earthquake specific attenuation relationships are illustrated in Figure 4.7.4 for a distance of 30 km. Spectral values as a function of distance for selected periods are shown in Figure 4.7.5. Values of the coefficients are listed in Table 4.7.2.

4.7.5.1 Evaluation of the proposed classification system

The three most common site types in Table 4.7.1: rock, soft weathered rock/shallow stiff soil, and deep stiff soil, have significantly different seismic response characteristics as shown in Figures 6.2.4 and 6.2.5. Site B (rock) and Site D (deep stiff soil)

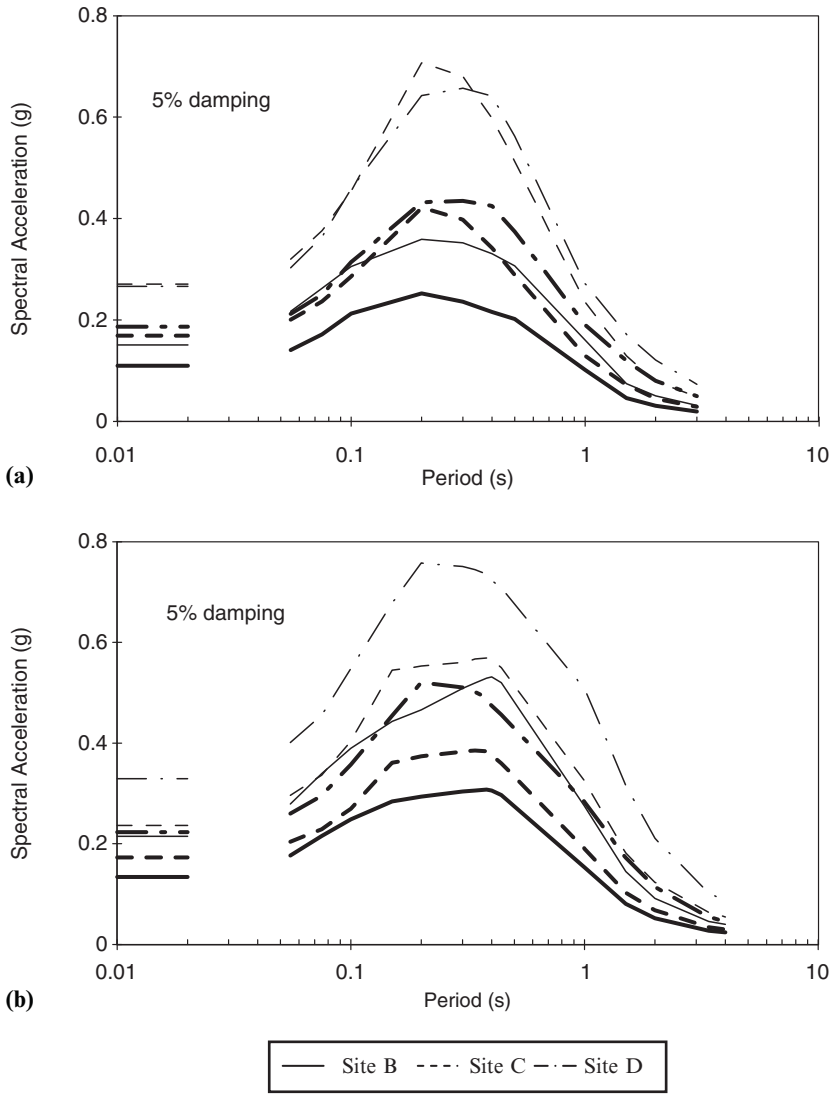

Fig. 4.7.4 Event-specific acceleration response spectra (5% damping) at a distance of 30 km: **(a)** Northridge earthquake, and **(b)** Loma Prieta earthquake. Thick lines represent median values, thin lines represent mean plus one standard error

have different response at all periods and distances. The difference decreases as the intensity of motion increases due to soil nonlinearity (Figure 4.7.5). Site C (soft weathered rock/shallow stiff soil) has a response between those of sites B and D. At short periods, the response of Site C approaches that of Site D, but at long periods, the response of Site D is larger due to the higher natural period of D sites (Figure 4.7.4).

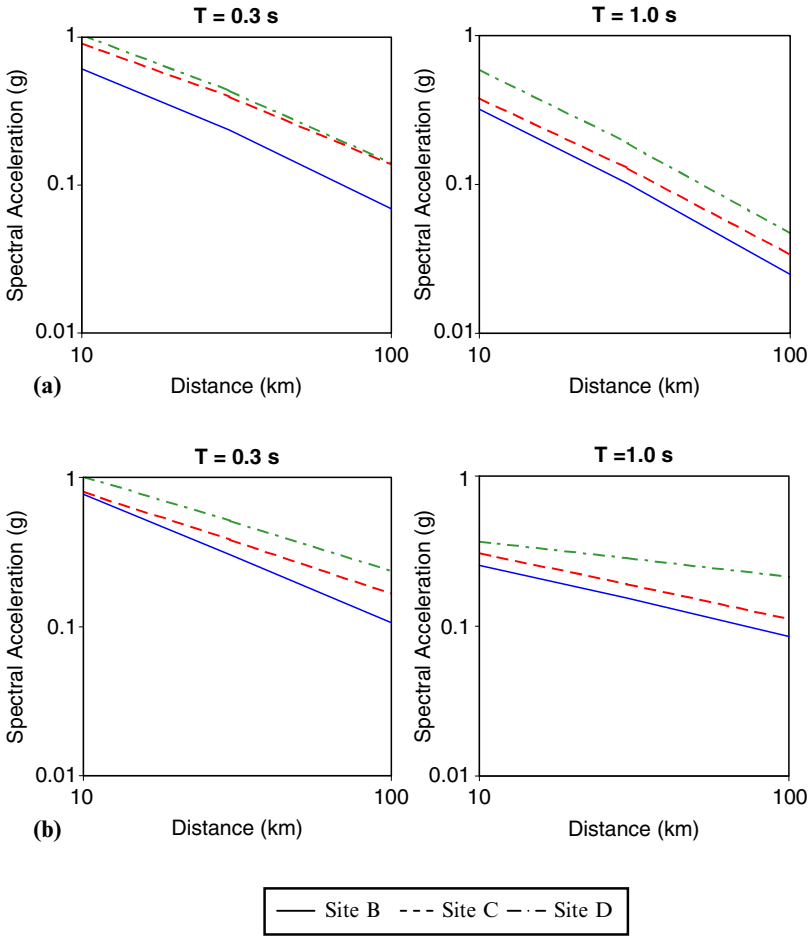

Fig. 4.7.5 Event-specific median spectral acceleration (5% damping) attenuation relationships for selected spectral periods: **(a)** Northridge earthquake, and **(b)** Loma Prieta earthquake

The relative benefits of subdividing C sites into the subcategories listed in Table 4.7.1 (C_1 = soft/weathered rock, C_2 = shallow stiff soil, and C_3 = intermediate depth stiff soil) were also evaluated. Figure 4.7.6 shows the residuals of Site C for the Northridge earthquake. Sites are identified by their classification into subcategories C_1, C_2 and C_3. Observe that no definite trend in the residuals is observed. In general, mean residuals are significantly lower than the standard error and do not show a bias. These results are representative of the results for the Loma Prieta earthquake as well. This implies that current data do not support this subdivision.

A further subdivision for deep stiff soil sites (Site D) according to age and soil type was also investigated. As shown in the classification system (Table 4.7.1), Site D is subdivided as either Holocene or Pleistocene, and as primarily clayey or sandy. Figure 4.7.7 shows the residuals for D sites for the Northridge earthquake. Mean

Table 4.7.2 Regression coefficients and standard error for the earthquake-specific attenuation relationship for selected spectral acceleration values at 5% damping

(a) Northridge earthquake

	B sites				C sites				D sites			
T	a	b	c	σ	a	b	c	σ	a	b	c	σ
PGA	2.3718	−1.2753	6.3883	0.3209	2.3718	−1.1538	6.3883	0.4686	2.6916	−1.2161	6.3883	0.3559
0.1	4.9768	−1.6855	18.0000	0.3615	4.9768	−1.6089	18.0000	0.4642	5.3000	−1.6679	18.0000	0.3774
0.2	3.4048	−1.2891	10.8444	0.3531	3.4048	−1.1508	10.8444	0.5174	3.7044	−1.2249	10.8444	0.3974
0.3	2.5178	−1.1149	4.9000	0.3983	2.5178	−0.9682	4.9000	0.5372	2.8087	1.0250	−4.9000	0.4129
0.5	2.4692	−1.1545	3.9890	0.4198	2.4692	−1.0526	3.9890	0.5739	2.7651	−1.0629	3.9890	0.4066
1.0	2.0734	−1.2443	3.2048	0.4538	2.0734	−1.1775	3.2048	0.6033	2.6601	−1.2333	3.2048	0.3551
1.5	1.7582	−1.3853	2.7461	0.4799	1.7582	−1.2588	2.7461	0.5850	2.3331	−1.2785	2.7461	0.3664
2.0	1.3896	−1.3970	2.4206	0.4799	1.3896	−1.2933	2.4206	0.5700	2.0500	−1.3154	2.4206	0.4130
3.0	0.6859	−1.3338	2.0000	0.4799	0.6859	−1.2207	2.0000	0.5200	1.3413	−1.2536	2.0000	0.3877

(b) Loma Prieta earthquake

	B sites				C sites				D sites			
T	a	b	c	σ	a	B	c	σ	a	b	c	σ
PGA	0.7219	−0.7954	1.0000	0.4713	0.8212	−0.7502	1.0000	0.3111	0.5716	−0.6032	1.0000	0.3896
0.1	2.2305	−1.0551	1.0000	0.4500	1.6419	−0.8595	1.0000	0.4027	1.5122	−0.7400	1.0000	0.4269
0.2	1.9861	−0.9352	1.0000	0.4626	1.8633	−0.8291	1.0000	0.3923	1.5961	−0.6551	1.0000	0.3761
0.3	1.8860	−0.8959	1.0000	0.5149	1.4800	−0.7104	1.0000	0.3812	1.5933	−0.6598	1.0000	0.3859
0.5	1.5766	−0.8357	1.0000	0.5658	1.0905	−0.6402	1.0000	0.4486	1.3791	−0.6481	1.0000	0.4659
1.0	−0.1915	−0.4913	1.0000	0.5854	−0.0967	−0.4555	1.0000	0.5354	−0.4193	−0.2456	1.0000	0.5852
1.5	−1.2503	−0.3703	1.0000	0.5874	−0.1493	−0.6191	1.0000	0.5697	−0.0722	−0.4911	1.0000	0.6087
2.0	−1.7950	−0.3397	1.0000	0.5674	−0.7453	−0.5663	1.0000	0.5950	−0.5395	−0.4756	1.0000	0.6160
3.0	−2.1924	−0.3596	1.0000	0.5428	−1.4567	−0.5011	1.0000	0.6189	−1.1824	−0.4400	1.0000	0.6268

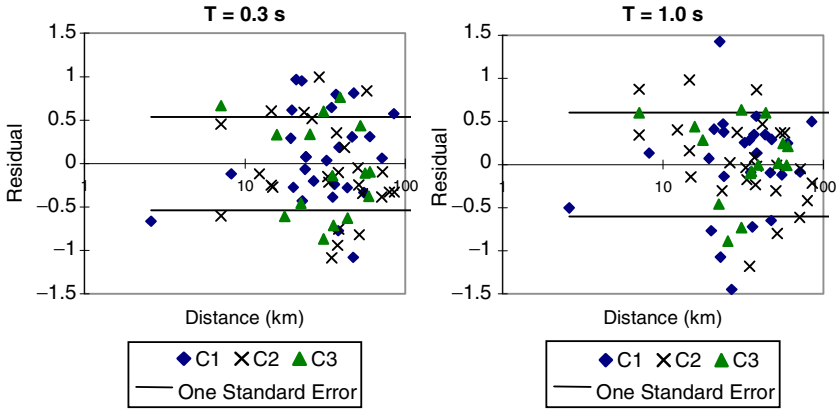

	PGA	T = 0.3	T=1	T=3
C1	0.08 (.09)	0.08 (.10)	0.10 (.13)	0.01 (.13)
C2	–0.08 (.09)	–0.10 (.10)	0.01 (.10)	0.05 (.09)
C3	–0.10 (.13)	–0.06 (.14)	0.05 (.12)	0.16 (.18)

Fig. 4.7.6 Residuals for B&R-M Site C, Northridge earthquake. Table gives mean of residuals and standard deviation of the sample mean (in parenthesis) for each subgroup

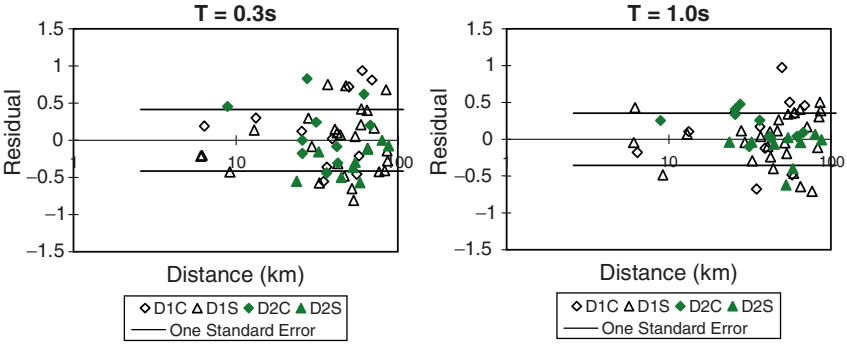

	PGA	T = 0.3	T=1	T=2
D1C	0.03 (.10)	0.14 (.16)	0.13 (.14)	0.15 (.13)
D1S	0.00 (.06)	–0.02 (.08)	0.01 (.06)	–0.07 (.09)
D2C	0.18 (.14)	0.13 (.13)	0.18 (.06)	0.04 (.14)
D2S	–0.26 (.09)	–0.29 (.07)	–0.13 (.08)	0.07 (.06)
D1	0.01 (.05)	0.02 (.07)	0.04 (.06)	–0.01 (.07)
D2	–0.03 (.10)	–0.07 (.09)	0.04 (.06)	0.05 (.08)
DC	0.10 (.09)	0.14 (.10)	0.16 (.08)	0.10 (.09)
DS	–0.06 (.05)	–0.09 (.06)	–0.02 (.05)	–0.04 (.07)

Fig. 4.7.7 Residuals for B&R-M Site D, Northridge earthquake. Table gives mean of residuals and standard deviation of the sample mean (in parentheses) for each subgroup

residuals consistently greater than zero are observed for clay sites at all periods. These mean residuals are considered important, but not overly significant when compared with the standard error for the entire distribution of around 0.4. This difference in residuals between clay and sand sites is magnified when only Pleistocene sites (D2) are considered. However, further studies are needed to confirm this trend, because the number of these sites is low. No apparent trend based solely on the age of the deposit is observed. The same general trends exist in the Loma Prieta data set, but the small number of D sites precludes a definitive finding. It appears that greater amplification occurs at clay sites, especially if Pleistocene, and this is consistent with the concept that higher plasticity soils have higher threshold strains and hence, exhibit less shear modulus reduction and less material damping at intermediate levels of ground motion. However, until additional ground motion and site classification data are obtained, the limited number of sites and records and the level of scatter associated with Site D precludes further subdivision at this time.

4.7.5.2 Comparison with a "rock vs. soil" classification system

Most current attenuation relationships use a broad site-classification system that divides sites into either rock/shallow soil or deep stiff soil, in addition to deep soft clay sites (e.g., Abrahamson and Silva, 1997). This "rock vs. soil" classification scheme is also often applied in design practice. Results from this study, however, indicate that this classification is an oversimplification, and further division into additional categories is warranted.

As a basis for comparison, the earthquake-specific attenuation model developed by P. Somerville and N. Abrahamson (P.G. Somerville, 1998, personal communication, denoted as S&A) is compared with the model developed in this study. The S&A model divides sites into rock (rock/shallow stiff soil) and soil (deep stiff soils). Deep soft clay sites are excluded. Figure 4.7.8 shows a comparison of the results at a distance of 20 km. Note that the spectra for soil sites in S&A generally match the spectra for Site D (deep stiff soils). However, the spectra for rock sites in S&A generally match the spectra for Site C (shallow and intermediate depth soils and weathered/soft rock). This result reflects the fact that for the joint database of rock and shallow soil sites, 83% of the sites are shallow soil or weathered rock sites, and only 17% of these sites actually belong to the Site B classification (competent rock sites). Note that the spectrum for Site B falls significantly below that for Site C (approximately 30% lower on average). Similar results were obtained independently by I.M. Idriss and W.J. Silva (1999, personal communication). These authors performed an analysis of strong motion at competent rock and weathered rock sites and concluded that acceleration response spectra at weathered rock sites are roughly 20% higher on average than those at competent rock sites.

Attenuation relationships are commonly used in engineering practice to predict ground motions at baseline "outcropping rock" sites. These baseline motions are often later modified for local soil conditions. The results presented herein point

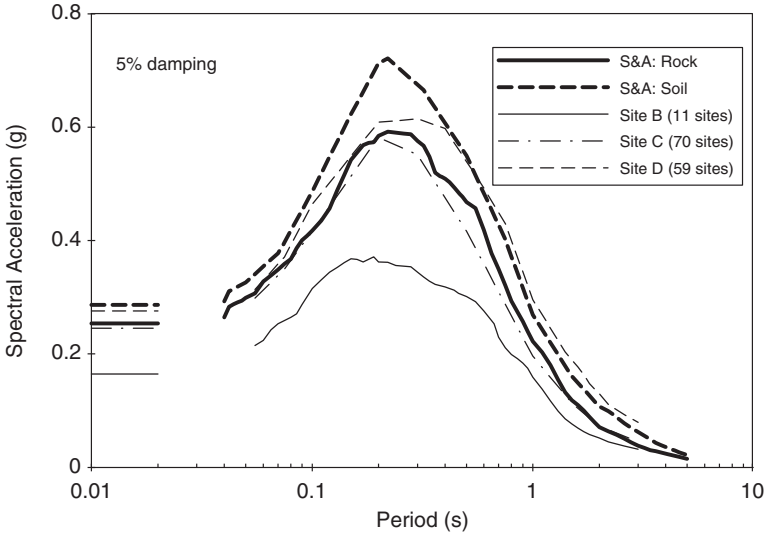

Fig. 4.7.8 Comparison of results with an earthquake-specific attenuation relationship by Somerville (1998, personal communication). Acceleration response spectra at 5% damping for the Northridge earthquake at R = 20 km

to the need of redefining the baseline "outcropping rock" condition into a more restrictive category. Many "rock" attenuation relationships used in practice actually correspond to a mix site condition that is dominated by shallow stiff soil and soft/weathered rock records due to the preponderance of these sites in the ground motion database. Hence, most "rock" attenuation relationships reflect the amplified response of soft/weathered rock and shallow stiff soil sites. The acceleration response spectrum at 5% damping for the true baseline rock condition (California rock) is consistently overestimated by that developed using currently available "rock" attenuation relationships. Thus, updated "rock" attenuation relationships that use a more restrictive baseline rock category are required.

As shown previously in Figures 6.2.4 and 6.2.5, Site B (California rock) data plot consistently below those for Site C (weathered rock/shallow stiff soil), which illustrates that a further subdivision from the "rock vs. soil" classification is warranted. More significant, however, is the reduction of uncertainty that results from the proposed classification system. Table 4.7.3 compares the standard errors from the S&A relationships with those from the relationships proposed in this report (B&R-M). The decrease in the standard error for B&R-M Site B compared with S&A rock sites is between 30% and 40%. A similar reduction is observed for soil sites (S&A Soil vs. B&R-M Site D). Standard errors for B&R-M Site C, however, remain high and are only marginally lower than standard errors for rock in the S&A model. A reduction in the uncertainty bands for sites B and D reflects the more selective grouping criteria applied in this study.

Table 4.7.3 Standard errors with standard deviations of the estimate of the standard error at selected periods (in parenthesis) for the earthquake-specific attenuation relationships for the Northridge earthquake by this study (B&R-M) and a previous study (S&A, P.G. Somerville, 1998, personal communication)

Period	B&R-M site B	B&R-M site C	B&R-M site D	Somerville & Abrahamson: Rock	Somerville & Abrahamson: Soil
PGA	0.32 (0.07)	0.47 (0.04)	0.36 (0.03)	0.53	0.48
0.3	0.40 (0.08)	0.54 (0.05)	0.41 (0.04)	0.60	0.51
1	0.45 (0.11)	0.60 (0.05)	0.36 (0.03)	0.62	0.48
2	0.48 (0.12)	0.57 (0.05)	0.41 (0.04)	0.57	0.60

4.7.5.3 Comparison with a shear wave velocity-based classification system

The proposed site classification system uses soil depth and stiffness as primary classification parameters. An alternative approach, the *1997 UBC* shear wave velocity-based classification system incorporates only the influence of soil stiffness. Ground motion sites from the Northridge earthquake were classified according to both classification systems to allow comparison of these two systems (Rodriguez-Marek et al., 1999). Although in many cases the two classification systems are consistent, they differ for some particular cases, namely:

- Weathered/soft rock sites lying on top of harder, intact rock (*UBC* Site B and B&R-M Site C)
- Shallow stiff soil or weathered/soft rock sites with depth to bedrock ranging from about 25 to 60 m (*UBC* Site D and B&R-M Site C) and
- Stiff clay or sand deposits with average shear-wave velocities only slightly larger than the boundary values determined by the *UBC* classification system (*UBC* Site C and B&R-M Site D)

More sites are classified differently for the Northridge earthquake than for the Loma Prieta earthquake. These differences result in different attenuation relationships depending on the classification system used.

Table 4.7.4 compares the standard errors at selected periods resulting from the regression analysis using both classification systems. For the Loma Prieta earthquake, standard errors for both classification systems are comparable, because site classifications generally agree. For the Northridge earthquake, standard errors vary slightly from one classification system to the other. Standard errors for Site B are slightly lower for the proposed classification system. For Sites C and D, standard errors are equal for a period of 0.3 s, but vary slightly at a period of 1.0 s. With the exception of Site D at a period of 1 s, the differences of the standard errors resulting from both classification systems are statistically insignificant. The exclusion of sites shallower than 60 m from Site D in the proposed classification system may lead to the observed reduction in the uncertainty levels. It is important to note, however,

Table 4.7.4 Standard errors with standard deviations of the estimate of the standard error at selected periods for proposed (B&R-M) and *1997 UBC* classification systems

	Northridge				Loma Prieta			
	T = 0.3 s		T = 1.0 s		T = 0.3 s		T = 1.0 s	
Site	B & R-M	UBC	B& R-M	UBC	B& R-M	UBC	B& R-M	UBC
B	0.40(0.08)	0.46(0.07)	0.45(0.11)	0.52(0.09)	0.51(0.10)	0.52(0.10)	0.58(0.11)	0.61(0.11)
C	0.54(0.05)	0.54(0.06)	0.60(0.05)	0.54(0.06)	0.38(0.05)	0.36(0.05)	0.53(0.08)	0.52(0.07)
D	0.41(0.04)	0.42(0.03)	0.36(0.03)	0.41(0.03)	0.39(0.07)	0.39(0.06)	0.59(0.11)	0.64(0.10)

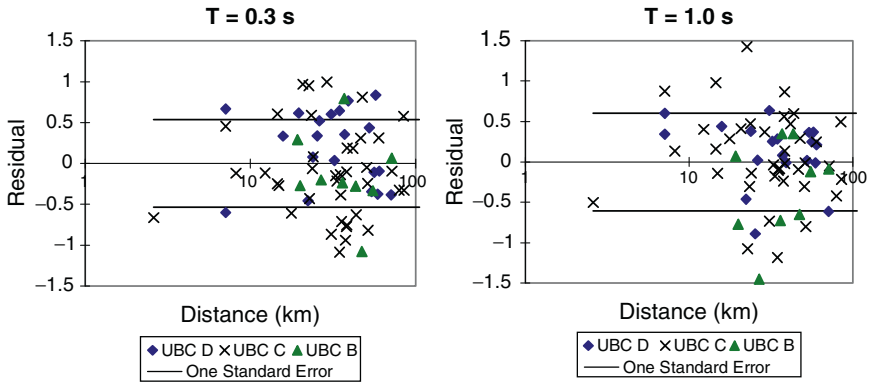

	PGA	T=0.3	T=1	T=2
UBC B	–0.08 (.14)	–0.14 (.17)	–0.34 (.20)	–0.44 (.18)
UBC C	–0.08 (.08)	–0.09 (.09)	0.08 (.09)	0.10 (.08)
UBC D	0.14 (.09)	0.19 (.11)	0.19 (.12)	0.18 (.14)

Fig. 4.7.9 Residuals for the Northridge earthquake with respect to regression analysis for proposed B&R-M Site C differentiated with respect to their corresponding *UBC* classification based on the average shear-wave velocity in the upper 30 m

the measure of soil depth introduced in the B&R-M classification scheme allows for a less exhaustive estimate of stiffness than actually measuring shear-wave velocity over the upper 30 m.

As was discussed previously, the data do not support subdividing Site C according to the guidelines given in Table 4.7.1. However, standard errors for Site C in the Northridge earthquake are relatively high. To investigate this, C sites were divided according to their average shear-wave velocity over the upper 30 m (Figure 4.7.9). In this case, significant trends in the data are observed. Relatively stiff sites (*UBC* B sites) have lower residuals than softer sites (*UBC* D sites) within the B&R-M site C class. Whereas a classification scheme based solely on average shear-wave velocity did not result in a reduction of uncertainty when compared to the

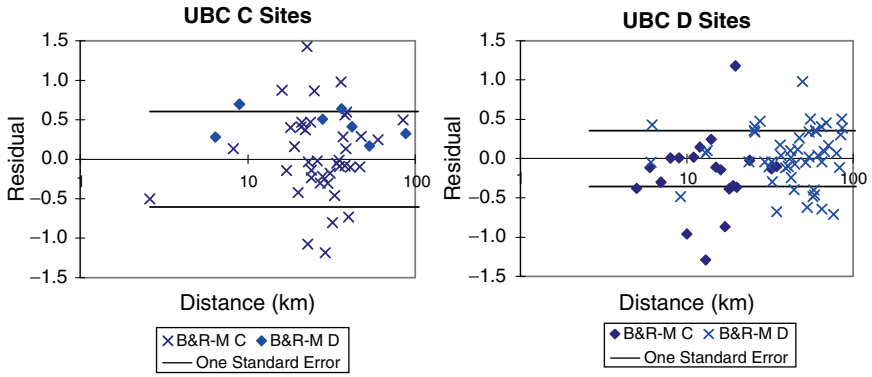

UBC C	PGA	T = 0.3	T=1	T=2
B&R-M Site C	–0.08 (.08)	–0.09 (.09)	0.08 (.09)	0.10 (.08)
B&R-M Site D	0.04 (.16)	0.02 (.18)	0.43 (.07)	0.67 (.20)
UBC D	PGA	T=0.3	T=1	T=2
B&R-M Site C	.04 (.09)	.11 (.10)	–.20 (.11)	–.40 (.15)
B&R-M Site D	.01 (.05)	.00 (.06)	.04 (.05)	.00 (.06)

Fig. 4.7.10 Residual spectral acceleration values (5% damping) from the Northridge earthquake at T = 1 s for *UBC* sites C and D differentiated by soil depth (B&R-M Site C has depth less than 60 m, B&R-M Site D has depth larger than 60 m)

proposed classification system, it appears that for shallow stiff soil sites (i.e., soil depth <60 m), refinement of the estimate of profile stiffness in the form of average shear-wave velocity does reduce uncertainty levels.

To illustrate the effect of soil depth, Figure 4.7.10 shows residuals for sites belonging to the same average shear-wave velocity group (i.e., *UBC* C or D based on average shear-wave velocity). Sites are also classified as either B&R-M Site C or Site D, corresponding to sites with soil depths lower or larger than 60 m, respectively. Deeper sites (B&R-M Site D) clearly plot above the mean for sites with intermediate average shear-wave velocity. Sites with a soil depth lower than 60 m are systematically low compared with all other *UBC* D sites. Thus, soil depth is a discriminating factor in site response. Results presented in this section point to the need to incorporate both soil depth and soil stiffness in an evaluation of seismic site response.

4.7.6 Amplification factors

The attenuation relationships developed in this paper are event-specific relations that cannot be generalized to other events. To extend the applicability of the results presented in this work, amplification factors with respect to a baseline site

condition (Site B) were obtained. The amplification factors are obtained by dividing Equation (4.7.1) for the two site conditions. The resulting relationship can be written as

$$ln\left(F_{C/B}\right) = a_{C/B} + b_{C/B} ln(R+c) \tag{4.7.2}$$

where $F_{C/B}$ is the spectral acceleration amplification factor at period T for Site C with respect to Site B, R is the closest distance to the rupture plane, and $a_{C/B}$ and $b_{C/B}$ are coefficients defined by:

$$a_{C/B} = a\,(Site\ C) - \mathrm{a}\,(Site\ B) \tag{4.7.3a}$$

$$b_{C/B} = b\,(Site\ C) - b\,(Site\ B) \tag{4.7.3b}$$

The regression coefficient c was assumed to be independent of site conditions and therefore no site-dependent ratio is necessary for this coefficient. These two coefficients were smoothed for all periods. The resulting amplification factors are shown in Figure 4.7.11. For the Loma Prieta earthquake, a reduction in spectral amplification factors for increasing levels of base rock motion is observed for periods shorter than 1 s. This trend is consistent with nonlinear soil behavior. At periods greater than 1 s, spectral amplification values do not necessarily decrease with increasing levels of base rock motion, as soil response nonlinearity would also tend to increase the response at larger periods as the site softened. Other issues may have affected the data in this period range, such as basin effects and surface waves. In addition, rather than a reflection of soil response, these observations may be a result of the significant scatter of the data at long periods. Moreover, for high values of PGA, the attenuation relationships are not well constrained due to the lack of near-fault data for the Loma Prieta earthquake.

Amplification factors from the Northridge earthquake do not show the same degree of nonlinearity in Figure 4.7.11, as do the results from Loma Prieta. Because the current *UBC* is based mainly on observational data from the Loma Prieta earthquake (e.g., Borcherdt 1994), amplification factors presented in the *UBC* may lead to underestimation of high amplitude ground motions.

The spectral amplification factors from each earthquake were combined to develop a set of recommended amplification factors. The factors were combined at equal PGA values. The relationship between PGA and distance is not unique for both earthquakes, because event-specific attenuation relationships are used for each earthquake. The two earthquakes were combined using a weighting scheme that gives to each earthquake a weight inversely proportional to the variance of the sample mean. The equations and coefficients used to determine the amplification factors are provided in Rodriguez-Marek et al. (1999). The resulting amplification factors are shown in Figure 4.7.12. The standard errors for each site condition were averaged using the same weighting scheme (Rodriguez-Marek et al., 1999).

For the sake of comparison with current code provisions, the spectral amplification factors were averaged over a range of periods to obtain short-period and mid-period amplification factors. The period range for the short-period amplification factor (Fa) is 0.1 to 0.5 s, and the period range for the mid-period amplification factor (Fv) is 0.4 to 2.0 s (Borcherdt, 1994). The mean factors were averaged from a double

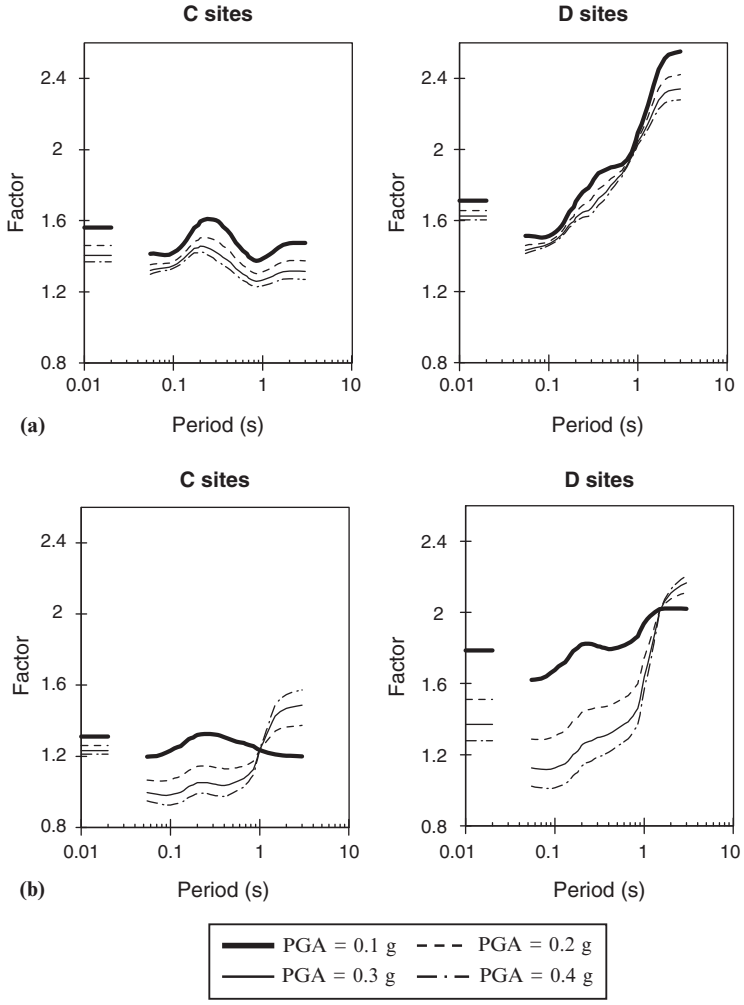

Fig. 4.7.11 Spectral amplification factors (5% damping) with respect to site B (rock): (a) Northridge earthquake, and (b) Loma Prieta earthquake

logarithmic plot of amplification factors versus period. The values of the code factors (UBC, 1997) and the factors obtained in this work are given in Table 4.7.5. The UBC and proposed schemes generally group sites into the same site categories, so this comparison offers useful insights regarding the relative magnitude of the site factors.

The short-period amplification factors (Fa) obtained in this work are larger than the code values. This is due in large part to the larger levels of motion observed in the Northridge earthquake, which was not included in the studies that led to the adoption of the 1997 UBC factors. Additionally, the site classification scheme adopted for the 1997 UBC differs from that proposed in this study, so that some sites are classified

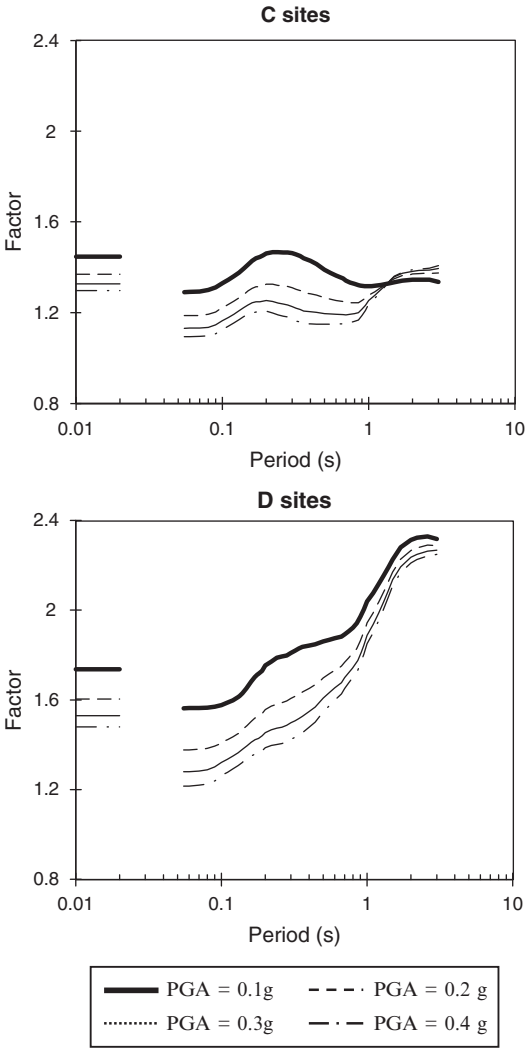

Fig. 4.7.12 Generalized spectral amplification factors (5% damping) with respect to site B (rock) using weighted mean of the Northridge and Loma Prieta earthquakes

differently. In addition, the intermediate-period amplification factors from the proposed site classification show less nonlinearity than the code factors. This is consistent with "soil" to "rock" amplification factors obtained by Abrahamson and Silva (1997) using a much broader database. Overall, the differences in the amplification factors are generally less than 25%. However, the differences in the short-period amplification factors (Fa) for $Z = 0.4$ are judged to be significant, because changes in these factors in Zone 4 can significantly impact design, and this work indicates that the current code factors are low. As additional data becomes available, these two site classification systems warrant further comparisons.

4.7.7 Conclusion

The strong ground motion data from the Loma Prieta and Northridge earthquakes were analyzed and used to evaluate a new simplified geotechnical site classification scheme developed to account for site effects in probabilistic seismic hazard assessments. The proposed classification scheme is based on a general geotechnical characterization of the site that includes soil depth and stiffness.

The proposed classification scheme results in a significant reduction in standard error when compared with a simpler "rock vs. soil" attenuation relationship approach. Additionally, the generic "outcropping rock" category used in many current attenuation relationships groups competent rock and weathered soft rock/shallow stiff soils. The results shown herein indicate a significant difference in the seismic responses of these two site classes, with competent rock spectral ordinates being about 30% lower than the corresponding spectral ordinates for weathered soft rock/shallow stiff soil sites for the same magnitude and distance. Moreover, "rock" attenuation relationships used in practice are dominated by the weathered soft rock/shallow stiff soil site category due to the preponderance of these sites in the database. The results presented herein point to the need of redefining the baseline "outcropping rock" condition into a more restrictive site category.

The standard errors resulting from the proposed classification system are comparable to the standard errors obtained using the 1997 UBC shear wave velocity-based classification system. However, for profiles within the same UBC classification (i.e., equal average shear-wave velocity), the inclusion of soil depth leads to a significant reduction of uncertainty. Conversely, for sites with a shallow soil depth (i.e., <60 m), refinement of the estimate of profile stiffness in the form of average shear-wave velocity reduces uncertainty levels. For deep stiff soil sites, measurement of the shear-wave velocity over the upper 30 m of the site does not significantly reduce uncertainty in the prediction of seismic site response. These observations indicate that a classification scheme including both soil stiffness and depth leads to better estimates of ground motion.

The relative merits of subdividing deep stiff clay sites (Site D) by soil type (e.g., either sand or clay) and depositional age (e.g., either Holocene or Pleistocene) was also evaluated. Results indicate a trend of higher response for clay sites, especially if Pleistocene. This is consistent with the concept that higher plasticity soils have higher threshold strains and hence, exhibit less shear modulus reduction and less material damping at intermediate levels of ground motion.

Spectral amplification factors with respect to competent bedrock were developed. Overall, the differences between the proposed and 1997 UBC site amplification factors are not large; however, the differences are sufficient, especially for Zone 4, to warrant further re-evaluation of the code factors. Additionally, the spectral amplification factors presented herein can be used in probabilistic seismic hazard assessments, because, unlike the code site factors, the proposed site amplification factors include quantification of the underlying uncertainty in the site-dependent ground motion estimate. However, caution should be exercised when using these factors, because they are obtained from a data set containing only two earthquakes.

Hence, intra-event scatter could be assessed for these two earthquakes, but inter-event scatter could not be evaluated satisfactorily. Moreover, due to the scarcity of the data, results are not well defined for near-fault conditions. Finally, the two earthquakes used in this study are shallow crustal events from a tectonically active region. Caution should be exercised when applying these amplification factors to regions with significantly different geologic and tectonic conditions.

Acknowledgments Financial support was provided by the Pacific Gas & Electric Company through the Pacific Engineering Earthquake Research Center, and by the David and Lucile Packard Foundation. The authors also wish to thank Dr. Walter Silva of Pacific Engineering and Analysis for his assistance in providing the ground motion database used in this study; Dr. François E. Heuze of the Lawrence Livermore National Laboratory for his assistance in sharing their geotechnical database; Dr. Paul Somerville for providing event-specific attenuation relationships for the Northridge and Loma Prieta earthquakes; Dr. Mladen Vucetic, Dr. Sands Figuers, and Dr. David Rogers for providing essential geotechnical data for ground motion sites; Dr. Jonathan Stewart for the information on the Oakland BART Station site and numerous sites in Southern California; and Dr. Susan Chang for her willingness to share knowledge and information on ground motion site classification.

References

Abrahamson, N. A. and Silva, W. J., 1997, Empirical response spectral attenuation relationships for shallow crustal earthquakes, *Seismol. Res. Lett*. **68**(1), 94–127.

Abrahamson, N. A. and Somerville, P. G., 1996, Effects of the hanging wall and footwall on ground motions recorded during the Northridge earthquake, *Bull. Seismol. Soc. Am*. **86**(1B), S93–S99.

Benjamin, J. R. and Cornell, A., 1970, *Probability, Statistics, and Decision for Civil Engineers*, Mc Graw-Hill, New York.

Borcherdt, R. D., 1994, Estimates of site-dependent response spectra for design (methodology and justification), *Earthq. Spectra* **10**(4), 617–653.

Bray, J. D. and Rodriguez-Marek, A., 1997, Geotechnical site categories, *Proceedings of the First PEER-PG&E Workshop on Seismic Reliability of Utility Lifelines*, San Francisco, CA, August.

Campbell, K. W., 1997, Empirical near-source attenuation relationships for horizontal and vertical components of peak ground acceleration, peak ground velocity, and pseudo-absolute acceleration response spectra, *Seismol. Res. Lett*. **68**(1), 154–179.

Chang, W. S., Bray, J. D., Gookin, W. B., and Riemer, M. F., 1997, Seismic response of deep stiff soil deposits in the Los Angeles, California area during the 1994 Northridge earthquake, *Report No. UCB/GT 97/01*, Geotechnical Engineering, Department of Civil and Environmental Engineering, University of California, Berkeley, CA.

Dobry, R., Martin, G. M., Parra, E., and Bhattacharyya, A., 1994, Development of site-dependent ratios of elastic response spectra (RRS) and site categories for building seismic codes, *Proceedings of the 1992 NCEER/SEAOC/BSSC Workshop on Site Response During Earthquakes and Seismic Code Provisions*, University of Southern California, Los Angeles, CA, November 18–20, 1992, G. R. Martin, ed.

Idriss, I. M., 1991, *Procedures for Selecting Earthquake Ground Motions at Rock Sites*, Report to the National Institute of Standards and Technology, University of California at Davis, September, revised March 1993.

Idriss, I. M. and Silva, W. J., 1999, personal communication.

ICBO (International Council of Building Officials), 1997, *Uniform Building Code*, Whittier, CA.

Rodriguez-Marek, A., Bray, J. D., and Abrahamson, N., 1999, Task 3: Characterization of site response, general site categories, *Pacific Earthquake Engineering Research Center Report 1999/03*, College of Engineering, University of California, Berkeley, CA.

Sadigh, K., Chang, C. Y., Egan, J. A., Makdisi, F., and Youngs, R. R., 1997, Attenuation relationships for shallow crustal earthquakes based on California strong motion data, *Seismol. Res. Lett*. **68**(1), 180–189.

Seed, H. B., and Idriss, I. M., 1982, Ground motions and soil liquefaction during earthquakes, *Engineering Monographs on Earthquake Criteria, Structural Design, and Strong Motion Records*, Vol. 5., Earthquake Engineering Research Institute.

Seed, H. B., Whitman, R. V., Dezfulian, H., Dobry, R., and Idriss, I. M., 1972, Soil conditions and building damage in the 1967 Caracas earthquake, *J. Soil Mech. Found. Div*. ASCE **98**(SM8), 787–806.

Seed, R. B., Dickenson, S. E., and Mok, C. M., 1991, Seismic response analysis of soft and deep cohesive sites: A brief summary of recent findings, *Proceedings of the CALTRANS First Annual Seismic Response Workshop*, Sacramento, CA, December 3–4.

Silva, W. J., 1998, personal communication.

Somerville, P. G., 1998, personal communication.

Somerville, P. G., Smith, N. F., Graves, R. W., and Abrahamson, N. A., 1997, Modification of empirical strong ground motion attenuation relations to include the amplitude and duration effects of rupture directivity, *Seismol. Res. Lett*. **68**(1), 199–222.

Trifunac, M. D. and Todorovska, M. I., 1996, Nonlinear soil response – 1994 Northridge, California, earthquake, *J. Geotech. Eng*. ASCE **122**(9), 725–735.

Vucetic, M. and Dobry, R., 1991, Effect of soil plasticity on cyclic response, *J. Geotech. Eng*. ASCE **117**(1), 89–107.

Appendix

Table A1 Ground motion stations from the Loma Prieta earthquake used in this study indicating site classification according to Table 4.7.1 (? indicates uncertainty about the classification)

Agency	Station	Class
CDMG	47006	C2
CDMG	47125	C2?
CDMG	47179	D?1C?
CDMG	47189	B
CDMG	47377	C1?
CDMG	47379	B
CDMG	47380	D1C
CDMG	47381	D1C
CDMG	47524	D1C?
CDMG	57007	C1
CDMG	57064	D?2S
CDMG	57066	D1C
CDMG	57191	C2?
CDMG	57382	D1C
CDMG	57383	C1
CDMG	57425	C2
CDMG	57476	C2?
CDMG	57504	C3?
CDMG	57563	B?

(continued)

Table A1 (continued)

Agency	Station	Class
CDMG	58043	B
CDMG	58065	C2?
CDMG	58117	F
CDMG	58127	B
CDMG	58130	C1
CDMG	58131	B
CDMG	58132	B?
CDMG	58133	B?
CDMG	58135	C1
CDMG	58151	B?
CDMG	58163	C1
CDMG	58219	C?1?
CDMG	58222	C1
CDMG	58223	E1
CDMG	58224	D2C
CDMG	58235	C2?
CDMG	58262	C1
CDMG	58264	E1
CDMG	58338	B
CDMG	58373	C1
CDMG	58375	E2
CDMG	58378	C1
CDMG	58393	D2C
CDMG	58471	C1
CDMG	58472	D1C
CDMG	58498	D?2C
CDMG	58505	C3?
CDMG	58539	B
Navy	NAS	E1
UCSC	13	B?
UCSC	15	C2?
UCSC	16	C?1
USGS	PNM	B
USGS	SNF	D?2S
USGS	1002	E1
USGS	1028	D1C
USGS	1032	B
USGS	1129	B
USGS	1161	C3?
USGS	1474	C2
USGS	1479	C2
USGS	1481	D1C
USGS	1515	E1
USGS	1590	E2
USGS	1601	C2
USGS	1652	C3?
USGS	1656	D1C?
USGS	1675	B
USGS	1678	C?1
USGS	1686	D?2S
USGS	1695	D1C?

(continued)

Table A1 (continued)

Agency	Station	Class
CDMG	12673	D1C?
CDMG	13122	D?1S?
CDMG	13123	C2
CDMG	13160	D?2S?
CDMG	13197	D2S?
CDMG	13610	C1
CDMG	13660	D1C?
CDMG	14159	C?1
CDMG	14196	D2S?
CDMG	14242	D2S?
CDMG	14368	D1S?
CDMG	14403	D2C
CDMG	14404	C1
CDMG	14405	C1
CDMG	14560	D2S?
CDMG	14578	D2S
CDMG	23497	D1S
CDMG	23542	D?1S
CDMG	23572	C?1
CDMG	23573	C2?
CDMG	23574	C2?
CDMG	23590	B?
CDMG	23595	B?
CDMG	23597	D1S?
CDMG	23598	B?
CDMG	23672	D?1S?
CDMG	24047	B?
CDMG	24055	C2?
CDMG	24087	D1S
CDMG	24088	C1
CDMG	24092	D?1S?
CDMG	24157	D2C?
CDMG	24207	B
CDMG	24207	B
CDMG	24271	D2C
CDMG	24278	C?1
CDMG	24279	C3
CDMG	24281	D1S
CDMG	24283	D1S
CDMG	24303	D1C
CDMG	24305	B
CDMG	24306	C2?
CDMG	24307	B?
CDMG	24308	C1?
CDMG	24309	C?1
CDMG	24310	C?1
CDMG	24389	D2C?
CDMG	24396	C1?
CDMG	24399	C1

(continued)

Table A1 (continued)

Agency	Station	Class
CDMG	24400	F?
CDMG	24401	C3?
CDMG	24436	C2?
CDMG	24461	C3?
CDMG	24469	B
CDMG	24475	D1S
CDMG	24514	D1C?
CDMG	24521	C3?
CDMG	24523	B
CDMG	24538	D2C
CDMG	24575	C?2
CDMG	24576	C?2
CDMG	24586	D1S?
CDMG	24592	C?1
CDMG	24605	C1
CDMG	24607	C?1
CDMG	24611	C1
CDMG	24612	D1S
CDMG	24644	C?1
CDMG	24688	C2
CDMG	25091	C1
CDMG	25147	D1C?
CDMG	25148	C?1
CDMG	25169	C2?
CDMG	25282	D1C?
CDMG	25340	D1C
CDMG	34093	D?1?S?
CDMG	34237	D?1?S?
DWP	74	D1S
DWP	75	D1S?
DWP	77	C2
USC	90003	D1C
USC	90006	C2
USC	90009	C2
USC	90011	F
USC	90013	C1
USC	90014	C1
USC	90015	C1
USC	90016	C1
USC	90017	B
USC	90018	D2C
USC	90019	C?2
USC	90020	D2S
USC	90021	C2
USC	90022	D?1S
USC	90025	D1C?
USC	90032	C2
USC	90033	C2
USC	90034	D?1S
USC	90040	D2S

(continued)

Table A1 (continued)

Agency	Station	Class
USC	90044	C1?
USC	90045	D2C?
USC	90046	D1S
USC	90047	F
USC	90049	C2
USC	90051	C2
USC	90053	C3
USC	90054	C3
USC	90055	C2
USC	90056	C2?
USC	90057	D?1S
USC	90058	C3
USC	90059	C?1
USC	90060	C3
USC	90061	C1
USC	90063	C3?
USC	90065	C3?
USC	90066	F
USC	90067	C2?
USC	90068	C3
USC	90069	C2
USC	90070	C3
USC	90071	C2
USC	90072	D?1S?
USC	90073	C3?
USC	90074	D2C?
USC	90075	C2
USC	90077	C3?
USC	90078	F
USC	90079	D1S
USC	90081	F
USC	90082	D1C
USC	90083	D1C?
USC	90084	D1S?
USC	90085	D?1C
USC	90086	D1S (F?)
USC	90087	D?2C
USC	90088	D1S?
USC	90089	F
USC	90090	C?2
USC	90091	F
USC	90093	D?1S?
USC	90094	D1S?
USC	90095	C3?
USC	90096	D1C
USC	90099	D?1S?
USGS	LA Dam	C1
USGS	127	C?1
USGS	637	D2C
USGS	638	D?2S?

(continued)

Table A1 (continued)

Agency	Station	Class
USGS	655	F
USGS	5080	B?
USGS	5081	C2?
USGS	5108	C1

Chapter 5
Conclusions

After 3 days of lectures and discussions, 30 participants from 14 countries agreed on the following answers to the questions posed before the workshop:

Q – Can we use ambient noise for building and soil characterization, and to extract useful information for engineers?
A – There is general agreement that noise allows the estimation of fundamental frequency of soils and mode shapes for linear elastic-behaving buildings. There is no consensus on the use of amplitudes retrieved from HVSR for soils. Investigation should be devoted to understand why in some cases there is a good agreement with SSR while in other cases HVSR fails to predict spectral amplitudes. More reliable classification schemes of soil aimed to seismic code can be obtained including soil fundamental frequency together with other parameters (e.g. Vs30). Noise measurements may help to export soil classification systems and building period-to-height relationships from one region to another. Furthermore, it is desirable to develop relationships to extrapolate determination of fundamental frequencies during stronger shaking from those determined using low-amplitude (ambient noise) data.
Q – How can we tell apart a frequency decrease due to a distributed damage, concentrated damage, or time-varying building and soil behaviour? How to couple soil and building non-linear behaviour?
A – At the moment there are very few data available to reach an answer. It would be desirable to have public links to data in order to allow different groups to share information. Moreover, long term building monitoring will provide control points for comparison and to envisage which strategy is better for single structures or large sets of buildings. In order to facilitate this, specific recommendations for permanent monitoring arrays ought to be developed.
Q – Which is the role of transients in ambient noise analysis?
A – There is no consensus in the seismological community about the effects of transients on noise measurement in the free-field. For engineering purposes, transient in buildings are standard practice (e.g. vibrodyne and shock tests, wind

M. Mucciarelli et al., (eds.), *Increasing Seismic Safety by Combining Engineering Technologies and Seismological Data,* NATO Science for Peace and Security Series C: Environmental Security, © Springer Science+Business Media B.V. 2009

gusts). This is one of the topics that point out the need for standardised techniques of data collection and processing on soil and in buildings.

Q – Can we quantify the influence of existing buildings on ground-motion recordings (both of noise and of earthquakes)?

A – At the moment there is empirical evidence of the importance of the effect of a single building on free-field recordings, while only numerical evidence is provided for the effect of a large set of building. To gather experimental evidence, new monitoring strategies have to be implemented, as well as dedicated data-processing techniques. In addition, transients in recorded strong-motion responses of buildings may indicate damage and propagation of damage. Uncertainty still exists for soil structure interaction, if it is visible in noise measurements or it becomes evident only with strong motion.

Q – To which extent is soil-building resonance a cause of damage enhancement?

A – There is general agreement that soil-building resonance can be a cause of damage enhancement. There are suggestions that peculiar damage patterns (e.g. the collapse of a single building in a set of identical ones) could be due to city-soil interaction. There is the need to better quantify the occurrence of resonance taking into account the time-varying, non-linear behaviour of soil and building subjected to strong ground motion.